UNIVERSITY OF
OXFORD

Blood transcriptomic profiles associated with fatal melioidosis and type 2 diabetes induced susceptibility to intracellular pathogens

Patpong Rongkard

St Hugh's College

University of Oxford

A thesis submitted for the degree of

Doctor of Philosophy

Trinity Term 2022

Supervisors: Susanna Dunachie, Paul Klenerman, Barbara Kronsteiner-Dobramysl

Abstract

Blood transcriptomic profiles associated with fatal melioidosis and type 2 diabetes-induced susceptibility to intracellular pathogens

Patpong Rongkard

St Hugh's College

Submitted for the degree of Doctor of Philosophy

Trinity Term 2022

Background: Melioidosis is caused by the Gram-negative bacterium *Burkholderia pseudomallei,* and is a leading cause of death from community-acquired infections in Northeast Thailand with a case fatality rate of up to 50%. Most melioidosis patients have one or more comorbidities, and more than half of patients have diabetes which confers a 12-fold increased susceptibility to melioidosis. A similar, but less marked, relationship is seen in tuberculosis (TB) patients, with a 3-fold increased risk of developing TB in people with diabetes. Little is known regarding the mechanisms underlying the increased susceptibility in diabetes to these intracellular pathogens. Likewise, the host response associated with fatal melioidosis remains to be fully elucidated.

Methods: Whole blood RNA sequencing data were generated from three independent melioidosis cohorts from Northeast Thailand and one global multi-site tuberculosis study. Both supervised and unsupervised data analysis approaches were performed including differential gene expression (DGE) analysis, pathway analyses, upstream regulator analysis, weighted gene co-expression network analysis (WGCNA), and hub gene analysis.

Results: Firstly, principal component analysis (PCA) revealed clear separation between fatal and surviving melioidosis patients. DGE analysis identified profound changes in the transcriptome of fatal melioidosis cases with over 600 up- and 1,000 down-regulated genes compared to survivors. Pathway analyses following DGE analysis identified exaggerated

inflammation and up-regulated type 2 immune responses concurrent with massively down-regulated T cell signalling cascades in fatal melioidosis. Upstream regulator analysis identified potential key regulators associated with fatality during melioidosis including *TNF, IL4, IL1A*, *PTGER2*, and *OSM*. Likewise, the unsupervised analysis by WGCNA confirmed that several co-expressed gene modules enriched for inflammatory immune responses driven by the innate immune compartment were associated with 28-day mortality. Furthermore, hub genes associated with fatal melioidosis such as *CEACAM1, SERPINB1* and *SORT1* may play deleterious roles during melioidosis.

Secondly, the impact of diabetes on the transcriptome was subtle in acute melioidosis, with similar but more pronounced changes in TB, which is a more chronic disease. Diabetes status was associated with enhanced non-specific inflammatory responses for both melioidosis and TB, alongside failure to fully switch on interferon-mediated responses for TB.

Conclusion: The transcriptomic signature in fatal melioidosis is characterised by concomitant excessive inflammation, a pronounced anti-inflammatory response, and a stunted T cell response. These results highlight the pivotal role of adaptive immunity during fatal melioidosis. Furthermore, diabetes is associated with increased activation of innate pathways and reduced interferon responses which may contribute to the increased susceptibility observed for these intracellular pathogens.

Publications

Published

Fidler S, Fox J, Tipoe T, Longet S, …, **Rongkard R**,…, Frater J. **Booster vaccinations against SARS-CoV-2 induce potent immune responses in people with HIV**. Clinical Infectious Diseases. 2022 Sep. Accepted.

Tomic A, Skelly DT, Ogbe A, …, **Rongkard P**, …, Dunachie SJ. **Divergent trajectories of antiviral memory after SARS-CoV-2 infection**. Nat Commun. 2022 Mar 10;13(1):1251.

Angyal A, Longet S, Moore SC, …, **Rongkard P**, …, de Silva TI; PITCH Consortium. **T-cell and antibody responses to first BNT162b2 vaccine dose in previously infected and SARS-CoV-2-naive UK health-care workers: a multicentre prospective cohort study**. Lancet Microbe. 2022 Jan;3(1):e21-e31.

Frater J, Ewer KJ, Ogbe A, …, **Rongkard P**, …, Lambe T; Oxford COVID Vaccine Trial Group. **Safety and immunogenicity of the ChAdOx1 nCoV-19 (AZD1222) vaccine against SARS-CoV-2 in HIV infection: a single-arm substudy of a phase 2/3 clinical trial**. Lancet HIV. 2021 Aug;8(8):e474-e485.

Ogbe A, Kronsteiner B, Skelly DT, …, **Rongkard P,** …, Dunachie S. **T cell assays differentiate clinical and subclinical SARS-CoV-2 infections from cross-reactive antiviral responses**. Nat Commun. 2021 Apr 6;12(1):2055.

Skelly DT, Harding AC, Gilbert-Jaramillo J, Knight ML, et al., **Two doses of SARS-CoV-2 vaccination induce robust immune responses to emerging SARS-CoV-2 variants of concern.** Nat Commun. 2021 Aug 17;12(1):5061. Listed as author within Protective Immunity T cells in Health Care Worker (PITCH) consortium.

Payne RP, Longet S, Austin JA, Skelly DT, et al. **Immunogenicity of standard and extended dosing intervals of BNT162b2 mRNA vaccine.** Cell. 2021 Nov 11;184(23):5699-5714.e11. Listed as author within Protective Immunity T cells in Health Care Worker (PITCH) consortium.

Manuscripts in preparation

Patpong Rongkard, Lu Xia, Barbara Kronsteiner-Dobramysl, Thatcha Yimthin, Rungnapa Phunpang, Adul Dulsuk, Viriya Hantrakun, Gumphol Wongsuvan, Prapit Teparrukkul, Lara Lovelace-Macon, Nicholas P.J. Day, Paul Klenerman, Direk Limmathurotsakul, Narisara Chantratita, Susanna J. Dunachie, Sina A. Gharib, T. Eoin West. **T-cell dysregulation is associated with fatality in community-acquired melioidosis.** *In preparation.*

Patpong Rongkard, Lu Xia, Barbara Kronsteiner-Dobramysl, Thatcha Yimthin, Rungnapa Phunpang, Adul Dulsuk, Viriya Hantrakun, Gumphol Wongsuvan, Prapit Teparrukkul, Lara Lovelace-Macon, Nicholas P.J. Day, Paul Klenerman, Direk Limmathurotsakul, Narisara

Chantratita, Susanna J. Dunachie, Sina A. Gharib, T. Eoin West**. Multi-omic signature of melioidosis in community acquired infection.** *In preparation.*

Patpong Rongkard, Barbara Kronsteiner-Dobramysl, Gumphol Wongsuvan, Prapit Teparrukkul, Nicholas P.J. Day, Paul Klenerman, Direk Limmathurotsakul, Narisara Chantratita, Susanna J. Dunachie. **Increased inflammatory immune response associated with poor outcome and type II diabetes in melioidosis.** *In preparation.*

The impact of COVID-19 pandemic on this thesis

This thesis was partially affected by the COVID-19 pandemic. Originally, I planned to spend at least 6 months at the University of Washington from June 2020 for training and work on the transcriptomic data of Chapter 5, including development of predictive models and multi-omic data integration. This visit was cancelled and the collaboration continued remotely. Therefore, the development of my techniques to include a predictive model of case fatality in melioidosis and to distinguish melioidosis from other infections is still underway and not included in this thesis. Nevertheless, in parallel to undertaking my transcriptomic analysis I have contributed my time and expertise in 2020-21 to several COVID-19 projects based at the Peter Medawar Building for Pathogen Research as a part of the Protective Immunity T cells in Health Care Worker (PITCH) consortium. My contributions have been recognised with authorship on the listed publications from the COVID-19 studies.

Acknowledgements

I would like to express my deepest gratitude to Professor Susanna Dunachie, for giving me the opportunity to work on this project. This project would not have been possible without her support and guidance. I would also like to thank my co-supervisors Professor Paul Klenerman and Dr. Barbara Kronsteiner-Dobramysl. Likewise, I am deeply indebted to Professor Eoin West and Professor Direk Limmathurotsakul for giving me the opportunity to work on the untouched, largest transcriptomic data set of human melioidosis. Also, I would like to thank Professor Narisara Chantratita and Thatcha Timthin for the validation data set and Dr. Jackie Cliff and Professor Gregory Bancroft for the tuberculosis data set.

From the start of my DPhil, I have been supported by the Klenerman group including Dr. Emanuele Marchi, Dr. Lucy Garner, and Dr. Narayan Ramamurthy on RNA-seq data analyses and setting up my experiments. Furthermore, I have received support from Professor Sina Gharib and Dr. Lu Xia from University of Washington for advice, assistance, and opportunity to learn new analysis techniques. I have been tremendously supported by colleagues from the Dunachie group, especially Dr. Mohammad Ali, Dr. Jennifer Hill, Dr. Martha Zewdie and Hossian Akther from the Klenerman group for their helpful thoughts and discussions. Also, I would like to thank Dr. Barbara Kronsteiner and Carl-Philipp Hackstein for the thoughts and support for the validation experiments.

Of course, I would not have completed this journey without the motivation and mental support from my family; my mom Chuennapha, my grandmother Yen, my sister Patcharin, and my nephews Prem and Peun who were always there when I needed. I also would like to thank MORU including Professor Nick Day for financial support, career development and support from the colleagues, friends, and colleagues at Peter Medawar building. This project would not have been possible without everyone who were involved in running all the studies

in Thailand including doctors, nurses, lab staff, and project management teams; I am deeply appreciated all the efforts had been made to make all the studies so successful.

Statement of responsibility

All work presented in this thesis is my own, unless stated otherwise. In **Chapter 3**, I prepared RNA samples for RNA sequencing which was performed by the Oxford Genomics Centre, Wellcome Centre for Human Genetics, and I undertook the first and primary analysis. In **Chapter 4**, data from the TANDEM (TB and Diabetes Mellitus) study were kindly provided by Dr. Jackie Cliff and Professor Gregory as a collaborative project, published in Eckold *et al.*, Impact of Intermediate Hyperglycemia and Diabetes on Immune Dysfunction in Tuberculosis. *Clin Infect Dis* 72, 69-78 (2021). I re-analysed and compared with data from **Chapter 3**. In **Chapter 5**, data were generated by the University of Washington Northwest Genomics Centre and kindly provided by Professor Eoin West as a collaborative project, and my work represents the first and primary analysis. In **Chapter 6**, data were kindly provided by Professor Narisara Chantratita as a validation data set for **Chapter 5** from a publication: Yimthin *et al.*, Blood transcriptomics to characterize key biological pathways and identify biomarkers for predicting mortality in melioidosis. *Emerg Microbes Infect* 10, 8-18 (2021).

List of abbreviations

AGE	Advanced Glycation End product
AhpC	Alkyl hydroperoxidase reductase subunit C
APC	Antigen Presenting Cell
BCG	*Mycobacterium bovis* Bacillus Calmette-Guérin
Bp	Burkholderia pseudomallei
CAP	Community-Acquired Pneumoniae
CPS	Capsular Polysaccharide
CRP	C-Reactive Protein
CTLA-4	Cytotoxic T-lymphocyte associated protein 4
DAMP	Damage-Associated Molecular Pattern
DEG	Differentially Expressed Gene
DGE	Differential Gene Expression
DIC	Disseminated Intravascular Coagulation
DPP-4	Dipeptidyl Peptidase 4
E. coli	*Escherichia coli*
ELISpot	Enzyme-Linked Immunosorbent Spot
ER	Endoplasmic Reticulum
FDR	False Discovery Rate
GHS	Glutathione
GLP-1	Glucagon-Like Peptide-1
GSEA	Gene Set Enrichment Analysis
H. influenzae	*Haemophilus influenzae*
HbA1c	Glycated haemoglobin
Hcp1	Hemolysin co-regulated protein 1
HIV	Human Immunodeficiency Virus
HLA	Human Leukocyte Antigen
ICU	Intensive Care Unit
IL	Interleukin
iNOS	inducible Nitric Oxide Synthase
Interferon	IFN
IPA	Ingenuity Pathway Analysis
IRAK-M	Interleukin-1R-associated-kinase-M
K. pneumoniae	*Klebsiella pneumoniae*
LADA	Latent Autoimmune Diabetes
LMIC	Low- and Middle-Income Country
LPS	Lipopolysaccharide
LTBI	Latent TB infection
MALDI-TOF MS	Matrix-Assisted Laser Desorption/Ionisation—Time of Flight Mass Spectrometry
MD	Myeloid Differentiation factor
MDR-TB	Multi-Drug Resistant Tuberculosis
MDSC	Myeloid-Derived Suppressor Cell
ME	Module Eigengene
MHC	Major Histocompatibility Complex

MODY	Maturity Onset Diabetes of the Young
MPO	Myeloperoxidase
MRSA	Methicillin-Resistant *Staphylococcus aureus*
MsigDB	Molecular Signatures DataBase
Mtb	Mycobacterium tuberculosis
MyD88	Myeloid Differentiation primary response gene 88
NADH	Nicotinamide Adenine Dinucleotide
NADPH	Nicotinamide Adenine Dinucleotide Phosphate
NCD	Non-Communicable Disease
NET	Neutrophil Extracellular Trap
NE	Neutrophil Elastase
NF-κB	Nuclear Factor kappa B
NK	Natural Killer
NLR	Nucleotide-binding and Oligomerisation Domain (NOD)-Like Receptor
NLRC4	Nod-Like Receptor family CARD domain Containing 4
NLRP3	Nod-Like Receptor family Pyrin domain containing 3
PAMP	Pathogen-Associated Molecular Pattern
PBMC	Peripheral Blood Mononuclear Cell
PCA	Principal Component Analysis
PD-1	Programmed cell Death protein-1
PD-L1	Programmed cell Death Ligand-1
PKC	Protein Kinase C
PRR	Pattern Recognition Receptor
RLR	Retinoic acid-Inducible Gene-I (RIG-I)-like receptor
RNS	Reactive Nitrogen Species
ROS	Reactive Oxygen Species
RPKM	Reads Per Kilobase of transcript per Million reads Mapped
S. aureus	*Staphylococcus aureus*
S. pneumoniae	*Streptococcus pneumoniae*
SARS-COV2	Severe Acute Respiratory Syndrome Coronavirus 2
SGLT2	Sodium-Glucose Co-Transporter-2
SOFA	Sequential Organ Failure Assessment
Spp.	Species
SRS	Sepsis Response Signature
STZ	Streptozotocin
T1DM	Type 1 Diabetes
T2DM	Type 2 Diabetes
TB	Tuberculosis
TCR	T-Cell Receptor
TLR	Toll-Like Receptor
TNF	Tumour Necrosis Factor
Treg	Regulatory T cell
TTSS3	Type III Secretion System
TTSS6	Type VI Secretion System
UPR	Unfolded Protein Response
VST	Variance Stabilising Transformation

WGCNA	Weighted Gene Co-expression Network Analysis
WHO	World Health Organisation
XDR-TB	Extensive multi-drug resistant tuberculosis

Table of Contents

Chapter 1: Introduction

1.1 Melioidosis, a neglected 'neglected tropical disease" that kills up to half of infected individuals in endemic regions

1.1.1 Melioidosis is more prevalent than we appreciated

Melioidosis is a fatal infectious disease caused by infection with the Gram-negative bacillus, *Burkholderia pseudomallei* (Bp) affecting both humans and animals (*1, 2*). The bacterium is an environmental saprophyte, commonly found in soil and surface water in endemic areas, particularly in tropical and subtropical climate countries (*3*). A prediction model of the global burden of melioidosis from 2015 estimated there were 165,000 cases with 89,000 deaths annually worldwide, with a much wider distribution in tropical countries across the globe than previously appreciated (**Figure 1.1**) (*4, 5*). In Thailand, melioidosis is highly endemic in the Northeast of Thailand, and melioidosis cases have been reported across the country as well as environmental isolates (*6-8*). Melioidosis can be acquired via inoculation, ingestion, and inhalation (*9, 10*). A case-control study conducted in Northeast Thailand identified activities associated with acquisition of melioidosis such as working in rice fields, outdoor exposure to rain, and eating/drinking contaminated food/water (*11*). Similar outcomes have been observed in other endemic regions, and melioidosis cases typically peak during rainy season with heavy rainfall associated with more severe disease and worse outcomes (*12-15*).

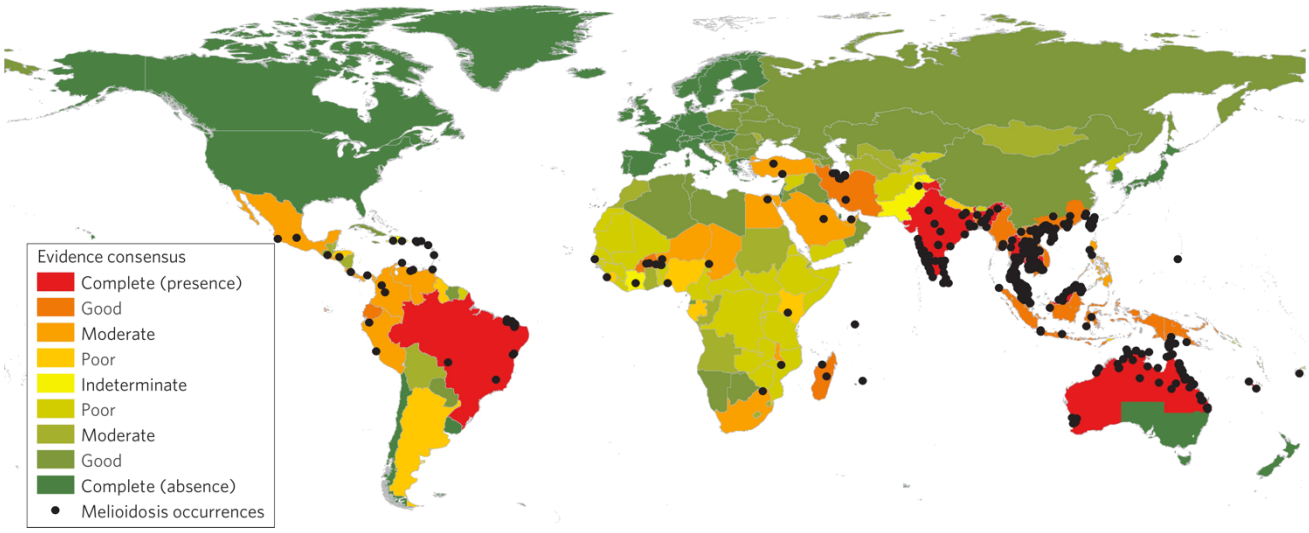

Figure 1.1 Global burden of melioidosis and *Burkholderia pseudomallei* between 1910 and 2014. Each country was labelled ranging from red to green indicating a complete consensus on presence to absence of Bp isolates. Each black dot represents identified melioidosis cases based on geographic locations (*4*). Reproduced with licence from Limmathurotsakul *et al.*, Predicted global distribution of Burkholderia pseudomallei and burden of melioidosis. *Nat Microbiol* 1, 15008 (2016). Licence number: 5380330406195.

1.1.2 Clinical manifestations of melioidosis are broad and ambiguous

Melioidosis usually presents as an acute infection (85%); however, the infection can result in chronic (11%) or latent (4%) disease (*9, 16, 17*). Clinical manifestations of melioidosis are broad and can resemble the clinical syndromes of other diseases such as TB, sepsis, and community-acquired pneumonia (*17*). In acute melioidosis, more than half of the patients are bacteraemic and / or present with pneumonia, and a sepsis syndrome is common with about 20% developing septic shock (*10*). Formation of abscesses in multiple organs such as liver, spleen, and skeletal muscle is also common (*2*), and more rarely melioidosis can occur in any organ system, with skin, cardiac and neurological manifestations described (*10*).

Recurrent melioidosis due to either relapse of latent infection or re-infection is common. The recurrence rate in Darwin, Australia was 5.7% over a 20-year prospective study (1989-2012) (*18*). Similarly, a prospective study in Northeast Thailand between 1986 and 2005 identified a recurrent rate of 5% (*19*). The in-hospital case fatality rate is up to 40% in northeast of Thailand and 14% in Australia (*9, 20, 21*). However, a recent prospective study between 1997 and 2020 in Townsville, Queensland identified higher case-fatality rates of 23% compared to the Northern Territory, Australia (*22*). Mortality rates in some endemic areas reach 50%, and the clinical presentations associated with poor outcome include pneumonia, bacteraemia, and septic shock (*2, 9, 23, 24*). Differences in case fatality rates between regions may reflect late presentation to hospital in some settings (*25*), differing critical care management (*26*), or regional variation in bacterial virulence factors (*27*).

1.1.3 Early diagnosis of melioidosis is critical for correct treatment

Bacterial culture remains the gold-standard for diagnosis of melioidosis, despite low sensitivity (<60%) as estimated by Bayesian latent class modelling (*28*). Bp grows relatively well on standard laboratory diagnostic agars, but it may take up to 4 days until the bacterial colony appears, and in the absence of experienced laboratory personnel the Bp colony may be dismissed as a contaminating environmental *Pseudomonas* species with no clinical importance (*10, 29*). Therefore, it is challenging in certain settings where melioidosis is less endemic or underappreciated. Bacterial culture from multiple specimens such as throat swabs, abscesses and urine, and the use of selective media may improve detection of Bp (*10, 30*), and the bacteria is correctly identified by Matrix-Assisted Laser Desorption/Ionisation–Time of Flight mass spectrometry (MALDI-TOF MS) if an appropriate database is used (*31*).

Prolonged and intensive use of antibiotics is the only treatment option and consists of two phases: intensive and eradication. The intensive phase is recommended following melioidosis-proven diagnosis with intravenous ceftazidime or meropenem for a minimum of 10 days. It is followed by the eradication phase with oral therapy for at least 3 months, with trimethoprim-sulfamethoxazole recommended (*32*). Currently, there is no licensed vaccine available although a Phase 1 clinical trial of a leading candidate (*33*) is due to take place in Oxford in 2023.

1.1.4 The host immune response against bacterial infection activates both innate and adaptive immune compartments

During the host immune response against a bacterial infection, innate immune cells (e.g., neutrophils, macrophages, dendritic cells), anti-microbial proteins and peptides are the first host defence mechanisms against an invading pathogen (**Figure 1.2**). Innate immune cells sense presence of Pathogen-Associated Molecular Patterns (PAMPs) expressed on or released from a pathogen via Pattern Recognition Receptors (PRRs), with broad specificity. These cells can also detect Damage-Associated Molecular Patterns (DAMPs) released from injured cells or damaged tissues (*34*). Subsequently, this activates a series of inflammatory immune responses leading to elimination of the pathogen, antigen processing and initiation of adaptive immunity (*35*). Within a lymph node, primed antigen presenting cells (chiefly dendritic cells) present a cognate antigen to T and B lymphocytes leading to activation, polarisation, and proliferation of antigen-specific lymphocytes. The activated adaptive immune cells migrate to the site of infection and perform effector functions such as activation of bactericidal activity in phagocytes and direct killing of infected cells (*36*). In parallel, the antigen-specific antibody works in a synergy with the innate and adaptive immune compartments using mechanisms such as neutralisation, opsonisation for

complement activation and phagocytosis. If successful, local, and contained inflammatory immune responses then contract and antigen-specific memory responses are developed for subsequent reinfection with the same pathogen (*37, 38*).

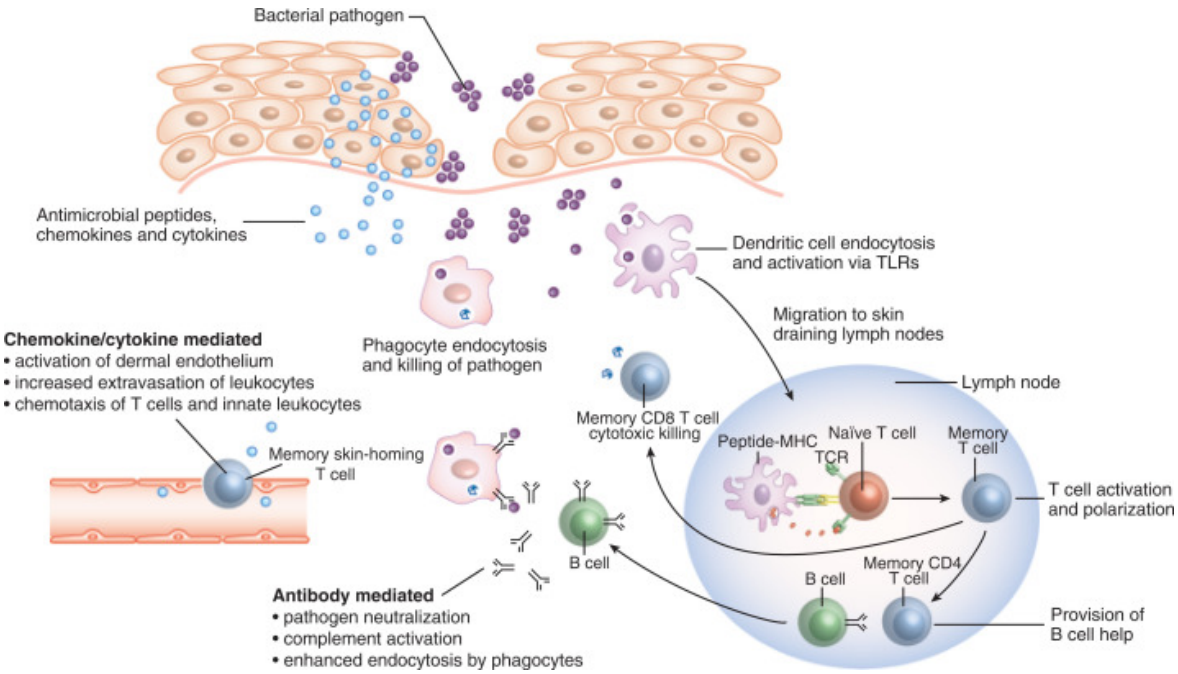

Figure 1.2 Interplay between innate and adaptive immunity during bacterial infection. Following infection, initial host innate immune responses such as anti-microbial peptides, chemokines, and cytokines are deployed to limit the infection and to communicate with other immune cells. At the infection site, innate immune cells such as neutrophils, macrophages and dendritic cells are the first line defenders that further eliminate the pathogen and initiate adaptive immune response. In the lymph node, activation of adaptive immunity is initiated, where a professional antigen presenting cell (APC) presents a cognate antigen to a naïve T lymphocyte. Subsequent events include activation and proliferation of T lymphocytes, activation of B lymphocytes, development of antigen-specific antibody, clearance of remaining pathogen and infected cells, and development of memory capacity in lymphocytes for the subsequent re-infection (*39*). Reproduced with licence from Clark and Kupper, Old meets new: the interaction between innate and adaptive immunity. *J Invest Dermatol* 125, 629-637 (2005). Licence number: 5398730229737.

1.1.5 *Burkholderia pseudomallei* expresses various virulence factors that modulate host immune response

During melioidosis, Bp has mechanisms for evasion of the host immune response. This intracellular bacterium can hide in a dormant state, with the longest reported latent period being 62 years since the first exposure (*16, 40-42*). Virulence factors expressed by Bp during infection include capsular polysaccharide (CPS), lipopolysaccharide (LPS), flagellin, and type III and type VI secretion systems (TTSS3/TTSS6) (*43-47*). For example CPS-expressed Bp is resistant to deposition of complement protein (C3b) and phagocytosis by polymorphonuclear leukocytes (*40*). LPS, one of the most potent immune activator derived from Gram-negative bacteria, is well established in the pathogenesis of sepsis (*48*). During melioidosis, LPS stimulates toll-like receptor-2 (TLR-2) and TLR-4 (in presence of myeloid differentiation factor 2 [MD-2]) to activate downstream pro-inflammatory signalling pathways e.g. via nuclear factor kappa B (NF-κB) leading to bacterial clearance (*49-51*).

1.1.6 *Burkholderia pseudomallei* infection can lead to an excessive host immune response

Persistence of Bp in the human host could potentially over-activate defensive immune response pathways, resulting in an exaggerated inflammatory immune response, onset of sepsis and death in melioidosis (*52-54*). Neutrophils are the most abundant innate myeloid cell and the first line defence against infections, increasing in frequency within hours of pathogenic insults. Neutrophils express broad PRRs (e.g. TLRs and NOD-like receptors [NLRs]), harbour cytotoxic granules (e.g. myeloperoxidase [MPO] and neutrophil elastase [NE]) and employ several key defence mechanisms such as degranulation, phagocytosis, and NETosis to eliminate invading pathogens (*55*). Fatal melioidosis patients show increased plasma cytokines including interleukin-6 (IL-6), IL-8, and IL-10 compared to

survivors (*56, 57*). Moreover, *ex vivo* stimulation with Bp LPS of whole blood obtained from melioidosis patients demonstrates reduced production of pro-inflammatory cytokines such as IL-1β, tumour necrosis factor (TNF), and IL-6 in non-survivors compared to survivors (*58*). Immunosuppression is associated with case fatality, with expression of interleukin-1R-associated-kinase-M (IRAK-M), a negative regulator of TLR being up-regulated in the non-survivors (*58, 59*). In line with evidence from clinical studies, a study by *Ceballos-Olvera et al.* (*60*) demonstrated improved survival, decreased neutrophil infiltration and lower bacterial burden in the lungs of IL-1β-deficient mice compared to wild type mice. In contrast, IL-18 knockout in mice was detrimental, suggesting a protective role of IL-18 while IL-1β may play a deleterious role during melioidosis potentially through recruitment of neutrophils leading to excessive inflammation and tissue damage (**Figure 1.3**).

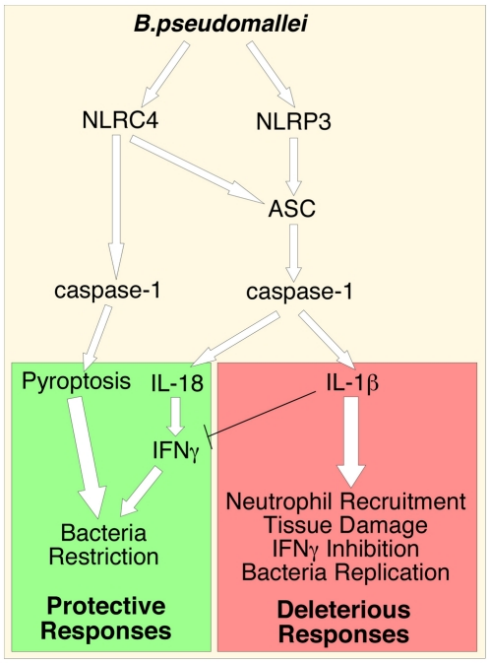

Figure 1.3 Inflammasome-mediated immune response in melioidosis. Following *Burkholderia pseudomallei* (Bp) infection, free-living Bp in the cytosol is recognised by the host intracellular pattern recognition receptors such as Nod-like receptor (NLR) family CARD domain containing 4 (NLRC4) and NLR family pyrin domain containing 3 (NLRP3) leading to activation of the caspase-1 inflammasome response. NLRC4 activates pyroptosis, an inflammatory programmed cell death that contains bacterial growth. While activation of NLRP3 leads to production of pro-inflammatory cytokines, IL-18, and IL-1β. IL-18 promotes IFN-γ production thus facilitating bacterial clearance, whereas IL-1β response leads to infiltration of neutrophils, increased inflammation, and inhibition of protective IFN-γ response (*60*). Reproduced from Ceballos-Olveraet *et al.,* Inflammasome-dependent pyroptosis and IL-18 protect against *Burkholderia pseudomallei* lung infection while IL-1beta is deleterious. *PloS Pathog* **7**, e1002452 (2011). Licence: CC BY 4.0

1.1.7 Genetic predispositions are associated with worse outcome in melioidosis

Host genetic variation of the innate immune system impacts the host immune response during melioidosis. Type I immune responses are indispensable for controlling intracellular infections (*61, 62*). In particular, interferon-γ (IFN-γ) is required for bacterial clearance

mediated by macrophages through bactericidal activities of inducible nitric oxide synthase (iNOS), reactive nitrogen species (RNS), and reactive oxygen species (ROS) in melioidosis (*63, 64*). An experimental melioidosis model identified reduced survival rates in mice treated with αIFN-γ antibody, and similar outcomes were observed when neutralised with αTNF and anti-interleukin-12 (αIL-12) (*61*). Increased frequency of the TNF2 allele in melioidosis and septic shock patients is associated with case fatality (*65, 66*). Increased frequency of human leukocyte antigen (HLA) DRB1*1602 allele but a decrease of DQA1*03 was associated with enhanced susceptibility to melioidosis and disease severity (*67*). Moreover, melioidosis patients with HLA-B*46 and HLA-C*01 were associated with poor outcome (*68*). Nevertheless, the balance of the innate immune response is important, with TLR-2 responses found to be detrimental during experimental melioidosis (*50*). Genetic variants of TLR-4 in humans are associated with increased susceptibility to melioidosis (*69*). Likewise, TLR-5 is key in host defence against melioidosis in flagellin-independent manner (*70*), in which melioidosis patients with TLR5 c.1174C>T variant were associated with survival (*71*).

1.1.8 Cellular immune responses are protective during melioidosis

Cellular immune responses against melioidosis are important, with type I immune responses (e.g. IFN-γ, TNF, IL-18) by T lymphocytes protective against disease progression, bacterial dissemination and clearance (*72*). An experimental melioidosis model (*73*) identified diminished protection against Bp infection in IFN-γ, IL-12-, and IL-18-knockout mice. The primary source of IFN-γ was from natural killer (NK) cells, NK T cells, and conventional T cells, which were dependent on IL-12 and IL-18 following Bp infection. In addition, Bp-specific CD4 T cells in particular were shown to have a protective role in mice following the initial period of infection. However, increased systemic inflammatory responses are

associated with poor outcome. One study identified elevated serum IFN-γ and soluble IL-2R in melioidosis patients with severe disease and associated with case fatality compared to milder cases (*74*). Similarly, another study identified elevated type I immune cytokines including IFN-γ, IL-18, IL-12p40, and IL-15 in melioidosis patients and those with bacteraemia compared to healthy donors (*53*). Melioidosis patients with bacteraemia show elevated plasma levels of CXCL9 and CXCL10, chemokines that regulate Th1 immune response, and found to be correlated with poor outcome (*75*).

In patient studies of acute melioidosis in Ubon Ratchathani, Thailand, patients who survived showed stronger Bp-specific IFN-γ responses and higher frequencies of Bp-specific CD4+ T and CD8+ T cells compared to non-survivors (*76*). Several studies since have identified protective Bp antigens that stimulate T cells and are associated with protection in clinical melioidosis including alkyl hydroperoxidase reductase subunit C (AhpC), the Type III secreted protein BopE, the Type IV pilus biosynthesis protein (PilO), ATP binding protein, BpOmpW, and hemolysin co-regulated protein 1 (Hcp1) (*33, 68, 77, 78*).

1.1.9 The humoral immune response is also important during melioidosis

Humoral immune responses to Bp are highly prevalent in people who live in endemic areas (e.g., Northeast Thailand, many parts of Southeast Asia, and South Asia) (*79-81*). Seropositive people may be at risk of developing the disease when one or more co-morbidities is present such as diabetes, chronic renal disease, and alcohol abuse (*10*). Whilst seropositivity is a marker of exposure to *Burkholderia* species, the role of antibodies in protection against clinical melioidosis is less established. In melioidosis-endemic areas of Thailand, Bp co-exists with its low-virulence *Burkholderia* species (*Burkholderia thailandensis* [Bt] and Bt-expressing Bp-like CPS) (*82*), and healthy people show immune cross-reactivity between Bp and its counterparts for both humoral and cellular immunity

(*83*). Environmental exposure to the low-virulence strains may be protective against melioidosis. A clinical study of Thai melioidosis patients demonstrated that phagocytosis of live Bp by macrophages was enhanced in the presence of serum from the survivors and bacterial growth was reduced, implicating antibody-dependent cellular phagocytosis as protective (*84*). A follow-up study identified elevated Bp-specific IgG2 levels in the survivors compared to non-survivors, with FcγRIIa-H/R131-expressing monocytes showing enhanced Bp uptake in the presence of serum from survivors (*85*).

1.1.10 People with type 2 diabetes are highly susceptible to *Burkholderia pseudomallei* infection and their immune responses were dysregulated during melioidosis

Protective immunity against melioidosis requires a competent host immune response in both the innate and adaptive immune compartments (*76, 86*). Established risk factors for melioidosis include type 2 diabetes (T2DM), chronic renal diseases, and excessive alcohol consumption (*9, 87*). Strikingly, people with T2DM have up to 12-fold increased risk for melioidosis, and half to two-thirds of patients with melioidosis have T2DM (frequently undiagnosed) (*20, 87, 88*). Interestingly, once admitted to hospital with melioidosis, having T2DM is not correlated with increased severity and mortality (*9, 87*).

An experimental melioidosis study using a streptozotocin (STZ)-induced diabetic model identified a delayed innate immune response following Bp challenge compared to normoglycemic mice (*89*). Furthermore, a study by *Hodgson et al.* (*90*) using genetically T2DM-induced mice model revealed increased susceptibility to Bp infection, increased bacterial burden, and an elevated pro-inflammatory response (TNF, IL1-β, IL-6) following Bp challenge compared to normoglycemic mice. Peritoneal macrophages isolated from the T2DM model showed reduced bactericidal activity of nitric oxide resulting in increased bacterial burden compared to non-diabetic model. A subsequent study from the same

research group (*91*) identified impaired pro-inflammatory response at the site of infection including IFN-γ, TNF, IL1-β, IL-12, and iNOS in the T2DM model compared to non-diabetic counterparts. As a result, T2DM-induced mice showed increased bacterial burden in the lungs, spleen, and subcutaneous adipose tissue 3-day following subcutaneous challenge. Glutathione (GSH) is an antioxidant that eliminates free radicals arisen during oxidative stress such as under chronic hyperglycaemia and T2DM (*92*). T2DM patients have been shown to have reduced GSH levels compared to normoglycemic healthy donors (*93, 94*). During the Th1 immune response, GSH is essential for production of type I immune response such as IL-12 and IFN-γ against intracellular infections (*95-97*). An *ex vivo* study by *Tan et al.* (*98*) showed reduced levels of IL-12, IFN-γ and bacterial killing against Bp infection in peripheral blood mononuclear cells (PBMCs) derived from melioidosis and TB patients with T2DM. However, IL-12 responses and bacterial killing activity against Bp infection were improved when supplemented with GSH and similar results were confirmed in T2DM-induced mice challenged with Bp infection (*98*).

1.1.11 Melioidosis causes wide activation of host inflammatory programmes

A study in melioidosis with sepsis using whole blood mRNA profiling targeting 35 inflammatory markers by *Wiersinga et al.* (*99*) identified up-regulation of genes for both pro-inflammatory cytokines such as *IL1β, IL6, TNF* and anti-inflammatory cytokines such as *IL4* and *IL10* in melioidosis compared to healthy controls. Additionally, monocyte-derived genes such as *IL1B*, *IL1RA*, *NFKB1* and *MIP1A* and *SERPINB9* from granulocytes were associated with fatal melioidosis. The first genome-wide transcriptomic study of melioidosis with sepsis by *Pankla et al.* (*100*) identified up-regulation of pathways involved in innate immune responses such as activation of neutrophils and IFN signalling in 32 melioidosis patients compared to uninfected controls. On the other hand, pathways involved

in the cell-mediated immune response such as by T cells, B cells, and cytotoxic cells were down-regulated in melioidosis. A later study by *Koh et al.* (*101*) demonstrated that the whole blood transcriptome in 30 melioidosis patients was dominated by an IFN-mediated response, and was indistinguishable from active TB patients (*101, 102*). However, the whole blood transcriptomic profile associated with increased susceptibility to melioidosis in people with T2DM melioidosis remains unaddressed.

1.2 The co-epidemic of tuberculosis and diabetes is an urgent global health issue

1.2.1 The burden of tuberculosis has returned to levels from a decade ago due to the COVID-19 pandemic

Tuberculosis (TB) is the leading cause of death from one single pathogen worldwide and is caused by the acid-fast bacillus *Mycobacterium tuberculosis* (Mtb). In 2021, approximately 10 million people were infected with Mtb and an estimated 1.3 million deaths occurred, including 214,000 deaths among the human immunodeficiency virus (HIV)-positive population (*103*). The COVID-19 pandemic has had a huge impact on the World Health Organization (WHO) End TB programme, leading to undiagnosed new cases, disrupted treatment regimes, untreated cases and consequently increased case fatality worldwide (*103*). Eight countries account for two-thirds (66.2%) of all cases globally, including India (26%), China (8.5%), Indonesia (8.4%), the Philippines (6%), Pakistan (5.8%), Nigeria (4.6%), Bangladesh (3.6%), and South Africa (3.3%) (**Figure 1.4**) (*103*).

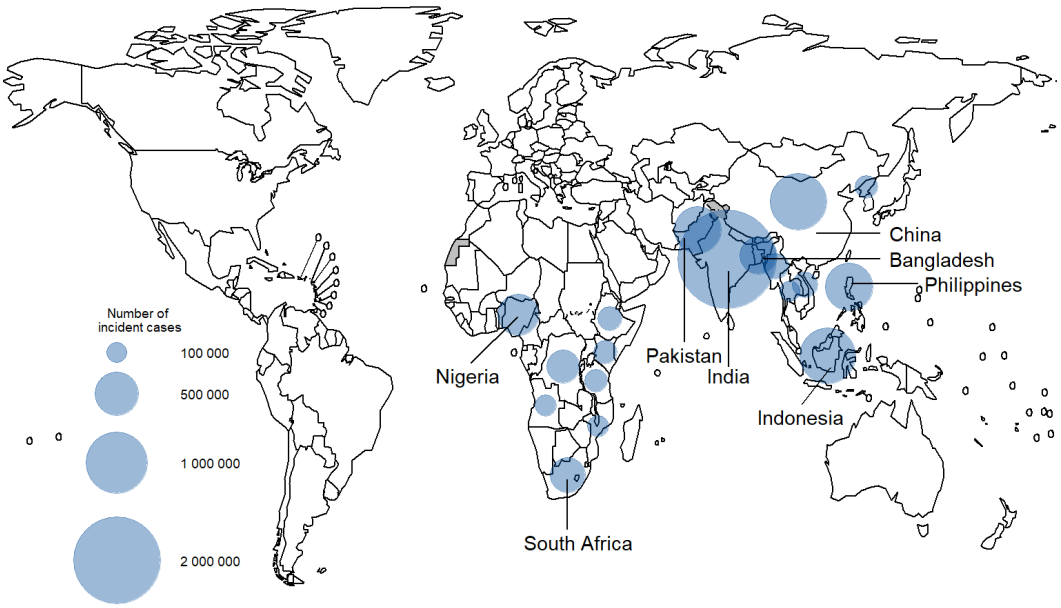

Figure 1.4 Estimated global TB incidence in 2020. Top 8 countries with the highest incidence of TB in at least 100,000 cases among the 18 high TB burden countries are shown (*103*). Reproduced from Global tuberculosis report 2021. Geneva: World Health Organization; 2021. Licence: CC BY-NC-SA 3.0 IGO.

1.2.2 Pathogenesis of tuberculosis and a steady rise of multi-drug resistant tuberculosis

Pulmonary TB is the most prevalent primary form of TB disease. The majority of Mtb-infected individuals are at the latent TB infection (LTBI) stage, which is an asymptomatic and non-transmissible state. However, when host immunity is compromised, about 5-10% of LTBI will progress to active TB in a life-time (*103*). On the other hand, a fast progressor may develop active TB within 2 years following initial exposure (*104*). Patients with active TB disease may manifest symptoms including persistent cough with or without blood, fever, lack of appetite, and weight loss (*105*). First-line drugs for TB treatment include isoniazid, rifampicin, ethambutol, and pyrazinamide. Drug resistance in TB is a global problem occurring in around 4% of newly diagnosed cases (*106*). Besides, multi-drug resistant TB

(MDR-TB, resistance to at least isoniazid or rifampicin) has become a global threat accounting for 14% of total TB-related deaths in 2017 (*107*) and extensive multi-drug resistant TB (XDR-TB) is now known (*108*).

1.2.3 People with diabetes are at risk of progression to active tuberculosis

Whilst it is well established that HIV infection confers the greatest risk of developing TB disease, with up to 20-fold increased risk (*109*), other key risk factors for TB include undernourishment, alcohol abuse, smoking and diabetes (*103, 110, 111*). In 2016, 1.7 billion people were estimated to have been infected with Mtb and a fraction of LTBI at 16.5 per 100,000 per year was projected to become an active TB infection in 2035 (*112*). People with diabetes have increased risk of progressing to active TB infection at a rate exceeding 10% annually compared to between 10% and 20% lifetime risk in those without diabetes (*113*).

1.2.4 The co-epidemic of tuberculosis and type 2 diabetes are a major global health challenge

T2DM confers up to three-fold increased risk of developing TB, contributing to 15% of global TB cases, or approximately one million TB cases worldwide in 2013 (*111, 114-117*). A systemic review focusing on co-prevalence of T2DM and TB in low- and middle-income countries (LMICs) from 1990 to 2016 (*118*) identified an estimated co-prevalence of between 10% and 30% in the majority of reviewed studies (**Figure 1.5**). The top three countries with the highest co-prevalence were India (20.2%), China (13.1%), and Mexico (8.3%). Moreover, TB patients with diabetes have up to three-fold increased risk of treatment failure and death, and up to four-fold enhanced risk of relapse compared to those without diabetes (*119-121*). The co-epidemic of TB and diabetes, especially in LMICs, will result in increased co-morbidity and mortality that will impact on healthcare expenditure

and socio-economic status. Therefore, an urgent plan is needed to mitigate the impact of the growing co-epidemics.

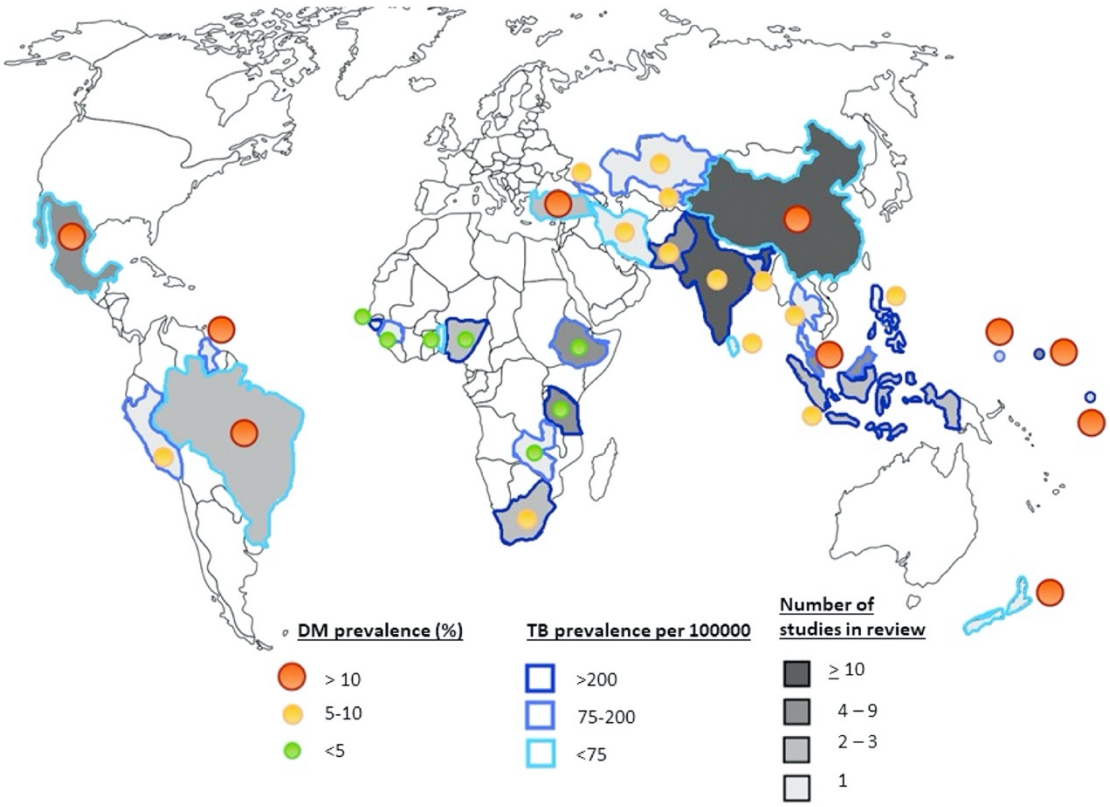

Figure 1.5 Estimated co-epidemic of diabetes and tuberculosis in low- and middle-income countries between 1990 and 2016 (*118*). Reproduced with licence from McMurry *et al.*, Coprevalence of type 2 diabetes mellitus and tuberculosis in low-income and middle-income countries: A systematic review. *Diabetes Metab Res Rev* 35, e3066 (2019). Licence number: 5380341047476.

1.2.5 Tuberculosis and melioidosis share some common features

Bp, the causative agent of melioidosis is a Gram-negative bacillus from the genus *Burkholderia* (previously the genus *Pseudomonas*) (*122*) whilst Mtb is a bacillus derived from the genus *Mycobacterium* (*123, 124*). Interestingly, Mtb expresses peptidoglycans that resemble that of Gram-positive bacterial cell wall components (*125*). Based on genetic evidence and taxonomy classification, Bp and Mtb are rather distinct from each other, but

both are intracellular infections (**Figure 1.6**). Clinically, melioidosis patients most commonly present as acute infection (85%) whereas TB is a chronic infection (*9*). Unlike melioidosis, sepsis in pulmonary TB is rare (*126*). However, clinical manifestations of the two diseases can overlap. In melioidosis, the majority of patients (up to 60%) present with lung disease (*10*). In TB, the lungs are primarily affected by Mtb infection. Like Bp, Mtb infection may occur in other part of the body such as lymph nodes, bones and joints, and central nervous system (*127*). Granuloma formation is a hallmark of TB, but can occur in melioidosis (*127, 128*). Melioidosis is an acute infection, in which sepsis is common and case fatality is up to 50% despite appropriate treatment. In contrast, the case-fatality rate in TB patients is around 15% based on current estimation (*103*).

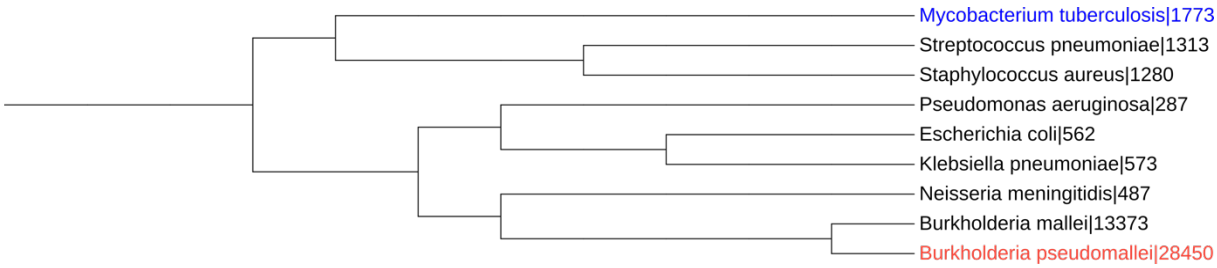

Figure 1.6 Simplified phylogenetic tree of selected pathogenic bacteria causing diseases in human. *Burkholderia pseudomallei* and *Mycobacterium tuberculosis* are labelled in red and blue respectively. The tree was constructed using phyloT (https://phylot.biobyte.de/) based on NCBI taxonomy or Genome Taxonomy Database with default setting. Bacterial species and corresponding taxonomy IDs are shown.

1.2.6 Tuberculosis and melioidosis utilise virulence determinants against host immune defence mechanisms

Despite different aetiology and biology, both pathogens employ similar immunomodulatory mechanisms for their own survival. In melioidosis, Bp expresses a number of carbohydrates

(e.g., CPS and LPS) and protein antigens (e.g. flagellin, TTSS3, and TTSS6) on their surface to facilitate host immune evasion (*10, 129*). Experimental melioidosis using the Syrian hamster model showed increased persistence of wild-type Bp in the blood with higher bacterial loads in multiple organs compared to hamsters challenged with CPS-mutant Bp strain. Moreover, complement factor C3b deposition on wild-type Bp and phagocytosis activity were reduced compared to the CPS-mutant strain (*40*). TTSS3 is a virulence factor that is deployed by Gram-negative bacteria to evade and modulate host immune responses during infection such as *Salmonella enterica* serovars, *Yersinia* species, and *Shigella* species (*130*). The structure of TTSS resembles a needle-like structure, allowing the pathogens to inject bacterial effector proteins into host cells for their own benefits such as cell adhesion, invasion, and intracellular survival (*130, 131*). During Bp infection, wild-type BP is able to escape the phagosome following phagocytosis. TTSS3-mutant Bp strains showed inability to escape from phagosomes compared to the wild-type and were targeted for killing by host phagolysosome (*45, 132*). On the other hand, cell wall components of Mtb are enriched with lipids such as lipoarabinomannan, mycolic acid and glycolipids (*133*). Macrophages and other phagocytes are known to play an important role in controlling Mtb infection. Sulfoglycolipids are abundantly expressed on the Mtb cell wall (*134*). An *in vitro* study of innate immune responses to Mtb by macrophages showed sulfoglycolipid-mutant Mtb increased activation of NF-κB and IL-8 compared to the wildtype strain. Moreover, sulfoglycolipids was found to inhibit activation of TLR-2 and its downstream signalling cascade by NF-κB (*135*). Similar to immune evasion mechanisms by Bp, lipid components of Mtb cell wall such as lipomannan, lipoarabinomannan, and phosphatidylinositol mannosides halt phagosome maturation and formation of phagolysosome, allowing them to replicate within macrophages (*136, 137*).

1.2.7 Type I immune responses are essential for controlling *Mycobacterium tuberculosis* infection

A small fraction of LTBI will develop into active disease when the host immune response is compromised due to either underlying conditions or immunomodulatory treatments (*138*). During LTBI, Mtb is contained within granulomas which are mediated by immune cells from both the innate and adaptive immune systems, such as neutrophils, macrophages, NK cells and T cells (*139*). Pro-inflammatory immune responses by Th1 cells are indispensable during Mtb infection, with type II interferon (IFN-γ) a key cell mediator that can activate bactericidal effector function within macrophages or via IFN-γ-independent mechanisms (*140-142*). Other pro-inflammatory cytokines such as TNF, IL-12, and IL-18 work synergistically in defence against Mtb infection (*143-145*). A number of studies have demonstrated the importance of TNF in regulating granuloma integrity, with blockade of TNF resulting in reactivation of LTBI (*146-148*). Suppressed IFN-γ responses are associated with increased risk of developing active TB, and worse outcomes (*149-151*). Interestingly, type I interferon (IFN-α/ IFN-β), which is important for controlling viral infections, does not appear to be protective during Mtb infection (*142*). The type I interferon response induces an anti-inflammatory cytokine (IL-10) that counteracts protective Th1 immune responses, leading to uncontrolled Mtb infection (*152*). Type II immune responses (i.e., IL-4, IL-5, and IL-13) are important for controlling parasitic and helminth infections, however, their protective roles during host immune response against intracellular infections are not favourable (*153, 154*). IL-10 is a potent anti-inflammatory cytokine that has a broad immunomodulating effects on many immune cells leading to poor control of infections such as chemotaxis, antigen presentation, activation, proliferation, and killing mechanisms (*155, 156*).

Inflammatory macrophages (M1) harbour bactericidal effector functions controlling Mtb infection and can be derived in presence of granulocyte-macrophage colony-stimulating factor (GM-CSF) (*157*). Upon type I immune response, IL-12 and IL-23 are primary cytokines that mediate Th1 differentiation and activation. On the other hand, anti-inflammatory macrophages (M2) are generated such as in presence of macrophage colony-stimulating factor (G-CSF) or some Mtb-derived antigens (*158, 159*). M2 macrophages produce IL-10, TGB-β, and arginase-1 which inhibits pro-inflammatory responses and down-regulate co-stimulatory molecules that are necessary for T cell activation leading to uncontrolled replication of Mtb, dissemination, and increased disease severity (*159, 160*). Nevertheless, a balanced pro- and anti-inflammatory immune responses against Mtb infection is crucial, in which excessive inflammation could potentially cause tissue damage and overactivated anti-inflammation may support bacterial growth and dissemination (*151, 161*).

1.2.8 Type 2 diabetes impairs innate immune responses against *Mycobacterium tuberculosis* and *Burkholderia pseudomallei* infection

T2DM is considered as a low-grade chronic inflammatory syndrome and it is known to enhance susceptibility to infections in general (*162, 163*). The impact of diabetes on the host immune response against Mtb has been demonstrated, with both innate and adaptive immune compartments are affected such as cell adhesion, chemotaxis, phagocytosis, bactericidal activity, T lymphocyte activation, effector function, and proliferation (**Figure 1.7**) (*164*). An *ex-vivo* phagocytosis model study of Mtb demonstrated increased frequency of neutrophils count in diabetes patients. However, phagocytosis activity of *Mycobacterium bovis* Bacillus Calmette-Guérin (BCG) in neutrophils and monocytes was reduced compared to healthy donors (*165*). Similarly, neutrophils derived from diabetes patients showed

reduced phagocytosis activity against Bp and cell migration in response to IL-8 stimulation compared to healthy donors (*166*). A follow-up study identified delayed NETosis in neutrophils derived from diabetes patients against Bp infection compared to healthy donors (*167*). Another study from the same laboratory identified impacts of anti-diabetic drugs on host immune response against Bp infection in diabetes patients. Production of pro-inflammatory cytokines from neutrophils following the infection including IL-1β and IL-18 were reduced in diabetes patients who received glibenclamide (sulfonylureas) compared to those who received metformin (biguanides), untreated group, or healthy control (*168*). This phenomenon was later discovered due to reduced glutathione level, which is essential for production of pro-inflammatory cytokines, thus bacterial growth (*98, 169*). A study by *Wong et al.* (*170*) identified elevated NETosis in diabetes patients and diabetic mice model. The increased NETosis in diabetic mice showed reduced wound healing compared to NETosis-deficient or normal-glycaemic mice.

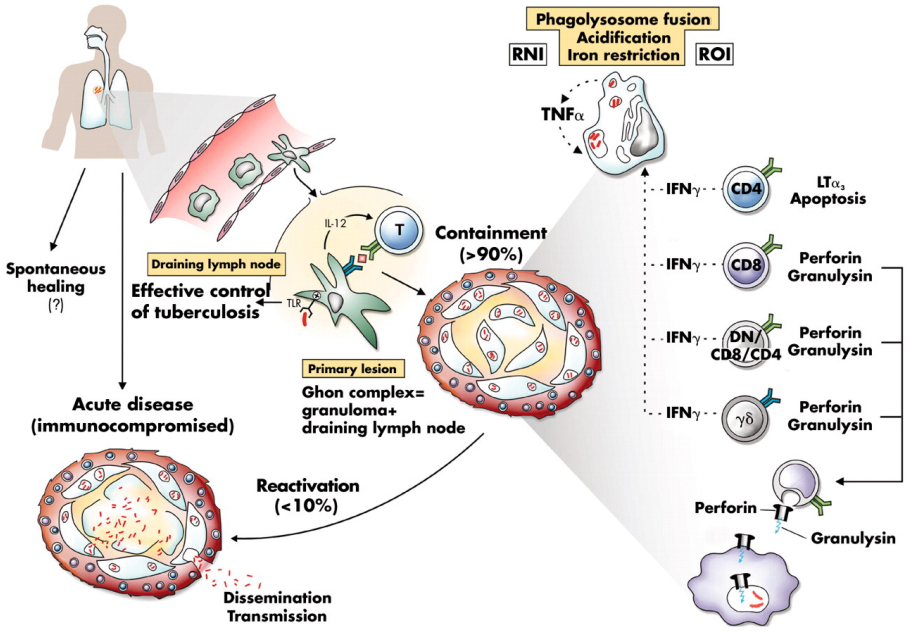

Figure 1.7 Impact of diabetes during host immune response against tuberculosis. A number of host immune responses including both innate and adaptive immune compartments are dysregulated in people with diabetes. Consequently, compromised host immune responses are predisposed to enhanced susceptibility, progression to active disease, and poor outcome (*171*). Reproduced with licence from Kaufmann, New issues in tuberculosis. *Ann Rheum Dis* 63 Suppl 2, ii50-ii56 (2004). Licence number: 5380341488680.

1.2.9 Type 2 diabetes dysregulates cellular immune response against *Mycobacterium tuberculosis* and *Burkholderia pseudomallei* infection

Dysregulation of cellular immune responses in people with diabetes during active TB have been demonstrated, in which TB patients with diabetes (TB-DM) showed lower production of IFN-γ and IL-12 compared to those without diabetes (*172*). Those with poor glycaemic control among TB-DM showed lower IFN-γ responses compared to those with good glycaemic control (*173*). An *ex vivo* study of PBMC isolated from TB patients with and without diabetes identified increased IL-10 production following *M. bovis* BCG and Mtb-

derived antigen stimulation. The Th1:Th2 cytokine ratio was also lower in TB-DM compared to non-diabetes and healthy donors, suggesting Th2 bias in the immune response in diabetes (*174*). Furthermore, T2DM has been shown to affect APCs, which are important for Th1 cell activation and the appropriate host immune response against Mtb infection (*175-177*). An *in vitro* study identified reduced expression of antigen presenting and costimulatory molecules (e.g., HLA-DR, CD80 and CD86) in monocyte-derived macrophages following infection with Mtb from TB-DM patients compared to those without diabetes (*178*). Similarly, another *in vitro* study identified increased frequency and production of IL-10, transforming growth factor-beta (TGF)-β, and IL-5 from myeloid-derived suppressor cells derived from T2DM patients (*179*). Moreover, reduced expression of CD14 and macrophage receptor with collagenous structure (MACRO) on alveolar macrophages and phagocytosis activity against Mtb were observed in diabetic compared to non-diabetic mice (*176*). Likewise, TB patients with T2DM showed increased plasma anti-inflammatory proteins including heme oxygenase-1 and tissue inhibitors of metalloproteinase-4, higher circulating neutrophils, and higher bacterial loads in sputum compared to non-diabetes (*180*). Impact on antigen presentation by dendritic cells in the diabetic mice model was demonstrated, with delayed migration to the lungs and activation of T cells due to reduced production of chemokine ligands (CCL5 and CCL2) in diabetic mice (*177*). In melioidosis, altered cell-mediated immune responses in people with diabetes has been reported, in which reduced Bp-specific IFN-γ responses were observed in the patients with T2DM compared to non-diabetes (*76*). Collectively, diabetes affects both innate and adaptive immune compartments. Dysregulation of innate immune cells, compromised Th1 immune response, increased anti-inflammatory immune with Th2-bias phenotype may be responsible for increased susceptibility to the infections in people with diabetes.

1.2.10 The host immune response against *Mycobacterium tuberculosis* infection is driven by interferon signalling

In 2010, a landmark whole blood transcriptomic study *Berry et al.* (*102*) identified a TB transcriptomic signature that could discriminate active TB from other inflammatory diseases and bacterial infections tested, and was characterised by an interferon-inducible neutrophil-driven signature. However, Bp was not one of the comparator infections. The study by *Koh et al.* in 2013 (*101*) showed that whole blood transcriptomic signatures between TB and melioidosis were indistinguishable, both being dominated by interferon-regulated pathways, although few of the TB patients in this cohort had DM. In 2017, *Prada-Medina et al.* (*181*) studied the impact of diabetes in TB using a systems immunology approach combining plasma cytokine and whole blood transcriptomic profiling. The integrative analysis of cytokines and transcriptomes identified 114 genes that explained the observed expression of cytokines in TB-DM. These genes are involved in innate and adaptive immunity, including neutrophil recruitment and activation, interferon signalling, antigen processing-cross presentation, regulation of complement cascades, and DNA methylation.

1.3 Community-acquired infections are complicated by sepsis leading to high case-fatality

1.3.1 Sepsis remains a global health challenge, especially in low- and middle-income countries

Sepsis is a leading cause of death in critically ill patients, caused by a dysregulated host response to infection (*182*). In 2017, approximately 50 million cases and 11 million deaths were estimated to be caused by sepsis globally, accounting for ~20% of all-cause mortality (*183*). Between 1990 and 2017, the incidence of sepsis declined by 37%, possibly due to better vaccine deployment, hygiene, and water progress, improved treatment, and management (*183*). A recent meta-analysis reported an estimated case fatality rate from sepsis of 27% in hospitalised patients, and up to 42% in patients admitted to intensive care units (*184*). Moreover, sepsis-related mortality is highly prevalent in young children and the elderly population (*183*). Strikingly, 85% of all sepsis cases and mortality (~85%) were estimated to have occurred in LMICs (**Figure 1.8**) (*183, 185*). However, due to limited data on the burden of sepsis in LMICs, the estimated sepsis-related incidence and mortality were extrapolated from high-income settings (*183*) and may underestimate the true incidence and sepsis-related mortality in LMICs. The high incidence and fatality rate in resource-limited settings remains a challenge for managing sepsis. Higher incidence and sepsis-related mortality were estimated to occur in countries with low and low-middle socio-demographic indices (*183*), potentially affected by such as low awareness, delayed diagnosis, socioeconomic status and resource-limited healthcare settings (*186*).

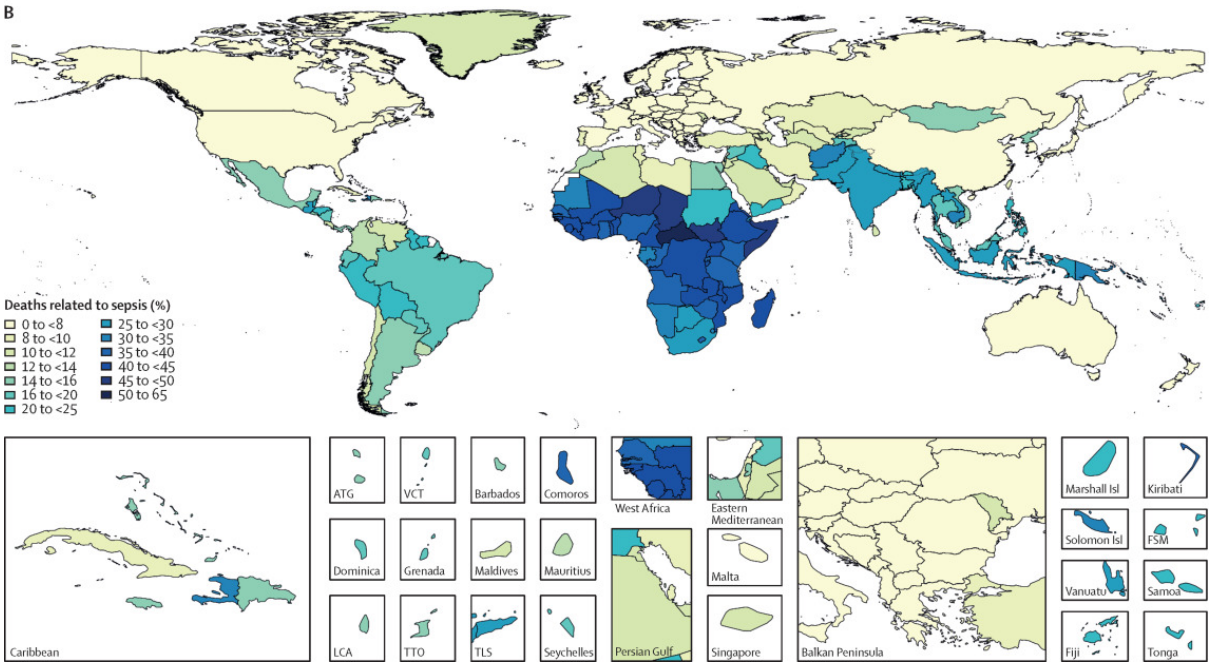

Figure 1.8 Estimated global sepsis-related mortality based on age-standardised sepsis incidence 100,000 population for both sexes in 2017 (*183*). Reproduced from Rudd *et al.*, Global, regional, and national sepsis incidence and mortality, 1990-2017: analysis for the Global Burden of Disease Study. *Lancet* 395, 200-211 (2020). Licence: CC BY 4.0.

1.3.2 *Burkholderia pseudomallei* is an important cause of death due to community-acquired infection in Southeast Asia

A systemic review of seventeen prospective studies in South and Southeast Asia between 1990 and 2010 (*187*) identified a wide range of Gram-negative and Gram-positive bacteria as the common causes of community-acquired bacteraemia in adults and children, including *Salmonella enterica* serotype Typhi, *Escherichia coli, Streptococcus pneumoniae, Haemophilus influenzae,* and *Staphylococcus aureus*. The case fatality ranges between 2% and 34% (9% overall). A multinational cross-sectional study across Southeast Asia between 2013 and 2015 (*188*) identified a wide range of infectious diseases such as dengue,

leptospirosis, and rickettsiosis as the commonest causes of community-acquired sepsis. Other emerging pathogens causing sepsis such as hantaviruses, non-typhoidal *Salmonella* species, and Bp were identified. The 28-day mortality was 13% in adults, with acute respiratory infection the leading cause of sepsis. A single-centre prospective observational study (Ubon-Sepsis) between 2013-2017 in Northeast Thailand identified *E. coli*, Bp*,* and coagulase-positive staphylococcus as the commonest causes of community-acquired infections. Bacteraemia is common in sepsis and is associated with increased mortality, presumably as it represents uncontrolled bacteria (*189-191*). Out of over 5,000 patients with suspected infection, 74% had confirmed sepsis as defined by a modified Sequential Organ Failure Assessment (SOFA) score ≥ 2 with high 28-day mortality at 21% (*192*). Moreover, exceptionally high 28-day mortality at 42% was seen in the sepsis patients who were admitted to intensive care units (ICUs) (*193*). Furthermore, a subset of the sepsis patients (*194*) had bacteraemia (~14%), in which *E. coli*, Bp*,* and *S. aureus* were the most frequent pathogens with overall 28-day mortality at 41%. Sepsis patients with bacteraemia caused by Bp have a staggering 28-day mortality at 66%. A Sepsis Fast Track programme (SFT) was introduced into the Ubon-Sepsis study (*195*), where patients with suspected sepsis were immediately admitted to ICUs. The SFT-implemented group showed an improved survival rate compared to the standard care group. This study highlights importance of early recognition and management of sepsis for improved outcomes.

1.3.3 Sepsis criteria have been redefined over the past 30 years

Definitions of sepsis have been evolved over the last three decades as a result of improved understanding of pathophysiology, immunopathology and aetiology leading to sepsis (*182*). In **Table 1.1,** Sepsis-1 is defined as a host's systemic inflammatory response syndrome (SIRS) as a result of infection (*196*). Severe sepsis, a subset of sepsis is defined as having

organ dysfunction or sepsis-induced hypotension (*196*). Furthermore, septic shock is the most serious form of sepsis that confers highest mortality approaching 50%, defined as having persistent hypotension in spite of adequate fluid resuscitation (*197, 198*). Sepsis-2 definition was proposed to facilitate early recognition of sepsis (*182*), in which additional clinical parameters and laboratory tests such as inflammatory, hemodynamic, and tissue perfusion parameters are included (*199*). Nevertheless, the SIRS criteria by Sepsis-1 and Sepsis-2 are unable to discriminate between infection-induced and sterile inflammation such as pancreatitis, trauma, and myocardial injury (*200, 201*). The latest sepsis definition (Sepsis-3) has removed SIRS criteria and incorporated SOFA score as an indication of organ dysfunction. Patients with suspected infection who manifest the total SOFA score of 2 or more, are considered as having sepsis (*197*).

Table 1.1 Definitions of sepsis over the past 30 years (*202*).

	Definitions	Comments
Sepsis-1, 1991		
Sepsis	SIRS* with infection (presumed or proven)	SIRS can be non-infectious in aetiology. Only infection plus SIRS is termed sepsis. Not all patients with serious infection necessarily show SIRS features despite having organ dysfunction
Severe sepsis	Sepsis (as above) with evidence of acute organ dysfunction	Gives a false impression that infection must go through the three stages of sepsis, severe sepsis, and septic shock; or that organ dysfunction must have SIRS
Septic shock	Sepsis with persistent hypotension after fluid resuscitation	Emphasis placed on circulation (blood pressure) alone without considering the metabolic (lactate) component
Sepsis-2, 2001	Unchanged	The list of signs and symptoms associated with sepsis was expanded
Sepsis-3, 2016		
Sepsis	Life-threatening organ dysfunction† caused by a dysregulated host response to infection	To recognise the finding that infections can result in local organ dysfunction (reflected by the SOFA score) without triggering a dysregulated host response (the old SIRS criteria)
Septic shock	A subset of sepsis with persistent hypotension requiring vasopressors to maintain MAP of ≥65 mm Hg and a serum lactate level of >2 mmol/L despite adequate volume resuscitation	The term 'severe sepsis' is deleted, and both circulatory and metabolic abnormalities are considered. Whether the new Sepsis-3 criteria improves clinical outcomes remains to be validated

Abbreviations: MAP = mean arterial pressure; SIRS = systemic inflammatory response syndrome; SOFA = Sequential Organ Failure Assessment

* ≥Two of the following: (a) temperature >38°C or <36°C, (b) heart rate >90/min, (3) respiratory rate >20/min or $PaCO_2$ <32 mm Hg (4.3 kPa), (4) white blood cell count >12 000/mm^3 or <4000/mm^3 or >10% immature bands

† Defined by an acute change of ≥2 points in the SOFA score; 6 components including: respiratory (partial pressure of oxygen in arterial blood/fractional inspired oxygen [PaO_2/FIO_2] ratio), neurological (Glasgow Coma Scale score), cardiovascular (MAP and vasopressor use), renal (serum creatinine and urine output), hepatic (bilirubin level), and platelet count

Reproduced from Lam *et al*, Clinical management of sepsis. *Hong Kong Med J* 23, 296-305 (2017). Licence: CC BY-NC-ND 4.0.

1.3.4 The host immune response during sepsis is heterogenous, with simultaneous hyper- and hypo-inflammation

A hyper-inflammatory immune response driven by the innate immune compartment (e.g. TLRs) against PAMPs (e.g. LPS), resulting in activation of the inflammatory response through elevation of cell mediators such as TNF, IL-1, and IL-6, alongside activation of leukocytes, was originally thought to play a deleterious role during sepsis in previous studies (*203, 204*). Therefore, several clinical trials attempted to reduce hyper-inflammation by neutralising pro-inflammatory mediators such as TNF, IL-1, and GM-CSF; however, little or no benefits were achieved (*205-207*). An exaggerated inflammatory immune response can cause collateral tissue damage. Consequently, DAMPs are released from injured cells and tissues which further attract and activate immune cells, therefore participating a vicious cycle of excessive inflammation (*208*).

A balanced immune response between pro- and anti-inflammation is the key for successful immune resolution following sepsis. Activation of the inflammatory immune response causes activation of compensatory anti-inflammatory immune mechanisms (*209*). Over-activation of anti-inflammatory responses has been shown to cause subsequent immunoparalysis, in which the cell-mediated immune response is compromised or reduced in number, leading to failure to clear the infection and secondary nosocomial infections (*210*). Key immune checkpoints such as IL-10, programmed cell death protein-1/programmed cell death ligand 1 (PD-1/PD-L1), and cytotoxic T-lymphocyte associated protein 4 (CTLA-4) are over-expressed in severe sepsis patients and are associated with poor outcomes (*211-213*). Several pre-clinical studies of PD-1/PD-L1 as an immunomodulatory target showed improved survival and cellular immune function in sepsis-induced models (*214-216*). However, implementation of anti-immune checkpoints in clinical settings must

be proceeded with caution because inhibition of anti-inflammatory mechanisms could result in harmful exaggeration of the inflammation and autoimmune-like conditions (*217*).

1.3.5 Host immune dysregulation during sepsis is due to the presence of bacterial-derived virulence factors

Sepsis and septic shock lead to collateral tissue damage, multiorgan failure, and lethality (*198, 218*). Some infectious diseases confer higher case fatality than others. For example, the case fatality in melioidosis is up to 50% in patients with septic shock, and mortality rate at ~30% was reported in patients with methicillin-resistant *S. aureus* (MRSA) bacteraemia (*10, 219, 220*). Pathogenic determinants play an important role of host-pathogen interactions and consequences during sepsis. LPS is an endotoxin released during Gram-negative-induced sepsis, and is recognised by the TLR-4 receptor complex (*221*). TLR-4 is abundantly expressed on many innate immune cells such as neutrophils, macrophages, and dendritic cells (*222*). Binding of LPS to TLR-4 induces activation of TLR signal transduction involving a series of phosphorylation of downstream signalling complex such as myeloid differentiation primary response gene 88 (MyD88), NF-κB, and ultimately production of pro-inflammatory cytokines and chemokines (*221*). Activation of the pro-inflammatory response is crucial for the host immune response against infections. However, exaggeration of the inflammatory response can be harmful to host tissues, potentially leading to SIRS. Several experimental sepsis studies have demonstrated that TLR4-deficient models were protected from *E. coli*-induced septic shock (*223-225*). In Gram-positive sepsis, *S. aureus* is the commonest cause of sepsis worldwide (*194, 226, 227*). In several experimental sepsis studies, staphylococcal enterotoxins-induced sepsis models displayed a severe from of the disease with increased frequencies of circulating leukocytes and elevated pro-inflammatory mediators and were associated with high mortality if left untreated (*228-230*).

1.3.6 Dysregulation of the innate immune response during sepsis leads to excessive inflammatory responses

The host innate immune system is dysregulated during sepsis. Factors from both host and pathogen such as host genetics, age, pregnancy, compromised immune system, comorbidities, and virulent determinants contribute to the development of sepsis (*231*). The innate immune system deploys various mechanisms to detect the presence of PAMPs and DAMPs within the host system, such as TLRs, nucleotide-binding and oligomerisation domain (NOD)-like receptors (NLRs), retinoic acid-inducible gene-I (RIG-I)-like receptors (RLRs) and the complement system (*232*). The innate immune response by TLRs has been extensively studied in the context of infectious diseases and sepsis. Location and combination of TLRs are important for host immune surveillance. Expression of cell surface TLRs such as TLR-1, TLR-2, TLR-4, TLR-5 and TLR-6 is essential for detection of PAMPs released from bacteria or fungi (*233*). For example, TLR-2 alone is specific for peptidoglycan from Gram-positive bacteria, whilst TLR2 from heterodimers with TLR-1 or TLR-6 can detect lipoprotein, lipoarabinomannan, glycolipids, and zymosan. TLR-4 and its complex including CD14 and MD-2 binds to LPS from Gram-negative bacteria, whilst TLR-5 detects flagellin (*233*). In contrast, endosomal TLRs such as TLR-3, TLR-7, TLR-8 and TLR-9 detect the presence of nucleic acids (single-stranded RNA and unmethylated DNA) derived from viruses and bacteria (*234*).

Hypofunction of TLRs can be associated with increased susceptibility to infections. However, over-activation of TLRs leads to hyperinflammation, SIRS, collateral tissue damage, and organ failure (*235*). DAMPs released following cell death or tissue damage can exert inflammatory effects (*34*). Examples of DAMPs are myeloid related protein 8/9 (MRP8/9) or S100A8/9, which are abundantly expressed in neutrophils and exert multiple

functions such as chemotaxis, inflammatory response, and anti-microbial activity (*236, 237*). S100A8/9 activates TLR-4 and its downstream signalling pathways (MyD88 and NF-κB) resulting in production of pro-inflammatory cytokines such as TNF, IL-1, and IL-17 (*238-240*). S100A8/9 activates advanced glycation end products (RAGE) receptors resulting in activation of NF-κB and pro-inflammatory responses (*241*). Elevated plasma levels of S100A8/9 were observed in septic shock patients and were associated with poor outcomes (*242*). Inhibition of the S100A8/9-mediated immune response by pharmaceutical agents (S100A8/9 inhibitors; ABR-238901 or paquinimod) was found to reduce inflammation and improve survival rates in animal models (*243-245*). Furthermore, perpetuation of inflammatory responses could be due to persistence of bacterial components as a result of bacteraemia, especially in Gram-negative sepsis, and is associated with increased severity and death (*246-248*).

1.3.7 Innate immune components are dysregulated during sepsis leading to complications and death

The complement system is another innate immune defence mechanism against infections and clearance of DAMPs. Complement proteins e.g., C3b can bind to the microbial surface for destruction by membrane attack complex or induction of opsonisation followed by phagocytosis (*249*). During infection, in particular as a result of bacteraemia, the complement system is activated, with C-reactive protein (CRP) involved in activation of the complement system via C1q molecules (*250*). Several clinical studies have identified increased plasma concentrations of complement protein, particularly C3 fragments or complement-CRP complex in septic shock patients and in those who succumb to death (*251-253*). During infection, the coagulation system is activated as a part of early host response to limit dissemination of pathogens. Coagulation and inflammation are closely regulated,

involving activation of the complement system, tissue factor, and platelets (*254*). Over-activation of coagulation can result in coagulation-related complications such as disseminated intravascular coagulation (DIC), thrombosis, and organ failure (*255*). An experimental *E. coli* sepsis using a baboon model identified reduced activation of complement pathway (C3a and C3b) after administration of C3 convertase inhibitor (compstatin). Moreover, a compstatin-treated baboon model showed reduced coagulation, infiltration of leukocytes, improved circulation, and organ functions (*256*). Collectively, during sepsis (particularly caused by microbial insults), a number of innate immune defence mechanisms are activated in order to eliminate invading pathogens, resulting in an overwhelmed inflammatory response. This innate response is closely interconnected involving complement, coagulation, and inflammation, potentially leading to systemic inflammation, tissue damages, multiorgan failure, and death (*257-259*).

1.3.8 Neutrophil dysregulation is a hallmark of sepsis

Lymphopenia and neutrophilia are a hallmark of sepsis, with an increased neutrophil-to-lymphocyte ratio associated with poor outcomes in sepsis patients in a meta-analysis (*260*). During sepsis, immature neutrophils ($CD16^{dim}$) are seen, with reduced expression of PRRs essential for pathogen recognition and functions such as CD14, MD2, and CXCR2 (*261*). Moreover, immature neutrophils have a longer lifespan and increased basal levels of pro-inflammatory cytokines (e.g., TNF and IL-1β), but reduced chemotaxis, phagocytosis, and reactive oxygen species (*261-263*). Dysregulation of chemotaxis, phagocytosis and NETosis play a deleterious role, contributing to immunopathogenesis during sepsis. For example, reduced expression of the chemokine receptor CXCR2 was observed in sepsis patients (*261*), leading to impaired migration to the site of infection, accumulation of circulating neutrophils and development of systemic inflammation (*261, 263*). Microbial killing following

phagocytosis by RNS/ROS is important for controlling infections; however, this process is dysregulated during sepsis (*264*). Excessive, uncontrolled production of ROS and RNS in sepsis is associated with organ failure as a result of oxidative stress-induced mitochondrial dysfunction (*265*). Likewise, excessive RNS/ROS and NETosis activity directly causes tissue damage and organ dysfunction in experimental sepsis and clinical studies (*266-268*). A study by *Poli et al.* (*269*) identified histone deacetylases (HDACs) as a key enzyme driving NETosis in humans and mouse models. Furthermore, a septic shock model in mice treated with an HDAC inhibitor showed reduced NETosis, inflammasome activation and pro-inflammatory cytokines (e.g., IL-1β, IL-6, and TNF), alongside protection against systemic inflammation (*270*).

1.3.9 Protective immunity by T lymphocytes is modulated by dysregulated innate immunity

An excessive inflammatory response by innate immune cells such as neutrophils and macrophages has been found to modulate the cellular immune response (*271, 272*). A competent cellular immune response requires cell-cell interaction between APCs and lymphocytes for activation, proliferation, effector functions and memory acquisition (*273*). During microbial infections (*274*), neutrophils deploy bactericidal mechanisms in which neutrophil granules such as NE, MPO, and defensins can be released extracellularly into the system and modulating host immune response (**Figure 1.9**). An experimental study of lung disease using a mice model (*275*) identified inhibition of dendritic cell maturation accompanying reduced expression of co-stimulatory molecules including CD40, CD80 and CD86 on NE-treated dendritic cells. The reduced expression of CD86 was due to proteolytic cleavage by NE. Moreover, NE induced production of TGF-β1 in dendritic cells, which promotes development of regulatory T cells (Tregs) (*276, 277*). Similarly, another murine

model study (*271*) demonstrated that MPO was able to suppress activation, function, and proliferation of CD4 T cell. Similar to NE, MPO was able to reduce activation of DC via cleavage of co-stimulatory molecules including CD40 and CD86, impair migration to lymph nodes, and antigen uptake and processing. Moreover, MPO was able to inhibit activation of DC via reduced expression of CD86 and HLA-DR on human DC.

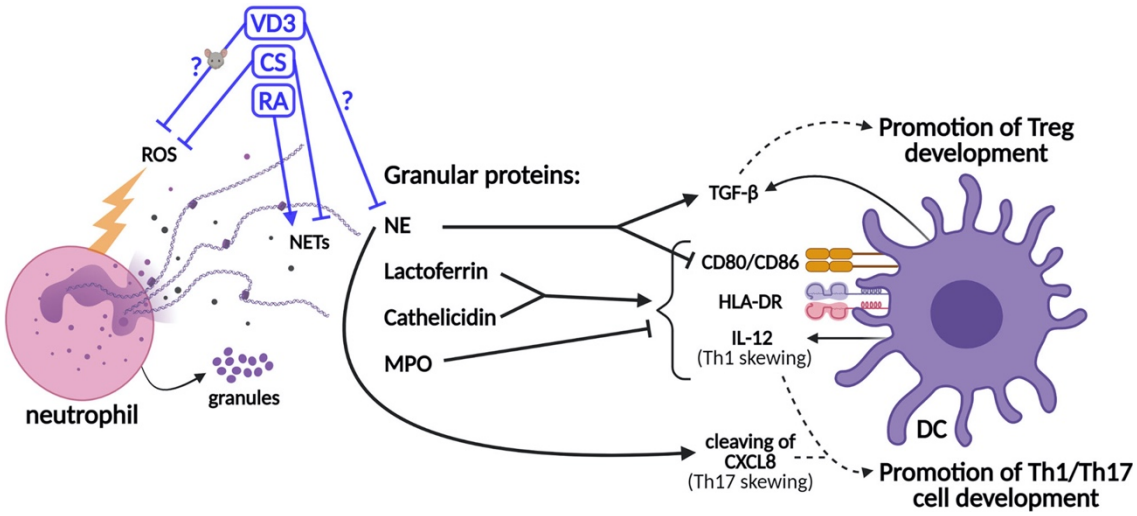

Figure 1.9 Neutrophil-mediated immunomodulation. Neutrophil granules are released during host immune response to infections or during inflammatory conditions. Neutrophil granules such as MPO and NE have been found to inhibit antigen presentation capability of dendritic cells and deviate polarisation of T cells into particular subsets (*274*). VD3=Vitamin D3. CS=Corticosteroids. RA=Retinoic acid. Reproduced from Hafkamp, Kormelink, and de Jong, Targeting DCs for Tolerance Induction: Don't Lose Sight of the Neutrophils. *Front Immunol* **12**, 732992 (2021). Licence: CC BY 2.0.

Likewise, other innate immune cells can inhibit or alter T lymphocyte function and differentiation. Myeloid-derived suppressor cells (MDSCs) derived from heterogenous populations of myeloid cells were found to modulate T cell responses via production of ROS/RNS and arginase (*278*). MDSC-like neutrophils were found to inhibit T cell

proliferation through inhibition of CD3 zeta-chain via arginase (*279*). Increased arginase production was found to compete L-arginine product which is required for T cell proliferation (*279, 280*). Mechanisms in which ROS mediates T cell suppression include interruption between T-cell receptor (TCR) and major histocompatibility complex (MHC) interaction, ROS-induced apoptosis, disruption of TCR signalling (*281*). Altogether, innate immune cells are able to modulate the adaptive immune response through various cell mediators such as NE, MPO, arginase and ROS resulting inhibition of T cell function, activation, and proliferation.

1.3.10 Impaired cellular immune responses lead to inefficient bacterial clearance and secondary infection

Cell-mediated immune responses, particularly by T cells and APCs are indispensable during infection and sepsis (*282, 283*). Depletion of lymphocytes is a hallmark of sepsis resulting in immune suppression and is associated with increased disease severity and mortality (*284*). Moreover, immune suppression during sepsis is associated with enhanced susceptibility to secondary or nosocomial infections and late mortality. Both pro- and anti-inflammatory immune response occurs concomitantly as early as the onset of sepsis (*285, 286*). Potential mechanisms involved in immune suppression include inflammation-associated immunomodulation, apoptosis of lymphocytes, and dysregulation of APCs (*208*).

Depletion of lymphocyte populations during acute infections and sepsis is primarily thought to be mediated by apoptosis and it has been associated with poor outcomes (*212, 287, 288*). Depleted lymphocyte population was observed in severe sepsis cases within 24 hours following confirmed-diagnosis (*289*). Correspondingly, host immune response fails to clear on-going infection while risk acquiring secondary infection is enhanced (*290*). During sepsis, reduced expression of HLA-DR on monocytes but increased frequency of CD64-

expressing neutrophils and Treg may be a prognostic marker of immune suppression (*291*). Increased active caspase-3 within splenic white pulp was identified in sepsis compared to non-sepsis patients (*292*). Similarly, increased apoptosis was identified in both T and B lymphocytes in septic shock patients within 3 days of disease onset and associated with case-fatality (*293*). Likewise, another study identified increased circulating Treg but reduced proliferative capacity of CD4 T cells in sepsis patients compared to healthy control (*294*). PD-1 and its ligand, PD-L1 have been found to mediate sepsis-induced immune suppression. During sepsis, expression of PD-1 is increased on T and B lymphocytes, and monocytes and it is correlated with increased apoptosis of lymphocytes, reduced cellular immune response, and poor outcomes (*214, 295*). Collectively, poor cellular immune response during sepsis is primarily mediated by suppressed APC response, increased apoptosis of lymphocytes, or through negative T cell co-stimulation.

1.3.11 Distinct transcriptomic signatures are associated with poor outcome in sepsis

Landmark genome-wide blood transcriptomic studies of sepsis (*296, 297*) identified two distinct blood transcriptomic signatures which distinguish sepsis patients based on clinical outcome. Patients with sepsis response signature 1 (SRS1) exhibit a higher mortality rate with an immunosuppressive profile such as T cell exhaustion, reduced MHC-II expression, endotoxin tolerance, and apoptosis. On the other hand, patients with SRS2 exhibit an immunocompetent phenotype. The SRS group assignment was based on the use of seven-gene set including *DYRK2, CCNB11P1, TDRD9, ZAP70, ARL14EP, MDC1*, and *ADGRE3*. Moreover, temporal changes of blood transcriptome were identified, in which majority of sepsis patients with SRS1 who moved to SRS2 survived compared to ~50% deaths in those who remained in SRS1 (*297*). Interestingly, sepsis patients with SRS2 showed reduced survival when treated with hydrocortisone possibly through immunosuppression of

competent and helpful immune responses (*298*). A similar whole blood transcriptomic study of sepsis patients with community-acquired pneumonia (CAP) (*299*) identified four distinct molecular endotypes of sepsis (Mars1-4) using a 140-gene signature. Sepsis patients with Mars-1 signature had the poorest outcome compared to other endotypes with suppressed phenotypes of both innate and adaptive immune responses such as TLRs, APCs, and T cell signalling cascades. In contrast, patients with Mars-3 and Mars-4 showed up-regulated pathways involved in TLR signalling, interferon signalling, co-stimulatory molecules, and effector functions of T lymphocytes.

A recent transcriptomic study identified five sepsis endotypes to predict disease progression and clinical outcome in patients admitted to the emergency department. The five sepsis endotype include Neutrophil-Suppressive (NPS), Inflammatory (INF), Innate-Host-Defence (IHD), Interferon (IFN), and Adaptive (ADA). Patients with NPS and INF endotypes had more severe disease and poor outcomes, whereas patients with ADA had the mildest disease and better outcomes. NPS endotype features up-regulation of neutrophil degranulation but down-regulation of adaptive immune responses involving in TCR signalling cascades such as CD28 co-stimulation, phosphorylation of CD3/TCR, translocation of ZAP-70 to immunological synapse and interferon signalling. Up-regulation of inflammatory responses such as TLR-4, IL-1 signalling, interferon signalling, and activation of platelet were dominated in INF endotype (*300*). A comparison between SRS and the five-sepsis endotype signatures showed agreeable results in which SRS1 and NPS signatures were mostly present in sepsis patients with poor outcomes (*300*). Another sepsis study (*301*) aimed to identify transcriptomic signatures associated with either Gram-negative or Gram-positive CAP and revealed largely similar transcriptomic profiles between the two groups of bacteria. However, plasma cytokine profiling showed distinct profiles, in which IL-8 and IL-10 responses were higher in *E. coli*-induced CAP patients whereas infection with *S.*

pneumoniae induced higher response of matrix metalloproteinase-8 (MMP-8) compared to *H. influenzae* and *Pseudomonas aeruginosa*.

1.4 Type 2 diabetes and dysregulation of host immune responses

1.4.1 Type 2 diabetes is on a rise and highly prevalent in low- and middle-income countries

Diabetes is a major global health issue, one of the top four non-communicable diseases (NCDs) alongside cardiovascular disease, cancer, and respiratory disease (*302*). Moreover, diabetes is a key co-morbid risk factor other NCDs and for infectious diseases (*303, 304*). In 2021, the prevalence of diabetes mellitus is currently at 536.6 million cases (aged 20-79 years) and killed over 6 million deaths worldwide, with 432.7 million cases (~80%) living in LMICs (**Table 1.2** and **Figure 1.10**). It is estimated that the prevalence of diabetes will reach 783.2 million cases (31% rise) by 2045 (**Table 1.2**) (*304*). Furthermore, it is projected that up to 94% of predicted diabetes cases will occur in LMICs by 2045, as a result of expected population growth and socio-economic changes. Although formal typing is rarely done in LMIC settings, over 90% of diabetes cases in LMICs are estimated to be T2DM (*305*).

Table 1.2 Estimated number of global diabetes cases aged 20-79 years based on World Bank income classification in 2021 and projection by 2045 (*304*). Reproduced with permission from the International Diabetes Federation (IDF Diabetes Atlas, 2021. http://www.diabetesatlas.org.)

At a glance	2021			2045		
World Bank income classification	**Number of people with diabetes (millions)**	**Diabetes prevalence[i] (%)**	**Comparative diabetes prevalence[ii] (%)**	**Number of people with diabetes (millions)**	**Diabetes prevalence[i] (%)**	**Comparative diabetes prevalence[ii] (%)**
World	**536.6**	**10.5%**	**9.8**	**783.2**	**12.2%**	**11.2**
High-income countries	103.9	11.1%	8.4	117.7	12.4%	10.3
Middle-income countries	414.0	10.8%	10.5	623.3	13.1%	12.0
Low-income countries	18.7	5.5%	6.7	42.2	6.1%	7.0
Number of deaths due to diabetes	6.7 million		–		–	

i Prevalence is standardised to each national population for the respective year
ii Prevalence is standardised to world population for the respective year

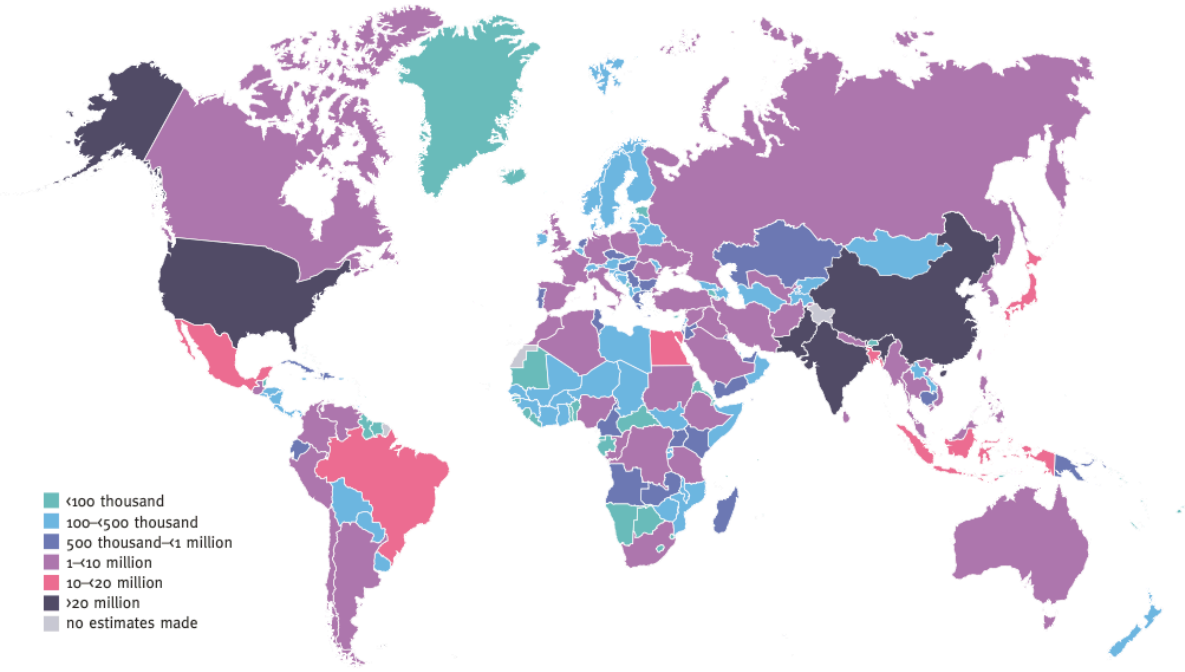

Figure 1.10 Estimated global burden of diabetes cases in adults aged 20-79 years in 2021. The total number of diabetes cases exceeded 20 million people in many low- and middle-income countries such as China, India, and Pakistan (*304*). Reproduced with permission from International Diabetes Federation (IDF Diabetes Atlas, 2021. http://www.diabetesatlas.org.)

1.4.2 Type 1 and Type 2 diabetes have different aetiologies

Clinically, people with concentrations of glycated haemoglobin (HbA1c) greater than or equivalent to 48 mmol/mol or 6.5% are considered as having T2DM (*306*). T2DM is a chronic metabolic disease resulting from dysregulation of insulin production and function leading to hyperglycaemia (*307*). The causes of T2DM are multifactorial, including obesity, pre-disposed genetics, imbalanced diet, and unhealthy lifestyle (*308*). T2DM is considered a low-grade chronic inflammatory disease, in which obesity is strongly associated with increased production of inflammatory mediators and insulin resistance (*309*). In healthy people, insulin is secreted by beta cells in the pancreas in response to high glucose concentration in the bloodstream e.g., after meals. Consequently, insulin binds to insulin receptors on cells allowing glucose molecules to enter cells for cellular energy source (*310*).

Constant secretion of insulin due to high blood glucose can cause insulin resistance when cells no longer respond to insulin and high demand insulin production (hyperinsulinemia) can lead to dysregulation and malfunction of the beta cells (*311*). People with T2DM secrete little or no insulin, leaving high blood sugar in the circulatory system (*312*). In parallel, excessive glucose is converted to fat and stored in multiple organs and tissues around the body. Altogether, high blood sugar, insulin resistance and high body fat content are thought to be key factors contributing to the development of T2DM (*313*). The majority of T2DM cases develop later in life; however, prevalence of T2DM in children and adolescents (aged below 20 years) can occur, up to 160-3,000 cases per 100,000 in some parts of the world (*304*). Treatment of T2DM ranges from diet, exercise and weight loss, a range of oral therapies including biguanides (metformin), sulphonylureas, thiazolidinediones, dipeptidyl peptidase 4 (DPP-4) inhibitors, glucagon-like peptide-1 (GLP-1) receptor agonists and

sodium-glucose co-transporter-2 (SGLT2) inhibitors, through to injectable insulin therapy (*314*).

In contrast, type 1 diabetes (T1DM) can occur at any age but has peak incidence in childhood. T1DM is thought to be caused by a combination of pre-disposed genetic susceptibility followed by an autoimmune-like response against the beta cells following an environmental trigger, leading to a complete loss of insulin production (*315*). Treatment for T1DM is limited to life-long insulin dependency usually through self-injection(*316*), unless receiving successful islet cell transplantation. Other types of diabetes include gestational diabetes, maturity onset diabetes of the young (MODY) and latent autoimmune diabetes in adults (LADA) (*317*). The majority of people with diabetes in the world have never undergone formal typing (e.g., with measurement of autoantibodies and C-peptide levels) but studies show that T2DM accounts for >90% of diabetes in the world, and higher in LMICs. For the purpose of this thesis, adults with diabetes in Thailand are assumed to have T2DM (*318, 319*).

1.4.3 Type 2 diabetes leads to other complications resulting in the global economic burden

People with T2DM develop secondary complications affecting many systems. Microvascular complications such as retinopathy, neuropathy and nephropathy are leading causes of T2DM-related morbidity (*320*). Moreover, T2DM is highly associated with development of macrovascular complications, primarily cardiovascular diseases, which are a major cause of death in diabetic patients (*321*). Therefore, management of patients with T2DM is complex due to its complications and costly as it requires life-long treatment and management. By 2021, the estimated global health expenditure on diabetes had increased

416% from USD $232 billion in 2007 to USD $966 billion. It is predicted that diabetes-related expenditure will surpass USD $1.05 trillion by 2045 (*304*).

1.4.4 Type 2 diabetes causes dysregulation of metabolic processes leading to elevated inflammation

Mechanisms underlying increased inflammation and oxidative stress leading to T2DM-induced complications in people with T2DM include alternative activation of the polyol pathway, elevated advanced glycation end products (AGEs), and enhanced protein kinase C (PKC) via diacylglycerol (DAG) (*322*). Excessive glucose under hyperglycaemic conditions activates the polyol pathway, in which glucose is converted to sorbitol (via aldose reductase) through oxidation of nicotinamide adenine dinucleotide phosphate (NADPH) and fructose (via sorbitol dehydrogenase) yielding nicotinamide adenine dinucleotide (NADH) (*323*). This causes depletion of NADPH, leading to reduced production of GSH (*324*), an important antioxidant which has been reported to be diminished in people with T2DM (*325, 326*). Moreover, activation of the polyol pathway can lead to accumulation of AGEs resulting in generation of ROS and RNS, and ultimately activation of NF-κB and pro-inflammatory cell mediators (*327-330*). Likewise, both free fatty acids and hyperglycaemia induce production of DAG that activates the PKC pathway, which in turn activates NF-κB pathway leading to production of pro-inflammatory cytokines (e.g. IL-1, TNF, and IL-6), superoxide, and ultimately contributing to oxidative stress (*331-333*). AGEs are elevated in T2DM patients, and include non-enzymatically glycosylated proteins and lipids that have been linked to increased inflammation and shown to promote diabetic complications such as cardiovascular diseases and atherosclerosis (*334*).

These aberrant mechanisms in T2DM have been shown to have impacts on host immune responses. A randomised-controlled study (*335*) on the effect of the aldose reductase

inhibitor (ponalrestat) on intracellular killing of *E. coli* by neutrophils firstly identified reduced bacterial killing by neutrophils derived from patients with DM compared to euglycemic matched controls. However, patients with DM treated with ponalrestat showed restoration of bacterial killing of *E. coli* to the level observed in euglycemic matched controls (*335*). Impacts of diabetes and its metabolic products on host immune responses were demonstrated including enhanced baseline inflammatory responses (*336, 337*), increased ROS production (*338*), impaired opsonophagocytosis of type III group B *Streptococcus* (*339*), reduced killing of *S. aureus* by neutrophils (*340*), reduced phagocytosis of yeast particles by neutrophils (*341*), and reduced phagocytosis of LPS by macrophages (*342*). Collectively, hyperglycaemia induces activation of the polyol and PKC pathway, and AGEs leading to activation of pathways involved in inflammation and dysregulation of innate immune functions, leading to a compromised host immune response against infection.

1.4.5 Altered functions of innate immune cells in people with type 2 diabetes led to increased inflammatory response

Besides well-known T2DM related complications, host immune response in people living with T2DM is altered (*163*). Neutrophil-mediated mechanisms are dysregulated in people with T2DM. Under homeostasis and upon LPS stimulation, production of pro-inflammatory cytokines from neutrophils including IL-1β, TNF and IL-8 were elevated in T2DM patients (*343*). In diabetic patients (both T1DM and T2DM) there is increased NETosis activity in freshly isolated neutrophils *ex vivo* with or without ionomycin stimulation (*170*). The same study identified higher level of citrullinate histone H3 which was associated with compromised wound healing in the diabetic mice model (*170*). Likewise, functions of macrophages are altered in diabetes for example, islet infiltration by macrophages is present in a T2DM mouse model with increased pro-inflammatory cytokine such as IL-6 and IL-8

and associated neutrophil and monocyte (*344*). Obesity is a major risk factor of T2DM development (*345*). A clinical study identified macrophages isolated from obese donors showed increased expressions of *IL1B* and *NOS2*, key pro-inflammatory regulated genes encoding IL-1β cytokine and nitric oxide synthase 2 (*346*). Altogether, elevated pro-inflammatory mediators and released cytotoxic compounds in circulation in diabetes contribute to dysregulation of immune responses and T2DM-related complications (*347*).

1.4.6 Dysregulated cellular immune responses in people with type 2 diabetes

Cell-mediated immune responses are crucial for controlling infections, generating memory for subsequent infections, and maintaining homeostasis (*72*). The low grade chronic inflammation of T2DM features elevated inflammatory mediators in circulation such as CRP, IL-6, and TNF (*348*). In line with increased inflammatory innate immune cells, frequencies of pro-inflammatory T cells subsets including Th1 and Th17 have been reported to be elevated in people with stable T2DM and obesity (*349-351*). One study identified reduced ratios of Treg/Th1 and Treg/Th17 populations in T2DM patients but increased inflammatory cytokine responses such as IFN-γ and IL-17 compared to healthy donors. The reduced circulating number of Treg cells appears to be due to increased susceptibility to apoptosis (*352*). A systemic review on the relationship between Treg and T2DM revealed reduced frequency of peripheral Treg (CD4+CD25+ Foxp3+) and serum IL-10 but increased serum IL-6, TGF-β, and TNF in patients with T2DM (*353*). *Jagannathan-Bogdan et al.* demonstrated similar findings, with increased peripheral Th17 cells and elevated production of IFN-γ from total T cells but reduced circulating Treg cells (*351*). However, people with T2DM showed reduced multifunctionality of CD8+ PD-1+ T cells (TNF, IFN-γ, IL-2), accompanied by reduced glycolysis and basal respiration, which was reversed by treatment

with metformin (*354*). Likewise, frequencies of PD-1 expressing CD4+ T and CD8+ T cells were increased in people with T2DM compared to healthy donors (*355, 356*).

1.4.7 T2DM increases susceptibility to intracellular infections and disease severity in viral infections

Generally, people with diabetes have increased susceptibility to infections including bacterial, viral, and fungal pathogens (*357*). People with type I and II diabetes are at higher risk from respiratory tract infection, urinary tract infection, and bacterial skin and mucous membrane infection (*358*). Mechanisms underlying the increased susceptibility to infections are complex and potentially involve both host conditions and pathogen factors (**Figure 1.11**) (*359*). Several clinical studies indicate that people with diabetes are at risk of increased colonisation of *S. aureus* (*360-362*) and *Candida* species *(363, 364).* In particular,T2DM patients are at increased risk of acquiring intracellular infections such as Mtb *(115),* Bp *(20),* and Hepatitis B virus (*365*). In TB, mycobacterial antigen-stimulated whole blood samples from TB patients with T2DM showed increased frequencies of both IFN-γ and IL-2 producing CD8 T cells and of TNF and IL-17 producing NK cells. In contrast, expression of cytotoxicity markers on CD8+ T cells including perforin, granzyme B, and CD107a (degranulation marker) was reduced compared to non-diabetic TB patients (*366*). People with T2DM showed an immunosenescent T cell phenotype with increased frequencies of effector memory CD45RA expression (EMRA) CD4+ T and CD8+ T cells, that express the pro-inflammatory marker CXCR2 and CX3CR1 but impair cell migration (*367*). Moreover, increased susceptibility and severity to viral infections is seen in T2DM. A prospective cohort study during the COVID-19 pandemic identified people with T2DM have about a three-fold increased susceptibility to severe acute respiratory syndrome coronavirus 2 (SARS-COV2) infection and hospitalisation (*368*). Moreover, SARS-COV2 patients with

diabetes co-morbidity showed increased disease severity and mortality (*368-370*). A metadata analysis identified an enhanced risk of severe dengue disease in people with diabetes (*371, 372*). People living with T2DM may be more susceptible to other viruses such as hepatitis C (*373*), varicella zoster virus (*374*), and Zika virus (*375*).

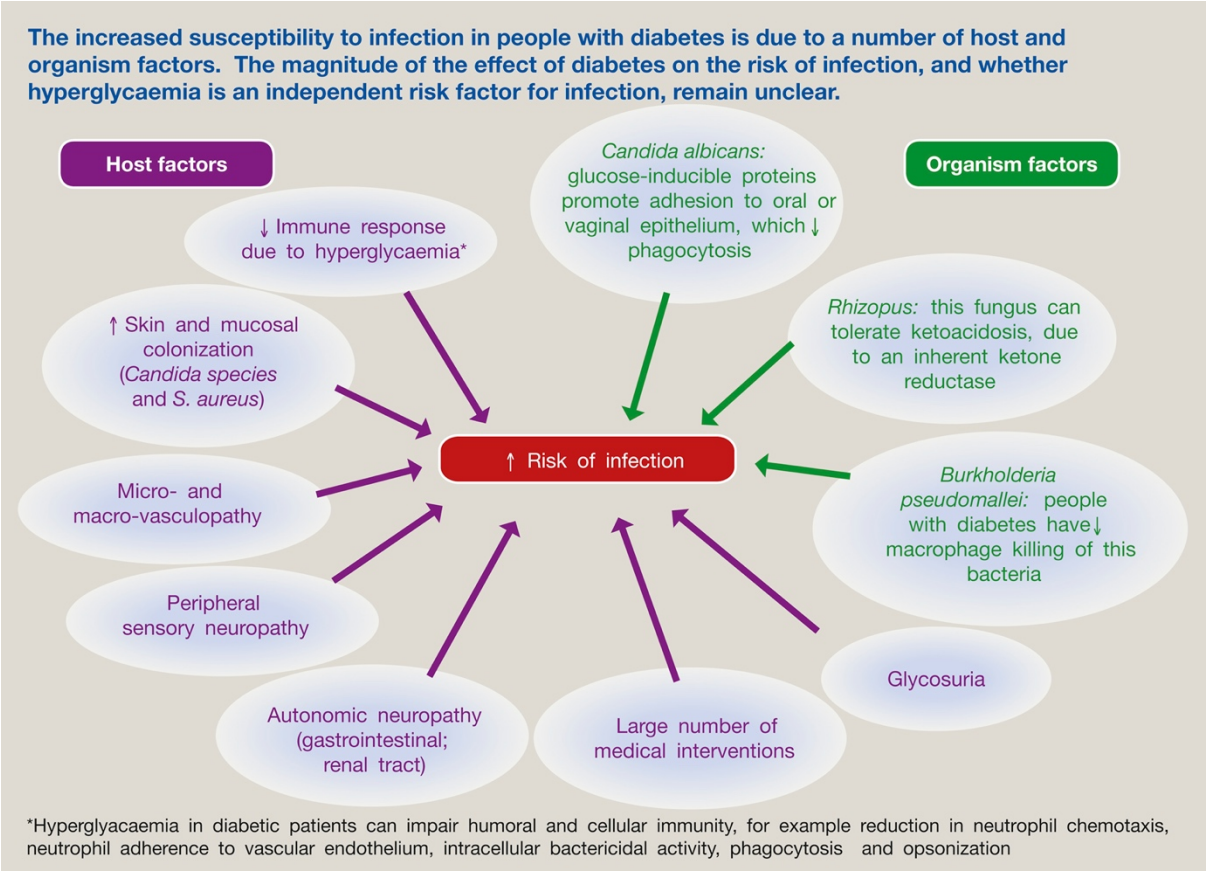

Figure 1.11 Host and pathogen factors implicated in increased susceptibility to infection in diabetes. A number of host immune mechanisms are dysregulated such as chemotaxis, phagocytosis, and bacterial killing, resulting in persistence of the invading pathogen. Pathogens can have a degree of intrinsic resistance to host immune responses, for example *Burkholderia pseudomallei*, the causative agent of melioidosis, displays evasion of multiple host innate immune systems including the complement system and phagocytosis (*359, 376*). Reproduced with licence from *Cooke,* Infections in people with diabetes. *Medicine* 47, 110-113 (2019). Licence number: 5380320935659.

1.5 Rationale for the thesis

To sum up, people living with T2DM are at higher risk of acquiring intracellular infections. Strikingly, people with T2DM are exceptionally susceptible to melioidosis (12-fold increased risk) and have a 3-fold increased risk of acquiring TB, with dysregulation of both innate and adaptive immunity due to diabetes likely to contribute to this phenomenon. Both diseases are caused by intracellular infections, with overlap of some clinical features, pathogenesis, and host immune responses. Therefore, underlying mechanisms leading to enhanced susceptibility in people with T2DM to melioidosis and TB may be common. To date, whole blood transcriptomic profiles associated with T2DM during melioidosis are yet to be elucidated. Furthermore, the high case fatality of melioidosis in endemic regions remains a great challenge despite improved healthcare facilities and clinical management. Host responses close to the onset of melioidosis are rarely evaluated systematically due to the requirement of diagnosis by bacterial culture. In this thesis, early whole blood transcriptomic profiles associated with fatal melioidosis are studied in a large, well-characterised cohort of melioidosis patients enrolled within 24 hours of hospital admission. Lastly, the identified transcriptomic profiles are validated using the independent melioidosis cohort.

1.6 Aims and objectives of this thesis

The aims of this thesis are to investigate the whole blood transcriptomic profiles associated with (i) diabetes in both melioidosis and TB, (ii) case-fatality in melioidosis, (iii) melioidosis compared to other community-acquired infections. The central objectives of this thesis are:

1. To study the whole blood transcriptome of melioidosis patients to reveal underlying mechanisms of increased susceptibility to melioidosis in diabetes, and to study the impact of diabetes on clinical outcomes.

2. To identify the whole blood transcriptomic profiles associated diabetes and intermediate hyperglycaemia in TB and common transcriptomic profiles associated with diabetes in both TB and melioidosis.

3. To identify the early whole blood transcriptomic profile associated with fatal melioidosis and transcriptomic signature of melioidosis compared to other community-acquired infections.

4. To validate the identified whole blood transcriptomic profiles associated with fatal melioidosis in community-acquired infections in the independent melioidosis cohort with similar study settings.

Chapter 2: Methods

This chapter will outline core RNA sequencing data analyses implemented across four main chapters (**Chapter 3-6**). Specific RNA sequencing approaches, data acquisitions, and data analyses will be described in detail within each chapter.

2.1 Rationale of experimental approach

The origin of this study came from a prospective observational study between 2013 and 2017 conducted at Sunpasitthiprasong Hospital, Ubon Ratchathani, a world-renowned study site for melioidosis. The study aimed to evaluate human immune response to melioidosis in adult patients, in which clinical samples such as peripheral blood mononuclear cell (PBMC), serum, and plasma were collected for studies using a wide range of humoral and cellular immune assays. Moreover, whole blood samples were collected for genomics and transcriptomics. As a result, key findings from this study identified importance of cellular immune responses during melioidosis and altered immune profiles in the patients with type 2 diabetes (T2DM) in PBMC samples (*76, 377*). Therefore, a full picture of host response during melioidosis is remained to be elucidated. This thesis, whole blood samples were studied using bulk RNA sequencing approach in melioidosis and tuberculosis, aiming to decipher whole blood transcriptomic profiles associated with (i) T2DM during the intracellular infection and (ii) case-fatality in melioidosis.

2.1.1 Why whole blood transcriptomics?

Transcriptomics is a study of the complete set of transcriptomes (coding and non-coding RNAs) within a cell or organism allowing decipherment of a relationship between the genome and observed phenotypes qualitatively and quantitively (*378*). Within each cell, a

fraction of genes are actively transcribed from the genome and influenced by both internal and external factors such as diseases, aging, or infections at a given time point (*379*). Therefore, whole blood transcriptomics provides a snapshot of global gene expression at genome-wide scales facilitating a comprehensive study between two or more phenotypes of interest within the biological systems (*380*). However, gene expression profiles may not fully reflect functions of protein and corresponding phenotypes, where functional proteins may undergo post-translational modifications (PTMs) such as glycosylation, methylation, and ubiquitylation (*381*).

2.1.2 Available tools for RNA transcriptomics

Multiple tools can be used to study gene expression such as real-time polymerase chain reaction (RT-PCR), microarray, and RNA sequencing. RT-PCR is a quick and robust tool to study gene expression, however, it is not applicable for genome-wide transcriptomics. In early 2000s, microarray had become a standard tool to study genome-wide gene expression, the technology was based on a fluorescent-based hybridization chip of known transcriptome (*382*). Nevertheless, microarray has several limitations including limit detects of known genes or transcripts, high background noise, low dynamic range, and low resolution (*383*). These limitations from microarray approach have led to the development of next-generation sequencing (NGS) and it has become a default approach for transcriptomics until nowadays. The NGS offers high-throughput and massively parallel sequencing of both DNA and RNA (*384*).

Likewise, RNA sequencing allows a study of global gene expression without a *priori* knowledge, providing higher dynamic ranges (*378*), and discovery of novel transcripts (*385*). A typical gene expression study usually targets messenger RNAs (mRNAs), therefore, poly-A tail or total RNA library preparation can be an option for RNA sequencing

(*386*). In fact, total RNA sequencing approach allows detection of other forms of RNAs and more suitable for samples with lower RNA quality e.g., preserved specimens (*387*). Nevertheless, total or bulk RNA sequencing measures averaged gene expression profile at population level, where cell-specific expression profile is natively indistinguishable but can be computationally estimated (*388*). In recent years, single-cell RNA sequencing (scRNA-seq) has become a widely adopted method to study gene expression at single-cell level, unravelling complexity of cellular heterogeneity and composition within an organism at a given condition and point in time (*389*). However, scRNA-seq is currently more expensive than bulk RNA sequencing and required enriched live cells to begin with (*390*). In this study, all-study cohorts were not designed for scRNA-seq experiment, in which cryopreserved PBMC samples were mostly unavailable or inapplicable due to low cell viability and poor recovery as a result of long-term storage (> 5 years) or a nature of acute PBMC samples.

2.1.3 Different choices of differential gene expression analysis

The emergence of high-throughput sequencing (HTS) data has led to the development of statistical R/Bioconductor packages. DESeq2 and edgeR are the most popular R packages developed to deal with large and complex HTS data generated from various sequencing platforms and approaches (*391, 392*). Differential gene expression analysis by DESeq2 and edgeR R packages assumes that genes are not differentially expressed between biological conditions. However, there are some key differences between the two packages including data normalisation and filtering of genes. DESeq2 estimates overdispersion of expression data utilising a statistical model based on a negative binomial distribution followed by a generalised linear model to estimate the mean and variance of each gene (*392*). DESeq2 uses a normalisation method called median of ratios method, in which counts are normalised by a scaling factor calculated from the median of the ratios of each gene over its geometric

mean across all samples (*393*). By default, DESeq2 employs the independent filtering method, in which differentially expressed genes are further filtered using the quantiles method (*392*). edgeR uses a similar statistical model based on the negative binomial distribution, in which data normalisation (trimmed mean of M-values method [TMM]) is based on a scaling factor calculated from a reference sample. By default, edgeR utilises a count-per-million (CPM) threshold to filter out genes that do not pass the minimum CPM in the smallest group sample size (*394*). Nevertheless, both methods provide similar results given sufficient biological replicates and are robust against low biological replicates, differences of library sizes, library compositions and outliers due to high variation of biological replicates (*395, 396*). However, the performance of DESeq2 has been shown to be slightly better in minimising false positivity, particularly in the presence of high variability of biological replicates and outliers (*392, 397*). I therefore chose DESeq2 to normalise read counts for downstream data analysis and perform DGE analysis.

2.2 Study cohorts

This thesis consists of whole blood RNA sequencing data derived from four independent studies including patients with melioidosis (**Chapter 3**: MICRO1501, N=110), tuberculosis (**Chapter 4**: The Concurrent Tuberculosis and Diabetes Mellitus [TANDEM], N=239), community-acquired infections (**Chapter 5**: Ubon-Sepsis, N=284), and an additional melioidosis cohort for validation (**Chapter 6**: Determinants of Outcome and Recurrent Infections in Melioidosis [DORIM], N=32) (**Figure 2.1**). Ethical approval information and participant demographics within each cohort will be described in detail within each chapter. In **Chapter 4**, the identified transcriptomic profiles associated with T2DM in melioidosis from **Chapter 3** were compared with tuberculosis patients. In **Chapter 6**, the identified transcriptomic profiles associated with fatality in melioidosis from **Chapter 5** were

validated in the independent melioidosis cohort. Although majority of diabetes cases in LMICs have T2DM, however, for accuracy of clinical data, the term "T2DM" was only used for the data associated with the study cohort from **Chapter 3**. Throughout this thesis, T2DM and diabetes were used interchangeably due to lack of formal diagnosis of diabetes in most studies.

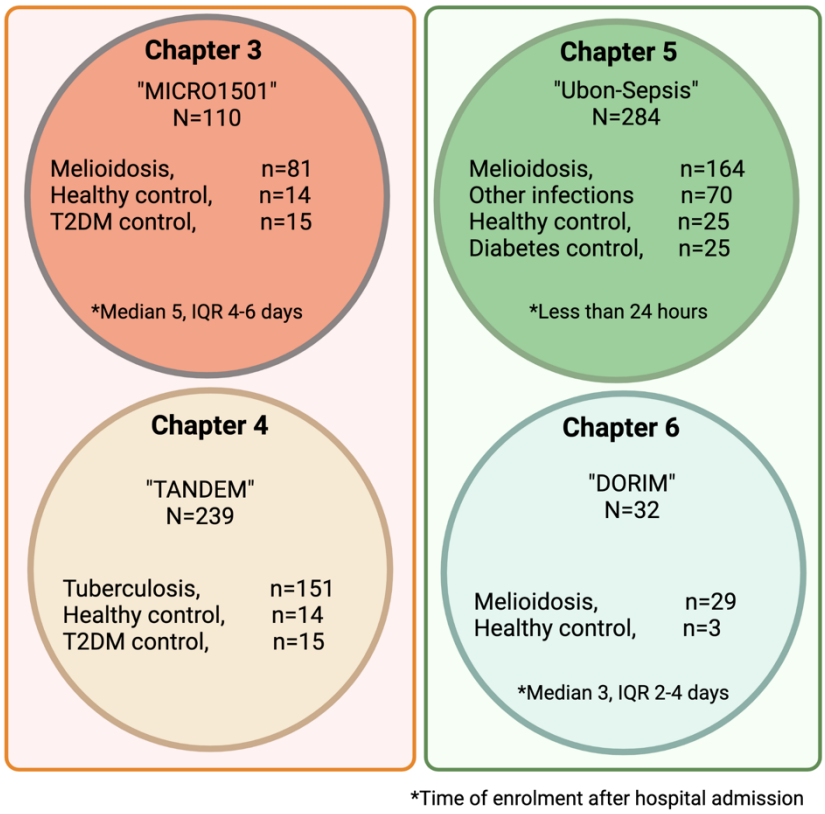

Figure 2.1 Study cohorts.

This thesis consists transcriptomic data derived from four independent study cohorts: (**Chapter 3**) melioidosis (MICRO1501), (**Chapter 4**) tuberculosis (TANDEM), (**Chapter 5**) community-acquired infections (Ubon-Sepsis), and (**Chapter 6**) melioidosis for validation (DORIM). Timing of participant enrolment into the study cohort relative to day of hospital admission (median in days after hospital admission and inter quartile range [IQR]) are indicated where appropriate (patients with tuberculosis were typically not admitted to hospital). The identified transcriptomic profiles associated with type 2 diabetes during melioidosis in **Chapter 3** were compared with tuberculosis patients in **Chapter 4**. The identified transcriptomic profiles associated with case fatality during

melioidosis in **Chapter 5** were validated in the independent melioidosis cohort in **Chapter 6**. Created with BioRender.com.

2.3 RNA sequencing data generation and data acquisition

This thesis, only RNA sequencing data from **Chapter 3** (MICRO1501) were generated locally. Briefly, RNA isolation and preparation for RNA sequencing was performed in Dunachie's laboratory at Peter Medawar Building for Pathogen Research, University of Oxford. Total RNA samples were sent for RNA sequencing at the Oxford Genomics Centre, Wellcome Centre for Human Genetics, University of Oxford. The RNA sequencing data from the remaining three chapters were kindly provided by our collaborators**. Chapter 4**: TANDEM, RNA sequencing data from tuberculosis study were kindly provided by Dr. Jackie Cliff and Professor Gregory Bancroft the London School of Hygiene and Tropical Medicine, UK. **Chapter 5**: Ubon-Sepsis, RNA sequencing data from community-acquired infections were provided by Professor Eoin West at University of Washington, USA. And **Chapter 6**: DORIM, RNA sequencing data for validation from melioidosis study were kindly provided by Professor Narisara Chantratita at Mahidol University, Thailand.

2.4 RNA sequencing data analyses

In this thesis, identical RNA sequencing data analysis approaches were applied to all study cohorts consisting of supervised and unsupervised approaches unless stated otherwise (**Figure 2.2**). The supervised data analysis approach or typical transcriptomic data analyses consisted of differential gene expression analysis (DGE), functional pathway analyses, and the Ingenuity Knowledge Base by QIAGEN Ingenuity Pathway Analysis (QIAGEN Inc., https://digitalinsights.qiagen.com/IPA) including canonical pathway and upstream regulator analyses. The unsupervised approach is based on weighted gene co-expression network

analysis (WGCNA), gene module enrichment, and identification of hub genes. To identify potential gene regulators, differentially expressed genes following DGE and identified hub genes from interesting gene modules were explored for overlapping genes using Venn diagrams by ggvenn R package (version 0.1.9).

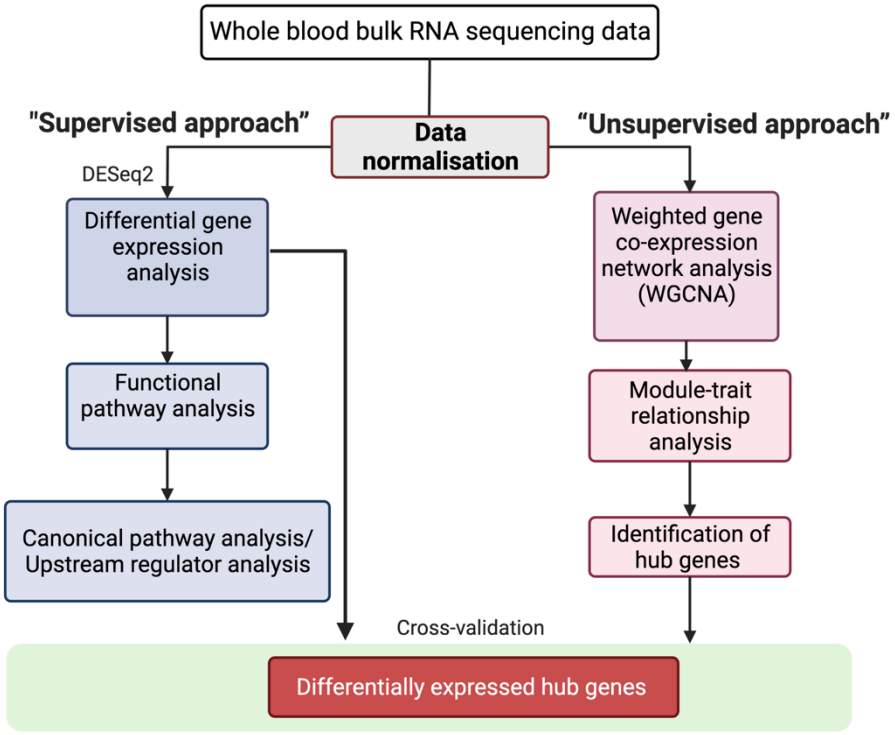

Figure 2.2 Overview of transcriptomic data analysis workflow.

The core data analysis pipeline consists of two independent approaches, supervised and unsupervised data analysis pipeline. The supervised approach employs a typical differential gene expression analysis and followed by functional pathway analysis. The unsupervised approach uses weighted gene co-expression network analysis and followed by module-trait and hub gene analysis within interesting gene modules. The two approaches are cross validated at the end of the pipeline in order to identify potential biomarkers.

2.5 Supervised approach

2.5.1 Differential gene expression analysis

All expression data were annotated to gene symbol (HGNC, HUGO Gene Nomenclature Committee). Genes with no counts or low counts were removed. Pre-filtered read counts were normalised using the median of ratios method within the DESeq2 R package that adjusts for different sequencing depth and RNA composition amongst samples (*393*). After normalisation, normalised read counts were transformed on the log2 scale using variance stabilising transformation (VST) function within the DESeq2 R package for data visualisation such as multi-dimensional scaling and heatmap (*392*). After the VST, unsupervised clustering by principal component analysis (PCA) was performed using the top 1,000 most variable genes to detect outliers and visualise biological variations among samples. Next, DGE analysis was carried out using negative binomial generalised linear modelling, implemented in the DESeq2 R package (*392*) adjusted for age and sex, unless otherwise stated. By default, the Wald test was applied to test the null hypothesis for comparison between two groups. To further reduce false positivity, independent filtering based on the mean of normalised counts and multiple testing correction using Benjamini-Hochberg/False discovery rate (FDR) was applied (*392, 398*). Finally, differentially expressed genes (DEGs) were deemed significant when satisfying absolute[Log2 fold-change] ≥ 1 and adjusted P-value (FDR) < 0.05, unless stated otherwise. DEGs were visualised on volcano plot using EnhancedVolcano R package (version 1.10.0) and heatmap using pheatmap R package (version 1.0.12).

2.5.2 Functional pathway analysis

Functional pathway analysis or over-representation analysis based on gene sets from the Molecular Signatures database (MSigDB, version 7.0, https://www.gsea-msigdb.org/gsea/msigdb/) such as Hallmark (*399*), Reactome (*400*), KEGG (*401*) and Gene Ontology (*402*) was performed using the clusterProfiler R package (version 4.0.5) (*403, 404*). To complement the result obtained from a particular gene set (e.g., Hallmark), an additional pathway analysis from another gene-sets collection (e.g., Reactome, KEGG, and Gene Ontology) was performed in most cases. Hallmark gene sets are the collection of summarised well-represented biological pathways from MSigDB database consisting of non-redundant 50 pathways (*399*). On the other hand, curated gene sets i.e., Reactome consists of 1,615 gene sets covering detailed biological pathways, disease, and processes in 24 major groups such as immune system, signal transduction, and metabolism (*400*). Following DGE analysis, a list of DEGs was filtered to remove any rows (genes) containing N/A values and ranked based on adjusted P-value (FDR)<0.05 and a cut-off of absolute [Log2 fold-change]≥ 1, unless stated otherwise. The analysis was based on determination of whether known gene sets were over-represented in the pre-ranked list of DEGs. The P-value was calculated using hypergeometric distribution (*405*). Gene sets or pathways were deemed significant when satisfying adjusted P-value (FDR)<0.05.

2.5.3 Gene set enrichment analysis (GSEA)

The over-representation analysis is only applicable when there are large differences of transcriptomic profiles between biologically distinctive phenotypes such as disease versus control or severe versus mild disease. On the other hand, gene set enrichment analysis (GSEA) can detect subtle but coordinated changes of gene expression patterns between comparative phenotypes (*406, 407*). A test result from DGE analysis was filtered to remove

any rows (genes) containing N/A values and ranked based on adjusted P-value. Pre-ranked data was used to perform the GSEA pre-ranked method based on the gene sets from MSigDB. GSEA analysis was performed and visualised using the fgsea R package version 1.18.0 (*408*) or GSEAPreranked mode on GSEA software with 1,000 permutations and classic scoring scheme setting (BROAD Institute, version 4.1.0).

2.5.4 Canonical pathway analysis

Ingenuity Pathway Analysis (IPA) was used to identify significant canonical pathways based on the Ingenuity Knowledge Base (QIAGEN Inc., https://digitalinsights.qiagen.com/IPA). Lists of DEGs were filtered to remove any rows (genes) containing N/A values and retained the DEGs with adjusted P-value (FDR)<0.05. Significant pathways satisfied overlap P-value<0.05 and z-score ≥2. The overlap P-value was calculated by the right-tailed Fisher's exact test to determine whether there was a significant overlap between the input expression data and pre-defined gene sets. A positive z-score indicates predicted activated pathways, and a negative z-score indicates predicted inhibited pathways.

2.5.5 Ingenuity upstream regulator analysis

IPA was used to identify genes, transcription factors or any molecules that may be responsible for changes of observed gene expression based on the Ingenuity Knowledge Base. Lists of DEGs were filtered to remove any rows (genes) containing N/A values and retained the DEGs with adjusted P-value (FDR)<0.05. Potential upstream regulators were based on overlap P-value<0.05 and z-score ≥2, unless stated otherwise. The overlap P-value was calculated using the right-tailed Fisher's exact test, to determine whether there was a significant overlap between the input expression data and known downstream target genes regulated by transcriptional regulators. The use of z-score is to infer activation status of

transcriptional regulators, where positive z-score indicates predicted activation of upstream regulators or negative z-score indicated predicted inhibition of upstream regulators (*409*).

2.6 Unsupervised approach

2.6.1 Weighted gene co-expression network analysis

In biological system, genes are usually co-expressed and functionally related. Gene expression may be controlled by a gene regulatory network such as transcription factors, RNA binding protein or gene products themselves (*410, 411*). There is evidence suggesting that biological networks are closed to "scale-free"(*412*), where a few genes (nodes) are connected to many nodes following distributions of a power law (*413, 414*). These highly connected genes are considered as hub genes that may regulate that particular gene network (*415*). Weighted gene co-expression network analysis (WGCNA) is a systems biology tool which can be used for studying the relationship between a group of highly interconnected genes and observed phenotypes (*416*). Genes with similar expression profiles (co-expression) form a cluster or gene module in an unsupervised manner. This significantly reduces a number of input genes and allows genes with biologically related functions forming a cluster and can be further studied for relationships to external traits. Finally, hub genes responsible for the observed phenotype can be identified (*415*). Therefore, WGCNA facilitates unbiased discovery of candidate biomarkers in high throughput data.

There are six major steps in performing WGCNA: (i) detection of outliers, (ii) construction of co-expressed gene network, (iii) identification of co-expressed gene modules, (iv) identification of module-trait relationships, (v) study of module relationships, and (vi) identification of hub genes within modules of interest (*415*). Firstly, outliers were detected and removed if present by hierarchical clustering using average method (*417*). Secondly, to

construct a weighted network, the correlation between every pair of genes was calculated to produce an adjacency matrix, where the strength of the connection between two genes in the network is graded from 0 (unconnected) to 1 (fully connected). Unlike a weighted network, an unweighted network uses a hard threshold resulting in a dichotomous relationships between a pair of genes, therefore, genes with low or moderate correlations below the threshold are disregarded (*416*).

There are three types of networks available: (i) unsigned, (ii) signed (*418*), and (iii) signed hybrid (*419*). The unsigned network considers genes with strong correlation regardless of the directions of association (*418*). The signed network only considers genes with positive correlation, and those genes with negative correlation are considered as unconnected (*418*). The signed hybrid considers genes with positive correlation and those with negative correlation considered as no correlation (*420*). Practically, signed and signed hybrid networks produce almost identical outcomes (*421*), but unsigned network was found to be less sensitive in a certain circumstance (*418*). In this thesis, the signed network was chosen for network construction as it was proven to be robust in identification of biologically meaningful biomarkers in several studies (*418, 422-424*). Thirdly, soft-threshold (power β) was chosen to obtain a scale-free network (*416*). Ideally, an approximate scale-free network is obtained when a minimal power reaches high R^2 (≥ 0.8) on the scale-free topology model. Moreover, the same power β should result in low mean connectivity (<100), avoiding influence of strong drivers that would invalid the assumption of scale-free topology (**Figure 2.3**). Fourthly, a topological overlap matrix (TOM) was calculated from the adjacency matrix in order to minimise effects of background noise and spurious correlations (*416*). Next, a dissimilarity of topological overlap matrix (DistTOM) was calculated and used to identify gene modules. Fifthly, co-expressed gene modules were identified via hierarchical

clustering using the Dynamic Tree Cut method (*425*). The one-step network construction and module detection function were performed with a minimal number of 50 genes per module.

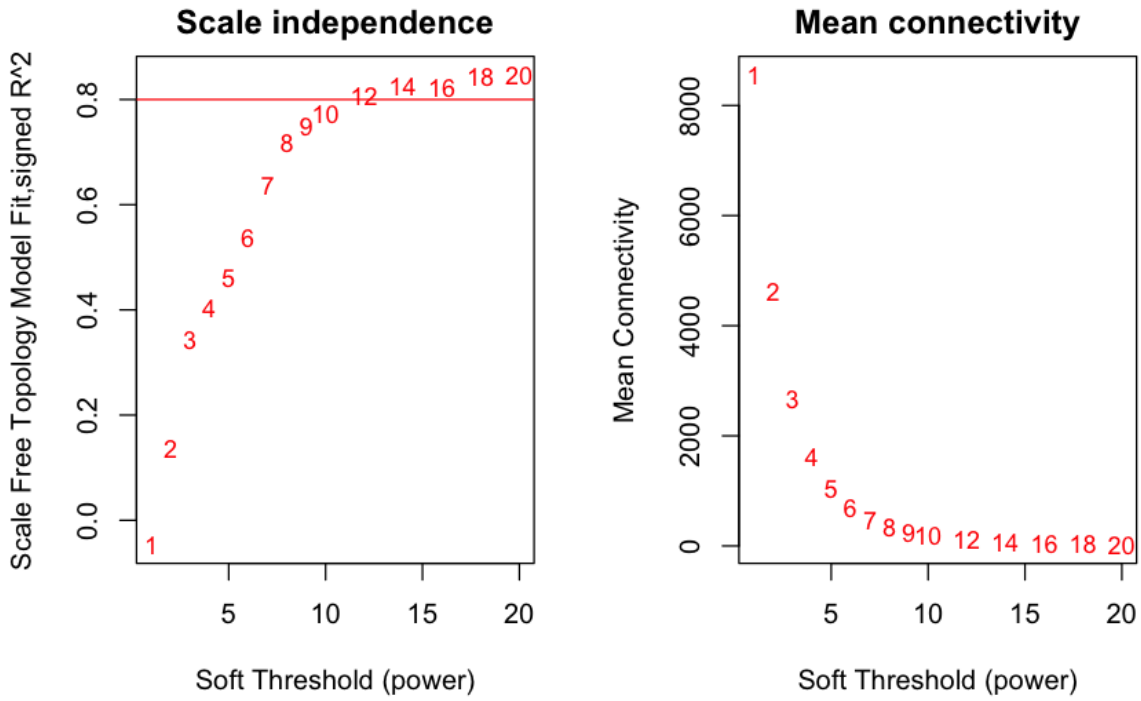

Figure 2.3 An example of scale free network topology analysis.

Scale-free network analysis with scale independence plot indicates scale free topology model fit (R^2) and mean connectivity plot, with the soft threshold displayed on the x-axis. Here, the power β of 14 was chosen based on high R^2 (0.82) with low mean connectivity (72).

As a result, co-expressed gene modules (module eigengenes, MEs) were generated and assigned with different colours (**Figure 2.4**). Each module eigengene can be described as the first principal component or a representative gene expression profile of a given module (**Figure 2.5**) (*426*). Finally, module-trait relationship analysis was performed to identify the correlations between module eigengenes and clinical traits (e.g. age, sex, diabetes status, mortality outcome). The module-trait relationship analysis accepts the clinical traits either

in binary or continuous outcomes. Correspondingly, a table of correlations where each row represents a gene module and each column represents a clinical trait was generated. Correlations were calculated by Pearson's correlation method and the corresponding correlation coefficients and P-values were displayed in each cell (*415*) (**Figure 2.6**). A high positive module-trait correlation indicates that the module eigengene increases with increasing trait values (i.e., increased frequency of neutrophils and SOFA scores). On the other hand, a high negative correlation of module-trait analysis implies that the module eigengene decreases with increasing trait values. In other words, within a gene module of a signed network, all genes are positively correlated with the eigengene. Therefore, a positive correlation of module-trait relationship implies an increase in expression profile within that particular module eigengene that correlates with increasing external trait values (**Figure 2.5, 2.6**). Interesting MEs (both positive and negative correlations) with significant module-trait correlations (P-value <0.05) were further studied with module enrichment analysis for pathways that are associated with observed phenotypes (i.e., clinical outcomes) and whether the same pathways were observed in the analyses by the supervised approach.

To facilitate identification of biologically meaningful gene modules, a co-expressed gene module that correlates with a given trait with a nominal P-value <0.05 is considered significant. This allows detection of gene modules associated with weaker or moderate correlations to other parameters (e.g., age, sex, and underlying conditions) which are typically hindered by transcriptional responses in drastic conditions (i.e., disease versus control or severe versus mild disease). To minimise false positive rates in identification of potential biomarkers, hub genes identified from interesting gene module must be present in the DEGs derived from the DGE analysis of interest (e.g., non-survivors versus survivors) and satisfy a threshold of DEGs with a fold change (FC) ≥ 1 (impact of diabetes in TB), FC

≥2 (impact of case fatality in melioidosis) and adjusted P-value <0.05 (**Figure 2.2**). In addition, the rationale behind identification of hub genes in a given gene module with positive correlation with trait values is robustness of increased expression of gene sets proven in many studies and settings providing higher sensitivity and specificity in discriminating one from another condition (*102, 427, 428*). Increased expression or presence of genes and gene products (i.e., proteins) are fundamentally important for development of diagnostic and prognostic tools in many conditions or diseases (*429*). In this thesis, the transcriptomic signature (gene sets) associated with fatal melioidosis may be useful for development of a point-of-care test that helps distinguish patients at high risk of developing severe disease.

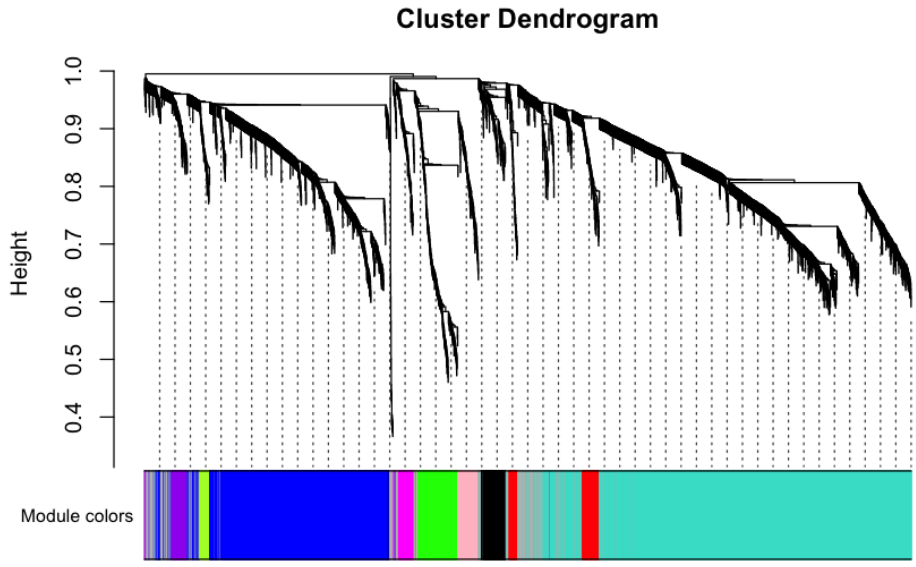

Figure 2.4. An example of cluster dendrogram and gene modules.

Cluster dendrogram of co-expressed gene modules by a hierarchical clustering of genes based on topological overlap using the Dynamic Tree Cut method. The corresponding modules assigned with different colours were displayed underneath. Here, 11 module eigengenes (MEs) were detected and are displayed with colours assigned in descending order based on size (number of genes) as follows: turquoise, blue, green, red, black, pink, magenta, purple and greenyellow.

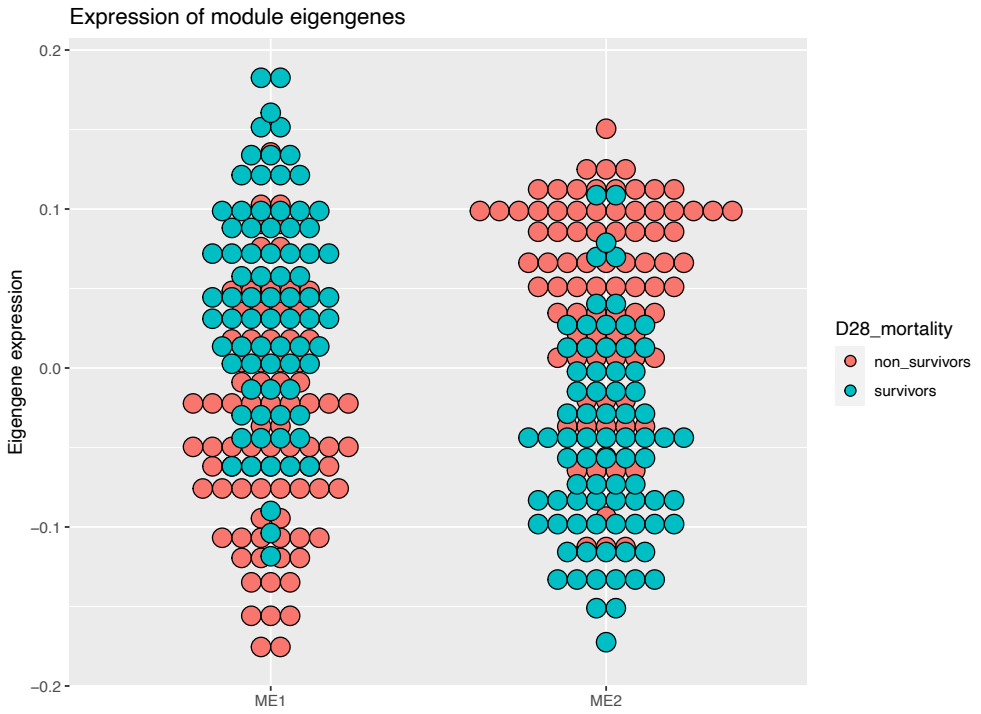

Figure 2.5 An example of module eigengene associated with 28-day mortality.

A module eigengene (ME) can be described as the first principal component or a representative gene expression profile of a given co-expressed gene module. For example, ME1 is associated with survivors whereas ME2 is associated with non-survivors. Accordingly, expression profiles of survivors are increased in ME1 but decreased in ME2 or *vice versa*.

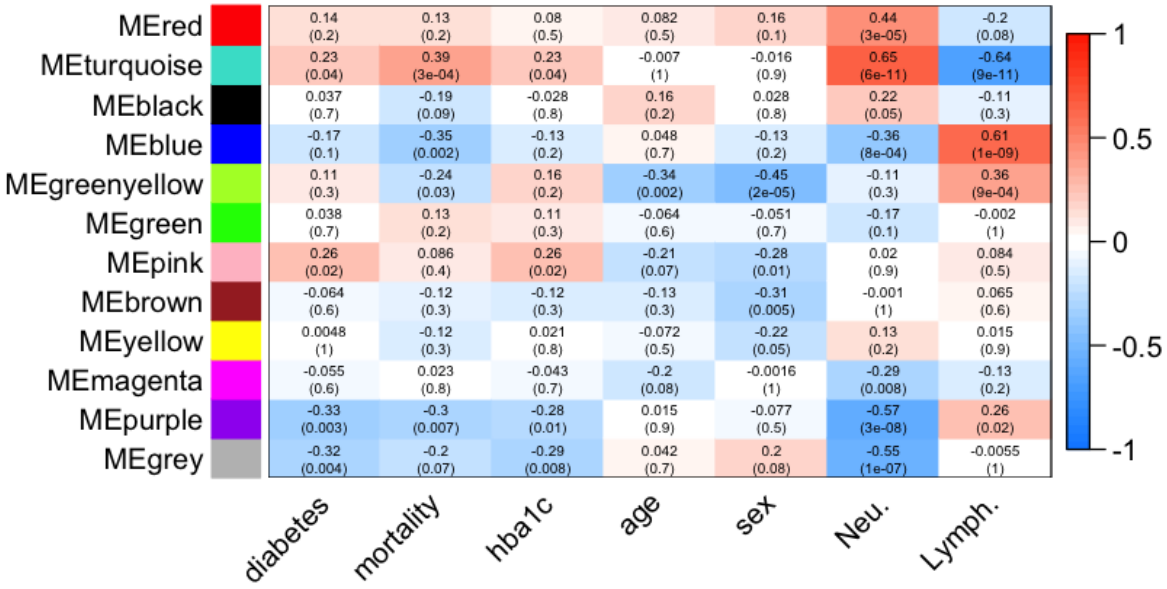

Figure 2.6 An example of module-trait correlations.

Module-trait relationship analysis. Each column represents clinical traits and each row presents module eigengenes, with corresponding Pearson's correlation coefficient and P-value in parenthesis for each module trait pair. The gradient colour bar indicates positive (+1, red) and negative (-1, blue) Pearson's correlation coefficient. Clinical traits analysed include diabetes status (binary - diabetes), 28-day mortality (binary - mortality), HbA1c level as percentage of haemoglobin (hba1c), age in years, sex (binary male or female), neutrophils percentage of total white cell count (Neu.), and lymphocyte percentage of total white cell count (Lymph.). Here, METurquoise was significantly correlated with %neutrophils and mortality (Pearson's correlation=0.65, P-value < 0.001).

2.6.2 Module enrichment analysis

Interesting modules with significant module-trait relationships (both positive and negative correlations) underwent module enrichment analysis based on the gene sets from MSigDB collection using clusterProfiler R package (version 4.0.5) (*399, 403, 404*).

2.6.3 Identification of hub genes within interesting gene modules

Interesting modules featuring the highest correlations with clinical traits of interest were used to identify hub genes. Co-expression gene network data containing edges (weights of network) and nodes (genes) were exported and visualised on Cytoscape software (version 3.9). Identification of hub genes within interesting modules was calculated using Maximal Clique Centrality method from CytoHubba plugin (version 0.1) on Cytoscape (*430*).

2.6.4 Identification of candidate biomarkers in fatal melioidosis, diabetes-induced susceptibility to tuberculosis, and validation experiments

In **Chapter 3** and **Chapter 5**, key regulators associated with fatal melioidosis were identified for overlapped genes among identified co-expressed gene modules associated with clinical parameters of interest, top 20 hub genes identified in the modules of interest, and up regulated genes following differential gene expression analysis between non-survivor and survivor melioidosis patients (**Figure 2.2)**. Similarly, In **Chapter 4**, key regulators associated diabetes and intermediate hyperglycaemia during tuberculosis were identified in similar fashion. Extensive literature research was performed to address potential contribution of each key hub gene in regulating host response associated with poor outcome during melioidosis. Likewise, key regulators potentially involving in increased susceptibility to Mtb infection in tuberculosis patients were discussed. In **Chapter 5**,

identified transcriptomic profiles associated with fatal melioidosis were validated in the independent melioidosis cohort and using functional assays in **Chapter 6**.

2.6.5 Deconvolution of bulk RNA sequencing data

As discussed previously, a scRNA-seq approach allows dissection of cell-type specific expression and cell compositions within a biological sample. Nevertheless, cell type abundances within whole blood population of bulk RNA-seq can be mathematically estimated using computational approaches. There are a number of available methods based on different algorithms and estimated cell types such as CIBERSORTx (*431*) (v-support vector regression, 22 immune cell types), EPIC (*432*) (constrained least square regression, 6 immune cell types), MCP-counter (*433*) (geometric mean of gene markers, 8 immune cell types), TIMER (*434*) (constrained least square fitting, 6 immune cell types), and xCell (*435*) (single sample gene-set enrichment analysis [ssGSEA], 64 immune and other cell types). Nevertheless, CIBERSORTx and xCell have shown decent performance in benchmark studies and provided more immune cell phenotyping compared to other methods (*388, 436*). This thesis deployed the two most popular deconvolution methods, CIBERSORTx (extended from CIBERSORT) (*431, 437*) and xCell (*435*). Firstly, CIBERSORTx uses a machine learning approach, with a linear support vector regression method for deconvolution of the mixture (*437*). In addition, a LM22 signature containing 547 genes that discriminate 22 human hematopoietic cells such as T cell subsets, B cell subsets, and myeloid subsets was used to deconvolute the RNA sequencing data using impute cell fractions analysis mode with 100 random permutations and other parameters set at default values (https://cibersortx.stanford.edu/) (*437*). Samples with P-value <0.05 were included for further analyses.

On the other hand, xCell employs ssGSEA algorithm to estimate the enrichment of 64 cell subsets such as lymphoids, myeloids, and stem cells using 489 gene signatures derived from six different sources (*435*). For xCell, read counts were normalised to Reads Per Kilobase of transcript per Million reads mapped (RPKM) using the DESeq2 package (*392*). Enrichment of 64 immune and stromal cells was performed using xCell (version 1.1.0) with default parameters. Both methods provide estimations of cell types using slightly different mathematical approaches, reference gene sets, and number of target cell types, in which the 22 immune cell types by CIBERSORTx were complimented and further phenotyped by 64 immune and stroma cell signatures by xCell. The imputed cell fractions and enrichment scores were compared using non-parametric Mann-Whitney tests in R programme.

Chapter 3: What is the impact of type 2 diabetes on the whole blood transcriptomic response during melioidosis?

3.1 Introduction

Melioidosis is a fatal infectious disease caused by an infection with a Gram-negative bacillus, *Burkholderia pseudomallei* (Bp). A recent prediction of global burden of melioidosis in 2015, estimated 165,000 cases with 89,000 deaths, and a much wider distribution in tropical countries across the globe than previously appreciated (*4*). The in-hospital case fatality rate is up to 40% in northeast of Thailand and 14% in Australia (*9, 20*). Established risk factors for melioidosis include diabetes, chronic renal diseases, and excessive alcohol consumption (*87*), in which people with diabetes have a 12-fold increased risk for melioidosis (*20*). In 2021, it was estimated that over 530 million people live with diabetes worldwide, and 77% live in LMICs. It was further estimated that the prevalence of diabetes will increase up to 31% by 2045 (*304*). Although formal typing is rarely done in LMIC settings, over 90% of diabetes cases in LMICs are estimated to be T2DM (*304*).

People with T2DM are known to have increased susceptibility to infections. There is established increased susceptibility in diabetes to many pathogens including both Gram-negative and Gram-positive bacteria and viruses (*357*). Host immune responses during infections in people with diabetes have been shown to be compromised including phagocytosis, cytokines, and chemokine response (*438*). Co-epidemics between the ever-growing burden of diabetes and individual infectious diseases, could result in more co-morbidity, mortality, and impact on global economy. In 2013, *Koh et al. (101)* demonstrated that the whole blood transcriptome in 30 melioidosis patients was dominated by interferon-mediated responses, and was indistinguishable from active TB patients (*102*). However, the

whole blood transcriptomic profile associated with increased susceptibility to melioidosis in people with T2DM melioidosis remains unaddressed.

A prospective observational study (MICRO1501) was conducted between 2015 and 2017 at Sunpasitthiprasong Hospital, a tertiary hospital, in Ubon Ratchathani, Thailand. The study aimed to investigate human cellular and humoral immune response during melioidosis using a wide range of assays including whole blood samples for bulk RNA sequencing. Firstly, a study of the functional cellular immune response to melioidosis using IFN-γ enzyme-linked immunosorbent spot (ELISpot) and intracellular staining demonstrated decreased Bp-specific IFN-γ responses in acute melioidosis patients with T2DM compared to non-diabetes (*76*). Secondly, *Kronsteiner et al. (377)* demonstrated that elevated humoral immune response and increased frequency of double-negative T cells were associated with survival in melioidosis with T2DM. Moreover, IFN-γ producing γδ T cells in response to Bp stimulation was also increased in recovered melioidosis patients with T2DM.

Based on the results of cellular immunity in melioidosis with T2DM, I hypothesised that stunted cellular immune response is one of underlying mechanisms leading to increased susceptibility in patients with T2DM to melioidosis. In this Chapter, whole blood transcriptomics in melioidosis (MICRO1501) will be studied for mechanisms behind the increased susceptibility to Bp infection in the patients with T2DM.

3.2 Specific objectives

1. To investigate whole blood transcriptomic profiles from acute melioidosis with and without T2DM.
2. To investigate whole blood transcriptomic profiles from fatal melioidosis compared to those who survived.
3. To correlate the identified transcriptomic signatures in T2DM cases with clinical outcomes.

3.3 Materials and Methods

3.3.1 Study design and ethical approval

RNA sequencing data used for this chapter were derived from a prospective observational study (MICRO1501) conducted between 2015 and 2017 at Sunpasitthiprasong Hospital, Ubon Ratchathani, Thailand. The study protocol was approved by the ethics committees of the Faculty of Tropical Medicine, Mahidol University (TMEC 12-014); Sunpasitthiprasong Hospital, Ubon Ratchathani (017/2559) and the Oxford Tropical Research Ethics Committee (OXTREC35-15). The study was conducted according to Good Clinical Practice, and all subjects gave written informed consent, including for export and storage of their blood samples. Adults aged 18 years and over were recruited into the Melioidosis Cohort of the study as soon as feasible after hospitalisation with melioidosis, defined as culture of Bp from any clinical specimen. Healthy household contacts of melioidosis cases enrolled in the study were recruited as endemic control participants, alongside people with T2DM recruited from diabetes out-patient clinic at Sunpasitthiprasong hospital. HbA1c was performed for all participants. Diabetes status for the Melioidosis Cohort was defined as holding a pre-existing diagnosis of DM and / or having an HbA1c $\geq$ to 6.5 %, as defined by WHO criteria (*439*).

This clinical immunology study aimed to evaluate human immune responses in melioidosis patients using a wide range of humoral and cellular immune assays. For RNA transcriptomics, 3 mL whole blood samples were collected into Tempus blood RNA tube (Applied Biosystems, Cat No. 4342792) from culture-confirmed melioidosis (Melioidosis Cohort, n=81) along with control cohorts, T2DM outpatients (T2DM, n=15), and household contacts of the melioidosis patients (HH, n=14). The tempus blood RNA tubes were store at -80°C at the study site, transferred on dry ice to the central laboratory at Mahidol Oxford Tropical Medicine Research Unit (MORU) in Bangkok for long-term storage. Then, the

samples were shipped on dry ice to Dunachie's research laboratory at Peter Medawar Building for Pathogen Research, University of Oxford, UK. The samples were stored at -80°C until use.

3.3.2 RNA isolation and preparation

RNA isolation, preparation, quantification, and qualification were performed according to the manufacturer's instructions unless otherwise stated. Total RNA was isolated from whole blood sample collected in Tempus blood RNA tube using the Tempus Spin RNA Isolation (Applied Biosystems, Thermo Fisher Scientific, Cat No. 4378926). Additionally, potential contaminating genomic DNA was removed using the TURBO DNase enzyme (Invitrogen, Cat No. AM1907). Isolated RNA samples were quantified and quality-checked using Qubit™ RNA IQ assay and RNA XR assay kits respectively. RNA samples with low concentrations of RNA were concentrated using GeneJET RNA cleanup and concentration micro kit (Thermo Fisher Scientific, Cat No. K0841). RNA samples were transferred to the Oxford Genomics Centre, Wellcome Centre for Human Genetics (OGC, WCHG) for library preparation and RNA sequencing.

3.3.3 Library preparation and RNA sequencing

Library preparation and RNA sequencing were performed at OGC, WCHG. Ribozero library preparation and the globin depletion workflow were chosen for library preparation. The library was sequenced for 75-base pair pair-end, 50 million reads using HiSeq4000 sequencer. Raw sequencing data (FASTQ files) were pre-processed, quality checked and data were accessed via secured file transfer protocol (ftp).

3.3.4 Upstream RNA sequencing analysis pipeline

The sequencing data (FASTQ files) were retrieved from the ftp server provided by OGC, WCHG sequencing provider. For upstream data analysis including mapping and counting mapped reads were performed on computer cluster provided by the Computational Biology Research Group, Weatherall Institute for Molecular Medicine, University of Oxford. Firstly, the raw sequencing data (FASTQ files) were quality checked using FastQC programme (version 0.11.9). Secondly, the raw data were mapped against human reference genome (UCSC hg38.p2 version 20201) using STAR aligner (version 2.6.1d) and binary alignment map (.bam) files were generated (*440*). Thirdly, mapped read files (.bam) were visualised using IGV programme (version 2.4.16). Fourthly, the .bam files were used as an input into Subread package using featureCounts function (version 1.6.2) for counting uniquely mapped reads (*441*) . Finally, read count files (tab delimited) were generated and compiled into a single expression data using Sartools R package version 1.6.8 (*442*). The expression data were used for subsequent data analyses.

3.3.5 Differential gene expression and functional pathway analysis

A total of 26,196 transcripts were generated and annotated to gene symbol (HGNC). Genes with no counts or lowly expressed were removed with a cut-off of row sum below 100. Pre-filtered genes (17, 594 features) were normalised and variance stabilising transformed using DESeq2 R package for downstream data analyses and visualisation (*392*). To assess whether melioidosis induces global transcriptional responses, multi-dimensional scaling by principal component analysis (PCA) using the top 1,000 most variable genes was performed in melioidosis (n=81) and control (n=29) subjects. Differential gene expression (DGE) analysis was carried out using negative binomial generalised linear model implemented in DESeq2 R package adjusted for age and sex covariates. Following DGE analysis, functional pathway

analysis was performed on pre-filtered differentially expressed genes (DEGs) with adjusted P-value <0.05 and absolute[Log2 fold-change]≥1. The functional pathway analysis based on MSigDB collection was performed using clusterProfiler R package (*403, 404*). Moreover, gene set enrichment analysis (GSEA) based on the MSigDB gene sets was performed using pre-ranked GSEA method (*406, 407*).

3.3.6 Weighted gene co-expression network analysis (WGCNA) and identification of hub genes

To identified co-expressed gene modules associated fatal melioidosis and T2DM, WGCNA was performed using pre-filtered, normalised and variance stabilising transformed expression data (17, 046 features) of melioidosis patients (n=81) (*415*). The remaining WGCNA workflow was performed as described in **Chapter 2**.

3.3.7 Deconvolution of bulk RNA sequencing data

Cell type abundances were estimated from bulk RNA sequencing data in 81 melioidosis patients using CIBERSORTx (*431*) and xCell (*435*). The imputed cell fractions and enrichment were compared between non-survivors (n=28) and survivors (n=53) using non-parametric Mann-Whitney tests in R programme.

3.4 Results

3.4.1 Study cohort

A total of 100 patients with culture-confirmed melioidosis (a median of 5 days after admission; interquartile range (IQR) 4 to 6 days) were enrolled into the melioidosis study (MICRO1501) along with control cohorts including healthy household contacts of melioidosis cases (healthy control, n = 96), T2DM outpatients (T2DM control, n = 98), and patients admitted to the hospital due to infections with other Gram-negative bacteria (other Gram-negative bacterial infections, n = 48). One patient from the Melioidosis Cohort was excluded from the study due to a positive diagnosis with tuberculosis (co-infection). Overall case fatality for this study was 30% and the proportion of melioidosis patients with T2DM was 67% (**Table 3.1**).

Table 3.1 Subject demographics for melioidosis study (MICRO1501)

Baseline characteristics	**Cohorts**			
	Melioidosis (n = 99)	**Healthy control (n = 96)**	**Diabetes control (n = 98)***	**Other Gram-negative bacterial infections (n = 48)**
Male (%)	63 (64%)	27 (28%)	25 (26%)	27 (56%)
Female (%)	36 (36%)	69 (72%)	73 (74%)	21 (44%)
Age in years; median (IQR)	55 (20-84)	48 (25-69)	53 (41-60)	64 (24-95)
***T2DM**	66 (67%)	NA	98 (100%)	NA
***Non-survivors**	30 (30%)	NA	NA	NA
Survivors	69 (70%)	NA	NA	NA

*T2DM is defined by those patients who were previously diagnosed with diabetes or having an HbA_1c level ≥ 6.5% on recruitment into the study. **Based on 28-day mortality. IQR, inter quartile range.

Of 99 samples, 81 whole blood samples from patients with culture-proven melioidosis were selected for RNA sequencing along with representative blood samples from uninfected individuals, 14 healthy blood donors and 15 T2DM outpatients. Sample selection for RNA sequencing for both melioidosis and control cohorts was based on matched DM and non-DM cases by age and sex where possible. **Table 3.2** shows the demographics of the participants for RNA sequencing. There was no statistically significant difference in the sex of melioidosis and control cohorts for RNA sequencing. 28-day mortality of the Melioidosis Cohort was not significantly different between the patients with/without T2DM. However, the age of melioidosis without T2DM was significantly higher than those with T2DM and control cohorts (P<0.001). Of 49 melioidosis patients who had T2DM, 26 patients (53%) had records of prescribed diabetic drugs including insulin (n=16), metformin (n=11), and sulphonylureas (n=11) (**Supplementary Figure 3.1**). Of the 26 patients, 8 patients were co-prescribed for metformin and sulphonylureas and 3 patients received all the treatments.

Table 3.2 Subject demographics for whole blood transcriptomic study from melioidosis and control cohort

Baseline characteristics (N=110)	*Non-survived melioidosis (n=28)	Survived melioidosis (n=53)	Diabetes control (n=15)	Healthy control (n=14)	P-value
Male	18 (64%)	36 (68%)	7 (47%)	8 (57%)	†0.48
Female	10 (36%)	17 (32%)	8 (53%)	6 (43%)	
Age in years; median (IQR)	61 (53-69)	54 (50-65)	49 (44-57)	47 (44-54)	¶<0.001
****T2DM**	18 (64%)	31 (59%)	NA	NA	†0.61
Non-T2DM	10 (36%)	22 (41%)	NA	NA	

*Case fatalities are based on 28-day mortality. ** Type 2 diabetes (T2DM) is defined by those patients who were previously diagnosed with diabetes or having an HbA_{1c} level ≥ 6.5% on recruitment into the study. †Chi-

square test. ¶Anova test. Comparisons among melioidosis patients and control cohort respectively. T2DM = Type 2 diabetes. NA= Not applicable.

3.4.2 High RNA quality for whole blood total RNA sequencing

To profile the whole blood transcriptome, total RNA was first isolated from whole blood samples collected into Tempus blood RNA tubes. Generally, RNA samples with a RIN score equivalent to 8 or higher are considered as high RNA quality for RNA sequencing (*443*). After RNA isolation, the RNA samples were quantified and qualified using Qubit™ RNA XR and IQ assay prior sending to OGC, WCHG for library preparation and RNA sequencing. Due to limited availability of Qubit™ RNA XR and IQ assay, total RNAs were randomly assayed. The RNA samples from 32 melioidosis patients had RNA integrity an average of 8.6 RNA IQ score (standard deviation (SD) = 0.55), and a mean quantity of 471 ng/µl (SD = 180) (**Supplementary Figure 3.2A, 3.2B**). RNA integrity from 29 uninfected donors (Control; 15 T2DM patients and 14 healthy donors) was comparable to the Melioidosis Cohort (RNA IQ score, median 8.7; SD = 0.28) (**Supplementary Figure 3.2C**). However, the quantity of total RNA isolated from the controls was significantly lower than the patients with a mean of 72 ng/µl (SD = 17) possibly due to lower total white cell count (**Supplementary Figure 3.2D)**. Afterwards, the RNA samples were diluted with nuclease-free water to obtain a total of 100 ng per sample. At the sequencing facility, the RNA samples were re-quantified and re-qualified using the Agilent TapeStation platform prior proceeding to library preparation. The RNA integrity by RIN score was slightly lower compared to the Qubit™ RNA IQ assay, with a mean of 8.2 (SD = 0.75) (**Supplementary Figure 3.2E)**; however, both methods confirmed high quality RNA for RNA sequencing with overall RIN score exceeding 8 (**Supplementary Figure 3.2F**). The final RNA input mass for library preparation was at a mean of 185 ng (SD = 74.7) (**Supplementary Figure 3.2G**).

3.4.3 High quality RNA sequencing data from the globin-depleted, Ribo-zero total RNA sequencing approach

RNA sequencing data were generated from whole blood samples of 81 melioidosis patients and 29 uninfected donors (controls) using the globin-depleted, Ribo-zero total RNA sequencing approach. Firstly, the quality of raw RNA sequencing data was primarily cleaned and checked by the sequencing facility and reports were provided. The raw RNA sequencing data were randomly double-checked and visualised using FastQC programme. The quality score is an indication of accuracy of base calling within a read, in which a score of 30 or higher considered high confidence in calling, with a probability of incorrect base-calling at the rate of 1 in 1,000 – or 99.9% accuracy (*444*). Overall, high quality raw RNA-sequencing data were achieved with a median quality score of 38.65 (interquartile range (IQR) 37.8-39.2) (**Supplementary Figure 3.3A**). Secondly, more than 50 million (M) high quality reads were generated from both cohorts (melioidosis: mean 65.2 M, SD = 5.6 M; controls: median 79.5 M, SD = 7.4) and mapped against the human reference genome, UCSC hg38.p2 version 20201 using STAR aligner (**Supplementary Figure 3.3B**). Thirdly, high, and comparable frequencies of uniquely mapped reads were achieved in both cohorts with an average of 69% mapped reads (melioidosis: median 69%, SD = 8.6; controls: median 66%, SD = 7.5) (**Supplementary Figure 3.3C, 3.3D**). Finally, the uniquely mapped reads were counted using the featureCounts function from Subread package to identify an average of 27.5 M reads per sample (melioidosis: mean 25 M, SD = 3.9 M; controls: median 29.7 M, SD = 2.8 M) (**Supplementary Figure 3.3E**). Consequently, the read counts were normalised by median of ratios method implemented in DESeq2 R package for the downstream RNA sequencing analysis pipeline including differential gene expression analysis, pathway analyses, and WGCNA (**Supplementary Figure 3.4**).

3.4.4 Melioidosis causes profound changes in the whole blood transcriptome

To evaluate whether melioidosis causes global transcriptional changes, principal component analysis (PCA) using 1,000 most variable genes was performed among Melioidosis and Control cohorts. Firstly, PCA identified clear separation between melioidosis cohort and control cohorts (**Figure 3.1**). Furthermore, there was some separation between healthy and T2DM controls. However, PCA coloured by diabetes status shows subtle differences between melioidosis with and without T2DM. In contrast, PCA coloured by 28-day mortality status shows better separation between non-survived and survived melioidosis patients. Secondly, differential gene expression (DGE) analysis was first performed between healthy and T2DM control cohorts. As expected from the PCA analysis, DGE analysis identified 94 up- and 2 down-regulated genes between T2DM and healthy controls (absolute[Log2 fold change]≥1, adjusted P-value<0.05) (**Supplementary Figure 3.5**). Therefore, healthy control was used as a baseline in subsequent analyses.

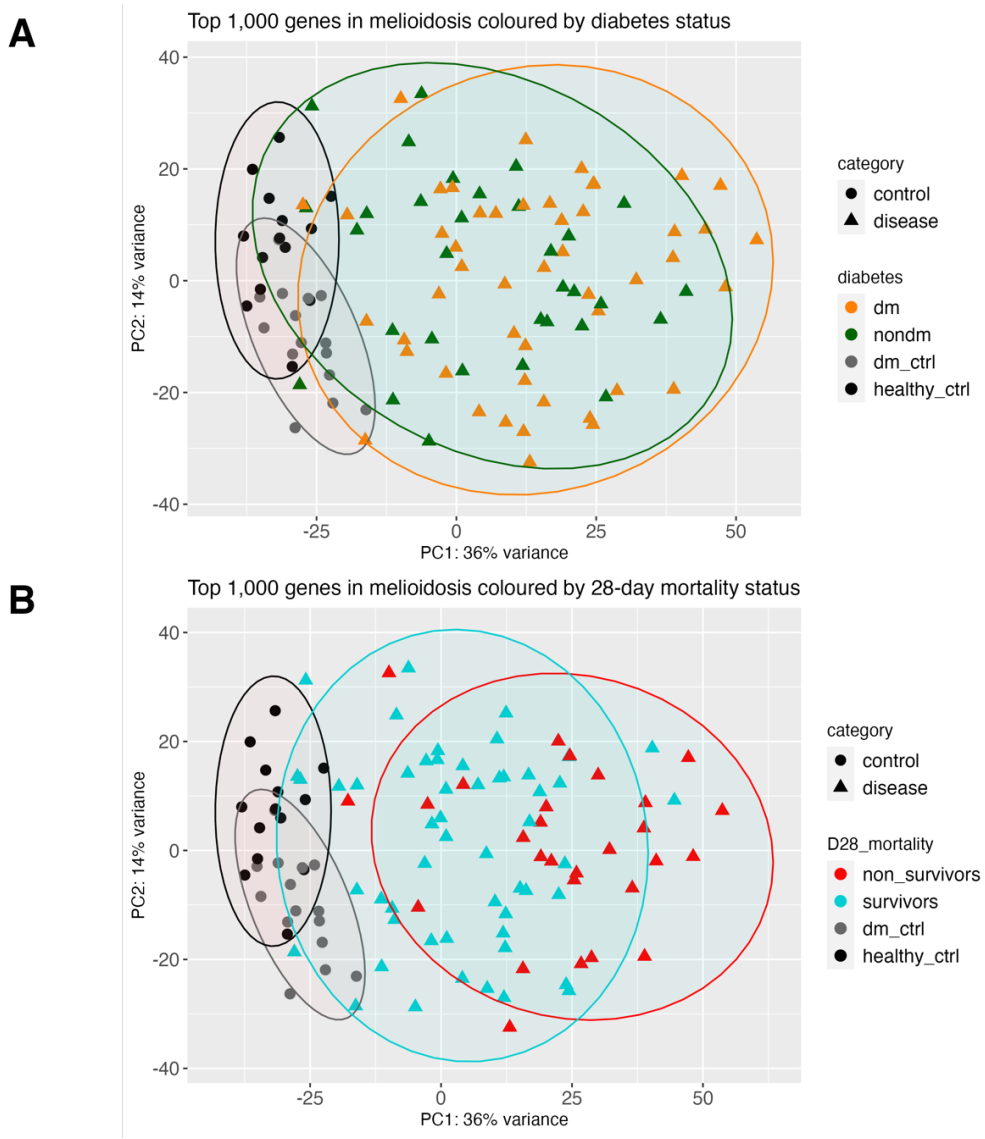

Figure 3.1 Principal component analysis (PCA) of the top 1,000 most variable genes in melioidosis and control cohorts coloured by (A) diabetes status and (B) 28-day mortality status. A: Cohorts: patients with melioidosis and T2DM ("dm", orange triangles, n=42), melioidosis patients without diabetes ("nondm", green triangles, n=39), healthy endemic controls ("healthy_ctrl", black circles, n=14), and T2DM endemic controls ("dm_ctrl", grey circles, n=15). B: Cohorts: patients with melioidosis who died ("non_survivors", red triangles, n=28), patients with melioidosis who survived ("survivors", turquoise triangles, n=53), healthy endemic controls ("healthy_ctrl", black circles, n=14), and T2DM endemic controls ("dm_ctrl", grey circles, n=15). PCA plots were generated using plotPCA function implemented in DESeq2 R package.

3.4.5 Profound changes in the whole blood transcriptome are associated with case fatality, however, subtle impacts by T2DM in melioidosis

DGE analysis identified large-scale changes of transcriptome between melioidosis patients and healthy donors with 1,537 up- and 610 down-regulated genes (**Figure 3.2**). People with T2DM confer 12-fold increased susceptibility to melioidosis (*20*). However, DGE analysis identified almost none of differentially expressed genes (3 down-regulated DEGs) between the melioidosis patients with and without T2DM (**Figure 3.3**), suggesting similar host immune responses during melioidosis regardless of diabetes status, at least by the time people were sampled for our study. To evaluate the impact of diabetic drugs on blood transcriptomics, DGE analysis between the melioidosis patients with and without T2DM identified no DEGs controlling for diabetic drugs prescribed in melioidosis patients with T2DM as a covariate (**Supplementary Figure 3.6A**). One major obstacle of bulk whole blood transcriptomic study especially whole blood samples derived from patients with acute infections is high proportion of neutrophils. Therefore, whole blood transcriptomic profiles are often dominated by neutrophil-driven transcriptional responses (*101*). Despite controlling for the frequency of neutrophils as a covariate, DGE analysis between melioidosis patients with and without T2DM did not increase sensitivity in detecting diabetes-driven transcriptional response during melioidosis (**Supplementary Figure 3.6B**). In Thailand, the hospitalised case fatality rate in melioidosis is up to 40% despite receiving recommended antibiotics (*20*). Here, DGE analysis identified 389 up- and 343 down-regulated genes between non-survived and survived melioidosis based on 28-day mortality (**Figure 3.4**).

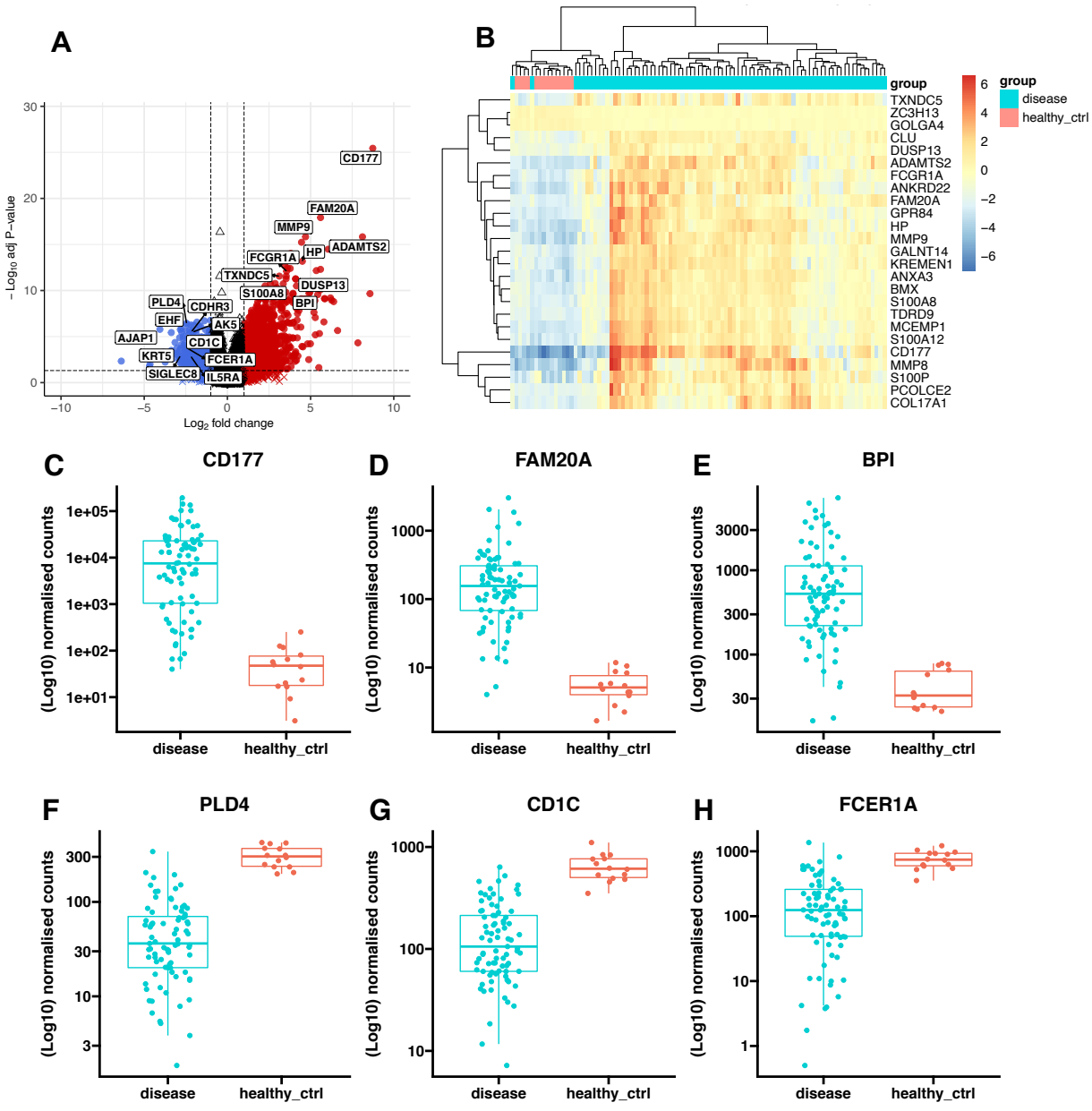

Figure 3.2 Visualisation of different differentially expressed genes (DEGs) between 81 melioidosis patients (disease) and 14 healthy endemic donors (healthy_ctrl). A: volcano plot of DEGs between melioidosis patients and healthy donors. Dotted lines define the cut-off for differentially expressed genes based on absolute[Log2 fold-change]≥ 1 (x-axis) and adjusted P-value < 0.05 (y-axis). B: heatmap of the top 25 DEGs between melioidosis patients and healthy endemic donors. Each column and row represent an individual participant (top bar) and gene respectively. The gradient colour bar indicates the magnitude of differentially expressed genes based on absolute[Log2 fold-change] and

adjusted P-value < 0.05. C-H: Representative expression profiles between melioidosis patients ("disease", turquoise dots) and healthy donors ("healthy_ctrl", coral dots). Each boxplot shows [log10] normalised counts of representative DEGs (both up- and down-regulated genes) derived from differential gene expression analysis between melioidosis patients and healthy donors. Each dot represents each participant. Box plots represent medians with interquartile range plus lines to minimum, maximum and potential outliers.

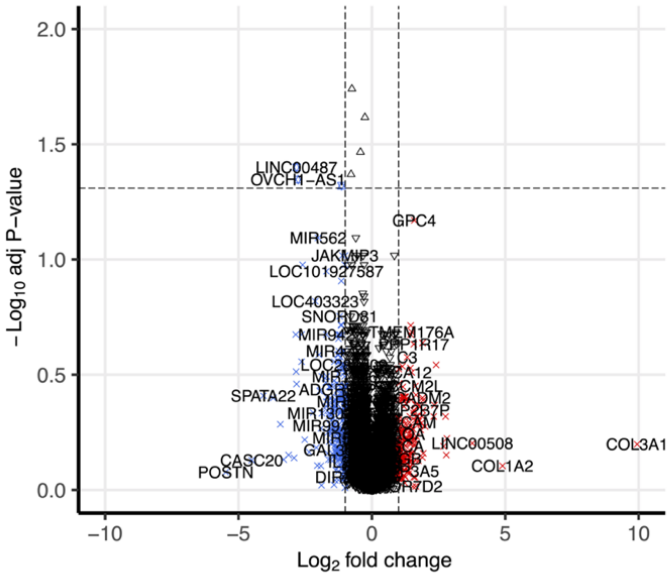

Figure 3.3 Volcano plot of differentially expressed genes between melioidosis with (n=49) and without (n=32) type 2 diabetes. Dotted lines define the cut-off for differentially expressed genes based on absolute[Log2 fold-change]≥ 1 (x-axis) and adjusted P-value < 0.05 (y-axis). Volcano plot was generated using EnhancedVolcano R package.

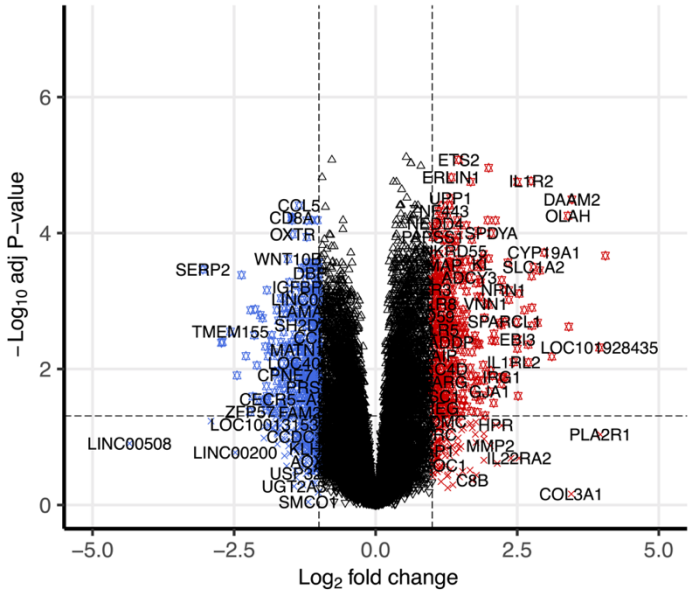

Figure 3.4 Volcano plot of differentially expressed genes between non-survivors (n=28) and survivors (n=53) of melioidosis based on 28-day mortality. Dotted lines define the cut-off for differentially expressed genes based on absolute[Log2 fold-change]≥ 1 (x-axis) and adjusted P-value < 0.05 (y-axis). Volcano plot was generated using EnhancedVolcano R package.

3.4.6 Melioidosis drives up-regulation of the inflammatory immune response, predominantly by innate immune compartment

To study the impact of melioidosis on transcriptomic profiles, functional pathway analysis was employed following DGE analysis by Hallmark and Reactome gene sets. Pathways involved in inflammatory immune responses such as inflammatory response, TNF signalling via NF-κB, neutrophil and platelet degranulation were highly up-regulated in melioidosis compared to healthy control (**Figure 3.5**). Immunoregulatory interactions between lymphoid and non-lymphoid cells, chemokine receptors bind chemokines and cell signalling pathways were down-regulated in melioidosis compared to healthy controls (absolute[Log2 fold-change]≥1, adjusted P-value < 0.05).

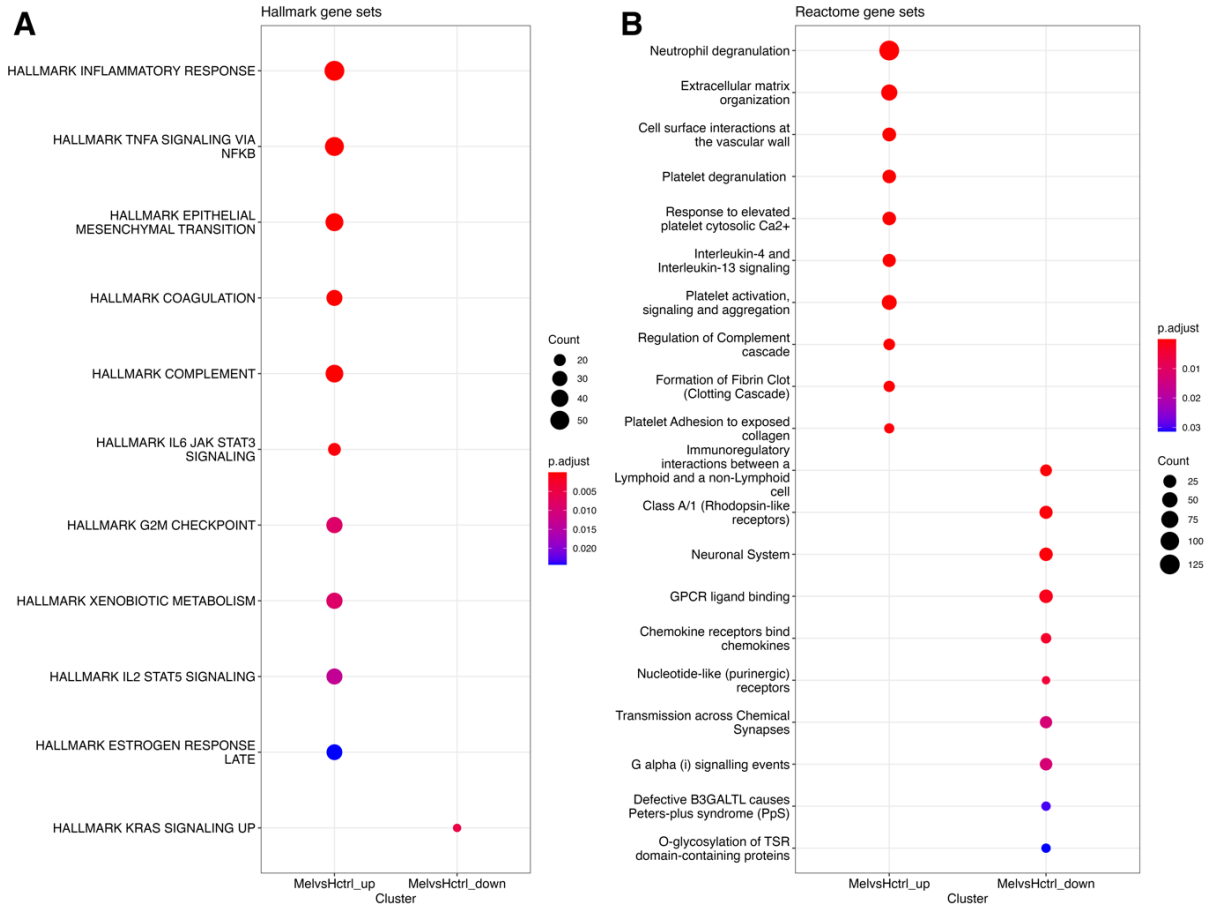

Figure 3.5 Functional pathway analysis comparing all melioidosis patients with healthy endemic controls. (A) Hallmark gene sets. (B) Reactome genes sets. The top 10 over-represented pathways are displayed. The gradient colour bar corresponds to the adjusted P-value. The size of each term is indicated by representative counts. Differentially expressed genes were pre-filtered based on a cut-off of absolute[Log2 fold-change]≥1 and adjusted P-value <0.05. MelvsHctrl_up: up-regulated pathways in melioidosis compared to healthy endemic controls. MelvsHctrl_down: down-regulated pathways in melioidosis compared to healthy endemic controls.

3.4.7 Increased innate pro-inflammatory immune responses but reduced T cell signalling are associated with poor outcome in melioidosis

To elicit pathways associated with fatality in melioidosis, functional pathway analysis based on Reactome, and Gene Ontology (biological process) was performed following DGE analysis between non-survived and survived melioidosis (absolute[Log2 fold-change]≥1, adjusted P-value < 0.05). Pathways involved in pro-inflammatory immune response such as neutrophil degranulation, cytokine mediated signalling, myeloid cell chemotaxis and TLR cascades were highly up-regulated in fatal melioidosis (**Figure 3.6**). On the other hand, pathways involved in adaptive immune responses such as T cell activation, T cell differentiation, immunoregulatory interactions between a lymphoid and non-lymphoid cell, and lymphocyte stimulation were down-regulated in non-survived compared to survived melioidosis patients.

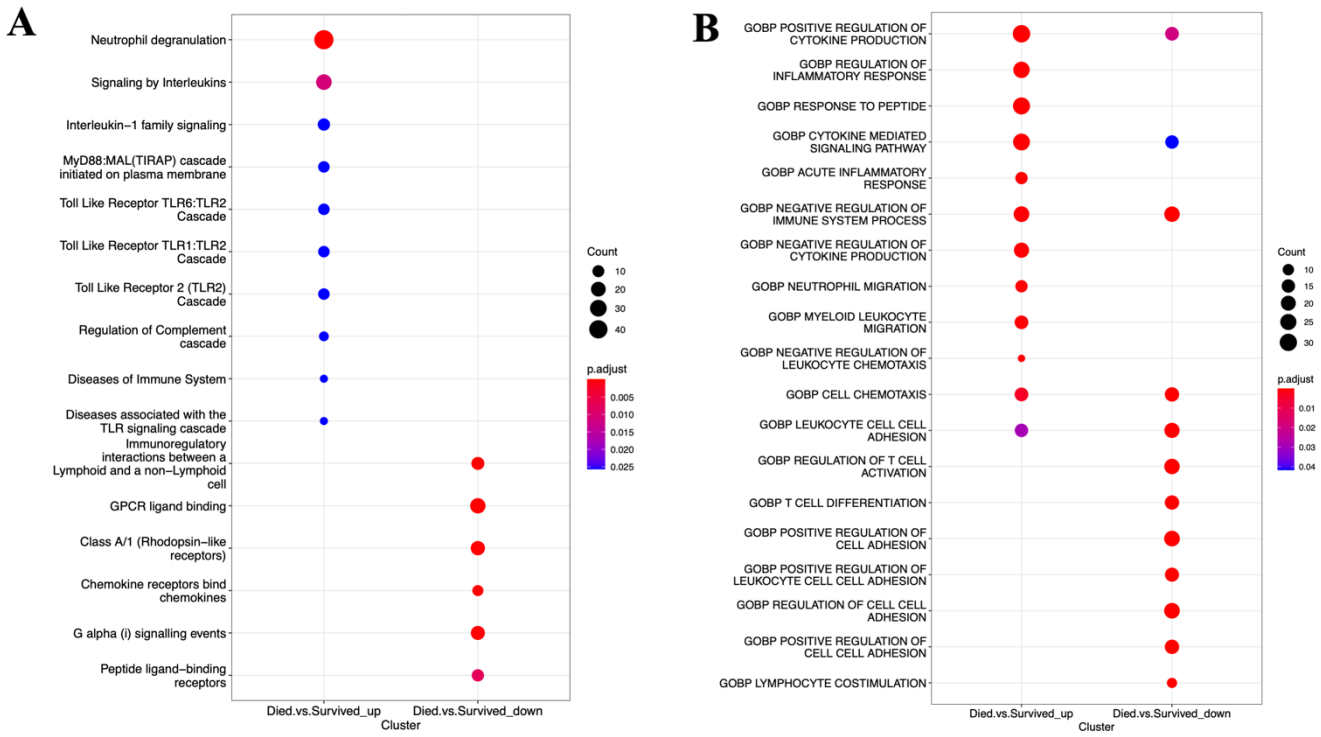

Figure 3.6 Functional pathway analysis between non-survived and survived melioidosis patients. A: Reactome genes sets. B: Gene Ontology (biological process) gene sets. The top 10 over-represented pathways are displayed. The gradient colour bar corresponds to the adjusted P-value. The size of each term is indicated by representative counts. Differentially expressed genes were pre-filtered based on a cut-off of absolute[Log2 fold-change]≥1 and adjusted P-value <0.05. Died.vs.Survived_up = up-regulated pathways in non-survived melioidosis compared to survivors. Died.vs.Survived_down = down-regulated pathways in non-survived melioidosis compared to survivors.

3.4.8 Increased non-specific inflammatory immune response and stress response in melioidosis with T2DM and having T2DM during melioidosis is not associated with worse outcome

To investigate the impact of T2DM on whole blood transcriptome, the genome-wide functional class scoring method was performed using pre-ranked GSEA following DGE analysis. Firstly, uninfected diabetes control cohort shows enriched pathways involved in heme metabolism and pro-inflammatory immune responses such as IFN-γ, TNF signalling via NF-κB, and IL-6 JAK STAT3 signalling compared to healthy donors (**Supplementary Table 3.1**). Secondly, the DGE analysis was unable to detect DEGs due to subtle differences of transcriptomic profiles in melioidosis patients with and without T2DM. However, GSEA revealed enriched pathways involved in inflammatory responses such as TNF signalling via NF-κB, inflammatory response, protein secretion, neutrophil degranulation, innate immune system, and endoplasmic reticulum stress responses in melioidosis with T2DM compared to non-diabetes cases (**Figure 3.7**). Thirdly, to evaluate the impact of T2DM on clinical outcome during melioidosis, pre-ranked GSEA following DGE analyses between the non-survivors and survivors within melioidosis with (n=49) and without (n=32) T2DM were performed. **Table 3.2,** melioidosis patients with and without T2DM had comparable outcome (Chi-square test, P-value = 0.61). Likewise, GSEA following DGE analyses between non-survivors compared to survivors of melioidosis within T2DM and non-T2DM group (**Table 3.3**), shows that both groups were enriched by immune-dominated pathways such as TNF signalling, inflammatory response, complement, and both interferon-γ and interferon-α. Nevertheless, the non-survivors compared to survivors within T2DM group show more enriched pathways involved in metabolisms, cell signalling, and proliferation.

Figure 3.7 Gene set enrichment analysis following differential gene expression analysis of melioidosis patients with type 2 diabetes compared to non-diabetes cases. (A) Hallmark gene sets. (B) Reactome genes sets. All significant Hallmark pathways are displayed. Pathways were deemed significant when adjusted P-value <0.05. Enriched pathways were calculated from the DESeq2 statistical test of pre-ranked gene list following DGE analysis using the fgsea R package.

Table 3.3 Pre-ranked gene set enrichment analysis (pre-ranked GSEA) by Hallmark gene sets following differential gene expression analysis (DGE) based on 28-days mortality status within a subset of melioidosis patients with and without type 2 diabetes (T2DM). The DGE analyses were performed within melioidosis with T2DM (18 non-survivors versus 31 survivors) and melioidosis without T2DM (10 non-survivors versus 22 survivors). Gene sets were deemed significant when satisfied false discovery rate (FDR q-value < 0.05) and ranked by normalised enrichment score and FDR. Enriched pathways were calculated from the DESeq2 statistical test of pre-ranked gene list following DGE analysis using GSEAPreranked mode on GSEA software.

Group		Rank	Hallmark pathways	NES	FDR q-val	Process category
Pre-ranked GSEA: non-survivors versus survivors	Melioidosis with T2DM	1	TNFA_SIGNALING_VIA_NFKB	6.08	0	Signalling
		2	INFLAMMATORY_RESPONSE	5.47	0	Immune
		3	INTERFERON_GAMMA_RESPONSE	5.26	0	Immune
		4	INTERFERON_ALPHA_RESPONSE	5.10	0	Immune
		5	IL6_JAK_STAT3_SIGNALING	4.42	0	Immune
		6	PROTEIN_SECRETION	4.16	0	Pathway
		7	MTORC1_SIGNALING	3.87	0	Signalling
		8	COMPLEMENT	3.68	0	Immune
		9	ANDROGEN_RESPONSE	3.24	0	Signalling
		10	IL2_STAT5_SIGNALING	2.97	0	Signalling
		11	OXIDATIVE_PHOSPHORYLATION	2.78	0	Metabolic
		12	APOPTOSIS	2.77	0	Pathway
		13	HYPOXIA	2.75	0	Pathway
		14	UV_RESPONSE_UP	2.74	0	DNA damage
		15	CHOLESTEROL_HOMEOSTASIS	2.69	0	Metabolic
		16	ADIPOGENESIS	2.59	1.14E-04	Development
		17	PI3K_AKT_MTOR_SIGNALING	2.40	9.69E-04	Signalling
		18	KRAS_SIGNALING_UP	2.38	9.16E-04	Signalling
		19	P53_PATHWAY	2.37	9.52E-04	Proliferation
		20	MITOTIC_SPINDLE	2.17	0.003	Proliferation
		21	GLYCOLYSIS	2.14	0.004	Metabolic
		22	UNFOLDED_PROTEIN_RESPONSE	2.08	0.005	Pathway
		23	FATTY_ACID_METABOLISM	1.88	0.018	Metabolic
		24	COAGULATION	1.86	0.019	Immune
		25	MYC_TARGETS_V1	1.86	0.019	Proliferation
		26	G2M_CHECKPOINT	1.82	0.022	Proliferation
		27	REACTIVE_OXYGEN_SPECIES_PATHWAY	1.68	0.046	Pathway
	Melioidosis-only	1	TNFA_SIGNALING_VIA_NFKB	4.58	0	Signalling
		2	COMPLEMENT	3.77	0	Immune
		3	INFLAMMATORY_RESPONSE	3.72	0	Immune
		4	IL6_JAK_STAT3_SIGNALING	3.57	0	Immune
		5	INTERFERON_GAMMA_RESPONSE	3.05	0	Immune
		6	HYPOXIA	2.98	0	Pathway
		7	PROTEIN_SECRETION	2.64	0	Pathway
		8	INTERFERON_ALPHA_RESPONSE	2.53	1.38E-04	Immune
		9	TGF_BETA_SIGNALING	2.13	0.007	Signalling
		10	P53_PATHWAY	2.12	0.006	Proliferation
		11	KRAS_SIGNALING_UP	2.07	0.010	Signalling
		12	HEME_METABOLISM	2.01	0.012	Metabolic
		13	ANDROGEN_RESPONSE	1.98	0.014	Signalling
		14	APOPTOSIS	1.97	0.014	Pathway
		15	PI3K_AKT_MTOR_SIGNALING	1.76	0.047	Signalling

NES= Normalised Enrichment Score. FDR q-val= False discovery rate.

3.4.9 Co-expressed gene modules correlated with case fatality were mutually shared with other clinical parameters associated with makers of disease severity

To complement the results obtained from DGE and pathway analyses as well as discovery of key regulators that may play a deleterious role during melioidosis, WGCNA was performed. A normalised variance-stabilising transformed expression dataset from the 81 melioidosis patients (17,046 features) was first constructed to identify potential outliers, and sample clustering was visualised based on their expression profiles and corresponding phenotypes (**Figure 3.8A**). Secondly, a power of $\beta = 14$ was chosen (soft-threshold $R^2 = 0.83$ and mean connectivity = 72) in order to achieve scale-free network (**Figure 3.8B**).

As a result, 22 co-expressed gene modules were identified based on dissimilarity of the topological overlap matrix via hierarchical clustering using the Dynamic Tree Cut method (**Figure 3.8C**). Module-trait relationship analysis identified significant correlations between the 28-day mortality clinical trait and the ME brown, black and blue modules, with ME brown (indicated in red boxes) showing the strongest correlation (Pearson's rho = 0.5, P-value=2e-06) (**Figure 3.9**). These modules were also positively correlated with %neutrophils, and reciprocally, %lymphocytes were negatively correlated with these modules. Interestingly, diabetes status was also correlated with ME brown and cyan (indicated in red boxes). The latter module was specifically correlated with both diabetes status and HbA1c level.

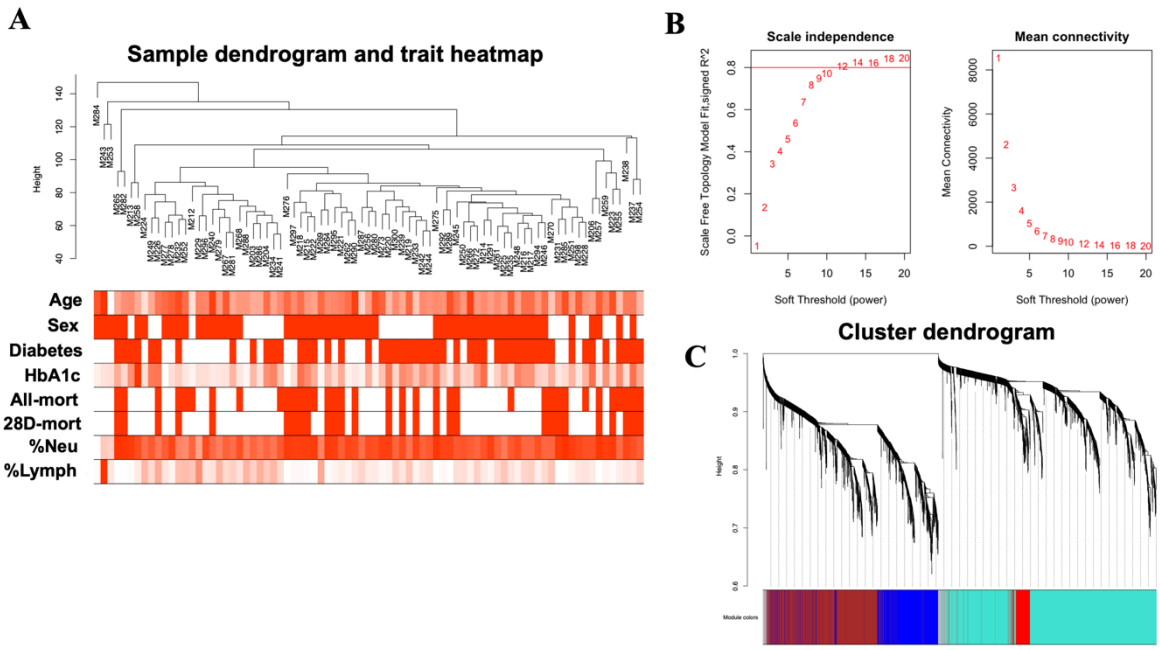

Figure 3.8 Weighted gene co-expression network analysis workflow in 81 melioidosis patients. A: Sample dendrogram with corresponding clinical trait heatmap. B: Scale-free network analysis, with scale independence plot displaying (left) scale free topology model fit (R^2) and (right) mean connectivity plot, with soft threshold on x-axis. Here, a power of β=14 resulted in soft-threshold R^2 = 0.83 indicating a scale-free topology obtained. C: Cluster dendrogram of co-expressed gene modules by hierarchical clustering of genes based on topological overlap and assigned module colours underneath.

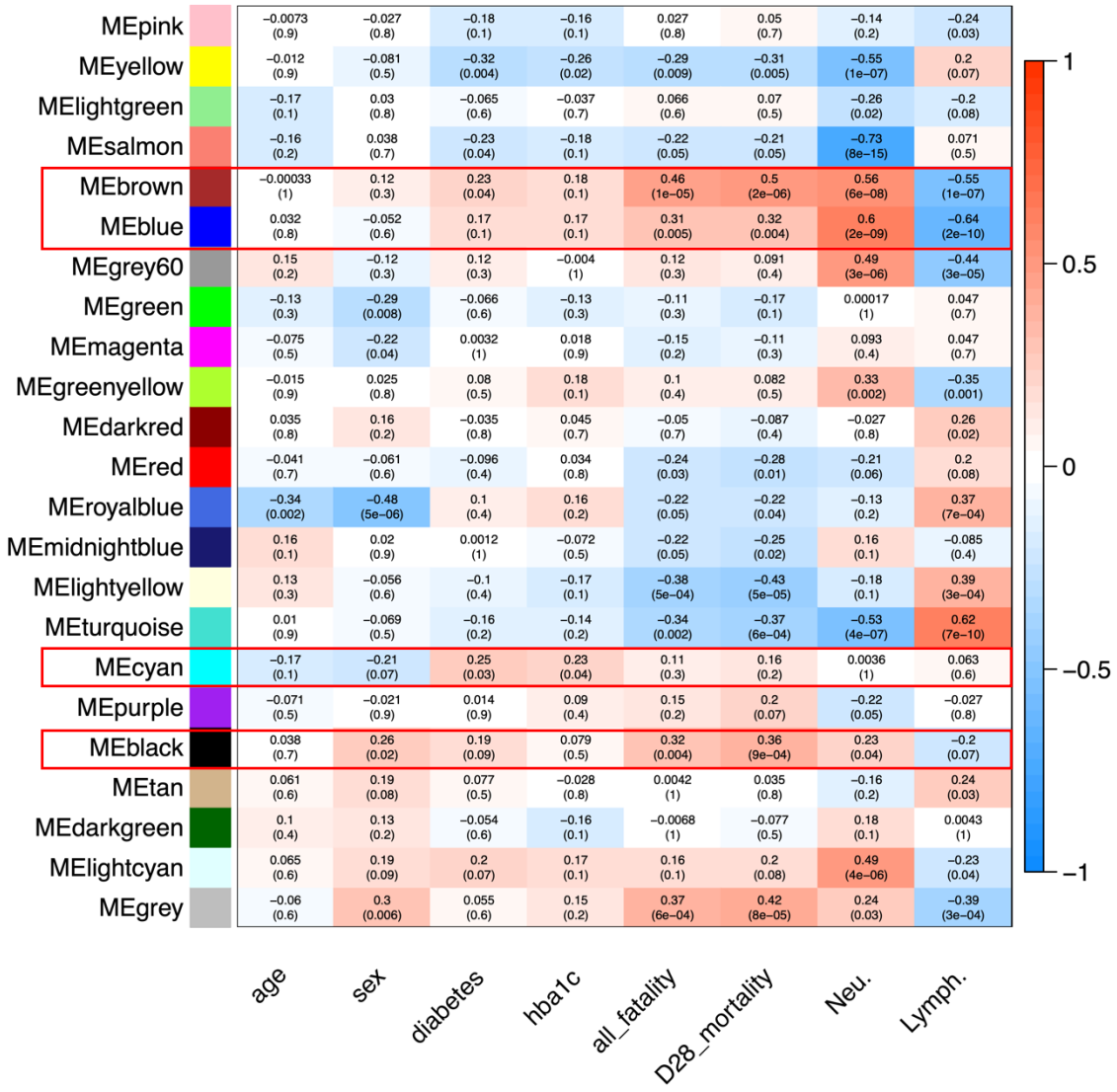

Figure 3.9 Module-trait relationship analysis in 81 melioidosis patients by weighted gene co-expression network analysis. A total of 22 co-expressed gene modules (module eigengenes, MEs) were identified. Each row represents an assigned module eigengene (ME) and each column represents a clinical trait of interest, with corresponding Pearson's correlation coefficient between each ME-trait pair displayed with P-value in parenthesis. The gradient colour bar indicates the degree of positivity (maximum +1, red) / negativity (minimum -1, blue) for the Pearson's correlation coefficient. Clinical traits include age (in years, continuous variable), sex (binary outcome), diabetes status (binary outcome), HbA1c level (hba1c, percentage of glycated haemoglobin in continuous variable), all-cause fatality (all_fatality, survived or dies over 1 year of follow-up in binary outcome), 28-day mortality (D28_mortality, survived or died over 28 days of follow-up in binary outcome), %

of total white cell count represented by neutrophils (Neu., continuous variable), and % of total white cell count represented by lymphocytes (Lymph., continuous variable).

3.4.10 Co-expressed gene modules enriched with inflammatory immune responses are associated with poor outcome

Enrichment analysis based on Reactome gene sets identified pathways involved in pro-inflammatory immune responses such as neutrophil degranulation, signalling by interleukins, TLR signalling and phagocytosis that were highly enriched within the ME brown and blue modules (**Figure 3.10**). On the other hand, ME black was enriched with pathways involved in cellular regulation such as protein degradation, respiratory electron transport, and regulation of apoptosis. Enrichment analysis based on Gene Ontology within the ME cyan module –which was associated with diabetes status and HbA1c level identified enriched pathways involved in regulation of endoplasmic reticulum and response to unfolded protein (**Table 3.4**).

Module eigengene (ME) can be considered as a representative expression profile or first principal component. MEs with significant correlations to 28-day mortality, %neutrophils, and %lymphocytes (both positive and negative) were visualised between non-survived and survived melioidosis. The expression profiles of ME brown, blue, black, and purple were associated with non-survivors. In contrast, the expression profile of ME salmon, yellow, red, turquoise, lightyellow and royalblue were associated with survivors (**Figure 3.11**). Enrichment analysis based on Gene Ontology in the modules positively correlated with %lymphocytes but negatively correlated with 28-day mortality (P-value <0.001) identified pathways involved in RNA regulation, B-cell and T-cell mediated immune responses (**Supplementary Figure 3.7**). Collectively, the results from WGCNA suggest that excessive

inflammatory immune response during melioidosis was associated with fatality, whereas cellular regulation and adaptive immune response were associated with survival. Diabetes status in melioidosis patients was associated with increased inflammation and unfolded protein response (UPR).

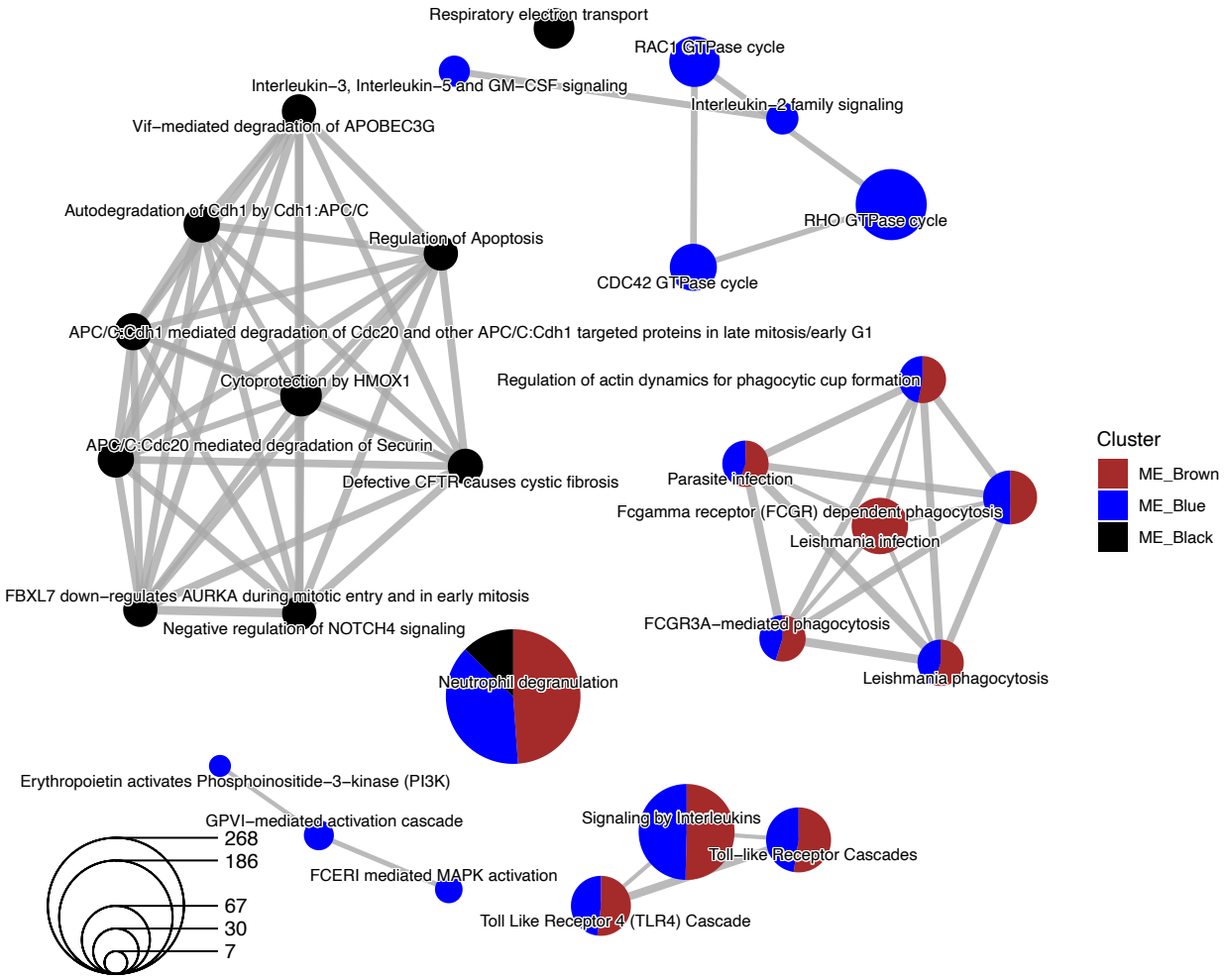

Figure 3.10 Enrichment analysis based on Reactome pathway in module eigengene (ME) brown, blue and black from **Figure 3.9** that were associated with 28-day mortality identified by module-trait relationship analysis in 81 melioidosis patients. Pathways with closely related functions were linked and clustered together. Line thickness indicates common genes shared among the pathways. The size of each term is indicated by representative counts. Enrichment plot was created using clusterProfiler R package.

Table 3.4 Gene Ontology enrichment analysis of module eigengene cyan associated with diabetes status and HbA1c level in module-trait relationship analysis by weighted gene co-expression network analysis of 81 melioidosis patients.

Module	Rank	dataSetID	dataSetName	nCommonGenes	adjusted P-value
cyan	1	GO:0005783	endoplasmic reticulum	99	1.80E-20
cyan	2	GO:0005789	endoplasmic reticulum membrane	69	1.36E-16
cyan	3	GO:0098827	endoplasmic reticulum subcompartment	69	1.70E-16
cyan	4	GO:0042175	nuclear outer membrane-endoplasmic reticulum membrane network	69	3.57E-16
cyan	5	GO:0034976	response to endoplasmic reticulum stress	36	2.02E-15
cyan	6	GO:0140534	endoplasmic reticulum protein-containing complex	25	3.09E-15
cyan	7	GO:0030968	endoplasmic reticulum unfolded protein response	24	8.26E-14
cyan	8	GO:0034620	cellular response to unfolded protein	25	2.48E-13
cyan	9	GO:0006986	response to unfolded protein	27	3.93E-13
cyan	10	GO:0035967	cellular response to topologically incorrect protein	26	5.62E-13
cyan	11	GO:0035966	response to topologically incorrect protein	28	8.92E-13
cyan	12	GO:0031984	organelle subcompartment	82	1.10E-12
cyan	13	GO:0005788	endoplasmic reticulum lumen	29	7.20E-12
cyan	14	GO:0006487	protein N-linked glycosylation	16	4.70E-10
cyan	15	GO:0012505	endomembrane system	136	7.46E-09
cyan	16	GO:0036498	IRE1-mediated unfolded protein response	14	2.31E-08

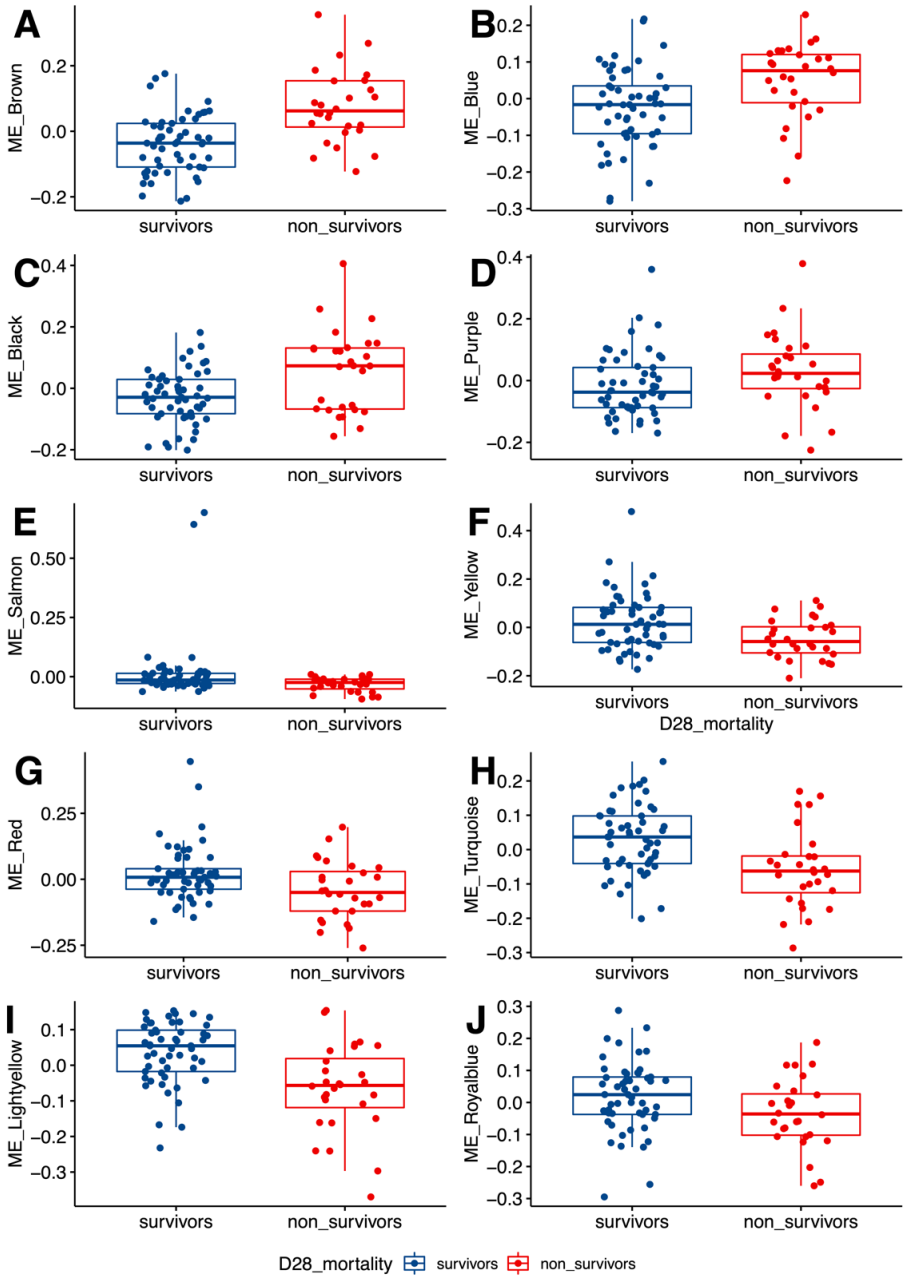

Figure 3.11 Comparison of module eigengene (ME) from **Figure 3.9** between non-survived (fatal) and survived melioidosis cases. ME is considered as a representative expression profile in each gene module. MEs with significant associations with 28-day mortality, %neutrophils, and %lymphocytes were compared between non-survived and survived melioidosis. Box plots represent medians with interquartile range plus lines to minimum, maximum and potential outliers.

3.4.11 Genes involved in the inflammatory immune response are potentially a key driver of the deleterious host immune response during melioidosis

To identify potential key regulators, the results from supervised (DGE analysis) and unsupervised (WGCNA) approaches were compared using Venn diagrams for overlapped genes. Top 20 hub genes were identified in ME brown and blue which were associated with fatal melioidosis (**Figure 3.12**). Out of a total of 2,222 genes within ME blue, 116 genes were differentially expressed between non-survived and survived melioidosis (as identified by the DGE analysis absolute[Log2 fold-change]≥1, adjusted P-value<0.05). Of 1336 gene members in ME brown, 210 genes were differentially expressed. Of 20 hub genes, 6 hub genes were differentially expressed between non-survived and survived melioidosis in the ME blue (5) and brown (1) respectively (**Figure 3.12B**). The 6 hub genes consist of *WDFY3* (WD Repeat and FYVE Domain Containing 3), *FCER1G* (Fc Epsilon Receptor Ig), *ACSL1* (Acyl-CoA Synthase Long Chain Family Member 1), *TLR4* (Toll Like Receptor 4), *AQP9* (Aquaporin 9) and *KLHL2* (Kelch Like Family Member2).

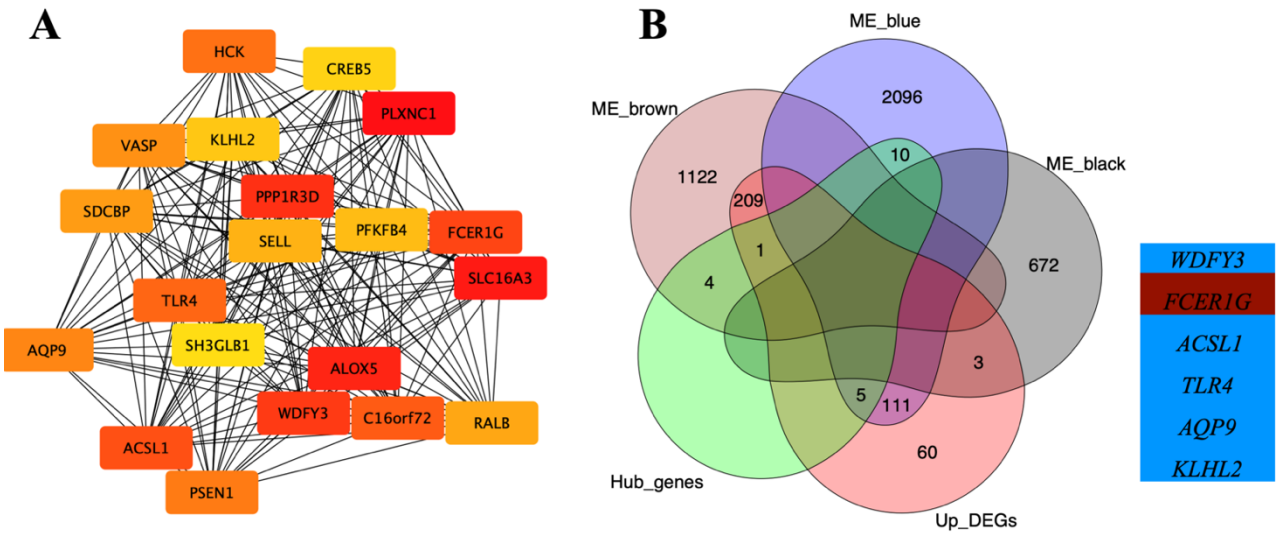

Figure 3.12 Top 20 hub genes with potential regulatory role in fatal melioidosis. A: The top 20 hub genes identified in the module eigengene (ME) brown, blue and black associated with 28-day mortality. B: Venn diagram of overlapping differentially expressed genes (DEGs), genes member of the ME brown, blue, and black identified by weighted gene co-expression network analysis (WGCNA) (**Figure 3.9**), and hub genes in the ME brown, blue, and black. DEGs were derived from up- and down-regulated genes between non-survived and survived melioidosis patients (**Figure 3.4**). ME brown, blue, and black were significantly associated with 28-day mortality by module-trait relationship analysis. 20 Hub genes within ME brown and blue were derived using the Maximal Clique Centrality (MCC) algorithm with the CytoHubba plugin on Cytoscape software. MCC scores of hub genes were ranked from high (red) to low (yellow).

3.4.12 Depleted adaptive immune cells, but increased innate immune cells were associated with poor outcome

To identify the distribution of immune cells associated with deleterious immune responses during melioidosis, whole blood RNA sequencing data were deconvoluted using xCell (*435*). Of 64 immune-cell signatures, 15 immune-cell subsets were significantly different between non-survived and survived melioidosis. Overall, T cell subsets, B cell subsets and dendritic cells were significantly enriched in the survivors compared to non-survivors, including CD4+ memory T cells, CD4+ effector memory T cells (CD4+ Tem), CD8+ T cells, CD8+ central memory T cells (CD8+ Tcm), CD8+ effector memory T cells (CD8+ Tem), memory B cells, naïve B cells, dendritic cells (DC), classical dendritic cells (cDC), and invariant dendritic cells (iDC) (**Figure 3.13**). In contrast, neutrophils, natural killer T cells (NKT), monocytes, macrophages, and M1 macrophages were significantly enriched in the non-survivors. The differential white cell count in the full blood count (FBC) measured in the hospital laboratory at Sunpasitthiprasong Hospital mostly confirmed the results obtained from the deconvolution technique in which higher neutrophil counts were observed in the non survivors with reduced lymphocytes (**Supplementary Figure 3.8**). In addition, Pearson's correlation analysis between enrichment scores of each cell type by the xCell method and frequency of white cell count obtained from 81 melioidosis patients shows significant correlations in most cases except monocytes (**Figure 3.14**). Interestingly, melioidosis patients with T2DM show enrichment of NKT cells, class switched memory B cells, and neutrophils, but reduced CD8+ naïve T cells (**Supplementary Figure 3.9**).

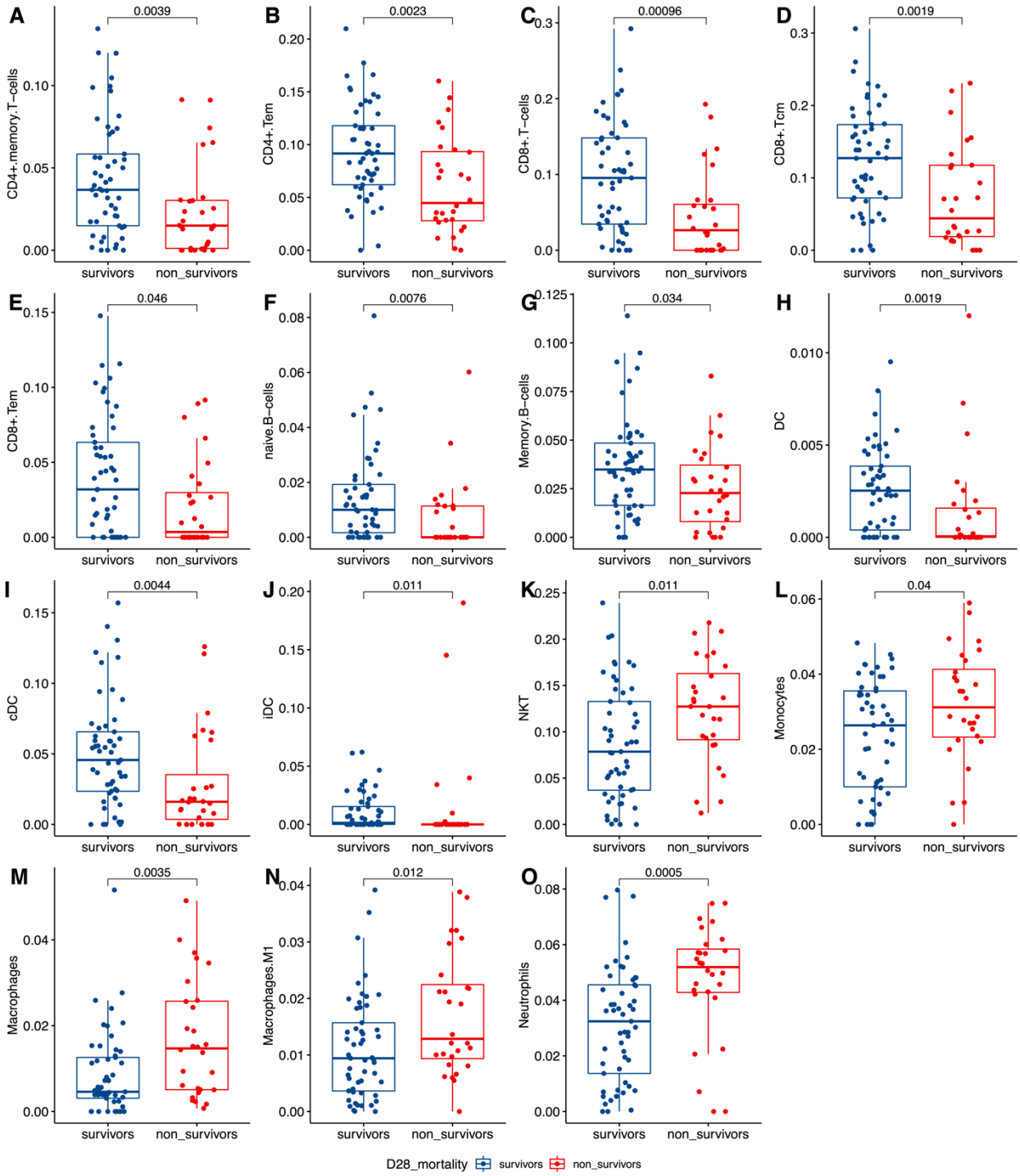

Figure 3.13 Scattered boxplots show comparisons of deconvoluted cell enrichment between survivor melioidosis patients (blue, n=53) and non-survivor (red, n=28) using the xCell deconvolution method (xCell R package version 1.1.0). The Y-axis displays each cell type defined by enrichment scores. Box plots represent medians with interquartile range plus lines to minimum, maximum and potential outliers. Non-parametric Mann-Whitney test was performed with its corresponding 2-tailed P-value displayed on each plot alongside median and inter-quartile range boxes.

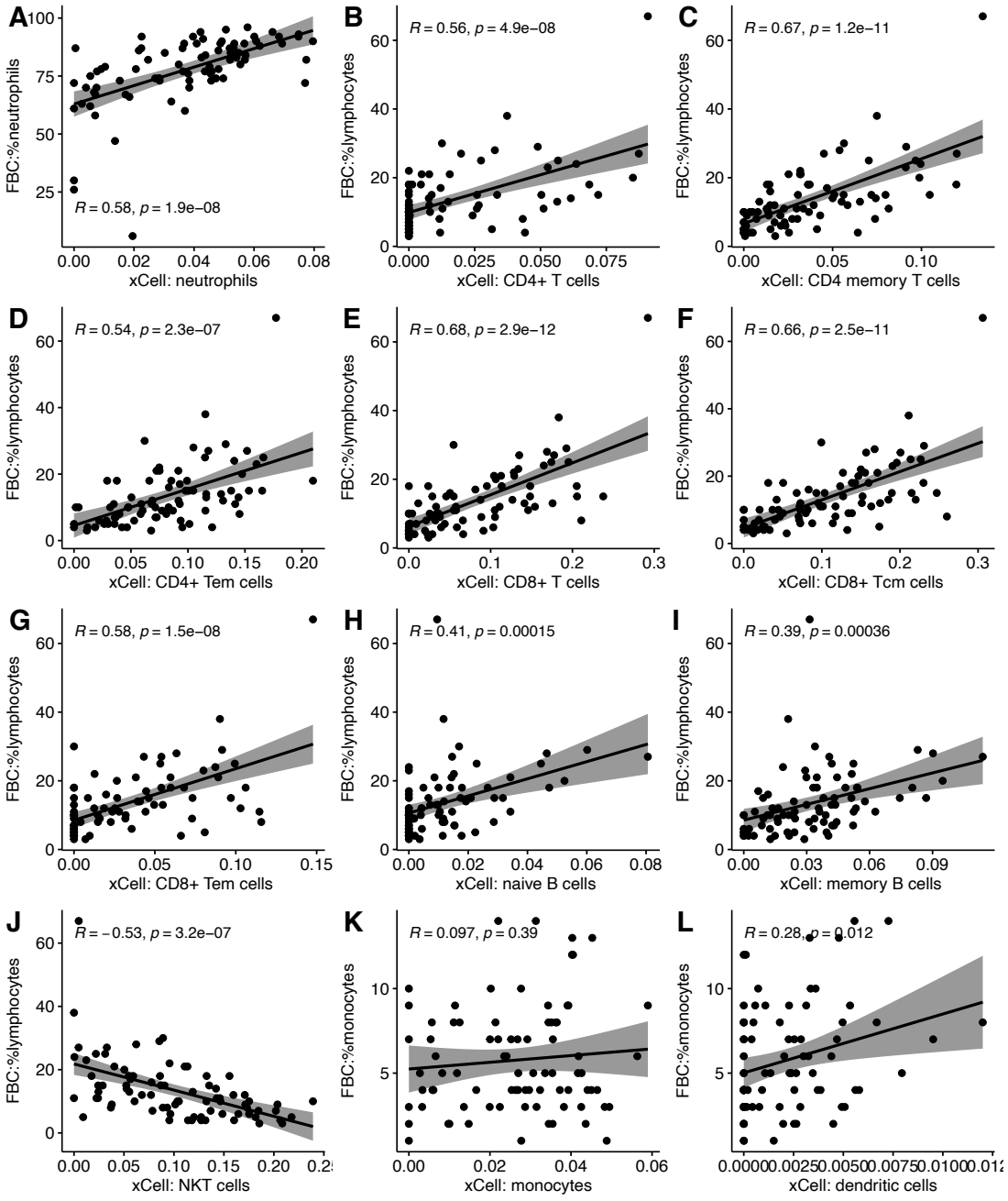

Figure 3.14 Scattered plots show correlations between deconvoluted cell enrichment scores by the xCell method and the results of full blood count (FBC) in 81 melioidosis patients. The x-axis displays enrichment scores of each cell type defined by the xCell method. The y-axis displays frequency of each cell type by FBC method. Pearson's correlation coefficient, corresponding P-value, and linear regression line with 95% confidence interval (shaded area) are displayed within each plot.

3.5 Discussion

In this chapter, the impacts of T2DM in melioidosis on whole blood transcriptome were studied. Melioidosis induces profound changes in the whole blood transcriptomic response compared to healthy controls, with over 2,000 differentially expressed genes. Despite an estimated twelve-fold increased risk of melioidosis in people with T2DM, transcriptomic profiles were largely similar between melioidosis patients with and without T2DM. However, analysis of case fatality based on 28-day mortality reveals profound transcriptomic changes in fatal melioidosis compared to survivors.

The 2013 transcriptomic study in melioidosis by *Koh et al.* (*101*) identified prominent interferon-signalling and inflammatory immune pathways in melioidosis and active tuberculosis relative to a healthy control group. In this chapter, I did not see such predominance of interferon signalling pathways in melioidosis compared to healthy controls, which may be due to differences in the timing of the sampling relative to participant's melioidosis journey but this information was unavailable from the *Koh et al.* study *(101).* In **Chapter 5**, predominant interferon signalling pathways were detected in melioidosis patients recruited at an earlier enrolment timepoint (less than 24 hours following hospital admission) compared to control group (*192*). These results suggest that interferon signalling is prominent during the early stages of melioidosis and resolves as the disease progresses.

People living with diabetes are known to have increased risk of infection from both extracellular and intracellular pathogens such as *S. aureus (360),* Dengue, and *Candida* species *(357, 445).* Firstly, DGE analysis between uninfected T2DM control and healthy

control cohort shows subtle difference, but moderately up-regulated genes in the T2DM control group. Following DGE analysis, GSEA analysis at baseline suggests increased pro-inflammatory immune responses in the T2DM control cohort. Secondly, DGE analysis identified almost none of DEGs between melioidosis patients with and without T2DM, despite the demonstrated twelve-fold increased risk (*20*), suggesting by the time of our sampling timepoint the host response was not hugely impacted by diabetes status. However, GSEA analysis drew out more subtle influences of diabetes status on transcriptomic profiles in acute melioidosis. Patients with T2DM show enrichment of multiple pathways involving the immune response, cell signalling and metabolism, especially TNF signalling, inflammatory response, and complement pathways, and compatible with the results from the xCell deconvolution method, in which NKT cells and neutrophils were highly enriched in the patients with T2DM. A study by *Lv et al.* (*446*) demonstrated increased frequency of NKT cells (CD3+CD56+) was observed in T2DM patients with increased production of IFN-γ and IL-4 compared to healthy control. Moreover, increased expression of IL-4 in NKT cells could inhibit proliferation of endothelial cells which are important for maintaining normal blood vessels (*446*). Thus, the increased IL-4 production may be involved in dysregulation of vascular endothelium in T2DM leading to T2DM-induced complications such as atherosclerosis and cardiovascular diseases (*447*). In line with baseline characteristics of uninfected T2DM patients, raised inflammatory mediators are frequently reported in people with T2DM, such as serum IFN-γ, CRP, TNF, and IL-1RA (*448-450*). An *in intro* study of T2DM in a macrophage cell line demonstrated induced expression of MMP-1, MMP-9, and IL-1β in the presence of IFN-γ under hyperglycaemic conditions (*451*). The increased inflammatory response may contribute to plague destabilisation leading to atherosclerosis and other cardiovascular complications (*452*).

There are established associations between neutrophils and T2DM supporting detrimental roles of neutrophilia via increasing inflammatory immune responses in diabetes (*343, 453*). Hyperglycaemia causes neutrophils dysfunction such as chemotaxis, phagocytosis, killing mechanisms and extracellular trap formation (*454*). In an experimental diabetes study, rats were treated with chemotactic agents where neutrophil migration and phenotype were observed. Rats with severe diabetes showed reduced migration and deformation of neutrophils (*455*). Hyperglycaemia can induce intracellular accumulation of Ca^{2+} which interferes with cellular energy production leading to reduced cellular activity including phagocytosis (*456*). Reactive oxygen species (ROS) are an essential killing mechanism in controlling intracellular infections. Increased ROS activity in diabetes patients compared to healthy individuals has been demonstrated both under resting and stimulation conditions (*457*). Neutrophils store resistin within granules and can be released upon inflammatory response (*458*). Resistin exerts pro-inflammatory activities and is associated with development of T2DM through its mechanism of inducing insulin resistance (*459*). Conversely, increased levels of resistin are associated with reduced ROS activity in severe tuberculosis patients with T2DM and patients with diabetes without infection (*460*). Thus, reduced ROS may be involved in increased susceptibility to infections in diabetes. Furthermore, studies have demonstrated that increased inflammation in hyperglycaemia produces microparticles under oxidative stress which stimulate the inflammasome leading to an increased inflammatory immune response (*461*).

Neutrophils under hyperglycaemic conditions are highly susceptible to NETosis - release of NETs which contain anti-microbial proteins such as MPO, NE and cathepsin G (*268*). Low-density neutrophils (LDNs, immature neutrophils) are especially susceptible to NETosis. A diabetic mice model to study increased susceptibility to *S. aureus* by *Cohen et al.*

demonstrated increased frequency of LDNs in diabetic mice with increased TGF-β expression, NETosis, and an association with poor outcome (*462*). Moreover, LDNs have been shown to suppress T cell activation and proliferation (*279, 463*). Taken together, my transcriptomic study and the underlying literature give mechanistic insight into how T2DM increases susceptibility to melioidosis, including via increased frequency of circulating neutrophils which are associated with increased inflammation and modulation of cell-mediated immune responses.

The unsupervised analysis approach by WGCNA identified two co-expressed gene modules including ME cyan and brown which were significantly associated with having diabetes. These modules were enriched with innate immune components and the stress response in endoplasmic reticulum (ER) respectively. As described above, there is growing evidence on how the innate immune compartment, particularly neutrophils, may increase susceptibility in people with T2DM during melioidosis. However, little is known about the ER stress response and its impact on the host immune response during infection. Under homeostasis, the ER functions to regulate protein production such as synthesis, folding, and transport (*464*). Pancreatic β cells produce insulin in response to high blood glucose such as after meal. To keep up with the demand, β cells produce large quantities of insulin resulting in high workload for ER machinery, causing in turn accumulation of misfolded and unfold proteins within the ER (termed "ER stress response"). The ER responds by either alleviating the ER stress response via a process called unfolded protein response (UPR), or if unsuccessful triggering apoptosis of the cell (*465*). Hyperglycaemia, elevated pro-inflammatory cytokines, and insulin resistance have all been found to contribute to development of T2DM. These conditions also contribute to increased ER stress response, especially in pancreatic β cells, leading to apoptosis and release of self-antigen (*466*).

Apoptotic β cells have been found to activate T cells, generating an autoimmune-like response targeting β cells. This contributes to auto-reactive T cells against β cells, destruction of β cells, and development of T2DM (*467*). The enriched ER stress response and UPR in the co-expressed gene module associated with having diabetes may be a hallmark for development of T2DM. However, the role of the ER stress response and its association with increased susceptibility to infections is unknown and requires further studies.

Nearly half of melioidosis cases die in some endemic regions despite receiving the recommended treatment (*468*). DGE analysis by 28-day mortality identified dramatic changes of transcriptomic profiles between non-survived and survived melioidosis patients, with over 700 DEGs. Pro-inflammatory pathways mediated by the innate immune compartment such as TNF signalling, inflammatory response, neutrophil degranulation and TLRs were up-regulated in the non-survivors. These deleterious immune responses have been reported to be associated with poor outcome and severe disease in melioidosis and other diseases (*50, 469, 470*). Furthermore, WGCNA revealed three co-expressed gene modules associated with 28-day mortality, with enrichment of pathways involved in inflammation dominated by innate immune compartments such as neutrophil degranulation, TLRs, and killing by phagocytosis. It is well-documented that excessive and uncontrolled inflammatory responses are associated with collateral tissue damage and fatality (*471*). On the other hand, pathways involved in T cell activation and differentiation were down-regulated in non-survived compared to survived melioidosis patients (or the corollary that non-survival is associated with failure to up-regulate crucial adaptive T cell pathways).

Depletion and dysregulation of lymphocytes including CD4+ T, CD8+ T and non-classical T cells have been reported as associated with poor outcomes in sepsis (*212, 472*). Our study identified that neutrophilia and lymphopenia were associated with the non-survivors by both hospital-measured FBC and the xCell deconvolution method. Neutrophilia and lymphopenia can be considered as a hallmark of sepsis (*473*). A meta-analysis (*260*) evaluating the prognostic value of neutrophil-to-lymphocyte ratio (NLR) in over 10,000 sepsis patients demonstrated that higher NLR is associated with poor outcome. Furthermore, deconvoluted immune cell enrichment identified large-scale depletions of CD4+ T, CD8+ T, and B cells. In line with our study, several studies have reported the impact of sepsis on T lymphocyte function and phenotype including increased apoptosis, exhaustion, reduced cytokine production and cytotoxicity (*474-476*).

The unsupervised analysis approach by WGCNA identified three co-expressed gene modules including ME brown, blue, and black which were significantly associated with 28-day mortality. Six hub genes including *WDFY3*, *FCER1G*, *ACSL1*, *TLR4*, *AQP9* and *KLHL2* were differentially expressed between non-survived and survived melioidosis. *FCER1G* encodes the high affinity immunoglobulin epsilon receptor subunit gamma (FcRγ) that plays several roles including allergic reaction, T cell regulation and tumour progression (*477-479*). *Yang et al.* (*480*) re-analysed transcriptomic data derived from sepsis and non-sepsis patients and identified *FCER1G* along with *SERPINA1* and *S100P* as potential biomarkers of sepsis. In line with this, in my study, *S100P* was up-regulated in non-survived compared to survived melioidosis patients (Fold change = 2.6, adjusted P-value = 0.035). An experimental peritonitis-induced study of *E.coli* (*481*) showed improved survival in FcRγ-deficient mice accompanying increased phagocytosis and bacterial killing with lower levels of TNF. Moreover, recognition of *E.coli* by CD16 (FcRIII) activated FcRγ inhibitory signalling

cascade resulting in decreased phagocytosis but increased production of TNF through TLR-4 signalling. Interestingly, another study (*479*) identified enhanced CD8+ T-cell function during lymphocytic choriomeningitis virus (LCMV) in FcRγ-deficient mice, i.e., wild-type mice expressing FcRγ showed reduced frequency and CD8+ T-cell function during LCMV infection mediated by FcRγ and NKp46 expressing NK cells. *ACSL1* encodes long-chain acyl-CoA synthetase family member 1, an enzyme that converts long chain fatty acids (FA) to FA acyl-CoAs essential for lipid synthesis such as triacylglycerol, cholesterol esters and sphingolipids (*482*). *Roekands et al.* comprehensively re-analysed and reviewed the roles of ACSL1 during sepsis from publicly available data sets and literature (*483*). Firstly, the expression of *ACSL1* in neutrophils was increased following stimulation with plasma derived from sepsis patients (*484*). Secondly, some studies have shown evidence supporting a link between increased expression of ACSL1 and elevated inflammatory immune responses by innate immune cells (*485, 486*). *ACSL1* is highly expressed in neutrophils and monocytes and can be induced with stimulation of several PAMPs and pro-inflammatory cytokines such as LPS, flagellin, IL-18 and TNF (*483, 487*). Taken together, the increased expression of *ACSL1* is tightly linked to an increased inflammatory immune response including higher frequency of circulating neutrophils.

AQP9 encodes Aquaporin 9, a membrane channel protein which allows small molecules such as water and glycerol to cross the cell membrane, and is highly expressed on leukocytes during inflammation and sepsis (*488, 489*). Experimental LPS-induced septic shock identified reduced inflammation via NF-κB p65 signalling through the production of reactive nitrogen species and superoxide anion in *AQP9* knockout mice (*488*). Similar observation was demonstrated in another study using an LPS-induced inflammation model, in which pro-inflammatory cytokines and chemokines such as IL-6, IL-1α, and CCL3 were

reduced in *AQP9* knockout mice compared to wide-type (*490*). In humans, patients with systemic inflammatory response syndrome have an increase in expression of AQP9 along with F-actin and oxidative activity compared to healthy donors (*491*). *TLR4* encodes Toll-like receptor 4, a transmembrane protein receptor highly expressed on many immune cells particularly those in the innate immune compartment such as neutrophils, monocytes and macrophages (*491*). During the innate immune response, TLR4 complexed with CD14 and MD-2 co-receptor binds LPS resulting in activation of pro-inflammatory immune signalling cascades, in particular MyD88 and subsequently the NF-κB mediated immune response (*492*). Excessive inflammatory immune response is a hallmark of sepsis, and in Gram-negative sepsis this is caused by dysregulation of the innate immune response to LPS via TLR4 signalling, leading to increased production of inflammatory mediators such as IL1β, TNF, and IL-6 and an association with severe disease and poor outcomes (*493, 494*). In melioidosis, plasma lactoferrin is elevated in non-survived melioidosis compared to survivors (*495*). *In vitro* infection with *Burkholderia thailandensis* (a closely related low-virulent species) of THP-1 cells and monocytes in presence of lactoferrin showed increased TNF and IL-1β production in TLR4 dependent manner (*495*). This suggests dysregulation of TLR4-mediated inflammatory immune response which is part of the chain leading to fatal melioidosis.

In this chapter, inflammatory pathways, especially those mediated via TLR signalling such as TLR2, TLR6, and MyD88 were up-regulated in fatal melioidosis. *Wiersinga et al.* (*50*) performed TLR phenotyping on monocytes and granulocytes derived from melioidosis patients and identified increased expression of TLR2, TLR4, CD14 and MD-2 compared to healthy controls. *In vivo* stimulation of alveolar macrophages and whole blood derived from TLR2- and TLR4-deficient mice with heat-killed Bp antigen showed reduced TNF

production suggesting both TLRs are important for host immune response to melioidosis. An *in vitro* study using stably transfected HEK293 cells with CD14/TLR2 showed activation of TLR2 signalling rather than TLR4 when stimulated with purified LPS from Bp. Interestingly, TLR2-deficient mice showed better survival when challenged with Bp compared to TLR4-deficient mice. This suggests TLR2 may play a deleterious role during melioidosis (*50*). In contrast, *West et al.* demonstrated that heat-killed Bp activates both TLR2 and TLR4 in HEK293 stably transfected with TLR2 (in combination with either TLR1 or TLR6) and TLR4 supplemented with CD14 and MD-2. The difference between the two studies could be due to the absence of MD-2 required for TLR-4 complex formation and signalling (*51*). Moreover, up-regulations of both *TLR2, TLR4* along with *TLR5, TLR8, TLR8-AS1* (absolute[Log2 fold-change]≥1, adjusted P-value <0.05) expression were identified in non-survived compared to survived melioidosis patients in this chapter.

As described earlier, Bp can activate both TLR2 and TLR4 which further activate downstream signalling cascades through MyD88:MyD88 adaptor-like(MAL)/TIR domain-containing adaptor protein (TIRAP) and ultimately NF-κB- mediated activation of pro-inflammatory immune responses (*496*). Interestingly, a study led by *Delano et al.* showed GR1+ CD11b+ myeloid-derived suppressor cells (MDSCs) inhibited both IFN-γ-producing CD8+ T cells and the proliferative capacity of CD4+ T cells via the MyD88 signalling pathway in a polymicrobial sepsis model using mice (*497*). Moreover, the MSDCs which were mainly composed of immature neutrophils and monocyte precursors are able to suppress and differentiate naïve CD4+ T cells toward a less protective Th2 phenotype (*497, 498*). In melioidosis, bacteraemia is a common clinical manifestation in up to 60% of all cases (*10*). The up-regulation of multiple TLRs is probably due to the presence of PAMP activity from bacterial components such as LPS resulting in activation of the inflammatory

immune response and release of cytokines and chemokines. Innate host defence by TLRs is important during infections, however, when dysregulated due to either host genetics or pathogen-mediated immune modulation may lead to excessive non-specific inflammation leading to increased disease severity and mortality in melioidosis and acute inflammatory condition such as during sepsis (*50, 69, 494*).

There were some limitations. This chapter utilised samples derived participants enrolled from a single centre study which might not well represent the general population in the region. The study site is a tertiary hospital, where melioidosis patients were transferred from adjacent provinces resulting in delayed enrolment, diagnosis, and treatment. The total number of whole blood samples for RNA sequencing may be under power in detecting a difference between melioidosis with and without diabetes. Moreover, most patients with melioidosis had one or more co-morbidities that may be a confounding factor to delineate transcriptomic profile associated with T2DM. Patients with T2DM in this study was not formally diagnosed, the length of the disease, as well as treatment might influence the outcome of this chapter. This study utilised whole blood bulk-RNA sequencing approach, and as a result whole blood transcriptome appears to be dominated by transcripts derived from neutrophils potentially obscuring transcriptome from other cell populations. Likewise, the cell-type signature for the deconvolution technique (CIBERSORTx) was initially derived from a cancer study, therefore its extrapolation to infection patients has limits, for example the presence of macrophage and mast cells in circulation detected in this study. Transcriptomic profiles associated with fatal melioidosis may require further validation experiment as transcriptome is regulated pre-translational and post-translational modifications. The impacts of diabetes in whole blood might be overwhelmed by neutrophils. To study the impacts of diabetes during melioidosis, an alternative approach

such as single cell RNA sequencing may be a more sensitive approach to detect cell-specific transcriptomic response. Lastly, module trait relationship analysis identified ME royal blue with negative correlations to age, sex and 28-day mortality suggesting the influence of age and sex during melioidosis. Therefore, the DGE analysis between non-survived and survived melioidosis patients were controlled for age and sex as covariates. Nevertheless, the impacts of age and sex are beyond the scope of this thesis.

In conclusion, this chapter demonstrates profound transcriptomic changes associated with fatal melioidosis involving excessive non-specific inflammation, but stunted T-cell responses. These findings highlight the importance of the cellular immune response by T cells during melioidosis. The inflammatory response in fatal melioidosis is chiefly driven by neutrophils - potentially via TLR signalling and other innate immune mediated responses such as MyD88 and IL-1 pathways. Subtle differences of whole blood transcriptomic profile between melioidosis with and without T2DM were detected after 5 days following hospital admission, despite diabetes being a major risk factor with up to 12-fold increased susceptibility to melioidosis. Moreover, having diabetes following hospital admission due to melioidosis was not associated with increased case fatality (*76, 499*). Despite having diabetes, other additional comorbidities such as older age, alcohol abuse, and chronic disease have been found to be confounding factors associated with hospitalisation making it difficult to delineate the true impact of diabetes during melioidosis (*68*). Moreover, information on self-medication or over-the-counter medicines (i.e., antibiotics, steroids, herbs) was unknown and it might affect the transcriptome (*500, 501*). Therefore, mechanisms underlying T2DM in increasing susceptibility require further studies. Transcriptomic study using single cell approach may be an appropriate choice in dissecting host immune response in melioidosis patients with T2DM.

Chapter 4: What are the whole blood transcriptomic profiles associated with diabetes and intermediate hyperglycaemia during tuberculosis?

4.1 Introduction

Tuberculosis (TB) is the leading cause of death from one single pathogen worldwide, caused by the Gram-negative bacillus *Mycobacterium tuberculosis* (Mtb) (*103*). In 2021, the World Health Organisation estimated approximately 10 million people were infected with Mtb and 1.3 million died including additional 214,000 deaths among the HIV-positive population (*103*). HIV infection confers the greatest risk factor of developing TB disease along with undernourishment, alcohol abuse, smoking and diabetes (*110, 111*). T2DM confers up to three-fold increased risk of developing TB (*111, 115*) which was attributable to approximately a million TB cases worldwide in 2013 (*114*). Interestingly, HIV infection is not a risk factor of acquiring melioidosis (*502*).

Melioidosis and TB share many common features. Both diseases are caused by intracellular Gram-negative bacteria and both pathogens preferentially affect the lungs and form granuloma (*128*). Type I immune responses are important for controlling both diseases (*76, 503*). In TB, type II immune responses and reduced IFN-γ response may be associated with poor Mtb control and severe disease (*149, 151, 504*). However, melioidosis patients most commonly present as acute infection (85%) (*9*) whereas TB is a chronic infection (*105*).

Impacts of diabetes (DM) on the cellular immune response against Mtb have been demonstrated. Lower IFN-γ and IL-12 responses were observed in TB-DM patients, and those who had poor glycaemic control showed lower IFN-γ response compared to those with good glycaemic control (*172, 173*). Furthermore, an increased IL-10 response in TB-DM

patients compared to either TB patients without diabetes or healthy subjects was identified (*174*). Likewise, reduced expression of antigen presenting and costimulatory molecules (e.g., HLA-DR, CD80 and CD86) in macrophages and higher neutrophils counts in response to Mtb infection was demonstrated in TB-DM compared to non-diabetes (*180*). Collectively, diabetes affects both innate and adaptive immune compartments. Dysregulation of innate immune cells compromised Th1 immune response and an increased anti-inflammatory immune may be responsible for increased susceptibility to the infections in people with diabetes.

In 2010, *Berry et al.* (*102*) reported an 86-gene signature of active TB that could discriminate active TB from some autoimmune diseases and bacterial infections, and was characterised by an interferon-inducible neutrophil-driven signature. However, this *Berry et al. (102)* report did not include cases of melioidosis, and a later study by *Koh et al.* (*101*) showed that whole blood transcriptomic signatures between tuberculosis and melioidosis were indistinguishable.

In this chapter, whole blood bulk RNA sequencing data were generated from newly diagnosed, bacteriologically confirmed pulmonary TB with and without diabetes along with uninfected patients with diabetes and healthy donors from a four-year prospective study (The Concurrent Tuberculosis and Diabetes Mellitus [TANDEM], http://tandem-fp7.eu/project/) between 2013 and 2016 across four-study sites: South Africa, Indonesia, Romania and Peru. The TANDEM project aimed to study the casual relationship between diabetes and TB, and the impact of diabetes on TB susceptibility, prevention, treatment, and prognosis (*505*). This data set were published by *Eckold et al.* in early 2021 (*506*), they identified increased innate inflammatory but decreased adaptive immune responses in TB patients with diabetes and intermediate hyperglycaemia compared to those TB patients without the conditions. Furthermore, genes involving in interferon responses were down-regulated compared to the

patients without diabetes and intermediate hyperglycaemia. In this chapter, the data set were reanalysed including DGE and pathway analysis for a direct comparison between TB and melioidosis cohorts. Furthermore, the unsupervised approach by WGCNA was performed to identify potential gene regulators and mechanisms underlying increased susceptibility in TB patients with diabetes and intermediate hyperglycaemia.

To date, little is known about common pathways underlying susceptibility to melioidosis and TB in patients with T2DM. With several common features and pathogenicity between the two diseases, I hypothesised that the increased susceptibility in patients with T2DM to melioidosis and TB is underlined by common transcriptomic profiles. In this chapter, I aim to unravel the relationship between whole blood transcriptomic profiles associated with T2DM and increased susceptibility to melioidosis and TB. The identified transcriptomic profiles in melioidosis (**Chapter 3**) and TB were studied.

4.2 Specific objectives

1. To investigate whole blood transcriptomic profiles in TB patients with and without diabetes and intermediate hyperglycaemia compared to healthy donors.
2. To identify pathways associated with diabetes that are shared between melioidosis and TB with diabetes.

4.3 Materials and Methods

4.3.1 Study design and RNA sequencing data acquisition

Whole blood bulk RNA sequencing data were kindly provided by Dr. Jackie Cliff and Professor Gregory Bancroft at the London School of Hygiene and Tropical Medicine as a part of collaborative project funded by the VALIDATE network entitled "Vaccines to target people with diabetes: characterising the pathways of immune response to *Mycobacterium tuberculosis* (TB) and *Burkholderia pseudomallei* in people with diabetes compared to non-diabetics". This chapter contains re-analysis of the data set published in the journal Clinical Infectious Diseases entitled "*Impact of Intermediate Hyperglycaemia and Diabetes on Immune Dysfunction in Tuberculosis*" (*506*). A total of 239 adults participants aged 18 years or older with newly diagnosed, bacterial-culture confirmed pulmonary TB with and without diabetes, along with uninfected diabetes patients and healthy donors from four study sites including South Africa, Romania, Indonesia, and Peru were enrolled into the study (TANDEM) (*505*). The TB patients were further classified as 1) "TB-only": TB without diabetes (HbA1c level < 5.7%), 2) "TB-IH": TB with intermediate hyperglycaemia or IH (HbA1c level between ≥5.7 and < 6.5%), and 3) "TB-DM": TB with diabetes (HbA1c level between ≥ 6.5%).

4.3.2 RNA isolation, library preparation and sequencing

RNA sequencing data were generated from 2.5 mL whole blood RNA collected into PAXgene Blood RNA Tubes (PreAnalytix). Total RNAs were extracted using a PAXgene blood miRMA kit (Qiagen) using QIAcube extraction platform. A poly-A tail library was prepared using the NEXTflex Rapid Directional RNA-Seq kit with the Caliper SciClone technology (PerkinElmer). The samples were sequenced for a single-ended 75 base pairs

using the NectSeq500 High Output kit V2 for 75 cycles (Illumina) (*506*). The RNA sequencing data (FASTQ files) were pre-quality checked and only those that passed the QC process were included into the subsequent analyses.

4.3.3 Upstream RNA sequencing analysis pipeline

The provided read counts were generated using older version human reference genome (UCSC hg19). To obtain the most comparable read counts, the sequencing data (FASTQ files) were re-aligned using the same pipeline as described in the Material and Methods section in **Chapter 3**.

4.3.4 Differential gene expression and functional pathway analysis

Differential gene expression analysis (DGE) was performed separately for three different cohorts: the South African cohort (discovery dataset, n=102), the Romanian cohort (validation dataset, n=66), and all-study-site combined dataset (N=239). DGE analysis within the South African and Romanian cohorts was adjusted for age and sex as covariates. For the combined data set, DGE analysis was adjusted for age, sex, and ethnicity as covariates. A total of 26,196 transcripts were generated from the sequencing and annotated to the gene symbol. Genes with no counts or lowly expressed were removed. Subsequently, the expression data were normalised, and variance stabilizing transformed using DESeq2 R package for down-stream data analyses and data visualization as described in **Chapter 2** (*392*).

4.3.5 Weighted gene co-expression network analysis (WGCNA) and identification of hub genes

To identify co-expressed gene modules associated with diabetes and IH in TB patients and corresponding hub genes, WGCNA was performed separately between TB-DM compared to TB-only and TB-IH compared to TB-only. For TB-DM (n=61) compared to TB-only (n=46), pre-filtered 15, 325 features, normalised and variance stabilizing transformed expression data were used for the analysis using WGCNA R package (*415*). For TB-IH (n=44) compared to TB-only (n=46), 15,058 features were included for the analysis. The remaining WGCNA workflow was performed as described in **Chapter 2**.

4.3.6 Deconvolution of bulk RNA sequencing data using xCell

Enriched cell type abundances were estimated from bulk RNA sequencing data of the TB cohorts and control cohorts (N=239) using xCell (R package version 1.1.0) (*435*). The enriched cell fractions were compared among TB patients: without diabetes (n=61), with intermediate hyperglycaemia (n=44), without diabetes (n=46), healthy control (n=36), and diabetes control (n=52) using non-parametric Mann-Whitney test on R programme.

4.4 Results

4.4.1 Demographics of study cohort

In this chapter, a total of 151 newly diagnosed, bacterial-culture confirmed pulmonary TB adult patients with and without diabetes along with uninfected diabetes patients (n=52) and healthy donors (n=36) were included in the data analyses. The participants were recruited from four study sites across the world including South Africa, Romania, Indonesia, and Peru (**Table 4.1**). The proportion of male was significant higher in the TB patients (Chi-square test, P-value = 0.03). The distribution of age was significantly different between the TB and control cohorts (Kruskal-Wallis test, P-value = 0.02), in which the age of TB-DM group was significantly higher than healthy control (Mann-Whitney, P-value=0.003). The study consists of participants from various ethnic backgrounds including Coloured, Sunda, Mestizo, and Romania which accounted for more than 80% of all participants.

Table 4.1 Subject demographics for whole blood transcriptomic study from tuberculosis patients across four study sites and corresponding control cohort.

Baseline characteristics	Study site (N=239)	TB-DM* (n=61)	TB-IH** (n=44)	TB-only (n=46)	Diabetes control (n=52)	Healthy control (n=36)	¶P-values	†P-values
No. participants (%)	South Africa	15	19	11	33	24	§0.15	§0.06
	Romania	15	10	10	19	12		
	Indonesia	19	6	14	NA	NA		
	Peru	12	9	11	NA	NA		
Sex, (male/ female)	South Africa	(7/8)	(12/7)	(2/9)	(15/18)	(12/12)	‡**0.03**	‡0.13
	Romania	(13/2)	(9/1)	(6/4)	(14/5)	(10/2)		
	Indonesia	(11/8)	(5/1)	(7/7)	NA	NA		
	Peru	(6/6)	(5/4)	(5/6)	NA	NA		
Age in years; median (IQR)	South Africa	46 (40-53)	45 (33-54)	48 (34-50)	49 (42-57)	42 (37-45)	§0.43	§**0.02**
	Romania	47 (43-55)	49 (40-57)	43 (39-53)	55 (46-58)	46 (40-53)		
	Indonesia	52 (45-58)	51 (38-57)	47 (39-58)	NA	NA		
	Peru	51 (48-54)	52 (41-57)	55 (33-64)	NA	NA		
Distribution of ethnic groups	South Africa	Two (1/14)	One (19)	One (11)	One (33)	Two (1/23)	NA	NA
	Romania	Two (1/14)	One (10)	One (10)	One (19)	Three (1/1/10)		
	Indonesia	Three (1/1/17)	Two (1/5)	Two (5/9)	NA	NA		
	Peru	One (12)	One (9)	Two (1/10)	NA	NA		

*Diabetes (DM) is defined as patients who were previously diagnosed with diabetes or having an HbA1c level ≥6.5% on recruitment into the study (*507*).**Intermediate hyperglycaemia (IH) is defined by having an HbA1c level between 5.7 and <6.5% on recruitment into the study. ¶P-values were derived from statistical analyses among TB patients. †P-values were derived from statistical analyses in all participants. §Kruskal-Wallis test. ‡Chi-square test. This table was adapted from Eckold *et al.*, Impact of Intermediate Hyperglycemia and Diabetes on Immune Dysfunction in Tuberculosis. *Clin Infect Dis* **72**, 69-78 (2021).

4.4.2 Re-alignment of RNA sequencing data

RNA sequencing data (FASTQ files) were re-aligned against the human reference genome, UCSC hg38.p2 (version 20201) and uniquely mapped reads were counted using the featureCounts function. High frequencies of uniquely mapped reads were achieved and comparable between TB (mean 72.3%, SD = 8.7) and control cohorts (mean 71%, SD = 8.5) (**Supplementary Figure 4.1A**). An average of 10 million (M) reads per sample were obtained for both TB (mean 10.5 M, SD = 1.9 M) and control cohorts TB (mean 10.4, SD = 2.1 M) (**Supplementary Figure 4.1B**). The expression data were normalised using median

of ratios method implemented in DESeq2 R package for down-stream data analyses (**Supplementary Figure 4.1C, 4.1D)**.

4.4.3 An inflammatory immune response driven by the innate immune compartment was more prominent in TB patients with diabetes and intermediate hyperglycaemia compared to the patients without diabetes

To investigate the impact of diabetes and intermediate hyperglycaemia on the whole blood transcriptome in TB patients, DGE analysis was carried out for the South African cohort (discovery) and validated with the Romanian cohort (validation). A total of 15,445 pre-filtered features were normalised and variance-stabilising transformed for subsequent data analyses. Firstly, PCA using the top 1,000 most variable genes identified some separation between TB patients and control subjects in the discovery cohort (**Figure 4.1**). However, PCA coloured by diabetes status and intermediate hyperglycaemia shows only subtle differences amongst the TB patients. Similar PCA clustering profiles were observed in the validation cohort (**Supplementary Figure 4.2**). In addition, PCA symbolized by ethnicities and countries among all TB patients and their respective control cohorts show unified clusters regardless of their origins (**Supplementary Figure 4.3A, 4.3B**). Nevertheless, covariates including age, sex, and ethnicity were included during DGE analysis as possible confounding factors.

Secondly, DGE analysis was performed among the TB patients relative to healthy controls. DGE analysis in the South African cohort identified more profound transcriptomic changes for TB-DM and TB-IH compared to healthy controls than for the TB-only group. DGE analysis of TB-IH shows 506 up- and 472 down-regulated genes, followed by TB-DM with 347 up- and 321 down-regulated genes compared to healthy controls (absolute[Log2 fold change]≥1, adjusted P-value<0.05) (**Figure 4.2**). DGE analysis in the validation cohort

shows similar trends of DEGs where TB-IH shows the highest number of DEGs followed by TB-DM, and TB-only relative to healthy control respectively (**Supplementary Figure 4.4**). More than 50% of the up-regulated genes found in the DGE analyses of TB-DM and TB-IH compared to healthy controls (discovery cohort) was identified in the validation cohort (**Supplementary Figure 4.5**). Of note, 109 genes involved in innate immune response such as *S100A8, CEACAM1, CD177*, and *GRP84* were mutually up-regulated in both TB-DM and TB-IH across both discovery and validation cohorts (**Supplementary Figure 4.6**). Lastly, to observe the correlation of the differential gene expression effects between discovery and validation cohort, Pearson's correlation analysis was performed on log2 fold-change of the DEGs. The correlation analyses identified strong correlations of the DEGs in all comparisons between the two studied cohorts (Pearson's correlation coefficient $R > 8$, P-value $< 2x10^{-16}$) (**Figure 4.3**).

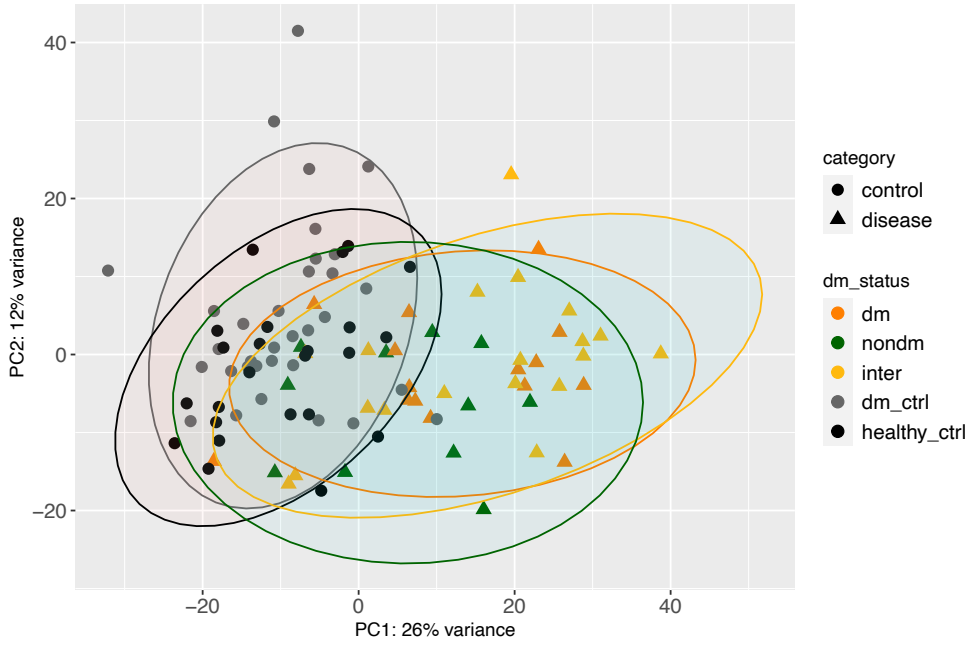

Figure 4.1 Principal component analysis (PCA) of the top 1,000 most variable genes in tuberculosis (TB) patients and controls from the South African cohort coloured by diabetes status and intermediate hyperglycaemia classification based on HbA1c level. (A) TB patients were divided into diabetes ("dm", orange triangles, n=15), intermediate hyperglycaemia ("inter", yellow triangles, n=19), non-diabetes ("nondm", green triangles, n=11), uninfected diabetes group ("dm_ctrl", grey circles, n=33), and healthy donors ("healthy_ctrl", black circles, n=24). Group classification based on HbA1c level: diabetes (HbA1c ≥6.5%), intermediate hyperglycaemia (HbA1c ≥5.7% and <6.5%), non-diabetes (HbA1c ≤ 5.6%). PCA plots were generated using plotPCA function implemented in DESeq2 R package.

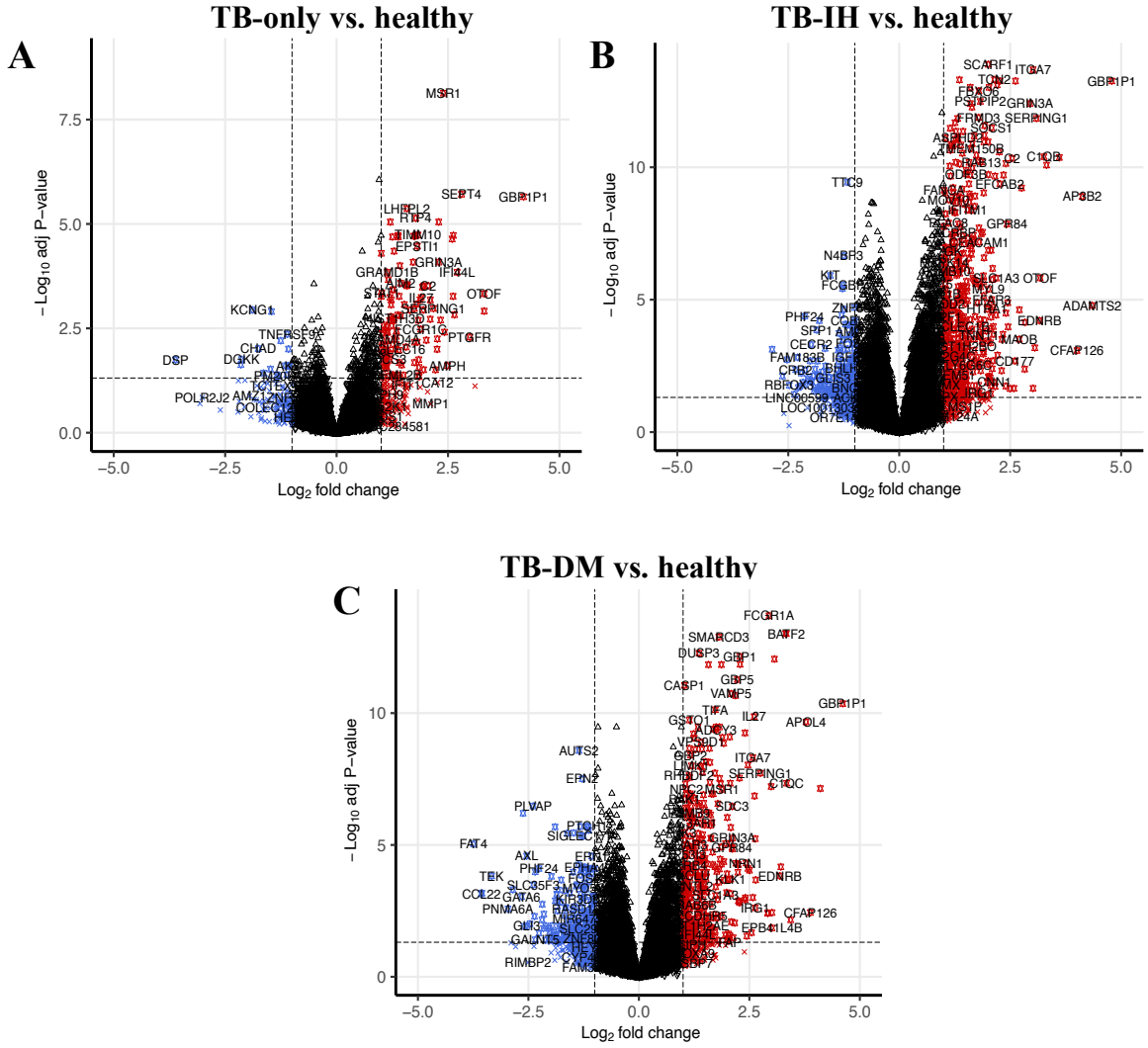

Figure 4.2 Volcano plots showing differentially expressed genes among tuberculosis (TB) patient groups and healthy controls from the South African cohort. A: Differential gene expression (DGE) analysis between TB patients only (TB-only, n=11) compared to healthy control (n=24). B: DGE analysis between TB patients with intermediate hyperglycaemia (TB-IH, n=19) compared to healthy control (n=24). C: DGE analysis between TB patients with diabetes (TB-DM, n=15) compared to healthy control (n=24). Dotted lines define the cut-off for differentially expressed genes based on absolute[Log2 fold-change]≥ 1 (x-axis) and adjusted P-value < 0.05 (y-axis). Volcano plot was generated using EnhancedVolcano R package.

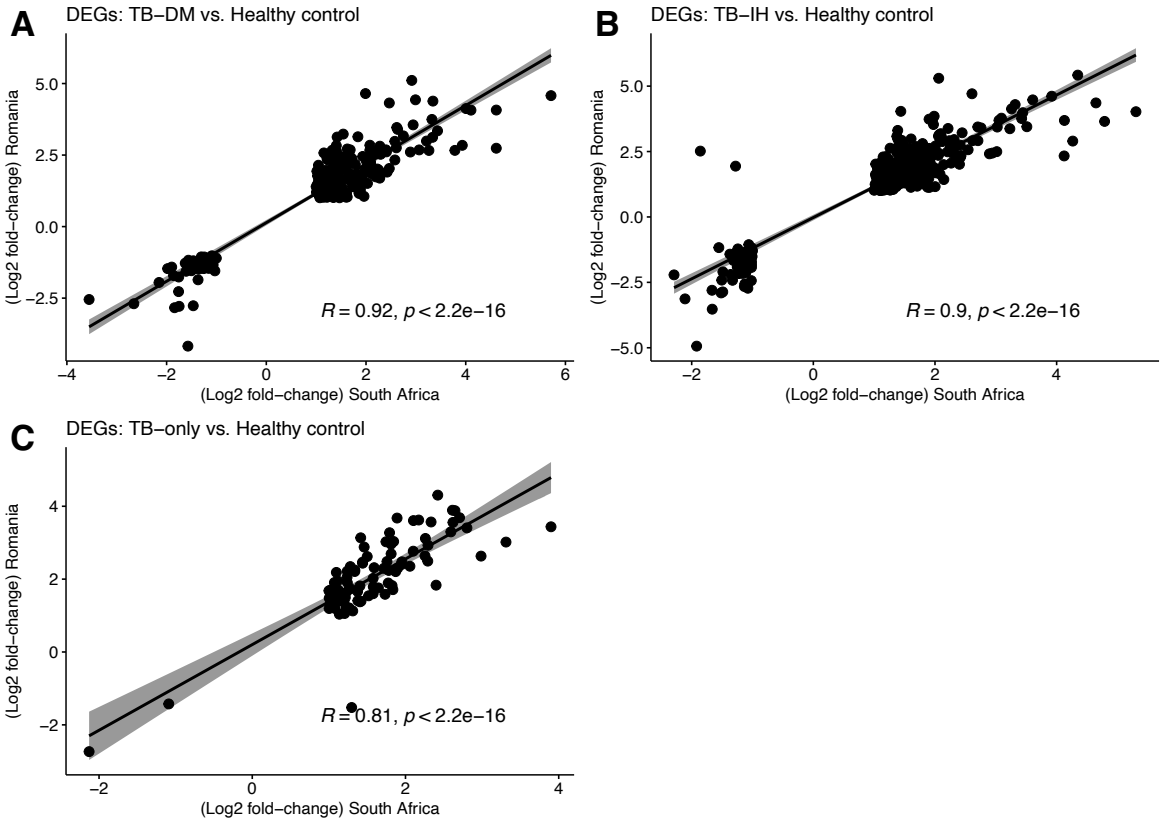

Figure 4.3 Scattered plots show correlations of differentially expressed genes (based on log2 fold-change) among TB patients compared to uninfected healthy donors between South African (x-axis, discovery) and Romania (y-axis, validation) cohort. A: Differentially expressed genes (DEGs) derived from differential gene expression (DGE) analysis between TB patients with diabetes (DM) compared to healthy donors. B: DEGs derived from DGE analysis between TB patients with intermediate hyperglycaemia (IH) compared to healthy donors. C: DEGs derived from DGE analysis between TB patients only compared to healthy donors. DEGs were based on absolute[Log2 fold-change]≥ 1 and adjusted P-value < 0.05. Pearson's correlation coefficient, corresponding P-value, and linear regression line with 95% confidence interval (shaded area) are displayed within each plot.

4.4.4 Diabetes is associated with an increased pro-inflammatory immune response, but suppressed interferon responses in TB patients

To investigate the impact of diabetes and intermediate hyperglycaemia on the whole blood transcriptome among TB patients, DGE analysis was carried out in all TB patients across all four study sites. A total of 16,407 pre-filtered features were normalised and variance-stabilising transformed for subsequent data analyses. PCA using the top 1,000 most variable genes identified some separation between TB patients and control subjects (**Figure 4.4A**). DGE analysis in TB-DM compared to TB-only patients identified a stronger impact of diabetes on the whole blood transcriptome (194 up- and 143-down regulated genes, adjusted P-value <0.05) compared to TB-IH relative to TB-only (59 up- and 14-down regulated genes) (**Figure 4.4B-D**). Moreover, 19 genes involved in the pro-inflammatory immune response such as *ADAMTS2, IL10RB-AS1, IL1R2*, and *PI3* were commonly up-regulated in TB-DM and TB-IH compared to TB-only patients.

GSEA based on Hallmark gene sets following DGE analysis identified pathways involved in inflammatory immune responses and metabolism such as coagulation, IL-6 JAK STAT3 signalling, complement, interferon signalling, oxidative phosphorylation, and reactive oxygen species were highly enriched in TB-IH compared to TB-only patients (**Figure 4.5**). In contrast, both interferon alpha and gamma pathways were enriched in TB-only compared TB-DM patients. Pathways involved in metabolism and the innate immune response such as oxidative phosphorylation, reactive oxygen species, coagulation, and complement were highly enriched in TB-DM compared to TB-only patients.

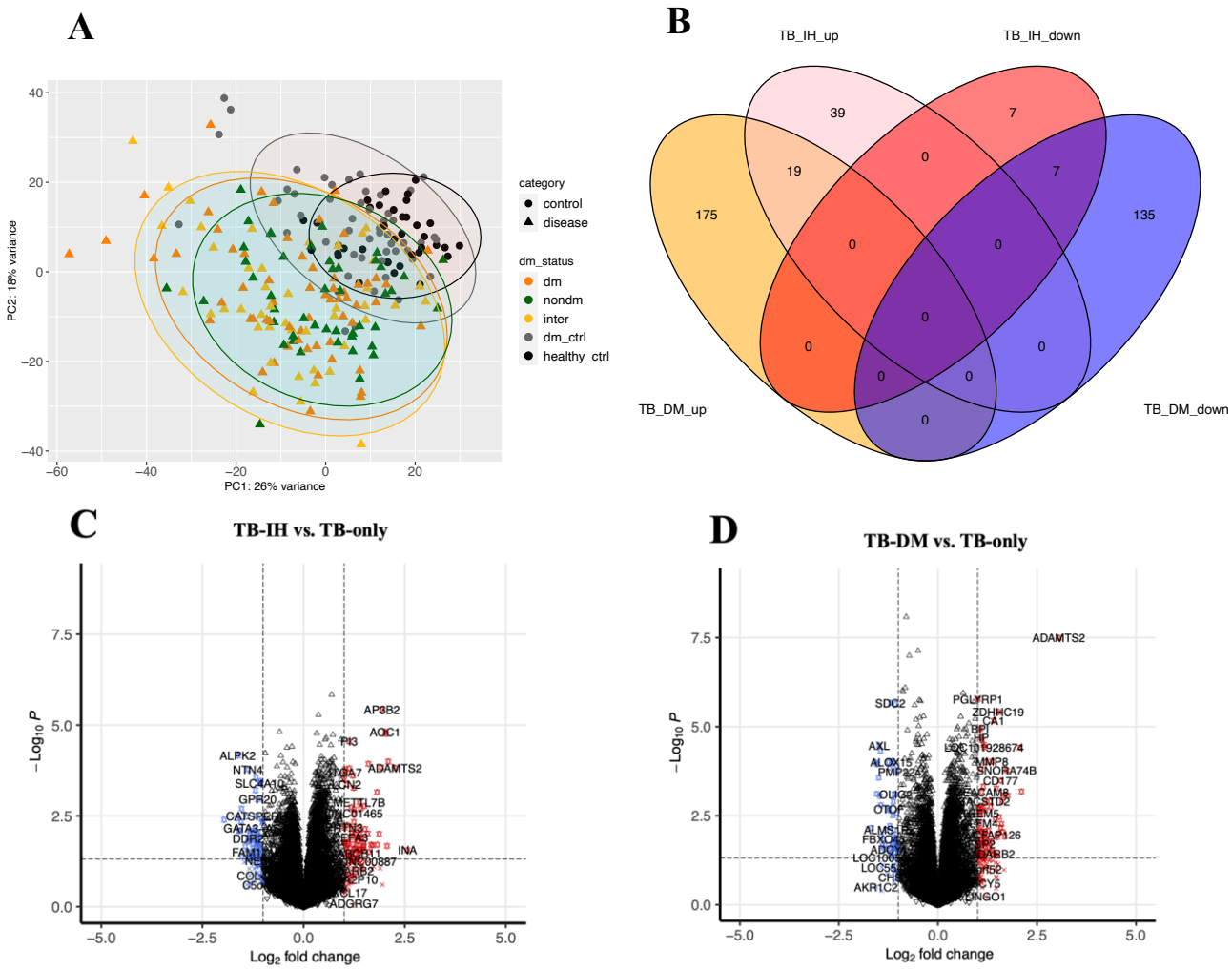

Figure 4.4 Principal component analysis (PCA) of the top 1,000 most variable genes, Venn diagram and volcano plots showing differentially expressed genes (DEGs) among 239 tuberculosis (TB) patient groups and controls from all-study sites combined. A: PCA plot of 239 TB patients and controls coloured by groups divided into TB with diabetes ("dm", orange triangles, n=61), TB with intermediate hyperglycaemia (IH) ("inter", yellow triangles, n=44), TB without diabetes ("nondm", green triangles, n=46), uninfected diabetes group ("dm_ctrl", grey circles, n=52), and healthy donors ("healthy_ctrl", black circles, n=36). B: Venn diagram of DEGs based on adjusted P-value < 0.05. C, D: Volcano plots show DEGs between TB patients with IH (TB-IH, n=44) and TB patients with diabetes (TB-DM, n=61) compared to TB-only group (n=46) respectively. For visualisation purpose only, dotted lines define the cut-off for DEGs based on absolute[Log2 fold-change]≥ 1 (x-axis) and P-value < 0.05 (y-axis). Venn diagram was generated using ggvenn R package.

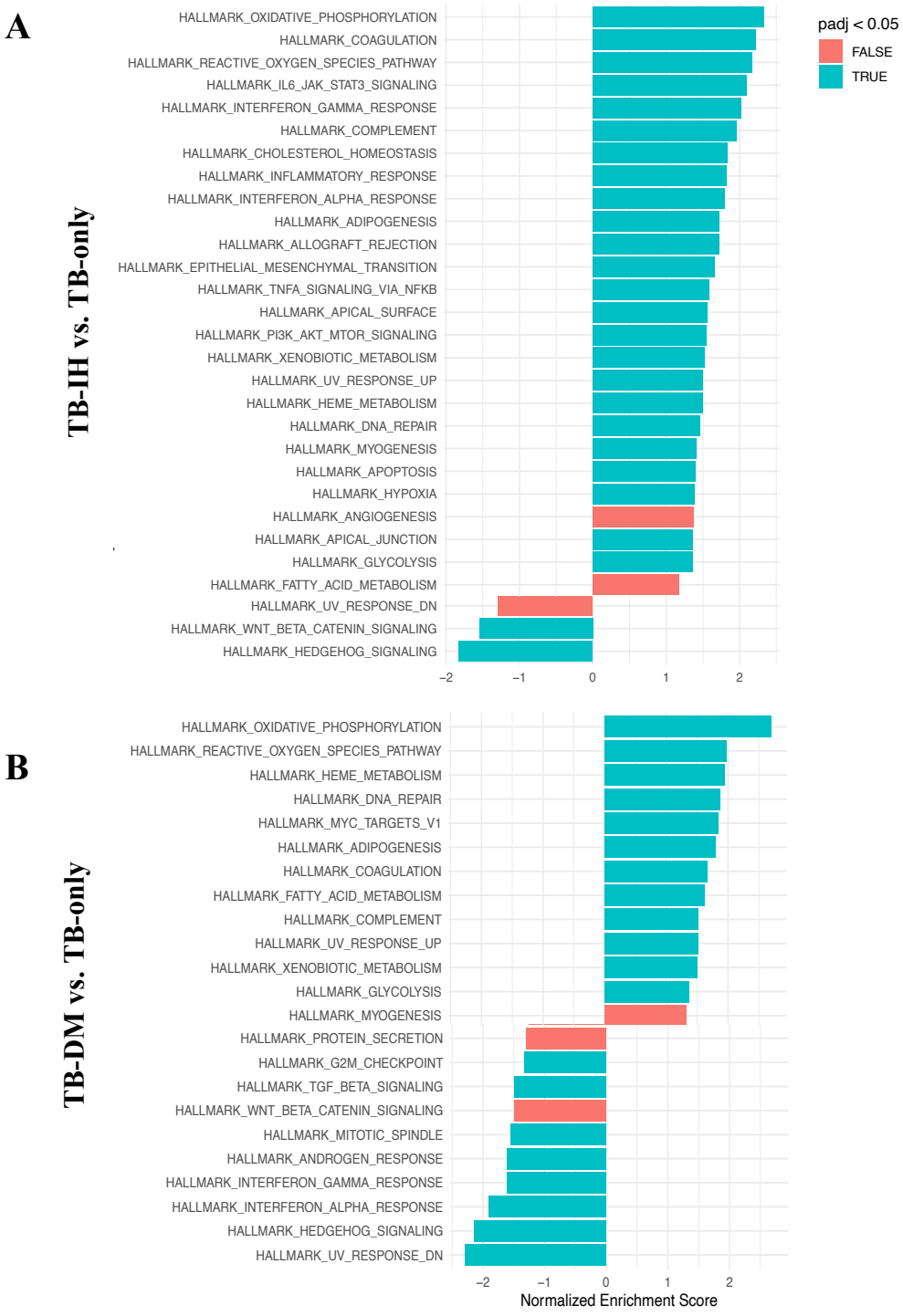

Figure 4.5 Gene set enrichment analysis based on Hallmark gene sets following differential gene expression (DGE) analysis among tuberculosis patients across four study sites. A: TB-IH (n=44) compared to TB-only (n=46). B: TB-DM (n=61) compared to TB-only (n=46). Pathways were deemed significant when adjusted P-value <0.05. Enriched pathways were calculated from DESeq2 test statistics of pre-ranked gene list following DGE analysis using fgsea R package.

4.4.5 Hyperglycaemia and diabetes drive an increased inflammatory immune response in both melioidosis and TB patients

To study the impact of diabetes and intermediate hyperglycaemia on the whole blood transcriptomic of both TB (discovery cohort) and melioidosis, functional pathway analysis was employed following DGE analysis by Reactome and KEGG pathway (absolute[Log2 fold-change]≥1, adjusted P-value < 0.05). Pathways involved in type I immune responses such as interferon signalling, interferon alpha/beta signalling and interferon gamma signalling were up-regulated in all TB groups compared to healthy controls (**Figure 4.6** and **Figure 4.7**). However, anti-viral mechanisms by IFN-stimulated genes, ISG15 antiviral mechanisms, hepatitis C, measles, and creation of C4 and C2 activators pathways were exclusively up-regulated in the TB-only group (**Figure 4.6**). Moreover, pathways classically described as involved in the immune response to viral infections including influenza A and Epstein-Barr virus infection were not up-regulated in the TB-DM group (**Figure 4.7**).

Pathways involving inflammatory immune responses including neutrophil degranulation and platelet degranulation were only up-regulated in TB-DM, TB-IH, and melioidosis. Interestingly, the clotting cascade and binding and uptake of ligands by scavenger receptors pathway were only up-regulated in TB-DM, TB-IH, and melioidosis with T2DM. Whereas, extracellular matrix organisation and cell cycle pathways were exclusively up-regulated in melioidosis. Distinctively, pathways involved in inflammation and immune responses in response to infections including TNF signalling, leishmaniasis, legionellosis, were only up-regulated in melioidosis with T2DM. Lastly, the PI3K-Akt signalling pathway was down-regulated in the TB-IH, TB-DM, and melioidosis with T2DM (**Figure 4.7**).

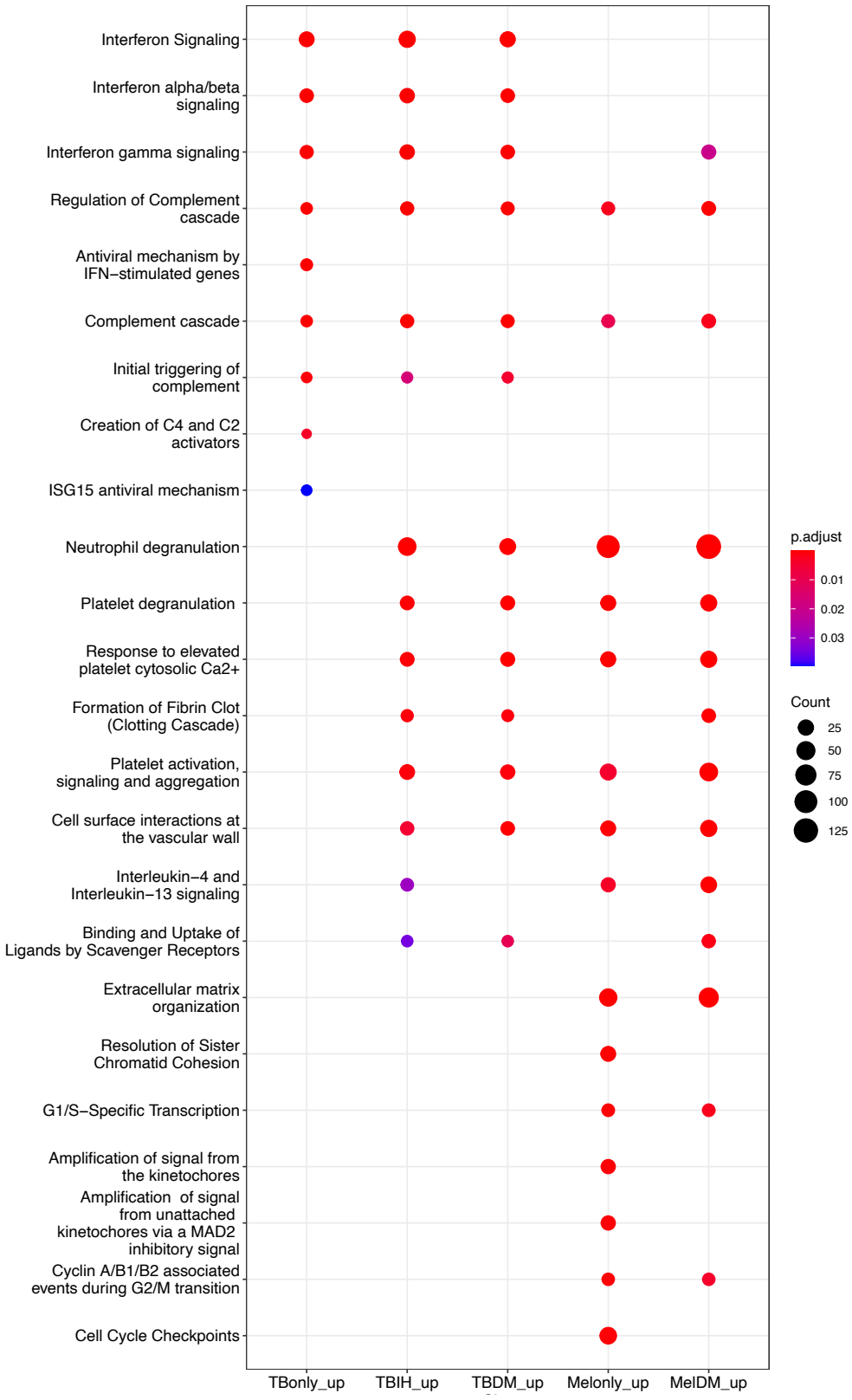

Figure 4.6 Functional pathway analysis based on Reactome gene sets following differential gene expression (DGE) analyses between tuberculosis (TB) cohort (South African cohort) and melioidosis

(**Chapter 3**). The pathways were derived from separate DGE analyses among TB and melioidosis cohorts compared to their respective control cohorts. The gradient colour bar corresponds to the adjusted P-value. The size of each term is indicated by representative counts. Differentially expressed gene were pre-filtered based on a cut-off of absolute[Log2 fold-change] ≥1 and adjusted P-value <0.05. TBonly_up, TBIH_up, and TBDM_up = up-regulated genes following DGE analysis among TB without diabetes, TB with intermediate hyperglycaemia, and TB with diabetes compared to healthy control respectively. Melonly_up and MelDM_up = up-regulated genes following DGE analysis among melioidosis without diabetes and with diabetes compared to healthy control respectively.

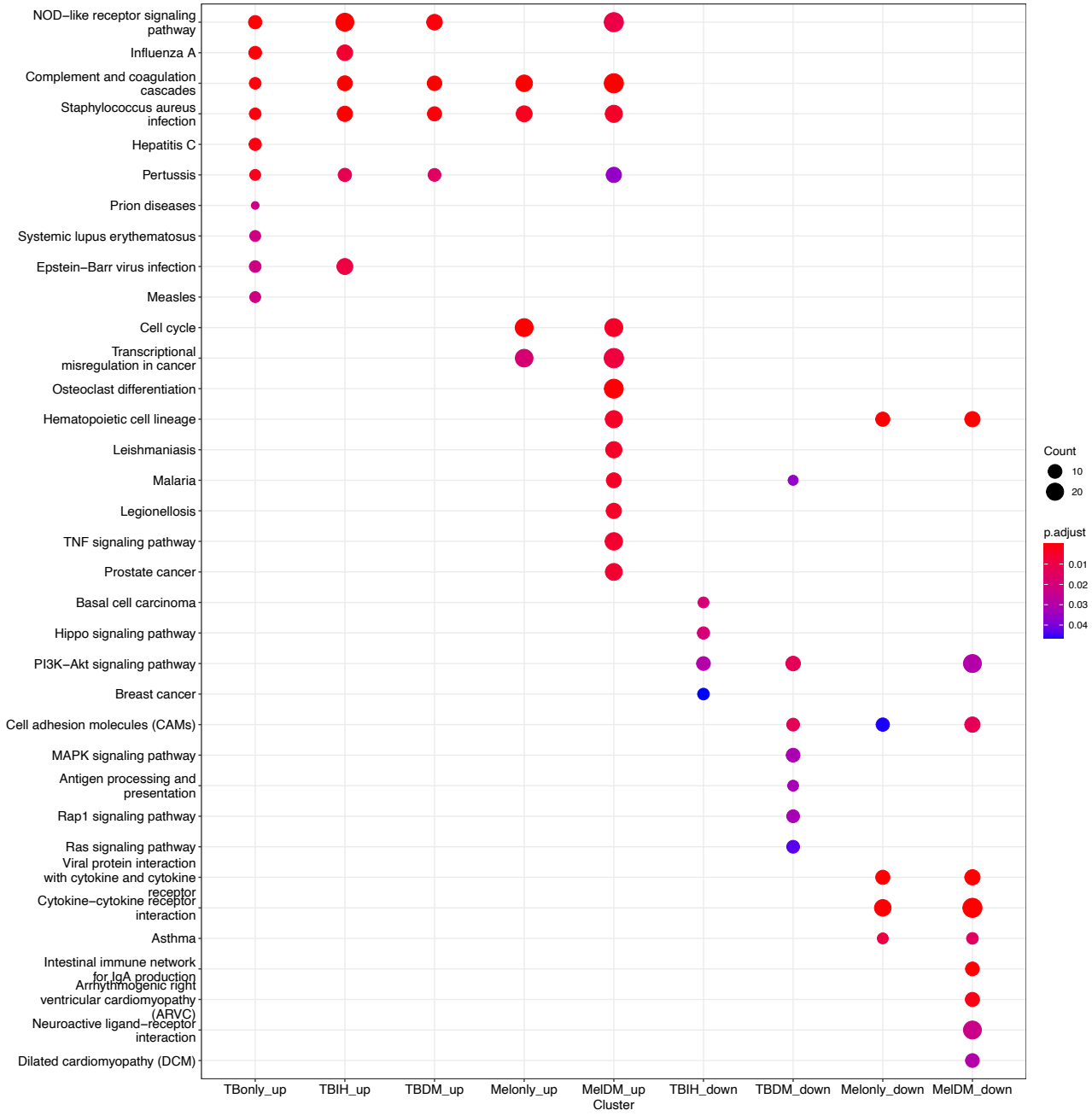

Figure 4.7 Functional pathway analysis based on KEGG gene sets following differential gene expression (DGE) analyses between tuberculosis (TB) cohort (South African cohort) and melioidosis (**Chapter 3**). The pathways were derived from separate DGE analyses among TB and melioidosis cohorts compared to their respective control cohorts. Pathways were derived from differentially expressed genes based on a cut-off of absolute[Log2 fold-change]≥1 and adjusted P-value <0.05. The gradient colour bar corresponds to the adjusted P-value. The size of each term is indicated by representative counts. TBonly_up, TBIH_up, and TBDM_up = up-regulated genes following DGE

analysis among TB without diabetes, TB with intermediate hyperglycaemia, and TB with diabetes compared to healthy control respectively. TBonly_down, TBIH_down, and TBDM_down = down-regulated genes following DGE analysis among TB patients without diabetes, TB patients with intermediate hyperglycaemia, and TB patients with diabetes compared to healthy control respectively. Melonly_up and MelDM_up = up-regulated genes following DGE analysis among melioidosis without diabetes and with diabetes compared to healthy control respectively. Melonly_down and MelDM_down = down-regulated genes following DGE analyses among melioidosis without diabetes and melioidosis with diabetes compared to healthy control respectively.

4.4.6 Co-expressed gene modules enriched with innate-driven inflammatory immune responses are associated with diabetes in TB patients

To identify co-expressed gene modules and hub genes that are associated diabetes, WGCNA was performed in the TB-DM and TB-only cohorts. Firstly, a sample dendrogram was constructed using normalised variance-stabilising transformed data (15, 325 features) to identify potential outliers (**Figure 4.8A**). One outlier from the TB-DM group was removed and the sample dendrogram was constructed on the remaining 106 participants with corresponding clinical traits (**Figure 4.8B**). Secondly, a power of $\beta = 14$ was chosen (soft-threshold $R^2 = 0.87$ and mean connectivity = 80) in order to achieve a scale-free network (**Figure 4.8C**). Subsequently, a total of 23 co-expressed gene modules (module eigengene, ME) were identified based on dissimilarity of topological overlap matrix via hierarchical clustering using Dynamic Tree Cut method (**Figure 4.8D, 4.9**). Module-trait relationship analysis identified significant correlations of ME darkturquoise with HbA1c level and diabetes status (indicated in a red box) (**Figure 4.9**). Moreover, ME magenta was significantly correlated with BMI (indicated in a red box). Module eigengene (ME) is considered as a representative expression profile or first principal component of a particular co-expressed gene module. MEs with significant correlations to diabetes were compared

between TB-DM and TB-only groups. ME darkturquoise was significantly higher in TB-DM compared TB-only group. In contrast, ME purple, lightyellow, lightcyan, darkred, and lightgreen were significantly higher in the TB-only group (**Supplementary Figure 4.7**). Functional analysis based on Reactome and Gene Ontology gene sets within ME darkturquoise (correlated with either diabetes status or continuous HbA1c level) identified enriched pathways involved in defence against infections driven by the innate immune compartment such as neutrophil degranulation, antimicrobial peptides, and defence response to bacterium (**Figure 4.10**). On the other hand, pathways involved in erythrocyte development and metabolism were enriched in ME magenta (correlated with BMI).

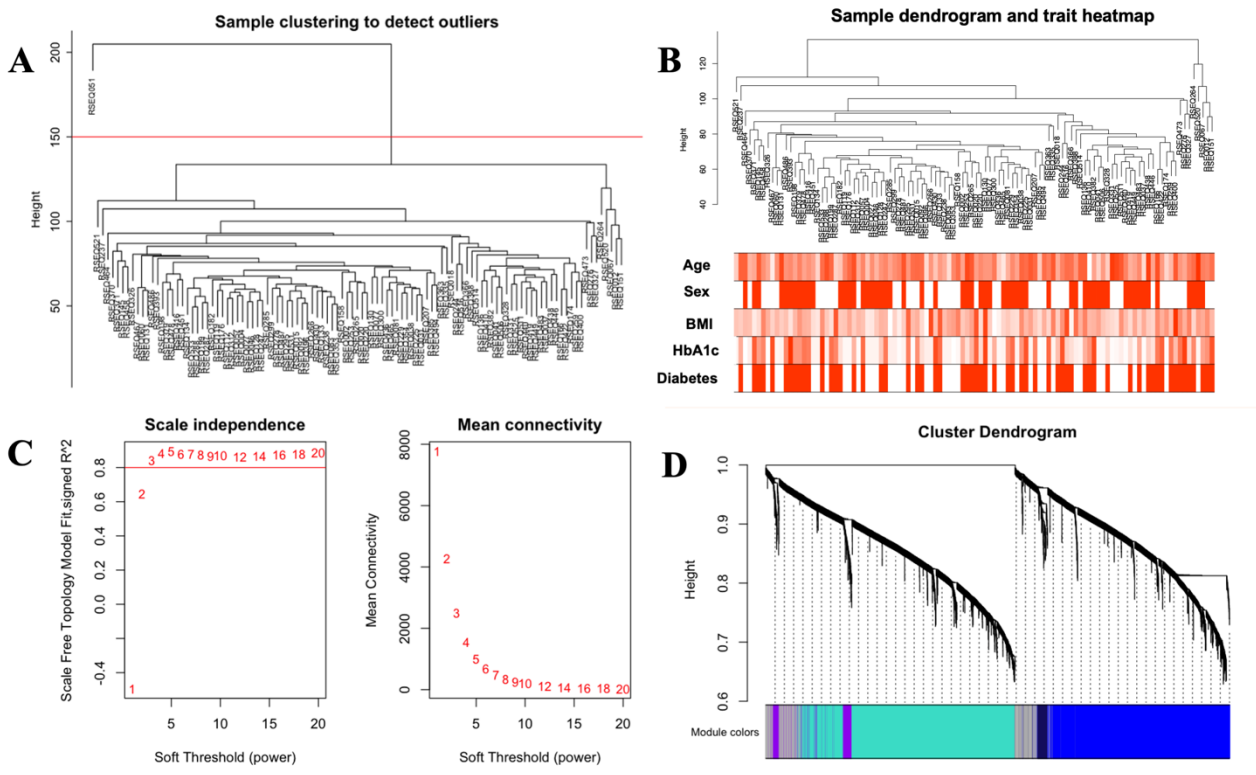

Figure 4.8 Weighted gene co-expression network analysis workflow in 107 TB patients with diabetes (n=61) and without diabetes (n=46). A: Sample dendrogram identified one outlier and removed. B: Sample dendrogram with corresponding clinical trait heatmap. C: Scale-free network analysis, with scale independence plot indicates scale free topology model fit (R^2) and mean connectivity plot with soft threshold on x-axis. Here, a power of β=14 resulted in soft-threshold R^2 = 0.87 indicating a scale-free topology obtained. D: Cluster dendrogram of co-expressed gene modules by a hierarchical clustering of genes based on topological overlap and assigned module colours underneath.

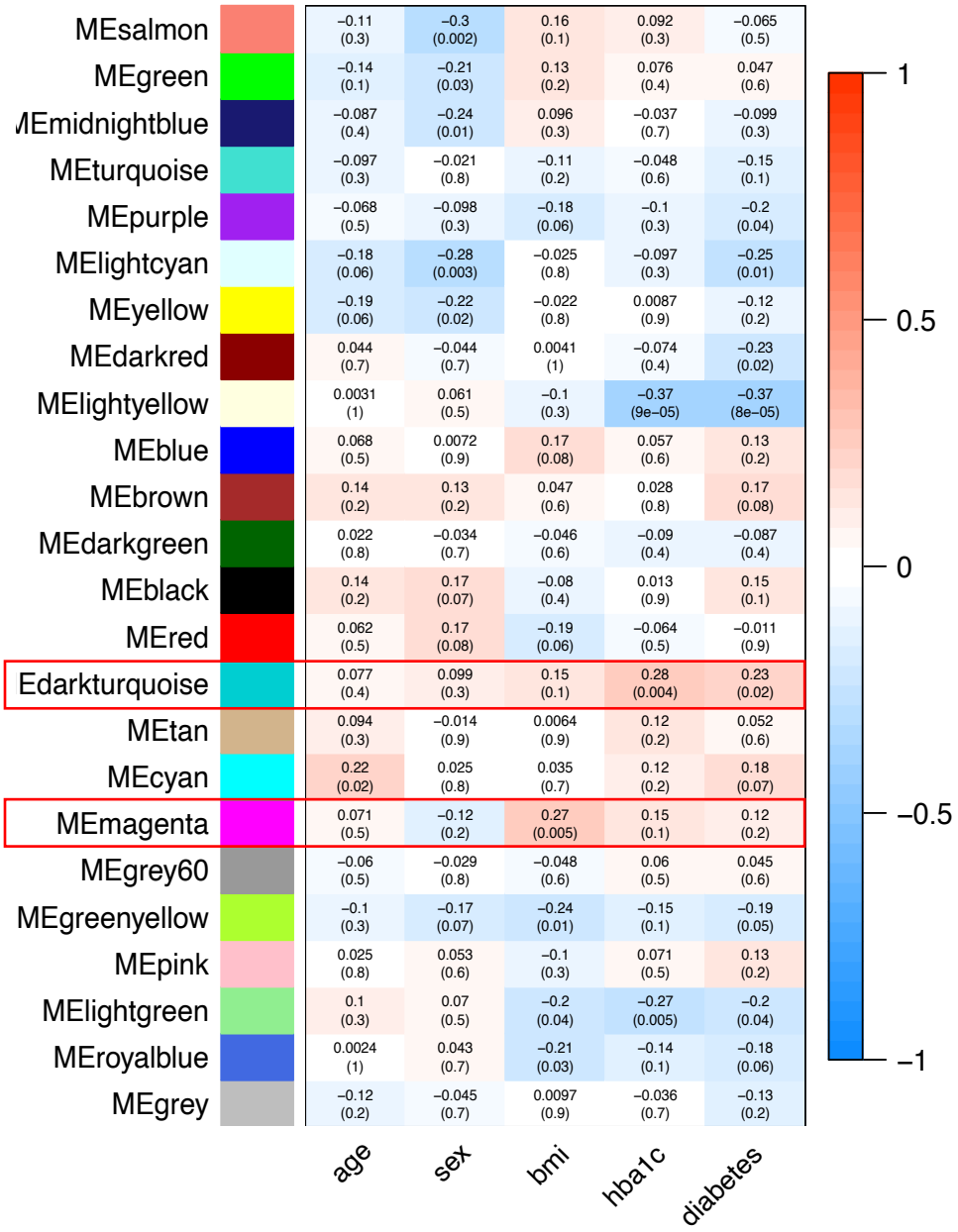

Figure 4.9 Module-trait relationship analysis in tuberculosis (TB) patients with (n=60) and without (n=46) diabetes by weighted gene co-expression network analysis. Each row represents an assigned module eigengene (ME) and each column represents a clinical trait of interest, with corresponding Pearson's correlation coefficient between each ME-trait pair displayed with P-value in parenthesis. The gradient colour bar indicates the degree of positivity (maximum +1, red) / negativity (minimum -1, blue) for the Pearson's correlation coefficient. Clinical traits include age (in years, continuous variable), sex (binary outcome), body mass index (bmi, percentage of the body mass in continuous variable), HbA1c level (hba1c, percentage of glycated haemoglobin in continuous variable), and diabetes status (binary outcome).

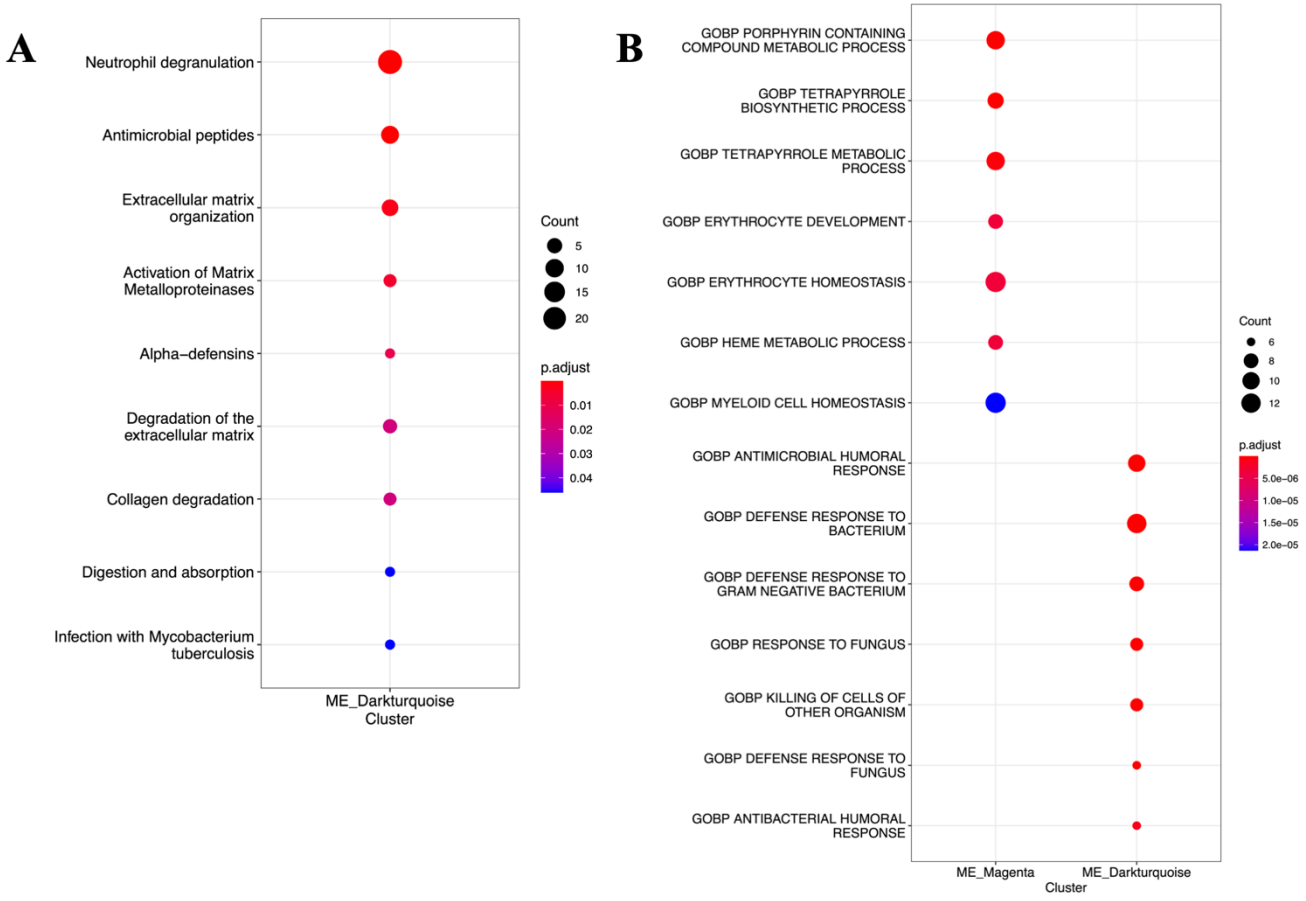

Figure 4.10 Enrichment analysis based on Reactome and Gene Ontology in ME darkturquoise and magenta that were significantly associated with HbA1c level, diabetes status and body mass index identified by module-trait relationship analysis in tuberculosis patients with and without diabetes respectively. A: Enriched pathways based on Reactome genes sets. B: Enriched pathways based on Gene Ontology genes sets. The gradient colour bar corresponds to the adjusted P-value. The size of each term is indicated by representative counts.

4.4.7 Multiple co-expressed gene modules enriched with broad inflammatory immune responses are associated with intermediate hyperglycaemia in TB patients

To identify gene modules and hub genes that are associated intermediate hyperglycaemia, WGCNA was performed for the TB-IH (n=44) and TB-only (n=46) cohorts. Firstly, a sample dendrogram was constructed using a normalised variance-stabilising transformed

data (15,058 features) to identify potential outliers (**Figure 4.11A**). One outlier from the TB-IH group was removed and the sample dendrogram was constructed on the remaining 89 participants with corresponding clinical traits (**Figure 4.11B**). Secondly, a power of $\beta = 14$ was chosen (soft-threshold $R^2 = 0.82$ and mean connectivity = 74) in order to achieve a scale-free network (**Figure 4.11C**). Subsequently, a total of 19 co-expressed gene modules (module eigengene, ME) were identified based on dissimilarity of topological overlap matrix via hierarchical clustering using Dynamic Tree Cut method (**Figure 4.11D, 4.12**). Module-trait relationship analysis identified significant correlations of ME pink, magenta, and tan (indicated in a red box) with HbA1c level (**Figure 4.12**). Moreover, ME tan was significantly correlated with IH status along with ME yellow (indicated in a red box). On the other hand, ME purple was correlated with BMI (indicated in a red box). MEs with significant (positive and negative) correlations to intermediate hyperglycaemia were compared between TB-IH and TB-only groups. ME magenta, yellow and tan were significantly higher in TB-IH compared TB-only group. Functional analysis based on Reactome gene sets in ME pink, magenta, and yellow (correlated with HbA1c) identified enriched pathways involved in pro-inflammatory immune responses such as neutrophil degranulation, interferon signalling, antigen presentation, signalling by interleukins, inflammasomes, and phagocytosis (**Figure 4.13**). Furthermore, pathways involved in platelet degranulation and coagulation were enriched in ME tan and yellow (correlated with IH). Similarly, ME purple (correlated with BMI) was enriched with neutrophil degranulation, antimicrobial peptides, and heme biosynthesis. In contrast, ME red, lightyellow, and salmon were significantly higher in the TB-only group (**Supplementary Figure 4.8**). Interestingly, module enrichment based on KEGG and Gene ontology identified pathways enriched in B cell signalling, natural killer cells and leukocytes mediated

cytotoxicity in ME lightyellow and red which were negatively correlated with TB-IH patients (**Supplementary Figure 4.9**).

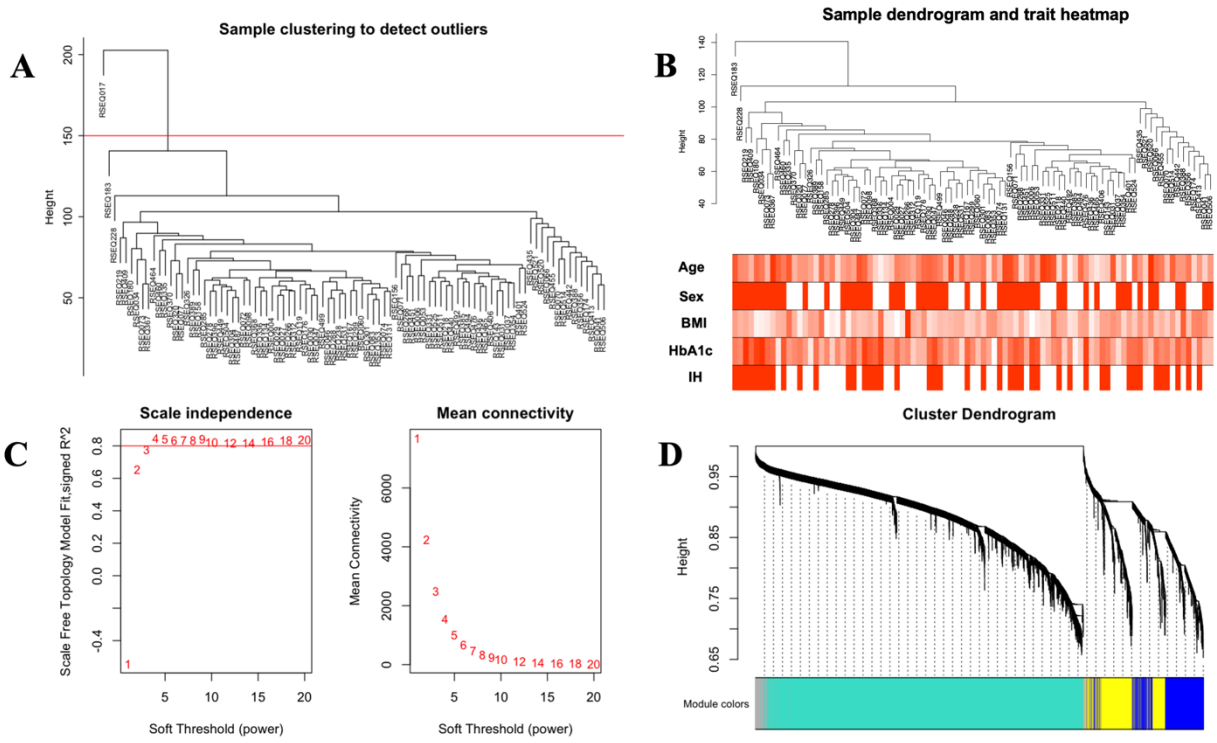

Figure 4.11 Weighted gene co-expression network analysis workflow in 90 tuberculosis patients with and without intermediate hyperglycaemia. A: Sample dendrogram identified one outlier and removed. B: Sample dendrogram with corresponding clinical trait heatmap. C: Scale-free network analysis, with scale independence plot indicates scale free topology model fit (R^2) and mean connectivity plot with soft threshold on x-axis. Here, a power of β=14 resulted in soft-threshold R^2=0.82 indicating a scale-free topology obtained D: Cluster dendrogram of co-expressed gene modules by a hierarchical clustering of genes based on topological overlap and assigned module colours underneath.

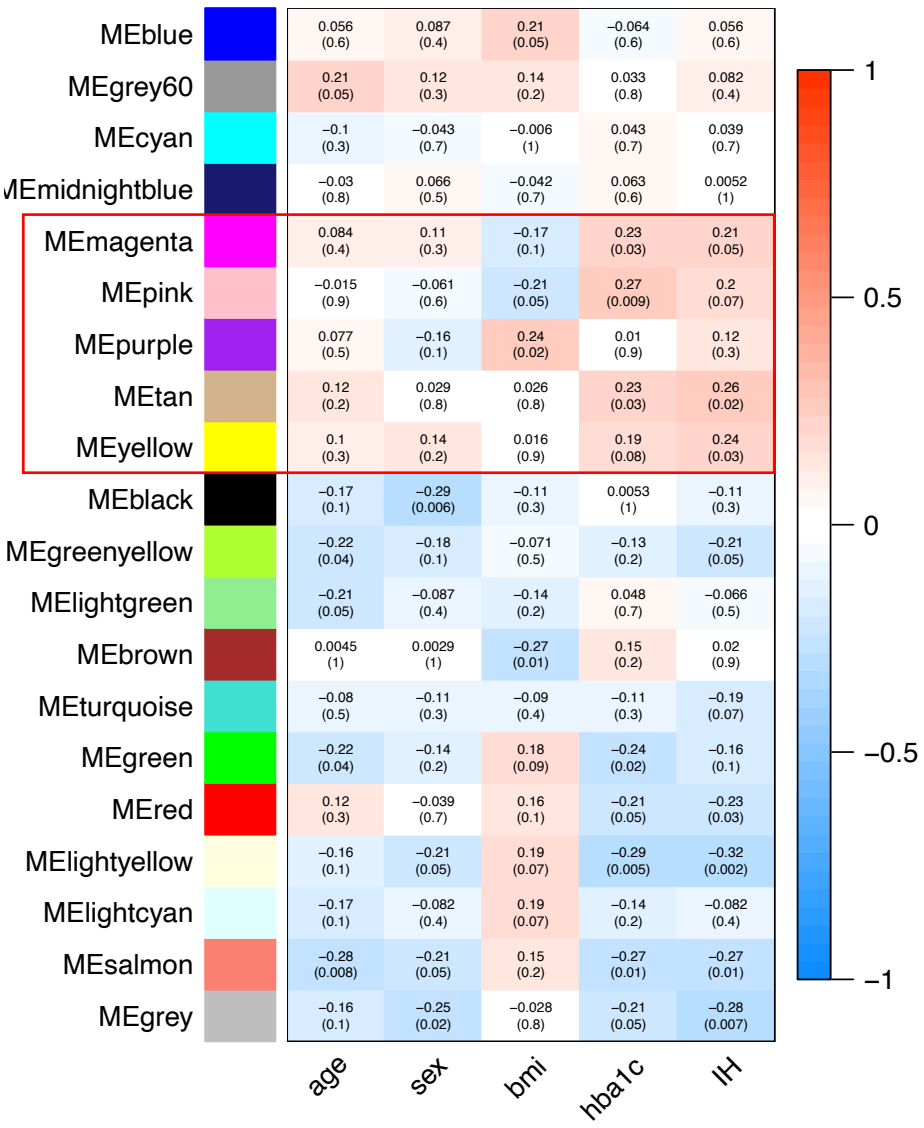

Figure 4.12 Module-trait relationship analysis in tuberculosis (TB) patients with (n=43) and without (n=46) intermediate hyperglycaemia (IH) by weighted gene co-expression network analysis. Each row represents an assigned module eigengenes (ME) and each column represents a clinical trait of interest, with corresponding Pearson's correlation coefficient between each ME-trait pair displayed with P-value in parenthesis. The gradient colour bar indicates the degree of positivity (maximum +1, red) / negativity (minimum -1, blue) for the Pearson's correlation coefficient. Clinical traits include age (in years, continuous variable), sex (binary outcome), body mass index (BMI, percentage of the body mass in continuous variable), HbA1c level (hba1c, percentage of glycated haemoglobin in continuous variable), and intermediate hyperglycaemia status (IH, binary outcome).

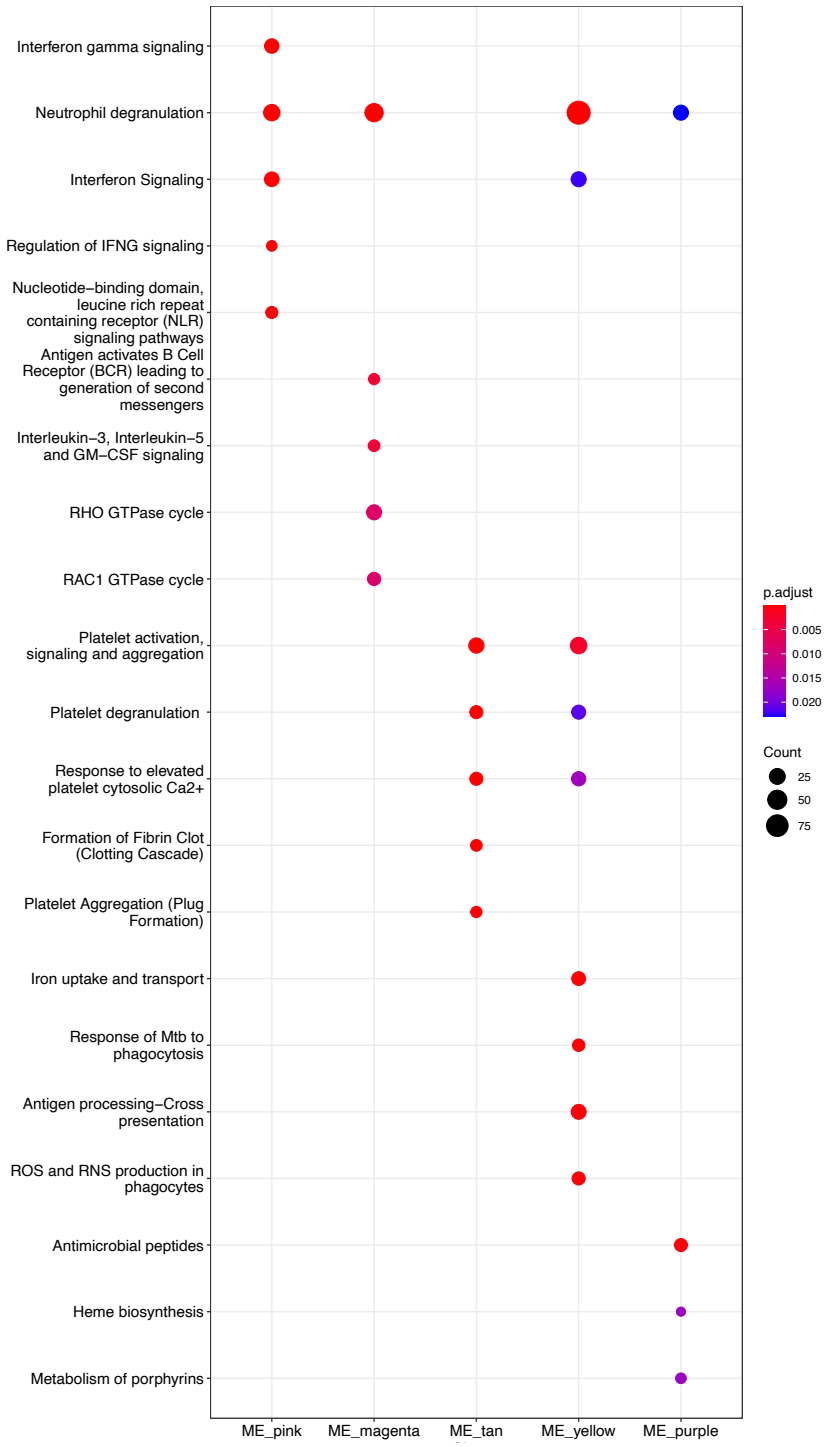

Figure 4.13 Enrichment analysis based on Reactome gene sets in module eigengene (ME) pink, magenta, tan, yellow, and purple that were significantly associated with HbA1c level, intermediate hyperglycaemia status and body mass index identified by module-trait relationship analysis in tuberculosis patients with and without intermediate hyperglycaemia respectively. The top 5 over-

represented pathways are displayed. The gradient colour bar corresponds to the adjusted P-value. The size of each term is indicated by representative counts.

4.4.8 Genes involved in inflammatory immune responses driven by innate immune responses are associated with intermediate hyperglycaemia and diabetes

To identify potential key regulators, the results from supervised (DGE analysis) and unsupervised (WGCNA) approaches were compared using Venn diagram to determine overlapping genes identified by different analyses (**Figure 4.14**). Firstly, 2 hub genes identified in ME darkturquoise were also up-regulated in TB-DM compared to TB-only patients including *CEACAM8* (Carcinoembryonic Antigen-related Cell Adhesion Molecule 8) and *BPI* (Bactericidal Permeability Increasing Protein) (Log2 fold-change ≥0.5 and adjusted P-value <0.05) (**Figure 4.14B**). Secondly, 2 hub genes identified in ME yellow were also up-regulated in TB-IH compared to TB-only patients including *S100A11* (S100 Calcium Binding Protein A11) and *TRAPPC1* (Trafficking Protein Particle Complex Subunit 1) (**Figure 4.15B**). Thirdly, 2 hub genes identified in ME tan that associated with HbA1c, were up-regulated in TB-IH compared to TB-only patients including *TREML1* (Triggering Receptor Expressed on Myeloid Cells Like 1) and *GP9* (Glycoprotein IX Platelet) (**Supplementary Figure 4.10**).

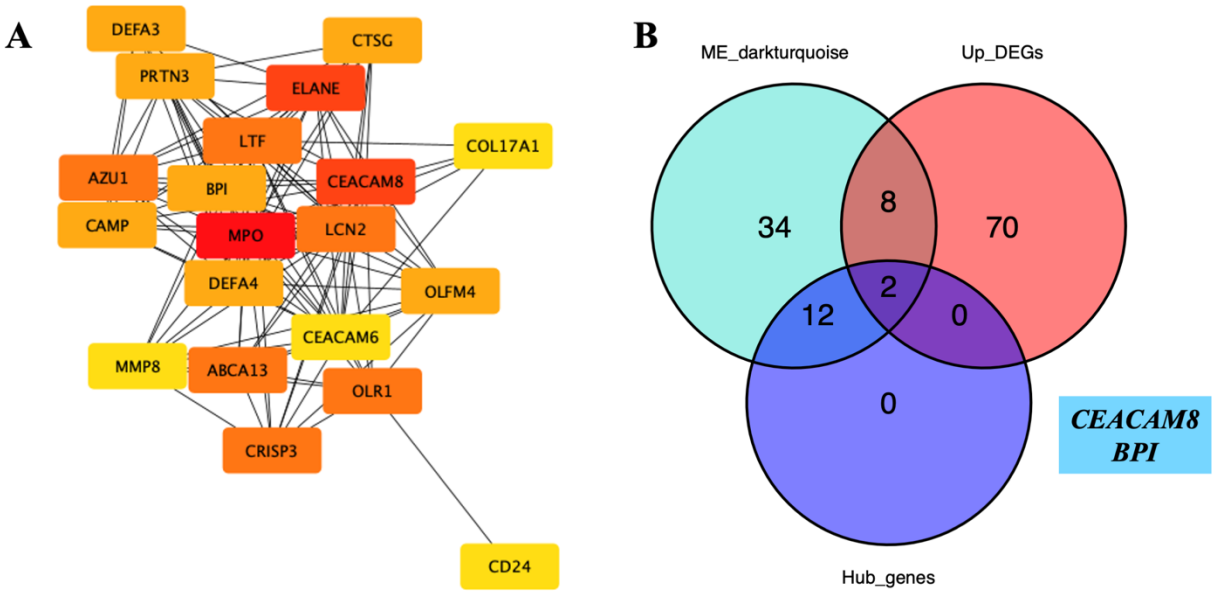

Figure 4.14 Top 20 hub genes with potential regulatory role of host immune response in tuberculosis (TB) patients with diabetes. A: The top 20 hub genes identified in the module eigengene (ME) darkturquoise associated with diabetes status. B: Venn diagram of overlapping differentially expressed genes (DEGs), gene membership of the ME darkturquoise identified by weighted gene co-expression network analysis, and hub genes identified in the ME darkturquoise. DEGs were derived from up-regulated genes between TB patients with and without diabetes based on absolute[Log2 fold-change]≥0.5 and adjusted P-value <0.05 (**Figure 4.4D**). ME darkturquoise was significantly associated with diabetes status by module-trait relationship analysis (**Figure 4.9**). 14 hub genes within ME darkturquoise were derived from Maximal Clique Centrality (MCC) algorithm using CytoHubba plugin on Cytoscape software. MCC scores of hub genes were ranked from high (red) to low (yellow). 6 hub genes with no score of MCC were excluded.

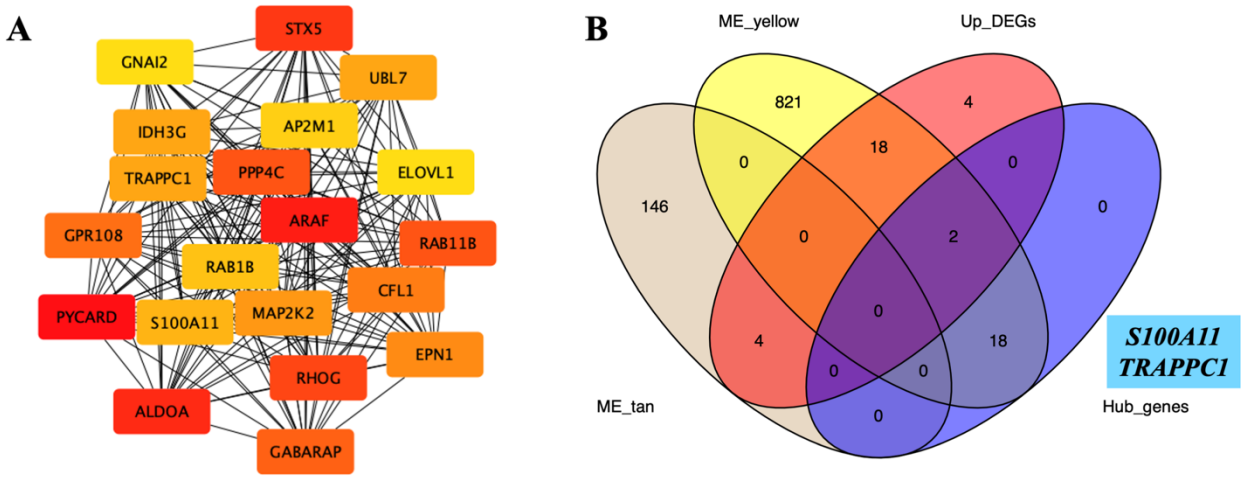

Figure 4.15 Top 20 hub genes with potential regulatory role of host immune response in TB patients with intermediate hyperglycaemia. A: The top 20 hub genes identified in the module eigengene (ME) tan and yellow associated with intermediate hyperglycaemia status. B: Venn diagram of overlapping differentially expressed genes (DEGs, gene membership of the ME tan and yellow identified by weighted gene co-expression network analysis, and hub genes in the ME tan and yellow. DEGs were derived from up-regulated genes between TB patients with intermediate hyperglycaemia and without diabetes based on an absolute[Log2 fold-change]≥0.5 and adjusted P-value <0.05 (**Figure 4.4C**). ME tan and yellow associated with intermediate hyperglycaemia by module-trait relationship analysis (**Figure 4.12)**. 20 hub genes within ME tan and yellow were derived from Maximal Clique Centrality (MCC) algorithm using CytoHubba plugin on Cytoscape software. MCC scores of hub genes were ranked from high (red) to low (yellow).

4.4.9 Increased neutrophils and Th2 cells in TB patients with intermediate hyperglycaemia and diabetes

To estimate the abundance of immune cells associated with intermediate hyperglycaemia and diabetes, whole blood RNA sequencing data were deconvoluted using xCell (*435*). TB-DM and TB-IH patients compared to TB-only group showed significant enrichment of Th2

cells. Moreover, TB-DM showed significant enrichment neutrophils compared to TB-only group (**Supplementary Figure 4.11**).

4.5 Discussion

In this chapter, the impact of diabetes and intermediate hyperglycaemia on the whole blood transcriptome during active TB and melioidosis was studied. Diabetes confers a 3-fold increased susceptibility to develop active TB (*111*), whereas people with diabetes are exceptionally prone melioidosis with a 12-fold increased susceptibility (*20*). In this chapter, the whole blood transcriptome in TB-DM and TB-IH was compared to uninfected non-diabetic healthy individuals. DGE analysis identified a higher magnitude of DEGs in TB-IH, followed by TB-DM and TB-only compared to healthy control. This suggests that altered host immune responses during active TB are influenced by intermediate hyperglycaemic which is considered a pre-diabetic condition (HbA1c level between 5.7% to 6.4%).

The altered transcriptomic profiles in TB-DM and TB-IH relative to healthy subjects include up-regulation of neutrophil degranulation, platelet degranulation, and coagulation. Moreover, deconvoluted whole blood transcriptome analysis identified enriched neutrophils in TB-DM compared to TB-only. Neutrophil functions such as cell migration, phagocytosis, and killing mechanisms have been reported to be compromised in people with diabetes and under hyperglycaemic conditions (*508-510*). Diabetes is a dependent risk factor of micro- and macrovascular complications such as atherosclerosis, nephropathy, and myocardial infarction (*321, 511*). During neutrophil activation, toxic granules, ROS, and pro-inflammatory cytokines are released in response to stimuli or under stress (*512*). In diabetes, neutrophils are more susceptible to degranulation, in which cell mediators such as NE and MPO are released (*513*). Many studies have shown increased MPO levels in T2DM patients which are associated with increased risk of diabetes-induced complications such as coronary artery disease and atherosclerosis (*514-517*). Neutrophil-derived mediators including NE

and cathepsin G have been found to inhibit activation of T lymphocytes, in which NE is able to cleave IL-2 receptor and cathepsin G can deplete IL-6 receptor preventing activation of T lymphocytes (*518*). Moreover, arginase I, another neutrophil-derive granule was found to deplete L-arginine and can cause inactivation of T cell through the CD3ζ mediated T cell signalling cascade (*519*). Altogether, increased neutrophil degranulation could be a key mechanism leading to a compromised adaptive immune response during active TB in those with diabetes and intermediate hyperglycaemia, and disordered neutrophil responses to infection could contribute to the known vascular complications of diabetes.

Platelet degranulation is an innate defence mechanism in response to tissue injury, releasing different types of cell mediators such as fibrinogen, von Willebrand factor (vWF), adenosine di/triphosphate (ADP/ATP), and serotonin (*520*). Activated platelets undergo morphological changes and release of other granules which promote coagulation such as fibrinogen and vWF (*521*). Other cell surface receptors and cytokines such as P-selectin, β2/β2 integrin and CXCL4 (Platelet Factor 4, PF4) were found to promote inflammatory immune responses by recruiting more leukocytes to the site of injury, further exaggerating inflammation (*522, 523*). As already mentioned, patients with T2DM are highly susceptible to the development of macrovascular complications such as atherosclerosis, thrombosis, and carotid artery (*524-526*). Interestingly, thrombin activation may induce increased inflammatory response by cleaving pro-IL-1α into an active form (IL-1α) leading to recruitment of leukocytes, and activation of pro-inflammatory Th17 cells (*527, 528*). In this chapter, TB-DM and TB-IH patients show up-regulation of *IL1R2*, a decoy receptor of IL-1 indicating a counterbalanced anti-inflammatory mechanism against IL-1 activity (*529*).

Moreover, neutrophil-derived genes such as *S100A8, CEACAM1,* and *CD177* are mutually up-regulated in TB-DM and TB-IH compared to healthy controls. *S100A8* encoding S1000

calcium-binding proteins A8 secretes from myeloid cells primarily neutrophils and monocytes upon activation. S100A8 and S100A9 form a heterodimer and exerts multiple biological activities during inflammatory immune responses (*237*). Increased production of S100A8/A9 enhances production of thrombopoietin, which in turn promotes thrombocytosis and atherosclerosis (*530, 531*). In diabetes patients, elevated plasma S100A8/A9 and high HbA1c level are correlated with reticulated thrombocytosis (*526*). Immune cell profiling by xCell identified enriched Th2 cells in TB-DM and TB-IH patients compared to TB-only. Moreover, functional pathway analysis identified up-regulation of IL-4 and IL-13 signalling in TB-IH patients. There is evidence that Th2 cytokines such as IL-4 and IL-13 divert the protective Th1 immune response against Mtb infection, resulting in uncontrolled infection and progression to active TB (*532, 533*).

Type I immune responses, in particular IFN-γ, are essential for controlling the intracellular infection during active TB and melioidosis (*76, 534*). In TB, CD4+ T cells are the primary source of IFN-γ during adaptive immune response against Mtb infection (*535*). This reflects the important role of cellular immunity mediated by CD4+ T cell against Mtb infection, in which HIV+ individuals are exceptionally susceptible to TB. On the other hand, type I immune response by CD4+ T cells during melioidosis may be compensated by other immune cells in particular CD8+ T cells (*76*), in which one study reported poor evidence of enhanced susceptibility to melioidosis in HIV+ population (*502*). Furthermore, having HIV during melioidosis is not associated with increased disease severity, however, the study might be underpowered (*502*).

This chapter confirms that whole blood transcriptomic profiles from TB patients were dominated by interferon signalling pathways and complement cascade. However, TB-DM

and TB-IH patients show reduced expressions of interferon signalling genes and pathways, particularly interferon stimulated genes compared to TB-only patients. Moreover, TB-DM and TB-IH show up-regulated pathways involved in innate inflammation such as neutrophil and platelet degranulation and coagulation. Melioidosis patients show similar transcriptomic profiles. Pathways involved in inflammatory immune responses such as neutrophil degranulation, platelet activation, and complement cascades were highly up-regulated in melioidosis regardless of diabetes status. Interestingly, melioidosis with T2DM shows up-regulation of interferon-γ and NOD-like receptor signalling pathways which was absent in melioidosis without T2DM. Moreover, KEGG pathways involved in inflammatory immune responses such as TNF signalling, immune response to leishmaniasis and legionellosis were up-regulated in melioidosis with T2DM reflecting excessive an inflammatory immune response in melioidosis with T2DM.

Interestingly, pathways involved in coagulation (formation of fibrin clot) and binding and uptake of ligands by scavenger receptors were up-regulated in TB-DM, TB-IH, and melioidosis patients with T2DM. Under hyperglycaemic condition, scavenger receptors (i.e. class A scavenger receptor) and proinflammatory cytokines (IL-6 and IL-12) are highly expressed in dendritic cells and macrophages, leading to increased uptake of oxidised low-density lipoproteins that initiate local inflammatory response, and development of atherosclerosis (*536, 537*).

The phosphatidylinositol 3-kinase (PI3K)-Akt signalling pathway was mutually down-regulated in TB-DM, TB-IH, and melioidosis patients with T2DM. The PI3K-Akt signalling pathway regulates many cellular functions such as cell growth and proliferation, glucose metabolism, apoptosis, and immune response (*538*). Insulin resistance, hyperglycaemia and

excess free fatty acids (FFAs) have been linked to dysregulation of the PI3K-Akt signalling pathway (*539*). For example, FFAs are able to inhibit activation of insulin pathway, but activate protein kinase C which triggers the NK-κB pathway (*540*). The latter pathway may play a major role in increased inflammatory immune response in diabetes (*541*). A *vitro* study of the PI3K-Akt signalling pathway in human endothelial model under hyperglycaemia identified reduced activity of the PI3K-Akt signalling pathway, reduced proliferation, and increased apoptosis of endothelial cells (*542*). Similar observation in diabetes and high-fat diet model using pigs identified decreased phosphorylation of Akt related signalling, but increased activation of NF-κB and apoptosis in those that developed advanced atherosclerosis (*543*).

The unsupervised analysis approach by WGCNA identified one co-expressed gene module, ME darkturquoise which was significantly correlated with diabetes status and HbA1c level in TB-DM patients. Two hub genes including *CEACAM8* and *BPI* were identified and differentially expressed in TB-DM compared to TB-only. *CEACAM8* (Carcinoembryonic Antigen-Related Cell Adhesion Molecule 8) encodes a cell adhesion module (CD66b) which is highly expressed on neutrophils during activation i.e. degranulation and production of reactive species (*544*) and was linked to increased disease severity and poor outcome in inflammatory diseases and acute infections (*544-546*). Several studies have demonstrated that expression of CD11b on monocytes, together with CD66b on neutrophils, are increased in diabetes patients compared to healthy donors (*547, 548*). The increased cell adhesion molecules on neutrophils may be associated with increased risk of developing diabetes-related complications i.e. atherosclerosis (*547*).

BPI encodes Bactericidal Permeability Increasing Protein (BPI) which is found in the azurophilic granules of neutrophils and has binding specificity and neutralisation activity against lipopolysaccharide (LPS) from Gram-negative bacteria (*549*). In TB, BPI can recognise lipoarabinomannan (LAM) of Mtb which shares some similar properties to LPS, thus BPI-mediated immune response to Mtb can be detectable in TB patients (*550-552*). BPI has regulatory roles such as induction of apoptosis, inhibition of angiogenesis, and lipid metabolism (*553*). Plasma BPI was found to positively correlate with lipid metabolites in people with glucose intolerance such as total cholesterol, low- and high-density lipoprotein cholesterol, and endothelial-dependent vasodilation (*554*). A study in patients with myocardial infarction identified significant increased plasma BPI along with inflammatory markers such as IL-1β, MPO, and S100A8/A9 compared to healthy control group and correlated with severity of coronary artery disease (*555*).

Furthermore, WGCNA identified four co-expressed gene module, ME tan and yellow, pink, and magenta which were positively associated with intermediate hyperglycaemia status and HbA1c level in TB patients respectively. Four potential regulators including *S100A11, TRAPPC1, TREML1,* and *GP9* were identified in TB-IH compared to TB-only patients. *S100A11* encodes S100 Calcium Binding Protein A11 (Calgizzarin) that is released from neutrophils during NETosis and promotes pro-inflammatory immune responses in rheumatoid arthritis (*556*). Furthermore, pro-inflammatory cytokines such as IL-1β and TNF-α can induce expression of *S100A11* that binds to receptor for advanced glycation end product (RAGE) receptor and activates p38 MAPK signalling pathway (*557*). Binding of S100A11 to RAGE promotes arterial calcification, a hallmark of atherosclerosis in mice model (*558*). *TRAPPC1* encodes Trafficking Protein Particle Complex 1 (TRAPPC1) which is known to participate in protein trafficking between endoplasmic reticulum and Golgi

complex (*559*). *Ex vivo* stimulation of LPS in human macrophages drives up-regulation of *TRAPPC1* genes along with other genes involved in inflammatory immune responses such as *ISG15, IFIT2* and *CXCL10 (560).* As described earlier, the immune response to LPS may indicate LAM-induced immune response. The up-regulation of *TRAPPC1* thus reflects host immune response against LAM during active TB. However, a role of *TRAPPC1* in diabetes during infection remains to be further elucidated. *TREML1* encoding for Triggering Receptor Expressed on Myeloid Cells Like 1 or TREM-Like transcript 1 (TLT-1) is a type 1 single Ig domain receptor expressed in megakaryocytes and on alpha-granule membranes of platelet, translocating to membranes of platelet during platelet activation. Moreover, TLT-1 and its soluble form have anti-inflammatory properties, dampening leukocyte activation and promoting platelet aggregation in sepsis (*561, 562*). Expression of TLT-1 was shown to be a more sensitive marker of platelet activation than its co-expressed adhesion molecule, P-selectin (CD62P) (*563*). Increased platelet activation is a hallmark of diabetes and its related complications such as atherosclerosis and coronary artery disease. High levels of P-selectin and soluble TLT-1 were found in the patients with acute myocardial infarction compared to healthy control group (*564*). One study identified increased expression of TLT-1 on monocytes during active TB and could induce platelet-monocyte aggregates (PMAs) and pro- and anti-inflammatory cytokines including IL-1β, IL-6 and IL-10 from B cells (*564*). *GP9* encodes Glycoprotein IX Platelet (CD42a) highly expressed on platelet during activation and adhered to blood vessels via binding to vWF (*565*). Like other platelet related genes, the increased expression of *GP9* may indicate hyper-coagulation of platelets in TB-IH patients and an increased risk of developing diabetes-related complications as discussed earlier. Moreover, a direct interaction between activated platelet and lymphocytes impacts lymphocyte functions under different conditions (*566*). A study in multiple sclerosis and

experimental autoimmune encephalitis in mice model identified reduced IFN-γ production, CD4 T cell activation, and proliferation in platelet-T-cell aggregate condition (*567*).

In summary, TB patients with diabetes and intermediate hyperglycaemia exhibit reduced interferon response, but increased inflammatory responses compared to TB without diabetes, with key dysfunctions of neutrophil function, clotting cascades and platelet function linked to well-described diabetes-induced complications. The reduced interferon immune response in TB patients with diabetes could be a potential underlying mechanism of increased susceptibility to Mtb infection. On the other hand, melioidosis is an acute infection where sepsis is common. As expected, the inflammatory immune response, in particular neutrophil degranulation, extracellular matrix organisation, coagulation, and platelet activation pathways, is more pronounced in melioidosis compared to TB. However, the impact of diabetes on the whole blood transcriptome during melioidosis may be overwhelmed by non-specific inflammatory immune response and confounded by other co-morbidities as described in **Chapter 3**. Increased pro-inflammatory immune responses such as neutrophil degranulation, coagulation and platelet degranulation were observed in TB patients with diabetes compared with no diabetes. Probable underlying mechanisms of increased susceptibility to infections may include immunomodulation by inflammatory mediators, compromised function of innate immune cells particularly neutrophils, and dysregulation of the cellular immune response.

Chapter 5: What are the transcriptomic profiles associated with melioidosis and poor outcomes from melioidosis during community-acquired infection in Northeast Thailand?

5.1 Introduction

Melioidosis remains a common cause of community-acquired infection in Northeast Thailand, with infection usually associated with the presence of at least one risk factor. The most common comorbidities are hypertension, diabetes, and chronic kidney disease (*192, 568*). Sepsis is common in melioidosis, with around 20% of patients developing septic shock and the hospitalised case fatality rate in endemic areas can exceed 50% despite appropriate treatment (*10, 468*). Sepsis is defined as life-threatening organ dysfunction caused by a dysregulation of host immune responses to infection (*182*). A prediction of global incidence and mortality caused by sepsis in 2017 reported almost 50 million cases and sepsis-related death accounted for 11 million deaths (~20% mortality). Strikingly, 85% of all sepsis cases occurred in low- and middle-income countries (*183*). The high mortality rate in resource-limited settings remains challenging for managing community-acquired sepsis.

The majority of melioidosis cases present to the hospital with acute infection, and the clinical presentations of melioidosis are broad. Pneumonia and bacteraemia are the most common manifestations accounting for 60% of all cases (*10*). In 2018, a 4-year clinical epidemiology study of community-acquired infection and sepsis in Northeast Thailand (Ubon-Sepsis) (*192*) enrolled almost 5,000 patients with suspected infection, of which 71% met criteria for sepsis. In this cohort, Bp was the second commonest cause of community-acquired bacteraemia after *E. coli*. Likewise, in 2021, a study by *Somayaji et al.* (*194*) identified Bp

as the second commonest cause of community-acquired bacteraemia in Northeast Thailand with a 66% 28-day mortality.

The host immune response during sepsis is heterogeneous and complex, and concomitant hyper- and hypo-inflammation may occur simultaneously (*569, 570*). Interestingly, population surveillance studies have revealed that most people who live in melioidosis-endemic areas such as Northeast Thailand develop a serological response to Bp (*571, 572*). However, people are most likely to acquire clinical melioidosis when they have the well-defined risk factors or due to a genetic predisposition (*65, 69, 573*). Host genetic pre-disposition is associated with increased susceptibility to melioidosis, disease severity and outcome. People with polymorphisms of TNF (TNF2 allele) are more susceptible to melioidosis. Moreover, melioidosis patients who did not survive show increased frequency of the TNF2 allele (*65*). Genetic variations in TLR4 are associated with increased susceptibility to melioidosis (*69*). In contrast, melioidosis patients with hypofunctional TLR-5 and NLRC4 variants demonstrate a reduced inflammatory immune response and an association with survival (*573, 574*). Therefore, pre-existing comorbidities and genetic predisposition play a pivotal role in enhanced host susceptibility to melioidosis and worse outcome.

Bacterial culture remains the gold standard for diagnosis of melioidosis; however, this takes several days. Most studies enrol participants following culture-confirmed melioidosis, therefore the host immune response close to disease onset is not typically captured. Moreover, transcriptomic signatures during sepsis are temporal and dynamic during the course of disease (*297, 575*). Hence, there are gaps between disease onset and how it determines clinical outcomes in melioidosis. Previous studies using whole blood transcriptomic approaches identified up-regulated inflammatory-related pathways such as

inflammation, interferon-inducible genes, and neutrophils in melioidosis in comparison to healthy controls (*100, 101*).

In this chapter, whole blood bulk RNA sequencing data was analysed from patients with community-acquired infections enrolled in the Ubon-Sepsis study. This was a prospective observational study conducted between 2013 and 2017 in a single centre study in Northeast Thailand. The study examined the clinical epidemiology and outcomes of patients within 24 hours of hospital admission with community-acquired infection. In this study, the largest whole blood RNA sequencing to date was performed with melioidosis patients enrolled within 24 hours after hospital admission. I hypothesised that the host immune response is dysregulated in fatal melioidosis, and that the transcriptomic signature associated with fatal cases can be used to predict the patients at high risk of death. In addition, I hypothesised that the transcriptomic signature of melioidosis is distinct from other community-acquired infections. Hereby, I aimed to investigate the whole blood transcriptomic profiles associated with fatality in melioidosis and the signature of melioidosis compared to other infections in the same study setting.

5.2 Specific objectives

1. To investigate the whole blood transcriptomic profiles associated with fatal melioidosis compared to those who survived.
2. To identify the pathways and upstream regulators associated with fatal melioidosis that are responsible for deleterious host immune responses.
3. To investigate the whole blood transcriptomic profiles associated with melioidosis compared to other community-acquired infections.

5.3 Materials and Methods

5.3.1 Study design, ethical approval, and participant enrolment

This chapter used whole blood (leukocyte) transcriptomic data generated from a prospective observational study conducted between 2013 and 2017 at Sunpasitthiprasong Hospital, Ubon Ratchathani, Thailand (Ubon-Sepsis, ClinicalTrials.gov identifier, NCT02217592). The study protocol was approved by the ethics committees of the Faculty of Tropical Medicine, Mahidol University (MUTM2012-024-01); Sunpasitthiprasong Hospital, Ubon Ratchathani (039/2556), the Oxford Tropical Research Ethics Committee (OXTREC172-12) and the University of Washington Institutional Review Board (42988). The study was conducted according to Good Clinical Practice, Declaration of Helsinki and all subjects gave written informed consent (*192*).

Participants 18 years of age and older who demonstrated at least three systemic manifestations of infection according to the criteria listed on the 2012 Surviving Sepsis Campaign were enrolled into the study and blood samples were collected (*576*). The transcriptomic study was performed on random samples selected from each of the following groups of patients in the Ubon-Sepsis study: (A) patients with melioidosis (as determined by a positive culture for Bp from any clinical specimen (n=164), (B) patients with *E. coli* bacteraemia (n=22), (C) patients with *S. aureus* bacteraemia (n=16), (D) patients with *Klebsiella pneumoniae* bacteraemia (n=13), or (E) patients with negative blood cultures and no positive culture of any clinical sample for Bp (n=19). For the uninfected control cohort, the study protocol was approved by the ethics committees of the Faculty of Tropical Medicine, Mahidol University (MUTM 2018-046-01) and Udon Thani Hospital Ethics Committee (6/2561). Uninfected non-hospitalised controls included in the study were randomly selected from groups of individuals with (A) diabetes (n=25) or (B) no relevant

medical conditions (n=25) recruited from the outpatient clinic and blood donation centre at Udon Thani Hospital, Udon Thani, Thailand

5.3.2 Sample collection

3 ml whole blood samples from all participants were collected at the time of enrolment into Tempus blood RNA tubes (Applied Biosystems), stored temporarily at -30°C at the study sites and shipped to Mahidol University in Bangkok on dry ice for long-term storage at -80°C. The samples were then shipped to University of Washington on dry ice and stored at -80°C until further processing.

5.3.3 RNA isolation

Total RNA was isolated from whole blood samples using the Tempus Spin RNA Isolation (Applied Biosystems, Thermo Fisher Scientific) by the team at University of Washington. Quantification of isolated RNA was performed using a Nanodrop ND-1000 spectrophotometer. The isolated RNA samples were stored at -80°C until processing.

5.3.4 Library preparation and RNA sequencing

The RNA sequencing was performed at the University of Washington's Northwest Genomics Centre core facility. For each sample, total RNA was normalised to 7.5ng/μL in a total volume of 50μL on the Perkin Elmer Janus Workstation (Perkin Elmer, Janus II). Poly-A selection and cDNA synthesis were performed using the TruSeq Stranded mRNA kit as outlined by the manufacturer (Illumina, cat#RS-122-2103). All steps were automated on the Perkin Elmer Sciclone NGSx Workstation to reduce batch to batch variability and to increase sample throughput. Final RNA sequencing libraries were quantified using the Quant-it dsDNA High Sensitivity assay, and library insert size distribution was checked

using a fragment analyser (Advanced Analytical; kit ID DNF474). Samples where adapter dimers constitute more than 4% of the electropherogram area were not proceeded to sequencing. Technical controls (K562,Thermo Fisher Scientific, cat# AM7832), were compared to expected results to ensure that batch to batch variability was minimised. Successful libraries were normalised to 10nM for submission to sequencing. RNA sequencing was performed using the NovaSeq 6000 system platform.

5.3.5 RNA sequencing analysis workflow

The processing workflow consisted of the following elements: (1) base calls generated in real-time on the NovaSeq6000 instrument (RTA 3.1.5); (2) demultiplexed, unaligned BAM files produced by Picard ExtractIlluminaBarcodes and IlluminaBasecallsToSam were converted to FASTQ format using SamTools bam2fq (v1.4); (3) sequence read and base quality were checked using the FASTX-toolkit (v0.0.13); (4) sequences were aligned to GRCh38 with reference transcriptome GENCODE release 30 using STAR (v2.6.1d). Gene level expression quantification was generated with RNA-SeQC (v2.3.3) and RSEM (v1.3.1). RPKM and TPM for transcript isoforms were quantitated on the merged lane-level data with RSEM (v1.3.1). Gene-level RPKMs were quantitated with RNA-SeQC (v2.3.3) on a standard collapsed reference annotation.

5.3.6 RNA sequencing quality check

Key expression QC metrics were reviewed for outliers. Marginal outliers in quality were identified using the interquartile ranges (IQR; ~1.5 * IQR) and flagged for further review. Principal component analysis (PCA) plots of meta data were generated using PCA analysis and were coloured and visualised using standard PCA plotting packages in Python for detection of confounding effects.

5.3.7 Differential gene expression and functional pathway analysis

A total of 58,673 transcripts were generated from the sequencing. Differential gene expression (DGE) analysis was performed on either a subset of melioidosis patients and controls (n=214) or a complete data set including all patients and controls (N=284). Initially, genes with no counts or lowly expressed with a cut-off of row sum below 500 were removed. Pre-filtered genes (melioidosis subset, n=19,919 features; full data set, n=20,697 feature) were normalised and variance stabilizing transformed using DESeq2 R package for subsequent data analyses and visualization (*392*). To assess the impact of melioidosis on the whole blood transcriptome, multidimensional scaling by principal component analysis (PCA) using the top 1,000 most variable genes was performed among patients and control subjects. DGE analysis was carried out using negative binomial generalised linear model implemented in DESeq2 R package adjusted for covariates of age and sex. The subsequent analyses were performed as described in **Chapter 2**. Ingenuity Pathway Analysis (IPA) was performed on DEGs to identify significantly enriched canonical pathways and upstream regulators (P-value <0.05, absolute[z-score]>2).

5.3.8 Weighted gene co-expression network analysis (WGCNA) and identification of hub genes

To identify co-expressed gene network and potential hub genes associated with fatal melioidosis, a signed network by WGCNA was performed among melioidosis patients. Pre-filtered, normalised and variance stabilizing transformed expression data (20, 609 features) of melioidosis cohort (n=162) were used for WGCNA and subsequent analyses (*415*). The remaining workflow was performed as described in **Chapter 2**.

5.3.9 Deconvolution of bulk RNA sequencing data

Cell type abundances were estimated from the bulk RNA sequencing data of 164 melioidosis patients using CIBERSORTx (*431*). To further identify immune cell subsets, enrichment of 64 cell subsets was performed using xCell R package (version 1.1.0) (*435*). The melioidosis patients were divided into non-survivors (n=84) and survivors (n=80). The imputed cell fractions and enrichment were compared using non-parametric Mann-Whitney test in R programme.

5.4 Results

5.4.1 Demographics of the study cohort

A total of 284 whole blood samples from patients with community-acquired infection including 164 culture-proven melioidosis, 35 culture-proven Gram-negative bacteria (22 *Escherichia coli* and 13 *Klebsiella pneumonia*), 16 culture-proven Gram-positive bacterium (*Staphylococcus aureus*), and 19 culture-negative were sequenced along with 50 blood samples from uninfected individuals in the community (25 healthy blood donors and 25 out-patient diabetes patients). **Table 5.1** shows the demographics of the participants. The age and sex were statistically significant among the patients. 28-day mortality was 44% among all the patients and 51% within the melioidosis cohort. About 40% of all the patients had diabetes, without significant difference between the groups (45% among melioidosis cohort). Of 164 melioidosis patients, 134 (79%) had bacteraemia upon enrolment. In this study all the patients from other Gram-negative and Gram-positive infections were selected with bacteraemia. All non-survivors based on 28-day mortality showed significantly higher modified SOFA score than the survivors (as expected).

Table 5.1 Characteristics of melioidosis, other community-acquired infection and control cohorts.

Characteristic (N=284)	Melioidosis (n=164)	Other Gram-negative (n=35)	Gram-positive (n=16)	Culture negative (n=19)	Healthy control (n=25)	Diabetes control (n=25)	P-value
Sex, Female (%)	53 (32)	19 (54)	4 (25)	11 (58)	10 (40)	10 (40)	0.059
Male (%)	111 (68)	16 (46)	12 (75)	8 (42)	15 (60)	15 (60)	
Age in years, median (interquartile range, IQR)	54 (46-64)	68 (58-75)	58 (45-69)	63 (46-76)	46 (41-49)	65 (54-71)	**<0.001**
28-day mortality, non-survivors (%)	84 (51)	9 (26)	6 (38)	4 (21)	NA	NA	**0.006**
survivors (%)	80 (49)	26 (74)	10 (62)	15 (79)	NA	NA	
Diabetes status, DM (%)	74 (45)	9 (26)	6 (38)	4 (21)	NA	NA	0.053
non-DM (%)	90 (55)	26 (74)	10 (62)	15 (79)	NA	NA	
Having bacteraemia, Yes (%)	130 (79)	35 (100)	16 (100)	0	NA	NA	**<0.001**
No (%)	34 (21)	0	0	19	NA	NA	
Having pneumonia, Yes (%)	52 (32)	5 (14)	2 (12)	4 (11)	NA	NA	0.08
No (%)	112 (68)	30 (86)	14 (88)	15 (79)	NA	NA	
Modified SOFA score, non-survivors (IQR)	8 (5-11)	7 (6-12)	11 (5-15)	5 (4-9)	NA	NA	**<0.001**
survivors (IQR)	2 (1-5)	3 (1-6)	4 (0-6)	4 (2-7)	NA	NA	

Abbreviations: SOFA, sequential organ failure assessment. Other Gram-negative group consists of patients infected with *Escherichia coli* (n=22) and *Klebsiella pneumoniae* (n=13). Gram-positive group consists of 16 patients with *Staphylococcus aureus* infection. Culture negative group refers to patients meeting the enrolment criteria but with blood culture negative for any bacteria (n=19). Binary and continuous variables were tested Chi-square and Kruskal-Wallis test respectively. Modified SOFA score and hospitalisation were expressed with median and interquartile range in parenthesis.

5.4.2 Distinct transcriptomic profiles in melioidosis are driven by clinical parameters associated with disease severity and poor outcome

An average of 34 million (M) and 30 M reads per sample (All-disease, SD = 6.8 M; Control, SD = 7.7 M) were generated from whole blood RNA sequencing (**Supplementary Figure 5.1A**). A total of 19, 919 (melioidosis and controls, n=214) and 20,697 transcripts (complete data set, N=284) following pre-filtering were used for subsequent data analyses. The pre-filtered genes were normalised using the median of ratios method implemented in DESeq2 R package (*392*) (**Supplementary Figure 5.1B, 5.1C**). The normalised expression data underwent variance-stabilising transformation for PCA and WGCNA analyses. To investigate the impact of case fatality by 28-day mortality status on the whole blood

transcriptome, the 1,000 most variable genes were selected for PCA analysis. Firstly, PCA identified a clear segregation between melioidosis and the healthy control group (**Figure 5.1**). Secondly, PCA coloured by 28-day mortality status shows some separation between non-survivors and survivors of melioidosis (**Figure 5.1**). Thirdly, PCA coloured by bacteraemia status shows some separation between melioidosis with and without bacteraemia (**Supplementary Figure 5.2A**). Fourthly, PCA coloured by pneumonia did not segregate the patients presenting with and without pneumonia among melioidosis patients (**Supplementary Figure 5.2B**). Finally, PCA coloured by diabetes status shows similar transcriptomic profiles between melioidosis with and without T2DM (**Supplementary Figure 5.3A**).

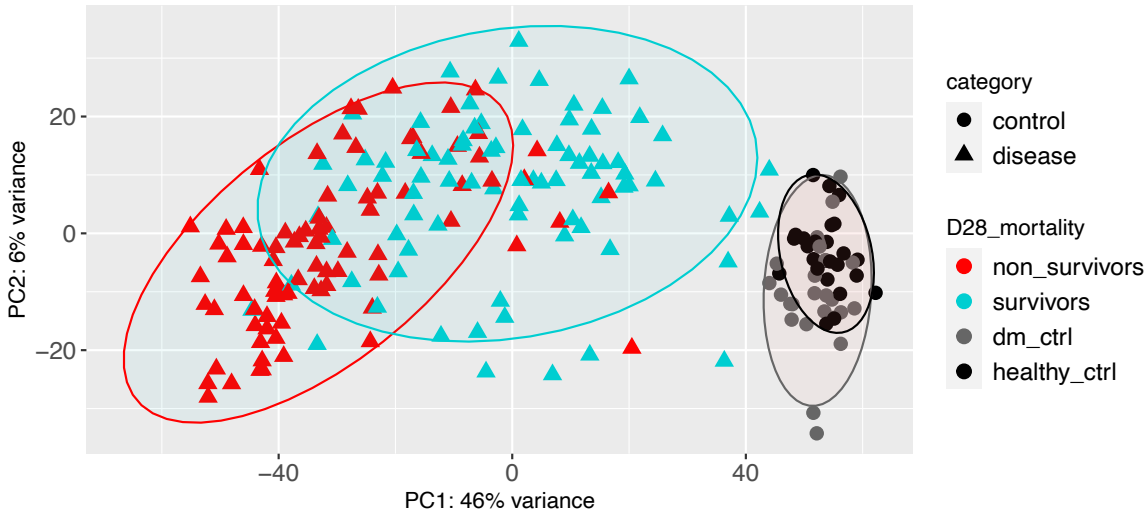

Figure 5.1. Multidimensional scaling by principal component analysis (PCA) of the 1,000 most variable genes in melioidosis and control cohorts. PCA in melioidosis and control cohorts was coloured by 28-day mortality status. Patients with melioidosis, divided into non-survivors ("non_survivors", red triangles, n=84), survivors ("survivors", turquoise triangles, n=80), uninfected diabetes group ("dm_ctrl", grey circles, n=25), and healthy donors ("healthy_ctrl", black circles, n=25). PCA plots were generated using plotPCA function implemented in DESeq2 R package.

5.4.3 Profound changes in the whole blood transcriptome are driven by case fatality and bacteraemia status

Differential gene expression (DGE) analysis was performed comparing healthy and diabetes controls. No differentially expressed genes were identified between diabetes and healthy controls (**Supplementary Figure 5.3B**). Hence, the two control groups were merged into one control group as a baseline for subsequent analyses. DGE analysis between melioidosis patients and control group was then performed and over 7,000 differentially expressed genes (DEGs) were identified in melioidosis compared to control group (absolute[Log2 fold-change]≥1, adjusted P-value<0.05) (**Figure 5.2A**). DGE analysis was performed between non-survivors and survivors of melioidosis and identified 633 up- and 1,109 down-regulated genes (**Figure 5.2B**).

In this study, bacteraemia was common in melioidosis whereas pneumonia was less common in melioidosis and other infections (**Table 5.1**). DGE analysis was performed to evaluate the impact of bacteraemia and pneumonia on whole blood transcriptome in melioidosis. The DGE analysis identified 644 up- and 543 down-regulated genes in melioidosis patients with bacteraemia compared to those without (**Figure 5.2C**). The impact of pneumonia on the whole blood transcriptome was less pronounced, with DGE analysis identifying 12 up- and 98-down-regulated genes in melioidosis presented with pneumonia compared to non-pneumonia cases (**Supplementary Figure 5.4A**). Despite a 12-fold increased risk of getting melioidosis in people who live with diabetes (*20*), DGE analysis identified no DEGs between melioidosis with and without diabetes (**Supplementary Figure 5.4B**). The identified DEGs within melioidosis were compared for overlap by Venn diagram. Over 400 DEGs were common between non-survivors compared to survivors and melioidosis patients with bacteraemia compared to non-bacteraemia (**Supplementary Figure 5.5**). In contrast,

small fractions of DEGs derived from melioidosis with pneumonia compared to non-pneumonia overlapped among other conditions of melioidosis.

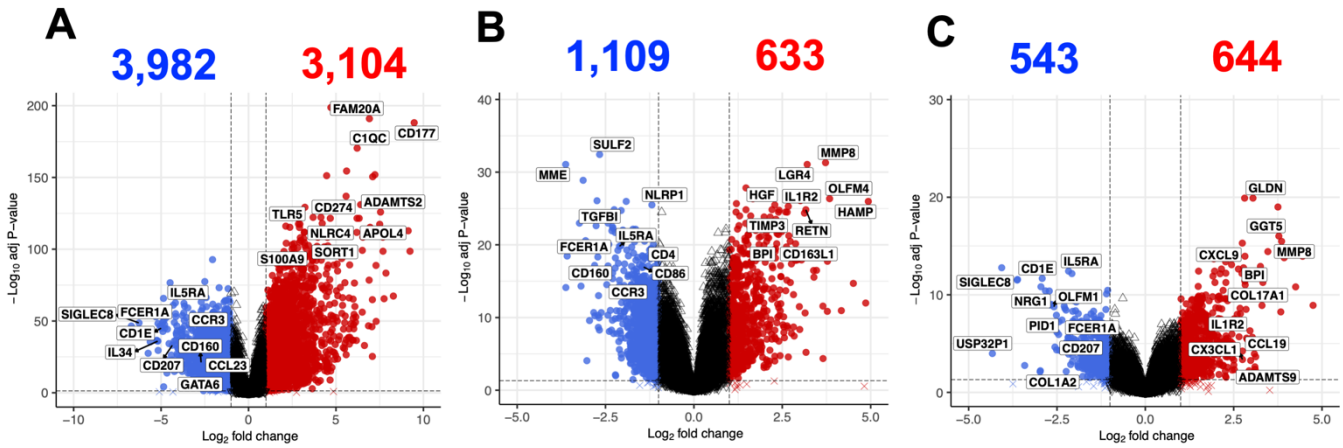

Figure 5.2 Volcano plots of differentially expressed genes between (A) melioidosis (n=164) compared to controls (n=50), (B) non-survivors of melioidosis (n=84) compared to survivors (n=80), and (C) melioidosis with bacteraemia (n=134) compared to those without bacteraemia (n=34). Dotted lines define a cut-off of differentially expressed genes based on absolute[Log2 fold-change]≥1 (x-axis) and adjusted P-value <0.05 (y-axis). Volcano plots were generated using EnhancedVolcano R package.

5.4.4 Melioidosis drives up-regulation of pro-inflammatory immune responses dominated by both type I and II interferon signalling

To identify the impact of melioidosis on the whole blood transcriptome, functional pathway analysis based on over-representation analysis by Hallmark and Reactome gene sets was performed following DGE analysis. Pathways involved in pro-inflammatory immune responses such as type I and type II interferon signalling, neutrophil degranulation, signalling by interleukins, and TNF signalling via NF-κB were highly up-regulated in melioidosis compared to healthy controls (**Figure 5.3**). On the other hand, pathways involved in cellular regulation such as immunoregulatory interactions between lymphoid

and non-lymphoid cells, T-cell signalling and cellular signalling were down-regulated in melioidosis compared to healthy controls.

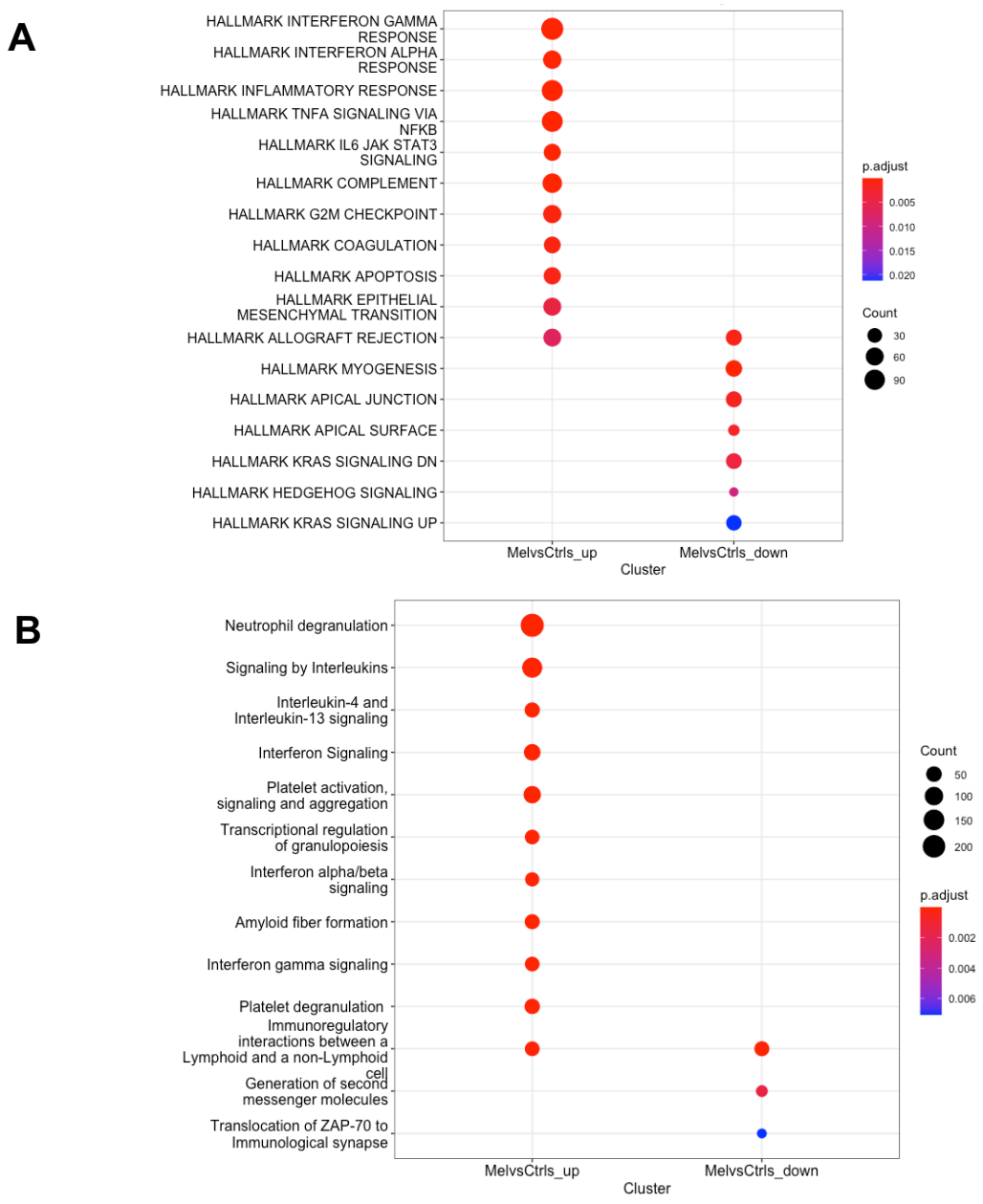

Figure 5.3 Functional pathway analysis of DEGs between melioidosis (n=164) and controls (n=50) (**Figure 5.2A**). A: Hallmark gene sets. B: Reactome gene sets. The top 10 over-represented pathways are displayed. The gradient colour bar corresponds to the adjusted P-value. The size of each term is indicated by representative counts. Differentially expressed genes were pre-filtered based on a cut-off of absolute[Log2 fold-change] and adjusted P-value <0.05. MelvsCtrls_up: up-regulated

pathways in melioidosis compared to controls. MelvsCtrls_down: down-regulated pathways in melioidosis compared to controls.

5.4.5 Excessive inflammatory immune responses but suppressed T-cell signalling are associated with poor outcome and bacteraemia in melioidosis

To identify how future case fatality (28-day mortality) induces transcriptional changes during melioidosis, functional pathway analysis following DGE analysis was performed between non-survived and survived melioidosis. Firstly, pathways involved in the inflammatory immune response such as neutrophil degranulation, signalling by interleukins, TNF signalling via NF-κB , and type II immune responses (IL-10, IL-4, and IL-13) were highly up-regulated in non-survivors of melioidosis (**Figure 5.4, Supplementary Figure 5.6**). Likewise, pathways involved in inflammation, cell cycle regulation, and interferon-γ response were up-regulated in melioidosis patients with bacteraemia compared to non-bacteraemia cases. Secondly, pathways involved in the adaptive immune response such as T-cell signalling and activation were down-regulated in non-survivors compared to survivors of melioidosis. Distinctively, melioidosis patients with bacteraemia show down-regulation of pathways involved in tissue homeostasis via erythropoietin-producing hepatocellular carcinoma (EPH) receptor signalling. Interestingly, pathways involved in pro-inflammatory immune responses such as chemokine signalling pathway, cytokine-chemokine receptor interaction, and natural killer cell mediated cytotoxicity were down-regulated in melioidosis with pneumonia compared to non-pneumonia cases (**Supplementary Figure 5.6**).

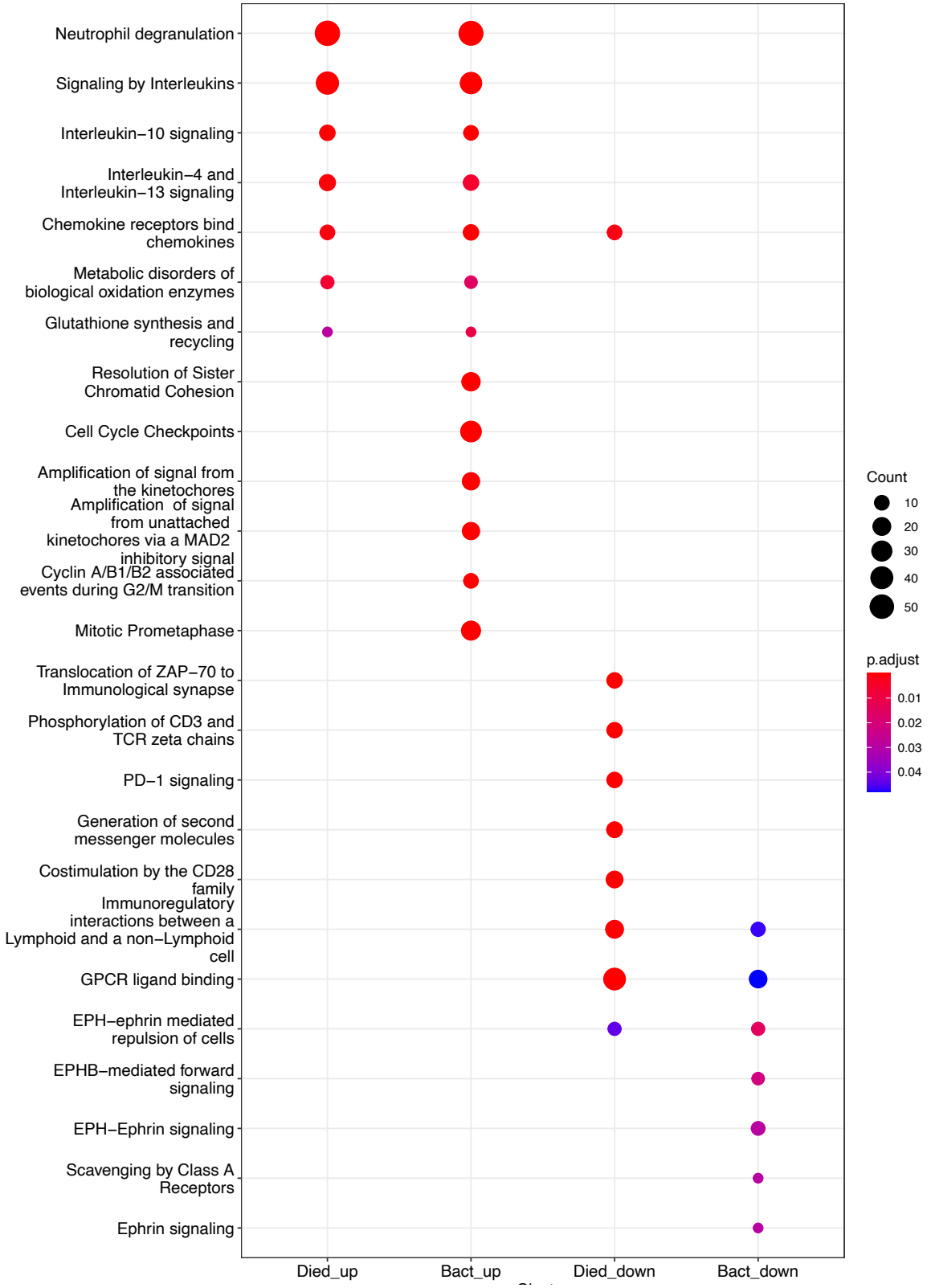

Figure 5.4 Functional pathway analysis based on Reactome gene sets following differential gene expression (DGE) analyses among melioidosis cases (**Figure 5.2B, 5.2C**). The DGE analyses among melioidosis patients include non-survivors (n=84) versus survivors (n=80) and bacteraemia (n=130)

versus non-bacteraemia (n=34). The gradient colour bar corresponds to the adjusted P-value. The size of each term is indicated by representative counts. Differentially expressed gene were pre-filtered based on a cut-off of absolute[Log2 fold-change] ≥1 and adjusted P-value <0.05. Died_up/down = up/down-regulated pathways in non-survivors compared to survivors. Bact_up/down = up/down-regulated pathways in the patients with bacteraemia compared to non-bacteraemia.

5.4.6 Excessive inflammatory immune responses driven by innate immune upstream regulators are associated with poor outcome and bacteraemia in melioidosis

In agreement with the results obtained from functional pathway analyses, canonical pathway analysis by Ingenuity Pathway Analysis (IPA) identified up-regulation of pathways involved in inflammation such as IL-6 signalling, hypercytokine/chemokine response, PD-1, and acute phase response signalling in non-survived melioidosis compared to survivors. Strikingly, several pathways involved in the adaptive immune response, particularly T-cell signalling cascades such as calcium-induced T lymphocyte apoptosis, ICOS-ICOSL signalling in T helper cells, and T cell receptor signalling as well as those involved in antigen presentation including dendritic cell maturation and phagosome formation were down-regulated in the non-survivors (**Table 5.2**). Likewise, the pathways involved in inflammatory immune responses such cell cycle regulation, IL-17 signalling, and p38 MAPK signalling were also up-regulated in melioidosis with bacteraemia compared to non-bacteraemia cases (**Table 5.3**).

Table 5.2 Canonical pathway analysis in fatal melioidosis patients. Differentially expressed genes were derived from DGE analysis between non-survivors and survivors of melioidosis and pre-filtered based on a cut-off of absolute[Log2 fold-change]≥1 and adjusted P-value <0.05. Significant pathways as ranked by P-value. Activated pathways (positive z-scores) are labelled in orange. Inhibited pathways (negative z-scores) are labelled in blue.

Ingenuity Canonical Pathways	P-value	Z-score
Calcium-induced T Lymphocyte Apoptosis	3.98E-54	-3.606
ICOS-ICOSL Signaling in T Helper Cells	3.98E-53	-3.606
PKCθ Signaling in T Lymphocytes	3.16E-51	-3.3
Dendritic Cell Maturation	3.16E-51	-2.746
CD28 Signaling in T Helper Cells	2.00E-50	-2.449
Role of NFAT in Regulation of the Immune Response	1.58E-47	-4.146
T Cell Receptor Signaling	7.94E-47	-10.823
Systemic Lupus Erythematosus In T Cell Signaling Pathway	6.31E-42	-3.13
Regulation of IL-2 Expression in Activated and Anergic T Lymphocytes	1.00E-41	-9.916
CREB Signaling in Neurons	3.55E-10	-3.825
Phagosome Formation	9.12E-09	-2.557
Th1 Pathway	2.51E-08	-3.13
Breast Cancer Regulation by Stathmin1	3.24E-07	-2.54
G-Protein Coupled Receptor Signaling	7.08E-07	-2.769
Neuroinflammation Signaling Pathway	1.45E-05	-2.268
Factors Promoting Cardiogenesis in Vertebrates	5.37E-05	-3.13
GPCR-Mediated Nutrient Sensing in Enteroendocrine Cells	5.37E-04	-2.5
Pulmonary Fibrosis Idiopathic Signaling Pathway	6.92E-04	-2.121
PD-1, PD-L1 cancer immunotherapy pathway	1.51E-03	3
IL-6 Signaling	3.47E-03	2.138
MSP-RON Signaling In Macrophages Pathway	3.80E-03	3.742
Basal Cell Carcinoma Signaling	4.79E-03	-2.646
Role of Hypercytokinemia/hyperchemokinemia in the Pathogenesis of Influenza	5.89E-03	2.111
Endocannabinoid Neuronal Synapse Pathway	6.03E-03	-2.673
Acute Phase Response Signaling	1.02E-02	2.138
IL-23 Signaling Pathway	3.47E-02	-2.449

Table 5.3 Canonical pathway analysis in melioidosis patients with bacteraemia. Differentially expressed genes were derived from DGE analysis between melioidosis with and without bacteraemia and pre-filtered based on a cut-off of absolute[Log2 fold-change]≥1 and adjusted P-value <0.05. Significant pathways were ranked by P-value. Activated pathway (positive z-scores) are labelled in orange. Inhibited pathways (negative z-scores) are labelled in blue.

Ingenuity Canonical Pathways	P-value	Z-score
Kinetochore Metaphase Signaling Pathway	5.25E-09	2.065
Mitotic Roles of Polo-Like Kinase	3.16E-05	2.53
Estrogen-mediated S-phase Entry	3.31E-04	2.449
Cyclins and Cell Cycle Regulation	1.17E-03	3
Regulation of IL-2 Expression in Activated and Anergic T Lymphocytes	1.35E-03	-4.49
Differential Regulation of Cytokine Production in Intestinal Epithelial Cells by IL-17A and IL-17F	1.41E-03	2.236
Acute Phase Response Signaling	1.70E-03	2.53
IL-6 Signaling	3.16E-03	2.714
Role of CHK Proteins in Cell Cycle Checkpoint Control	5.25E-03	-2.236
T Cell Receptor Signaling	5.75E-03	-5
p38 MAPK Signaling	1.32E-02	2.53
Role of Hypercytokinemia/hyperchemokinemia in the Pathogenesis of Influenza	1.51E-02	2.121

Moreover, T-cell related pathways including regulation of IL-2 expression in activated and anergic T lymphocytes and T cell receptor signalling were down-regulated in melioidosis with bacteraemia. Enriched upstream regulators based on patterns of differential gene expression in fatal compared to non-fatal melioidosis were identified using IPA (*409*). The top 5 upstream regulators including *TNF, IL4, IL1A, PTGER2*, and *OSM* were predicted to be activated in non-survivors compared to survivors (**Table 5.4**). Moreover, inhibited upstream regulators including *DUSP1*, *CIITA*, and *GATA3* were identified in the non-survivors compared to survivors (**Table 5.4**). On the other hand, top 5 upstream regulators identified in the patients with bacteraemia compared to non-bacteraemia cases included *TNF, PTGER2, CEBPB, FOXM1* and *CKAP2L*. Of the top 25, 7 upstream regulators were common between fatal melioidosis and those who had bacteraemia including *TNF* (**Figure 5.5**)*, IL4, IL1A, PTGER2, OSM, CEBPB* and *HGF* (**Table 5.4**).

Table 5.4 Top 25 predicted upstream regulators in fatal melioidosis compared survivors and melioidosis with bacteraemia compared to non-bacteraemia cases. Common predicted upstream regulators between the two groups are in bold. Significant upstream regulators were based on predicted absolute (activation z-score)≥2, and P-value of overlap <0.01.

Non-survivors versus survivors			Bacteremia versus non-bacteraemia		
Upstream Regulator	**Activation z-score**	**P-value of overlap**	**Upstream Regulator**	**Activation z-score**	**P-value of overlap**
TNF	**3.627**	**4.31E-35**	***TNF***	**4.431**	**5.73E-35**
IL4	**2.162**	**3.34E-23**	***PTGER2***	**4.848**	**1.01E-33**
IL1A	**3.705**	**6.32E-13**	***CEBPB***	**4.546**	**1.52E-25**
PTGER2	**2.14**	**6.13E-12**	*FOXM1*	4.417	1.61E-19
OSM	**4.607**	**6.18E-12**	*CKAP2L*	4.796	3.26E-19
C5	2.527	3.98E-11	***HGF***	**4.169**	**8.55E-19**
CEBPB	**2.243**	**1.45E-09**	***IL4***	**2.616**	**1.94E-18**
CAMP	2.977	2.48E-09	*CDKN1A*	-2.325	5.61E-17
HGF	**2.202**	**1.36E-08**	***IL1A***	**3.559**	**2.50E-15**
HIF1A	2.201	4.10E-08	*AREG*	4.081	1.33E-14
DUSP1	-2.4	5.52E-08	*H2AZ1*	3.606	2.88E-14
CD40LG	2.352	8.98E-08	*CHUK*	2.408	2.33E-13
TCL1A	2.186	9.27E-08	***OSM***	**4.408**	**6.42E-13**
S100A8	2.083	1.99E-07	*NFKBIA*	2.104	6.82E-13
GATA3	-2.026	4.82E-07	*MYD88*	4.136	2.05E-11
SAA1	2.414	7.93E-07	*FGF2*	3.194	7.81E-11
EGF	3.334	1.37E-06	*PCLAF*	2.998	9.69E-11
CD40	2.818	1.38E-06	*MYBL2*	2.765	2.01E-10
CIITA	-2.581	3.47E-06	*IL18*	3.391	3.13E-10
CEBPE	3.066	3.66E-06	*TGM2*	3.944	6.04E-10
TLR4	2.744	4.37E-06	*ZFP36*	-2.915	1.66E-09
F3	2.308	8.43E-06	*NFKB1*	2.591	2.54E-09
C3	2.455	1.78E-05	*EP400*	3.582	2.81E-09
PPRC1	2.734	2.33E-05	*E2F3*	2.898	4.29E-09
IL1R1	3.265	4.28E-05	*TGFBR2*	-3.259	6.72E-09

Upstream Regulator	Molecule Type	Predicted Activation State	Activation z-score	p-value of overlap	Target Molecules in Dataset
TNF	cytokine	Activated	3.627	4.31E-35	230

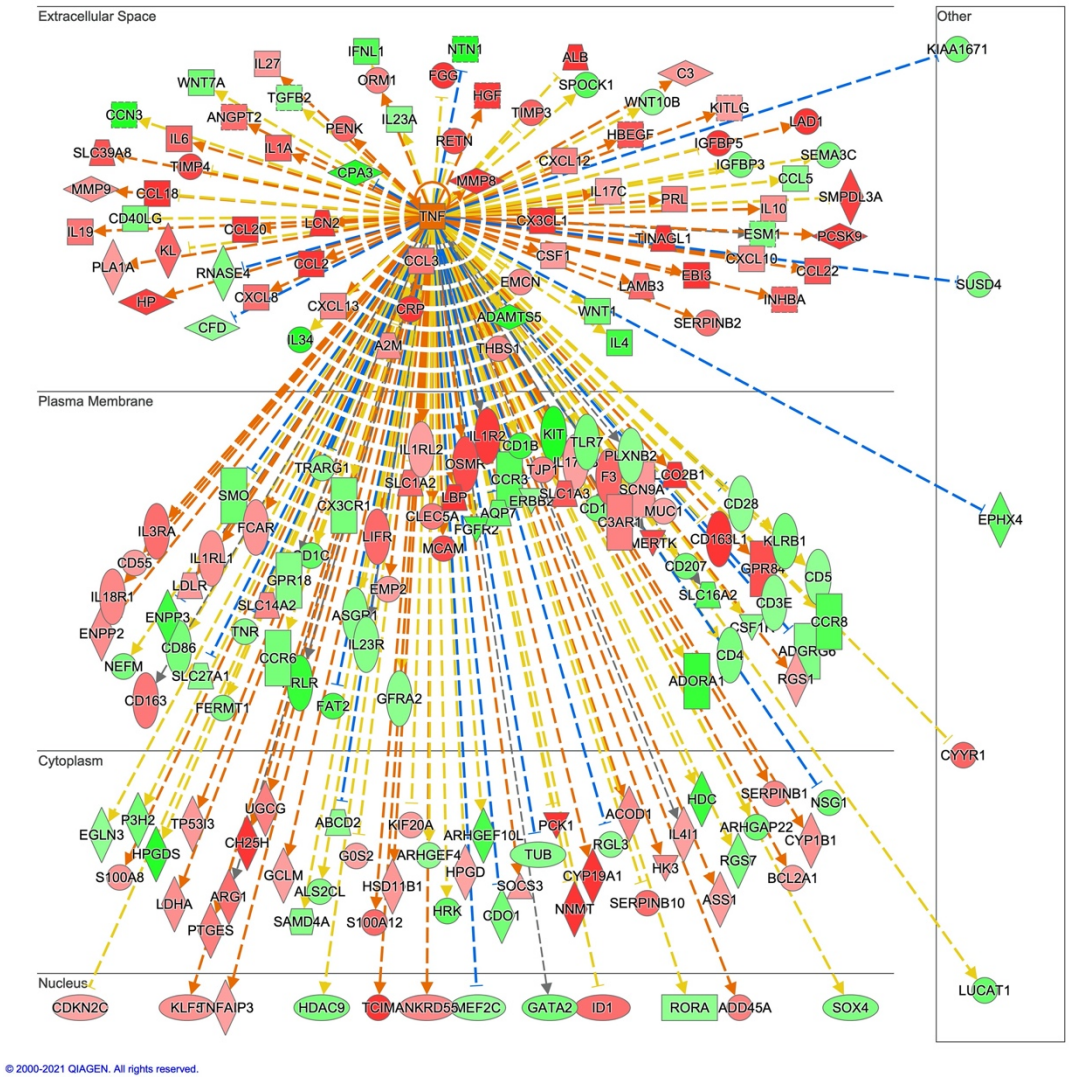

Figure 5.5 The upstream regulatory network of *TNF* predicted to be activated in fatal melioidosis. Upstream regulator analysis was performed based on patterns of differential gene between non-survivors and survivors of melioidosis expression (**Figure 5.2B**) using Ingenuity Pathway Analysis software (version 01-20-04). Differentially expressed genes used for this analysis were based on adjusted P-value < 0.05. Genes labelled with green indicate decreased expression. Genes labelled with red indicate increased expression. Intensities of colours represent a degree of confidence (darker = more confidence, lighter = less confidence). Dotted lines: in orange = leads to activation, in blue = leads to inhibition, and in yellow = findings inconsistent. Each symbol presents different roles: square = cytokine, diamond = enzymes, horizontal oval = transcription factor, vertical oval =

transmembrane receptor, and circle = complex/group/other. Significant upstream regulators were based on predicted absolute (activation z-score)≥2, and P-value of overlap <0.01.

5.4.7 Co-expressed gene modules enriched with inflammatory immune responses are associated with poor outcome

To complement the results obtained from DGE and pathway analyses, and to identify hub genes that may play a deleterious role during melioidosis, WGCNA was performed on the genome-wide expression profile from 162 melioidosis patients in an unsupervised fashion, following removal of two outliers. Firstly, the sample dendrogram shows two distinct clusters by 28-day mortality (**Supplementary Figure 5.7A**). Secondly, a power of $\beta = 12$ was chosen (soft-threshold $R^2 = 0.83$ and mean connectivity = 107) in order to achieve scale-free network (**Supplementary Figure 5.7B**). As a result, 27 co-expressed gene modules were identified (**Supplementary Figure 5.7C**). Module-trait relationship analysis identified several co-expressed genes modules such as ME blue, darkturquoise, and brown (indicated in red boxes) significantly correlated with clinical traits associated with 28-day mortality and markers of disease severity such as increased percentage of neutrophils, higher SOFA score, and having bacteraemia. Among the co-expressed gene modules with significant correlations to 28-day mortality, ME blue shows the strongest correlation (Pearson's rho = 0.6, P-value = 4e-17) (**Figure 5.6**). Module enrichment analysis identified enriched pathways involved in inflammatory immune responses, in particular activation and chemotaxis of innate immune cells were enriched within the ME blue, darkturquoise and brown (**Figure 5.7**).

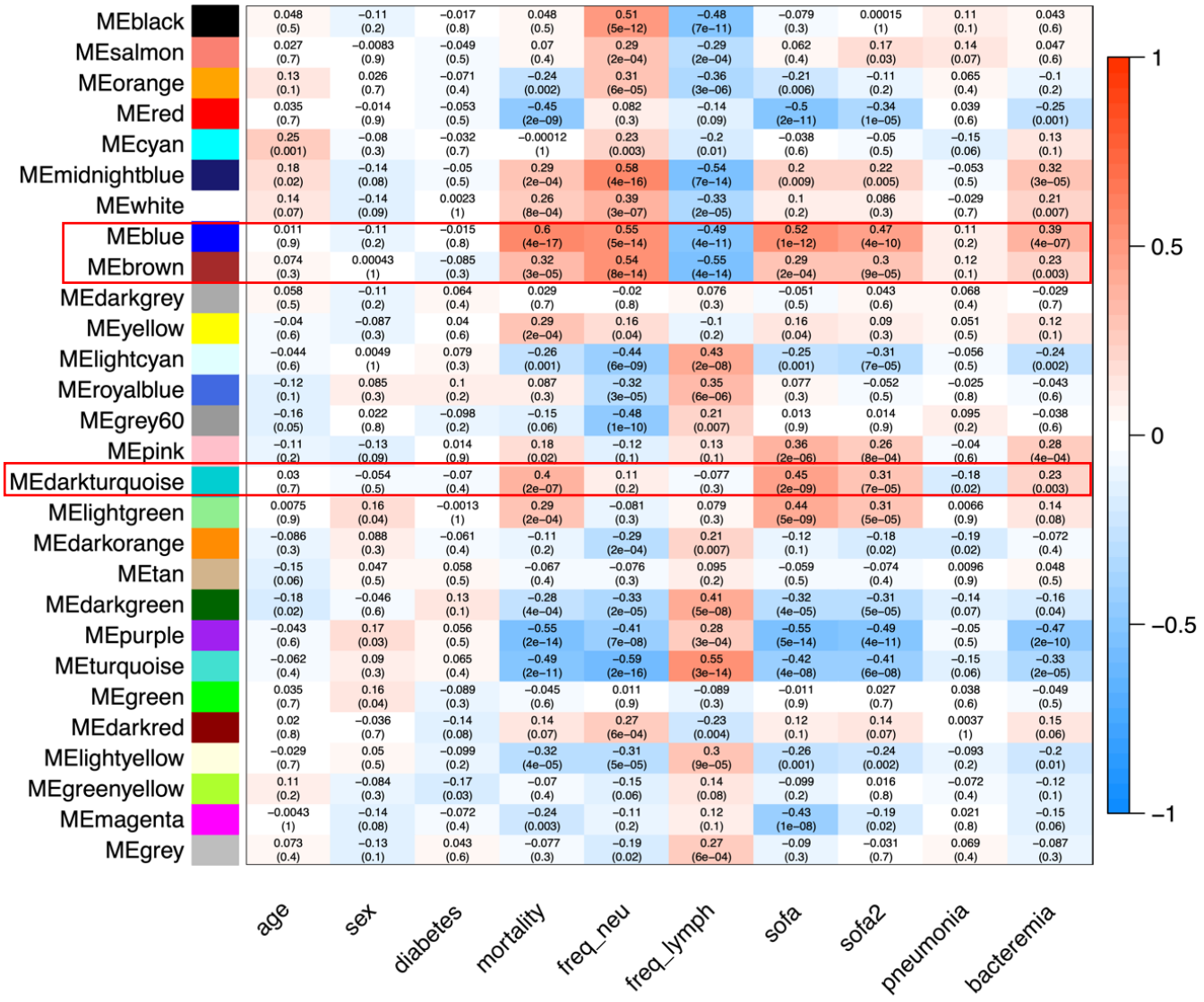

Figure 5.6 Module-trait relationship analysis in 162 melioidosis patients by weighted gene co-expression network analysis. A total of 27 co-expressed gene modules (module eigengenes, MEs) were identified. Each column and row represent clinical traits and MEs with corresponding Pearson's correlation coefficient between each ME-trait pair displayed with P-value in parenthesis. The gradient colour bar indicates the degree of positivity (maximum +1, red) / negativity (minimum -1, blue) for the Pearson's correlation coefficient. Clinical traits include age (in years, continuous variable), sex (binary outcome), diabetes status (binary outcome), 28-day mortality (mortality, binary outcome), % of total white cell count represented by neutrophils (freq_neu, continuous variable), % of total white cell count represented by lymphocytes (freq_lymph, continuous variable), modified

SOFA scores (sofa, continuous variable), modified SOFA scores at least 2 (sofa2, binary outcome), pneumonia (binary outcome), and bacteraemia (binary outcome).

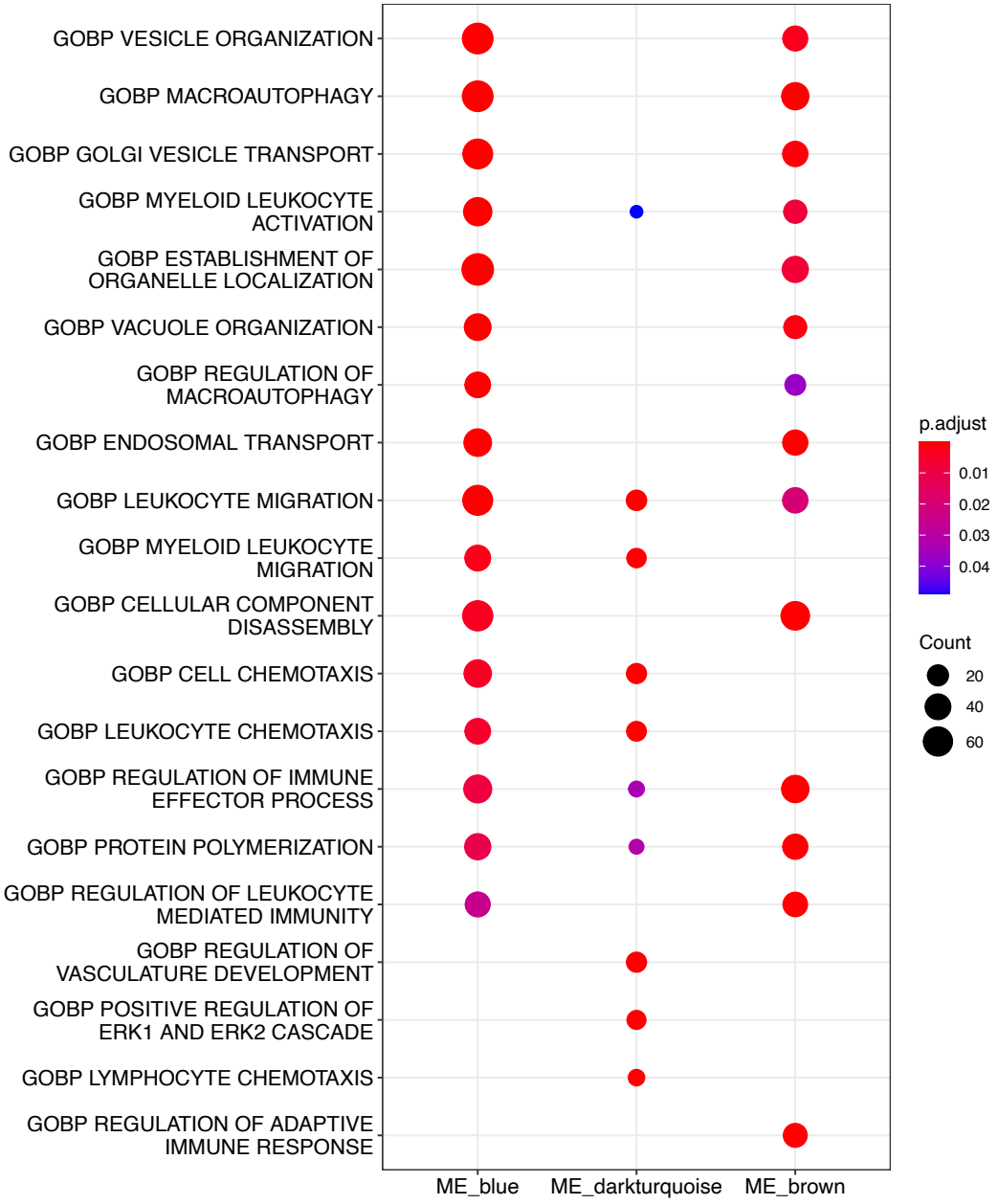

Figure 5.7 Enrichment analysis based on Gene Ontology (biological process) gene sets in module eigengene (ME) blue, darkturquoise and brown that were associated with 28-day mortality identified by module-trait relationship analysis in 162 melioidosis patients (**Figure 5.6**). The gradient colour bar corresponds to the adjusted P-value. The size of each term is indicated by representative counts. Enrichment plot was created using clusterProfiler R package.

Module eigengene (ME) or co-expressed gene module can be considered as a representative expression profile or first principal component and can be used to visualise expression profile associated with phenotypes. Here, MEs demonstrating significant correlations with 28-day mortality (both positive and negative correlations) were visualised between non-survived and survived melioidosis. Of 27, 8 MEs including ME blue, darkturquoise, brown, midnightblue, yellow, lightgreen, white and pink were higher in the non-survivors compared to survivors (**Supplementary Figure 5.8A-H**). On the other hand, 7 MEs including ME purple, turquoise, red, darkgreen, lightyellow, and orange were higher in the survivors compared to non-survivors (**Supplementary Figure 5.8I-N**). Module enrichment analysis within MEs associated with survival including ME purple, turquoise, lightyellow and darkgreen were highly enriched with pathways involved in T-cell signalling, mitochondrial regulation, cellular regulation, and B-cell receptor signalling (**Figure 5.8**).

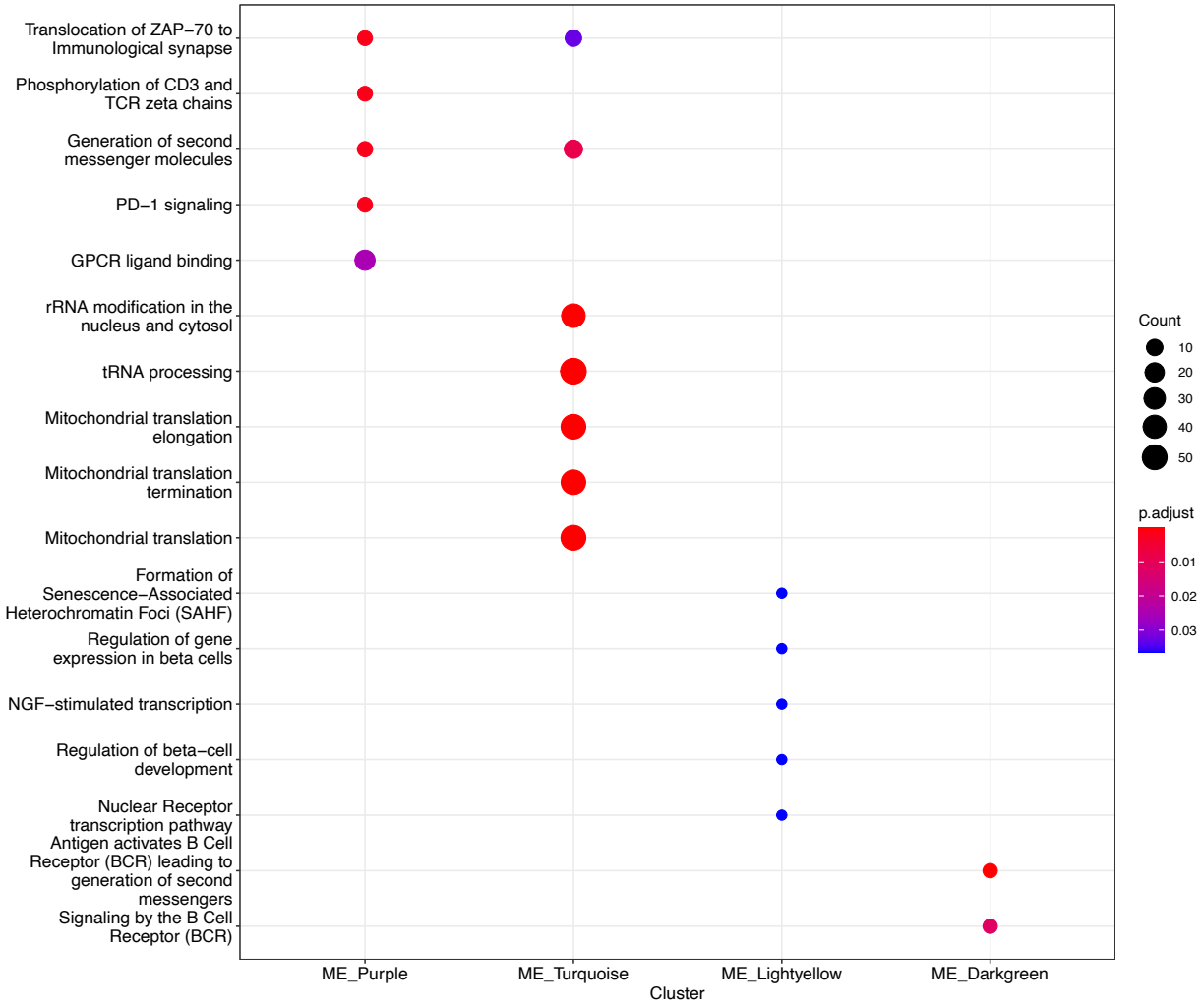

Figure 5.8 Enrichment analysis based on Reactome gene sets in four module eigengenes (MEs) which were associated with survival identified by module-trait relationship analysis in 162 melioidosis patients. The top 5 over-represented pathways are displayed. The gradient colour bar corresponds to the adjusted P-value. The size of each term is indicated by representative counts.

5.4.8 Hub genes involved in inflammation and immune regulation may be responsible for the deleterious host immune response in fatal cases of melioidosis

To identify hub genes associated with poor outcome, the results from supervised (DGE analysis) and unsupervised (WGCNA) approaches were compared using a Venn diagram for overlapped genes. Top 20 hub genes such as *SORT1, EXOC6, ATP11B* and *NLRC4* were identified from the ME blue module using Maximal Clique Centrality (MCC) algorithm (**Figure 5.9A**). Of 2,143 gene members within ME blue, 431 genes were differentially expressed identified by DGE analysis between fatal and surviving melioidosis patients (absolute[Log2 fold-change]≥1, adjusted P-value<0.05). Of the top 20, 6 hub genes were identified in the up-regulated DEGs (**Figure 5.9B**). The 6 hub genes including *CEACAM1* (CEA Cell Adhesion Molecule 1), *SERPINB1* (Serpin Family B Member 1), *SORT1* (Sortilin 1), *PGD* (Phosphogluconate Dehydrogenase), *ATP11B* (ATPase Phospholipid Transporting 11B), and *TBC1D8* (TBC1 Domain Family Member 8).

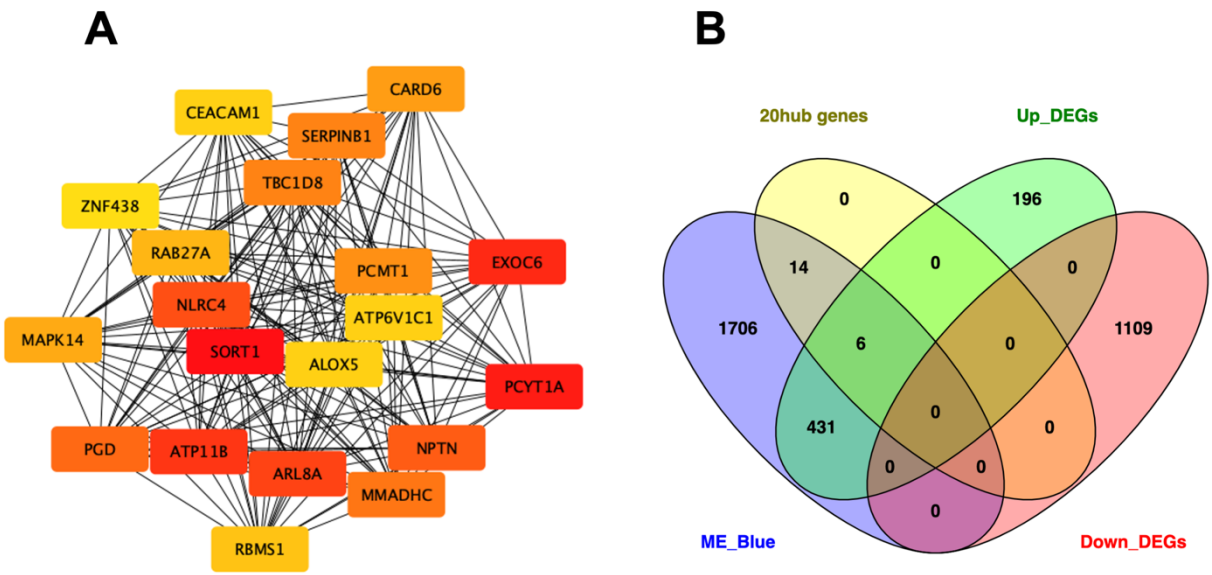

Figure 5.9 Top 20 hub genes with potential regulatory role in fatal melioidosis. A: Top 20 hub genes identified in the module eigengene (ME) blue associated with 28-day mortality (**Figure 5.6**). B: Venn diagram of overlapping differentially expressed genes (DEGs), genes member of the ME blue identified by weighted gene co-expression network analysis (WGCNA). DEGs derived from up- and down-regulated genes between non-survived and survived melioidosis patients (**Figure 5.2B**). ME blue was significantly associated with 28-day mortality by module-trait relationship analysis. 20 Hub genes within ME Blue were derived from Maximal Clique Centrality (MCC) algorithm using CytoHubba plugin on Cytoscape software. MCC scores of hub genes were ranked from high (red) to low (yellow).

5.4.9 Depleted adaptive immune cells, but increased innate immune cells were associated with poor outcome

To identify which immune cells are associated with poor outcome during melioidosis, whole blood RNA sequencing data were deconvoluted using CIBERSORTx and xCell. In general, the results obtained from both methods were comparable and higher proportions of lymphoid

cells were observed in the survivors compared to non-survivors (**Figure 5.10**, **Supplementary Figure 5.9**). Of 22-immune cell populations identified by CIBERSORTx, increased frequencies of neutrophils and γδ T cells but lower frequencies of T cell subsets including CD8 T cells, resting memory CD4 T cells, and resting NK cells were seen in the non-survivors compared to survivors (**Figure 5.10**). Of 64-cell signature by xCell, 12 lymphoid cell subsets were significantly enriched in survivors including CD4+ memory T cells, CD4+ naïve T cells, CD4+ central memory T cells (CD4+ Tcm), CD4+ effector memory T cells (CD4+ Tem), CD8+ T cells, CD8+ central memory T cells (CD8+ Tcm), CD8+ effector memory T cells (CD8+ Tem), B cells, memory B cells, naïve B cells, NK cells and NK T cells (**Supplementary Figure 5.9**). Likewise, monocytes, dendritic cells (DC), classical dendritic cells (cDC), immature dendritic cells (iDC) and plasmacytoid dendritic cells (pDC) were enriched in the survivors (**Supplementary Figure 5.10**). On the other hand, immune cells associated with fatal cases were regulatory T cells (Tregs), neutrophils, macrophages, M1 macrophages and basophils (**Supplementary Figure 5.9, 5.10**). The results obtained from the deconvolution methods agreed with the results from the local hospital laboratory full blood count taken upon enrolment in Ubon Ratchathani, in which higher frequency of neutrophils but lower frequencies of lymphocytes and monocytes were observed in the non-survivors (**Supplementary Figure 5.11**). Interestingly, melioidosis patients who had pneumonia show reduced CD8+ T cells, Th1 cells, and NK cells (**Supplementary Figure 5.12**). Lastly, Pearson's correlation analyses between white cell counts from 164 melioidosis patients and the deconvolution methods show significant correlations in all cell types (**Supplementary Figure 5.13, 5.14**).

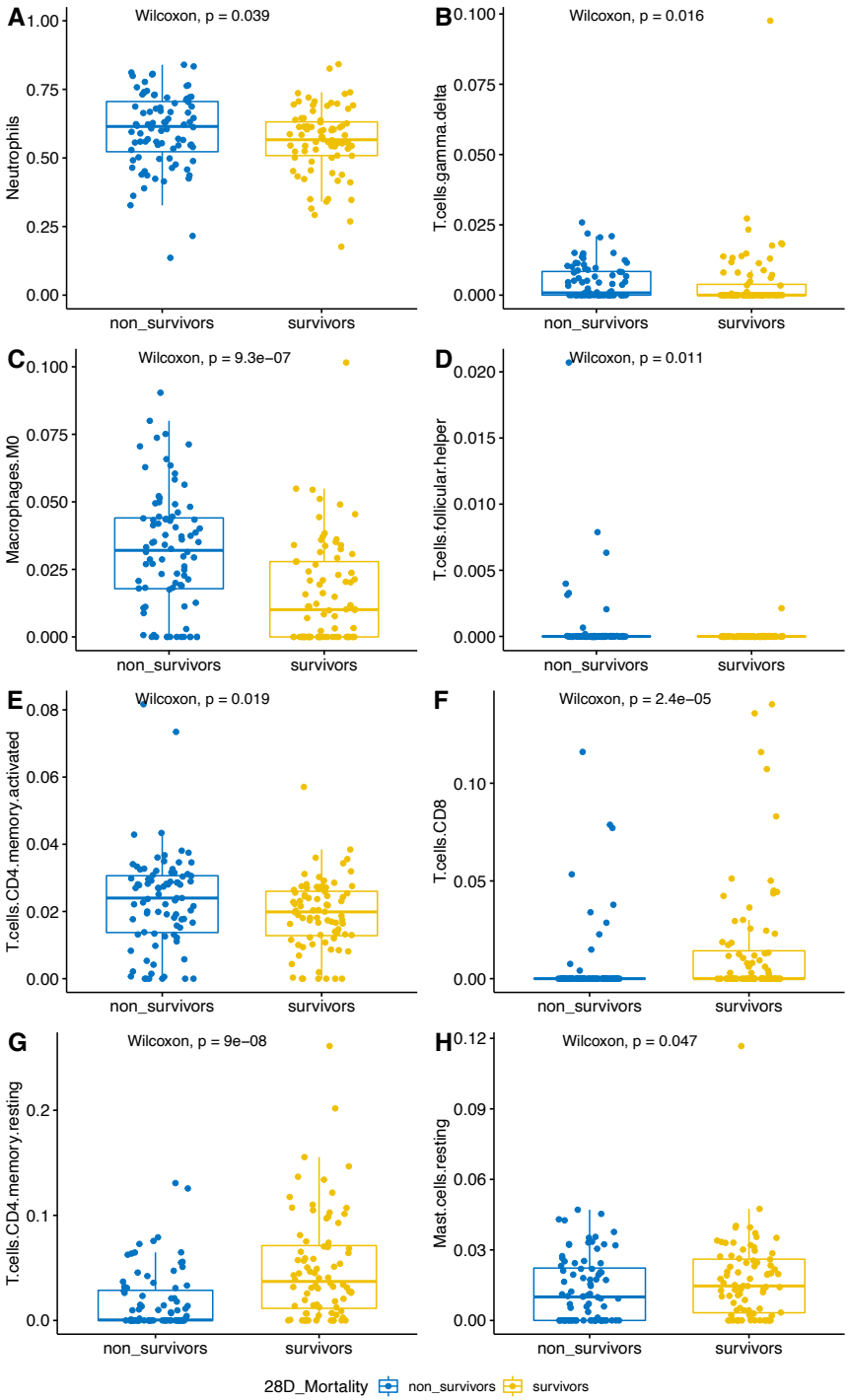

Figure 5.10 Scattered boxplots show comparisons of imputed cell fractions between non-survivor (blue, n=84) and survivor melioidosis patients (yellow, n=80) using CIBERSORTx. The Y-axis displays each cell type proportion. Box plots represent medians with interquartile range plus lines to minimum, maximum and potential outliers. Non-parametric Mann-Whitney test was performed with its corresponding 2-tailed P-value displayed on each plot alongside median and inter-quartile range boxes.

5.4.10 Melioidosis shows distinct transcriptomic profiles compared with other community-acquired infections

A total of 20,697 transcripts (complete data set, N=284) following pre-filtering were used to compare gene expression profiles between melioidosis and other infections (*E. coli, K. pneumoniae*, *S. aureus,* and blood culture-negative). To investigate the impact of different infection groups on the whole blood transcriptome, the 1,000 most variable genes were selected for PCA analysis. By colouring among infection groups, PCA shows clear separation of melioidosis compared to other infections (**Figure 5.11**). To identify transcriptomic signatures in melioidosis, separate DGE analysis was performed among melioidosis and patients with other community-acquired infections including other Gram-negative infections (*E. coli* and *K. pneumoniae*), Gram-positive infection (*S. aureus*), and blood culture-negative and had all clinical samples negative for Bp. Firstly, DGE analysis between melioidosis and other Gram-negative infections identified 486 up- and 510 down-DEGs (**Figure 5.12A**). Secondly, DGE analysis between melioidosis and Gram-positive infection group identified 139 up- and 86 down-DEGs (**Figure 5.12B**). Thirdly, DGE analysis between melioidosis and blood culture negative group identified 364 up- and156 down-DEGs (adjusted P-value<0.05, absolute[Log2 fold change]≥1) (**Figure 5.12C**). Fourthly, almost 700 DEGs were unique to melioidosis compared to other Gram-negative infections, 58 DEGs compared to Gram-positive infection group, and 249 DGEs compared to culture negative group. Of 1,298 DEGs, 77 up- and 17-down regulated were unique to melioidosis compared to all other infections (**Supplementary Figure 5.15**).

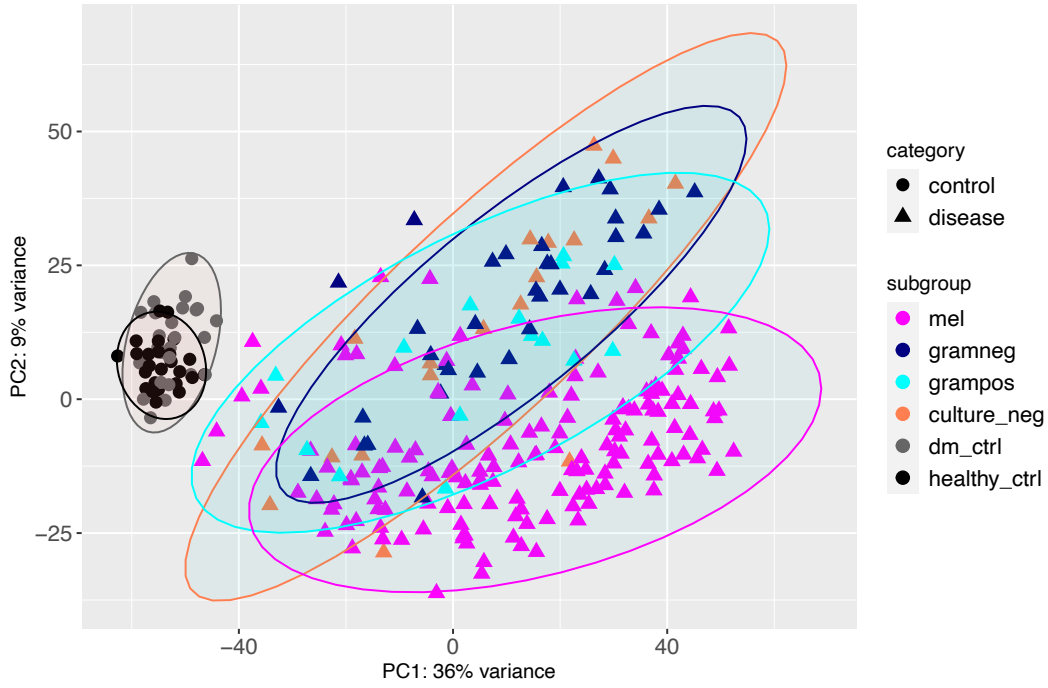

Figure 5.11 Multidimensional scaling by principal component analysis (PCA) of the 1,000 most variable genes in all-disease and control cohorts. PCA in all patients and control cohorts was coloured by infection, divided into melioidosis ("mel", magenta triangles, n=164), other Gram-negative infections ("gramneg", navy triangles, n=35), Gram-positive infection ("grampos", cyan triangles, n=16), culture negative ("culture_neg", coral triangles, n=19), uninfected diabetes group ("dm_ctrl", grey circles, n=25), and healthy donors ("healthy_ctrl", black circles, n=25). PCA plots were generated using plotPCA function implemented in DESeq2 R package.

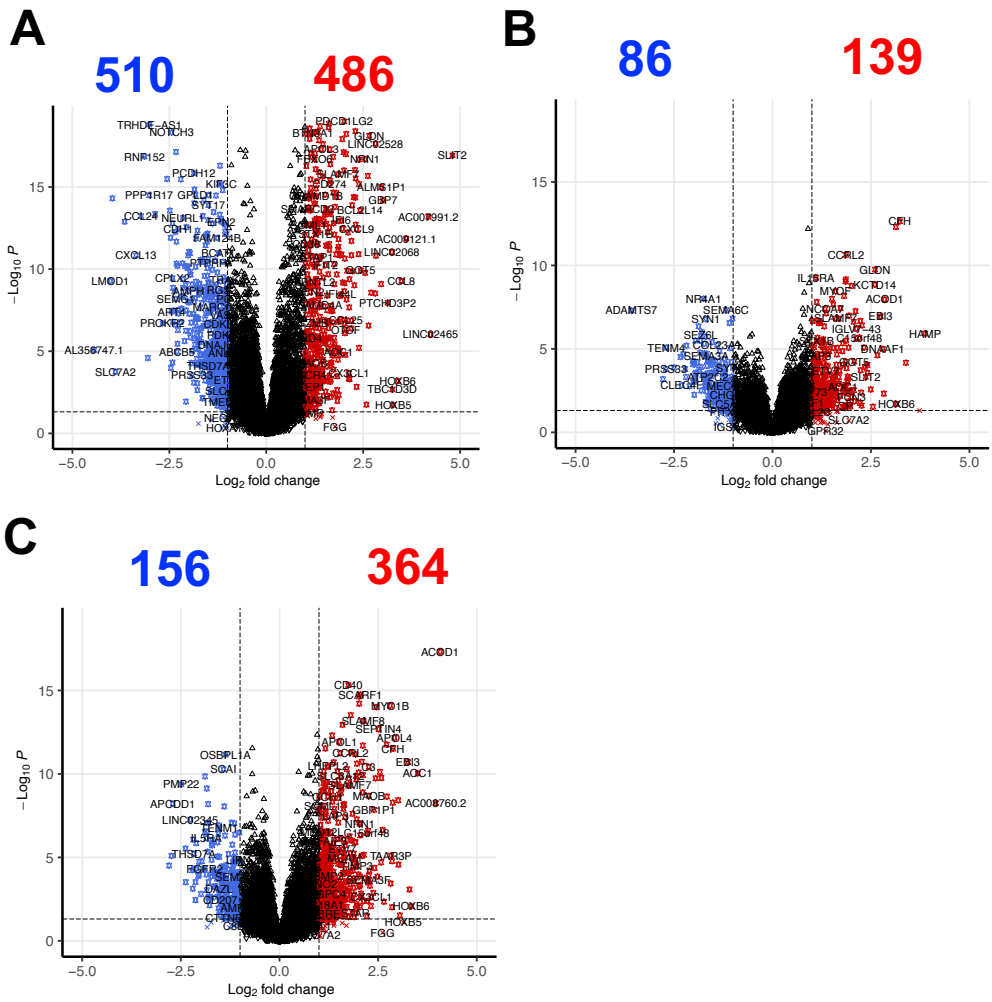

Figure 5.12 Volcano plots showing differentially expressed genes among melioidosis and other community-acquired infection. A: Melioidosis (n=164) versus other Gram-negative infections (n=35). B: Melioidosis versus Gram-positive infection (n=16). C: Melioidosis versus patients with culture-negative results (n=19). Dotted lines define a cut-off of differentially expressed genes based on absolute[Log2 fold-change]≥ 1 (x-axis) and P-value < 0.05 (y-axis). Volcano plot was generated using EnhancedVolcano R package.

5.4.11 Melioidosis causes profound up-regulation of interferon signalling compared with other community-acquired infections

To identify transcriptomic signatures that discriminate melioidosis from other community-acquired infections, functional pathway analysis following DGE analyses was performed. In general, pathways involved in type I immune responses - predominantly both type I and type II interferon signalling were up-regulated in melioidosis compared to all other community-acquired infections (**Figure 5.13**). Likewise, gene set enrichment analysis following DGE analyses show complementary results to the functional pathway analysis, with both interferon gamma and alpha responses were highly enriched in the melioidosis cohort compared to all other infections (**Figure 5.14**).

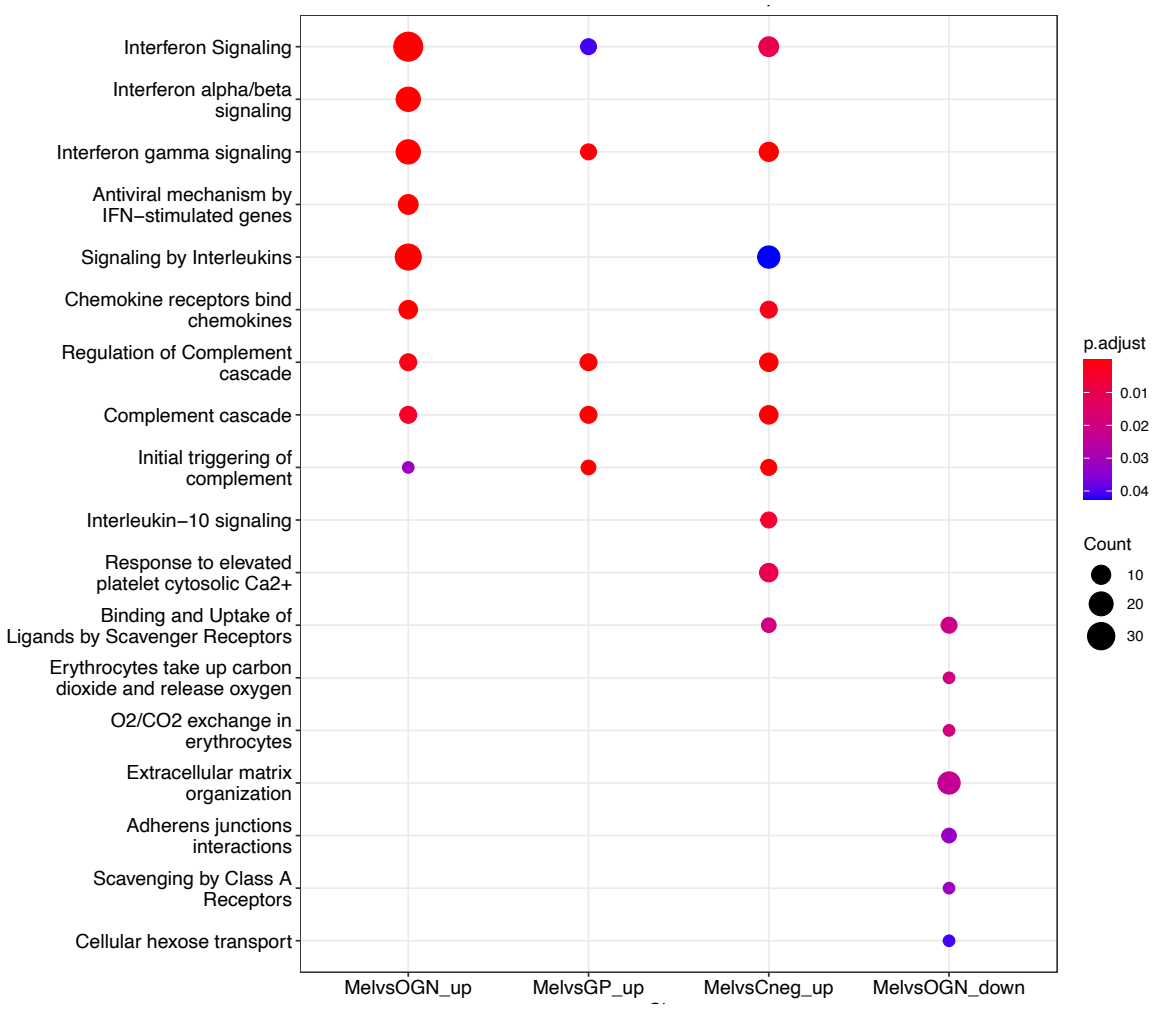

Figure 5.13 Functional pathway analysis based on Reactome gene sets following differential gene expression analyses among melioidosis and other infections (**Figure 5.12**). The gradient colour bar corresponds to the adjusted P-value. The size of each term is indicated by representative counts. Differentially expressed gene were pre-filtered based on a cut-off of absolute[Log2 fold-change] ≥1 and adjusted P-value <0.05. MelvsOGN_up/down = up/down-regulated pathways in melioidosis compared to other Gram-negative infections. MelvsGP_up = up-regulated pathways in melioidosis compared to Gram-positive infection. MelvsCneg_up = up-regulated pathways in melioidosis compared to patients with culture-negative. Enrichment plot was created using clusterProfiler R package.

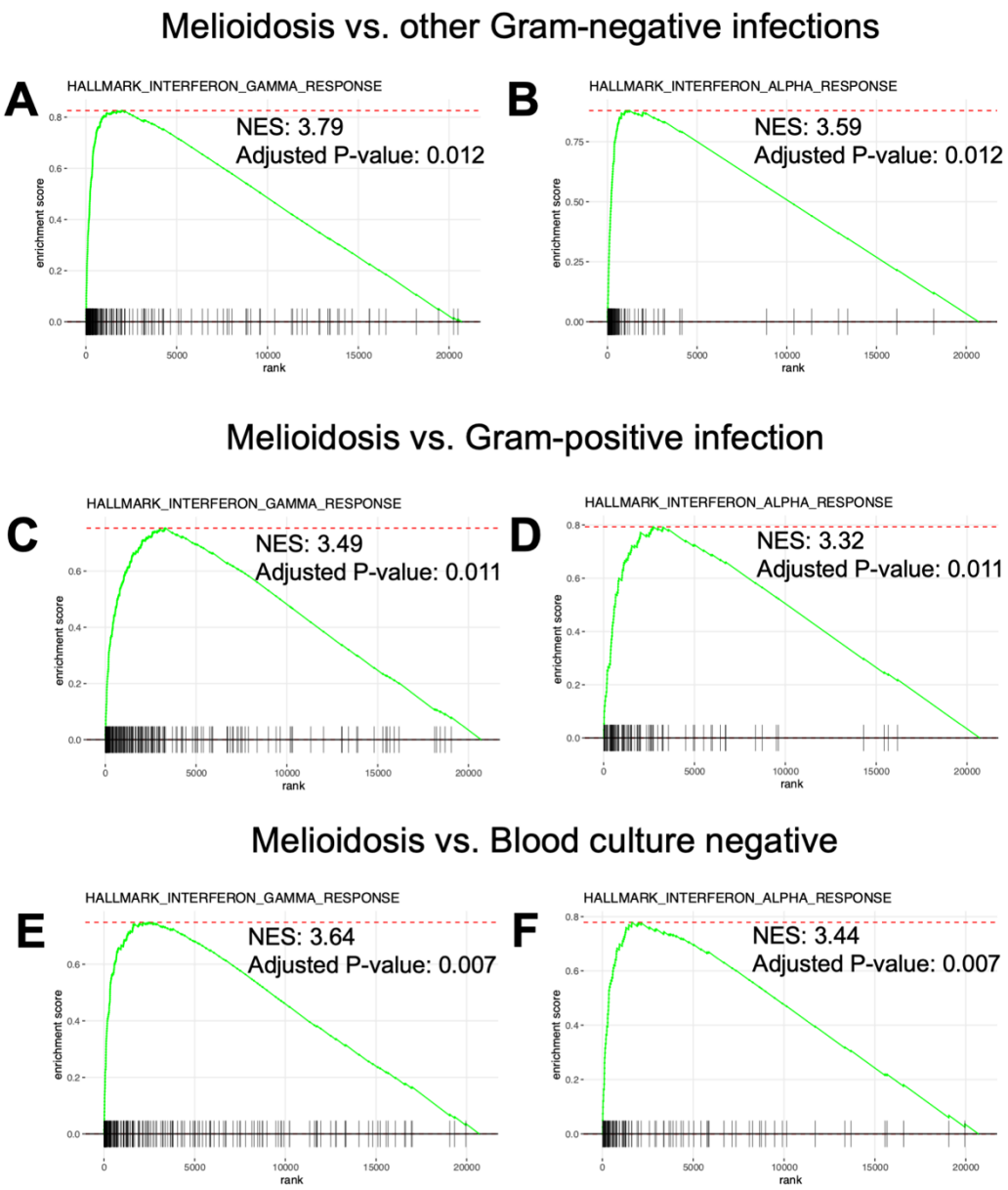

Figure 5.14 Pre-ranked gene set enrichment analysis (pre-ranked GSEA) of interferon gamma and alpha response based on Hallmark gene sets following differential gene expression analyses among melioidosis compared to other community-acquired infections using fgsea R package **(Figure 5.12)**. A, B: Melioidosis compared to other Gram-negative infections. C, D: Melioidosis compared to Gram-positive infection. E, F: Melioidosis compared to culture negative patients. Each enrichment plot displays normalised enrichment score (NES) and adjusted P-value.

5.5 Discussion

In this study, whole blood samples from patients with community-acquired infections were derived from the four-year prospective observational study conducted at Sunpasitthiprasong hospital, Ubon Ratchathani, in Northeast Thailand. This study enrolled participants with suspected community-acquired infection within 24-hours after admission based on the criteria proposed by 2012 Surviving Sepsis Campaign (*576*). This allows identification of early transcriptomic profiles that are associated with case fatality in melioidosis, compared to other studies (including **Chapter 3**) where enrolment of participants usually occurs after culture-proven melioidosis (*76*). Correspondingly, this study identified melioidosis amongst the top three leading causes of community-acquired bacteraemia in Northeast Thailand, with the highest 28-day hospitalised case fatality rate at 66% (*194*). Therefore, it is important that patients with higher risk of developing severe disease potentially leading to poor outcome, are recognised rapidly allowing appropriate interventions and management.

In this chapter, profound changes of the whole blood transcriptome were observed with over 3,000 DGEs in melioidosis patients compared to controls. Melioidosis causes wide-spread activation of inflammatory immune pathways dominated by innate immune responses and both type I and II interferon responses but suppressed cellular immune response by T cells. Furthermore, fatal melioidosis demonstrated concomitant inflammation and type II immune responses, but a suppressive phenotype of T cell signalling, activation, and antigen presentation compared to survivors. Likewise, melioidosis with bacteraemia was associated with increased fatality. Several pathways were common to both bacteraemia and fatal melioidosis such as excessive inflammation and stunted T cell signalling, likely reflecting

the fact that the presence of bacteraemia in melioidosis is closely correlated with the risk of death as it represents uncontrolled sepsis (*76*).

Sepsis is common in melioidosis (*10*). During sepsis, a high neutrophil-to-lymphocyte ratio is a hallmark of increased disease severity and fatality risk in many infection-causing sepsis settings (*577, 578*). Moreover, sepsis patients who develop lymphopenia are likely to have worse clinical outcomes (*579*). In this study, the depletion and dysregulation of T cells during melioidosis could be due to an over-compensatory anti-inflammatory immune response particularly by IL-10 and PD-1. IL-10 is a potent anti-inflammatory immune modulator that acts by inhibiting activation of many immune cells such as phagocytes and T lymphocytes (*580*). During sepsis, neutrophils are the major source of circulating IL-10, and both are elevated in those who develop more severe disease and associated with increased fatality (*581-583*). Programme death 1 (PD-1) is a cell-cell contact anti-inflammatory mechanism that functions to regulate activation, tolerance, immunomodulation of T cells during infections, inflammatory conditions, and cancers (*584*). Increased expression of PD-1 has been demonstrated in sepsis patients (*212, 295*). PD-1 deficient mice in a polymicrobial sepsis model showed improved survival, increased bacterial clearance and a lower inflammatory immune response. Likewise, monocytes isolated from sepsis patients showed increased PD-1 expression on monocytes compared to uninfected control (*585*). Altogether, excessive inflammation, dysregulated anti-inflammatory response, and impaired T cell-responses during sepsis lead to poor prognosis and worse clinical outcome (*472*).

Host immune responses during sepsis can be heterogenous, in which both pro- and anti-inflammation may occur simultaneously making sepsis management exceptionally

challenging (*569, 570*). Sepsis response signatures (SRSs) have been proposed to classify and predict clinical outcomes in community-acquired sepsis. Sepsis patients with sepsis response signature (SRS1) exhibit immunosuppressed phenotypes, with T-cell exhaustion and reduced capability of class-II antigen presentation and have an increased mortality rate (*296*). In contrast, immunocompetent phenotypes that are associated with better outcomes have been reported in sepsis patients with SRS2 (*296-298*). In the Ubon-Sepsis cohort, non-survivors of melioidosis exhibited suppressed T-cell signalling and antigen presentation compared to survivors. This transcriptomic profile resembles that of the SRS1 signature associated with increased mortality during sepsis (*297*). During severe sepsis, the presence of PAMPs such as LPS in circulation can cause excessive immune activation mediated by TLRs which were highly expressed on leukocytes such as neutrophils (*586*). Consequently, activation of TLR signalling by neutrophils can cause up-regulation of G protein-coupled protein kinase 2 (GRK2) expression that leads to reduced expression of chemokine receptor CXCR2 (*587*). The loss of CXCR2 expression impairs neutrophil migration to the site of infection leading to high circulating neutrophils, increased systemic inflammation, collateral tissue damage, organ dysfunction and death (*588*). In this study, we confirmed the up-regulation of *GRK2* (1.2-fold-increased, adjusted P-value = 0.03), but down-regulation of *CXCR2* (1.3-fold-decreased, adjusted P-value = 0.004) in the non-survivors compared to survivors. This represents a potential mechanism leading to excessive yet ineffective inflammation and associated fatality during melioidosis.

Apoptosis of lymphocytes is thought to be a primary mechanism of depletion of lymphocyte populations during sepsis (*589, 590*). In this chapter, increased frequency of neutrophils, but reduced frequencies of lymphocytes and monocytes were seen in fatal melioidosis compared to survivors. Moreover, increased frequencies of innate immune compartment such as

neutrophils, γδ T cells and unpolarised macrophages (M0), but depletion of lymphocytes including CD8 T cells and resting memory CD4 T cells were observed in fatal cases. Our previous study by *Jenjaroen et al* demonstrated that frequencies of both IFN-γ producing CD4 and CD8 T cells are significantly higher in surviving melioidosis patients (*76*).

Interestingly, γδ T cells were enriched in non-survivors and their roles during melioidosis are less well-known . γδ T cells are unconventional T cells that express unique T cell receptor γ and δ chain and ability to mediate both innate and adaptive immune responses (*591*). A source of IL-17 during the innate immune response is mainly from γδ T cells and NKT cells, with IL-17 functioning as a neutrophil chemoattractant (*592, 593*). However, an expansion of γδ T cells during innate immune response requires IL-23 which is primarily produced by activated macrophages and dendritic cells (*594*). A subset of γδ T cells expressing TLR-1, TLR-2, and dectin-1 have been found to produce IL-17 in response to heat-killed *M. tuberculosis* and *Candida albicans* (*593*). Moreover, increased frequency of the γδ1 T cell subset with pro-inflammatory phenotype has been found in sepsis patients and associated with severe disease (*595*). Therefore, the increased frequencies of γδ T cells observed in the non-survivors could be from γδ1 T cell subset which mainly produces IL-17, in line with KEGG pathway analysis which identified up-regulation of IL-17 signalling pathway in the non-survivors and those with bacteraemia. The increased IL-17 production could attract more neutrophils into the circulation which further exacerbate inflammation leading to an uncontrolled host immune response, potentially collateral tissue damage, organ dysfunction and death (*596*). Interestingly, *Kronsteiner et al. (377)* identified increased frequency of double negative T cells and antibody response in particular IFN-γ producing γδ T cells in response to Bp stimulation were associated with survival in melioidosis patients with T2DM.

In agreement with CIBERSORTx, the deconvolution method by xCell identified enrichment of multiple lymphocyte subsets from both CD4+ and CD8+ T cell compartments in survivors. Moreover, subsets of dendritic cells and monocytes were enriched in the survivors. Of note, Tregs, along with neutrophils and basophils, were enriched in non-survivors compared to survivors. Until now, the role of Tregs during melioidosis is largely unknown. Tregs are known to inhibit activation and function of various immune cell types such as CD4+ T cells, CD8+ T cell, NK cells, NKT cells, monocytes, and dendritic cells (*597*). Immunoinhibitory mechanisms mediated by Tregs include secretion of immunosuppressive cell mediators (e.g. IL-10, adenosine, TGF-β), down-regulation of co-stimulatory molecules via cell-cell contact (e.g. CTLA-4 and Lag3), and induction of cell apoptosis (*598*). *Huang et al.* identified increased serum and transcripts of IL-10 and TGF-β in burn-induced sepsis patients that were significantly higher in non-survivors compared to survivors (*599*). *Chaichana et al*. identified a non-sense mutation in *TLR5* (c.1174C>T) that was associated with survival in melioidosis, with plasma IL-10 and TNF significantly elevated in non-survivors compared to survivors (*71*). Therefore, suppressive T-cell signalling and function in fatal melioidosis may be partly regulated by Tregs.

Up to 60% of melioidosis patients present with pneumonia and bacteraemia manifestation (*10*). Pathways involved in inflammation such as neutrophil degranulation, interleukin signalling, IL-17 signalling and granulocyte migration, but down-regulation of lymphocyte-mediated immune pathways were shared between fatal melioidosis and those with bacteraemia. In agreement with the results from canonical pathway analysis, IL-17, p38 mitogen-activated protein kinase (p38 MAPK), and hypercytokine/hyperchemokine response were activated in the patients with bacteraemia. The aforementioned involvement of IL-17 in regulating the innate immune response due to the presence of Bp in the blood

could cause systemic inflammation leading to tissue damage, organ dysfunction, and associated poor outcomes (*600*). Furthermore, the up-regulation of p38 MAPK could promote chemotaxis of neutrophils and other innate immune cells to the sites of infection and into the circulation in response to the infection (*601*). Interestingly, melioidosis patients with pneumonia show reduced pro-inflammatory immune responses such as cytokine-chemokine receptor interaction and natural killer cell mediated cytotoxicity responses compared to non-pneumonia cases. In line with the pathway analysis, immunophenotyping by xCell identified key immune cells that may explain reduced pro-inflammatory immune response such as NK cells, Th1 cells, and CD8+ T cells in melioidosis presenting with pneumonia. Type I immune responses are indispensable during intracellular infections (*602*). IFN-γ, a key type I immune response cytokine, is mainly produced from Th1 cells, cytotoxic T cells, and NK cells (*603, 604*). An experimental severe pneumonia model of *Legionella pneumophila* (LPN) infection demonstrated that IFN-γ-producing NK cells in mice were protected against LPN infection, and this effect was diminished in NK cell-depleted mice (*605*). Moreover, lower counts of CD8+ T cells ($\leq$ 400 cells/mm^3) were found to be associated with increased risk of acquiring bacterial pneumonia and morality rate in HIV+ individuals (*606*). Altogether, this chapter supports the importance of cell-mediated immune response against development of pneumonia during melioidosis. Nevertheless, further in-depth study of the underlying immunopathology associated with pneumonia in melioidosis is warranted.

The module-trait relationship analysis by WGCNA was used to identify co-expressed gene modules associated with 28-day mortality and hub genes that may be responsible for the deleterious immune response in fatal melioidosis. The top 3 co-expressed gene modules associated with 28-day mortality were highly enriched with pathways involved in

inflammatory immune responses such as activation and chemotaxis of leukocytes, inflammatory response, and interferon signalling. By focusing on the ME blue module with the highest correlation to 28-day mortality, 6 hub genes *CEACAM1*, *SERPINB1*, *SORT1*, *PGD, ATP11B* and *TBC1D8* were found to be up-regulated in fatal melioidosis. *CEACAM1* encodes a cell adhesion molecule which is widely expressed on numerous cell types including epithelial, endothelial, innate and adaptive immune cells (*607, 608*). Along with other PRRs, various Gram-negative bacteria such as *E. coli*, *Salmonella* spp., and *Neisseria gonorrhoeae* (*N. gonorrhoeae*) have been found to utilise this cell surface molecule as a binding site to enter cells (*609, 610*). Upon binding to CEACAM1, it activates the cytosolic tail and recruits Src homology region-2 domain-containing phosphatase (SHP)-1 and SHP2 resulting in suppressed TCR signal transduction via CD3ζ chain and ZAP-70 and inhibition of T cell function and activation (*610, 611*). This mechanism, together with up-regulation of IL-10 and PD-1 pathways, may explain down-regulated T-cell signalling cascades in fatal melioidosis.

SERPINB1 encodes serine protease inhibitor B1 (SerpinB1) which plays a regulatory role in inhibiting several neutrophil serine proteases (NSPs) during activation of neutrophils such as neutrophil elastase (NE), cathepsin G (CG), and proteinase-3 (*612*). Several animal studies have demonstrated that SerpinB1 limits excessive activity of NSPs, in turn preventing tissue damage, thus serving a protective role during inflammatory responses (*612-614*). The up-regulation of *SERPINB1* in the non-survivors could be a marker of high activity of NSPs during melioidosis. Nevertheless, a role for SerpinB1 during melioidosis requires further study. *SORT1* encodes Sortilin 1 protein which is widely expressed on many immune cell types (*615*). Sortilin 1 has been reported to regulate production of pro-inflammatory cytokines (e.g., IL-6, IFN-α and IFN-γ) and intracellular trafficking in

inflammatory conditions and infectious diseases (*616, 617*). A metadata analysis on sepsis derived from whole blood microarray data identified *SORT1* to be dysregulated within lysosomal membrane protein pathways in sepsis patients compared to controls (*618*). An experimental model of atherosclerosis demonstrated reduced IL-6 and IFN-α production from macrophages and Th1 cells and reduced atherosclerotic lesions in sortilin-deficiency mice (*617*). This suggests the pro-inflammatory immune response can be regulated by sortilin expressed by macrophages and Th1 cells. *ATP11B* encodes ATPase, class VI, type 11B that functions in ion channels and calcium regulation. A study of necrosis in neutrophils by *Kobayashi et.* identified enhanced virulence mechanisms of community-associated MRSA during phagocytosis in neutrophils through up-regulation of *ATP11B* among other genes that regulate of ion-channel homeostasis (*619*). Furthermore, identification of biomarkers associated with septic shock in acute kidney injury study by *Tang et al*. identified pathways involved in inflammation particularly those mediated by neutrophils, that were highly enriched in the septic shock group. Moreover, they proposed *ATP11B* as one of the hub genes which may be associated with septic shock (*620*).

Bp infection may cause dysregulation of intracellular homeostasis leading to necrotic destruction of cells and tissues during acute melioidosis (*621*). As a result, damage-associated molecular patterns (DAMPs) are released into the circulation. The release of DAMP-associated antigens further induces systemic inflammation, thus exaggerating on-going host immune response (*231*). PGD encodes a third enzyme in the oxidative pentose phosphate pathway (PPP), phosphogluconate dehydrogenase (6PGD) that catalyses 6-phosphogluconate to ribose 5-phosphate during anti-oxidative process and cell proliferation (*622*). Up-regulation of 6PGD and glucose-6-phosphatedyhydrogenase (G6PD) have been reported in sepsis patients and in an experimental sepsis model suggesting an alteration of

normal immunometabolism with an increase of glycolysis and PPP (*623*). *Daneshmandi et al.* identified increased frequency and function of effector CD8+ T cell in 6PGD-deficient model with increased mitochondrial respiratory by reactive oxygen species (*624*). A follow-up study using the same model identified a shift in T cell polarization towards Th1, Th2 and Th17, but reduced Treg development in 6PGD-deficiency model(*625*). Taken together, the host immune response during infection via production of cytokines and chemokines requires high levels of energy. To keep up with the demand, activated immune cells switch metabolic pathways from oxidative phosphorylation to glycolysis and PPP (*626*). Over-expression of *PGD* might favour the development of Treg and anti-inflammatory immune responses during melioidosis. In agreement with the results from functional pathways and deconvolution, up-regulation of the IL-10 pathway and enrichment of Treg cells were associated with fatal melioidosis.

The aforementioned hub genes were derived from the most significant co-expressed gene module associated with 28-day mortality. To complement these findings, knowledge-based upstream regulator analysis was performed on all DEGs following DGE analysis between non-survived compared to survived melioidosis cases. In this study, melioidosis patients with bacteraemia were associated with increased fatality. The top 5 activated upstream regulators including *TNF, IL4, IL1A, PTGER2*, and *OSM* were common between fatal melioidosis and those who had bacteraemia. *TNF* encodes tumour necrosis factor (TNF), a key pro-inflammatory cytokine known to regulate host immune responses in both innate and adaptive immune compartments during infection (*627*). TNF is mainly produced from activated macrophages, monocytes, neutrophils and T cells which initiate a number of host immune responses such inflammation, chemotaxis and apoptosis (*628*). A number of studies have reported elevated serum TNF in non-survivors and associated with increased case

fatality (*629-631*). Therefore, it has been one of the therapeutic targets aiming to reduce disease severity during sepsis. Unfortunately, many clinical trials targeting TNF were not successful, indicating complexity of host immune response during sepsis (*205, 632, 633*). Moreover, TNF can induce apoptosis of mature CD4 T and CD8 T cells (*634, 635*). Thus, the activation of *TNF* could potentially cause apoptosis of T cells leading to depletion of T cells in the fatal melioidosis group. *IL4* encodes IL-4 cytokine, a Th2 cytokine mainly secretes from mast cells, CD4 T cells, NKT cells and type 2 innate lymphoid cells (*636*). IL-4 is known to regulate (inhibit) Th1 immune responses and has been shown to play a detrimental role during infections (*637, 638*). IL-4 inhibits neutrophil recruitment, migration to the site of infection and pro-inflammatory signalling (*639*). Therefore, up-regulation of *IL4* might restrict protective immunity by type I immune response during melioidosis.

Of note, *OSM* encodes oncostatin M, a member of the IL-6 family which is produced by many immune cells such as neutrophils, macrophages and T lymphocytes and is known to play an essential role during inflammation and infection (*640-642*). A recent study by *Gong et al.* identified elevated serum oncostatin M in sepsis patients compared to non-sepsis ICU patients and healthy controls. Moreover, increased serum oncostatin M correlated with markers of disease severity such as SOFA score, white blood cell count, and 28-day mortality (*643*). Therefore, oncostatin M has been proposed as a diagnostic and prognosis biomarker of sepsis and other in inflammatory conditions (*643-645*). The 3 inhibited upstream regulators including *DUSP1, GATA3*, and *CIITA* may be involved in dysregulation of host immune response during melioidosis. For example, *DUSP1* encodes for Mitogen-Activated Protein Kinase Phosphatase 1 or Dual Specificity Phosphatase 1, the protein that regulates inflammatory immune response essential for control of infection (*646*). An experimental sepsis study by *Hammer et al* (*647*) using *DUSP1*-deficient mice showed

increased serum CCL-4, IL-10, and IL-6, but failed to clear bacterial infection and had poorer outcome compared to wild-type mice. Altogether, the identified upstream regulators suggest broad activation of inflammatory programmes leading to an excessive inflammatory immune response with systemic inflammation, tissue damages and organ dysfunction in fatal melioidosis (*208*).

During acute melioidosis, Bp infection drives profound up-regulation of both type I and II interferons and inflammatory responses mediated by the innate immune compartment (*101*). Bp is an intracellular bacterium which can infect many cell types and replicate within the cytosol (*648*). Type I immunity, particularly the IFN-γ-mediated immune response, is important for controlling intracellular pathogens such as Bp, Mtb and *Salmonella spp*. (*76, 649, 650*). An earlier transcriptomic study by *Koh et al.* identified profound up-regulation of both type I and II interferon signalling pathways in melioidosis and tuberculosis (*101, 102*). In this chapter I sought to identify a transcriptomic signature that discriminates melioidosis from other infections from the same study setting. I identified a transcriptomic signature of 94 genes (77-up and 17-down DEGs) that distinguished melioidosis from other infections. Moreover, the results from GSEA confirmed that melioidosis drives up-regulation of both IFN-γ and IFN-α responses compared to other community-acquired infections within the same study setting. This work provides the springboard for further development of a biomarker set to discriminate melioidosis from other infections, with diagnostic applications.

This study has several strengths including a relatively large sample size of well-characterised patients with suspected sepsis enrolled systemically and prospectively over four years of study, providing the largest collection of melioidosis samples for RNA-sequencing,

alongside early enrolment of participants within 24-hours of admission. However, there are some limitations. This study utilised the whole blood bulk-RNA sequencing approach, and as a result there is heavy dominance of transcripts derived from neutrophils which could potentially obscure transcriptome from other cell populations. Nevertheless, the whole blood approach allows unbiased analysis of the entire circulating blood compartment, and inclusion of neutrophils that are difficult to preserve and study by conventional cellular immunology approaches due to their labile nature. Likewise, the cell-type signature for the deconvolution technique (CIBERSORTx) was initially derived from a cancer study, therefore its extrapolation to infection patients has limits, for example the presence of macrophage and mast cells in circulation detected in this study may fundamentally differ between cancer and infection cohorts. These drawbacks may be addressed by a single cell RNA sequencing approach in future studies.

In conclusion, this chapter demonstrates profound changes in the whole blood transcriptome during melioidosis. Fatal melioidosis patients show distinct transcriptomic profiles involving excessive and uncontrolled inflammation and concomitant Th2 responses, but impeded fine-tuning of T-cell response and antigen presentation. These heterogenous host immune responses highlight a complex relationship between pro- and anti-inflammatory immune response during melioidosis. Depletions of many lymphocyte subsets and dendritic cells were associated with poor outcome, in which γδ T cells and Tregs, in addition to neutrophils and inflammatory macrophages, may be responsible for a deleterious immune response. The suppressed cell-mediated immune compartment could be due to over-compensatory anti-inflammatory mechanisms or immunomodulation by Bp as suggested by the identified hub genes. Moreover, the transcriptomic signature of melioidosis was dominated by type I and II interferon responses which discriminate melioidosis from other

community-acquired infections. Ultimately, the identified transcriptomic profiles associated with fatal melioidosis can be useful for diagnostic and prognostic tool development aiming for rapid detection of patients at higher risk of severe disease. Therefore, appropriate treatments and interventions can be initiated early and efficiently.

Chapter 6: Validation of transcriptomic profiles associated with fatal melioidosis in the independent melioidosis cohort

6.1 Introduction

Sepsis is common in melioidosis where case fatality in endemic areas may exceed 50% despite recommended treatment (*10, 468*). In melioidosis, elevated pro-inflammatory cytokines such as IL-1β, TNF-α, IL-6, IL-8, IL-17A and anti-inflammatory IL-10 response have been observed in fatal melioidosis (*52, 56, 60, 651*). Moreover, impaired cellular immune responses to melioidosis by IFN-γ secreting CD4+ T and CD8+ T lymphocytes have been reported in fatal melioidosis compared to survivors (*76*). In **Chapter 5**, the whole blood transcriptomic profile associated with fatal melioidosis was identified in melioidosis patients admitted within 24 hours after hospital admission. The transcriptomic profile features up-regulation of pathways involved in pro- and anti-inflammatory immune responses and down-regulation of cell-mediated immune responses in particular T cells in fatal melioidosis.

In 2021, *Yimthin et al.* reported up-regulation of innate immune pathways such as activation of myeloid leukocyte and TLR cascades in non-survived melioidosis patients compared to the survivors. Moreover, increased expression of genes involved in inflammation such as *IL1R2, GAS7*, *IRAK3* and *NFKBIA* was proposed to be a hallmark of fatal melioidosis (*428*). Correspondingly, the proposed signature genes were also found to be up-regulated in non-survivors compared to survivor melioidosis patients in **Chapter 3**.

In this chapter, the identified transcriptomic profile from **Chapter 5** was validated using the independent whole blood transcriptomic data generated from acute melioidosis patients from a multi-centre study (DORIM) in seven provinces in Northeast Thailand with similar

study settings to the Ubon-Sepsis Cohort of **Chapter 5**, but excluding Ubon Ratchathani province (*428, 651*). Of note, participants from the validation cohort were enrolled following culture-confirmed melioidosis with a median of 3 days after hospital admission. I hypothesised that the transcriptomic profile associated fatal melioidosis is prominent prior initiation of treatment. Hereby, I aimed to compare the transcriptomic profiles associated with fatal melioidosis between the discovery (**Chapter 5**) and validation (**Chapter 6**) cohorts. Having identified the transcriptomic signatures associated with death, it would facilitate the development of a prognostic tool to identify patients at high risk of death for targeted therapy, thus reducing the number of case fatalities in resource-limited settings.

6.2 Specific objectives

1. To investigate the whole blood transcriptomic profile associated with fatal melioidosis compared to the patients who survived, in the validation cohort.
2. To compare the identified whole blood transcriptomic profile between the discovery and validation cohort.
3. To identify pathways and upstream regulators associated with fatal melioidosis that may be responsible for the deleterious host immune response during melioidosis.

6.3 Materials and Methods

6.3.1 Study design, ethical approval, and data acquisition

Whole blood bulk RNA sequencing data were kindly provided by Professor Narisara Chantratita and Thatcha Yimthin from the Department of Microbiology and Immunology, Faculty of Tropical Medicine, Mahidol University, Bangkok, Thailand. This dataset was published in the journal *Emerging Microbes and Infections* entitled "Blood transcriptomics to characterise key biological pathways and identify biomarkers for predicting mortality in melioidosis" (*428*). Whole blood transcriptomic data were generated from a prospective longitudinal study, as part of multi-centre study conducted between 2015 and 2019 across seven provincial hospitals in the Northeast of Thailand. Participants aged ≥ 15 years with culture-confirmed melioidosis were prospectively enrolled (*428, 651*). 3 ml of whole blood was collected into Tempus blood RNA tubes within 24 hours after a positive culture of Bp was obtained in the hospital laboratory. The patients were enrolled into the study with a median of 3 days following hospital admission (interquartile range [IQR], 4-6). As a baseline control, uninfected healthy donors aged ≥ 18 years were enrolled at provincial hospitals in Udon Thani and Mukdhahan provinces. This study was approved by the ethical committee of the Faculty of Tropical Medicine, Mahidol University (MUTM2015-022-03), the Udon Thani Hospital Ethics Committee (6/2561), and the Mukdhahan Hospital Ethics Committee (MEC 010/59) (*651*). For this chapter, a total of 29 culture-proven melioidosis and 3 healthy donors from blood donation centre at Udon Thani Hospital in Udon Thani province were included into transcriptomic study.

6.3.2 Sample collection, preparation, and RNA sequencing

For full details regarding materials and methods used in this study, please refer to *Yimthin et al.* "Blood transcriptomics to characterize key biological pathways and identify biomarkers for predicting mortality in melioidosis." *Emerging microbes & infections* vol. 10,1 (2021): 8-18. Briefly, 3 ml whole blood samples were collected from melioidosis patients following culture-proven melioidosis and healthy blood donors into Tempus blood RNA tubes (Applied Biosystems). The samples were stored at either -20°C or -80°C at the study sites until further processing. RNA isolation was performed using MagMAX™ for Stabilised Blood Tubes RNA Isolation Kit (Life technologies) and RNA concentration was measured using the NanoDrop Spectrophotometer (Thermo Fisher Scientific). The RNA quality was assessed using the Agilent RNA 6000 Pico kit on 2100 Bioanalyzer (Agilent Technologies). RNA libraries were prepared using Ion AmpliSeq™ Transcriptome Human Gene Expression Kit (Thermo Fisher Scientific). The final libraries were loaded onto Ion PI v3 chips and sequenced using Ion PI Hi-Q Sequencing 200 Kit chemistry (Life Technologies) on Ion Proton System for 200 bp read length (*428*).

6.3.3 Differential gene expression and functional pathway analysis

A total of 20,812 transcripts were generated from the sequencing and annotated to gene symbol. Genes with no counts or lowly expressed were removed with a cut-off of row sum below 10. Pre-filtered genes (16,532 features) were normalised and variance stabilising transformed using the DESeq2 R package for subsequent data analyses (*392*). To assess whether melioidosis induces global transcriptional changes, multidimensional scaling by principal component analysis (PCA) using the top 1,000 most variable genes was performed in 29 melioidosis patients and 3 healthy control subjects. Differential gene expression (DGE) analysis was carried out using negative binomial generalised linear model implemented in

DESeq2 R package adjusted for age and sex. The subsequent analyses were performed as described in **Chapter 2**. Additionally, Ingenuity Pathway Analysis (IPA) following DGE analysis was performed on DEGs (adjusted P-value <0.05) to identify significant canonical pathways and upstream regulators (P-value <0.05, absolute(z-score)>2).

6.3.4 Weighted gene co-expression network analysis (WGCNA) and identification of hub genes

To identify co-expressed gene modules and hub genes associated with fatality in melioidosis, a signed network by WGCNA was performed followed by module enrichment analysis and identification of hub genes in 29 melioidosis patients (*415*). Pre-filtered, normalised and variance stabilizing transformed expression data (16, 522 features) of melioidosis cohort (n=29) were analysed using WGCNA R package (*415*). The remaining workflow was performed as described in **Chapter 2**.

6.3.5 Deconvolution of bulk RNA sequencing data

Cell type abundances were estimated from the bulk RNA sequencing data using CIBERSORTx (*431*) and xCell (*431*) as described in **Chapter 2**. The melioidosis patients were divided into non-survivors (n=15) and survivors (n=14). The imputed cell fractions and enrichment were compared using non-parametric Mann-Whitney test in R programme.

6.3.6 Gamma-delta T cell phenotyping

To validate increased frequency of gamma-delta (γδ) T cells in fatal melioidosis patients, immunophenotyping of γδ T cells by flow cytometry was performed. Cryopreserved peripheral blood mononuclear cells (PBMCs) from acute melioidosis patients derived from the MICRO1501 study (**Chapter 3**) were thawed at 37°C and washed one time with RPMI

medium supplemented with 10% heat-inactivated fetal calf serum (R10). Afterwards, cells were rested in R10 medium supplemented with Benzonate Nuclease (Cat no#E1014-5KU, Millipore) at 37°C for one hour and washed with R10 afterwards. For extracellular staining, cell were stained for 20 min on ice in the dark with following anti-human antibodies: CD3-BV510 (Clone:UCHT1, Cat no#300448, Becton Dickinson), CD69-PE (Clone:FN50, Cat no#310906, Biolegend), TCR-γδ1-VioBlue (Clone:REA173, Cat no#130-120-443, Miltenyi Biotec), TCR-γδ2-FITC (Clone:B6, Cat no#555738, Becton Dickinson), Live/Dead fixable near-IR dead cell staining kit (Cat no#L10119, Invitrogen). Cells were then fixed and permed for 20 minutes using BD Cytofix/Cytoperm kit (Cat no#554714, Becton Dickinson) and followed by intracellular staining with Granzyme-B-AF647 (Clone:GB11, Cat no#515406, Biolegend) for 20 minutes on ice in the dark. Cells were then acquired using a MACSQuant X flow cytometer (Miltenyi Biotec). Flow cytometry data were analysed using FlowJo software version 10.8.1 on Mac OS X Catalina version 10.15.7. PBMCs were first gated based on forward (FSC-A) and side (SSC-A) scatter followed by single cell gating using FSC-H and FSC-A. Live CD3+ populations were gated within the single-live cell gate ($CD3^+ LD^-$). Subsets of γδ T cells populations were based on the expression of the following cell surface markers: γδ1 T cells ($CD3^+\gamma\delta1^+$), CD69+ γδ1 T cells ($CD3^+\gamma\delta1^+$ $CD69^+$), Granzyme-B+ γδ1 T cells ($CD3^+\gamma\delta1^+$ Granzyme-B^+), γδ2 T cells ($CD3^+\gamma\delta2^+$), CD69+ γδ2 T cells ($CD3^+\gamma\delta2^+$ $CD69^+$), and Granzyme-B+ γδ2 T cells ($CD3^+\gamma\delta2^+$ Granzyme-B^+) (**Supplementary Figure 6.1**).

6.3.7 Phospho-flow cytometry in T cells

To validate reduced T cell signalling in fatal melioidosis patients, phospho-flow cytometry in T cells was performed. Matched cryopreserved PBMCs were thawed and rested as described previously. Cells were then stimulated with recommended concentration of cell

activation cocktail (phorbol myristate acetate (PMA)/ionomycin, Cat no#423301, Biolegend), ImmunoCult human T cell activator (soluble anti- CD3/CD28/CD2, Cat no#10970, STEMCELL technologies), and R10 medium at 37°C for 20 minutes. Stimulations were stopped by adding ice-cold phosphate saline buffer and immediately centrifuged at 4°C. Cells were then fixed for 20 minutes on ice with True-Nuclear fixing buffer from True-Nuclear Transcription Factor Buffer Set (Cat no#424401, Biolegend). Afterwards, cells were permed for 20 minutes on ice with True-Nuclear perm buffer. Cells were stained for 20 minutes on ice in the dark with following anti-human antibodies: CD3-PerCP (Clone:UCHT1, Cat no#300428, Biolegend), CD4-V450 (Clone:RPA-T4, Cat no#560345, Becton Dickinson), CD8a-BV510 (Clone:RPA-T8, Cat no#301047, Biolegend), FITC anti-ERK1/2- Phospho (Thr202/Tyr204, Clone:6B8B69, Cat no#369520, Biolegend), ZAP70-PE (Clone:1E7.2, Cat no#313404, Biolegend), PE-Cy7 anti-RPS6 Phospho (Ser235/Ser236, Clone:A17020B, Cat no#608606, Biolegend). Cells were then acquired and analysed as previously described. Median Fluorescence Intensity (MFI) was detected for each marker expressing in CD4+ T, CD8+ T and double negative (DNT) T cells. Relative Fluorescent Intensity (RFI) was used for a comparative analysis and calculated by subtracting with MFI from the negative control (R10 medium). PBMCs were first gated based on forward (FSC-A) and side (SSC-A) scatter followed by single cell gating using FSC-H and FSC-A. CD3+ populations were gated within the single cell gate ($CD3^+$). Subsets of T cells populations were based on the expression of the following cell surface markers: CD4+ T cells ($CD3^+$ $CD4^+$), CD8+ T cells ($CD3^+$ $CD8^+$), double negative T cells ($CD3^+$ $CD4^-$ $CD8^-$). Expression of each intracellular markers including ZAP-70, RPS6, and ERK1/2 were detected by MFI within each T cell subset (**Supplementary Figure 6.2**).

6.4 Results

6.4.1 Demographics of the validation cohort

RNA sequencing data were generated from the independent cohort of 29 patients with culture-confirmed melioidosis along with 3 uninfected healthy donors as a baseline control. **Table 6.1** shows the demographics of the participants. The age and sex were not significantly different between non-survivors, survivors, and healthy controls. The proportions of patients with and without diabetes was similar between non-survivors and survivors. The main difference between the discovery (**Chapter 5**) and validation cohort (this chapter) was the timing of participant enrolment with respect to hospital admission, with the validation cohort enrolled the participants following culture-confirmed melioidosis with a median of 3 days after hospital admission (**Figure 6.1**). On the other hand, the discovery cohort enrolled the participants within 24 hours after hospitalisation because this was a large NIH-funded study sampling 5000 consecutive admissions with sepsis, enabling later identification of those with culture-confirmed melioidosis.

Table 6.1 Characteristics of melioidosis patients and healthy donors.

Characteristic (N=32)	Non-survived Melioidosis (n=15)	Survived Melioidosis (n=14)	Healthy control (n=3)	P-value
Sex, Female (%)	4 (27)	4 (29)	2 (67)	
Male (%)	11 (73)	10 (71)	1 (33)	0.9
Age in years, median (interquartile range)	55 (46-65)	50 (44-62)	28 (28-34)	0.3
Diabetes status, DM (%)	8 (53)	7 (50)	0	
non-DM (%)	7 (47)	7 (50)	3 (100)	0.85

Binary and continuous variables were tested with Chi-square and Kruskal-Wallis tests respectively.

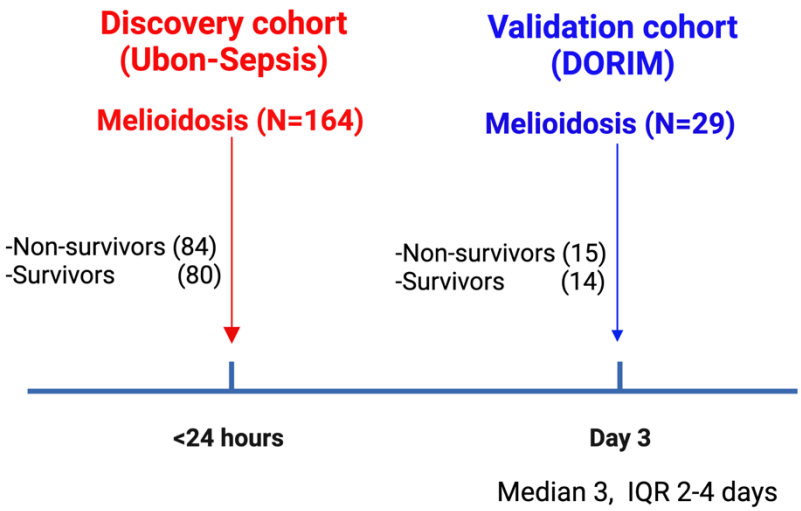

Figure 6.1 Timelines of participant enrolment for discovery and validation cohort. Discovery cohort (Ubon-Sepsis) consists of 84 non-survived and 80 survived melioidosis patients. The patients from discovery cohort were enrolled within 24-hour after hospital admission. Validation cohort (DORIM) consists of 15 non-survived and 14 survived melioidosis patients. The patients from validation cohort were enrolled following culture-proven melioidosis with a median of 3 days after hospital admission. IQR= Interquartile Range. Created with BioRender.com.

6.4.2 Whole blood transcriptomic profiles are distinct in fatal melioidosis

An average of 20 million reads per sample (IQR 18-22M) was generated from whole blood RNA sequencing for the validation cohort (**Supplementary Figure 6.3A)**. A total of annotated 16,532 transcripts following pre-filtering for lowly expressed genes were used for subsequent data analyses. The pre-filtered genes were normalised using median of ratios method implemented in DESeq2 R package (*392*) (**Supplementary Figure 6.3B, 6.3C**). The normalised expression data were variance-stabilising transformed for data visualisation. To evaluate the impact of case fatality by 28-day mortality measurement on whole blood transcriptome, the 1,000 most variable genes were selected for PCA analysis. Firstly, PCA identified clear separation between disease and control groups, in which healthy donors were

grouped together and adjacent to survived melioidosis patients (**Figure 6.2**). Secondly, PCA coloured by 28-day mortality status shows some separation between non-survived and survived melioidosis patients (**Figure 6.2**). Diabetes is a major risk factor of having melioidosis. However, PCA coloured by diabetes status did not segregate between melioidosis with and without diabetes, similar to the lack of distinction by diabetes status I saw in **Chapter 3** and **Chapter 5** (**Supplementary Figure 6.4**).

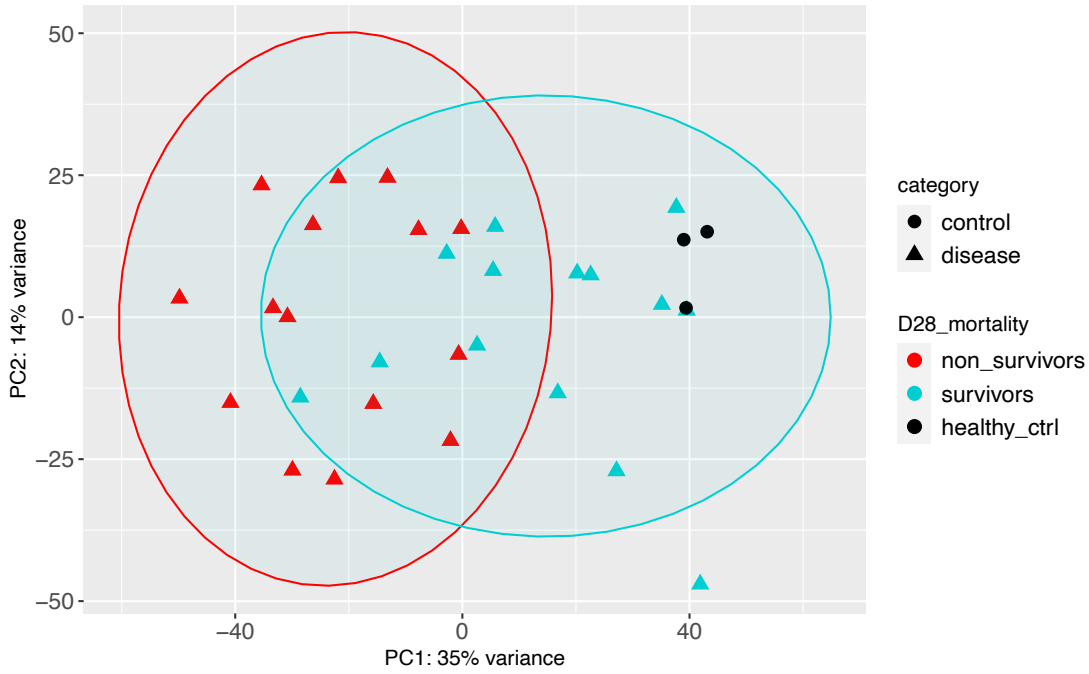

Figure 6.2 Multidimensional scaling by principal component analysis (PCA) of the 1,000 most variable genes. PCA in melioidosis and control cohorts coloured by 28-day mortality status. Patients with melioidosis, divided into non-survivors ("non_survivors", red triangles, n=15), survivors ("survivors", turquoise triangles, n=14), and healthy donors ("healthy_ctrl", black circles, n=3). PCA plots were generated using plotPCA function implemented in DESeq2 R package.

6.4.3 Profound down-regulation of adaptive immune responses by T cells are associated with case fatality in melioidosis

To identify the impact of subsequent case fatality on the whole blood transcriptome of melioidosis patients, DGE analysis was performed between non-survived and survived melioidosis patients in the validation cohort. DGE analysis identified 838 up- and 914 down-DEGs in non-survivors compared to survivors (absolute[Log2 fold-change]≥1, adjusted P-value<0.05) (**Figure 6.3 A**). A total of 449 genes (188 [15%] up- and 261 [15%] down-DEGs) were common between discovery and validation cohort (**Supplementary Figure 6.5**). Likewise, Pearson's correlation analysis of DEGs based on log2 fold-change identified highly concordant expression profiles (Pearson's correlation coefficient R=0.93, P-value =2.2x10^{-16}) of the non-survivors compared to survivor between discovery (**Chapter 5**) and validation (this chapter) (**Figure 6.3B**).

Following DGE analysis, functional pathway analysis based on Reactome gene sets identified up-regulation of pathways involved in inflammatory immune responses including neutrophil degranulation, signalling by interleukins, and IL-4 and IL-13 signalling, common between both the discovery and the validation cohort (**Figure 6.4**). Distinctively, pathways involved in TLR cascades such as TLR4, TLR2, and TLR6:TLR2 were only up-regulated in non-survivors compared to survivors from validation cohort. Strikingly, almost all pathways involved in T-cell signalling cascades were down-regulated in non-survivors compared to survivors from both discovery and validation cohorts.

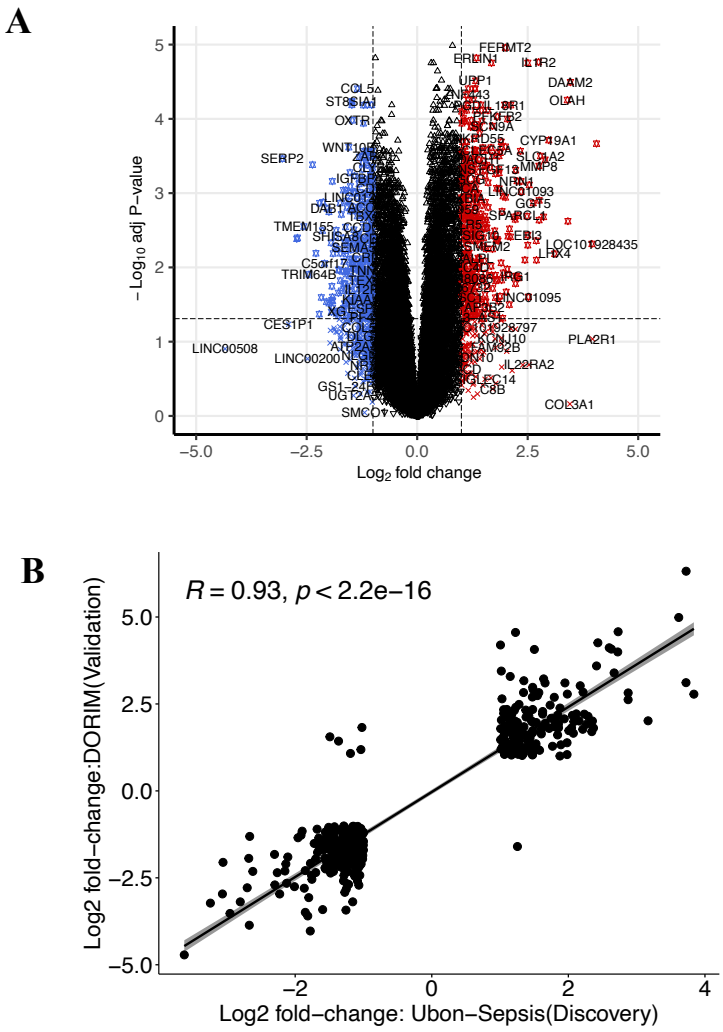

Figure 6.3 Volcano plot of differentially expressed genes in fatal melioidosis and correlation analysis of the differentially expressed genes (DEGs) derived from discovery (**Chapter 5**) and validation (this chapter). A: Differential gene expression (DGE) analysis between non-survived (n=15) and survived melioidosis patients (n=14) from the validation cohort. B: Pearson's correlation analysis of DEGs based on log2 fold-change derived from DGE analyses between non-survived and survived melioidosis patients of the discovery cohort (x-axis, Ubon-Sepsis) and validation cohort (y-axis, DORIM). DEGs were based on absolute[Log2 fold-change]≥ 1 (x-axis) and adjusted P-value <0.05 (y-axis). Pearson's correlation coefficient, corresponding P-value, and linear regression line with 95% confidence interval (shaded area) are displayed within the plot.

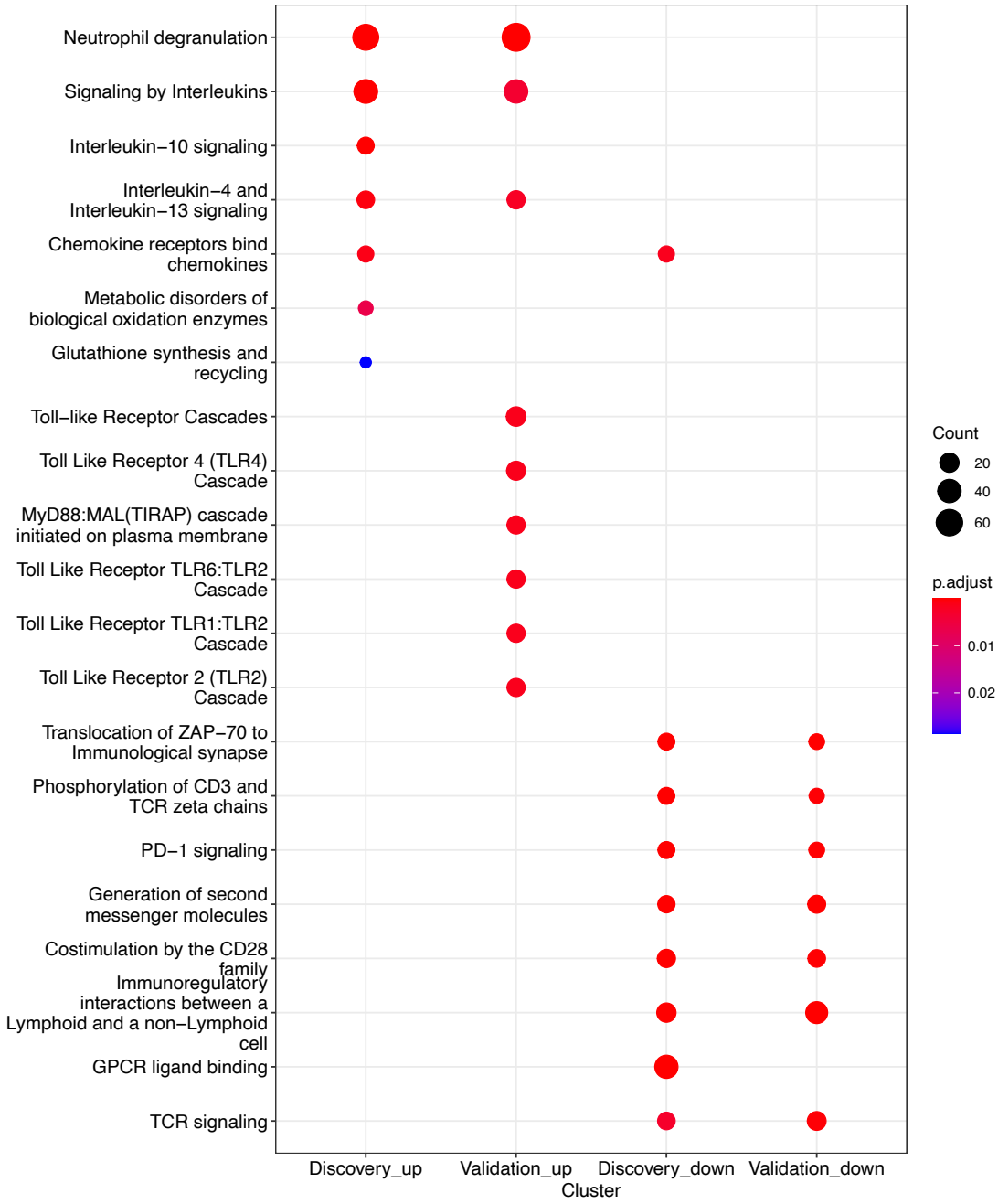

Figure 6.4 Functional pathway analysis based on Reactome gene sets following differential gene expression analysis between non-survived and survived melioidosis patients from discovery (**Figure 5.2B**) and validation cohort (**Figure 6.3**). The top 7 over-represented pathways are displayed. The gradient colour bar corresponds to the adjusted P-value. The size of each term is indicated by representative counts. Differentially expressed genes were pre-filtered based on a cut-off of absolute[Log2 fold-change]≥1 and adjusted P-value <0.05.

In agreement with functional pathway analysis, canonical pathway analysis identified pathways involved in T cell signalling such as T cell receptor signalling, ICOS-ICOSL signalling in T helper cells, and Th1 pathway were down-regulated in non-survivors compared to survivors in both discovery and validation cohorts (**Table 6.2**). On the other hand, PD-1/PD-L1, MSP-RON signalling in macrophages, and IL-6 signalling pathways were up-regulated in fatal melioidosis across both cohorts. Of the top 25 genes, 10 activated upstream regulators were common between the discovery and validation cohorts including *TNF, IL1B, IL4, CEBPA*, *CSF3, IFNG, IL6, OSM, IL17A, STAT3* (**Table 6.3**).

Table 6.2 The top 20 common canonical pathways in fatal melioidosis patients from the discovery and validation cohorts. Differentially expressed genes were derived from differential gene expression analyses between non-survived and survived melioidosis patients and pre-filtered based on a cut-off of absolute[Log2 fold-change]≥1 and adjusted P-value <0.05. Significant pathways were ranked by P-value. Activated pathways (positive z-scores) are labelled in orange. Inhibited pathways (negative z-scores) are labelled in blue.

Canonical Pathways	Discovery	Validation
T Cell Receptor Signaling	-10.823	-4.217
Regulation of IL-2 Expression in Activated and Anergic T Lymphocytes	-9.916	-2.236
ICOS-ICOSL Signaling in T Helper Cells	-3.606	-4.472
Calcium-induced T Lymphocyte Apoptosis	-3.606	-4
Role of NFAT in Regulation of the Immune Response	-4.146	-3.157
CREB Signaling in Neurons	-3.825	-3.263
PKC (theta) Signaling in T Lymphocytes	-3.3	-2.6
Systemic Lupus Erythematosus In T Cell Signaling Pathway	-3.13	-2.646
Th1 Pathway	-3.13	-2.646
PD-1, PD-L1 cancer immunotherapy pathway	3	2.558
CD28 Signaling in T Helper Cells	-2.449	-3
Factors Promoting Cardiogenesis in Vertebrates	-3.13	-2.183
MSP-RON Signaling In Macrophages Pathway	3.742	1.387
Crosstalk between Dendritic Cells and Natural Killer Cells	-1.897	-3
IL-6 Signaling	2.138	2.683
GPCR-Mediated Nutrient Sensing in Enteroendocrine Cells	-2.5	-2
G-Protein Coupled Receptor Signaling	-2.769	-1.668
Glioblastoma Multiforme Signaling	-2.496	-1.886
Dendritic Cell Maturation	-2.746	-1.633
Basal Cell Carcinoma Signaling	-2.646	-1.633

Table 6.3 The top 25 predicted upstream regulators in fatal melioidosis patients from the discovery and validation cohorts. Common predicted upstream regulators between the cohorts are in bold and labelled in orange. Differentially expressed genes were derived from differential gene expression analyses between non-survived and survived melioidosis patients and pre-filtered based on adjusted P-value <0.05. Significant upstream regulators are based on predicted absolute (activation z-score)≥2 and P-value of overlap <0.01.

Discovery cohort			Validation cohort		
Upstream Regulator	Predicted Activation State	Activation z-score	Upstream Regulator	Predicted Activation State	Activation z-score
TNF	**Activated**	**3.627**	***TNF***	**Activated**	**2.484**
IL1B	**Activated**	**4.383**	***IL4***	**Activated**	**3.104**
IL4	**Activated**	**2.162**	***IFNG***	**Activated**	**2.276**
CEBPA	**Activated**	**3.199**	***IL1B***	**Activated**	**3.571**
CSF3	**Activated**	**2.134**	Immunoglobulin	Inhibited	-4.484
IFNG	**Activated**	**2.663**	***CEBPA***	**Activated**	**3.71**
IL6	**Activated**	**4.696**	***CSF3***	**Activated**	**4.662**
IL1	Activated	3.24	***IL6***	**Activated**	**4.202**
Tnf (family)	Activated	2.419	*CSF2*	Activated	2.169
EZH2	Activated	2.868	TCR	Inhibited	-2.701
IL1A	Activated	3.705	*PGR*	Activated	3.007
PTGER2	Activated	2.14	***STAT3***	**Activated**	**2.872**
OSM	**Activated**	**4.607**	***OSM***	**Activated**	**3.44**
TGFBR2	Inhibited	-2.489	*CSF1*	Activated	2.109
C5	Activated	2.527	*SP1*	Activated	2.237
AGT	Activated	2.433	*KLF2*	Inhibited	-2.368
NOD2	Activated	3.346	***IL17A***	**Activated**	**3.793**
IL17A	**Activated**	**3.746**	*EGF*	Activated	4.093
IL33	Activated	2.142	*PPARG*	Activated	3.087
IKBKB	Activated	4.059	*TGM2*	Activated	5.549
CEBPB	Activated	2.243	Akt	Activated	2.614
NFkB (complex)	Activated	3.331	*MYD88*	Activated	2.045
STAT1	Activated	2.226	*NR3C1*	Activated	2.18
STAT3	**Activated**	**2.046**	*STAT6*	Activated	2.069
IL22	Activated	2.958	*HIF1A*	Activated	2.003

6.4.4 Co-expressed gene modules enriched with inflammatory immune responses are associated with poor outcome

To complement the results obtained from DGE and pathway analyses as well as identification of hub genes that may drive deleterious immune responses during melioidosis, WGCNA was performed on the genome-wide expression profile from 29 melioidosis patients in an unsupervised fashion. To identify potential outliers, firstly a sample dendrogram was constructed from normalised variance-stabilising transformed expression data (16,522 features) (**Supplementary Figure 6.6A**). Secondly, a power of β=16 was

chosen (soft-threshold $R^2 = 0.79$ and mean connectivity = 83) in order to achieve scale-free network (**Supplementary Figure 6.6B**). As a result, 25 co-expressed gene modules were identified based on dissimilarity of the topological overlap matrix via hierarchical clustering using the Dynamic Tree Cut method (**Supplementary Figure 6.6C**). Thirdly, module-trait relationship analysis identified several co-expressed genes modules significantly correlated with clinical traits associated with 28-day mortality such as ME blue, darkred, lightgreen, and yellow (indicated in a red box) (**Figure 6.5**). In particularly, ME blue gene module was highly correlated with 28-day mortality (highest Pearson's rho = 0.66, P-value=1e-04) Moreover, ME darkred was highly correlated with bacteraemia status (highest Pearson's rho = 0.66, P-value=1e-04). Distinct expression profiles between non-survivors and survivors within each module (module eigengene, ME) were visualised based on significant correlations to 28-day mortality (both positive and negative). Of 25, 5 co-expressed gene modules including ME blue, darkred, yellow, red, and lightgreen were highly expressed in non-survivors compared to survivors (**Figure 6.6 A-E**). On the other hand, 5 co-expressed gene modules negatively correlated with 28-day mortality including ME turquoise, purple, lightyellow, darkgreen, and darkgrey were highly expressed in survivors compared to non-survivors (**Figure 6.6 F-J**).

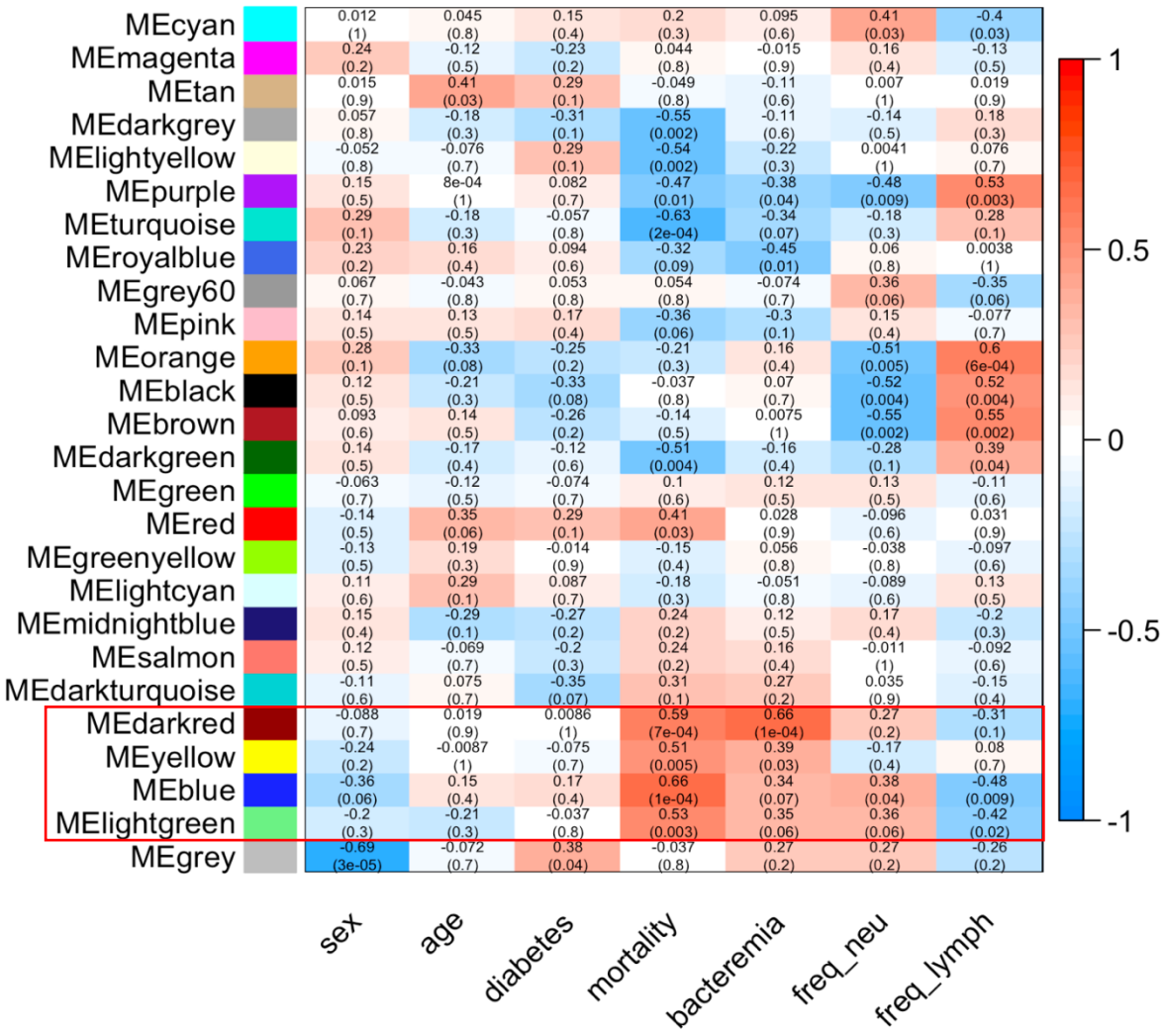

Figure 6.5 Module-trait relationship analysis in 29 melioidosis patients by weighted gene co-expression network analysis. A total of 25 co-expressed gene modules (module eigengenes, MEs) were identified. Each column and row represent clinical traits and MEs with corresponding Pearson's correlation coefficient between each ME-trait pair displayed with P-value in parenthesis. The gradient colour bar indicates the degree of positivity (maximum +1, red) / negativity (minimum -1, blue) for the Pearson's correlation coefficient. Clinical traits include sex (binary outcome), age (in years, continuous variable), diabetes status (binary outcome), 28-day mortality (mortality, binary outcome), bacteraemia (binary outcome), % of total white cell count represented by neutrophils (freq_neu, continuous variable), and % of total white cell count represented by lymphocytes (freq_lymph, continuous variable).

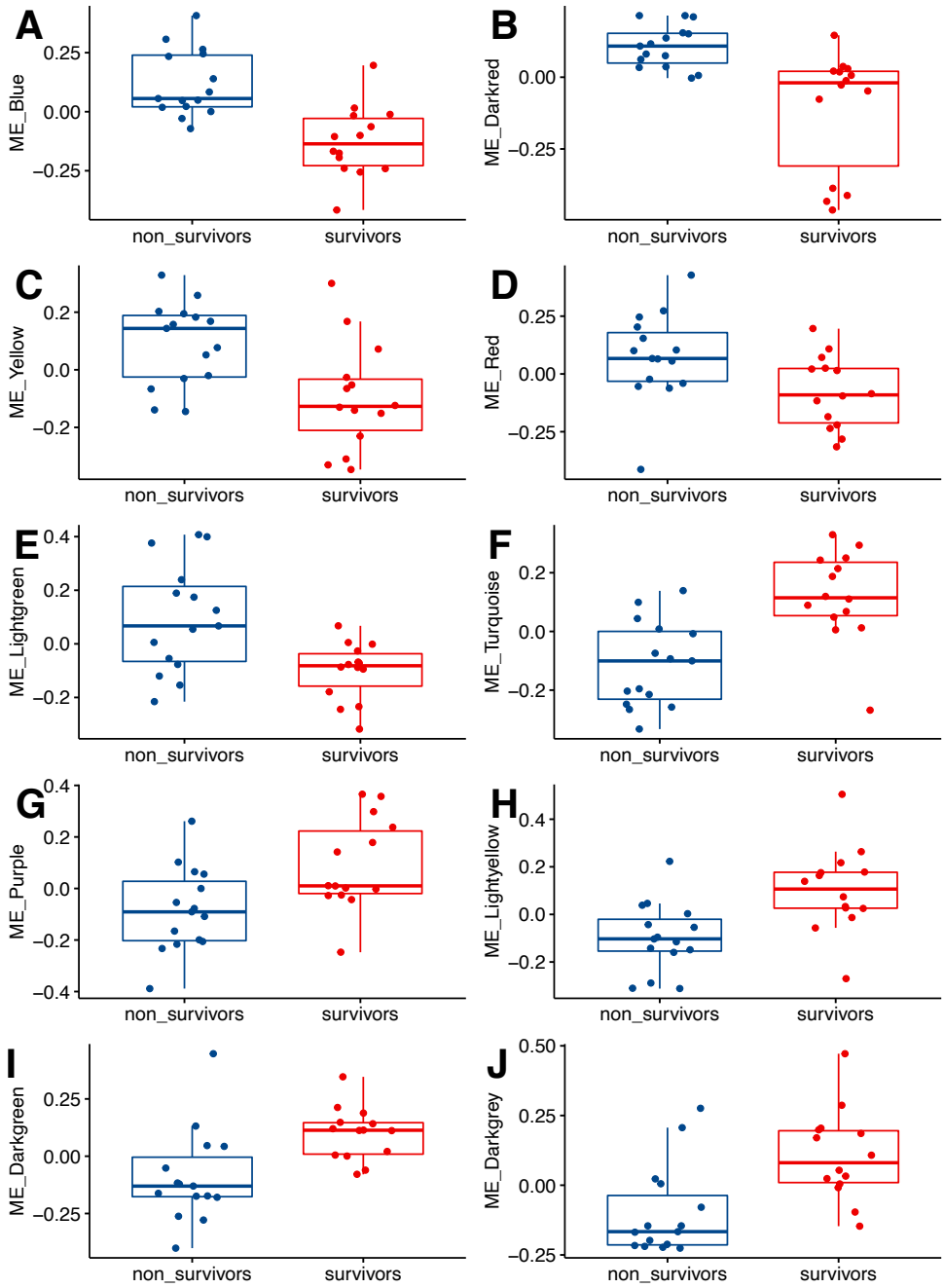

Figure 6.6 Scattered box plots show comparison of co-expressed gene modules (module eigengene, ME) between non-survived (n=15) and survived (n=14) melioidosis based on 28D mortality. ME is considered as a representative expression profile in each gene module. MEs with significant associations with 28-day mortality based on module trait relationship analysis were shown. Box plots represent medians with interquartile range plus lines to minimum, maximum and potential outliers.

6.4.4 Co-expressed gene modules enriched with inflammatory immune responses are associated with poor outcome (continued)

Module enrichment analysis based on Hallmark gene sets within the co-expressed gene modules associated with 28-day mortality identified enriched pathways involved in inflammatory immune responses such as TNF signalling via NF-κB, IL6 JAK STAT3 signalling, inflammatory response, myeloid leukocyte activation and differentiation, and IFN-γ response (**Figure 6.7**). On the other hand, pathways involved in T cell differentiation, antigen processing and presentation, and B cell activation and proliferation were enriched in the co-expressed gene modules associated with survival (**Supplementary Figure 6.7**). Taken together, as found in the discovery cohort, an excessive inflammatory immune response was associated with fatal outcomes at 28 days, whereas cellular regulation and cellular immune response were associated with survival.

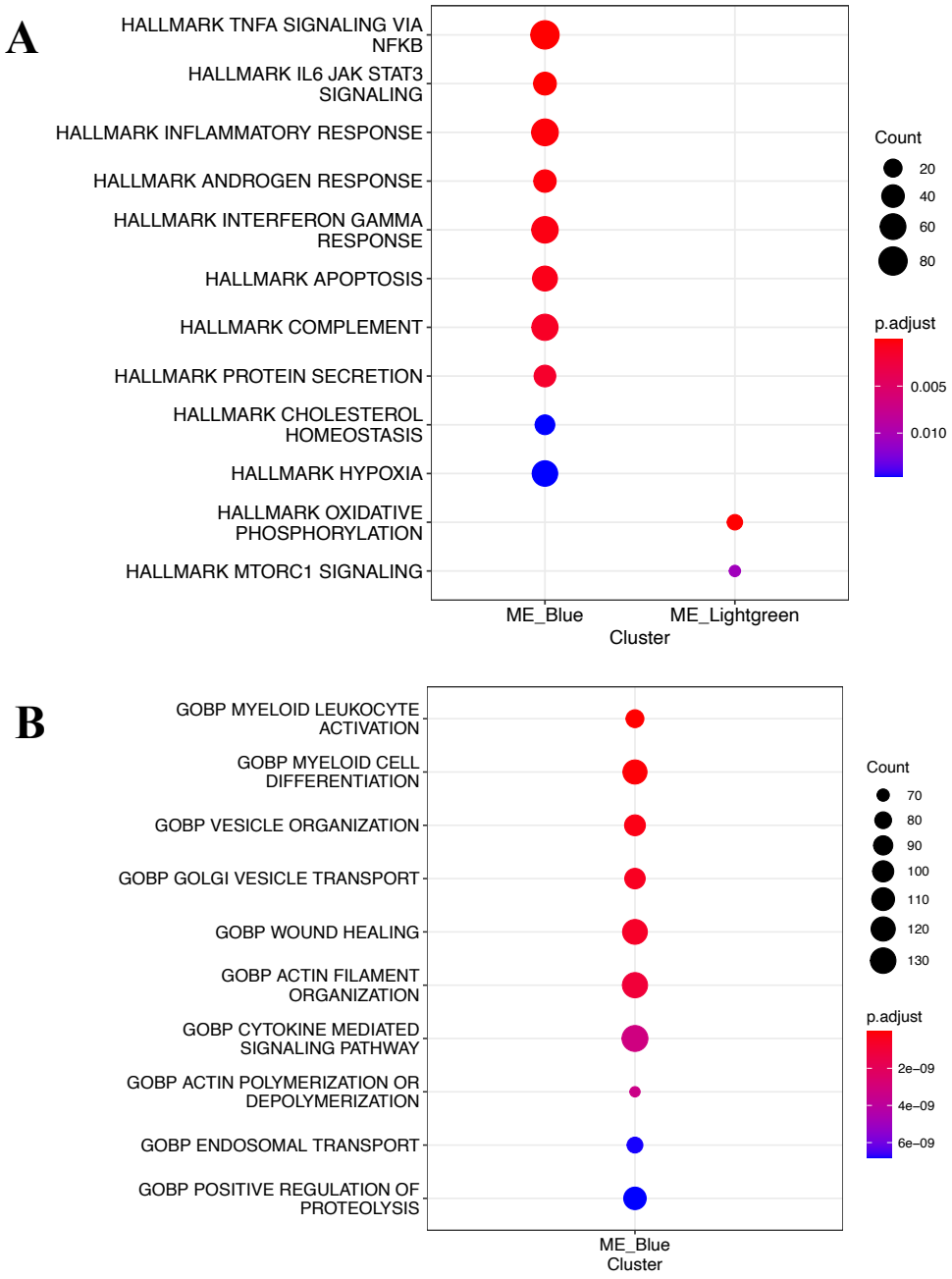

Figure 6.7 Module enrichment analysis based on Hallmark and Gene Ontology gene sets in the module eigengene (ME) blue and lightgreen that were associated with 28-day mortality in 29 melioidosis patients. The top 10 enriched pathways are displayed. A: Hallmark gene sets. B: Gene Ontology gene sets. The gradient colour bar corresponds to the adjusted P-value. The size of each circle indicates representative counts.

6.4.5 Depletion of adaptive immune cells, particularly T lymphocytes, is associated with fatal melioidosis

To explore the frequency of immune cells associated with fatal melioidosis, whole blood RNA sequencing data were deconvoluted using CIBERSORTx and xCell. Of 22-immune cells by CIBERSORTx, proportions of lymphocytes both T and B cells were reduced, but increased neutrophils and γδ T cells in non-survivors compared to survivors (**Figure 6.8**). Similarly, deconvolution by xCell identified depletion of lymphocytes and professional antigen presenting cells such as CD4+ T cells, CD8+ T cells, Th1 cells, NK cells and dendritic cells in non-survivors compared to survivors (**Supplementary Figure 6.8**, **6.9**). In contrast, myeloid cells such as macrophages, M1 and M2 macrophages and monocytes were highly enriched in non-survivors (**Supplementary Figure 6.9**). In line with the results from the full blood count from the hospitals' laboratories, lower frequencies of lymphocytes but higher neutrophils counts were observed in non-survivors (**Supplementary Figure 6.10**). Nevertheless, Pearson's correlation analyses between white cell counts from 29 melioidosis patients and the deconvolution scores show some significant correlations mostly within lymphocyte populations, whereas frequency of monocytes and different myeloid cells were not correlated possibly due to insufficient sample size (**Supplementary Figure 6.11, 6.12**).

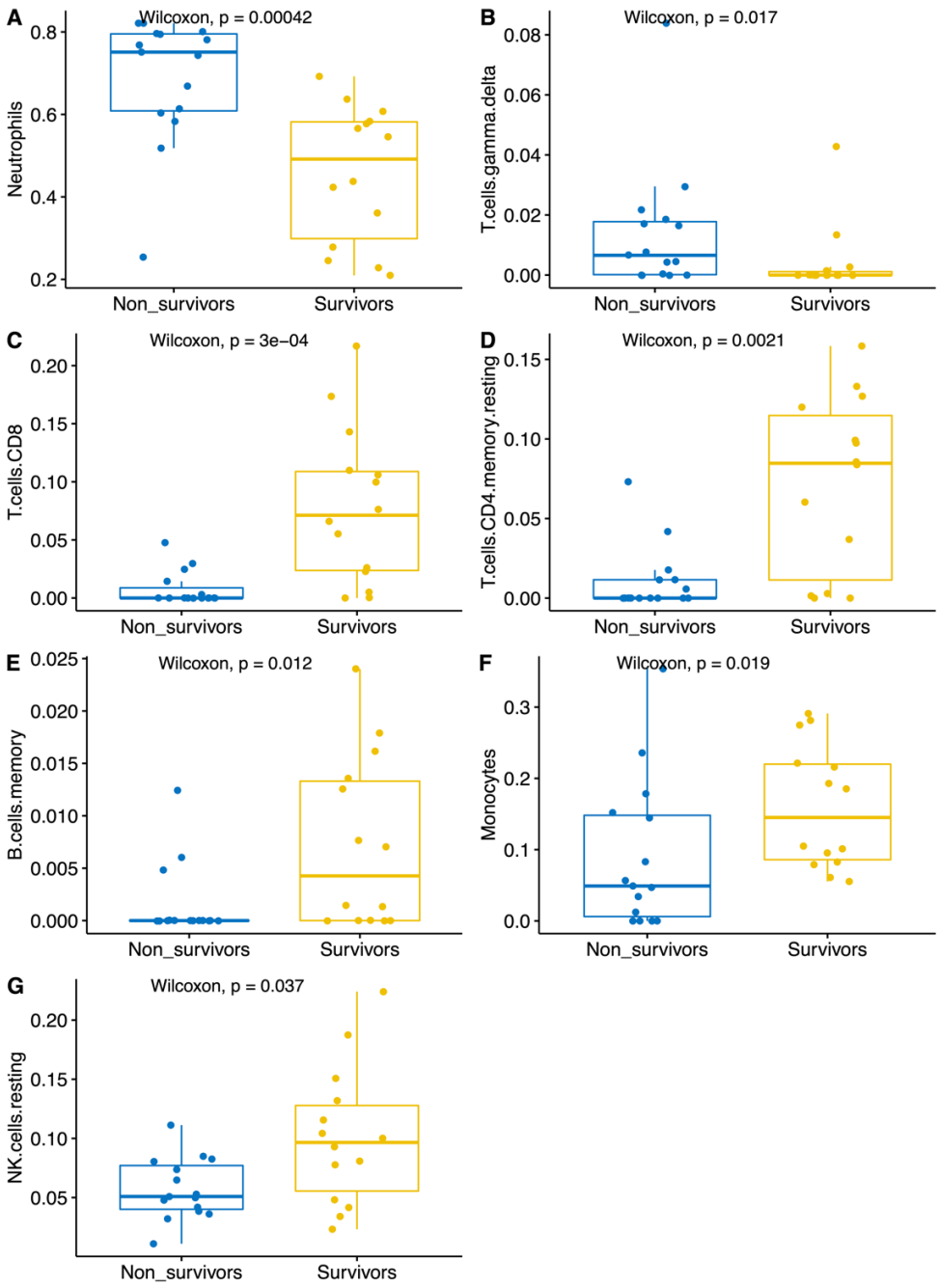

Figure 6.8 Scattered boxplots show comparisons of imputed cell fractions between non-survived (blue, n=15) and survived (yellow, n=14) melioidosis patients in the validation cohort using CIBERSORTx. The Y-axis displays each cell type proportion. Box plots represent medians with interquartile range plus lines to minimum, maximum and potential outliers. Non-parametric Mann-Whitney test was performed with its corresponding 2-tailed P-value displayed on each plot alongside median and inter-quartile range boxes.

6.4.6 Activated gamma-delta 1 T cells may play a deleterious role during melioidosis

In sepsis, increased circulating γδ1 T cell subset was associated with case fatality whereas higher frequency of γδ2 T cell subset was associated with survival (*595*). In this study, deconvolution of whole blood RNA sequencing data by CIBERSORTx identified increased frequencies of γδ T cells in non-survivors compared to survivors in both the discovery (**Chapter 5**) and validation (**Chapter 6**) cohorts (**Supplementary Figure 6.13A, 6.13B**). There was a trend of higher γδ T cells in non-survivors compared to survivors of melioidosis cohort from **Chapter 3 (Supplementary Figure 6.13C**). To validate this finding and further study contribution of specific γδ T cell subset during melioidosis, immunophenotyping of γδ T cell subsets including γδ1 T and γδ2 T cells was performed on PBMC samples derived from an independent cohort of acute melioidosis patients, where the samples were drawn a median of 5 days after hospitalisation (**Chapter 3**). The immunophenotyping shows comparable frequencies of γδ1 T and γδ2 T cells between non-surviving and surviving melioidosis patients at this timepoint (**Figure 6.9A, 6.9D**). There was trend of higher CD69+ γδ1 T cells in non-survivors compared to survivors (**Figure 6.9B**). In addition, frequencies of granzyme B-expressing γδ1 and γδ2 T cells were not different between non-survivors and survivors (**Figure 6.9C, 6.9F**).

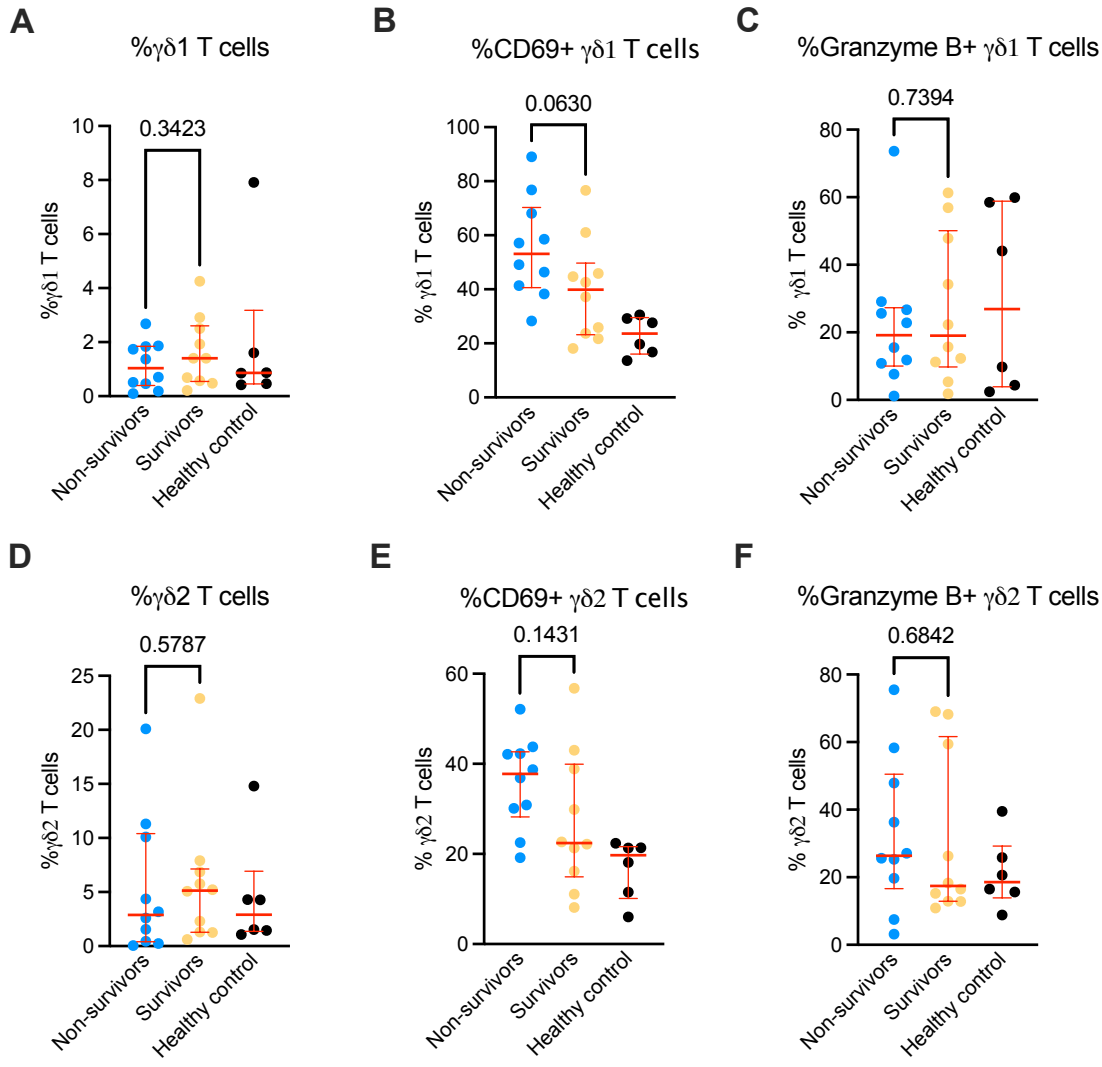

Figure 6.9 Scatter plots show frequencies of γδ T cell subsets in peripheral blood mononuclear cells from acute melioidosis patients by immunophenotyping using flow cytometry. A-C: Frequencies of γδ1 T cells, CD69+ γδ1 T cells and granzyme B+ γδ1 T cells within live CD3+ cells among non-survivors (n=10), survivors (n=10) of melioidosis, and healthy control (n=6) respectively. D-F: Frequencies of γδ2 T cells, CD69+ γδ2 T cells and granzyme B+ γδ2 T cells within live CD3+ cells among non-survivors (n=10), survivors (n=10) of melioidosis, and healthy control (n=6) respectively. Non-parametric Mann-Whitney test was performed with its corresponding 2-tailed P-value displayed on each plot alongside median and inter-quartile range boxes.

6.4.7 Unchanged T cell signalling upon T cell receptor stimulation in PBMC from acute melioidosis patients

According to canonical and functional pathway analyses, pathways involved in T cell signalling cascades were profoundly down-regulated in non-survivors compared to survivors. To validate this finding, phospho-flow cytometry of phosphorylated T cell signalling molecules were performed on PBMC samples derived from the independent cohort of acute melioidosis patients (**Chapter 3**). PBMC samples from acute melioidosis patients from the independent cohort were stimulated with T cell receptor (TCR)-dependent stimulator (αCD3/CD28/CD2), TCR-independent stimulator (PMA/Ionomycin), and R10 medium served as a negative control. Expression of phospho-ZAP-70, phospho-ERK1/2 (Thr202/Tyr204), and phosphor-S6 ribosomal protein (RPS6, Ser235/236) were measured within CD4+ T, CD8+ T, and double negative (DN) T cells.

Firstly, to identify the composition of T cell subsets, T cell phenotyping was performed for unstimulated PBMC derived from the melioidosis patients and healthy donors. Surprisingly, frequencies of T-cell subsets including CD4+ T, CD8+ T, and DN T cells were not different between non-survivors and survivors of melioidosis, and healthy donors (**Figure 6.10**). However, there was a trend of higher frequency of DN T cells in the survivors compared to non-survivors. Secondly, to assess whether TCR-dependent and independent stimulators induce phosphorylation of TCR signalling molecules, expression of phospho-ZAP-70, phospho-ERK1/2 and phosphor-S6 ribosomal protein (RPS6) were compared against baseline stimulation with R10 medium. All T cells subsets including CD4+ T, CD8+ T, and DN T cells show increased expression of phospho-ZAP70 in melioidosis patients when stimulated with αCD3/CD28/CD2 (**Supplementary Figure 6.14A, 6.14D, 6.14G**). Moreover, stimulations with either αCD3/CD28/CD2 or PMA/Ionomycin could induce expression of phosphor-RPS6 in all T cell subsets in melioidosis patients (**Supplementary**

Figure 6.14B, 6.14E, 6.14H). However, expression of phosphor-ERK1/2 was slightly increased but not statistically significant in any stimulations or T cell subsets (**Supplementary Figure 6.14C, 6.14F, 6.14I**). Thirdly, to assess the impact of subsequent case fatality on TCR signalling cascades, expression of phospho-ZAP-70, phospho-ERK1/2 and phosphor-S6 ribosomal protein (RPS6) were compared between non-survivors and survivors. Similar expressions of all TCR signalling molecules were observed between non-survivors and survivors regardless of T cell subsets and stimulations (**Figure 6.11**). Interestingly, expression of all TCR signalling molecules were higher in melioidosis patients compared to healthy controls.

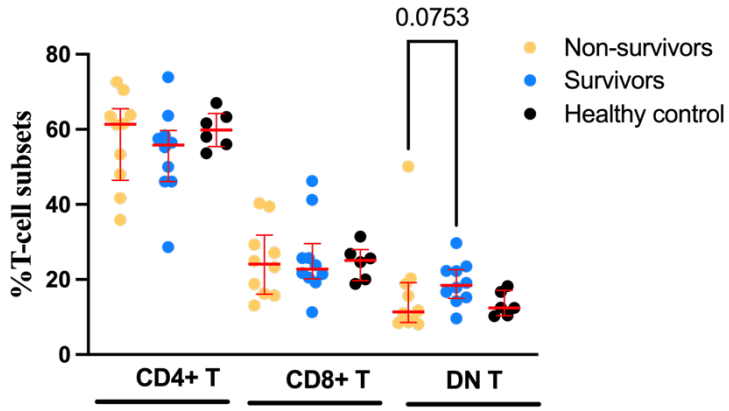

Figure 6.10 Frequencies of baseline T-cell subsets within peripheral blood mononuclear cells (PBMCs) derived from acute melioidosis patients (**Chapter 3**). PBMCs were rested in R10 medium for an hour prior immunophenotyping. Frequencies of CD4+ T, CD8+ T, and double negative (DN) T cells (see gating strategy in **Supplementary Figure 6.2**) were compared among non-survivors (yellow, n=10), survivors (blue, n=10) of melioidosis patients, and healthy donors (black, n=6). Non-parametric Mann-Whitney test was performed with its corresponding 2-tailed P-value displayed on each plot alongside median and inter-quartile range boxes.

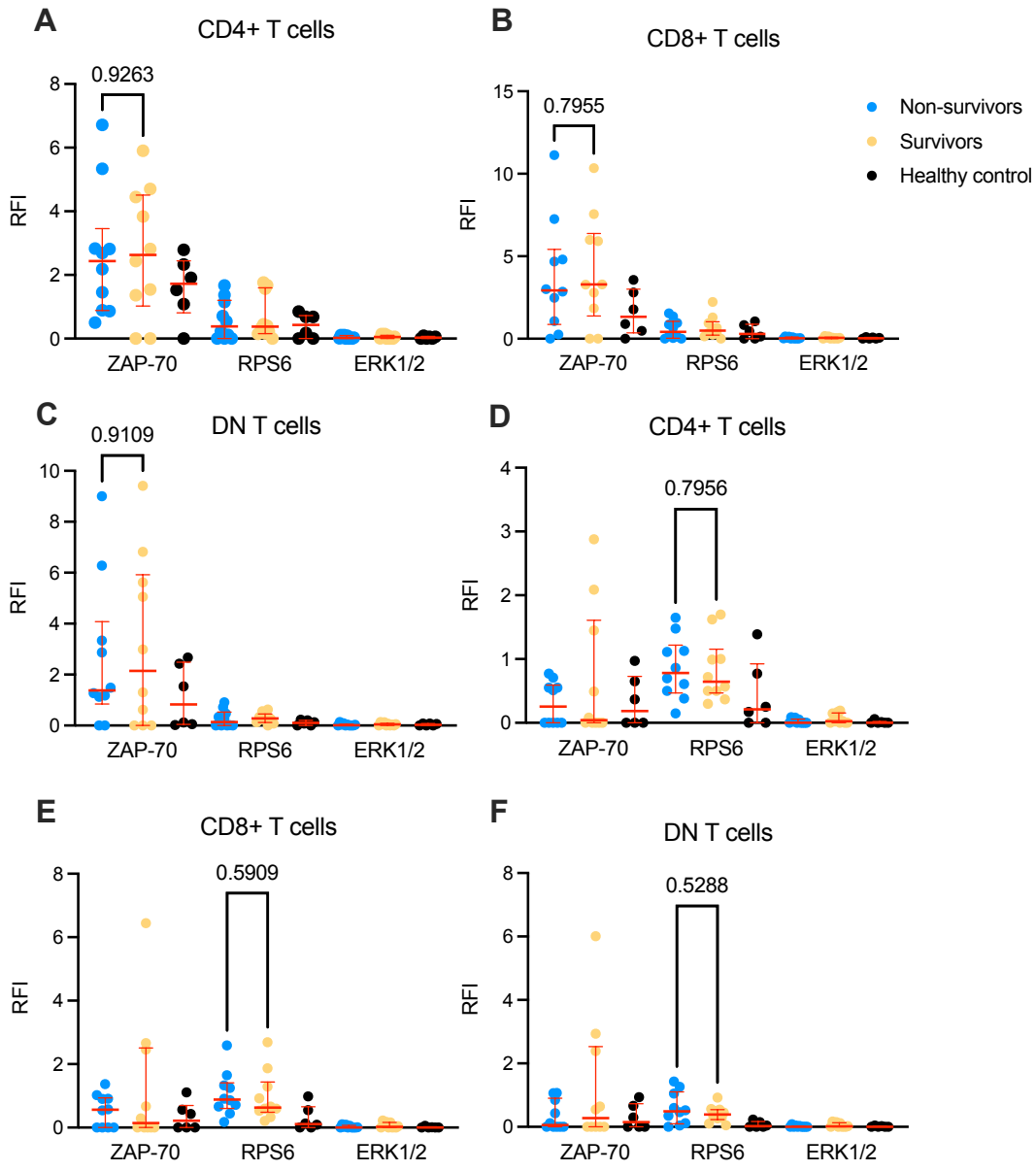

Figure 6.11 Scatter plots show phosphorylation of T cell receptor (TCR) signalling cascade proteins in peripheral blood mononuclear cells (PBMCs) from acute melioidosis patients using phospho-flow cytometry. PBMCs were stimulated with (A-C) α-CD3/CD28/CD2 or (D-F) PMA/Ionomycin. The expression of phosphorylated ZAP-70, RPS6, and ERK1/2 were measured within CD4+ T, CD8+ T cells and double negative (DN) T cells amongst non-survivors (n=10), survivors (n=10), and healthy control (n=6). Non-parametric Mann-Whitney test was performed with its corresponding 2-tailed P-value displayed on each plot alongside median and inter-quartile range boxes. RFI = Relative Fluorescent Intensity.

6.5 Discussion

In this chapter, the whole blood transcriptomic profile associated with subsequent case fatality from a large single-centre study of community-acquired melioidosis (**Chapter 5**, "discovery cohort") was validated using an independent cohort of melioidosis patients derived from a multi-centre study of melioidosis in similar study settings. Despite the different enrolment timepoint, the whole blood transcriptomic profile associated with fatal melioidosis was largely consistent between the two cohorts. The transcriptomic profile in both cohorts consisted of excessive inflammatory immune responses, predominately driven by innate immune compartment including neutrophils, with profound down-regulation of T cell signalling cascades prominent in both cohorts. Accordantly, several co-expressed gene modules enriched with inflammatory immune responses were associated with poor outcome in melioidosis.

Likewise, the majority of upstream regulators involved in pro-inflammatory immune responses were activated in fatal melioidosis both cohorts. Of the top 25, 10 key regulators including *TNF, IL1B, IL4, CEBPA*, *CSF3, IFNG, IL6, OSM, IL17A, STAT3* were common between the two cohorts. Possible detrimental roles of the upstream regulators including *TNF, IL4,* and *OSM* were extensively discussed in **Chapter 5**. Here, deleterious immune responses regulated by *STAT3*, *IL6*, and *IL17A* are discussed. *STAT3* encodes the signal transducer and activator of transcription 3 (STAT3) that exerts multiple functions such as inflammatory immune response, cell differentiation, and proliferation (*652*). STAT3 signalling cascades can be activated by external stimuli such as cytokines, chemokines, and infections (*653*). As a result, the activated STAT3 regulates host immune responses such as phagocytosis, cytokine production and host defence mechanisms (*652*). For example,

binding of LPS to its receptor (TLR-4) can activate STAT3 leading to increased production of inflammatory mediators such as IL-1β, TNF, and IL-6 (*654*). A sepsis model study by *Xu et al.* identified phosphorylation of STAT3 at Tyr705 (pY-STAT3) causing increased pro-inflammatory immune response, coagulation, and tissue injury. However, administration of pY-STAT3 phosphorylation inhibitor reduces inflammation, tissue injury and improved survival rate (*655*). Cell differentiation can be regulated by STAT3 activity. For example activation of STAT3 and retinoic acid receptor-related orphan receptor gamma-T (RORγt) can differentiate naïve CD4+ T cells into inflammatory helper T cells (Th17), which mainly produce IL-17 cytokine in response to infections or during inflammatory conditions (*656-658*). Moreover, increased production of IL-17 has been found to be associated with development of sepsis, inflammatory immune response, tissue damages, and poor outcome (*659-661*).

IL6 encodes a pro- and anti-inflammatory interleukin-6 (IL-6) cytokine that is primarily produced from activated myeloid cells and lymphocytes during infection and tissue damage (*662-664*). Effects of IL-6 are broad, for example IL-6 can activate production of IL-17 from neutrophils and increase microbiocidal activity (*665*). IL-6 in combination with transcription factors such as T-bet, GATA3, or RORγt can differentiate naïve CD4+ T cells into Th1, Th2, and Th17 cells respectively (*666*). There is strong evidence to support involvement of IL-6 in mediating detrimental host immune response during sepsis and acute infections, in which elevated levels of IL-6 in sepsis patients have been associated with increased disease severity and mortality (*667-669*). Moreover, high levels of circulating IL-6 and IL-10 were associated with increased disease severity and fatality rate in community-acquired pneumonia (*670*). *IL17A* encodes a pro-inflammatory IL-17A cytokine that is primarily produced from Th17 cells, innate lymphoid cell group 3 (ILC3), and γδ T cells (*671*). IL-

17A participates in inflammatory immune response during infection and in inflammatory conditions (*657, 672*). High levels of IL-17A during infection have been shown to cause systemic inflammation through influx of neutrophils into the circulation (*673*). Several studies have demonstrated that depletion of IL-17A in a caecal ligation and puncture (CLP) induced sepsis model could reduce proinflammatory cytokines such as TNF, IL1-β and IL-6, and improve survival rate (*659, 674, 675*). Taken together, the detrimental host immune response during melioidosis may be regulated by a number of upstream regulators that work in a concerted manner resulting in excessive inflammation and dysregulation of the host immune response.

Host immune responses associated with fatal melioidosis are dysregulated (*10*). Certain immune cells may play detrimental roles, leading to severe disease and poor outcome. Here, fatal melioidosis patients from both cohorts show increased abundance of γδ T cells based on the deconvolution method by CIBERSORTx. The host immune response by γδ T cells in melioidosis is not well characterised. A previous preliminary study of γδ T cells in melioidosis identified lower frequency of circulating γδ2 T cells with effector memory phenotype ($CD45RA^{-}$ $CCR7^{-}$) in non-survivors compared to survivors (*676*). During bacterial sepsis, the frequency of γδ T cells has been found to be reduced in severe disease and in fatal cases (*677, 678*). However, immune phenotyping of γδ T cells in sepsis patients by *Wang et al.* identified increased frequency of the γδ1 T cell subset in sepsis patients compared to healthy controls, whereas the frequency of the γδ2 T cell subset was higher in healthy controls. Moreover, the frequency of γδ1 T cells was higher in fatal cases compared to those who survived (*595*). In this chapter, the γδ T cells subset (γδ1 T and γδ2 T cells) findings were validated based on the deconvolution method with the transcriptomic data.

However, wet laboratory γδ T cell immunotyping using PBMC from an independent cohort (from MICRO1501, **Chapter 3**) did not identify any altered frequencies of either γδ1 T or γδ2 T cells in non-survived compared to survived melioidosis patients, in agreement with a previous published study using the same patient cohort (*377*). However, there was a trend of higher frequency of CD69-expressing γδ1 T and γδ2 T cells in non-survivors compared to survivors. A study by *Liao et al.* reported reduced NKG2D but increased expression of CD69 on γδ T cells, along with pro- and anti-inflammatory cytokines including IFN-γ, IL-17, IL-10 and TGB-β in sepsis patients compared to healthy controls. However, *ex-vivo* stimulation with PMA/ionomycin of PBMC obtained from the sepsis patients showed reduced function of γδ T cells including decreased IFN-γ and CD69 expression compared to healthy controls (*678*). Altogether, increased activated γδ T cells in fatal melioidosis may be involved in increased inflammation possibly via IL-17-mediated immune response as suggested by the activation of *IL17A* upstream regulator as discussed earlier.

Depletion of the cell-mediated immune response, in particular lymphocyte populations, alongside elevated neutrophils counts are a hallmark of sepsis and melioidosis and they are established as associated with poor prognosis and outcome (*76, 600, 679, 680*). In this chapter, the distinct whole blood transcriptomic profile associated with fatal melioidosis gives further mechanistic insight, revealing down-regulation of T-cell signalling pathways and antigen presentation in both the discovery and validation cohorts. As discussed in **Chapter 5**, the identified transcriptomic profile associated with subsequent case fatality resembles that of the sepsis response signature 1 (SRS1) associated with an exhaustive T cell phenotype and reduced antigen presentation (*296, 297*). Moreover, *Baghela et al.* have recently proposed five transcriptomic sepsis endotypes corresponding to immune mechanisms and disease severity, including Neutrophilic-Suppressive (NSP), Inflammatory

(INF), Innate-Host-Defence (IHD), Interferon (IFN), and Adaptive (ADA) (*300*). Patients with NSP and INF has profiles resembling the host immune response in fatal melioidosis, including up-regulated inflammation such as neutrophil degranulation, TLRs, and TNF-α and down-regulated T cell signalling cascades and activation (*300*). There is growing evidence supporting immunosuppression and worse clinical outcome in sepsis patients whose immune responses are skewed towards Th2 phenotypes (*497, 681, 682*). Moreover, concomitant inflammatory immune responses and the Th2 pathway (IL-4, IL-13, and IL-10) were up-regulated in fatal melioidosis. In contrast, the canonical Th1 pathway was down-regulated in fatal melioidosis. Moreover, digital immunophenotyping by the xCell deconvolution method identified an enriched Th1 cell subset in survivors compared to non-survivors. A study by *Xue et al.* identified increased frequency of Th2 cells and Th2/Th1 ratio in severe sepsis patients and those who did not survive compared to survivors (*682*). As previously described in **Chapter 5**, there could be several mechanisms that potentially contribute to immunosuppression of T lymphocytes leading to poor outcome in melioidosis. These include unbalanced neutrophil-to-lymphocyte ratio, over compensatory anti-inflammation, inhibition of T cells and antigen presenting cells, immunomodulation by certain immune cell subsets, and immunomodulation by Bp.

Despite strong evidence from my transcriptomic approach supporting defective TCR signalling transduction in fatal melioidosis, flow cytometry analysis of phosphorylation of TCR signalling molecules (ZAP70, RPS6, and ERK1/2) within CD4+ T, CD8+ T and DNT cells from PBMC samples were not different between non-survivors and survivors. ZAP70 is a cytoplasmic protein tyrosine kinase, expressed in T cells essential for TCR signalling cascades leading to T cell activation and development (*683*). Following the recognition of antigen presented on MHC molecules, Lck is recruited to CD3 and TCR complex leading to

phosphorylation of tyrosine molecule in the immunoreceptor tyrosine-based activation motifs (ITAMs). Subsequently, phosphorylated ITAMs recruit ZAP-70 resulting in activation of ZAP-70 which further phosphorylates downstream signalling proteins such as T cell p38 MAP kinase (MAPK), activation of T cells (LAT), and SH2-domain-containg leukocytes protein of 76 kDa (SLP-76) (*683, 684*). Interestingly, there are visible trends of increased phosphorylation of ZAP70 and RPS6 in all T cell subsets in melioidosis patients compared to healthy controls. This might suggest functional and pre-activated TCR signalling molecules in melioidosis patients during acute disease.

The unexpected results in the flow cytometry experiments, which largely did not validate the transcriptomic findings from the discovery and validation cohorts, may be due to a number of reasons. Firstly, I found poor cell recovery and viability from the cryopreserved PBMC (on average, <50% viability) potentially as a result of (i) long-term storage of PBCM samples (5 years), (ii) collection of PBMC in Northeast Thailand followed by several journeys and periods of shipping on dry ice to reach the UK, (iii) impact of acute sepsis and immune activation on cell viability. Secondly, the PBMC from the MICRO1501 study (**Chapter 5**) were drawn later in the disease course than the other two cohorts, when cellular proportions may have changed. Thirdly, the relationship between gene transcripts and expression of cell surface markers used to identify cell subsets in flow cytometry may not be directly proportional. Nevertheless, a study by *Roquetaillade et al. (685)* demonstrated unaltered TCR signalling molecules (CD3ζ and AMPK) that are proximal to TCR complex in CD4+ T cells between sepsis patients and controls. However, phosphorylation of distal TCR signalling molecules such as RPS6 and ERK were reduced compared to controls.

In conclusion, the transcriptomic profile associated with fatal melioidosis consists of concomitant pro- and anti-inflammatory immune responses but suppressed phenotypes of T lymphocytes and antigen presenting cells as identified in both discovery and validation cohorts. For example, pathways involved in inflammation such as neutrophil degranulation, signalling by interleukins, IL-6 signalling and anti-inflammation such as type-II immunity (IL-4 and IL-13) and PD-1/PD-L1 signalling were concomitantly up-regulated in the non-survivors. A similar phenomenon is also observed in other acute infections, and in sepsis in general (*686, 687*). Moreover, activated upstream regulators i.e., *TNF* may exaggerate on-going inflammation and meanwhile modulate protective cellular immune response in fatal melioidosis (*71, 635*). This highlights the complex interplay between hyper- and hypo-inflammatory immune responses, leading to suppressed T cell functions during melioidosis. In agreement with functional pathway analyses, multiple subsets of CD4+ and CD8+ T cells were depleted in the non-survivors. On the other hands, myeloid cells such as neutrophils, macrophages, and γδ T cells were enriched in the non-survivors. Despite improved clinical settings, awareness, and diagnosis of melioidosis, the case fatality rate of melioidosis in Thailand remains high making clinical management challenging. Ultimately, development of a rapid prognostic tool may be useful as guidance for appropriate treatment and clinical management.

Chapter 7: General discussion and conclusions

7.1 How does type 2 diabetes increase susceptibility to intracellular infections?

People with T2DM are highly susceptible to melioidosis with 12-fold increased risk and show a 3-fold enhanced risk of developing TB. For the first part of my thesis, I hypothesised that people with T2DM share common underlying mechanisms leading to increased susceptibility to melioidosis and TB. I sought to study and compare transcriptomic profiles derived from melioidosis and TB patients who lived with diabetes using whole blood RNA sequencing approach.

In **Chapter 3**, the impact of T2DM on the whole blood transcriptome during acute melioidosis (a median of 5 days after hospital admission) was studied. This study was the first study to utilise a genome-wide transcriptomic approach to unravel whole blood gene expression profiles associated with T2DM in melioidosis patients. The PCA did not reveal significant differences in transcriptomic profiles between the melioidosis patients with and without T2DM. This lack of difference was also observed in the other two independent melioidosis cohorts (**Chapter 5** and **Chapter 6**). In keeping with this, DGE analyses was unable to identify DEGs between the melioidosis with and without T2DM in any of the three cohorts studied, suggesting that any differences in transcriptomic profiles associated with diabetes were subtle by the time that people are admitted to hospital with melioidosis. This is in contrast to the impact of mortality status on the transcriptome, with the results of PCA, DGE, functional analysis, and WGCNA demonstrating a strong impact of mortality status on the whole blood transcriptomic responses during melioidosis, for all cohorts studied

(**Chapter 3, Chapter 5**, and **Chapter 6**). The lack of major difference in the transcriptome between people with and without diabetes hospitalised with melioidosis is compatible with past clinical studies by our group and others where diabetes status in hospitalised melioidosis patients is not associated with differences in disease severity or mortality. This is in contrast with studies in viral infections such as SARS-COV2 and dengue virus, in which people with diabetes were at increased risk of developing more severe disease and associated with increased case fatality compared to normoglycaemic cases.

I next used more detailed transcriptomic analysis techniques to draw out more subtle impacts of diabetes on the transcriptome during melioidosis. One such approach, Gene Set Enrichment Analysis (GSEA), assesses up- or down-regulation in all genes mapping to a given pathway to determine enrichment. This is in contrast to standard overrepresentation analysis whereby only the subset of DGEs is assessed for enrichment. Since genes do not work in isolation, but are often highly coordinated in functionally overlapping processes, GSEA is a more powerful approach for investigating pathway enrichment especially when the transcriptional signal is weak. At baseline, the result from GSEA shows increased inflammatory responses such as TNF, interferons, and IL-6 in uninfected T2DM control compared to healthy control cohort from **Chapter 3**. Likewise, the results from GSEA following DGE analysis in melioidosis (**Chapter 3**) revealed that multiple pathways involving the immune response, cell signalling and metabolism were altered in melioidosis patients with T2DM. The top enriched pathways such as TNF signalling, neutrophil degranulation, inflammatory response, innate immune system, heme metabolism, and IRE1alpha activates chaperones suggest elevated inflammatory immune responses, dysregulation of metabolism and an increased ER stress response in the patients with T2DM. Similarly, the results from module enrichment following WGCNA analysis identified

increased inflammatory response such as neutrophil degranulation, TLR cascades, and signalling by interleukins in melioidosis with T2DM. This increased pro-inflammatory milieu with heavy neutrophil dominance may directly modulate the cell-mediated immune response which is required for controlling intracellular infection.

Overall, the effects of T2DM on the host immune system are complex and heterogenous, with baseline dysregulated host metabolism, increased inflammation, hyperglycaemia, and insulin resistance likely contributors to the increased susceptibility to Bp infection. Studying the impact of diabetes on the transcriptome earlier in the course of infection is likely to further illuminate the mechanisms of how the initial innate immune response fails to control the infection and instead leads to an excessive pro-inflammatory response. Future use of a diabetic mouse model alongside studying early transcriptomic responses to a new vaccine in people with and without diabetes is likely to build on my findings.

7.2 Shared whole blood transcriptomic signatures between melioidosis and tuberculosis in people with diabetes and intermediate hyperglycaemia

In this thesis (**Figure 7.1**), the transcriptomic signature associated with T2DM during melioidosis (**Chapter 3**) and TB (**Chapter 4**) were identified and compared. In general, melioidosis patients show higher magnitudes of pro-inflammatory responses compared with TB patients. Melioidosis is typically an acute infection, where sepsis is common and there is high mortality of up to 50%. In contrast, TB is more typically a chronic disease with mortality recently estimated at 15%. Nevertheless, the two diseases are both caused by intracellular bacteria, share the inhalational route of transmission and predominance of pulmonary presentations. My findings show that in TB, the whole blood transcriptome was dominated by interferon responses (α/β and γ). In contrast, interferon signalling pathways

in melioidosis patients sampled at a median of 5 days after hospital admission (**Chapter 3**) were less dominant compared to TB cohorts. DGE analysis of a different melioidosis cohort sampled within 24 hours of hospital admission (**Chapter 5)** revealed profound up-regulation of both interferon-α/β and interferon-γ signalling pathways compared to the healthy control cohort. The data suggest that the interferon response is more prominent during early melioidosis. The diminished interferon response by median of day 5 could be due to reduced bacterial load in the system following antibiotic treatment with decreased number of infected cells, therefore, the interferon responses.

Unlike melioidosis, there were substantial differences in transcriptomic profiles between TB patients with and without diabetes or intermediate hyperglycaemia. TB patients with diabetes and intermediate hyperglycaemia show up-regulation of pathways involved in inflammatory responses pre-dominated by neutrophil degranulation, platelet degranulation, and coagulation. However, it is interesting that many interferon-related pathways such as antiviral mechanisms by IFN-stimulated genes, interferon-stimulated gene 15 (ISG15) antiviral mechanism, and pathways previously defined as associated with hepatitis C response were not up-regulated in the TB patients with diabetes/intermediate hyperglycaemia. It is possible that mechanisms underlying increased susceptibility to TB in people with diabetes/intermediate hyperglycaemia are mainly due to defective interferon response in combination with increased inflammatory response. It is well-studied that interferon-γ response is dispensable during Mtb infection. The degree to which the increased inflammatory response to TB, in particular by neutrophils, is compensatory as a result of uncontrolled infection or causal for the lower interferon responses via modulation of protective cellular immunity requires animal models to dissect.

Overall, my work has identified that diabetes result in increased pro-inflammatory responses to both melioidosis and TB, and abrogation of interferon pathways in TB. The more chronic nature of TB may allow better identification of the transcriptomic response, because the transcriptomic signature of acute melioidosis is dominated by the acute inflammatory response.

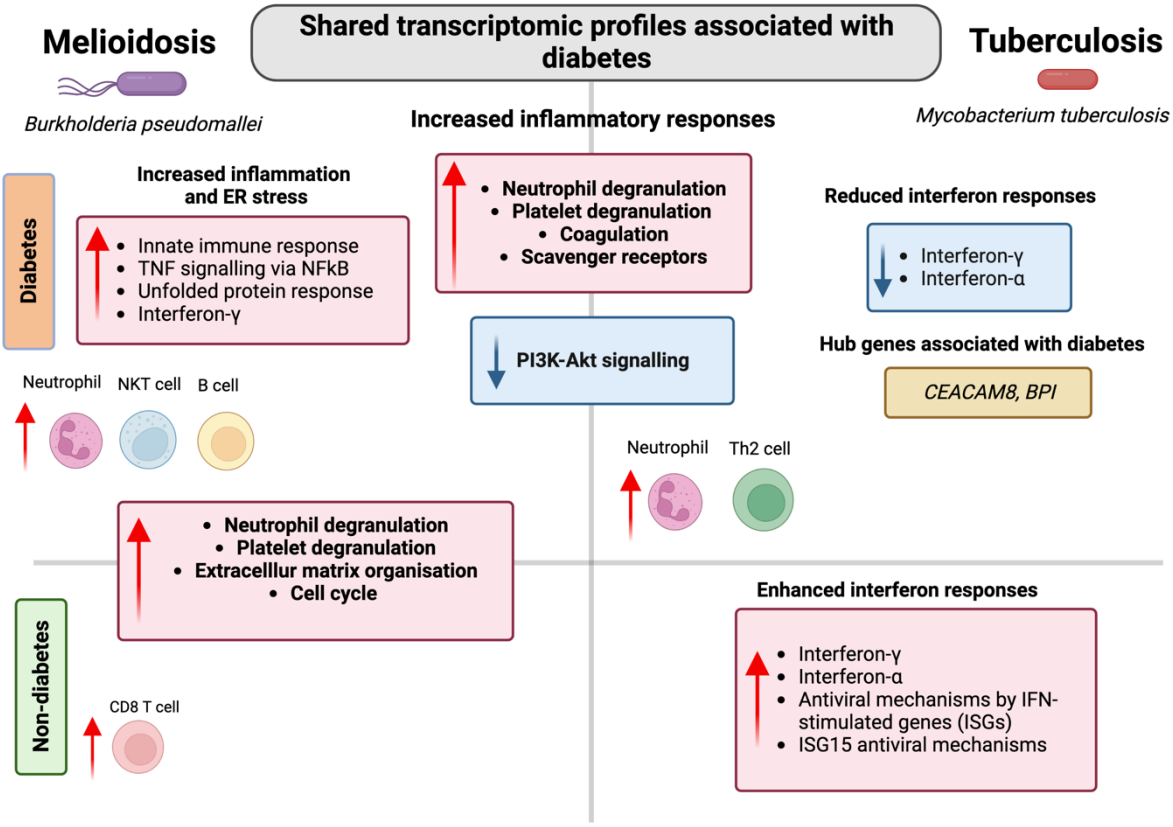

Figure 7.1 Schematic summary of whole blood transcriptomic profiles associated with increased susceptibility to melioidosis and tuberculosis in people who live with type 2 diabetes compared with respective healthy control cohorts. Created with BioRender.com.

7.3 What are the transcriptomic profiles associated with case fatality in community-acquired melioidosis?

Melioidosis is a leading cause of death from community-acquired infection in Northeast Thailand, and earlier diagnosis and identification of those at greatest risk of death would facilitate concentration of limited resources in critical care to save lives. In addition, deeper understanding of the mechanisms of pathogenicity of Bp and protective immune responses enables development of novel therapies and vaccines. For the next part of my thesis, I hypothesised that Bp infection causes profound dysregulation of the host response during melioidosis leading to high 28-day mortality with identifiable features. I aimed to (i) investigate the whole blood transcriptomic profile associated with fatal melioidosis and (ii) compare whole blood gene expression patterns in melioidosis to patients hospitalised with other community-acquired infections.

This thesis was the first study to define the transcriptomic profile associated with fatal melioidosis in a well-characterised cohort with blood samples obtained within 24 hours of hospital admission. My main goal was to identify features that could potentially discriminate those who will progress to severe disease and death from those who recover. This information will be useful in development of a prognostic tool for community-acquired melioidosis. The identified transcriptomic profiles associated with fatal melioidosis (**Chapter 5**) was validated in an independent, multi-centre cohort study of melioidosis (**Chapter 6**).

Firstly, the full blood count measured in the local hospital laboratory can provide a simple prognostic tool in identifying those who will develop severe disease and lethality. All three melioidosis cohorts (**Chapter 3, Chapter 5**, and **Chapter 6**) showed similar outcomes, in

which non-survivor melioidosis patients had higher neutrophil, but reduced lymphocyte counts compared to survivors. These full blood count measurements agreed with the deconvolution of whole blood RNA sequencing data, in which depletion of lymphocytes and increased circulating neutrophils were associated with poor outcome. Nevertheless, more detailed mechanisms associated with case fatality were elucidated.

The whole blood transcriptomic profiles associated with fatal melioidosis were largely consistent between the discovery (**Chapter 5**) and validation cohort (**Chapter 6),** despite the different participant enrolment timepoints (less than 24 hours versus a median of 3 days, respectively). Fatal melioidosis patients exhibit increased inflammation with a pronounced neutrophil-driven inflammatory response concomitant with type 2 immune responses (IL-4, IL-13, and IL-10) (**Figure 7.2**). Strikingly, depleted cellular immune responses, in particular T cell signalling, were identified in the non-survivors. However, there were some differences between the two cohorts - for example IL-10 signalling was up-regulated in the non-survivors in discovery cohort (**Chapter 5**, < 24 hours after admission) and down-regulated in the validation cohort (**Chapter 6**, median 3 days after admission). Likewise, TLR signalling was up-regulated only in the non-survivors from the validation cohort. Similar findings were observed in the melioidosis cohort from **Chapter 3** (median of 5 days after hospital admission), in which TLR signalling was up-regulated in the non-survivors. The data suggest that IL-10-mediated anti-inflammatory mechanisms are prominent at admission to hospital melioidosis patients who do not survive, but are replaced within days by pro-inflammatory responses from TLRs and neutrophils leading to exaggerated inflammation, onset of sepsis, multiorgan failure and early death. Moreover, the observed excessive inflammation and over-compensatory mechanisms by IL-10 and PD-1/PD-L1 could be the cause of depleted lymphocytes leading to unbalanced pro- and anti-inflammatory responses

that pose an increased risk of uncontrolled Bp and secondary infections. This thesis demonstrates the importance of both the innate and adaptive immune system early in infection, highlighting the impact of dysregulated innate immune responses resulting in depletion and dysfunction of cellular immunity.

Potential hub genes that may mediate deleterious host immune responses in fatal melioidosis were also identified (**Chapter 5**). For example, *CEACAM1,* which encodes a cell adhesion molecule widely expressed on many immune cells was up-regulated in the non-survivors compared to survivors. A number of Gram-negative bacteria such as *E. coli, Salmonella* spp., and *N. gonorrhoeae* utilise CEACAM1 to enter cells. Interestingly, binding to CEACAM1 on T cells can activate an immunoreceptor tyrosine-based inhibitory motif (ITIM) leading to inhibition of T cell signalling and function which may represent a mechanism for defective cell-mediated immune responses in fatal melioidosis.

Several up-stream regulators potentially involved in the detrimental host immune response in fatal melioidosis identified in the discovery cohort (**Chapter 5**) were then confirmed in the validation cohort (**Chapter 6**), with up-regulation in non-survivors of *TNF, IL1B, IFNG, IL6,* and *OSM*. *TNF* is a key regulator of many downstream genes involved in the inflammatory response such as *IL6, IL1A, CCL2*, and *MMP8*, and inhibits genes involved in activation of T cell signalling such as *CD4, CD28*, and *CD86*. Additionally, TNF induces apoptosis in T cells resulting in depletion of the T cell compartment. *TNF* up-regulation may therefore be a further mechanism of detrimental lymphocyte depletion in fatal melioidosis.

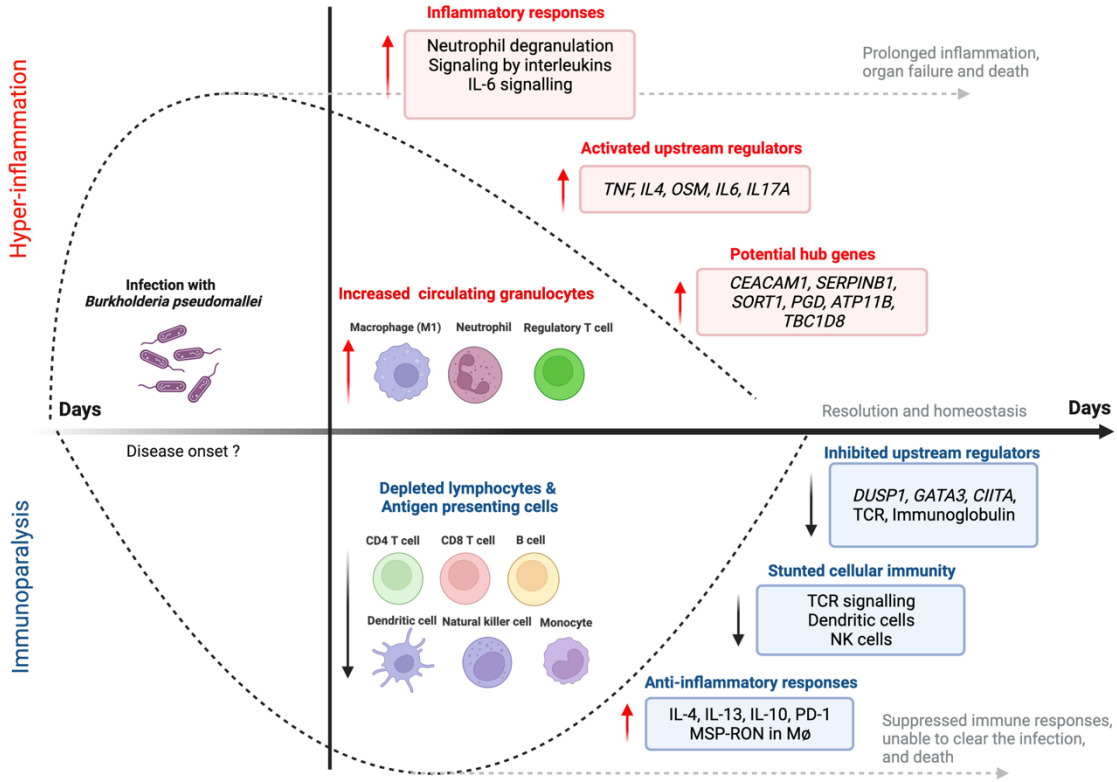

Figure 7.2 Schematic summary of whole blood transcriptomic profiles associated with fatal melioidosis compared with those who survive. Created with BioRender.com.

7.4 Whole blood transcriptomic signatures associated with melioidosis compared with other community-acquired infections

In **Chapter 5**, to identify the transcriptomic profile associated with melioidosis, DGE analyses were performed to compare patients with melioidosis, and three groups of community-acquired bacteraemia: Gram-negative (*E. coli* and *K. pneumonia*), Gram-positive (*S. aureus*), and sepsis patients with negative blood cultures. Generally, melioidosis patients show marked up-regulation of pathways involving pro-inflammatory immune responses compared to the other three groups, dominated by both interferon-α/β and -γ responses. I derived a "77-gene signature" that distinguishes melioidosis from other

community-acquired infections in Northeast Thailand. Interestingly, the "melioidosis signature" genes were not present in the 86-gene TB signature proposed by *Berry et al.* for distinguishing active TB patients from other infections and inflammatory autoimmune diseases, and this new melioidosis signature may be used to discriminate melioidosis from TB, which is of great potential value. This would facilitate discrimination of melioidosis from TB as the clinical presentations may overlap and can form the foundation for further refinement towards a novel biomarker based diagnostic test.

7.5 Limitations of this study

7.5.1 Bulk RNA sequencing detects averaged expression profile

All data used for this study were derived from whole blood bulk RNA sequencing (bulk RNA-seq). While bulk RNA-seq technologies allow study of the averaged global transcriptional profile at a cell population level, cell-specific expression profile and contribution of each cell subpopulation to the observed phenotypes cannot be derived. The whole blood RNA sequencing datasets were dominated by neutrophil pathways which may mask more subtle changes in the lymphocyte-derived transcriptome. Nevertheless, the overall findings of neutrophil enrichment and suppression of cellular pathways in diabetes status and in fatal cases matches the hospital full blood count measurements and the parallel clinical immunology studies of melioidosis by our group. To mitigate this limitation, we did perform "in silico" deconvolution analysis on whole blood transcriptional signals to explore immune cell subtype contributions.

7.5.2 Differences in time of enrolment of melioidosis cohorts

In this study, three independent melioidosis cohorts enrolled the participants differently. In **Chapter 5**, suspected sepsis patients were enrolled within 24-hour following hospital admission, based on the 2012 Surviving Sepsis Campaign prior melioidosis-confirmed diagnosis. This well-funded sampling study of 5000 sepsis patients enabled retrospective selection of culture-confirmed melioidosis patients alongside other bacteraemias. Thus, this cohort allowed identification of the early transcriptomic profiles associated with melioidosis and fatal melioidosis. In contrast, for **Chapter 3** and **Chapter 6,** study funding enabled only recruitment of melioidosis patients with a culture-confirmed diagnosis, with culture usually taking several days, thus the time of enrolment was delayed to a median of 5 and 3 days respectively. The cohort described in **Chapter 3** was reliant on the availability of a single team member for enrolment, hence the longer median recruitment time compared to **Chapter 5**. Despite the broadly consistent transcriptomic profiles associated with fatal melioidosis, discrepancies of the transcriptomic profiles between **Chapter 5** and **Chapter 6** could be due to the different timings and enrolment criteria – for example not all melioidosis patients meet the criteria for sepsis. Moreover, **Chapter 3** and **Chapter 5** enrolled the participants from the same single centre, which might not well represent the general population in the region, although some were referred from adjacent hospitals.

7.5.3 Unknown time of disease onset

In **Chapter 5,** despite early enrolment of the participants into the study, it was estimated that a third of patients reported having symptoms for approximately one week, and half of the remaining patients felt unwell between one week to one month previously. Therefore, the transcriptomic profiles associated with fatal melioidosis cannot represent the host immune response to melioidosis at disease onset. This might partly explain downregulation

of T cell response, with advanced, well-established disease leading to malfunction of cellular immunity and case-fatality.

7.5.4 Unknown pre-intervention prior to enrolment and use of diabetic drugs

Due to a lack of information on interventions or treatments received prior to enrolment into the studies, the impact of drugs on the observed transcriptomic profiles is unknown. The use of over-the-counter antibiotics and steroids from pharmacies in Thailand is common, alongside use of traditional Thai and Chinese remedies of unknown composition. Moreover, information on diabetic drug use by participants was unavailable in **Chapter 5** and **Chapter 6,** and incomplete for **Chapter 3.** Therefore, the impact of diabetic drugs was not considered during the analyses. In Thailand, metformin (80%) and sulfonylureas are commonly prescribed for patients with T2DM. Metformin has anti-inflammatory and immunomodulatory properties that may regulate the transcriptomic response in melioidosis patients with T2DM independent of diabetes. Additionally, melioidosis patients usually have one or more comorbidity such as chronic kidney or lung disease; hence the impact of diabetes on whole blood transcriptome could be confounded by other comorbidities.

7.5.5 Limited number of participants from other community-acquired infections

In **Chapter 5**, the study was not primarily designed to differentiate the transcriptomic signature of non-melioidosis community-acquired infections from each other due to insufficient number of participants from other groups (*E. coli*, n=22, ; *K. pneumoniae*, n=13; *S. aureus*, n=16; blood culture-negative, n=19). To develop a classifier to discriminate different bacterial infections, the participants within each group should be randomised and allocated into discovery and validation sets (e.g., with 70:30 ratio). The number of other community infections within each subgroup may limit the reliability of such a classifier.

7.5.6 Comparable composition of γδ T cells and T-cell signalling cascades

Deconvolution of the whole blood transcriptome using the CIBERSORTx method identified increased frequencies of γδ T cells in melioidosis patients who did not survive compared to survivors in both the discovery (**Chapter 5**) and validation (**Chapter 6**) cohorts. I sought to explore these findings using flow cytometry in cryopreserved PBMC samples of acute melioidosis derived from **Chapter 3** (selected as an independent cohort with PBMC samples available). However, this validation experiment identified comparable frequencies of γδ T cells (both γδ1 T and γδ2 T cells) in the non-survivors compared to survivors. Nevertheless, this "wet lab" finding matched the deconvolution of RNA-seq data from **Chapter 3** which confirmed comparable circulating γδ T cells in the acute melioidosis patients at this timepoint (median 5 days after hospitalisation). Collectively, the data suggest γδ T cells may play a detrimental role during melioidosis in the early stage of infection. Furthermore, frequencies of T-cell subsets were comparable between the non-survivors and survivors, and phosphorylation of proteins downstream TCR signalling cascades were not associated with case fatality. This is despite an earlier study in 2015 by our group (*Jenjaroen et al.)* found depletion of both CD4+ T and CD8+ T cells by immunophenotyping of PBMCs from the same **Chapter 3** cohort. Collectively, the unchanged frequencies of γδ T cells and TCR signalling cascades could be due to underpowered samples, lower quality PBMC, or the samples from **Chapter 3** being drawn later in the clinical course of melioidosis compared to **Chapter 5** and **Chapter 6**.

7.6 On-going work and future directions

7.6.1 Single-cell RNA sequencing to dissect cell-specific expression profile associated with T2DM

The data used in this study were derived from whole blood bulk RNA sequencing, and as a result, signatures were dominated by neutrophil-enriched transcriptional signals. Moreover, the depleted lymphocyte populations during melioidosis further limited the detection of lymphocyte-derived expression profiles. Unlike bulk RNA sequencing, single-cell RNA sequencing (scRNA-seq) technologies offer the study of transcriptional expression at single-cell level allowing the dissection of a relationship between cell-specific gene expression and observed phenotype. Moreover, scRNA-seq facilitates discovery of rare cell populations that are traditionally obscured by the transcriptomes from dominant cell types by bulk RNA-seq. Our research group is currently doing a pilot study of scRNA-seq of recovered COVID-19 patients with and without type 2 diabetes led by Dr. Mohammad Ali and Dr. Barbara Kronsteiner-Dobramysl. This should allow a dissection of which cell-specific expression profiles are altered during T2DM and possibly leading to an increased risk of infection and poor outcome.

7.6.2 Identification of a predictive transcriptomic signature associated with fatal melioidosis, and integration with the signatures derived from proteomic and metabolomic approaches

Aims for the Ubon-Sepsis study (**Chapter 5**) include identifying the blood transcriptomic signature associated with fatal melioidosis and development of biomarker tests to identify patients at high risk of severe disease and death. In collaboration with Professor Eoin West, Professor Sina Gharib, and Dr. Lu Xia at Division of Pulmonary, Critical Care and Sleep

Medicine, University of Washington, Seattle, US, we are working on a predictive model to identify the transcriptomic signature associated with fatal melioidosis from the whole blood RNA transcriptomic data. Meanwhile, these collaborators are working on identification of proteomic and metabolomic signature associated with fatal melioidosis generated from matched plasma samples from the participants in my RNA-seq study (**Chapter 5**). Ultimately, we aim to integrate the signature associated with fatal melioidosis derived from the multiple-omic approaches.

7.6.3 Additional RNA-sequencing for other community-acquired infections

As per discussion in the limitations of this study, the number samples from participants deriving from each other community-acquired infections other than melioidosis is probably insufficient to confidently derive transcriptomic signatures associated with fatal cases within each group of the infection. Further work to study a larger dataset of other community-acquired infections in this geographical location would allow me to confidently identify a transcriptomic signature that could discriminate patients with melioidosis from other infections.

7.7 Final Conclusions

This thesis represents the largest transcriptomic survey of the host response to melioidosis to date, with 274 melioidosis patients studied in total. In my thesis, the impact of diabetes on the whole blood transcriptomic profile during acute melioidosis was subtle, despite T2DM conferring the highest risk of acquiring melioidosis. On the other hand, the whole blood transcriptomic profile associated with diabetes in TB patients was distinctive, suggesting that reduced interferon responses in diabetes could be a potential mechanism leading to increased susceptibility to Mtb infection in TB patients with diabetes and

intermediate hyperglycaemia. Nevertheless, both melioidosis and TB patients with diabetes exhibit an elevated, neutrophil-driven inflammatory response. This highlights a potential detrimental role of excessive inflammatory immune responses and associated reduced cellular responses to intracellular pathogens in people with diabetes. Meanwhile, in community-acquired melioidosis, excessive inflammation concomitant with anti-inflammatory immune response and stunted cellular immune responses were associated with fatal infection. This implicates the need for a delicate balance between innate responses and finely tuned, effective adaptive responses for survival from melioidosis.

Appendices

Supplementary information for Chapter 3

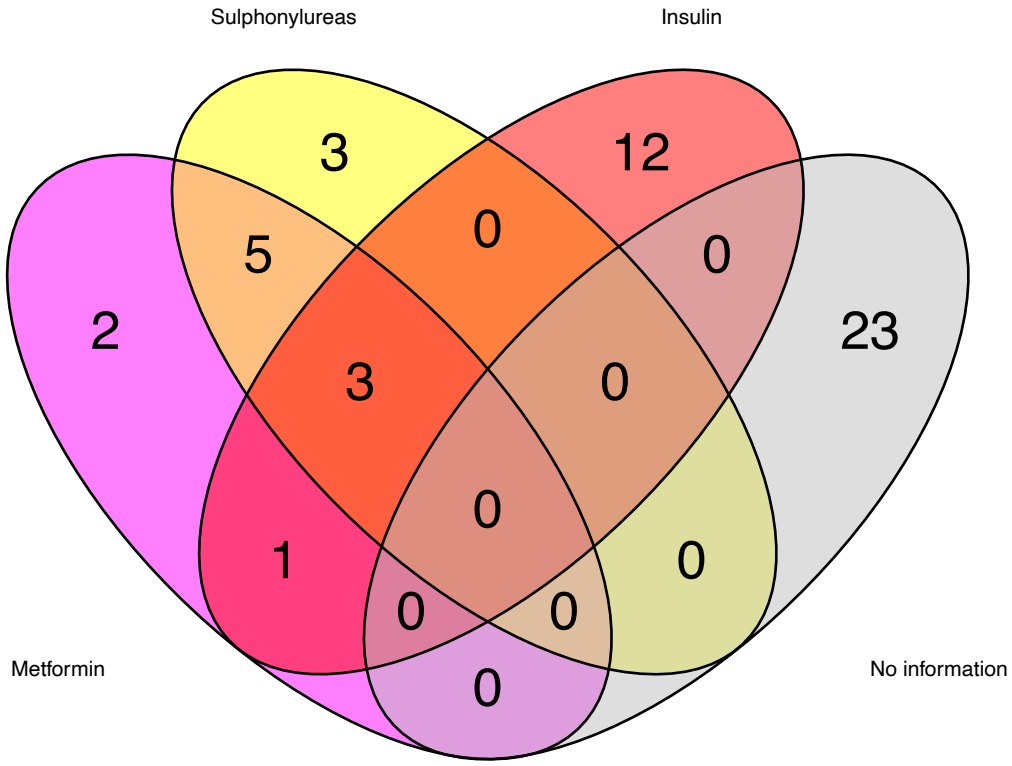

Supplementary Figure 3.1 A Venn diagram shows proportions of melioidosis patients with type 2 diabetes (T2DM) who received different diabetic drug regimens. A total of 49 melioidosis patients with T2DM, 26 patients had records on prescribed diabetic drugs following enrolment into the study. 3 main groups of diabetic drugs are shown including metformin, sulphonylureas, and insulin.

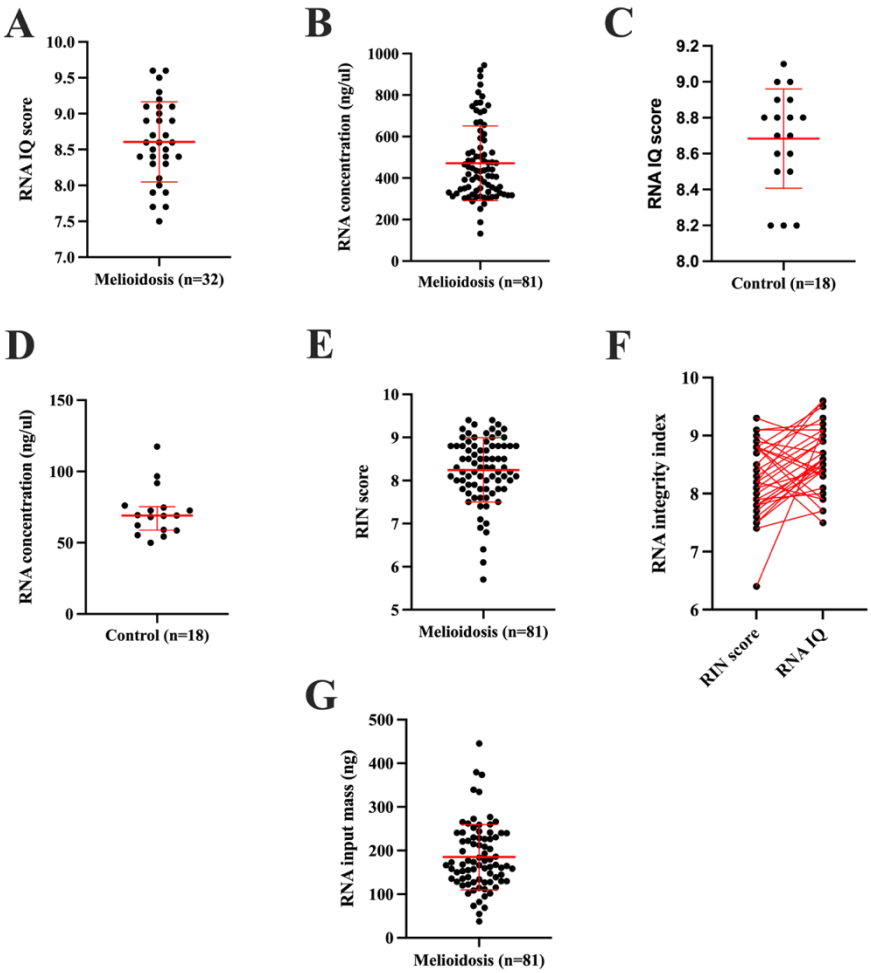

Supplementary Figure 3.2 Quality control of total RNA derived from melioidosis and control cohorts. Total RNAs were isolated from cryopreserved whole blood in Tempus blood RNA tubes. A, B: RNA samples from melioidosis patients measured for RNA integrity by Qubit™ RNA IQ and quantity by Qubit™ XR assay. C, D: RNA samples from uninfected control donors measured for RNA integrity by Qubit™ RNA IQ and quantity by Qubit™ XR assay. E: RNA samples from melioidosis patients measured for RNA integrity by Agilent TapeStation. F: Comparison of RNA integrity index measured by Agilent TapeStation and Qubit™ RNA IQ of matched samples. G: Total RNA input mass for RNA-sequencing by Agilent TapeStation. Bars represent mean and standard deviation.

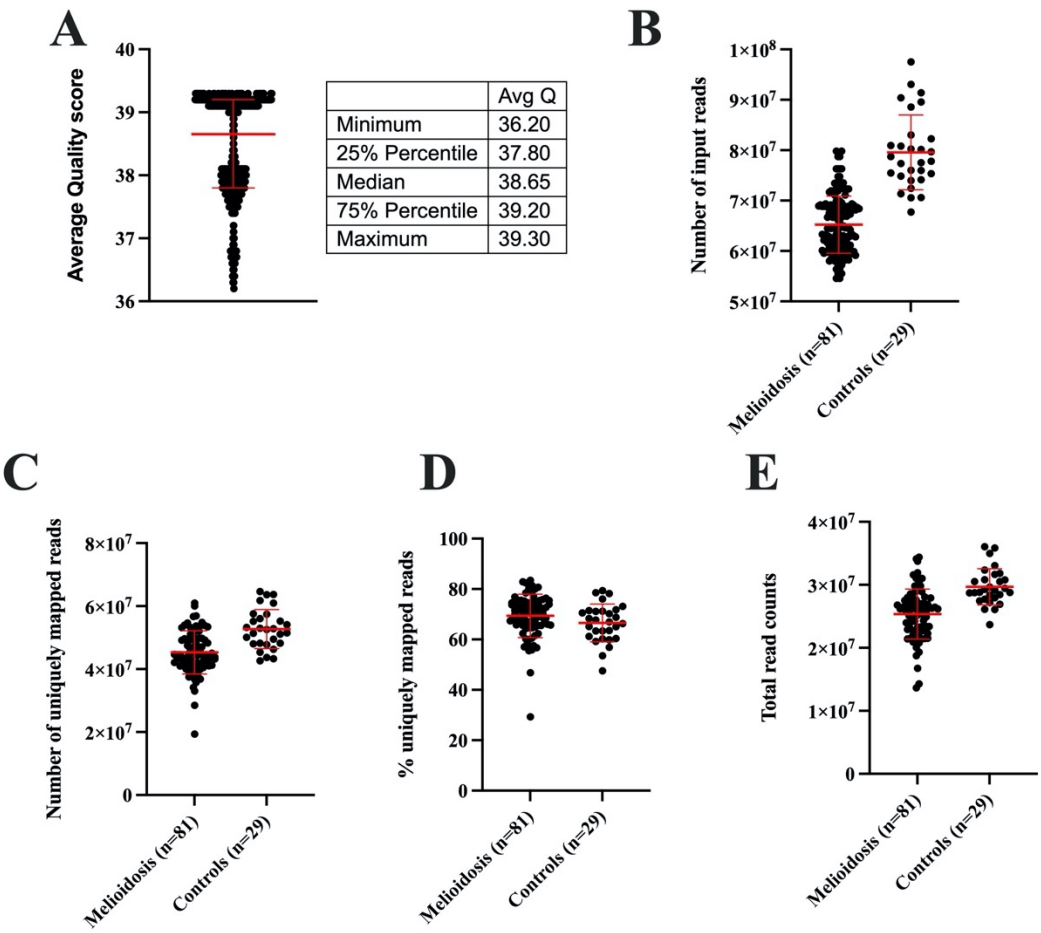

Supplementary Figure 3.3 Quality control of raw RNA sequencing data. RNA sequencing data were generated from whole blood samples of 81 melioidosis patients and 29 uninfected control donors using globin-depleted, Ribo-zero total RNA sequencing approach. A: Representative plot of average quality score of raw RNA sequencing data. B: Total RNA sequencing reads for mapping using STAR aligner against human reference genome, UCSC hg38.p2 version 20201. C, D: Total mapped and frequencies of uniquely mapped reads respectively. E: Total read counts per sample. Bars represent mean and standard deviation.

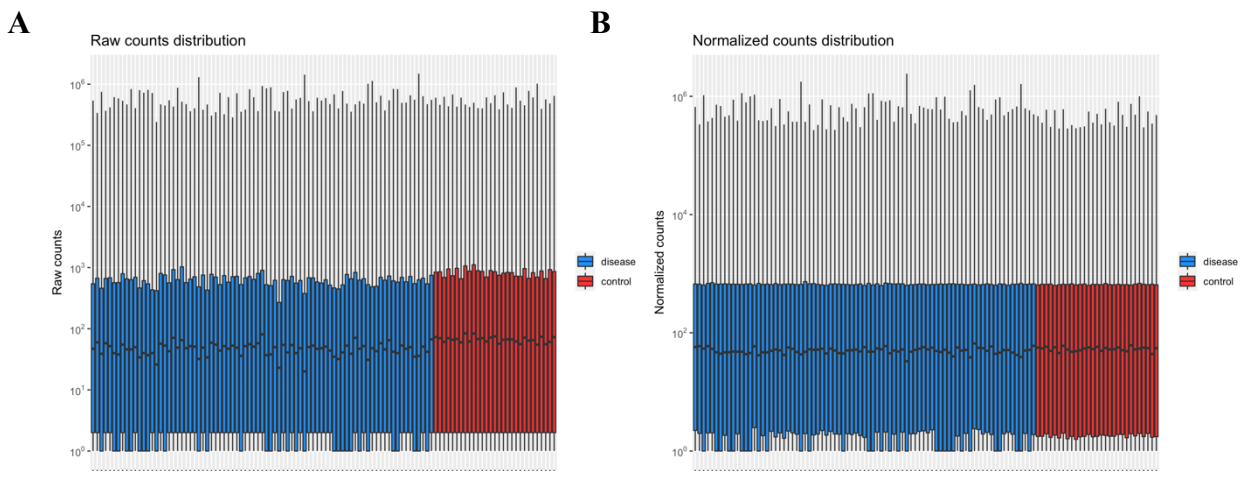

Supplementary Figure 3.4 Normalisation of RNA sequencing data by DESeq2.

Pre-filtered 17,594 genes after removal of lowly expressed genes were normalised using median of ratios method implemented in DESeq2 R package, accounting for differences in sequencing depth and RNA composition among samples. A: Raw read counts before normalisation. B: Normalised expression data. Disease: 81 melioidosis patients. Control: 29 uninfected donors.

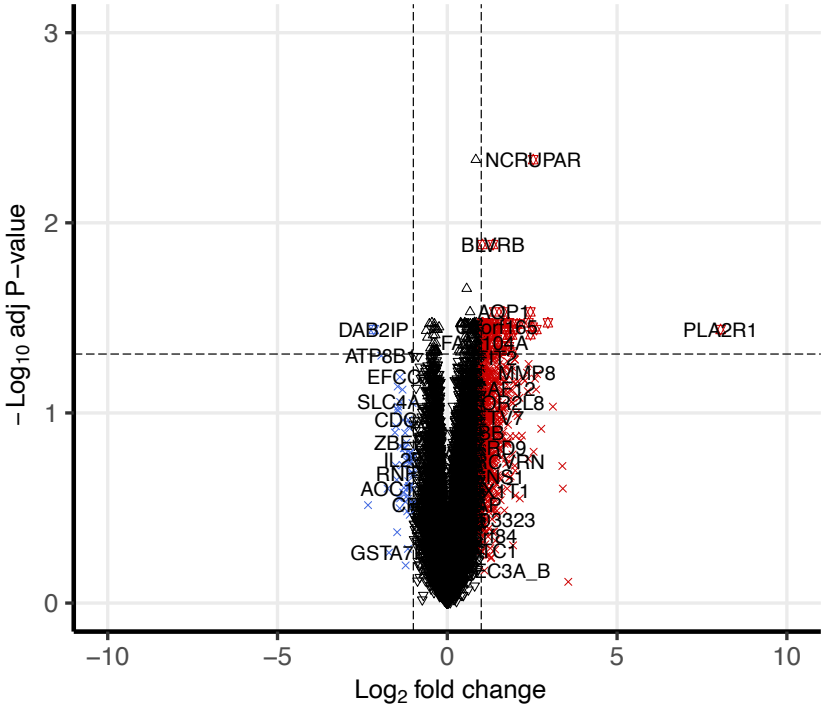

Supplementary Figure 3.5 Volcano plot of differentially expressed genes between diabetes (n=15) and healthy (n=14) controls. Dotted lines define a cut-off of differentially expressed genes based on absolute (log2 fold-change)≥ 1 (x-axis) and adjusted P-value < 0.05 (y-axis). Volcano plot was generated using EnhancedVolcano R package.

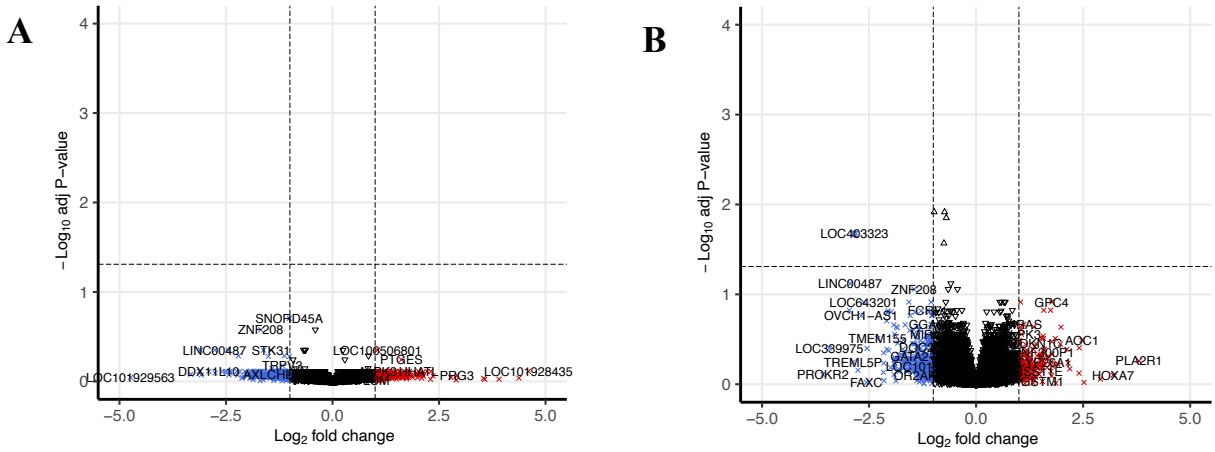

Supplementary Figure 3.6 Volcano plot of differentially expressed genes between melioidosis patients with (n=49) and without diabetes (n=32). A: Differential gene expression analysis between melioidosis with and without diabetes controlling for prescribed diabetic drugs in the patients with diabetes (26/49) as a covariate. B: Differential gene expression analysis between melioidosis with and without diabetes controlling for frequency of neutrophils as a covariate. Dotted lines define a cut-off of differentially expressed genes based on absolute (log2 fold-change)≥ 1 (x-axis) and adjusted P-value < 0.05 (y-axis). Volcano plot was generated using EnhancedVolcano R package.

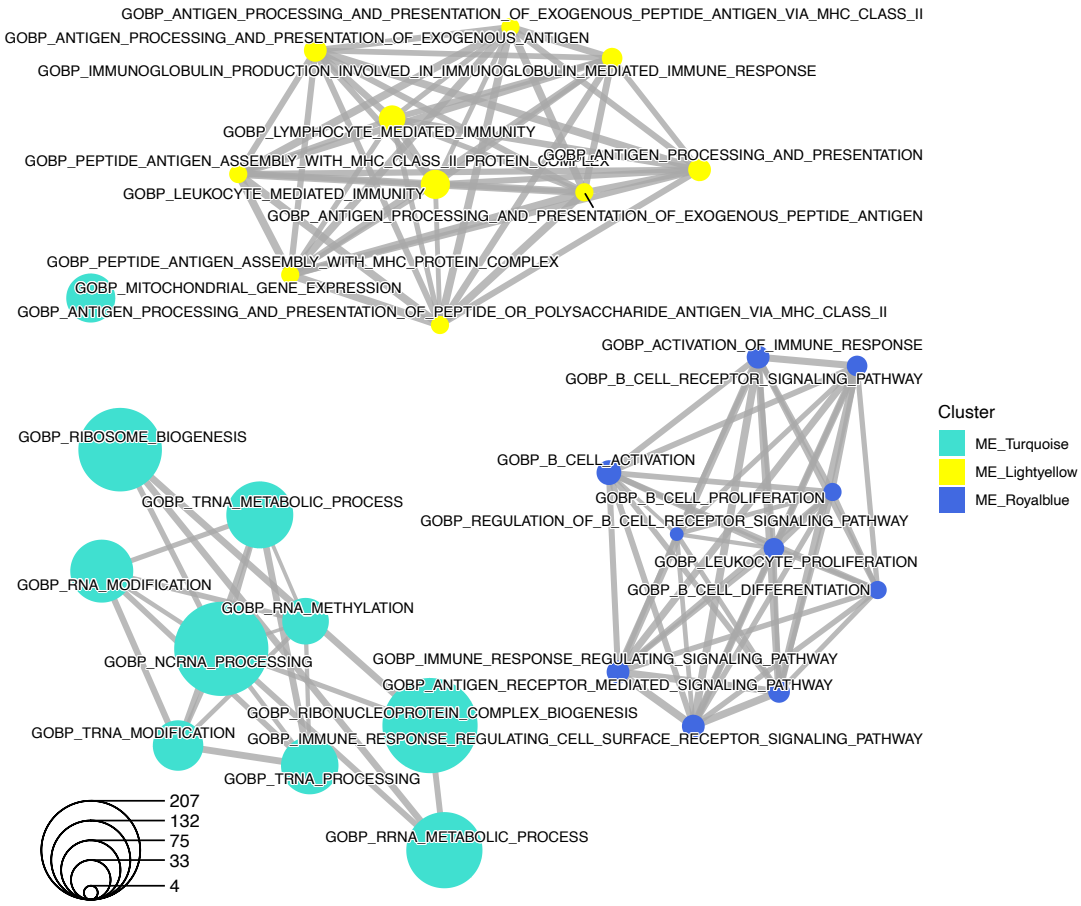

Supplementary Figure 3.7 Enrichment analysis based on Gene Ontology (biological process) gene sets in 3 module eigengenes (MEs) including ME turquoise, lightyellow, and royalblue which were associated with %lymphocytes identified by module-trait relationship analysis in 81 melioidosis patients. Pathways with closely related functions were linked and clustered together. The thickness of line indicates common genes shared among the pathways. The size of each term is indicated by representative counts. Enrichment plot was created using clusterProfiler R package.

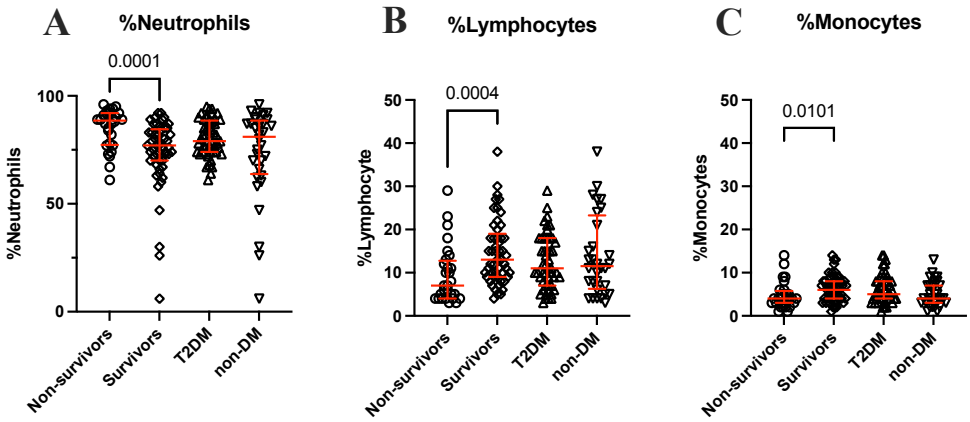

Supplementary Figure 3.8 Scatter plots show the frequencies of (A) neutrophils, (B) lymphocytes and (C) monocytes from full blood count (FBC) upon enrolment of 81 melioidosis patients. The comparisons were made between 28-day mortality (non-survivors versus survivors) and diabetes status (type 2 diabetes [T2DM] versus non-diabetes [non-DM]). Non-parametric Mann-Whitney test was performed with its corresponding P-value displayed on each plot and median and inter-quartile range bars.

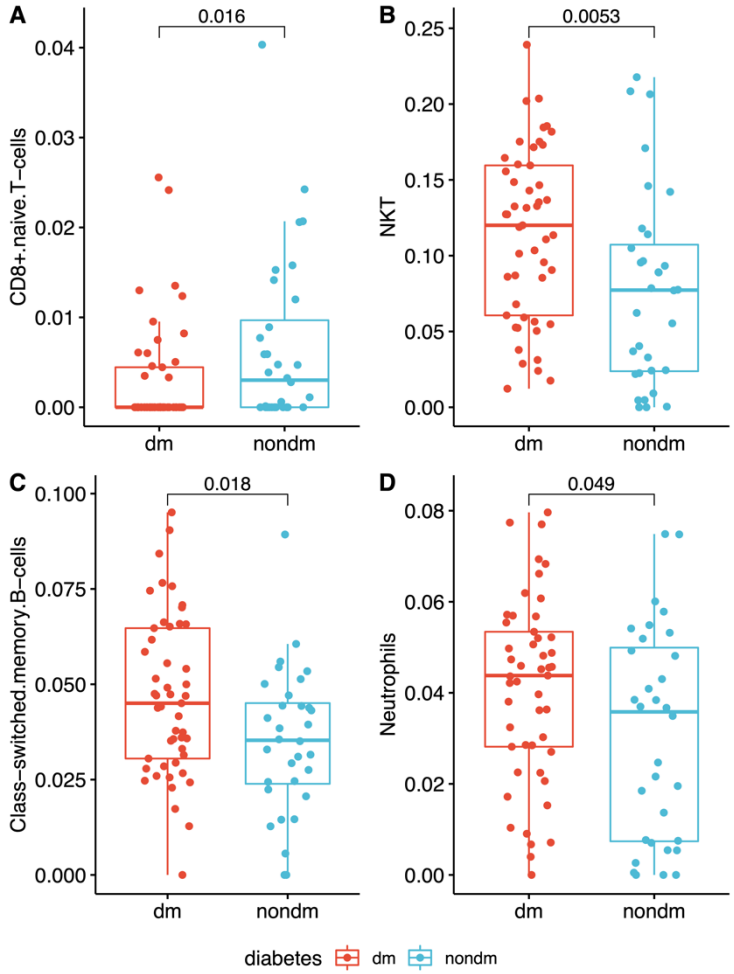

Supplementary Figure 3.9 Scattered boxplots show comparisons of deconvoluted cell fractions between melioidosis patients with (red, n=49) and without type 2 diabetes (blue, n=32) using xCell deconvolution method (xCell R package version 1.1.0). The Y-axis displays each cell type by enrichment scores. Box plots represent medians with interquartile range plus lines to minimum, maximum and potential outliers. Non-parametric Mann-Whitney test was performed with its corresponding 2-tailed P-value displayed on each plot alongside median and inter-quartile range boxes.

Supplementary Table 3.1 Pre-ranked gene set enrichment analysis (pre-ranked GSEA) by Hallmark gene sets following differential gene expression analysis (DGE) of uninfected control cohorts. The DGE analyse was performed on type 2 diabetes control cohort (n=15) compared to healthy donors (n=14). Gene sets were deemed significant when satisfied false discovery rate (FDR q-value < 0.05) and ranked by normalised enrichment score and FDR. Enriched pathways were calculated from the DESeq2 statistical test of pre-ranked gene list following DGE analysis using GSEAPreranked mode on GSEA software.

Group		Rank	Hallmark pathways	NES	FDR q-val	Process category
Pre-ranked GSEA: T2DM control versus healthy control	Enriched in T2DM control	1	HEME_METABOLISM	7.01	0	Metabolic
		2	INTERFERON_ALPHA_RESPONSE	5.23	0	Immune
		3	INTERFERON_GAMMA_RESPONSE	3.56	0	Immune
		4	TNFA_SIGNALING_VIA_NFKB	2.43	0.002	Signalling
		5	INFLAMMATORY_RESPONSE	2.21	0.005	Immune
		6	IL6_JAK_STAT3_SIGNALING	2.02	0.013	Immune
	Enriched in healthy control	1	MYC_TARGETS_V1	-7.90	0	Proliferation
		2	OXIDATIVE_PHOSPHORYLATION	-6.35	0	Metabolic
		3	E2F_TARGETS	-5.75	0	Proliferation
		4	MTORC1_SIGNALING	-4.67	0	Signalling
		5	MYC_TARGETS_V2	-4.08	0	Proliferation
		6	UNFOLDED_PROTEIN_RESPONSE	-3.86	0	Pathway
		7	GLYCOLYSIS	-3.54	0	Metabolic
		8	G2M_CHECKPOINT	-3.27	0	Proliferation
		9	ADIPOGENESIS	-3.07	0	Development
		10	FATTY_ACID_METABOLISM	-3.05	0	Metabolic
		11	DNA_REPAIR	-2.94	0	DNA damage
		12	PEROXISOME	-2.43	4.50E-04	Cellular component
		13	WNT_BETA_CATENIN_SIGNALING	-2.04	0.010	Signalling
		14	BILE_ACID_METABOLISM	-1.91	0.021	Metabolic
		15	ESTROGEN_RESPONSE_LATE	-1.85	0.027	Signalling
		16	CHOLESTEROL_HOMEOSTASIS	-1.79	0.035	Metabolic
		17	IL2_STAT5_SIGNALING	-1.76	0.040	Signalling
		18	ALLOGRAFT_REJECTION	-1.74	0.043	Immune
		19	ANDROGEN_RESPONSE	-1.74	0.041	Signalling

Supplementary information for Chapter 4

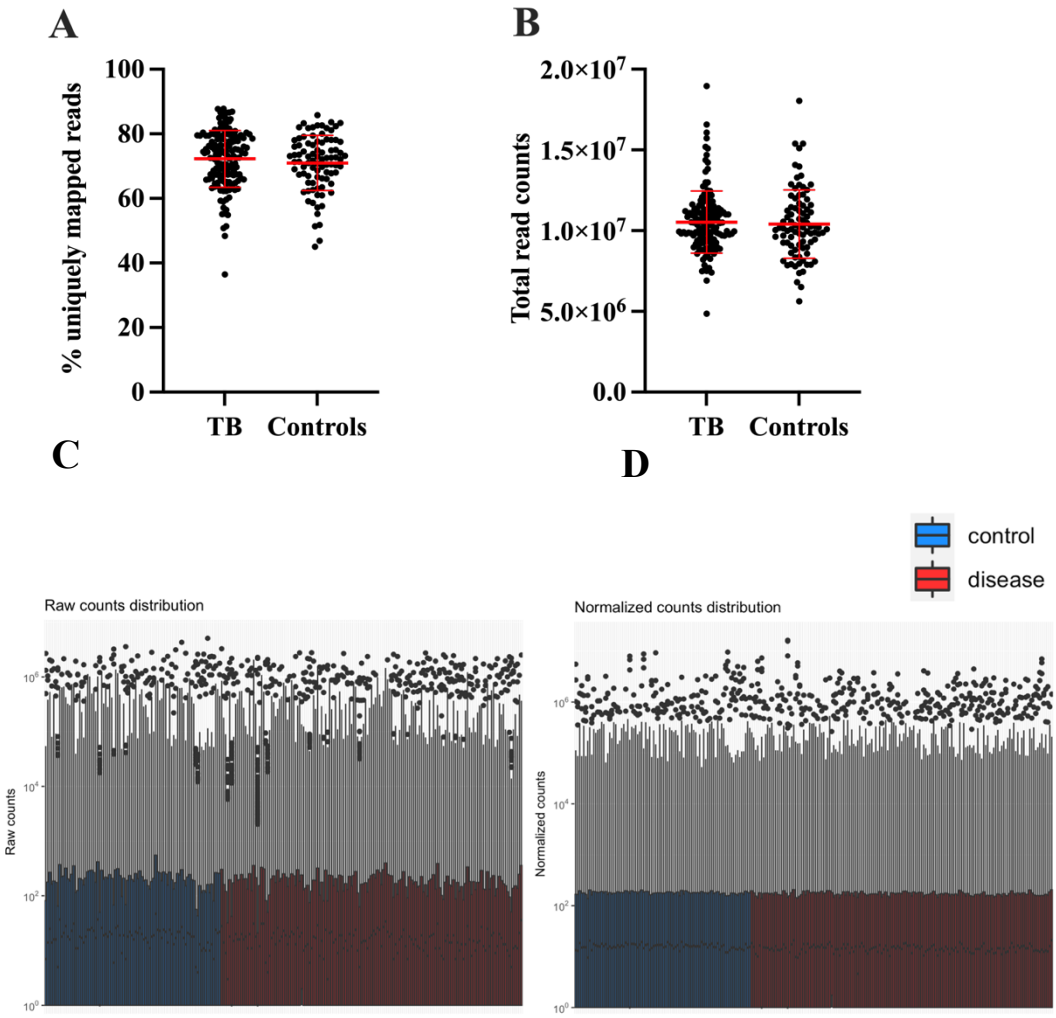

Supplementary Figure 4.1 Summary of raw counts and distribution of RNA sequencing data generated from whole blood sample of tuberculosis (TB) and control cohorts. A: Frequencies of uniquely mapped reads in TB (n=151) and control cohorts (n=88) using STAR aligner against human reference genome, UCSC hg38.p2 version 20201. B: Total read counts per sample between TB and control cohorts. C: unnormalised and (D) normalised total read counts using median of ratios method implemented in DESeq2 R package. Bars represent mean and standard deviation.

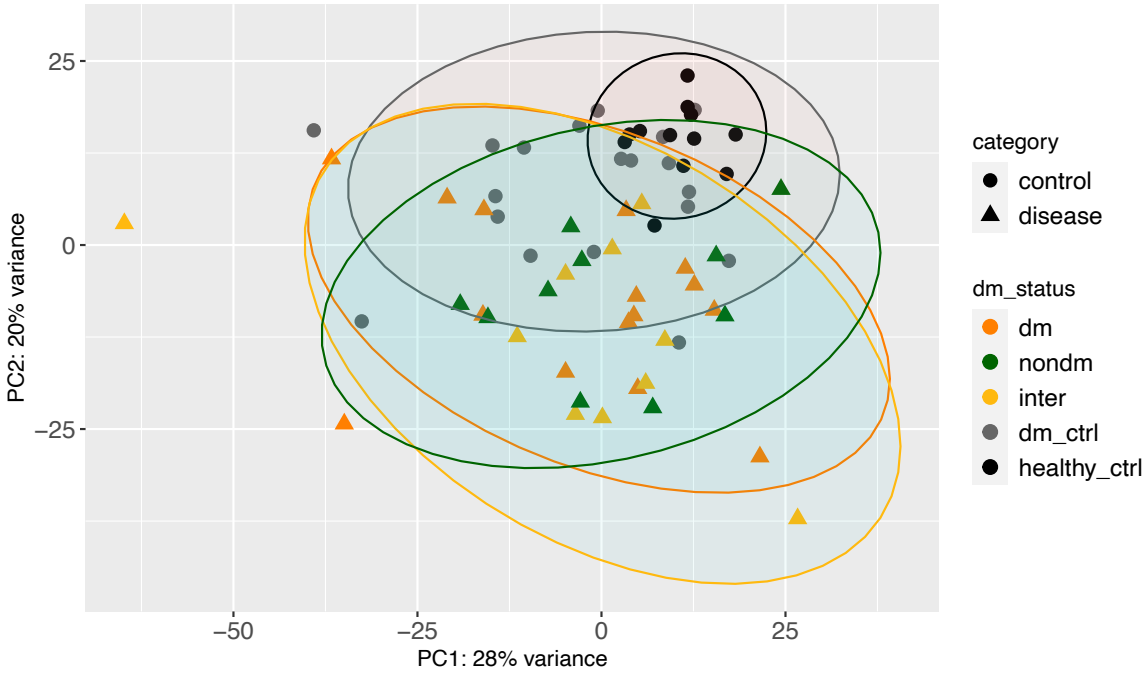

Supplementary Figure 4.2 Principal component analysis (PCA) of the top 1,000 most variable genes in tuberculosis (TB) patients and controls from Romanian cohort coloured by diabetes status and intermediate hyperglycaemia classification based on HbA1c level. TB patients were divided into diabetes ("dm", orange triangles, n=15), intermediate hyperglycaemia ("inter", yellow triangles, n=10), non-diabetes ("nondm", green triangles, n=10), uninfected diabetes group ("dm_ctrl", grey circles, n=19), and healthy donors ("healthy_ctrl", black circles, n=12). Group classification based on HbA1c level: diabetes (HbA1c ≥6.5%), intermediate hyperglycaemia (HbA1c ≥5.7% and <6.5%), non-diabetes (HbA1c ≤ 5.6%). PCA plots were generated using plotPCA function implemented in DESeq2 R package.

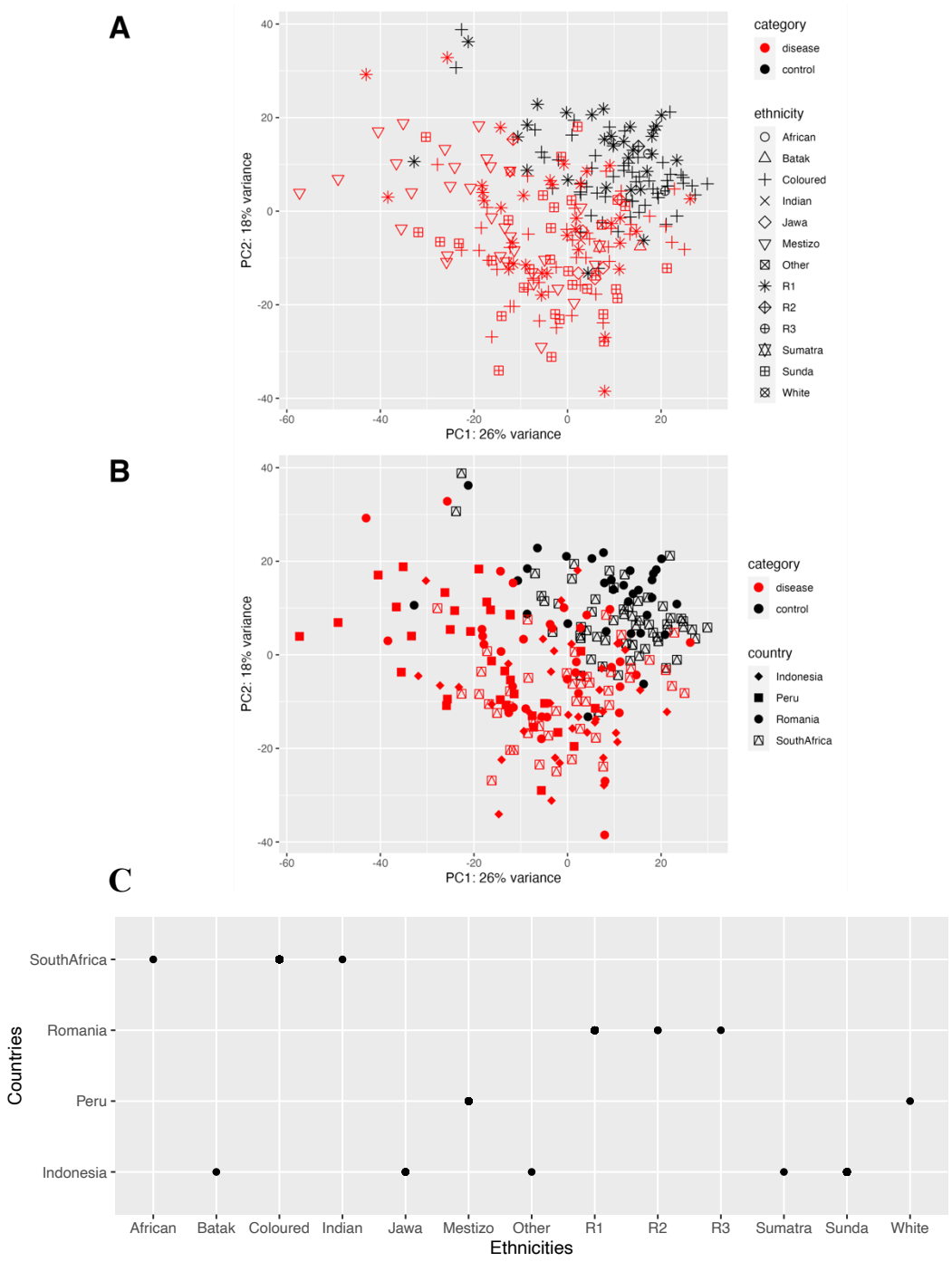

Supplementary Figure 4.3 Principal component analysis (PCA) of the top 1,000 most variable genes among 239 tuberculosis (TB) patients and controls from all-study sites combined and distribution of ethnicities in each of the study sites. For PCA plots, TB patients and control cohorts were labelled in red and black respectively. A: PCA symbolised by ethnicity across all-four study sites divided into Africa (opened circle, n=1), Batak (opened triangle point up, n=1), Coloured (plus sign, n= 100), Indian (cross sign, n=1), Jawa (opened diamond, n=5), Mestizo (opened triangle point

down, n=31), other (opened square cross, n=1), R1 (star, n= 63), R2 (opened diamond plus, n=2), R3 (opened circle plus, n=1), Sumatra (opened triangle up and down, n=1), Sunda (opened square plus, n=31), and White (opened circle cross, n=1). B: PCA symbolised by country across all-four study sites divided into Indonesia (filled diamond, n=39), Peru (filled square, n=32), Romania (filled circle, n=66), and South Africa (opened square and triangle up, n=102). C: A plot shows distribution of each ethnicity in each of the study sites.

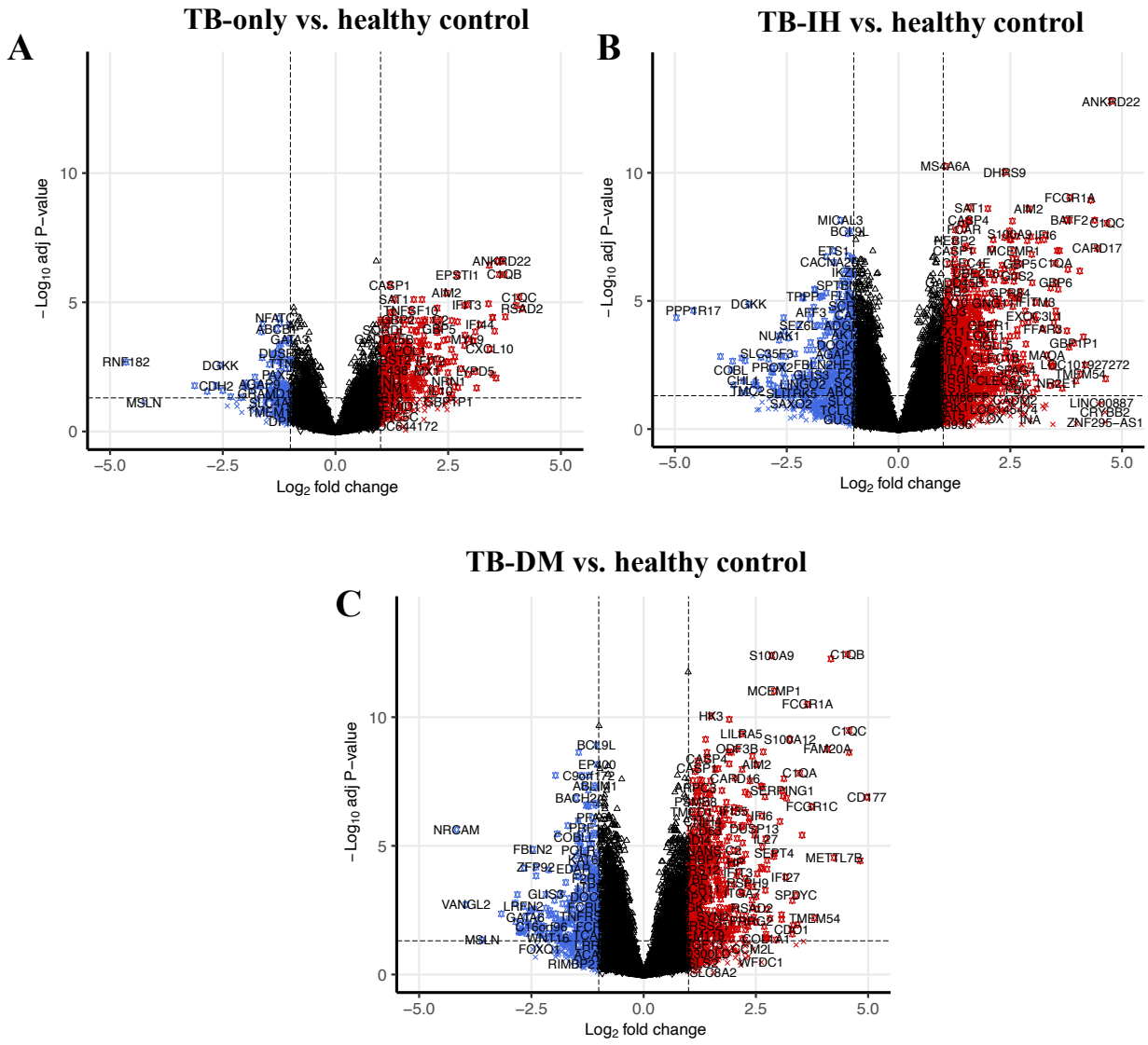

Supplementary Figure 4.4 Volcano plots showing differentially expressed genes among tuberculosis (TB) patient groups and healthy controls from the Romanian cohort. A: Differential gene expression (DGE) analysis between TB patients only (TB-only, n=10) compared to healthy control (n=12). B: DGE analysis between TB patients with intermediate hyperglycaemia (TB-IH, n=10) compared to healthy control (n=12). C: DGE analysis between TB patients with diabetes (TB-DM, n=15) compared to healthy control (n=12). Dotted lines define the cut-off for differentially expressed genes based on absolute (log2 fold-change)≥ 1 (x-axis) and adjusted P-value < 0.05 (y-axis). Volcano plot was generated using EnhancedVolcano R package.

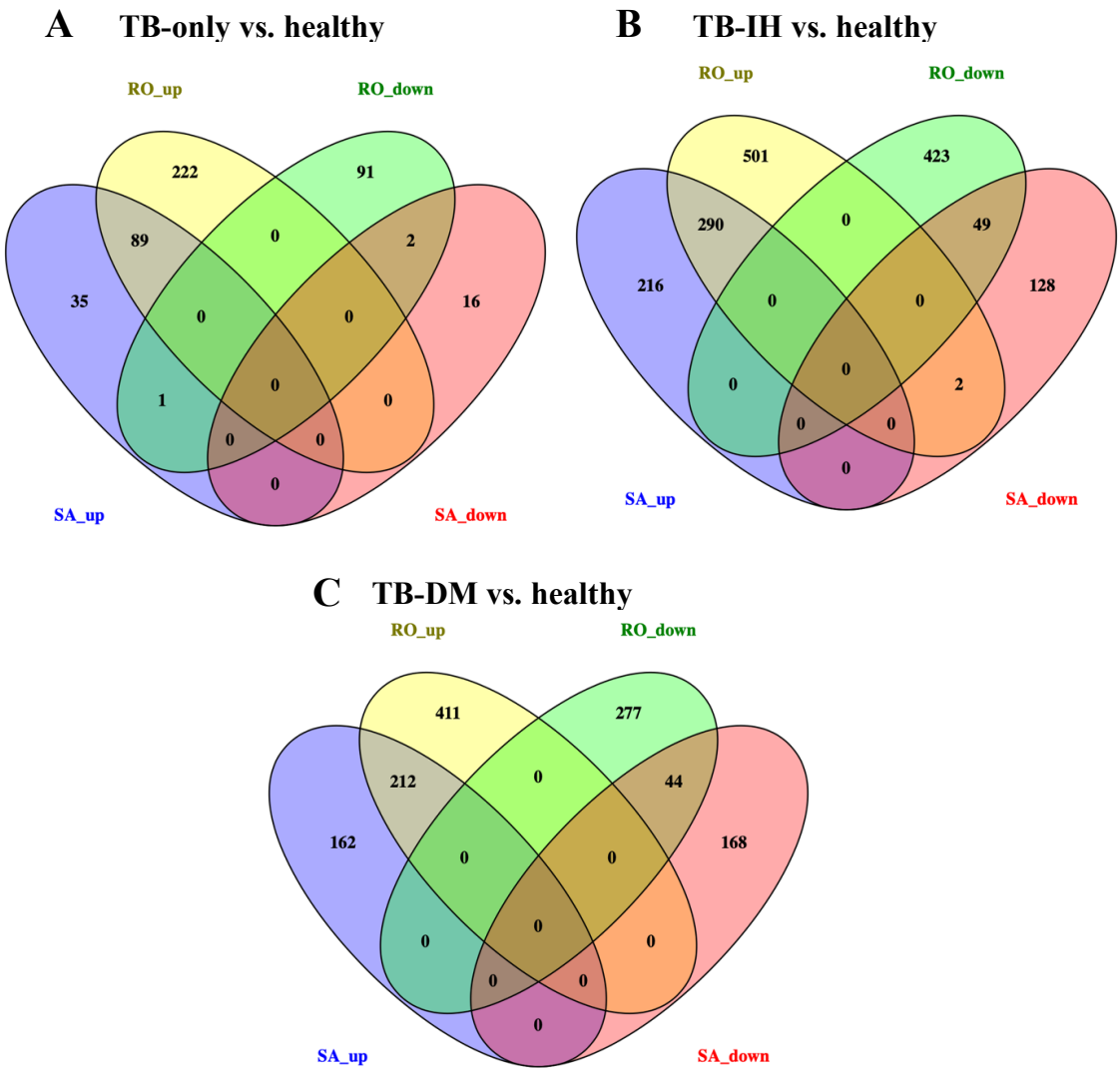

Supplementary Figure 4.5 Overlapping differentially expressed genes (DEGs) identified following differential gene expression (DGE) analyses of tuberculosis (TB) patients and control cohorts between South African (discovery) and Romanian (validation) cohort. A: DGE analysis between TB patients without diabetes and healthy controls. B: DGE analysis between TB patients with intermediate hyperglycaemia and healthy control. C: DGE analysis between TB patients with diabetes and healthy control. DEGs were deem significant when satisfied absolute (log2 fold-change)≥1 and adjusted P-value <0.05. SA_up = up-regulated genes in South African cohort. SA_down = down-regulated genes in South African cohort. RO_up = up-regulated genes in Romanian cohort. RO_down = down-regulated genes in Romanian cohort.

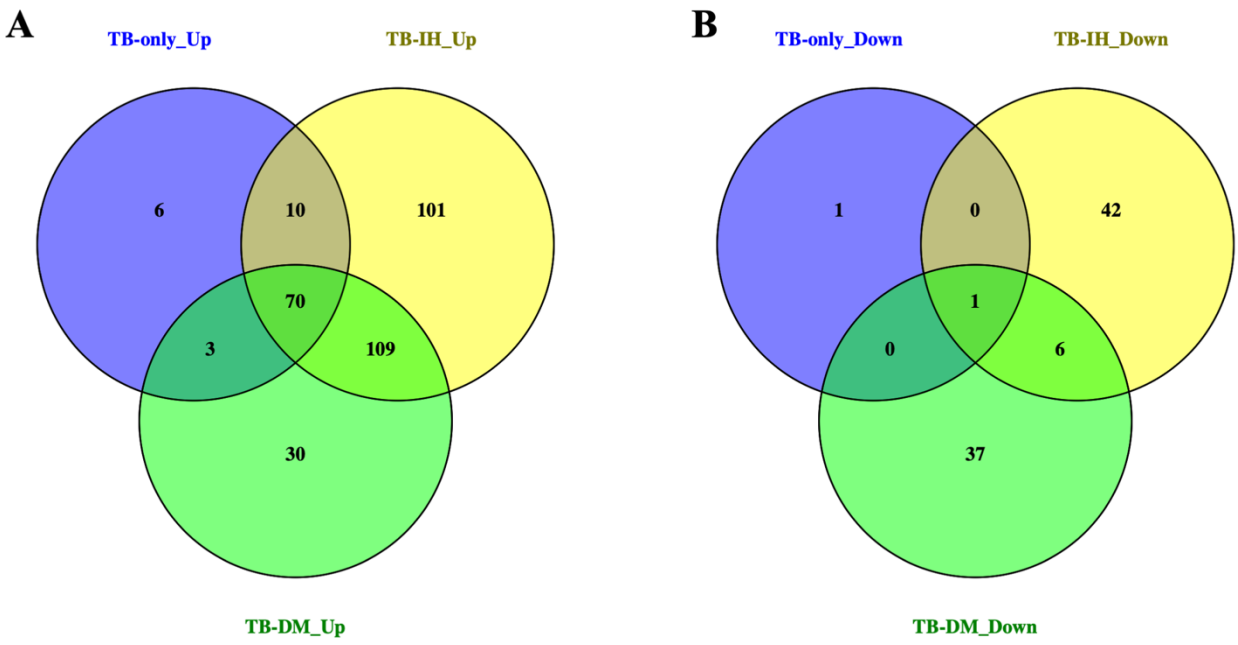

Supplementary Figure 4.6 Overlapping differentially expressed genes (DEGs) identified in South African (discovery) and Romanian (validation) cohorts. A: Up-regulated DEGs. B: Down-regulated DEGs. DEGs were derived from DGE analyses: TB compared to healthy control (TB-only_up and TB-only_down), TB-IH compared to healthy control (TB-IH_up and TB-IH_down), and TB-DM compared to healthy control (TB-DM_up and TB-DM_down). Significant DEGs are based on absolute (log2 fold-change)≥1 and adjusted P-value <0.05.

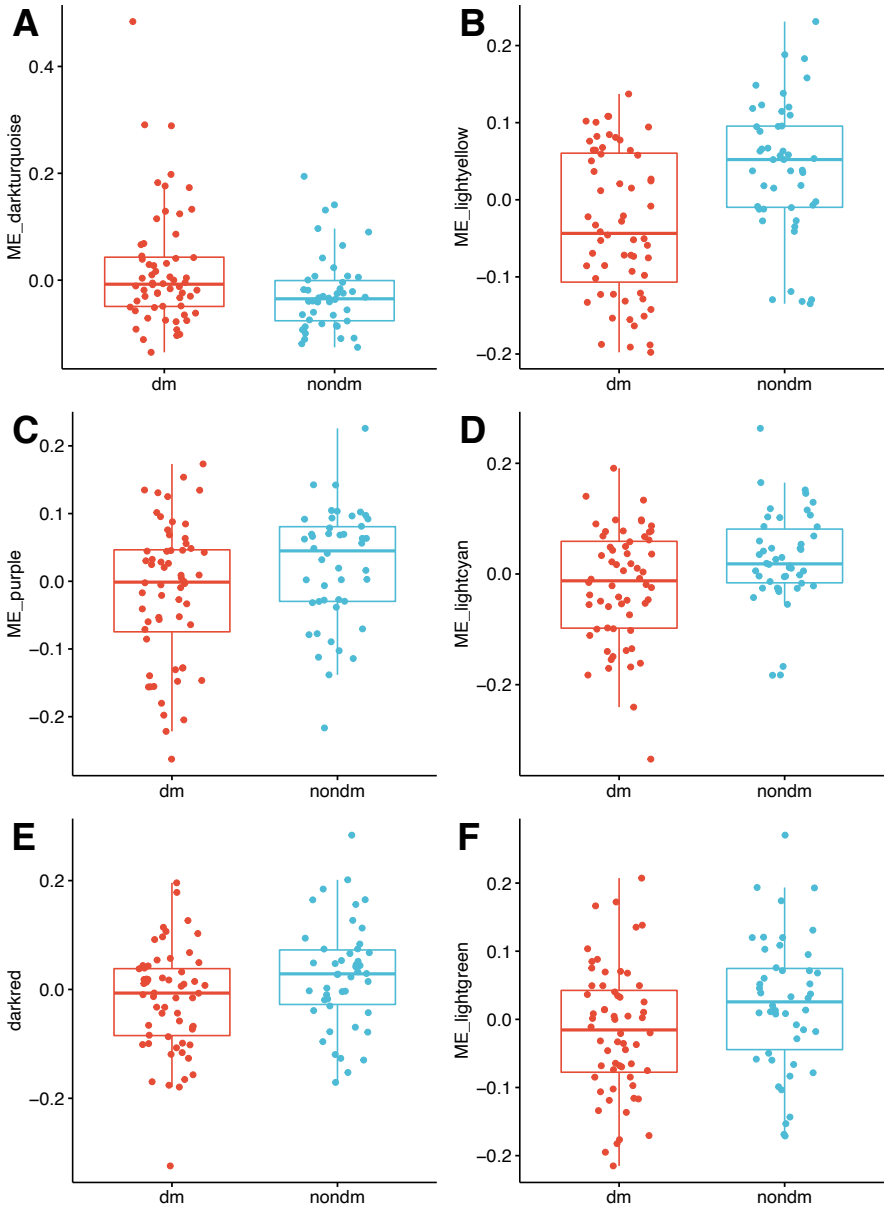

Supplementary Figure 4.7 Comparison of module eigengenes (MEs) between TB patients with and without diabetes from **Figure 4.9**. MEs with significant associations with diabetes status and HbA1c level were compared between TB patients with diabetes (red, n=61) and without diabetes (blue, n=46). Box plots represent medians with interquartile range plus lines to minimum, maximum and potential outliers.

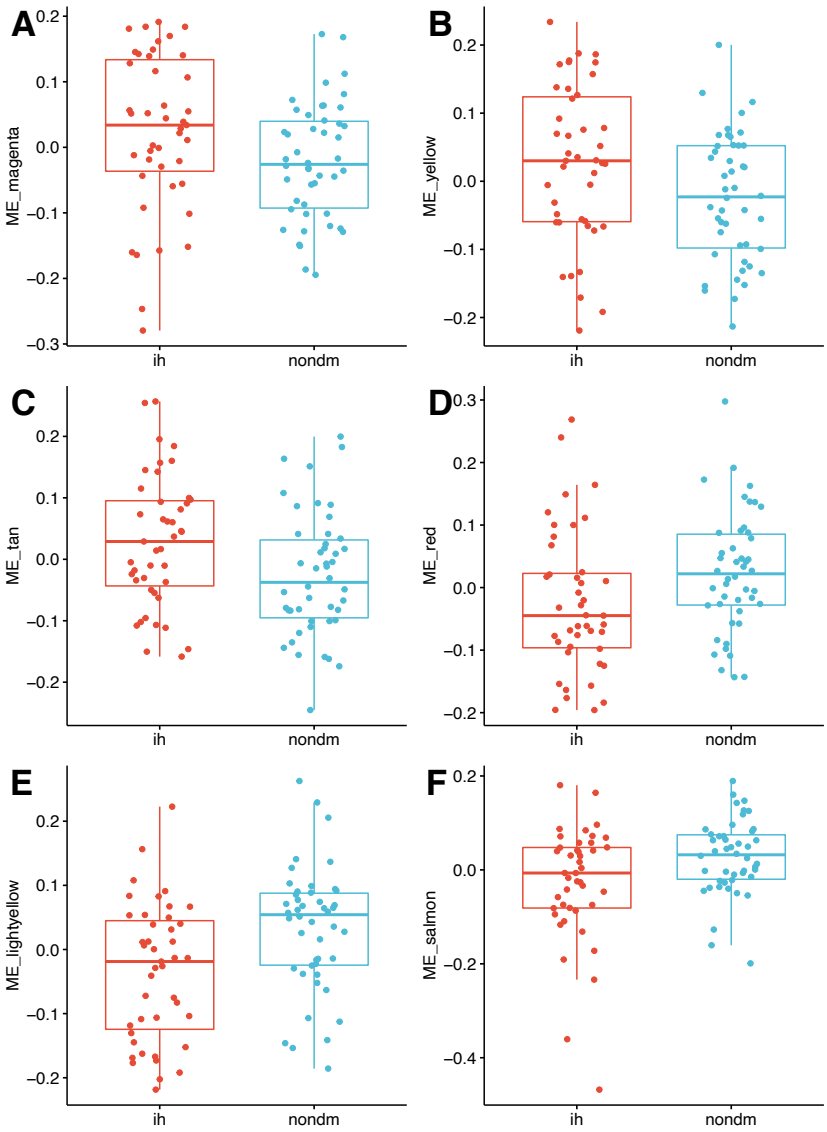

Supplementary Figure 4.8 Scattered box plots show comparisons of co-expressed gene modules (module eigengenes, MEs) between TB patients with and without intermediate hyperglycaemia (IH) from **Figure 4.12**. MEs with significant associations with intermediate hyperglycaemia status and HbA1c level were compared between TB patients with IH (red, n=44) and without diabetes (blue, n=46). Box plots represent medians with interquartile range plus lines to minimum, maximum and potential outliers.

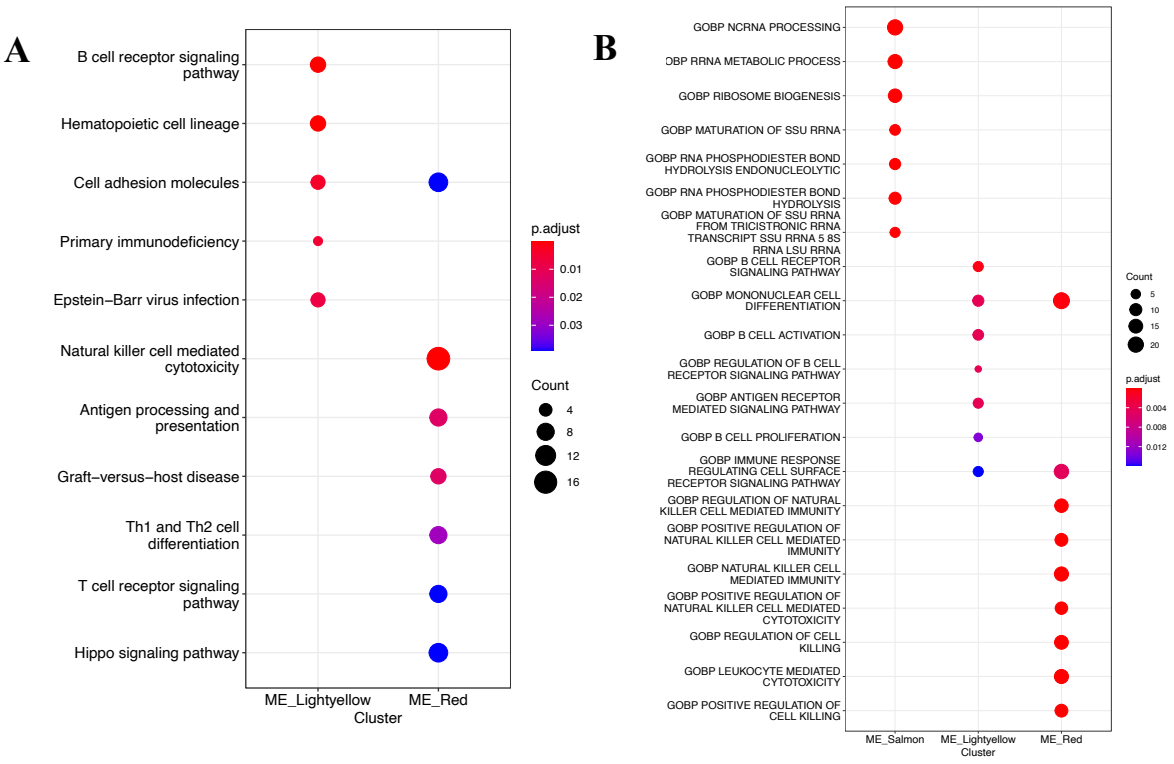

Supplementary Figure 4.9 Enrichment analysis based on Reactome and Gene Ontology in ME lightyellow, red and salmon that were negatively correlated with intermediate hyperglycaemia (IH) status and HbA1c level identified by module-trait relationship analysis in tuberculosis patients with and without IH respectively. A: Enriched pathways based on KEGG genes sets. B: Enriched pathways based on Gene Ontology genes sets. The gradient colour bar corresponds to the adjusted P-value. The size of each term is indicated by representative counts.

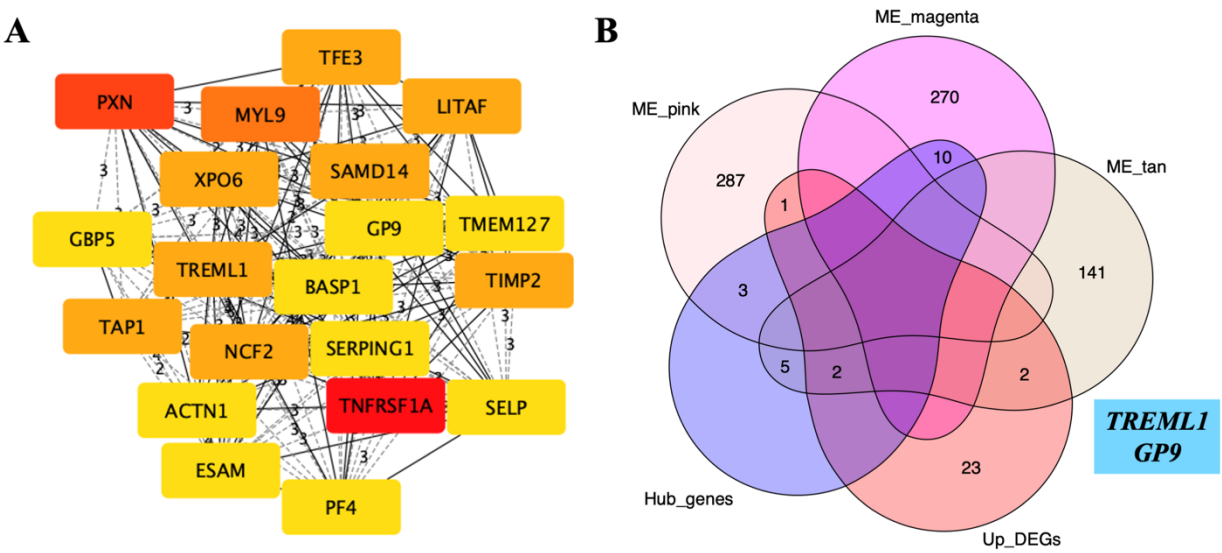

Supplementary Figure 4.10 Top 20 hub genes with potential regulatory role of host immune response in tuberculosis with intermediate hyperglycaemia (TB-IH). A: The top 20 hub genes identified in the eigengene (ME) pink, magenta and tan associated with HbA1c level. B: Venn diagram of overlapping differentially expressed genes (DEGs), gene membership of the ME pink, magenta and tan identified by weighted gene co-expression network analysis, and hub genes in the ME pink, magenta and tan. DEGs were derived from up-regulated genes between TB-IH and TB without diabetes patients based on absolute (log2 fold-change≥0.5 and adjusted P-value <0.05). ME pink, magenta and tan which were associated with HbA1c level by module-trait relationship analysis (**Figure 4.12**). 20 hub genes within ME pink, magenta and tan were derived from Maximal Clique Centrality (MCC) algorithm using CytoHubba plugin on Cytoscape software. MCC scores of hub genes were ranked from high (red) to low (yellow).

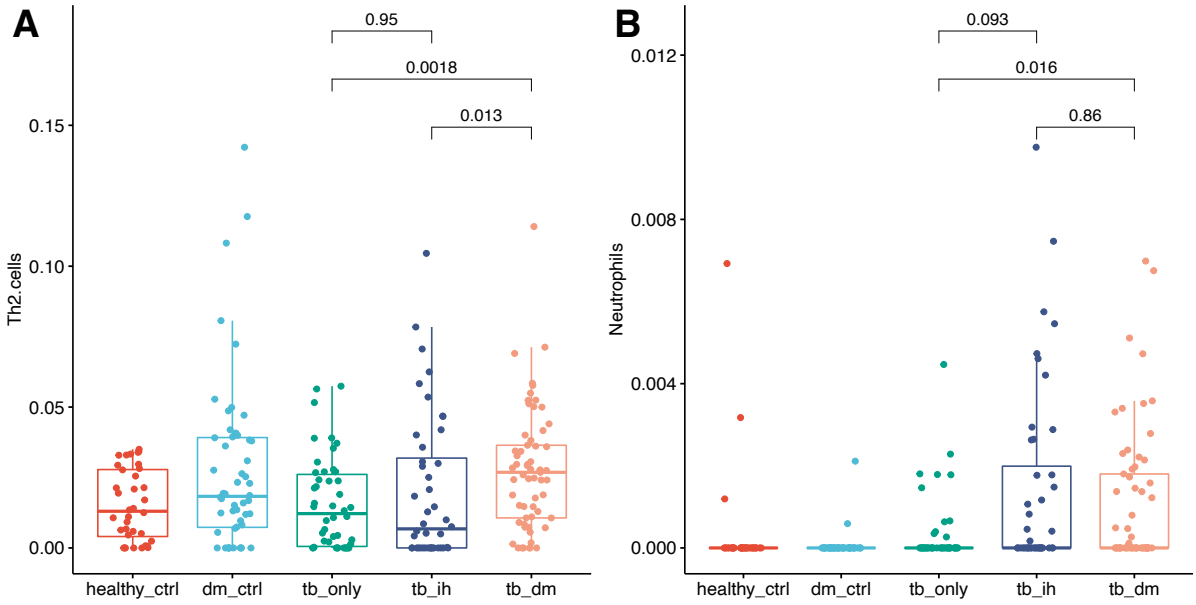

Supplementary Figure 4.11 Scattered boxplots show comparisons of enriched cell subsets among all TB patients across four study sites using xCell deconvolution method (xCell R package version 1.1.0). The Y-axis displays each cell type defined by enrichment scores. Box plots represent medians with interquartile range plus lines to minimum, maximum and potential outliers. Non-parametric Mann-Whitney test was performed with its corresponding 2-tailed P-value displayed on each plot alongside median and inter-quartile range boxes. healthy_ctrl = healthy controls (red, n=36). dm_ctrl = diabetes control (blue, n=52). tb_only = TB patients without diabetes (green, n=46). tb_ih = TB patients with intermediate hyperglycaemia (dark blue, n=44). tb_dm = TB patients with diabetes (salmon, n=61).

Supplementary information for Chapter 5

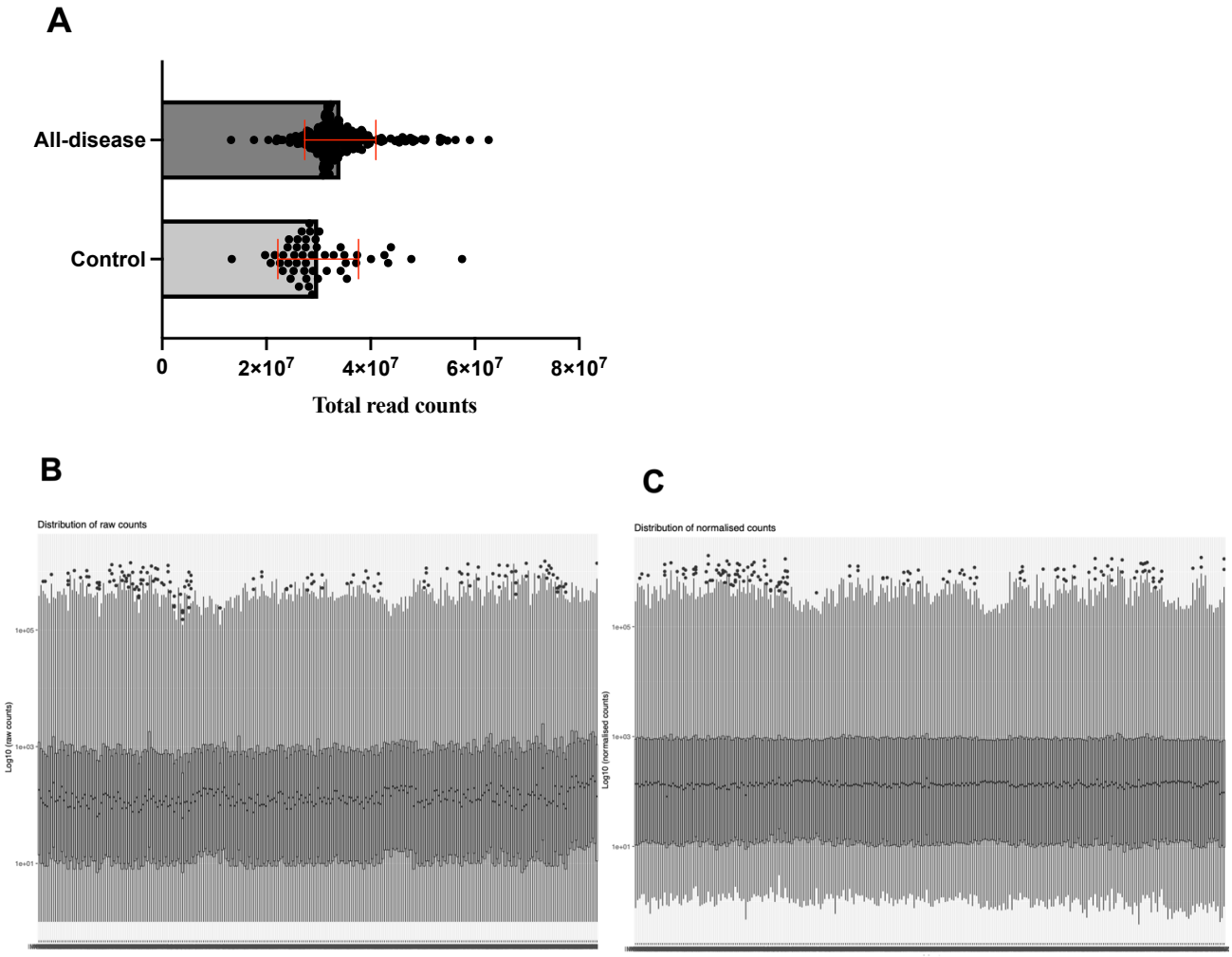

Supplementary Figure 5.1 Total read counts and distribution of raw and normalised counts from whole blood RNA sequencing of melioidosis and control cohort (N=284). A: Scatter plot shows total read counts in all-disease (n=234) and control cohort (n=50) with bars represent mean and standard deviation. B: Distribution of raw counts. C: Distribution of normalised counts. Read counts were generated using STAR aligner against human reference genome GRCh38 with reference transcriptome GENCODE release 30 respectively. The raw counts were normalised using median of ratios method implemented in DESeq2 R package. Bars represent mean and standard deviation.

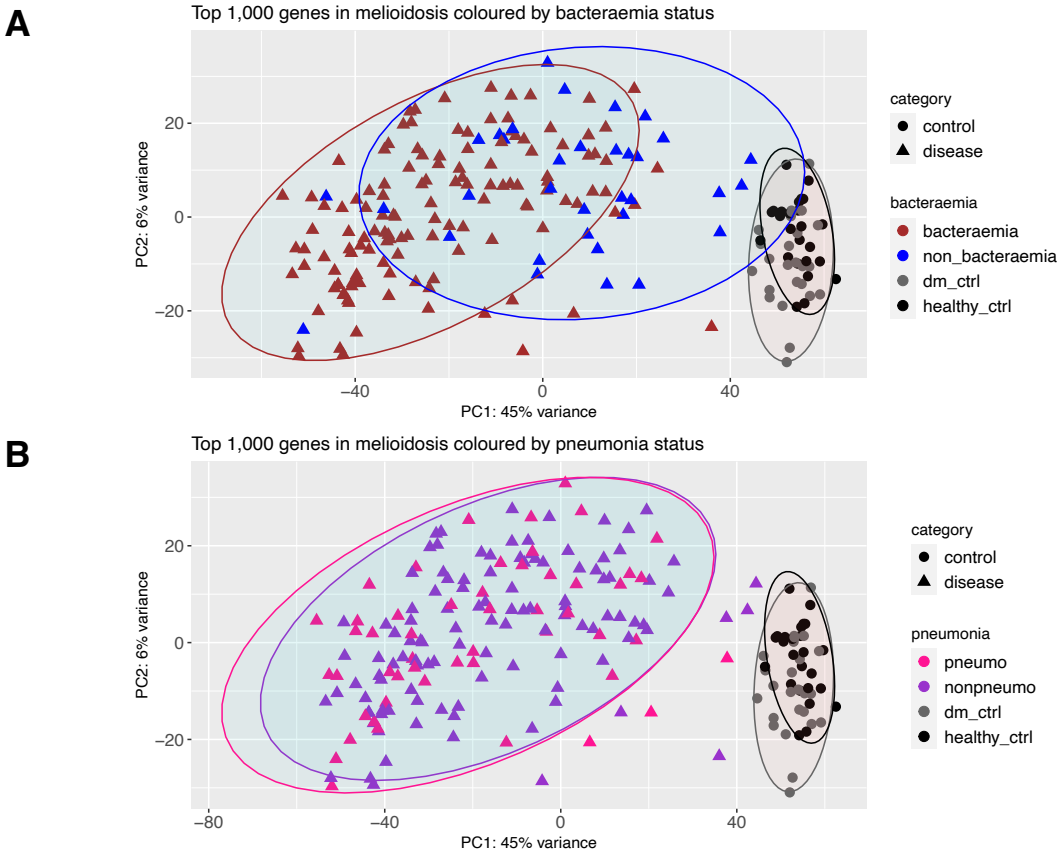

Supplementary Figure 5.2 Multidimensional scaling by principal component analysis (PCA) of the 1,000 most variable genes among melioidosis and control cohort. PCA in melioidosis and control cohorts were coloured by (A) bacteraemia and (B) pneumonia status. A: Patients with melioidosis, divided into bacteraemia ("bacteraemia", brown triangles, n=130), non-bacteraemia ("non_bacteraemia", blue triangles, n=30), uninfected diabetes group ("dm_ctrl", grey circles, n=25), and healthy donors ("healthy_ctrl", black circles, n=25). B: Patients with melioidosis, divided into those presented with pneumonia ("pneumo", pink triangles, n=52), without pneumonia ("nonpneumo", purple triangles, n=112), uninfected diabetes group ("dm_ctrl", grey circles, n=25), and healthy donors ("healthy_ctrl", black circles, n=25). PCA plots were generated using plotPCA function implemented in DESeq2 R package.

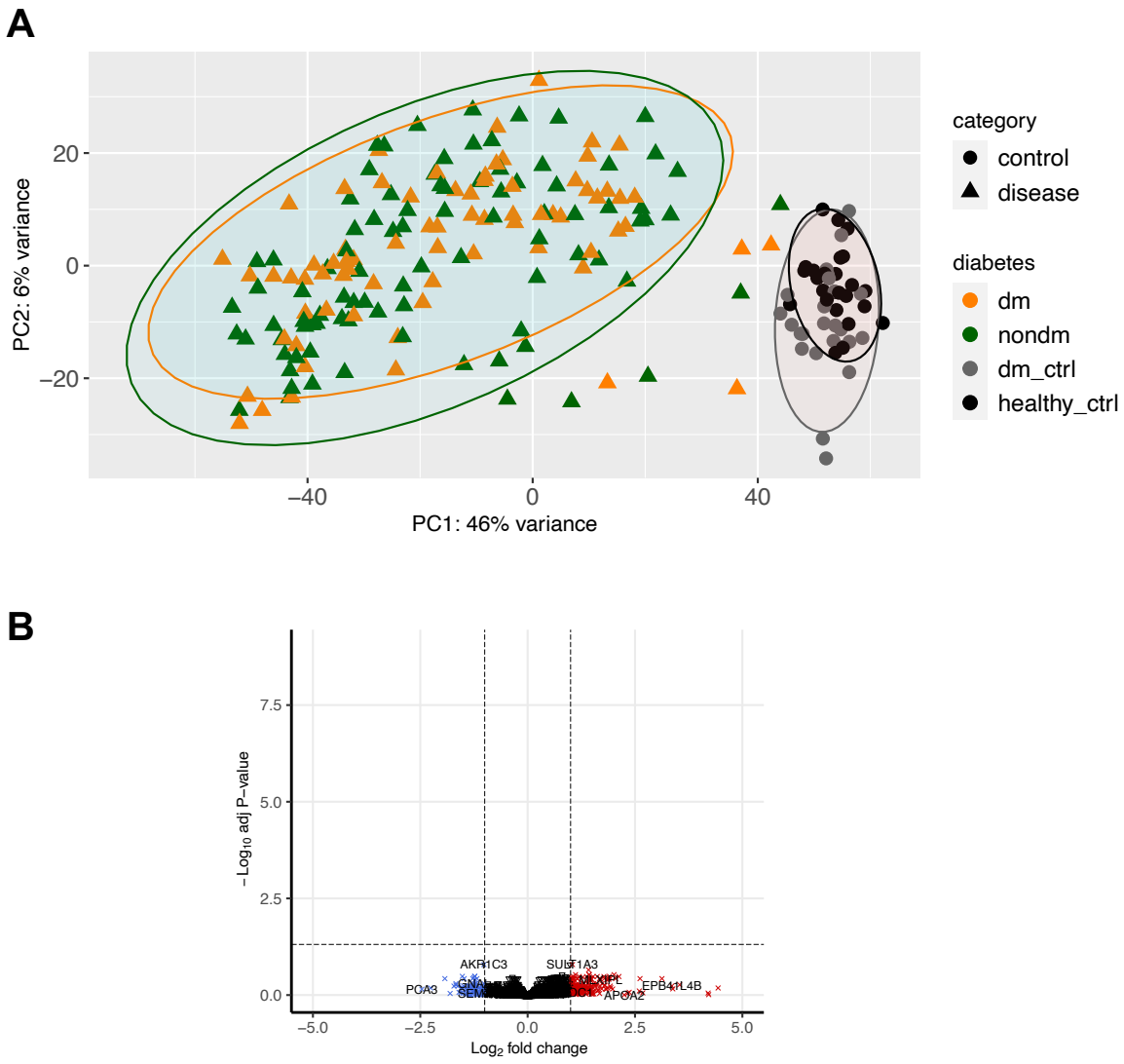

Supplementary Figure 5.3 Multidimensional scaling by principal component analysis (PCA) and differential gene expression analysis among melioidosis and control cohorts. A: PCA of the 1,000 most variable genes in melioidosis patients, divided into patients with diabetes ("dm", orange triangles, n=74), without diabetes ("nondm", green triangles, n=90), uninfected diabetes group ("dm_ctrl", grey circles, n=25), and healthy donors ("healthy_ctrl", black circles, n=25). B: Volcano plot of differentially expressed genes between uninfected diabetes group (n=25) and healthy donors (n=25). Dotted lines define a cut-off of differentially expressed genes based on absolute (log2 fold-change)≥ 1 (x-axis) and adjusted P-value < 0.05 (y-axis). PCA plots were generated using plotPCA function implemented in DESeq2 R package. Volcano plot was generated using EnhancedVolcano R package.

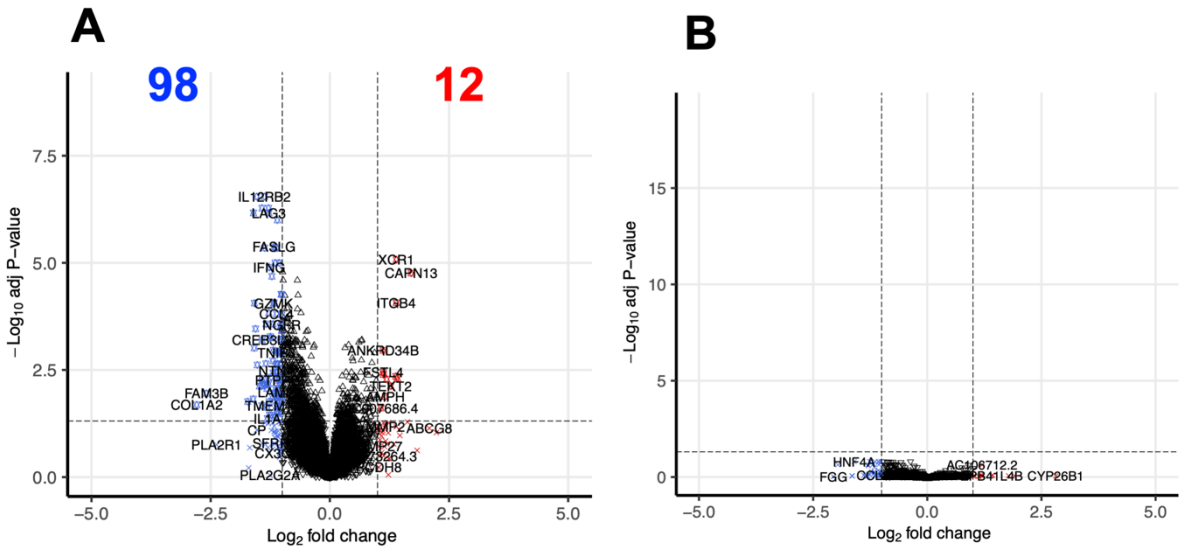

Supplementary Figure 5.4 Volcano plots of differentially expressed genes between among melioidosis with pneumonia and by diabetes status. A: Volcano plot of differentially expressed genes between melioidosis presented with pneumonia (n=52) and without pneumonia (n=112). B: Volcano plot of differentially expressed genes between melioidosis with diabetes (n=74) and without diabetes (n=90). Dotted lines define a cut-off of differentially expressed genes based on absolute[Log2 fold-change]≥ 1 (x-axis) and adjusted P-value < 0.05 (y-axis). Volcano plots were generated using EnhancedVolcano R package.

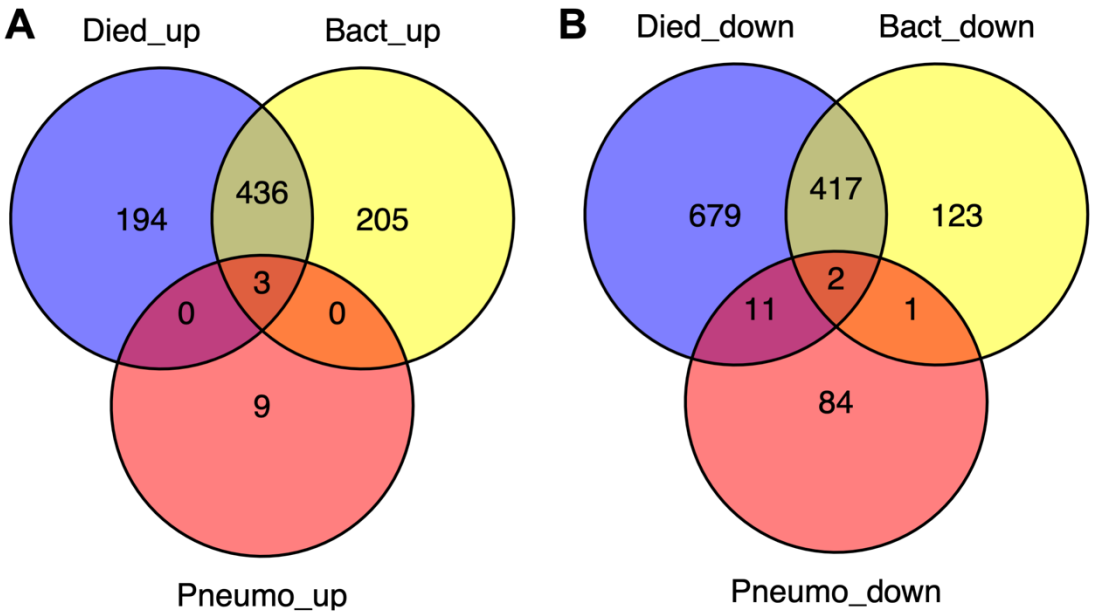

Supplementary Figure 5.5 Venn diagrams of overlapping differentially expressed genes (DEGs) within melioidosis patients. A: Overlapping up-regulated genes. B: Overlapping down- regulated genes. DEGs were derived from differential gene expression analyses: non-survivors (n=84) compared to survivors (n=80) (**Figure 5.2B**), bacteraemia (n=130) compared to non-bacteraemia cases (n=34) (**Figure 5.2C**), and pneumonia (n=53) compared to non-pneumonia cases (n=112) (**Supplementary Figure 5.4A**). Significant DEGs were based on absolute[Log2 fold-change]≥1 and adjusted P-value <0.05. Died_Up/Down: up/down-regulated DEGs in non-survivors compared to survivors. Bact_Up/Down: up/down-regulated DEGs in melioidosis with bacteraemia compared to non-bacteraemia cases. Pneumo_Up/Down: up/down-regulated DEGs in melioidosis with pneumonia compared to non-pneumonia cases.

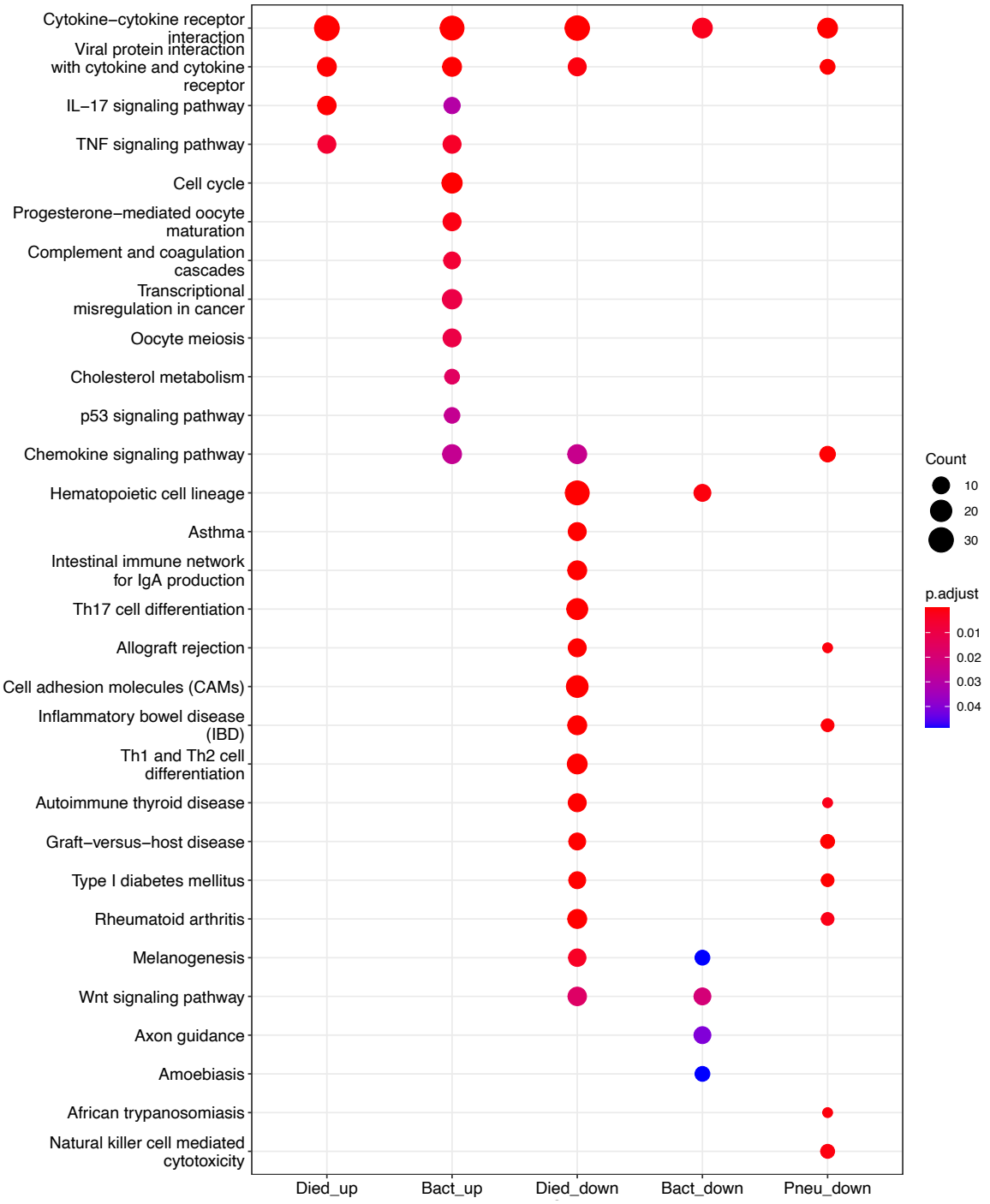

Supplementary Figure 5.6 Functional pathway analysis based on KEGG gene sets following differential gene expression analyses among melioidosis patients. Differentially expressed genes were derived from differential gene expression analyses: non-survivors (n=84) compared to survivors (n=80) (**Figure 5.2B**), bacteraemia (n=130) compared to non-bacteraemia cases (n=34) (**Figure 5.2C**), and pneumonia (n=53) compared to non-pneumonia cases (n=112) (**Supplementary Figure 5.4A**). The gradient colour bar corresponds to the adjusted P-value. The size of each term is

indicated by representative counts. Differentially expressed gene were pre-filtered based on a cut-off of absolute[Log2 fold-change] ≥1 and adjusted P-value <0.05. Died_up/down, up/down-regulated pathways in non-survivors compared to survivors. Bact_up/down= up/down-regulated pathways in the patients with bacteraemia compared to non-bacteraemia. Pneu_down= down-regulated pathways in the patients with pneumonia compared to non-pneumonia.

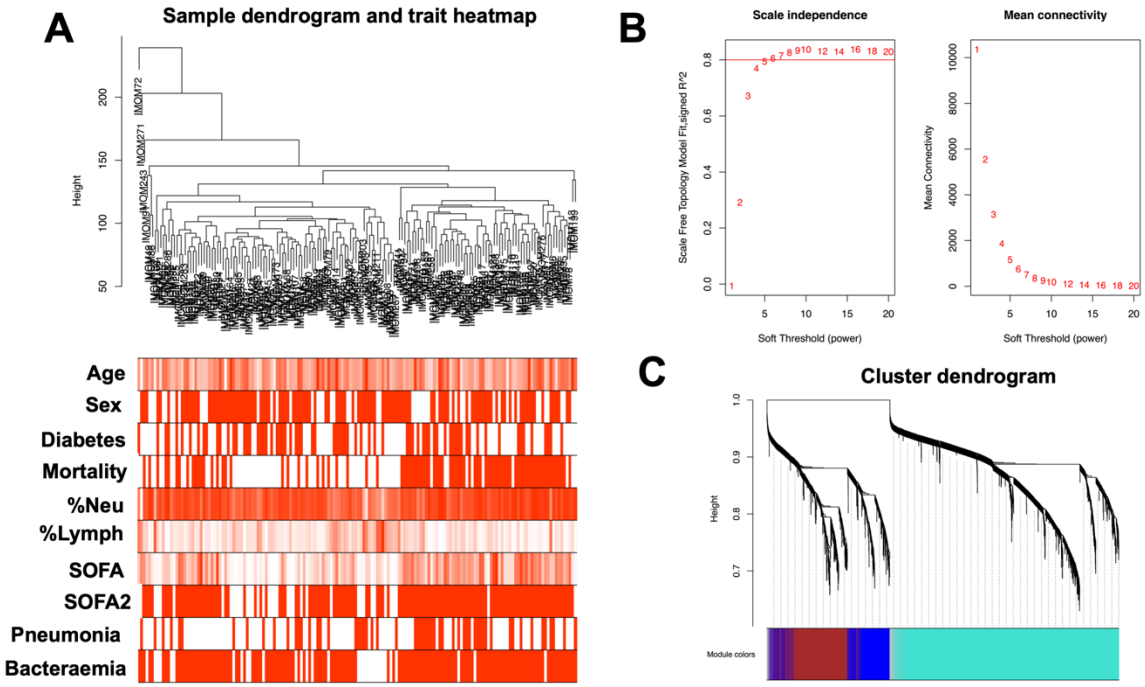

Supplementary Figure 5.7 Workflow of weighted gene co-expression network analysis (WGCNA) in 162 melioidosis patients. A: Sample dendrogram with corresponding trait heatmap. B: Scale-free network analysis identifying a β (soft power) in order to achieve scale free topology network (R^2 ≥8). C: Cluster dendrogram of co-expressed gene modules (assigned with different colours) by a hierarchical clustering of genes based on topological overlap.

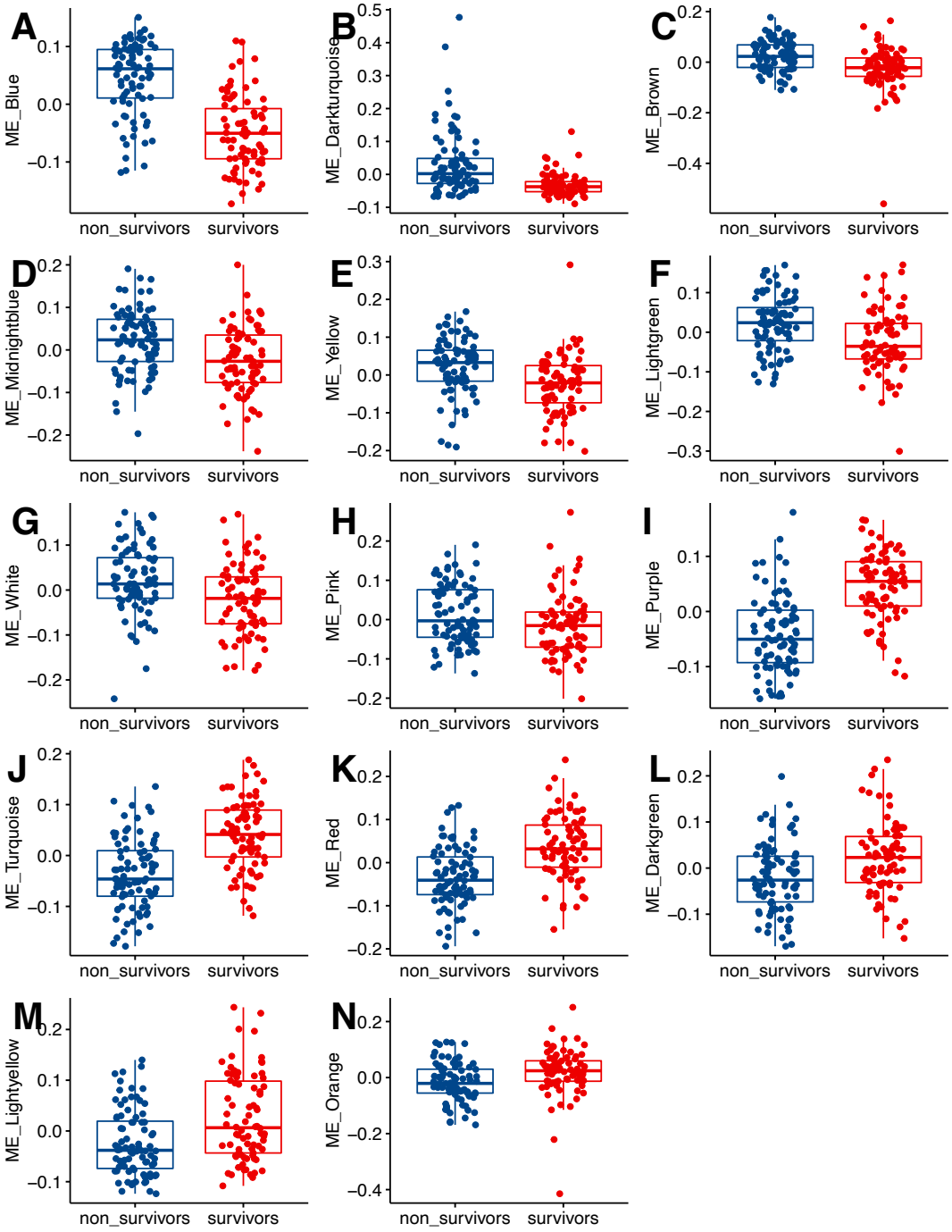

Supplementary Figure 5.8 Scattered box plots show comparisons of co-expressed gene modules (module eigengene, ME) between non-survived (n=84) and survived (n=78) melioidosis based on 28D mortality. ME is considered as a representative expression profile in each gene module. MEs with significant associations with 28-day mortality based on module trait relationship analysis were compared. Box plots represent medians with interquartile range plus lines to minimum, maximum and potential outliers.

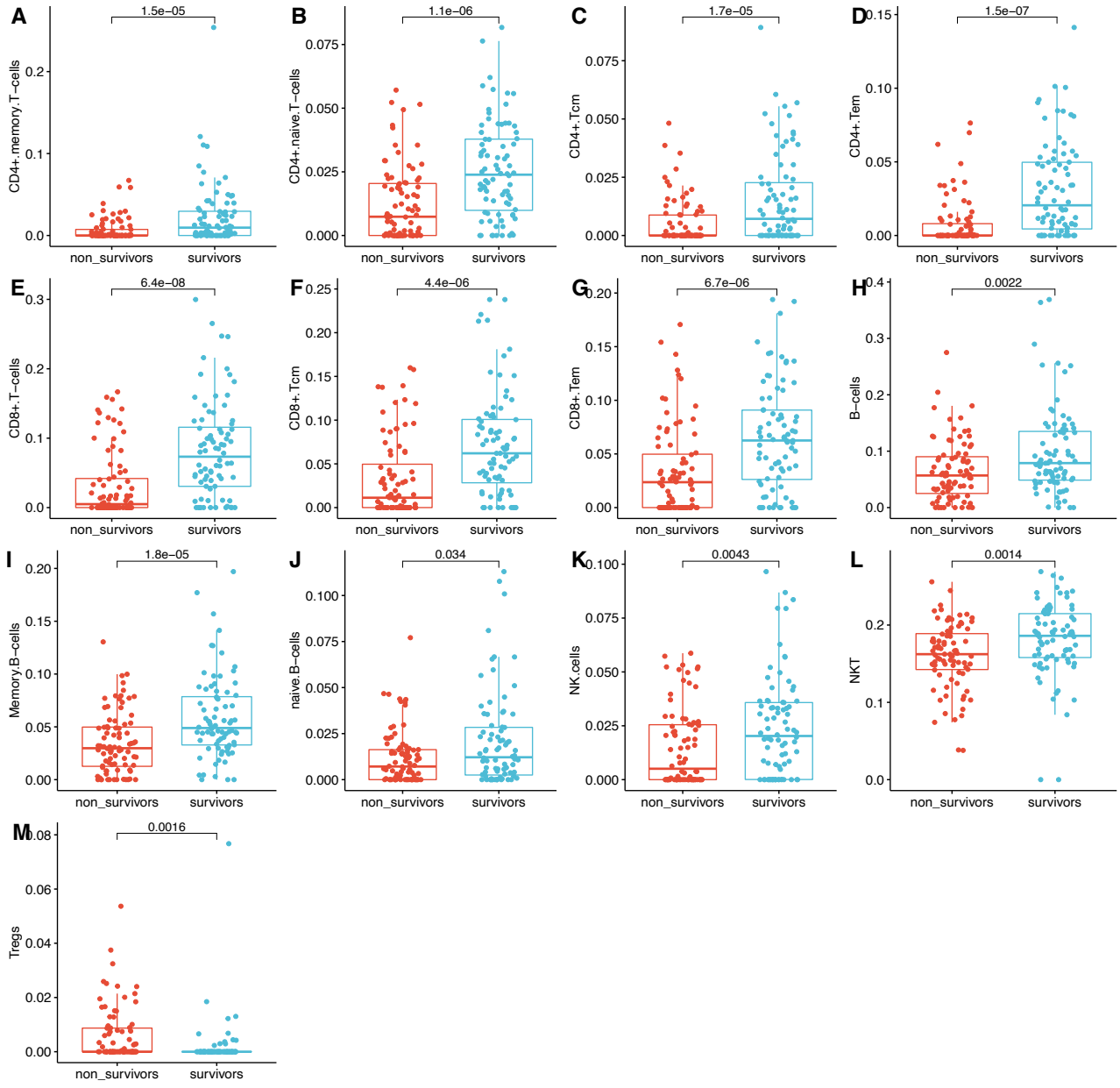

Supplementary Figure 5.9 Scattered boxplots show comparisons of deconvoluted cell enrichment in lymphoid cells between non-survived (red, n=84) and survived melioidosis patients (blue, n=80) using xCell deconvolution method (xCell R package version 1.1.0). The Y-axis displays each cell type by enrichment scores. Box plots represent medians with interquartile range plus lines to minimum, maximum and potential outliers. Non-parametric Mann-Whitney test was performed with its corresponding 2-tailed P-value displayed on each plot alongside median and inter-quartile range boxes.

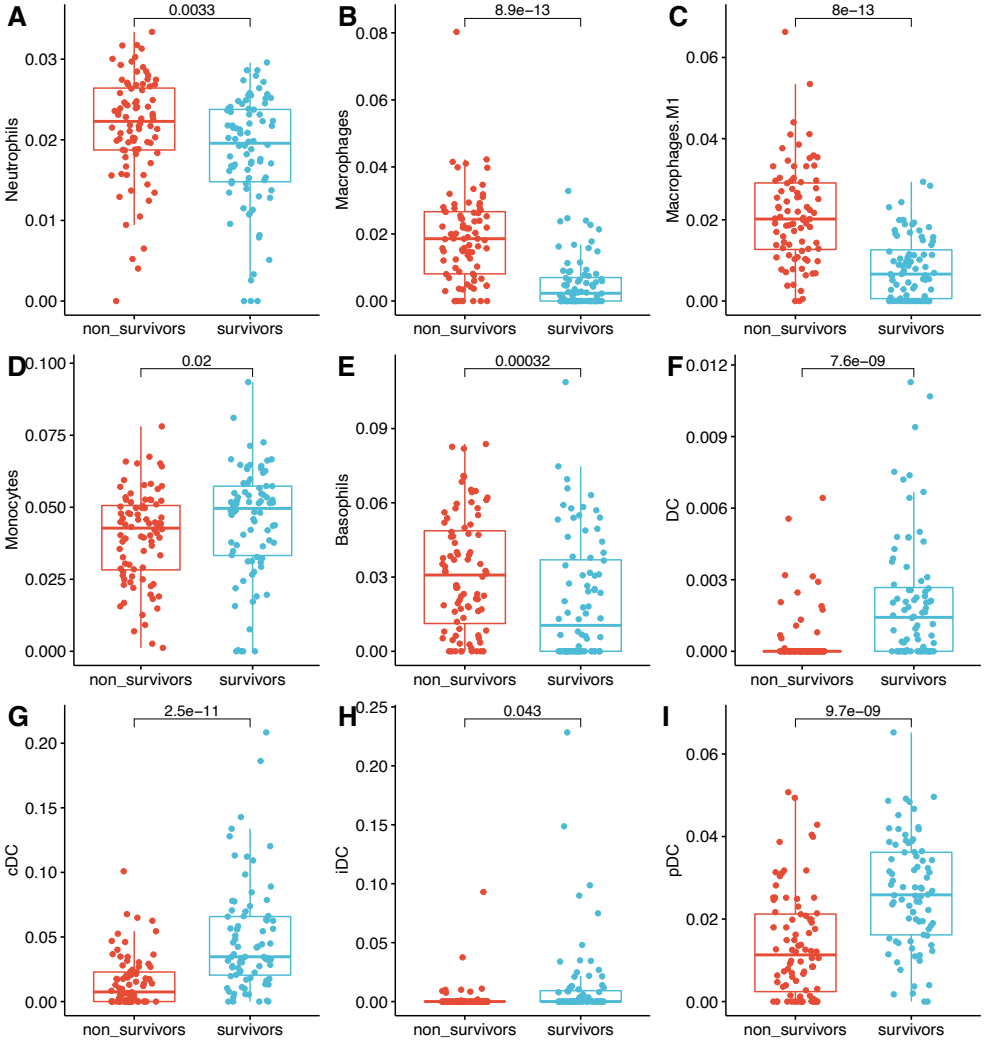

Supplementary Figure 5.10 Scattered boxplots show comparisons of deconvoluted cell enrichment in myeloid populations between non-survived (red, n=84) and survived melioidosis patients (blue, n=80) using xCell deconvolution method (xCell R package version 1.1.0). The Y-axis displays each cell type by enrichment scores. Box plots represent medians with interquartile range plus lines to minimum, maximum and potential outliers. Non-parametric Mann-Whitney test was performed with its corresponding 2-tailed P-value displayed on each plot alongside median and inter-quartile range boxes.

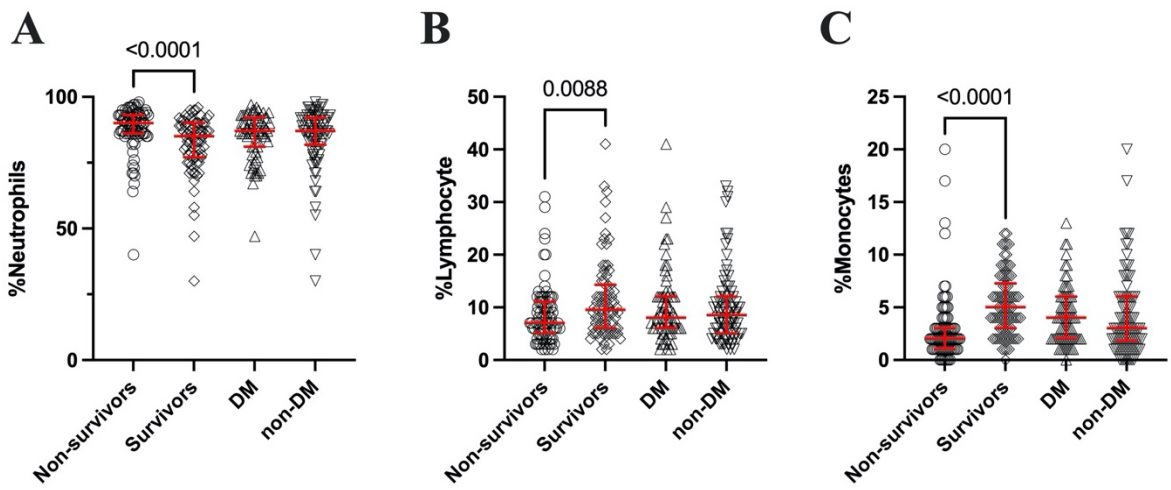

Supplementary Figure 5.11 Scatter plots show the frequencies of (A) neutrophils, (B) lymphocytes and (C) monocytes from full blood count (FBC) upon enrolment of 164 melioidosis patients. The comparisons were made between 28-day mortality (non-survivors versus survivors) and diabetes status (diabetes [DM] versus non-diabetes [non-DM]). Non-parametric Mann-Whitney test was performed with its corresponding P-value displayed on each plot and median and inter-quartile range bars.

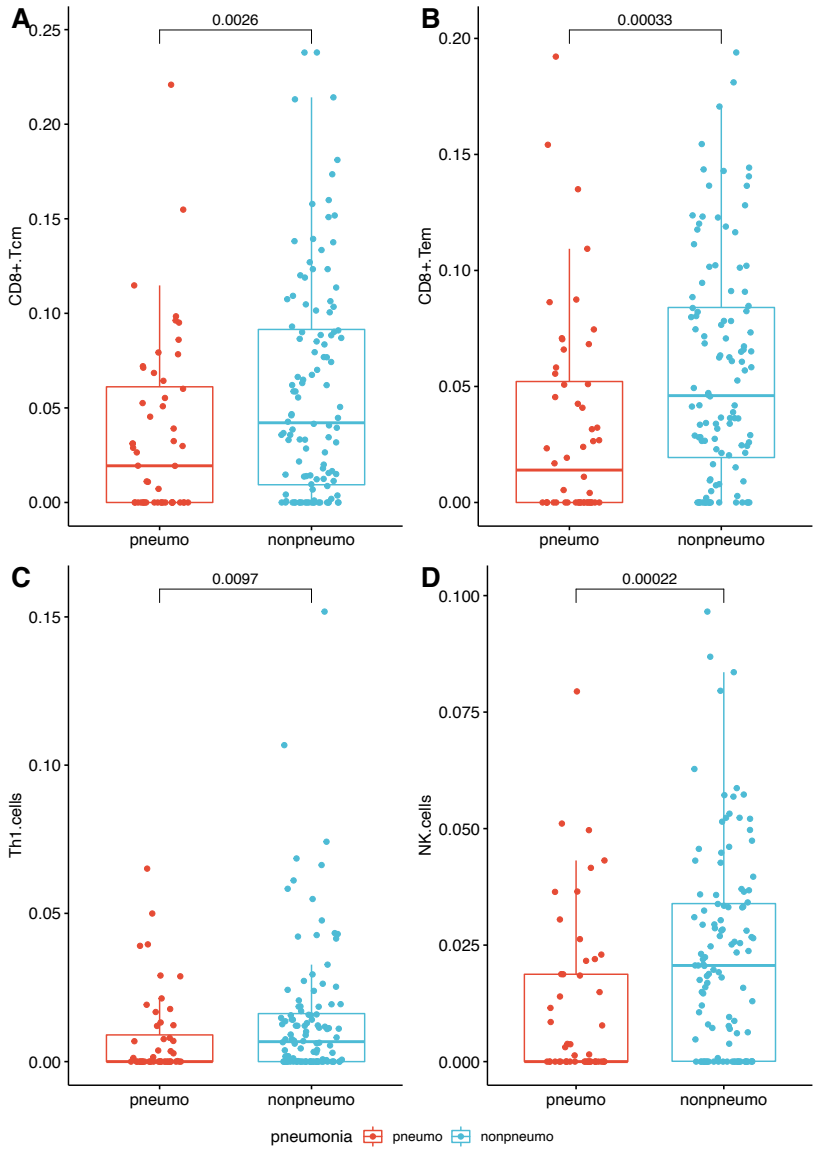

Supplementary Figure 5.12 Scattered boxplots show comparisons of deconvoluted cell enrichment in lymphoid cells between melioidosis patients with (red, n=52) and without (blue, n=112) pneumonia using xCell deconvolution method (xCell R package version 1.1.0). The Y-axis displays each cell type by enrichment scores. Box plots represent medians with interquartile range plus lines to minimum, maximum and potential outliers. Non-parametric Mann-Whitney test was performed with its corresponding 2-tailed P-value displayed on each plot alongside median and inter-quartile range boxes.

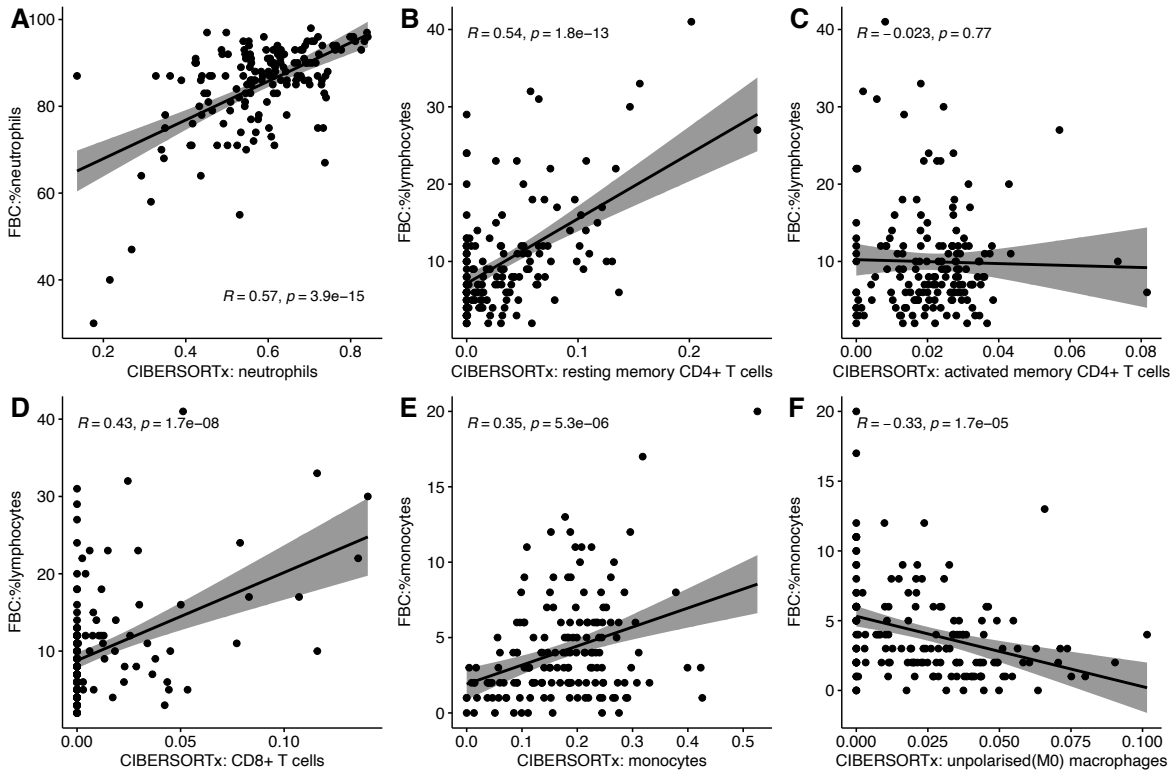

Supplementary Figure 5.13 Scattered plots show correlations between imputed cell fractions by the CIBERSORTx deconvolution method and the results of full blood count (FBC) in 164 melioidosis patients. The X-axis displays each cell type proportion. The Y-axis displays frequency of each cell type by FBC method. Pearson's correlation coefficient, corresponding P-value, and linear regression line with 95% confidence interval (shaded area) are displayed within each plot.

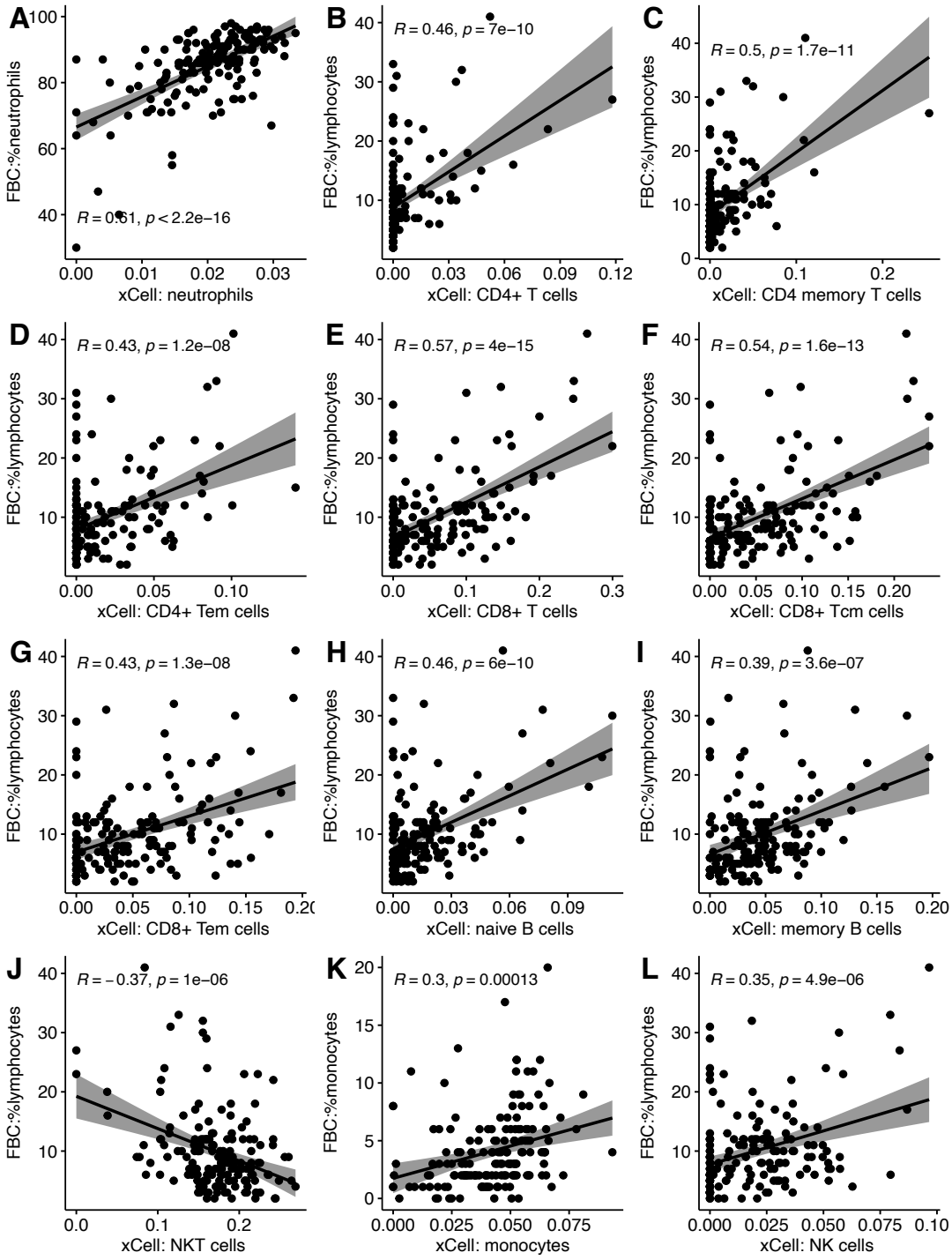

Supplementary Figure 5.14 Scattered plots show correlations between deconvoluted cell enrichment scores by the xCell deconvolution method and the results of full blood count (FBC) in 164 melioidosis patients. The X-axis displays enrichment scores of each cell type defined by the xCell method. The Y-axis displays frequency of each cell type by FBC method. Pearson's correlation

coefficient, corresponding P-value, and linear regression line with 95% confidence interval (shaded area) are displayed within each plot.

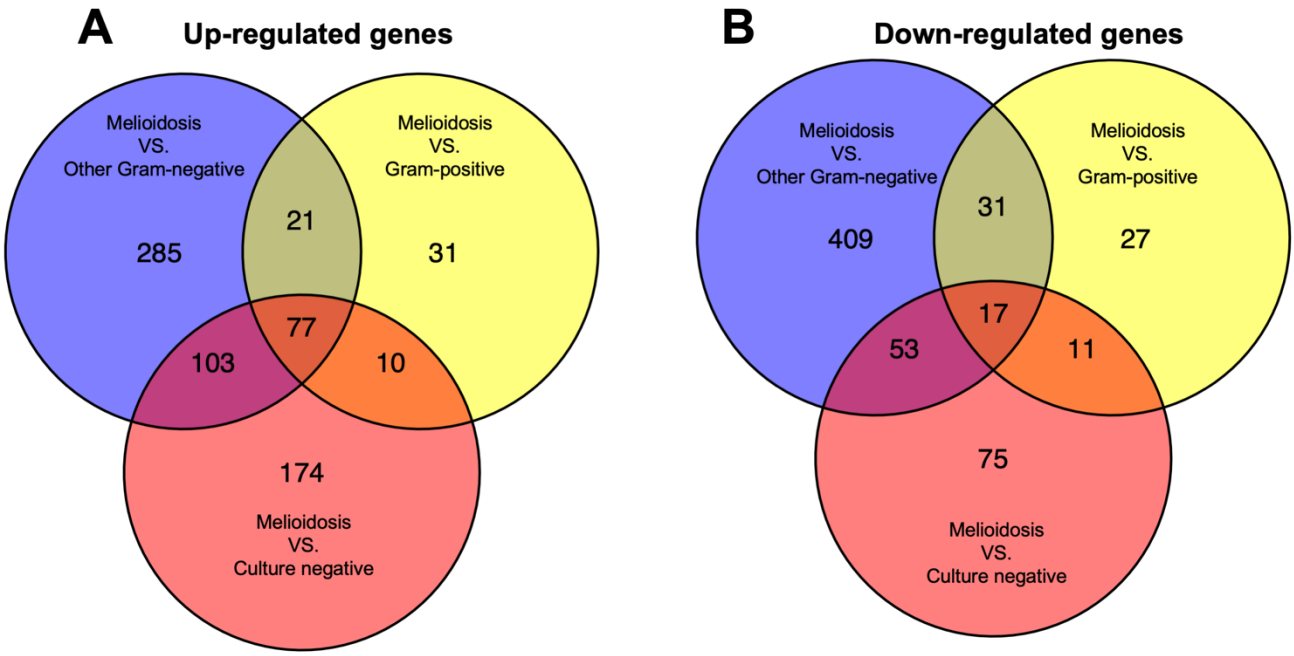

Supplementary Figure 5.15 Venn diagrams of overlapping differentially expressed genes (DEGs) among melioidosis and other community-acquired infections. A: Overlapping up-regulated genes. B: Overlapping down- regulated genes. DEGs were derived from differential gene expression analyses: melioidosis (n=164) compared to other Gram-negative infections (n=35) (**Figure 5.12A**), melioidosis (n=164) compared to Gram-positive infection (n=35) (**Figure 5.12B**), and melioidosis (n=164) compared patients with culture-negative results (n=19) (**Figure 5.12C**). Significant DEGs were based on absolute[Log2 fold-change]≥1 and adjusted P-value <0.05.

Supplementary information for Chapter 6

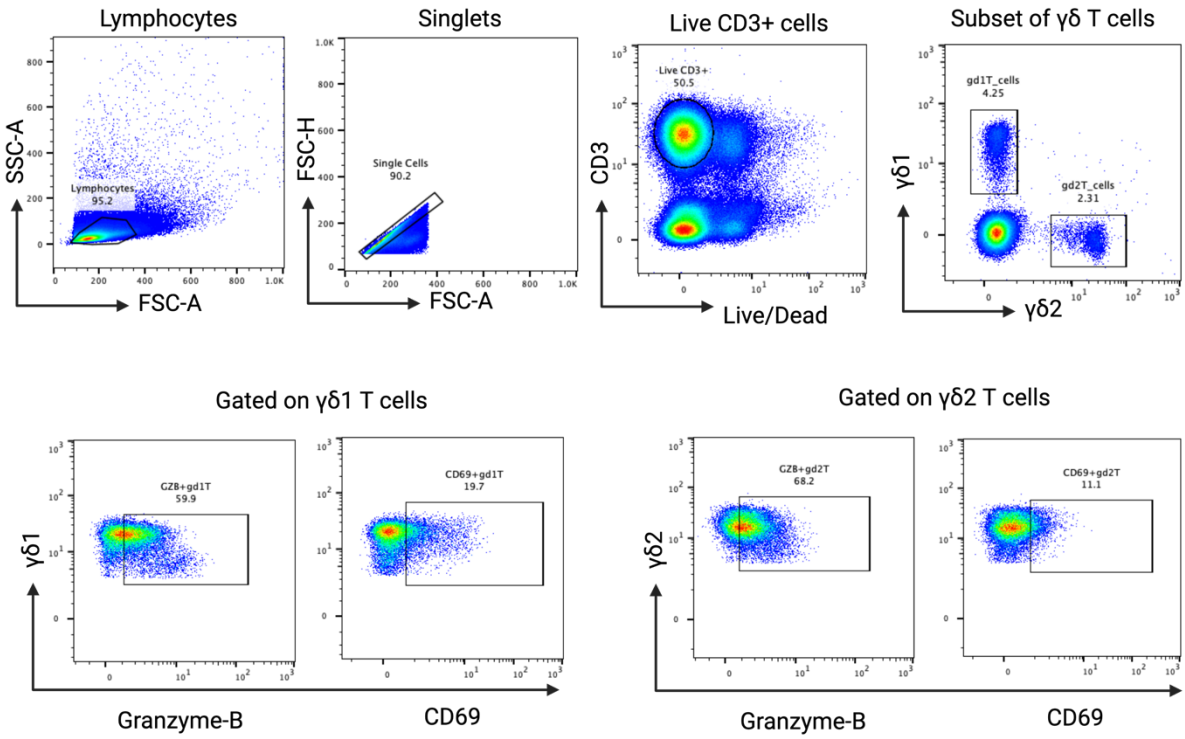

Supplementary Figure 6.1 A representative of gating strategy used for γδ T cell phenotyping by flow cytometry. PBMC were first gated based on forward (FSC-A) and side (SSC-A) scatter followed by single cell gating using FSC-H and FSC-A. Live CD3+ cells were gated on CD3-positive, Live/Dead negative populations. Subsets of γδ T cells populations were gated based on the expression of the following cell surface markers: γδ1 T cells ($CD3^+$γδ1+), CD69+ γδ1 T cells ($CD3^+$γδ1+ CD69+), Granzyme-B+ γδ1 T cells ($CD3^+$γδ1+ Granzyme-B+), γδ2 T cells ($CD3^+$γδ2+), CD69+ γδ2 T cells ($CD3^+$γδ2+ CD69+), and Granzyme-B+ γδ2 T cells ($CD3^+$γδ2+ Granzyme-B+).

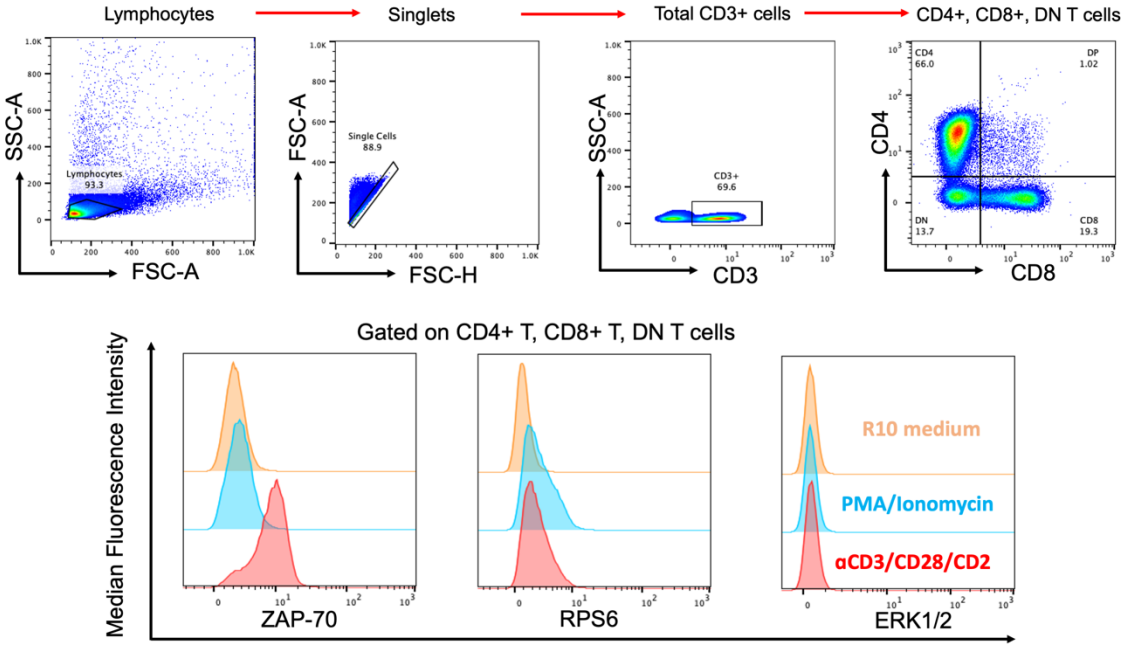

Supplementary Figure 6.2 A representative of gating strategy used for T cell receptor signalling based on phospho-flow cytometry. PBMCs were first gated based on forward (FSC-A) and side (SSC-A) scatter followed by single cell gating using FSC-H and FSC-A. Single CD3+ cells populations were gated within the single cells. Subsets of T cells populations were based on the expression of the following cell surface markers: CD4+ T cells ($CD3^+$ $CD4^+$), CD8+ T cells ($CD3^+$ $CD8^+$), double negative (DN) T cells ($CD3^+$ $CD4^-$ $CD8^-$). Expression of each intracellular marker including ZAP70, RPS6, and ERK1/2 was detected by median inflorescence intensity.

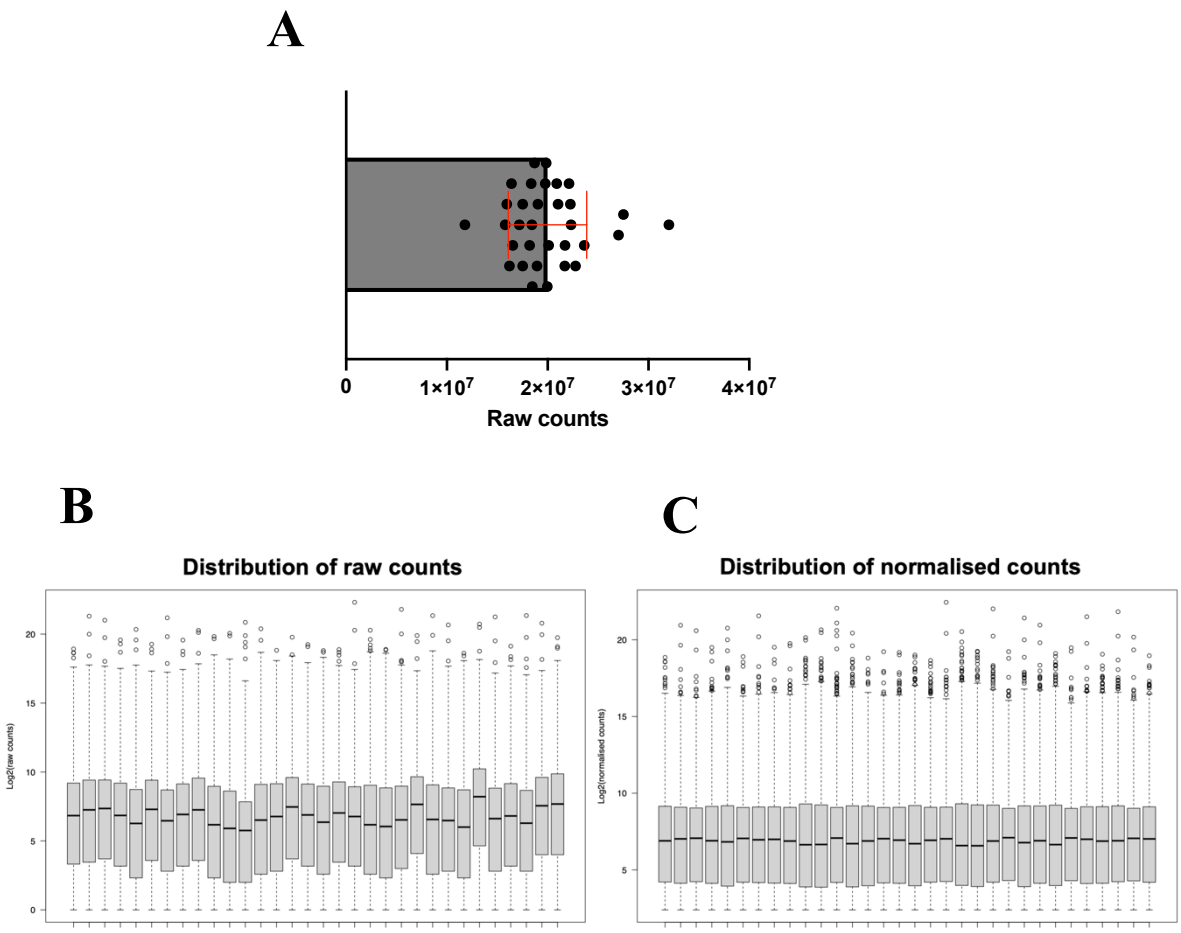

Supplementary Figure 6.3 Distribution of raw and normalised counts of RNA sequencing data generated from whole blood samples of melioidosis (n=29) and control (n=3) cohort in validation cohort (N=32). A: Total raw counts in 32 participants (mean with standard deviation). B: Distribution of raw counts. C: Distribution of normalised counts. The raw counts were normalised using median of ratios method implemented in DESeq2 R package.

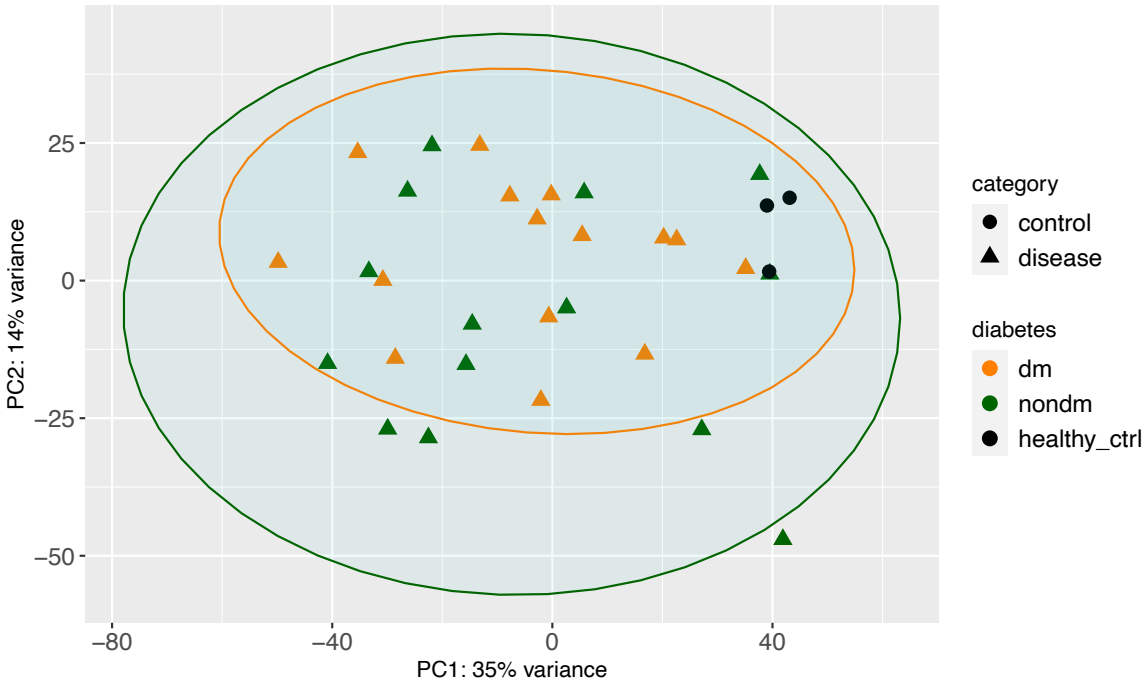

Supplementary Figure 6.4 Multidimensional scaling by principal component analysis (PCA) of the 1,000 most variable genes among melioidosis patients and healthy donors coloured by diabetes status from the validation cohort. Patients with melioidosis, divided into those with diabetes ("dm", orange triangles, n= 15), without diabetes ("nondm", green triangles, n= 14), and healthy donors ("healthy_ctrl", black circles, n=3). PCA plot was generated using plotPCA function implemented in DESeq2 R package.

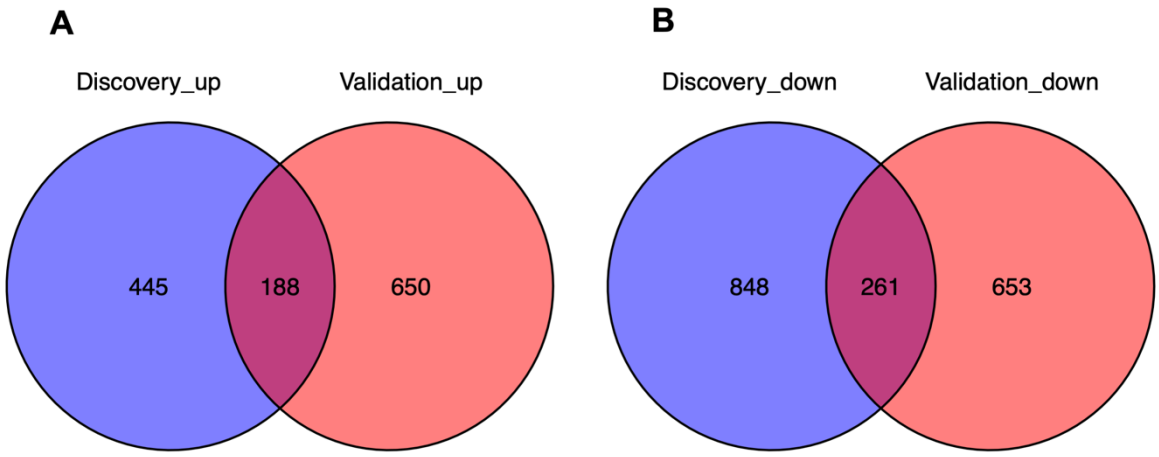

Supplementary Figure 6.5 Venn diagrams of overlapping differentially expressed genes (DEGs) among melioidosis patients between discovery and validation cohort. A: Overlapping up-regulated genes between discovery and validation cohort. B: Overlapping down- regulated genes between discovery and validation cohort. DEGs were derived from differential gene expression analyses: non-survivors (n=84) compared to survivors (n=80) from discovery cohort (**Figure 5.2B**) and non-survivors (n=15) compared to survivors (n=14) from validation cohort (**Figure 6.3**). Significant DEGs were based on absolute (log2 fold-change)≥1 and adjusted P-value <0.05.

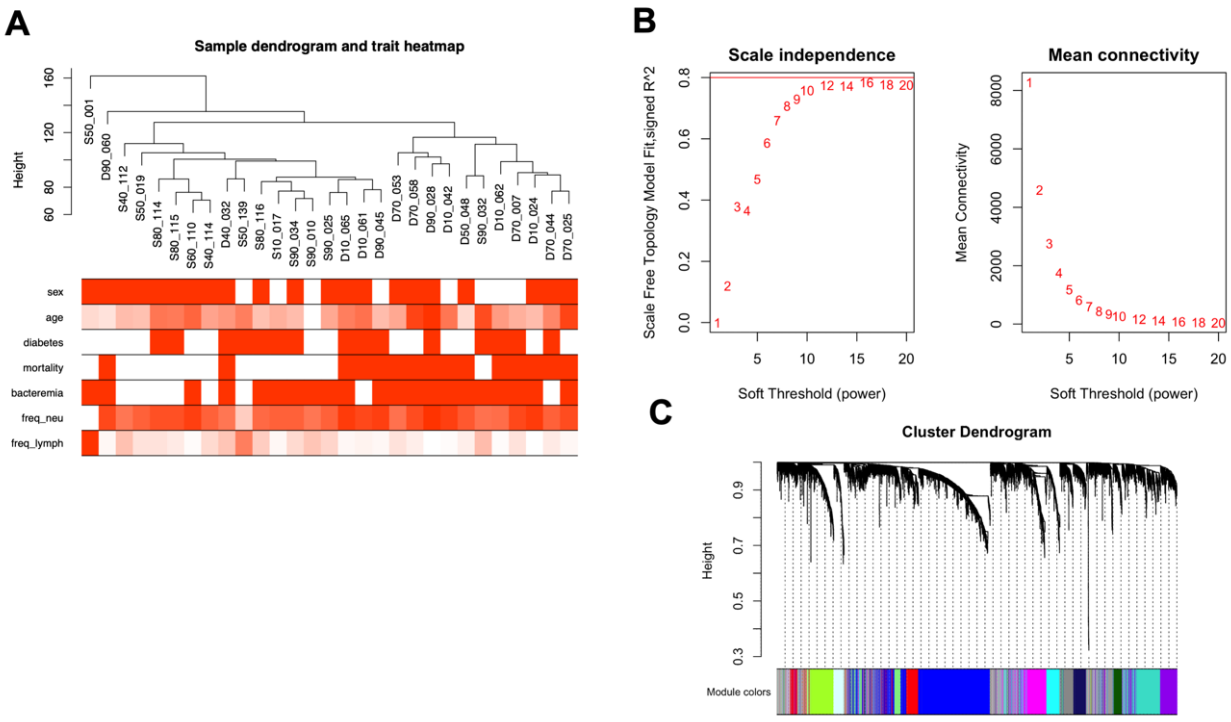

Supplementary Figure 6.6 Workflow of weighted gene co-expression network analysis (WGCNA) in 29 melioidosis patients from validation cohort. A: Sample dendrogram with corresponding trait heatmap. B: Scale-free network analysis identifying a β (soft power) in order to achieve scale free topology network. C: Cluster dendrogram of co-expressed gene modules (assigned with different colours) by a hierarchical clustering of genes based on topological overlap.

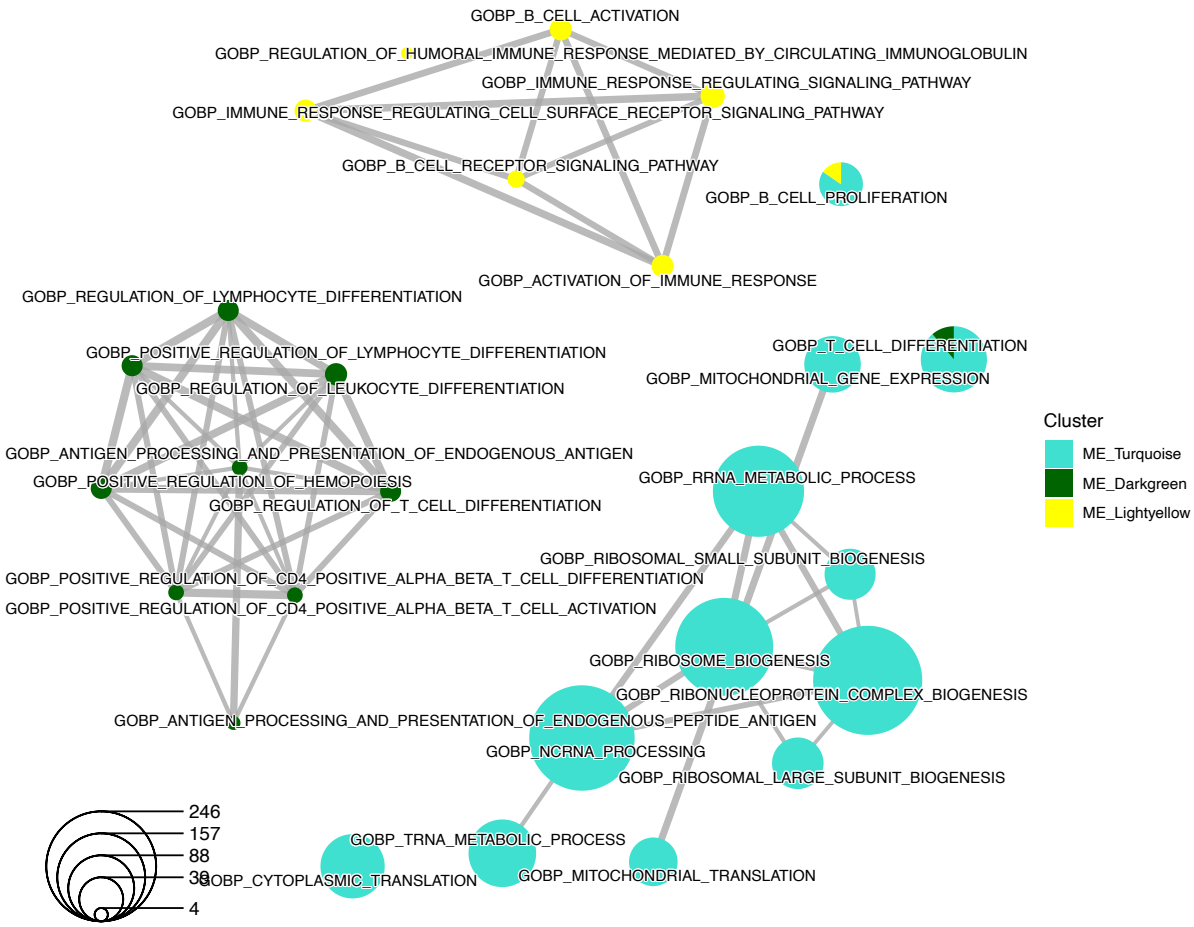

Supplementary Figure 6.7 Enrichment analysis based on Gene Ontology (biological process) gene sets in three module eigengene (MEs) which were associated with survival identified by module-trait relationship analysis in 29 melioidosis patients. Pathways with closely related functions were linked and clustered together. The thickness of line indicates common genes shared among the pathways. The size of each term is indicated by representative counts. Enrichment plot was created using clusterProfiler R package.

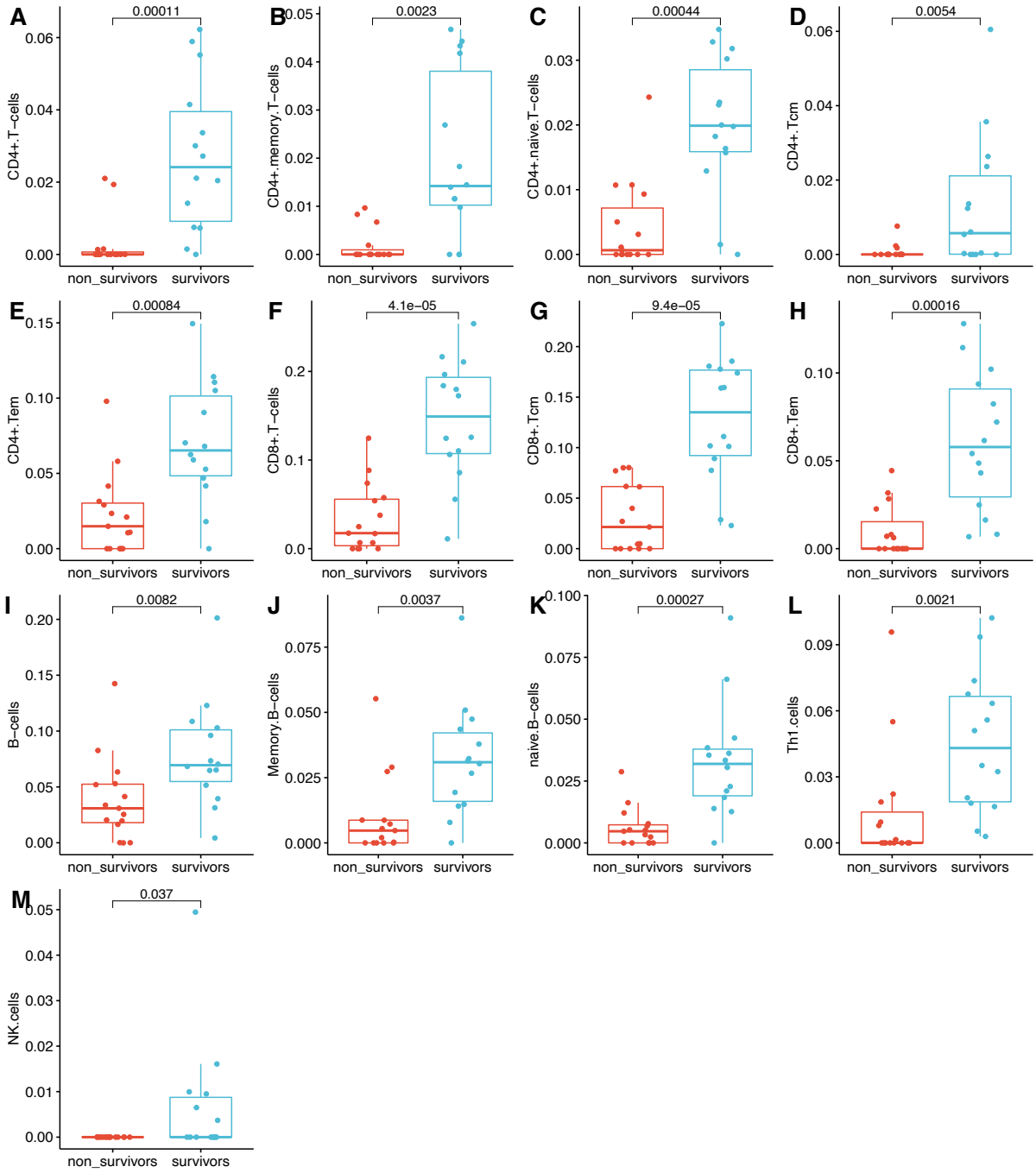

Supplementary Figure 6.8 Scattered boxplots show comparisons of deconvoluted cell enrichment in lymphoid cells between non-survived (red, n=15) and survived (blue, n=14) melioidosis patients using xCell deconvolution method (xCell R package version 1.1.0). The Y-axis displays each cell type by enrichment scores. Box plots represent medians with interquartile range plus lines to minimum, maximum and potential outliers. Non-parametric Mann-Whitney test was performed with its corresponding 2-tailed P-value displayed on each plot alongside median and inter-quartile range boxes.

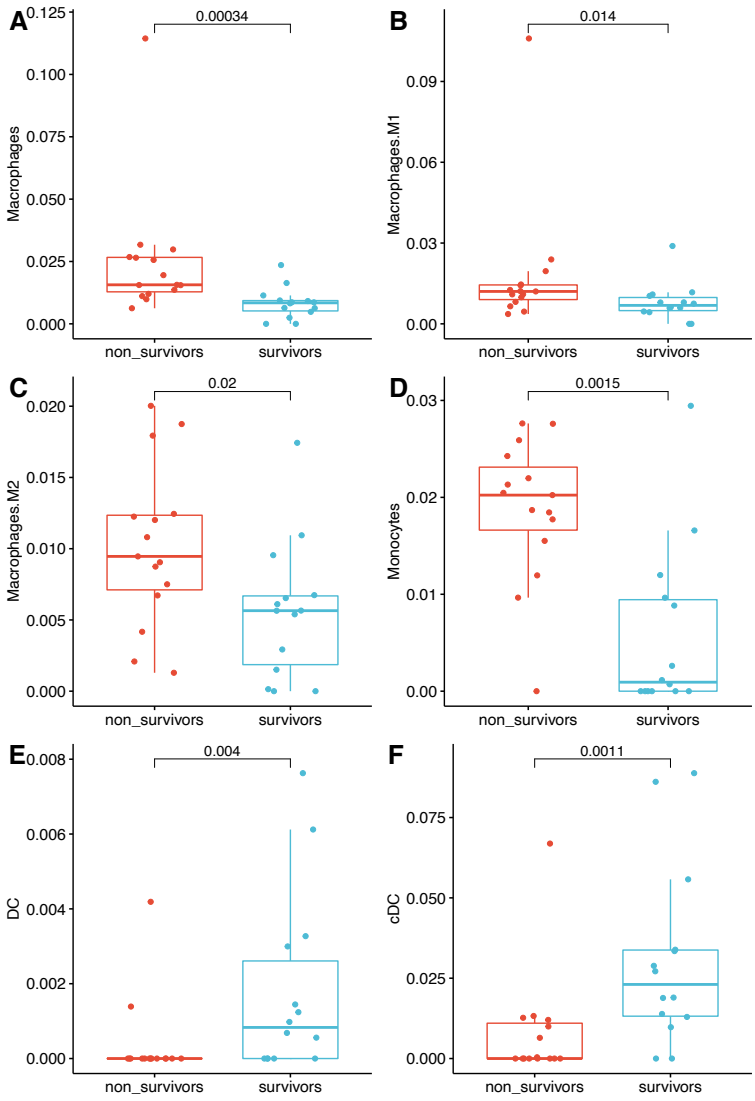

Supplementary Figure 6.9 Scattered boxplots show comparisons of deconvoluted cell enrichment in myeloid cells between non-survived (red, n=15) and survived (blue, n=14) melioidosis patients using xCell deconvolution method (xCell R package version 1.1.0). The Y-axis displays each cell type by enrichment scores. Box plots represent medians with interquartile range plus lines to minimum, maximum and potential outliers. Non-parametric Mann-Whitney test was performed with its corresponding 2-tailed P-value displayed on each plot alongside median and inter-quartile range boxes.

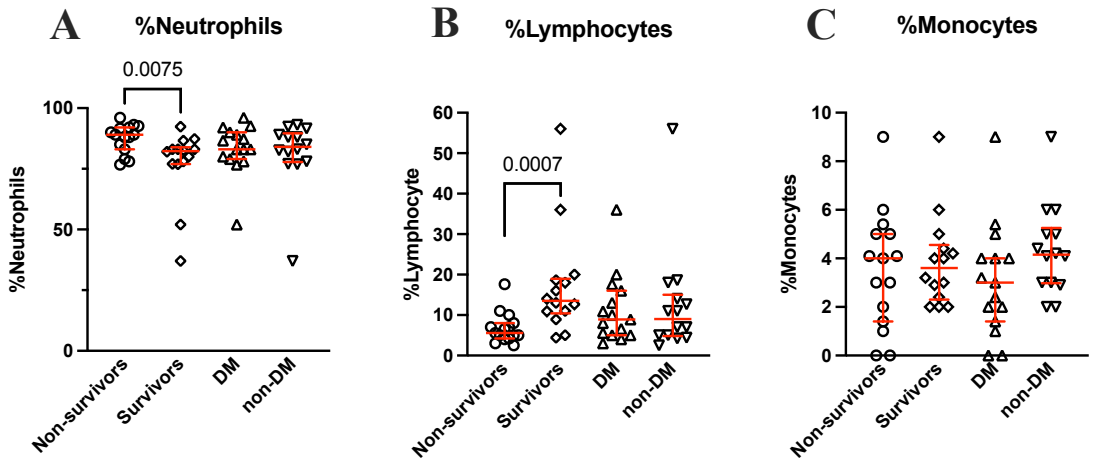

Supplementary Figure 6.10 Scatter plots show the frequencies of (A) neutrophils, (B) lymphocytes and (C) monocytes from full blood count (FBC) upon enrolment of 29 melioidosis patients. The comparisons were made between 28-day mortality (non-survivors versus survivors) and diabetes status (diabetes [DM] versus non-diabetes [non-DM]). Non-parametric Mann-Whitney test was performed with its corresponding P-value displayed on each plot and median and inter-quartile range bars.

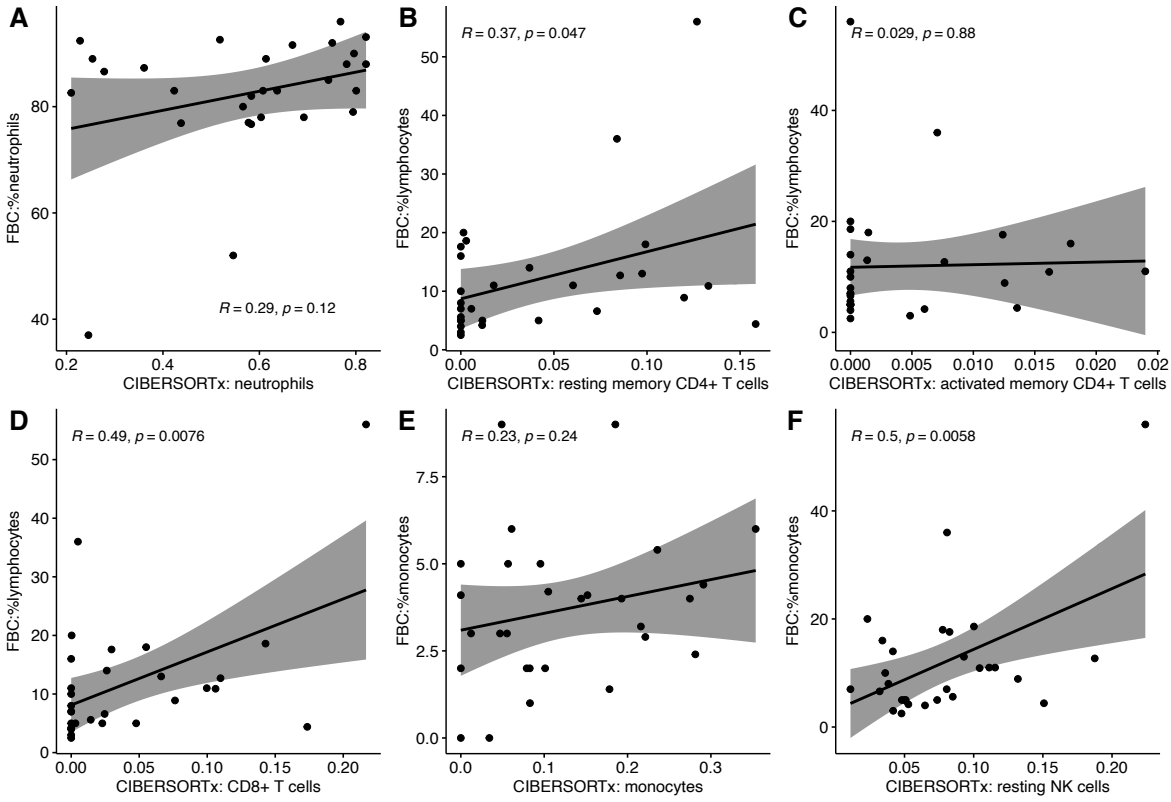

Supplementary Figure 6.11 Scattered plots show correlations between imputed cell fractions by the CIBERSORTx deconvolution method and the results of full blood count (FBC) in 29 melioidosis patients. The X-axis displays each cell type proportion. The Y-axis displays frequency of each cell type by FBC method. Pearson's correlation coefficient, corresponding P-value and linear regression line with 95% confidence interval (shaded area) are displayed within each plot.

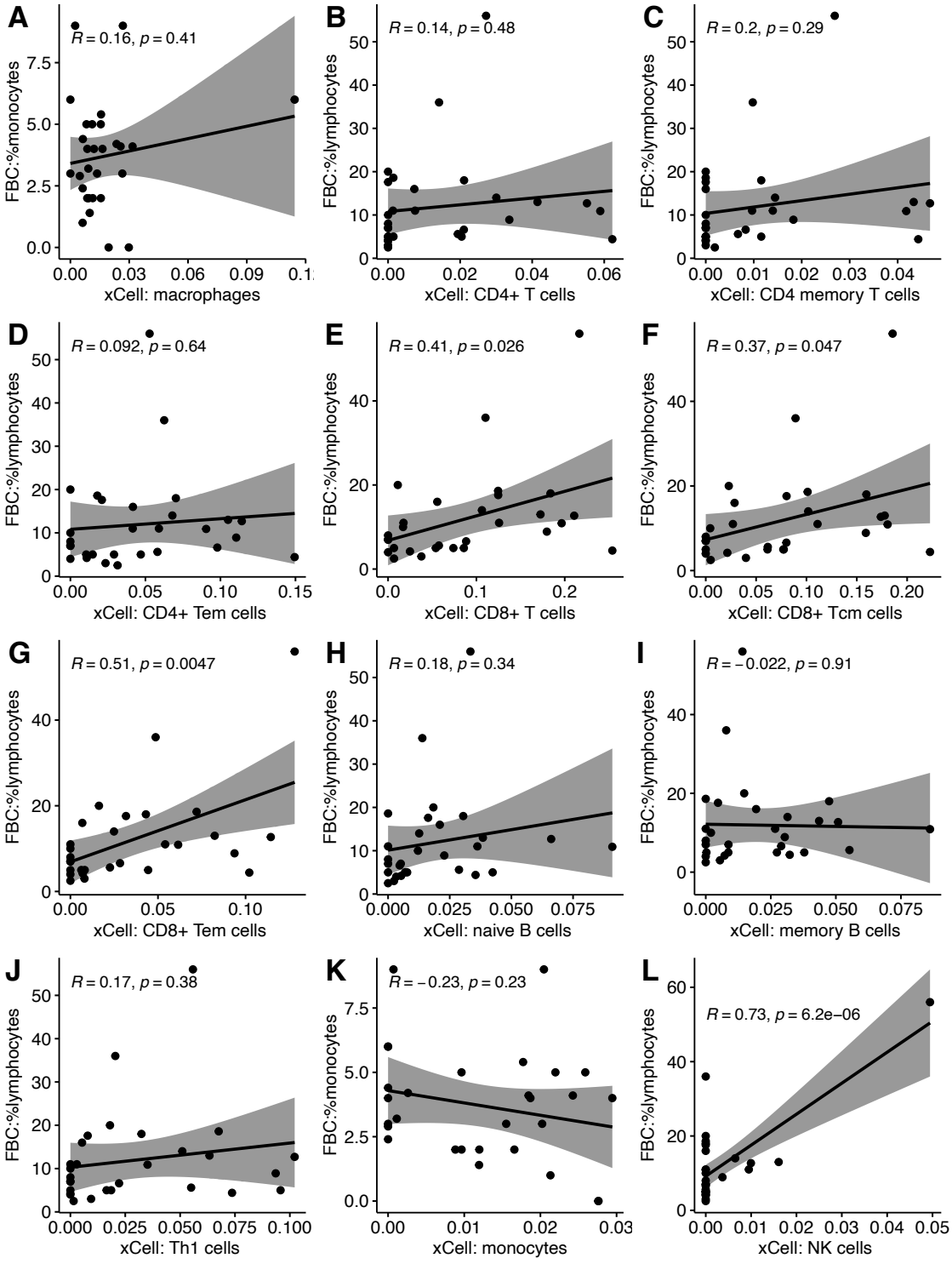

Supplementary Figure 6.12 Scattered plots show correlations between deconvoluted cell enrichment scores by the xCell deconvolution method and the results of full blood count (FBC) in 29 melioidosis patients. The X-axis displays enrichment scores of each cell type defined by the xCell method. The Y-axis displays frequency of each cell type by FBC method. Pearson's correlation

coefficient, corresponding P-value and 95% confidence interval (shaded area) are displayed within each plot.

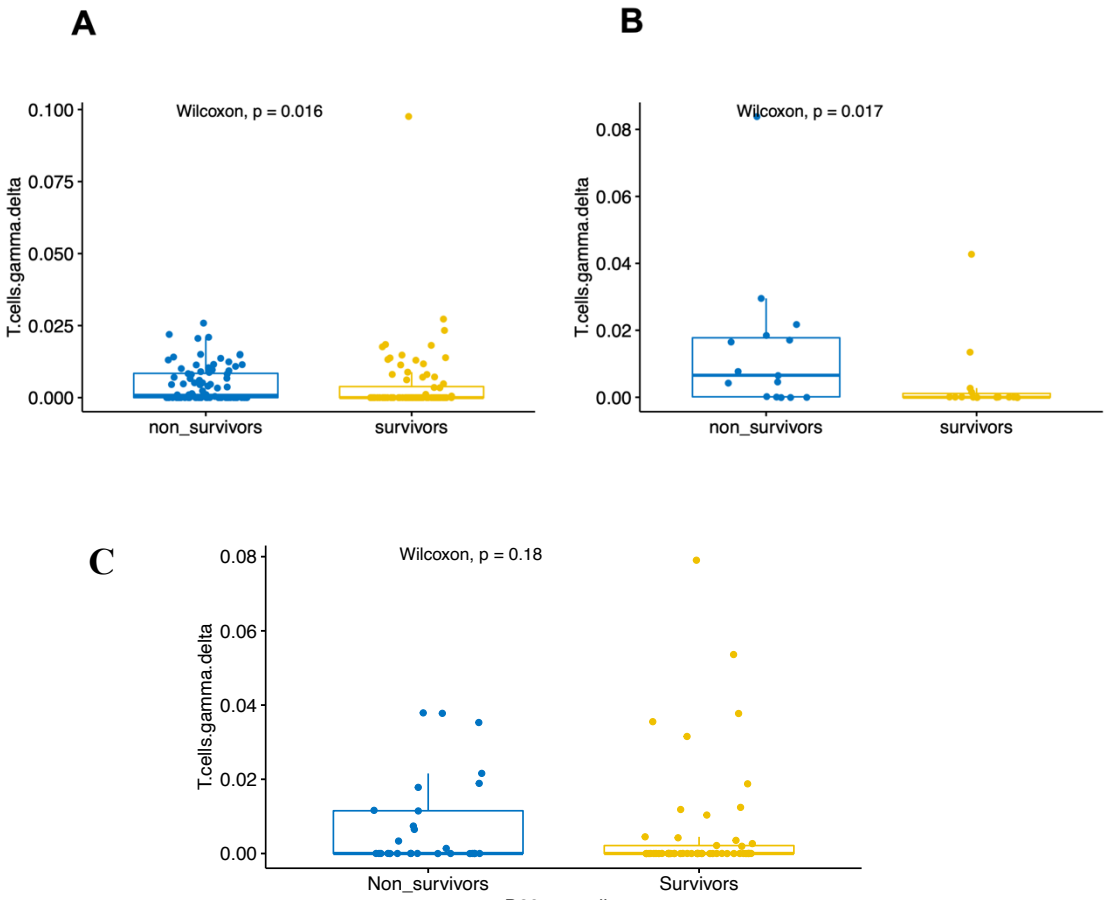

Supplementary Figure 6.13 Deconvoluted frequencies of γδ cells in melioidosis patients between (A) discovery (**Chapter 5**), (B) validation (**Chapter 6**) cohort, and (C) MICRO1501 (**Chapter 3**). Scattered boxplots show comparisons of imputed cell fractions of γδ T cells between non-survivor and survivor melioidosis patients using CIBERSORTx in discovery (A, n=164), validation cohort (B, n=29), and MICRO1501 (C, n=81) respectively. Non-parametric Mann-Whitney test was performed with its corresponding P-value displayed on each plot and median and inter-quartile range bars.

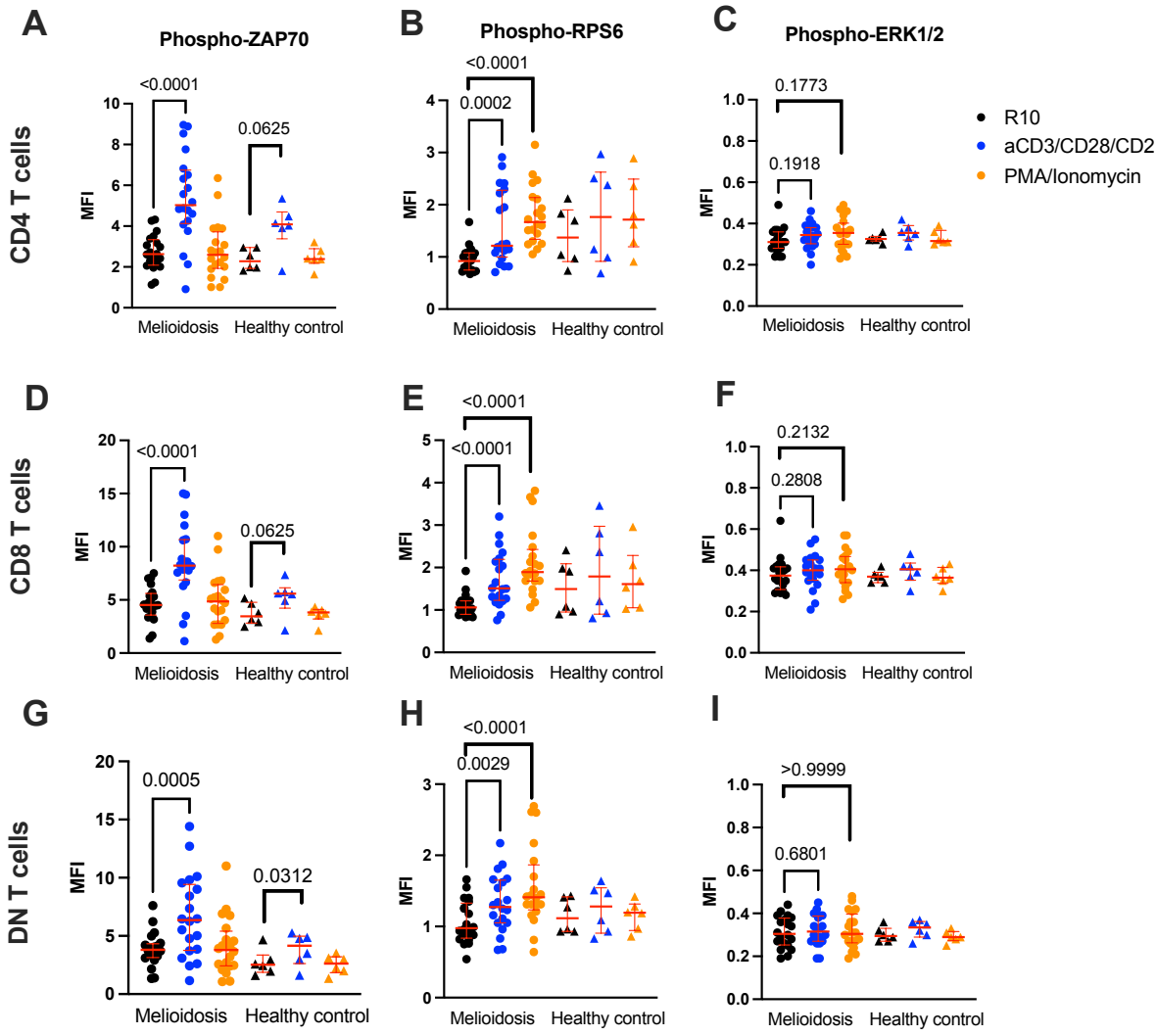

Supplementary Figure 6.14 Scattered plots show phosphorylation of T cell receptor (TCR) signalling cascade proteins in peripheral blood mononuclear cells (PBMCs) from acute melioidosis patients and healthy donors using phospho-flow cytometry. PBMCs were stimulated with α-CD3/CD28/CD2 cocktail (blue), PMA/Ionomycin (orange), or medium only (R10, black). The expression of phosphorylated ZAP-70, RPS6, and ERK1/2 were measured within (A-C) CD4+ T, (D-F) CD8+ T cells and (G-I) double negative (DN) T cells amongst melioidosis patients (circle, n=20) and healthy control (triangle, n=6) respectively. Non-parametric Mann-Whitney test was performed with its corresponding 2-tailed P-value displayed on each plot alongside median and inter-quartile range boxes. MFI= Median Fluorescent Intensity.

Bibliography

1. D. Limmathurotsakul *et al.*, Melioidosis in animals, Thailand, 2006-2010. *Emerg. Infect. Dis.* **18**, 325-327 (2012).

2. N. J. White, Melioidosis. *Lancet* **361**, 1715-1722 (2003).

3. D. Limmathurotsakul *et al.*, Systematic review and consensus guidelines for environmental sampling of Burkholderia pseudomallei. *PLoS Negl Trop Dis* **7**, e2105 (2013).

4. D. Limmathurotsakul *et al.*, Predicted global distribution of Burkholderia pseudomallei and burden of melioidosis. *Nat Microbiol* **1**, 15008 (2016).

5. J. E. Gee *et al.*, Multistate Outbreak of Melioidosis Associated with Imported Aromatherapy Spray. *N Engl J Med* **386**, 861-868 (2022).

6. S. Hinjoy *et al.*, Melioidosis in Thailand: Present and Future. *Trop Med Infect Dis* **3**, 38 (2018).

7. V. Hantrakun *et al.*, Soil Nutrient Depletion Is Associated with the Presence of Burkholderia pseudomallei. *Appl Environ Microbiol* **82**, 7086-7092 (2016).

8. V. Vuddhakul *et al.*, Epidemiology of Burkholderia pseudomallei in Thailand. *Am J Trop Med Hyg* **60**, 458-461 (1999).

9. B. J. Currie, L. Ward, A. C. Cheng, The epidemiology and clinical spectrum of melioidosis: 540 cases from the 20 year Darwin prospective study. *PLoS Negl. Trop. Dis.* **4**, e900 (2010).

10. W. J. Wiersinga *et al.*, Melioidosis. *Nat Rev Dis Primers* **4**, 17107 (2018).

11. D. Limmathurotsakul *et al.*, Activities of daily living associated with acquisition of melioidosis in northeast Thailand: a matched case-control study. *PLoS Negl Trop Dis* **7**, e2072 (2013).

12. B. J. Currie, S. P. Jacups, Intensity of rainfall and severity of melioidosis, Australia. *Emerg Infect Dis* **9**, 1538-1542 (2003).

13. X. Liu *et al.*, Association of melioidosis incidence with rainfall and humidity, Singapore, 2003-2012. *Emerg Infect Dis* **21**, 159-162 (2015).

14. L. Y. A. Chai, D. Fisher, Earth, wind, rain, and melioidosis. *Lancet Planet Health* **2**, e329-e330 (2018).

15. W. Chaowagul *et al.*, Melioidosis: a major cause of community-acquired septicemia in northeastern Thailand. *J. Infect. Dis.* **159**, 890-899 (1989).

16. V. Ngauy, Y. Lemeshev, L. Sadkowski, G. Crawford, Cutaneous melioidosis in a man who was taken as a prisoner of war by the Japanese during World War II. *J Clin Microbiol* **43**, 970-972 (2005).

17. A. Chakravorty, C. H. Heath, Melioidosis: An updated review. *Aust J Gen Pract* **48**, 327-332 (2019).

18. D. S. Sarovich *et al.*, Recurrent melioidosis in the Darwin Prospective Melioidosis Study: improving therapies mean that relapse cases are now rare. *J Clin Microbiol* **52**, 650-653 (2014).

19. D. Limmathurotsakul *et al.*, A simple scoring system to differentiate between relapse and re-infection in patients with recurrent melioidosis. *PLoS Negl. Trop. Dis.* **2**, e327 (2008).

20. D. Limmathurotsakul *et al.*, Increasing incidence of human melioidosis in Northeast Thailand. *Am J Trop Med Hyg* **82**, 1113-1117 (2010).

21. W. Chaowagul *et al.*, Relapse in melioidosis: incidence and risk factors. *J Infect Dis* **168**, 1181-1185 (1993).

22. I. Gassiep, V. Ganeshalingam, M. D. Chatfield, P. N. A. Harris, R. E. Norton, The epidemiology of melioidosis in Townsville, Australia. *Trans R Soc Trop Med Hyg* **116**, 328-335 (2022).

23. K. P. Chan, J. G. Low, J. Raghuram, S. M. Fook-Chong, A. Kurup, Clinical characteristics and outcome of severe melioidosis requiring intensive care. *Chest* **128**, 3674-3678 (2005).

24. A. Zueter *et al.*, The epidemiology and clinical spectrum of melioidosis in a teaching hospital in a North-Eastern state of Malaysia: a fifteen-year review. *BMC Infect Dis* **16**, 333 (2016).

25. P. V. Kingsley, G. Arunkumar, M. Tipre, M. Leader, N. Sathiakumar, Pitfalls and optimal approaches to diagnose melioidosis. *Asian Pac J Trop Med* **9**, 515-524 (2016).

26. D. Limmathurotsakul, S. J. Peacock, Melioidosis: a clinical overview. *Br Med Bull* **99**, 125-139 (2011).

27. C. Chewapreecha *et al.*, Genetic variation associated with infection and the environment in the accidental pathogen Burkholderia pseudomallei. *Commun Biol* **2**, 428 (2019).

28. D. Limmathurotsakul *et al.*, Defining the true sensitivity of culture for the diagnosis of melioidosis using Bayesian latent class models. *PLoS One* **5**, e12485 (2010).

29. N. Chantratita *et al.*, Biological relevance of colony morphology and phenotypic switching by Burkholderia pseudomallei. *J Bacteriol* **189**, 807-817 (2007).

30. S. J. Peacock *et al.*, Comparison of Ashdown's medium, Burkholderia cepacia medium, and Burkholderia pseudomallei selective agar for clinical isolation of Burkholderia pseudomallei. *J Clin Microbiol* **43**, 5359-5361 (2005).

31. V. Walewski *et al.*, MALDI-TOF MS contribution to diagnosis of melioidosis in a nonendemic country in three French travellers. *New Microbes New Infect* **12**, 31-34 (2016).

32. D. Dance, Treatment and prophylaxis of melioidosis. *Int J Antimicrob Agents* **43**, 310-318 (2014).

33. M. N. Burtnick *et al.*, Development of Subunit Vaccines That Provide High-Level Protection and Sterilizing Immunity against Acute Inhalational Melioidosis. *Infect. Immun.* **86**, (2018).

34. J. S. Roh, D. H. Sohn, Damage-Associated Molecular Patterns in Inflammatory Diseases. *Immune Netw* **18**, e27 (2018).

35. J. S. Marshall, R. Warrington, W. Watson, H. L. Kim, An introduction to immunology and immunopathology. *Allergy Asthma Clin Immunol* **14**, 49 (2018).

36. A. Thakur, H. Mikkelsen, G. Jungersen, Intracellular Pathogens: Host Immunity and Microbial Persistence Strategies. *J Immunol Res* **2019**, 1356540 (2019).

37. R. Medzhitov, Inflammation 2010: new adventures of an old flame. *Cell* **140**, 771-776 (2010).

38. R. Medzhitov, Recognition of microorganisms and activation of the immune response. *Nature* **449**, 819-826 (2007).

39. R. Clark, T. Kupper, Old meets new: the interaction between innate and adaptive immunity. *J Invest Dermatol* **125**, 629-637 (2005).

40. S. L. Reckseidler-Zenteno, R. DeVinney, D. E. Woods, The capsular polysaccharide of Burkholderia pseudomallei contributes to survival in serum by reducing complement factor C3b deposition. *Infect Immun* **73**, 1106-1115 (2005).

41. S. Arjcharoen *et al.*, Fate of a Burkholderia pseudomallei lipopolysaccharide mutant in the mouse macrophage cell line RAW 264.7: possible role for the O-antigenic polysaccharide moiety of lipopolysaccharide in internalization and intracellular survival. *Infect Immun* **75**, 4298-4304 (2007).

42. D. DeShazer, P. J. Brett, D. E. Woods, The type II O-antigenic polysaccharide moiety of Burkholderia pseudomallei lipopolysaccharide is required for serum resistance and virulence. *Mol Microbiol* **30**, 1081-1100 (1998).

43. K. L. Chua, Y. Y. Chan, Y. H. Gan, Flagella are virulence determinants of Burkholderia pseudomallei. *Infect. Immun.* **71**, 1622-1629 (2003).

44. M. N. Burtnick *et al.*, Development of capsular polysaccharide-based glycoconjugates for immunization against melioidosis and glanders. *Front Cell Infect Microbiol* **2**, 108 (2012).

45. L. Gong *et al.*, The Burkholderia pseudomallei type III secretion system and BopA are required for evasion of LC3-associated phagocytosis. *PLoS One* **6**, e17852 (2011).

46. S. Schwarz *et al.*, Burkholderia type VI secretion systems have distinct roles in eukaryotic and bacterial cell interactions. *PLoS Pathog* **6**, e1001068 (2010).

47. P. Utaisincharoen, N. Tangthawornchaikul, W. Kespichayawattana, P. Chaisuriya, S. Sirisinha, Burkholderia pseudomallei interferes with inducible nitric oxide synthase (iNOS) production: a possible mechanism of evading macrophage killing. *Microbiol Immunol* **45**, 307-313 (2001).

48. S. M. Opal, Endotoxins and other sepsis triggers. *Contrib Nephrol* **167**, 14-24 (2010).

49. T. A. Weehuizen *et al.*, Differential Toll-Like Receptor-Signalling of Burkholderia pseudomallei Lipopolysaccharide in Murine and Human Models. *PLoS One* **10**, e0145397 (2015).

50. W. J. Wiersinga *et al.*, Toll-like receptor 2 impairs host defense in gram-negative sepsis caused by Burkholderia pseudomallei (Melioidosis). *PLoS Med.* **4**, e248 (2007).

51. T. E. West, R. K. Ernst, M. J. Jansson-Hutson, S. J. Skerrett, Activation of Toll-like receptors by Burkholderia pseudomallei. *BMC Immunol* **9**, 46 (2008).

52. Y. Suputtamongkol, D. Kwiatkowski, D. A. Dance, W. Chaowagul, N. J. White, Tumor necrosis factor in septicemic melioidosis. *J Infect Dis* **165**, 561-564 (1992).

53. F. N. Lauw *et al.*, Elevated plasma concentrations of interferon (IFN)-gamma and the IFN-gamma-inducing cytokines interleukin (IL)-18, IL-12, and IL-15 in severe melioidosis. *J. Infect. Dis.* **180**, 1878-1885 (1999).

54. F. N. Lauw *et al.*, The CXC chemokines gamma interferon (IFN-gamma)-inducible protein 10 and monokine induced by IFN-gamma are released during severe melioidosis. *Infect Immun* **68**, 3888-3893 (2000).

55. C. Rosales, Neutrophil: A Cell with Many Roles in Inflammation or Several Cell Types? *Front Physiol* **9**, 113 (2018).

56. A. J. Simpson *et al.*, Prognostic value of cytokine concentrations (tumor necrosis factor-alpha, interleukin-6, and interleukin-10) and clinical parameters in severe melioidosis. *J. Infect. Dis.* **181**, 621-625 (2000).

57. J. S. Friedland *et al.*, Prolonged elevation of interleukin-8 and interleukin-6 concentrations in plasma and of leukocyte interleukin-8 mRNA levels during septicemic and localized Pseudomonas pseudomallei infection. *Infect Immun* **60**, 2402-2408 (1992).

58. W. J. Wiersinga *et al.*, Immunosuppression associated with interleukin-1R-associated-kinase-M upregulation predicts mortality in Gram-negative sepsis (melioidosis). *Crit Care Med* **37**, 569-576 (2009).

59. K. Kobayashi *et al.*, IRAK-M is a negative regulator of Toll-like receptor signaling. *Cell* **110**, 191-202 (2002).

60. I. Ceballos-Olvera, M. Sahoo, M. A. Miller, L. Del Barrio, F. Re, Inflammasome-dependent pyroptosis and IL-18 protect against Burkholderia pseudomallei lung infection while IL-1beta is deleterious. *PLoS Pathog* **7**, e1002452 (2011).

61. P. Santanirand, V. S. Harley, D. A. Dance, B. S. Drasar, G. J. Bancroft, Obligatory role of gamma interferon for host survival in a murine model of infection with Burkholderia pseudomallei. *Infect. Immun.* **67**, 3593-3600 (1999).

62. D. A. Lammas, J. L. Casanova, D. S. Kumararatne, Clinical consequences of defects in the IL-12-dependent interferon-gamma (IFN-gamma) pathway. *Clin Exp Immunol* **121**, 417-425 (2000).

63. K. Miyagi, K. Kawakami, A. Saito, Role of reactive nitrogen and oxygen intermediates in gamma interferon-stimulated murine macrophage bactericidal activity against Burkholderia pseudomallei. *Infect Immun* **65**, 4108-4113 (1997).

64. P. Utaisincharoen *et al.*, Induction of iNOS expression and antimicrobial activity by interferon (IFN)-beta is distinct from IFN-gamma in Burkholderia pseudomallei-infected mouse macrophages. *Clin Exp Immunol* **136**, 277-283 (2004).

65. S. Nuntayanuwat, T. Dharakul, W. Chaowagul, S. Songsivilai, Polymorphism in the promoter region of tumor necrosis factor-alpha gene is associated with severe meliodosis. *Hum Immunol* **60**, 979-983 (1999).

66. J. P. Mira *et al.*, Association of TNF2, a TNF-alpha promoter polymorphism, with septic shock susceptibility and mortality: a multicenter study. *JAMA* **282**, 561-568 (1999).

67. T. Dharakul *et al.*, HLA-DR and -DQ associations with melioidosis. *Hum Immunol* **59**, 580-586 (1998).

68. S. J. Dunachie *et al.*, Infection with Burkholderia pseudomallei - immune correlates of survival in acute melioidosis. *Sci Rep* **7**, 12143 (2017).

69. T. E. West *et al.*, Toll-like receptor 4 region genetic variants are associated with susceptibility to melioidosis. *Genes Immun.* **13**, 38-46 (2012).

70. E. Birnie *et al.*, Role of Toll-Like Receptor 5 (TLR5) in Experimental Melioidosis. *Infect Immun* **87**, (2019).

71. P. Chaichana *et al.*, A nonsense mutation in TLR5 is associated with survival and reduced IL-10 and TNF-alpha levels in human melioidosis. *PLoS Negl Trop Dis* **11**, e0005587 (2017).

72. A. M. Cooper, Cell-mediated immune responses in tuberculosis. *Annu Rev Immunol* **27**, 393-422 (2009).

73. A. Haque *et al.*, Role of T cells in innate and adaptive immunity against murine Burkholderia pseudomallei infection. *J Infect Dis* **193**, 370-379 (2006).

74. A. E. Brown *et al.*, Immune cell activation in melioidosis: increased serum levels of interferon-gamma and soluble interleukin-2 receptors without change in soluble CD8 protein. *J. Infect. Dis.* **163**, 1145-1148 (1991).

75. J. H. Dufour *et al.*, IFN-gamma-inducible protein 10 (IP-10; CXCL10)-deficient mice reveal a role for IP-10 in effector T cell generation and trafficking. *J Immunol* **168**, 3195-3204 (2002).

76. K. Jenjaroen *et al.*, T-Cell Responses Are Associated with Survival in Acute Melioidosis Patients. *PLoS Negl Trop Dis* **9**, e0004152 (2015).

77. J. Tomas-Cortazar *et al.*, BpOmpW Antigen Stimulates the Necessary Protective T-Cell Responses Against Melioidosis. *Front Immunol* **12**, 767359 (2021).

78. C. Reynolds *et al.*, T Cell Immunity to the Alkyl Hydroperoxide Reductase of Burkholderia pseudomallei: A Correlate of Disease Outcome in Acute Melioidosis. *J Immunol* **194**, 4814-4824 (2015).

79. P. Kanaphun *et al.*, Serology and carriage of Pseudomonas pseudomallei: a prospective study in 1000 hospitalized children in northeast Thailand. *J. Infect. Dis.* **167**, 230-233 (1993).

80. V. Wuthiekanun *et al.*, Burkholderia pseudomallei antibodies in children, Cambodia. *Emerg. Infect. Dis.* **14**, 301-303 (2008).

81. I. Gassiep, M. Armstrong, R. Norton, Human Melioidosis. *Clin Microbiol Rev* **33**, (2020).

82. V. Hantrakun *et al.*, Presence of B. thailandensis and B. thailandensis expressing B. pseudomallei-like capsular polysaccharide in Thailand, and their associations with serological response to B. pseudomallei. *PLoS Negl Trop Dis* **12**, e0006193 (2018).

83. P. Rongkard *et al.*, Human Immune Responses to Melioidosis and Cross-Reactivity to Low-Virulence Burkholderia Species, Thailand(1). *Emerg Infect Dis* **26**, 463-471 (2020).

84. P. Chaichana *et al.*, Serum From Melioidosis Survivors Diminished Intracellular Burkholderia pseudomallei Growth in Macrophages: A Brief Research Report. *Front Cell Infect Microbiol* **10**, 442 (2020).

85. P. Chaichana *et al.*, Role of Burkholderia pseudomallei-Specific IgG2 in Adults with Acute Melioidosis, Thailand. *Emerg Infect Dis* **27**, 463-470 (2021).

86. A. Easton, A. Haque, K. Chu, R. Lukaszewski, G. J. Bancroft, A critical role for neutrophils in resistance to experimental infection with Burkholderia pseudomallei. *J. Infect. Dis.* **195**, 99-107 (2007).

87. B. J. Currie *et al.*, Melioidosis epidemiology and risk factors from a prospective whole-population study in northern Australia. *Trop. Med. Int. Health* **9**, 1167-1174 (2004).

88. A. Merianos *et al.*, The 1990-1991 outbreak of melioidosis in the Northern Territory of Australia: epidemiology and environmental studies. *Southeast Asian J Trop Med Public Health* **24**, 425-435 (1993).

89. C. Y. Chin, D. M. Monack, S. Nathan, Delayed activation of host innate immune pathways in streptozotocin-induced diabetic hosts leads to more severe disease during infection with Burkholderia pseudomallei. *Immunology* **135**, 312-332 (2012).

90. K. A. Hodgson, J. L. Morris, M. L. Feterl, B. L. Govan, N. Ketheesan, Altered macrophage function is associated with severe Burkholderia pseudomallei infection in a murine model of type 2 diabetes. *Microbes Infect* **13**, 1177-1184 (2011).

91. K. A. Hodgson, B. L. Govan, A. K. Walduck, N. Ketheesan, J. L. Morris, Impaired early cytokine responses at the site of infection in a murine model of type 2 diabetes and melioidosis comorbidity. *Infect Immun* **81**, 470-477 (2013).

92. M. C. Bravi *et al.*, Insulin decreases intracellular oxidative stress in patients with type 2 diabetes mellitus. *Metabolism* **55**, 691-695 (2006).

93. I. Hakki Kalkan, M. Suher, The relationship between the level of glutathione, impairment of glucose metabolism and complications of diabetes mellitus. *Pak J Med Sci* **29**, 938-942 (2013).

94. V. Calabrese *et al.*, Oxidative stress, glutathione status, sirtuin and cellular stress response in type 2 diabetes. *Biochim Biophys Acta* **1822**, 729-736 (2012).

95. J. D. Peterson, L. A. Herzenberg, K. Vasquez, C. Waltenbaugh, Glutathione levels in antigen-presenting cells modulate Th1 versus Th2 response patterns. *Proc Natl Acad Sci U S A* **95**, 3071-3076 (1998).

96. K. Alam, S. Ghousunnissa, S. Nair, V. L. Valluri, S. Mukhopadhyay, Glutathione-redox balance regulates c-rel-driven IL-12 production in macrophages: possible implications in antituberculosis immunotherapy. *J Immunol* **184**, 2918-2929 (2010).

97. C. Guerra *et al.*, Glutathione and adaptive immune responses against Mycobacterium tuberculosis infection in healthy and HIV infected individuals. *PLoS One* **6**, e28378 (2011).

98. K. S. Tan *et al.*, Glutathione deficiency in type 2 diabetes impairs cytokine responses and control of intracellular bacteria. *J Clin Invest* **122**, 2289-2300 (2012).

99. W. J. Wiersinga *et al.*, High-throughput mRNA profiling characterizes the expression of inflammatory molecules in sepsis caused by Burkholderia pseudomallei. *Infect. Immun.* **75**, 3074-3079 (2007).

100. R. Pankla *et al.*, Genomic transcriptional profiling identifies a candidate blood biomarker signature for the diagnosis of septicemic melioidosis. *Genome Biol.* **10**, R127 (2009).

101. G. C. Koh *et al.*, Host responses to melioidosis and tuberculosis are both dominated by interferon-mediated signaling. *PLoS One* **8**, e54961 (2013).

102. M. P. Berry *et al.*, An interferon-inducible neutrophil-driven blood transcriptional signature in human tuberculosis. *Nature* **466**, 973-977 (2010).

103. "Global Tuberculosis report 2021," (Geneva: World Health Organisation, 2021).

104. M. A. Behr, P. H. Edelstein, L. Ramakrishnan, Revisiting the timetable of tuberculosis. *BMJ* **362**, k2738 (2018).

105. M. Pai *et al.*, Tuberculosis. *Nat Rev Dis Primers* **2**, 16076 (2016).

106. K. J. Seung, S. Keshavjee, M. L. Rich, Multidrug-Resistant Tuberculosis and Extensively Drug-Resistant Tuberculosis. *Cold Spring Harb Perspect Med* **5**, a017863 (2015).

107. G. M. Knight, C. F. McQuaid, P. J. Dodd, R. M. G. J. Houben, Global burden of latent multidrug-resistant tuberculosis: trends and estimates based on mathematical modelling. *Lancet Infect Dis* **19**, 903-912 (2019).

108. A. Rendon *et al.*, Classification of drugs to treat multidrug-resistant tuberculosis (MDR-TB): evidence and perspectives. *J Thorac Dis* **8**, 2666-2671 (2016).

109. A. Pawlowski, M. Jansson, M. Skold, M. E. Rottenberg, G. Kallenius, Tuberculosis and HIV co-infection. *PLoS Pathog* **8**, e1002464 (2012).

110. K. Lonnroth, E. Jaramillo, B. G. Williams, C. Dye, M. Raviglione, Drivers of tuberculosis epidemics: The role of risk factors and social determinants. *Soc Sci Med* **68**, 2240-2246 (2009).

111. S. Hayashi, D. Chandramohan, Risk of active tuberculosis among people with diabetes mellitus: systematic review and meta-analysis. *Trop Med Int Health* **23**, 1058-1070 (2018).

112. R. M. Houben, P. J. Dodd, The Global Burden of Latent Tuberculosis Infection: A Re-estimation Using Mathematical Modelling. *PLoS Med* **13**, e1002152 (2016).

113. K. Hodgson *et al.*, Immunological mechanisms contributing to the double burden of diabetes and intracellular bacterial infections. *Immunology* **144**, 171-185 (2015).

114. K. Lonnroth, G. Roglic, A. D. Harries, Improving tuberculosis prevention and care through addressing the global diabetes epidemic: from evidence to policy and practice. *Lancet Diabetes Endocrinol* **2**, 730-739 (2014).

115. C. Y. Jeon, M. B. Murray, Diabetes mellitus increases the risk of active tuberculosis: a systematic review of 13 observational studies. *PLoS Med* **5**, e152 (2008).

116. J. R. Foe-Essomba *et al.*, Diabetes mellitus and tuberculosis, a systematic review and meta-analysis with sensitivity analysis for studies comparable for confounders. *PLoS One* **16**, e0261246 (2021).

117. J. J. Noubiap *et al.*, Global prevalence of diabetes in active tuberculosis: a systematic review and meta-analysis of data from 2.3 million patients with tuberculosis. *Lancet Glob Health* **7**, e448-e460 (2019).

118. H. S. McMurry *et al.*, Coprevalence of type 2 diabetes mellitus and tuberculosis in low-income and middle-income countries: A systematic review. *Diabetes Metab Res Rev* **35**, e3066 (2019).

119. M. A. Baker *et al.*, The impact of diabetes on tuberculosis treatment outcomes: a systematic review. *BMC Med* **9**, 81 (2011).

120. P. Huangfu, C. Ugarte-Gil, J. Golub, F. Pearson, J. Critchley, The effects of diabetes on tuberculosis treatment outcomes: an updated systematic review and meta-analysis. *Int J Tuberc Lung Dis* **23**, 783-796 (2019).

121. M. E. Jiménez-Corona *et al.*, Association of diabetes and tuberculosis: impact on treatment and post-treatment outcomes. *Thorax* **68**, 214-220 (2013).

122. E. Yabuuchi *et al.*, Proposal of Burkholderia gen. nov. and transfer of seven species of the genus Pseudomonas homology group II to the new genus, with the type species Burkholderia cepacia (Palleroni and Holmes 1981) comb. nov. *Microbiol Immunol* **36**, 1251-1275 (1992).

123. M. A. Behr, Evolution of Mycobacterium tuberculosis. *Adv Exp Med Biol* **783**, 81-91 (2013).

124. L. M. Fu, C. S. Fu-Liu, Is Mycobacterium tuberculosis a closer relative to Gram-positive or Gram-negative bacterial pathogens? *Tuberculosis (Edinb)* **82**, 85-90 (2002).

125. A. Maitra *et al.*, Cell wall peptidoglycan in Mycobacterium tuberculosis: An Achilles' heel for the TB-causing pathogen. *FEMS Microbiol Rev* **43**, 548-575 (2019).

126. S. Kethireddy *et al.*, Mycobacterium tuberculosis septic shock. *Chest* **144**, 474-482 (2013).

127. R. Loddenkemper, M. Lipman, A. Zumla, Clinical Aspects of Adult Tuberculosis. *Cold Spring Harb Perspect Med* **6**, a017848 (2015).

128. K. T. Wong, S. D. Puthucheary, J. Vadivelu, The histopathology of human melioidosis. *Histopathology* **26**, 51-55 (1995).

129. M. N. Burtnick *et al.*, The cluster 1 type VI secretion system is a major virulence determinant in Burkholderia pseudomallei. *Infect. Immun.* **79**, 1512-1525 (2011).

130. B. Coburn, I. Sekirov, B. B. Finlay, Type III secretion systems and disease. *Clin Microbiol Rev* **20**, 535-549 (2007).

131. D. Hajra, A. V. Nair, D. Chakravortty, An elegant nano-injection machinery for sabotaging the host: Role of Type III secretion system in virulence of different human and animal pathogenic bacteria. *Phys Life Rev* **38**, 25-54 (2021).

132. T. D'Cruze *et al.*, Role for the Burkholderia pseudomallei type three secretion system cluster 1 bpscN gene in virulence. *Infect Immun* **79**, 3659-3664 (2011).

133. C. Ghazaei, Mycobacterium tuberculosis and lipids: Insights into molecular mechanisms from persistence to virulence. *J Res Med Sci* **23**, 63 (2018).

134. M. Mishra, P. Adhyapak, R. Dadhich, S. Kapoor, Dynamic Remodeling of the Host Cell Membrane by Virulent Mycobacterial Sulfoglycolipid-1. *Sci Rep* **9**, 12844 (2019).

135. L. Blanc *et al.*, Mycobacterium tuberculosis inhibits human innate immune responses via the production of TLR2 antagonist glycolipids. *Proc Natl Acad Sci U S A* **114**, 11205-11210 (2017).

136. S. Ehrt, D. Schnappinger, Mycobacterial survival strategies in the phagosome: defence against host stresses. *Cell Microbiol* **11**, 1170-1178 (2009).

137. J. Augenstreich, V. Briken, Host Cell Targets of Released Lipid and Secreted Protein Effectors of Mycobacterium tuberculosis. *Front Cell Infect Microbiol* **10**, 595029 (2020).

138. J. W. Ai, Q. L. Ruan, Q. H. Liu, W. H. Zhang, Updates on the risk factors for latent tuberculosis reactivation and their managements. *Emerg Microbes Infect* **5**, e10 (2016).

139. S. Ehlers, U. E. Schaible, The granuloma in tuberculosis: dynamics of a host-pathogen collusion. *Front Immunol* **3**, 411 (2012).

140. T. Prezzemolo *et al.*, Functional Signatures of Human CD4 and CD8 T Cell Responses to Mycobacterium tuberculosis. *Front Immunol* **5**, 180 (2014).

141. S. C. Cowley, K. L. Elkins, CD4+ T cells mediate IFN-gamma-independent control of Mycobacterium tuberculosis infection both in vitro and in vivo. *J Immunol* **171**, 4689-4699 (2003).

142. A. O'Garra *et al.*, The immune response in tuberculosis. *Annu Rev Immunol* **31**, 475-527 (2013).

143. R. Vankayalapati *et al.*, Production of interleukin-18 in human tuberculosis. *J Infect Dis* **182**, 234-239 (2000).

144. A. M. Cooper, J. Magram, J. Ferrante, I. M. Orme, Interleukin 12 (IL-12) is crucial to the development of protective immunity in mice intravenously infected with mycobacterium tuberculosis. *J Exp Med* **186**, 39-45 (1997).

145. P. L. Lin, H. L. Plessner, N. N. Voitenok, J. L. Flynn, Tumor necrosis factor and tuberculosis. *J Investig Dermatol Symp Proc* **12**, 22-25 (2007).

146. A. G. Bean *et al.*, Structural deficiencies in granuloma formation in TNF gene-targeted mice underlie the heightened susceptibility to aerosol Mycobacterium tuberculosis infection, which is not compensated for by lymphotoxin. *J Immunol* **162**, 3504-3511 (1999).

147. T. Botha, B. Ryffel, Reactivation of latent tuberculosis infection in TNF-deficient mice. *J Immunol* **171**, 3110-3118 (2003).

148. I. Solovic *et al.*, The risk of tuberculosis related to tumour necrosis factor antagonist therapies: a TBNET consensus statement. *Eur Respir J* **36**, 1185-1206 (2010).

149. M. Zhang *et al.*, T-cell cytokine responses in human infection with Mycobacterium tuberculosis. *Infect Immun* **63**, 3231-3234 (1995).

150. J. Y. Feng *et al.*, Depressed Gamma Interferon Responses and Treatment Outcomes in Tuberculosis Patients: a Prospective Cohort Study. *J Clin Microbiol* **56**, (2018).

151. E. Sahiratmadja *et al.*, Dynamic changes in pro- and anti-inflammatory cytokine profiles and gamma interferon receptor signaling integrity correlate with tuberculosis disease activity and response to curative treatment. *Infect Immun* **75**, 820-829 (2007).

152. M. L. Donovan, T. E. Schultz, T. J. Duke, A. Blumenthal, Type I Interferons in the Pathogenesis of Tuberculosis: Molecular Drivers and Immunological Consequences. *Front Immunol* **8**, 1633 (2017).

153. J. E. Allen, T. E. Sutherland, Host protective roles of type 2 immunity: parasite killing and tissue repair, flip sides of the same coin. *Semin Immunol* **26**, 329-340 (2014).

154. B. Spellberg, J. E. Edwards, Jr., Type 1/Type 2 immunity in infectious diseases. *Clin Infect Dis* **32**, 76-102 (2001).

155. K. N. Couper, D. G. Blount, E. M. Riley, IL-10: the master regulator of immunity to infection. *J Immunol* **180**, 5771-5777 (2008).

156. S. S. Iyer, G. Cheng, Role of interleukin 10 transcriptional regulation in inflammation and autoimmune disease. *Crit Rev Immunol* **32**, 23-63 (2012).

157. M. Gonzalez-Juarrero *et al.*, Disruption of granulocyte macrophage-colony stimulating factor production in the lungs severely affects the ability of mice to control Mycobacterium tuberculosis infection. *J Leukoc Biol* **77**, 914-922 (2005).

158. R. Guler *et al.*, IL-4Ralpha-dependent alternative activation of macrophages is not decisive for Mycobacterium tuberculosis pathology and bacterial burden in mice. *PLoS One* **10**, e0121070 (2015).

159. Y. Zhang *et al.*, Mycobacterium tuberculosis Heat-Shock Protein 16.3 Induces Macrophage M2 Polarization Through CCRL2/CX3CR1. *Inflammation* **43**, 487-506 (2020).

160. F. A. Verreck *et al.*, Human IL-23-producing type 1 macrophages promote but IL-10-producing type 2 macrophages subvert immunity to (myco)bacteria. *Proc Natl Acad Sci U S A* **101**, 4560-4565 (2004).

161. M. P. Etna, E. Giacomini, M. Severa, E. M. Coccia, Pro- and anti-inflammatory cytokines in tuberculosis: a two-edged sword in TB pathogenesis. *Semin Immunol* **26**, 543-551 (2014).

162. L. M. Frydrych, G. Bian, D. E. O'Lone, P. A. Ward, M. J. Delano, Obesity and type 2 diabetes mellitus drive immune dysfunction, infection development, and sepsis mortality. *J Leukoc Biol* **104**, 525-534 (2018).

163. A. Berbudi, N. Rahmadika, A. I. Tjahjadi, R. Ruslami, Type 2 Diabetes and its Impact on the Immune System. *Curr Diabetes Rev* **16**, 442-449 (2020).

164. B. Ayelign, M. Negash, M. Genetu, T. Wondmagegn, T. Shibabaw, Immunological Impacts of Diabetes on the Susceptibility of Mycobacterium tuberculosis. *J Immunol Res* **2019**, 6196532 (2019).

165. S. Raposo-Garcia *et al.*, Immunological response to Mycobacterium tuberculosis infection in blood from type 2 diabetes patients. *Immunol Lett* **186**, 41-45 (2017).

166. S. Chanchamroen, C. Kewcharoenwong, W. Susaengrat, M. Ato, G. Lertmemongkolchai, Human polymorphonuclear neutrophil responses to Burkholderia pseudomallei in healthy and diabetic subjects. *Infect. Immun.* **77**, 456-463 (2009).

167. D. Riyapa *et al.*, Neutrophil extracellular traps exhibit antibacterial activity against burkholderia pseudomallei and are influenced by bacterial and host factors. *Infect Immun* **80**, 3921-3929 (2012).

168. C. Kewcharoenwong *et al.*, Glibenclamide reduces pro-inflammatory cytokine production by neutrophils of diabetes patients in response to bacterial infection. *Sci Rep* **3**, 3363 (2013).

169. C. Kewcharoenwong *et al.*, Glibenclamide impairs responses of neutrophils against Burkholderia pseudomallei by reduction of intracellular glutathione. *Sci Rep* **6**, 34794 (2016).

170. S. L. Wong *et al.*, Diabetes primes neutrophils to undergo NETosis, which impairs wound healing. *Nat Med* **21**, 815-819 (2015).

171. S. H. Kaufmann, New issues in tuberculosis. *Ann Rheum Dis* **63 Suppl 2**, ii50-ii56 (2004).

172. K. Tsukaguchi *et al.*, [The relation between diabetes mellitus and IFN-gamma, IL-12 and IL-10 productions by CD4+ alpha beta T cells and monocytes in patients with pulmonary tuberculosis]. *Kekkaku* **72**, 617-622 (1997).

173. K. Tsukaguchi *et al.*, [Longitudinal assessment of IFN-gamma production in patients with pulmonary tuberculosis complicated with diabetes mellitus]. *Kekkaku* **77**, 409-413 (2002).

174. R. J. Al-Attiyah, A. S. Mustafa, Mycobacterial antigen-induced T helper type 1 (Th1) and Th2 reactivity of peripheral blood mononuclear cells from diabetic and non-diabetic tuberculosis patients and Mycobacterium bovis bacilli Calmette-Guerin (BCG)-vaccinated healthy subjects. *Clin Exp Immunol* **158**, 64-73 (2009).

175. B. I. Restrepo *et al.*, Tuberculosis in poorly controlled type 2 diabetes: altered cytokine expression in peripheral white blood cells. *Clin Infect Dis* **47**, 634-641 (2008).

176. N. Martinez, N. Ketheesan, K. West, T. Vallerskog, H. Kornfeld, Impaired Recognition of Mycobacterium tuberculosis by Alveolar Macrophages From Diabetic Mice. *J Infect Dis* **214**, 1629-1637 (2016).

177. T. Vallerskog, G. W. Martens, H. Kornfeld, Diabetic mice display a delayed adaptive immune response to Mycobacterium tuberculosis. *J. Immunol.* **184**, 6275-6282 (2010).

178. N. Lopez-Lopez *et al.*, Type-2 diabetes alters the basal phenotype of human macrophages and diminishes their capacity to respond, internalise, and control Mycobacterium tuberculosis. *Mem Inst Oswaldo Cruz* **113**, e170326 (2018).

179. J. C. Fernandez-Ruiz *et al.*, Myeloid-Derived Suppressor Cells Show Different Frequencies in Diabetics and Subjects with Arterial Hypertension. *J Diabetes Res* **2019**, 1568457 (2019).

180. B. B. Andrade *et al.*, Heightened plasma levels of heme oxygenase-1 and tissue inhibitor of metalloproteinase-4 as well as elevated peripheral neutrophil counts are associated with TB-diabetes comorbidity. *Chest* **145**, 1244-1254 (2014).

181. C. A. Prada-Medina *et al.*, Systems Immunology of Diabetes-Tuberculosis Comorbidity Reveals Signatures of Disease Complications. *Sci Rep* **7**, 1999 (2017).

182. M. Singer *et al.*, The Third International Consensus Definitions for Sepsis and Septic Shock (Sepsis-3). *JAMA* **315**, 801-810 (2016).

183. K. E. Rudd *et al.*, Global, regional, and national sepsis incidence and mortality, 1990-2017: analysis for the Global Burden of Disease Study. *Lancet* **395**, 200-211 (2020).

184. C. Fleischmann-Struzek *et al.*, Incidence and mortality of hospital- and ICU-treated sepsis: results from an updated and expanded systematic review and meta-analysis. *Intensive Care Med* **46**, 1552-1562 (2020).

185. O. World Health, *Global report on the epidemiology and burden of sepsis: current evidence, identifying gaps and future directions*. (World Health Organization, Geneva, 2020).

186. K. E. Rudd *et al.*, The global burden of sepsis: barriers and potential solutions. *Crit Care* **22**, 232 (2018).

187. J. Deen *et al.*, Community-acquired bacterial bloodstream infections in developing countries in south and southeast Asia: a systematic review. *Lancet Infect Dis* **12**, 480-487 (2012).

188. N. Southeast Asia Infectious Disease Clinical Research, Causes and outcomes of sepsis in southeast Asia: a multinational multicentre cross-sectional study. *Lancet Glob Health* **5**, e157-e167 (2017).

189. L. Mellhammar *et al.*, Bacteremic sepsis leads to higher mortality when adjusting for confounders with propensity score matching. *Sci Rep* **11**, 6972 (2021).

190. A. Mansur *et al.*, Primary bacteraemia is associated with a higher mortality risk compared with pulmonary and intra-abdominal infections in patients with sepsis: a prospective observational cohort study. *BMJ Open* **5**, e006616 (2015).

191. D. W. Bates, K. E. Pruess, T. H. Lee, How bad are bacteremia and sepsis? Outcomes in a cohort with suspected bacteremia. *Arch Intern Med* **155**, 593-598 (1995).

192. V. Hantrakun *et al.*, Clinical epidemiology and outcomes of community acquired infection and sepsis among hospitalized patients in a resource limited setting in Northeast Thailand: A prospective observational study (Ubon-sepsis). *PLoS One* **13**, e0204509 (2018).

193. K. E. Rudd *et al.*, Early management of sepsis in medical patients in rural Thailand: a single-center prospective observational study. *J Intensive Care* **7**, 55 (2019).

194. R. Somayaji *et al.*, Comparative clinical characteristics and outcomes of patients with community acquired bacteremia caused by Escherichia coli, Burkholderia pseudomallei and Staphylococcus aureus: A prospective observational study (Ubon-sepsis). *PLoS Negl Trop Dis* **15**, e0009704 (2021).

195. S. Booraphun *et al.*, Effectiveness of a sepsis programme in a resource-limited setting: a retrospective analysis of data of a prospective observational study (Ubon-sepsis). *BMJ Open* **11**, e041022 (2021).

196. R. C. Bone *et al.*, Definitions for sepsis and organ failure and guidelines for the use of innovative therapies in sepsis. The ACCP/SCCM Consensus Conference Committee. American College of Chest Physicians/Society of Critical Care Medicine. *Chest* **101**, 1644-1655 (1992).

197. M. Shankar-Hari *et al.*, Developing a New Definition and Assessing New Clinical Criteria for Septic Shock: For the Third International Consensus Definitions for Sepsis and Septic Shock (Sepsis-3). *JAMA* **315**, 775-787 (2016).

198. N. Shapiro *et al.*, The association of sepsis syndrome and organ dysfunction with mortality in emergency department patients with suspected infection. *Ann Emerg Med* **48**, 583-590, 590 e581 (2006).

199. M. M. Levy *et al.*, 2001 SCCM/ESICM/ACCP/ATS/SIS International Sepsis Definitions Conference. *Crit Care Med* **31**, 1250-1256 (2003).

200. J. F. Frencken *et al.*, Myocardial Injury in Patients With Sepsis and Its Association With Long-Term Outcome. *Circ Cardiovasc Qual Outcomes* **11**, e004040 (2018).

201. I. Cinel, S. M. Opal, Molecular biology of inflammation and sepsis: a primer. *Crit Care Med* **37**, 291-304 (2009).

202. S. M. Lam, A. C. Lau, R. P. Lam, W. W. Yan, Clinical management of sepsis. *Hong Kong Med J* **23**, 296-305 (2017).

203. C. E. Spooner, N. P. Markowitz, L. D. Saravolatz, The role of tumor necrosis factor in sepsis. *Clin Immunol Immunopathol* **62**, S11-17 (1992).

204. A. C. Muller Kobold *et al.*, Leukocyte activation in sepsis; correlations with disease state and mortality. *Intensive Care Med* **26**, 883-892 (2000).

205. E. Abraham *et al.*, Efficacy and safety of monoclonal antibody to human tumor necrosis factor alpha in patients with sepsis syndrome. A randomized, controlled, double-blind, multicenter clinical trial. TNF-alpha MAb Sepsis Study Group. *JAMA* **273**, 934-941 (1995).

206. S. M. Opal *et al.*, Confirmatory interleukin-1 receptor antagonist trial in severe sepsis: a phase III, randomized, double-blind, placebo-controlled, multicenter trial. The Interleukin-1 Receptor Antagonist Sepsis Investigator Group. *Crit Care Med* **25**, 1115-1124 (1997).

207. J. J. Presneill, T. Harris, A. G. Stewart, J. F. Cade, J. W. Wilson, A randomized phase II trial of granulocyte-macrophage colony-stimulating factor therapy in severe sepsis with respiratory dysfunction. *Am J Respir Crit Care Med* **166**, 138-143 (2002).

208. C. Nedeva, J. Menassa, H. Puthalakath, Sepsis: Inflammation Is a Necessary Evil. *Front Cell Dev Biol* **7**, 108 (2019).

209. N. S. Ward, B. Casserly, A. Ayala, The compensatory anti-inflammatory response syndrome (CARS) in critically ill patients. *Clin Chest Med* **29**, 617-625, viii (2008).

210. W. J. Frazier, M. W. Hall, Immunoparalysis and adverse outcomes from critical illness. *Pediatr Clin North Am* **55**, 647-668, xi (2008).

211. R. Abe *et al.*, Up-regulation of interleukin-10 mRNA expression in peripheral leukocytes predicts poor outcome and diminished human leukocyte antigen-DR expression on monocytes in septic patients. *J Surg Res* **147**, 1-8 (2008).

212. J. S. Boomer *et al.*, Immunosuppression in patients who die of sepsis and multiple organ failure. *JAMA* **306**, 2594-2605 (2011).

213. S. Inoue *et al.*, Dose-dependent effect of anti-CTLA-4 on survival in sepsis. *Shock* **36**, 38-44 (2011).

214. Y. Zhang *et al.*, PD-L1 blockade improves survival in experimental sepsis by inhibiting lymphocyte apoptosis and reversing monocyte dysfunction. *Crit Care* **14**, R220 (2010).

215. P. Brahmamdam *et al.*, Delayed administration of anti-PD-1 antibody reverses immune dysfunction and improves survival during sepsis. *J Leukoc Biol* **88**, 233-240 (2010).

216. K. C. Chang *et al.*, Blockade of the negative co-stimulatory molecules PD-1 and CTLA-4 improves survival in primary and secondary fungal sepsis. *Crit Care* **17**, R85 (2013).

217. Y. Wang *et al.*, Treatment-Related Adverse Events of PD-1 and PD-L1 Inhibitors in Clinical Trials: A Systematic Review and Meta-analysis. *JAMA Oncol* **5**, 1008-1019 (2019).

218. P. Comstedt, M. Storgaard, A. T. Lassen, The Systemic Inflammatory Response Syndrome (SIRS) in acutely hospitalised medical patients: a cohort study. *Scand J Trauma Resusc Emerg Med* **17**, 67 (2009).

219. O. Gasch *et al.*, Predictive factors for mortality in patients with methicillin-resistant Staphylococcus aureus bloodstream infection: impact on outcome of host, microorganism and therapy. *Clin Microbiol Infect* **19**, 1049-1057 (2013).

220. O. Gasch *et al.*, Epidemiology of methicillin-resistant Staphylococcus aureus (MRSA) bloodstream infection: secular trends over 19 years at a university hospital. *Medicine (Baltimore)* **90**, 319-327 (2011).

221. Y. C. Lu, W. C. Yeh, P. S. Ohashi, LPS/TLR4 signal transduction pathway. *Cytokine* **42**, 145-151 (2008).

222. T. Kawasaki, T. Kawai, Toll-like receptor signaling pathways. *Front Immunol* **5**, 461 (2014).

223. T. Roger *et al.*, Protection from lethal gram-negative bacterial sepsis by targeting Toll-like receptor 4. *Proc Natl Acad Sci U S A* **106**, 2348-2352 (2009).

224. G. Baumgarten *et al.*, Role of Toll-like receptor 4 for the pathogenesis of acute lung injury in Gram-negative sepsis. *Eur J Anaesthesiol* **23**, 1041-1048 (2006).

225. J. X. Liu *et al.*, Protective effect of forsythoside B against lipopolysaccharide-induced acute lung injury by attenuating the TLR4/NF-kappaB pathway. *Int Immunopharmacol* **66**, 336-346 (2019).

226. S. J. van Hal *et al.*, Predictors of mortality in Staphylococcus aureus Bacteremia. *Clin Microbiol Rev* **25**, 362-386 (2012).

227. S. Y. Tong, J. S. Davis, E. Eichenberger, T. L. Holland, V. G. Fowler, Jr., Staphylococcus aureus infections: epidemiology, pathophysiology, clinical manifestations, and management. *Clin Microbiol Rev* **28**, 603-661 (2015).

228. A. K. Varshney *et al.*, Staphylococcal Enterotoxin B-specific monoclonal antibody 20B1 successfully treats diverse Staphylococcus aureus infections. *J Infect Dis* **208**, 2058-2066 (2013).

229. R. A. Buonpane *et al.*, Neutralization of staphylococcal enterotoxin B by soluble, high-affinity receptor antagonists. *Nat Med* **13**, 725-729 (2007).

230. D. L. Hu *et al.*, A mutant of staphylococcal enterotoxin C devoid of bacterial superantigenic activity elicits a Th2 immune response for protection against Staphylococcus aureus infection. *Infect Immun* **73**, 174-180 (2005).

231. W. J. Wiersinga, S. J. Leopold, D. R. Cranendonk, T. van der Poll, Host innate immune responses to sepsis. *Virulence* **5**, 36-44 (2014).

232. G. Gasteiger *et al.*, Cellular Innate Immunity: An Old Game with New Players. *J Innate Immun* **9**, 111-125 (2017).

233. H. Kumar, T. Kawai, S. Akira, Toll-like receptors and innate immunity. *Biochem Biophys Res Commun* **388**, 621-625 (2009).

234. D. De Nardo, Toll-like receptors: Activation, signalling and transcriptional modulation. *Cytokine* **74**, 181-189 (2015).

235. H. Tsujimoto *et al.*, Role of Toll-like receptors in the development of sepsis. *Shock* **29**, 315-321 (2008).

236. A. Schiopu, O. S. Cotoi, S100A8 and S100A9: DAMPs at the crossroads between innate immunity, traditional risk factors, and cardiovascular disease. *Mediators Inflamm* **2013**, 828354 (2013).

237. C. Ryckman, K. Vandal, P. Rouleau, M. Talbot, P. A. Tessier, Proinflammatory activities of S100: proteins S100A8, S100A9, and S100A8/A9 induce neutrophil chemotaxis and adhesion. *J Immunol* **170**, 3233-3242 (2003).

238. J. M. Ehrchen, C. Sunderkotter, D. Foell, T. Vogl, J. Roth, The endogenous Toll-like receptor 4 agonist S100A8/S100A9 (calprotectin) as innate amplifier of infection, autoimmunity, and cancer. *J Leukoc Biol* **86**, 557-566 (2009).

239. T. Vogl *et al.*, Mrp8 and Mrp14 are endogenous activators of Toll-like receptor 4, promoting lethal, endotoxin-induced shock. *Nat Med* **13**, 1042-1049 (2007).

240. C. Christmann *et al.*, Interleukin 17 Promotes Expression of Alarmins S100A8 and S100A9 During the Inflammatory Response of Keratinocytes. *Front Immunol* **11**, 599947 (2020).

241. P. Ehlermann *et al.*, Increased proinflammatory endothelial response to S100A8/A9 after preactivation through advanced glycation end products. *Cardiovasc Diabetol* **5**, 6 (2006).

242. C. Dubois *et al.*, High plasma level of S100A8/S100A9 and S100A12 at admission indicates a higher risk of death in septic shock patients. *Sci Rep* **9**, 15660 (2019).

243. Q. Guo *et al.*, Induction of alarmin S100A8/A9 mediates activation of aberrant neutrophils in the pathogenesis of COVID-19. *Cell Host Microbe* **29**, 222-235 e224 (2021).

244. B. Zhao *et al.*, S100A9 blockade prevents lipopolysaccharide-induced lung injury via suppressing the NLRP3 pathway. *Respir Res* **22**, 45 (2021).

245. G. Sreejit *et al.*, Neutrophil-Derived S100A8/A9 Amplify Granulopoiesis After Myocardial Infarction. *Circulation* **141**, 1080-1094 (2020).

246. L. C. Casey, R. A. Balk, R. C. Bone, Plasma cytokine and endotoxin levels correlate with survival in patients with the sepsis syndrome. *Ann Intern Med* **119**, 771-778 (1993).

247. S. Takeshita, K. Nakatani, H. Tsujimoto, Y. Kawamura, I. Sekine, Detection of circulating lipopolysaccharide-bound monocytes in children with gram-negative sepsis. *J Infect Dis* **182**, 1549-1552 (2000).

248. S. M. Opal *et al.*, Relationship between plasma levels of lipopolysaccharide (LPS) and LPS-binding protein in patients with severe sepsis and septic shock. *J Infect Dis* **180**, 1584-1589 (1999).

249. N. S. Merle, R. Noe, L. Halbwachs-Mecarelli, V. Fremeaux-Bacchi, L. T. Roumenina, Complement System Part II: Role in Immunity. *Front Immunol* **6**, 257 (2015).

250. N. R. Sproston, J. J. Ashworth, Role of C-Reactive Protein at Sites of Inflammation and Infection. *Front Immunol* **9**, 754 (2018).

251. G. J. Wolbink *et al.*, Complement activation in patients with sepsis is in part mediated by C-reactive protein. *J Infect Dis* **177**, 81-87 (1998).

252. C. E. Hack *et al.*, Elevated plasma levels of the anaphylatoxins C3a and C4a are associated with a fatal outcome in sepsis. *Am J Med* **86**, 20-26 (1989).

253. S. Stove *et al.*, Circulating complement proteins in patients with sepsis or systemic inflammatory response syndrome. *Clin Diagn Lab Immunol* **3**, 175-183 (1996).

254. C. T. Esmon, J. Xu, F. Lupu, Innate immunity and coagulation. *J Thromb Haemost* **9 Suppl 1**, 182-188 (2011).

255. S. Antoniak, The coagulation system in host defense. *Res Pract Thromb Haemost* **2**, 549-557 (2018).

256. R. Silasi-Mansat *et al.*, Complement inhibition decreases the procoagulant response and confers organ protection in a baboon model of Escherichia coli sepsis. *Blood* **116**, 1002-1010 (2010).

257. R. S. Hotchkiss, I. E. Karl, The pathophysiology and treatment of sepsis. *N Engl J Med* **348**, 138-150 (2003).

258. E. Birnie *et al.*, Increased Von Willebrand factor, decreased ADAMTS13 and thrombocytopenia in melioidosis. *PLoS Negl Trop Dis* **11**, e0005468 (2017).

259. W. J. Wiersinga *et al.*, Activation of coagulation with concurrent impairment of anticoagulant mechanisms correlates with a poor outcome in severe melioidosis. *J Thromb Haemost* **6**, 32-39 (2008).

260. Z. Huang, Z. Fu, W. Huang, K. Huang, Prognostic value of neutrophil-to-lymphocyte ratio in sepsis: A meta-analysis. *Am J Emerg Med* **38**, 641-647 (2020).

261. G. Drifte, I. Dunn-Siegrist, P. Tissieres, J. Pugin, Innate immune functions of immature neutrophils in patients with sepsis and severe systemic inflammatory response syndrome. *Crit Care Med* **41**, 820-832 (2013).

262. R. Taneja, A. P. Sharma, M. B. Hallett, G. P. Findlay, M. R. Morris, Immature circulating neutrophils in sepsis have impaired phagocytosis and calcium signaling. *Shock* **30**, 618-622 (2008).

263. S. K. Lee *et al.*, Phospholipase D2 drives mortality in sepsis by inhibiting neutrophil extracellular trap formation and down-regulating CXCR2. *J Exp Med* **212**, 1381-1390 (2015).

264. S. Biswal, D. G. Remick, Sepsis: redox mechanisms and therapeutic opportunities. *Antioxid Redox Signal* **9**, 1959-1961 (2007).

265. H. F. Galley, Oxidative stress and mitochondrial dysfunction in sepsis. *Br J Anaesth* **107**, 57-64 (2011).

266. J. M. Alonso de Vega, J. Diaz, E. Serrano, L. F. Carbonell, Plasma redox status relates to severity in critically ill patients. *Crit Care Med* **28**, 1812-1814 (2000).

267. S. S. Santos *et al.*, Generation of nitric oxide and reactive oxygen species by neutrophils and monocytes from septic patients and association with outcomes. *Shock* **38**, 18-23 (2012).

268. V. Brinkmann *et al.*, Neutrophil extracellular traps kill bacteria. *Science* **303**, 1532-1535 (2004).

269. V. Poli *et al.*, Zinc-dependent histone deacetylases drive neutrophil extracellular trap formation and potentiate local and systemic inflammation. *iScience* **24**, 103256 (2021).

270. V. G. Magupalli *et al.*, HDAC6 mediates an aggresome-like mechanism for NLRP3 and pyrin inflammasome activation. *Science* **369**, (2020).

271. D. Odobasic *et al.*, Neutrophil myeloperoxidase regulates T-cell-driven tissue inflammation in mice by inhibiting dendritic cell function. *Blood* **121**, 4195-4204 (2013).

272. A. A. Filardy *et al.*, Proinflammatory clearance of apoptotic neutrophils induces an IL-12(low)IL-10(high) regulatory phenotype in macrophages. *J Immunol* **185**, 2044-2050 (2010).

273. G. M. Winslow, A. Cooper, W. Reiley, M. Chatterjee, D. L. Woodland, Early T-cell responses in tuberculosis immunity. *Immunol Rev* **225**, 284-299 (2008).

274. F. M. J. Hafkamp, T. Groot Kormelink, E. C. de Jong, Targeting DCs for Tolerance Induction: Don't Lose Sight of the Neutrophils. *Front Immunol* **12**, 732992 (2021).

275. A. Roghanian, E. M. Drost, W. MacNee, S. E. Howie, J. M. Sallenave, Inflammatory lung secretions inhibit dendritic cell maturation and function via neutrophil elastase. *Am J Respir Crit Care Med* **174**, 1189-1198 (2006).

276. P. C. Maffia *et al.*, Neutrophil elastase converts human immature dendritic cells into transforming growth factor-beta1-secreting cells and reduces allostimulatory ability. *Am J Pathol* **171**, 928-937 (2007).

277. Y. Belkaid, G. Oldenhove, Tuning microenvironments: induction of regulatory T cells by dendritic cells. *Immunity* **29**, 362-371 (2008).

278. D. I. Gabrilovich, S. Nagaraj, Myeloid-derived suppressor cells as regulators of the immune system. *Nat. Rev. Immunol.* **9**, 162-174 (2009).

279. C. J. Darcy *et al.*, Neutrophils with myeloid derived suppressor function deplete arginine and constrain T cell function in septic shock patients. *Crit Care* **18**, R163 (2014).

280. P. C. Rodriguez *et al.*, Arginase I production in the tumor microenvironment by mature myeloid cells inhibits T-cell receptor expression and antigen-specific T-cell responses. *Cancer Res* **64**, 5839-5849 (2004).

281. X. Chen, M. Song, B. Zhang, Y. Zhang, Reactive Oxygen Species Regulate T Cell Immune Response in the Tumor Microenvironment. *Oxid Med Cell Longev* **2016**, 1580967 (2016).

282. J. Brady, S. Horie, J. G. Laffey, Role of the adaptive immune response in sepsis. *Intensive Care Med Exp* **8**, 20 (2020).

283. C. A. Janeway, Jr., How the immune system works to protect the host from infection: a personal view. *Proc Natl Acad Sci U S A* **98**, 7461-7468 (2001).

284. A. M. Drewry *et al.*, Persistent lymphopenia after diagnosis of sepsis predicts mortality. *Shock* **42**, 383-391 (2014).

285. R. S. Hotchkiss, C. M. Coopersmith, J. E. McDunn, T. A. Ferguson, The sepsis seesaw: tilting toward immunosuppression. *Nat Med* **15**, 496-497 (2009).

286. M. Antonelli, Sepsis and septic shock: pro-inflammatory or anti-inflammatory state? *J Chemother* **11**, 536-540 (1999).

287. Z. Guo, Z. Zhang, M. Prajapati, Y. Li, Lymphopenia Caused by Virus Infections and the Mechanisms Beyond. *Viruses* **13**, (2021).

288. H. Okada *et al.*, Extensive lymphopenia due to apoptosis of uninfected lymphocytes in acute measles patients. *Arch Virol* **145**, 905-920 (2000).

289. J. S. Boomer, J. Shuherk-Shaffer, R. S. Hotchkiss, J. M. Green, A prospective analysis of lymphocyte phenotype and function over the course of acute sepsis. *Crit Care* **16**, R112 (2012).

290. K. M. Sundar, M. Sires, Sepsis induced immunosuppression: Implications for secondary infections and complications. *Indian J Crit Care Med* **17**, 162-169 (2013).

291. F. Venet, A. Lepape, G. Monneret, Clinical review: flow cytometry perspectives in the ICU - from diagnosis of infection to monitoring of injury-induced immune dysfunctions. *Crit Care* **15**, 231 (2011).

292. R. S. Hotchkiss *et al.*, Apoptotic cell death in patients with sepsis, shock, and multiple organ dysfunction. *Crit Care Med* **27**, 1230-1251 (1999).

293. Y. Le Tulzo *et al.*, Early circulating lymphocyte apoptosis in human septic shock is associated with poor outcome. *Shock* **18**, 487-494 (2002).

294. F. Venet *et al.*, Increased circulating regulatory T cells (CD4(+)CD25 (+)CD127 (-)) contribute to lymphocyte anergy in septic shock patients. *Intensive Care Med* **35**, 678-686 (2009).

295. Y. Zhang *et al.*, Upregulation of programmed death-1 on T cells and programmed death ligand-1 on monocytes in septic shock patients. *Crit Care* **15**, R70 (2011).

296. E. E. Davenport *et al.*, Genomic landscape of the individual host response and outcomes in sepsis: a prospective cohort study. *Lancet Respir Med* **4**, 259-271 (2016).

297. K. L. Burnham *et al.*, Shared and Distinct Aspects of the Sepsis Transcriptomic Response to Fecal Peritonitis and Pneumonia. *Am J Respir Crit Care Med* **196**, 328-339 (2017).

298. D. B. Antcliffe *et al.*, Transcriptomic Signatures in Sepsis and a Differential Response to Steroids. From the VANISH Randomized Trial. *Am J Respir Crit Care Med* **199**, 980-986 (2019).

299. B. P. Scicluna *et al.*, Classification of patients with sepsis according to blood genomic endotype: a prospective cohort study. *Lancet Respir Med* **5**, 816-826 (2017).

300. A. Baghela *et al.*, Predicting sepsis severity at first clinical presentation: The role of endotypes and mechanistic signatures. *EBioMedicine* **75**, 103776 (2022).

301. L. Pereverzeva *et al.*, Blood leukocyte transcriptomes in Gram-positive and Gram-negative community-acquired pneumonia. *Eur Respir J* **59**, (2022).

302. A. Budreviciute *et al.*, Management and Prevention Strategies for Non-communicable Diseases (NCDs) and Their Risk Factors. *Front Public Health* **8**, 574111 (2020).

303. J. Casqueiro, J. Casqueiro, C. Alves, Infections in patients with diabetes mellitus: A review of pathogenesis. *Indian J Endocrinol Metab* **16 Suppl 1**, S27-36 (2012).

304. International Diabetes Federation, "IDF Diabetes Atlas 10th edn.," (Brussels, Belgium:International Diabetes Federation, 2021. http://www.diabetesatlas.org).

305. International Diabetes Federation, "IDF Diabetes Atlas 8th edn.," (Brussels, Belgium:International Diabetes Federation, 2017. http://www.diabetesatlas.org).

306. N. N. Gholap, M. J. Davies, S. A. Mostafa, K. Khunti, Diagnosing type 2 diabetes and identifying high-risk individuals using the new glycated haemoglobin (HbA1c) criteria. *Br J Gen Pract* **63**, e165-167 (2013).

307. U. Galicia-Garcia *et al.*, Pathophysiology of Type 2 Diabetes Mellitus. *Int J Mol Sci* **21**, (2020).

308. R. A. DeFronzo *et al.*, Type 2 diabetes mellitus. *Nat Rev Dis Primers* **1**, 15019 (2015).

309. J. P. Bastard *et al.*, Recent advances in the relationship between obesity, inflammation, and insulin resistance. *Eur Cytokine Netw* **17**, 4-12 (2006).

310. G. Wilcox, Insulin and insulin resistance. *Clin Biochem Rev* **26**, 19-39 (2005).

311. L. I. Hudish, J. E. Reusch, L. Sussel, beta Cell dysfunction during progression of metabolic syndrome to type 2 diabetes. *J Clin Invest* **129**, 4001-4008 (2019).

312. Y. T. Wondmkun, Obesity, Insulin Resistance, and Type 2 Diabetes: Associations and Therapeutic Implications. *Diabetes Metab Syndr Obes* **13**, 3611-3616 (2020).

313. J. Ye, Mechanisms of insulin resistance in obesity. *Front Med* **7**, 14-24 (2013).

314. A. Chaudhury *et al.*, Clinical Review of Antidiabetic Drugs: Implications for Type 2 Diabetes Mellitus Management. *Front Endocrinol (Lausanne)* **8**, 6 (2017).

315. S. A. Paschou, N. Papadopoulou-Marketou, G. P. Chrousos, C. Kanaka-Gantenbein, On type 1 diabetes mellitus pathogenesis. *Endocr Connect* **7**, R38-R46 (2018).

316. A. L. McCall, L. S. Farhy, Treating type 1 diabetes: from strategies for insulin delivery to dual hormonal control. *Minerva Endocrinol* **38**, 145-163 (2013).

317. Y. N. Lee, M. S. Huda, Uncommon forms of diabetes. *Clin Med (Lond)* **21**, e337-e341 (2021).

318. C. Deerochanawong, A. Ferrario, Diabetes management in Thailand: a literature review of the burden, costs, and outcomes. *Global Health* **9**, 11 (2013).

319. J. C. Chan *et al.*, Diabetes in Asia: epidemiology, risk factors, and pathophysiology. *JAMA* **301**, 2129-2140 (2009).

320. E. J. Barrett *et al.*, Diabetic Microvascular Disease: An Endocrine Society Scientific Statement. *J Clin Endocrinol Metab* **102**, 4343-4410 (2017).

321. A. Chawla, R. Chawla, S. Jaggi, Microvasular and macrovascular complications in diabetes mellitus: Distinct or continuum? *Indian J Endocrinol Metab* **20**, 546-551 (2016).

322. D. T. Graves, R. A. Kayal, Diabetic complications and dysregulated innate immunity. *Front Biosci* **13**, 1227-1239 (2008).

323. L. J. Yan, Redox imbalance stress in diabetes mellitus: Role of the polyol pathway. *Animal Model Exp Med* **1**, 7-13 (2018).

324. A. D'Souza *et al.*, Pathogenesis and pathophysiology of accelerated atherosclerosis in the diabetic heart. *Mol Cell Biochem* **331**, 89-116 (2009).

325. F. K. Lutchmansingh *et al.*, Glutathione metabolism in type 2 diabetes and its relationship with microvascular complications and glycemia. *PLoS One* **13**, e0198626 (2018).

326. R. V. Sekhar *et al.*, Glutathione synthesis is diminished in patients with uncontrolled diabetes and restored by dietary supplementation with cysteine and glycine. *Diabetes Care* **34**, 162-167 (2011).

327. Y. Hamada *et al.*, Rapid formation of advanced glycation end products by intermediate metabolites of glycolytic pathway and polyol pathway. *Biochem Biophys Res Commun* **228**, 539-543 (1996).

328. S. Bansal *et al.*, Advanced glycation end products enhance reactive oxygen and nitrogen species generation in neutrophils in vitro. *Mol Cell Biochem* **361**, 289-296 (2012).

329. A. Gupta, A. K. Tripathi, R. L. Tripathi, S. V. Madhu, B. D. Banerjee, Advanced glycosylated end products-mediated activation of polymorphonuclear neutrophils in diabetes mellitus and associated oxidative stress. *Indian J Biochem Biophys* **44**, 373-378 (2007).

330. A. Bierhaus *et al.*, Diabetes-associated sustained activation of the transcription factor nuclear factor-kappaB. *Diabetes* **50**, 2792-2808 (2001).

331. A. C. Roberts, K. E. Porter, Cellular and molecular mechanisms of endothelial dysfunction in diabetes. *Diab Vasc Dis Res* **10**, 472-482 (2013).

332. E. Kontny, M. Ziolkowska, A. Ryzewska, W. Maslinski, Protein kinase c-dependent pathway is critical for the production of pro-inflammatory cytokines (TNF-alpha, IL-1beta, IL-6). *Cytokine* **11**, 839-848 (1999).

333. T. Inoguchi *et al.*, Protein kinase C-dependent increase in reactive oxygen species (ROS) production in vascular tissues of diabetes: role of vascular NAD(P)H oxidase. *J Am Soc Nephrol* **14**, S227-232 (2003).

334. A. Prasad, P. Bekker, S. Tsimikas, Advanced glycation end products and diabetic cardiovascular disease. *Cardiol Rev* **20**, 177-183 (2012).

335. O. M. Boland, C. C. Blackwell, B. F. Clarke, D. J. Ewing, Effects of ponalrestat, an aldose reductase inhibitor, on neutrophil killing of Escherichia coli and autonomic function in patients with diabetes mellitus. *Diabetes* **42**, 336-340 (1993).

336. K. V. Ramana, B. Friedrich, S. Srivastava, A. Bhatnagar, S. K. Srivastava, Activation of nuclear factor-kappaB by hyperglycemia in vascular smooth muscle cells is regulated by aldose reductase. *Diabetes* **53**, 2910-2920 (2004).

337. K. V. Ramana, A. Bhatnagar, S. K. Srivastava, Inhibition of aldose reductase attenuates TNF-alpha-induced expression of adhesion molecules in endothelial cells. *FASEB J* **18**, 1209-1218 (2004).

338. T. Inoguchi *et al.*, High glucose level and free fatty acid stimulate reactive oxygen species production through protein kinase C--dependent activation of NAD(P)H oxidase in cultured vascular cells. *Diabetes* **49**, 1939-1945 (2000).

339. M. A. Mazade, M. S. Edwards, Impairment of type III group B Streptococcus-stimulated superoxide production and opsonophagocytosis by neutrophils in diabetes. *Mol Genet Metab* **73**, 259-267 (2001).

340. K. S. Collison *et al.*, RAGE-mediated neutrophil dysfunction is evoked by advanced glycation end products (AGEs). *J Leukoc Biol* **71**, 433-444 (2002).

341. D. Saiepour, J. Sehlin, P. A. Oldenborg, Hyperglycemia-induced protein kinase C activation inhibits phagocytosis of C3b- and immunoglobulin g-opsonized yeast particles in normal human neutrophils. *Exp Diabesity Res* **4**, 125-132 (2003).

342. A. Kitaura *et al.*, Advanced glycation end-products reduce lipopolysaccharide uptake by macrophages. *PLoS One* **16**, e0245957 (2021).

343. E. Hatanaka, P. T. Monteagudo, M. S. Marrocos, A. Campa, Neutrophils and monocytes as potentially important sources of proinflammatory cytokines in diabetes. *Clin Exp Immunol* **146**, 443-447 (2006).

344. J. A. Ehses *et al.*, Increased number of islet-associated macrophages in type 2 diabetes. *Diabetes* **56**, 2356-2370 (2007).

345. A. S. Al-Goblan, M. A. Al-Alfi, M. Z. Khan, Mechanism linking diabetes mellitus and obesity. *Diabetes Metab Syndr Obes* **7**, 587-591 (2014).

346. W. He, T. Yuan, K. Maedler, Macrophage-associated pro-inflammatory state in human islets from obese individuals. *Nutr Diabetes* **9**, 36 (2019).

347. R. Njeim *et al.*, NETosis contributes to the pathogenesis of diabetes and its complications. *J Mol Endocrinol* **65**, R65-R76 (2020).

348. A. D. Pradhan, J. E. Manson, N. Rifai, J. E. Buring, P. M. Ridker, C-reactive protein, interleukin 6, and risk of developing type 2 diabetes mellitus. *JAMA* **286**, 327-334 (2001).

349. H. Madhumitha, V. Mohan, M. Deepa, S. Babu, V. Aravindhan, Increased Th1 and suppressed Th2 serum cytokine levels in subjects with diabetic coronary artery disease. *Cardiovasc Diabetol* **13**, 1 (2014).

350. I. Matia-Garcia *et al.*, Th1/Th2 Balance in Young Subjects: Relationship with Cytokine Levels and Metabolic Profile. *J Inflamm Res* **14**, 6587-6600 (2021).

351. M. Jagannathan-Bogdan *et al.*, Elevated proinflammatory cytokine production by a skewed T cell compartment requires monocytes and promotes inflammation in type 2 diabetes. *J Immunol* **186**, 1162-1172 (2011).

352. C. Zeng *et al.*, The imbalance of Th17/Th1/Tregs in patients with type 2 diabetes: relationship with metabolic factors and complications. *J Mol Med (Berl)* **90**, 175-186 (2012).

353. Y. C. Qiao *et al.*, Changes of Regulatory T Cells and of Proinflammatory and Immunosuppressive Cytokines in Patients with Type 2 Diabetes Mellitus: A Systematic Review and Meta-Analysis. *J Diabetes Res* **2016**, 3694957 (2016).

354. I. Nojima *et al.*, Dysfunction of CD8 + PD-1 + T cells in type 2 diabetes caused by the impairment of metabolism-immune axis. *Sci Rep* **10**, 14928 (2020).

355. Y. Jia, Y. Zhao, C. Li, R. Shao, The Expression of Programmed Death-1 on CD4+ and CD8+ T Lymphocytes in Patients with Type 2 Diabetes and Severe Sepsis. *PLoS One* **11**, e0159383 (2016).

356. B. Shi, X. Du, Q. Wang, Y. Chen, X. Zhang, Increased PD-1 on CD4(+)CD28(-) T cell and soluble PD-1 ligand-1 in patients with T2DM: association with atherosclerotic macrovascular diseases. *Metabolism* **62**, 778-785 (2013).

357. S. Dunachie, P. Chamnan, The double burden of diabetes and global infection in low and middle-income countries. *Trans. R. Soc. Trop. Med. Hyg.* **113**, 56-64 (2019).

358. L. M. Muller *et al.*, Increased risk of common infections in patients with type 1 and type 2 diabetes mellitus. *Clin Infect Dis* **41**, 281-288 (2005).

359. F. J. Cooke, Infections in people with diabetes. *Medicine* **47**, 110-113 (2019).

360. S. S. Kutlu *et al.*, Prevalence and risk factors for methicillin-resistant Staphylococcus aureus colonization in a diabetic outpatient population: a prospective cohort study. *Am J Infect Control* **40**, 365-368 (2012).

361. A. Reighard, D. Diekema, L. Wibbenmeyer, M. Ward, L. Herwaldt, Staphylococcus aureus nasal colonization and colonization or infection at other body sites in patients on a burn trauma unit. *Infect Control Hosp Epidemiol* **30**, 721-726 (2009).

362. D. K. Warren *et al.*, Epidemiology of methicillin-resistant Staphylococcus aureus colonization in a surgical intensive care unit. *Infect Control Hosp Epidemiol* **27**, 1032-1040 (2006).

363. B. Pallavan *et al.*, Comparison and correlation of candidal colonization in diabetic patients and normal individuals. *J Diabetes Metab Disord* **13**, 66 (2014).

364. M. Maisey, Evaluating the benefits of nuclear cardiology. *Q J Nucl Med* **40**, 47-54 (1996).

365. C. Cai *et al.*, Association between hepatitis B virus infection and diabetes mellitus: A meta-analysis. *Exp Ther Med* **10**, 693-698 (2015).

366. N. P. Kumar *et al.*, Type 2 diabetes mellitus is associated with altered CD8(+) T and natural killer cell function in pulmonary tuberculosis. *Immunology* **144**, 677-686 (2015).

367. E. Y. M. Lau *et al.*, Type 2 diabetes is associated with the accumulation of senescent T cells. *Clin Exp Immunol* **197**, 205-213 (2019).

368. J. M. Gregory *et al.*, COVID-19 Severity Is Tripled in the Diabetes Community: A Prospective Analysis of the Pandemic's Impact in Type 1 and Type 2 Diabetes. *Diabetes Care* **44**, 526-532 (2021).

369. Z. Wu, J. M. McGoogan, Characteristics of and Important Lessons From the Coronavirus Disease 2019 (COVID-19) Outbreak in China: Summary of a Report of 72314 Cases From the Chinese Center for Disease Control and Prevention. *JAMA* **323**, 1239-1242 (2020).

370. J. Yang *et al.*, Prevalence of comorbidities and its effects in patients infected with SARS-CoV-2: a systematic review and meta-analysis. *Int J Infect Dis* **94**, 91-95 (2020).

371. N. S. Htun *et al.*, Is diabetes a risk factor for a severe clinical presentation of dengue?--review and meta-analysis. *PLoS Negl. Trop. Dis.* **9**, e0003741 (2015).

372. I. K. Lee, C. J. Hsieh, C. T. Lee, J. W. Liu, Diabetic patients suffering dengue are at risk for development of dengue shock syndrome/severe dengue: Emphasizing the impacts of co-existing comorbidity(ies) and glycemic control on dengue severity. *J Microbiol Immunol Infect* **53**, 69-78 (2020).

373. A. Antonelli *et al.*, Hepatitis C virus infection and type 1 and type 2 diabetes mellitus. *World J Diabetes* **5**, 586-600 (2014).

374. K. Kawai, B. P. Yawn, Risk Factors for Herpes Zoster: A Systematic Review and Meta-analysis. *Mayo Clin Proc* **92**, 1806-1821 (2017).

375. S. R. Azar *et al.*, Aedes aegypti Shows Increased Susceptibility to Zika Virus via Both In Vitro and In Vivo Models of Type II Diabetes. *Viruses* **14**, (2022).

376. M. E. Woodman, R. G. Worth, R. M. Wooten, Capsule influences the deposition of critical complement C3 levels required for the killing of Burkholderia pseudomallei via NADPH-oxidase induction by human neutrophils. *PLoS One* **7**, e52276 (2012).

377. B. Kronsteiner *et al.*, Diabetes alters immune response patterns to acute melioidosis in humans. *Eur J Immunol* **49**, 1092-1106 (2019).

378. Z. Wang, M. Gerstein, M. Snyder, RNA-Seq: a revolutionary tool for transcriptomics. *Nat Rev Genet* **10**, 57-63 (2009).

379. M. C. Frith, M. Pheasant, J. S. Mattick, The amazing complexity of the human transcriptome. *Eur J Hum Genet* **13**, 894-897 (2005).

380. R. Lowe, N. Shirley, M. Bleackley, S. Dolan, T. Shafee, Transcriptomics technologies. *PLoS Comput Biol* **13**, e1005457 (2017).

381. Y. C. Wang, S. E. Peterson, J. F. Loring, Protein post-translational modifications and regulation of pluripotency in human stem cells. *Cell Res* **24**, 143-160 (2014).

382. R. Bumgarner, Overview of DNA microarrays: types, applications, and their future. *Curr Protoc Mol Biol* **Chapter 22**, Unit 22 21 (2013).

383. S. S. Chavan, M. A. Bauer, E. A. Peterson, C. J. Heuck, D. J. Johann, Jr., Towards the integration, annotation and association of historical microarray experiments with RNA-seq. *BMC Bioinformatics* **14 Suppl 14**, S4 (2013).

384. S. Behjati, P. S. Tarpey, What is next generation sequencing? *Arch Dis Child Educ Pract Ed* **98**, 236-238 (2013).

385. A. Roberts, H. Pimentel, C. Trapnell, L. Pachter, Identification of novel transcripts in annotated genomes using RNA-Seq. *Bioinformatics* **27**, 2325-2329 (2011).

386. A. Conesa *et al.*, A survey of best practices for RNA-seq data analysis. *Genome Biol* **17**, 13 (2016).

387. W. Zhao *et al.*, Comparison of RNA-Seq by poly (A) capture, ribosomal RNA depletion, and DNA microarray for expression profiling. *BMC Genomics* **15**, 419 (2014).

388. H. Jin, Z. Liu, A benchmark for RNA-seq deconvolution analysis under dynamic testing environments. *Genome Biol* **22**, 102 (2021).

389. D. Jovic *et al.*, Single-cell RNA sequencing technologies and applications: A brief overview. *Clin Transl Med* **12**, e694 (2022).

390. T. Ilicic *et al.*, Classification of low quality cells from single-cell RNA-seq data. *Genome Biol* **17**, 29 (2016).

391. M. D. Robinson, D. J. McCarthy, G. K. Smyth, edgeR: a Bioconductor package for differential expression analysis of digital gene expression data. *Bioinformatics* **26**, 139-140 (2010).

392. M. I. Love, W. Huber, S. Anders, Moderated estimation of fold change and dispersion for RNA-seq data with DESeq2. *Genome Biol* **15**, 550 (2014).

393. S. Anders, W. Huber, Differential expression analysis for sequence count data. *Genome Biol* **11**, R106 (2010).

394. C. W. Law *et al.*, RNA-seq analysis is easy as 1-2-3 with limma, Glimma and edgeR. *F1000Res* **5**, (2016).

395. M. A. Dillies *et al.*, A comprehensive evaluation of normalization methods for Illumina high-throughput RNA sequencing data analysis. *Brief Bioinform* **14**, 671-683 (2013).

396. N. J. Schurch *et al.*, How many biological replicates are needed in an RNA-seq experiment and which differential expression tool should you use? *RNA* **22**, 839-851 (2016).

397. D. Li *et al.*, An evaluation of RNA-seq differential analysis methods. *PLoS One* **17**, e0264246 (2022).

398. R. Bourgon, R. Gentleman, W. Huber, Independent filtering increases detection power for high-throughput experiments. *Proc Natl Acad Sci U S A* **107**, 9546-9551 (2010).

399. A. Liberzon *et al.*, The Molecular Signatures Database (MSigDB) hallmark gene set collection. *Cell Syst* **1**, 417-425 (2015).

400. B. Jassal *et al.*, The reactome pathway knowledgebase. *Nucleic Acids Res* **48**, D498-D503 (2020).

401. M. Kanehisa, M. Furumichi, M. Tanabe, Y. Sato, K. Morishima, KEGG: new perspectives on genomes, pathways, diseases and drugs. *Nucleic Acids Res* **45**, D353-D361 (2017).

402. C. The Gene Ontology, The Gene Ontology Resource: 20 years and still GOing strong. *Nucleic Acids Res* **47**, D330-D338 (2019).

403. G. Yu, Q. Y. He, ReactomePA: an R/Bioconductor package for reactome pathway analysis and visualization. *Mol Biosyst* **12**, 477-479 (2016).

404. G. Yu, L. G. Wang, Y. Han, Q. Y. He, clusterProfiler: an R package for comparing biological themes among gene clusters. *OMICS* **16**, 284-287 (2012).

405. E. I. Boyle *et al.*, GO::TermFinder--open source software for accessing Gene Ontology information and finding significantly enriched Gene Ontology terms associated with a list of genes. *Bioinformatics* **20**, 3710-3715 (2004).

406. V. K. Mootha *et al.*, PGC-1alpha-responsive genes involved in oxidative phosphorylation are coordinately downregulated in human diabetes. *Nat Genet* **34**, 267-273 (2003).

407. A. Subramanian *et al.*, Gene set enrichment analysis: a knowledge-based approach for interpreting genome-wide expression profiles. *Proc Natl Acad Sci U S A* **102**, 15545-15550 (2005).

408. V. S. Gennady Korotkevich, Nikolay Budin, Boris Shpak, Maxim N. Artyomov, Alexey Sergushichev, Fast gene set enrichment analysis. (2021).

409. A. Kramer, J. Green, J. Pollard, Jr., S. Tugendreich, Causal analysis approaches in Ingenuity Pathway Analysis. *Bioinformatics* **30**, 523-530 (2014).

410. C. A. Jackson, D. M. Castro, G. A. Saldi, R. Bonneau, D. Gresham, Gene regulatory network reconstruction using single-cell RNA sequencing of barcoded genotypes in diverse environments. *Elife* **9**, (2020).

411. M. Levine, E. H. Davidson, Gene regulatory networks for development. *Proc Natl Acad Sci U S A* **102**, 4936-4942 (2005).

412. M. Aldana, Boolean dynamics of networks with scale-free topology. *Physica D: Nonlinear Phenomena* **185**, 45-66 (2003).

413. A. D. Broido, A. Clauset, Scale-free networks are rare. *Nat Commun* **10**, 1017 (2019).

414. M. L. Siegal, D. E. Promislow, A. Bergman, Functional and evolutionary inference in gene networks: does topology matter? *Genetica* **129**, 83-103 (2007).

415. P. Langfelder, S. Horvath, WGCNA: an R package for weighted correlation network analysis. *BMC Bioinformatics* **9**, 559 (2008).

416. B. Zhang, S. Horvath, A general framework for weighted gene co-expression network analysis. *Stat Appl Genet Mol Biol* **4**, Article17 (2005).

417. S. Datta, S. Datta, Comparisons and validation of statistical clustering techniques for microarray gene expression data. *Bioinformatics* **19**, 459-466 (2003).

418. M. J. Mason, G. Fan, K. Plath, Q. Zhou, S. Horvath, Signed weighted gene co-expression network analysis of transcriptional regulation in murine embryonic stem cells. *BMC Genomics* **10**, 327 (2009).

419. A. Ghosh, A. Som, Decoding molecular markers and transcriptional circuitry of naive and primed states of human pluripotency. *Stem Cell Res* **53**, 102334 (2021).

420. J. A. Botia *et al.*, An additional k-means clustering step improves the biological features of WGCNA gene co-expression networks. *BMC Syst Biol* **11**, 47 (2017).

421. P. Langfelder. (2018, Signed and signed hybrid: what's the difference?: https://peterlangfelder.com/2018/11/25/__trashed/ (Accessed on: 20 June 2022)).

422. A. Hasankhani *et al.*, Differential Co-Expression Network Analysis Reveals Key Hub-High Traffic Genes as Potential Therapeutic Targets for COVID-19 Pandemic. *Front Immunol* **12**, 789317 (2021).

423. C. R. G. Willis *et al.*, Transcriptomic adaptation during skeletal muscle habituation to eccentric or concentric exercise training. *Sci Rep* **11**, 23930 (2021).

424. A. Hasankhani *et al.*, Integrated Network Analysis to Identify Key Modules and Potential Hub Genes Involved in Bovine Respiratory Disease: A Systems Biology Approach. *Front Genet* **12**, 753839 (2021).

425. P. Langfelder, B. Zhang, S. Horvath, Defining clusters from a hierarchical cluster tree: the Dynamic Tree Cut package for R. *Bioinformatics* **24**, 719-720 (2008).

426. P. Langfelder, S. Horvath, Eigengene networks for studying the relationships between co-expression modules. *BMC Syst Biol* **1**, 54 (2007).

427. T. E. Sweeney, L. Braviak, C. M. Tato, P. Khatri, Genome-wide expression for diagnosis of pulmonary tuberculosis: a multicohort analysis. *Lancet Respir Med* **4**, 213-224 (2016).

428. T. Yimthin *et al.*, Blood transcriptomics to characterize key biological pathways and identify biomarkers for predicting mortality in melioidosis. *Emerg Microbes Infect* **10**, 8-18 (2021).

429. T. Barichello, J. S. Generoso, M. Singer, F. Dal-Pizzol, Biomarkers for sepsis: more than just fever and leukocytosis-a narrative review. *Crit Care* **26**, 14 (2022).

430. C. H. Chin *et al.*, cytoHubba: identifying hub objects and sub-networks from complex interactome. *BMC Syst Biol* **8 Suppl 4**, S11 (2014).

431. A. M. Newman *et al.*, Determining cell type abundance and expression from bulk tissues with digital cytometry. *Nat Biotechnol* **37**, 773-782 (2019).

432. J. Racle, K. de Jonge, P. Baumgaertner, D. E. Speiser, D. Gfeller, Simultaneous enumeration of cancer and immune cell types from bulk tumor gene expression data. *Elife* **6**, (2017).

433. E. Becht *et al.*, Estimating the population abundance of tissue-infiltrating immune and stromal cell populations using gene expression. *Genome Biol* **17**, 218 (2016).

434. B. Li *et al.*, Comprehensive analyses of tumor immunity: implications for cancer immunotherapy. *Genome Biol* **17**, 174 (2016).

435. D. Aran, Z. Hu, A. J. Butte, xCell: digitally portraying the tissue cellular heterogeneity landscape. *Genome Biol* **18**, 220 (2017).

436. G. Sturm *et al.*, Comprehensive evaluation of transcriptome-based cell-type quantification methods for immuno-oncology. *Bioinformatics* **35**, i436-i445 (2019).

437. A. M. Newman *et al.*, Robust enumeration of cell subsets from tissue expression profiles. *Nat Methods* **12**, 453-457 (2015).

438. P. Kumar Nathella, S. Babu, Influence of diabetes mellitus on immunity to human tuberculosis. *Immunology* **152**, 13-24 (2017).

439. in *Use of Glycated Haemoglobin (HbA1c) in the Diagnosis of Diabetes Mellitus: Abbreviated Report of a WHO Consultation*. (Geneva, 2011).

440. A. Dobin *et al.*, STAR: ultrafast universal RNA-seq aligner. *Bioinformatics* **29**, 15-21 (2013).

441. Y. Liao, G. K. Smyth, W. Shi, featureCounts: an efficient general purpose program for assigning sequence reads to genomic features. *Bioinformatics* **30**, 923-930 (2014).

442. H. Varet, L. Brillet-Gueguen, J. Y. Coppee, M. A. Dillies, SARTools: A DESeq2- and EdgeR-Based R Pipeline for Comprehensive Differential Analysis of RNA-Seq Data. *PLoS One* **11**, e0157022 (2016).

443. A. Schroeder *et al.*, The RIN: an RNA integrity number for assigning integrity values to RNA measurements. *BMC Mol Biol* **7**, 3 (2006).

444. P. J. Cock, C. J. Fields, N. Goto, M. L. Heuer, P. M. Rice, The Sanger FASTQ file format for sequences with quality scores, and the Solexa/Illumina FASTQ variants. *Nucleic Acids Res* **38**, 1767-1771 (2010).

445. C. F. Rodrigues, M. E. Rodrigues, M. Henriques, Candida sp. Infections in Patients with Diabetes Mellitus. *J Clin Med* **8**, (2019).

446. X. Lv, Y. Gao, T. Dong, L. Yang, Role of Natural Killer T (NKT) Cells in Type II Diabetes-Induced Vascular Injuries. *Med Sci Monit* **24**, 8322-8332 (2018).

447. H. A. Hadi, J. A. Suwaidi, Endothelial dysfunction in diabetes mellitus. *Vasc Health Risk Manag* **3**, 853-876 (2007).

448. M. M. Bahgat, D. R. Ibrahim, Proinflammatory cytokine polarization in type 2 diabetes. *Cent Eur J Immunol* **45**, 170-175 (2020).

449. V. Grossmann *et al.*, Profile of the Immune and Inflammatory Response in Individuals With Prediabetes and Type 2 Diabetes. *Diabetes Care* **38**, 1356-1364 (2015).

450. R. Mesia *et al.*, Systemic inflammatory responses in patients with type 2 diabetes with chronic periodontitis. *BMJ Open Diabetes Res Care* **4**, e000260 (2016).

451. A. Nareika *et al.*, High glucose and interferon gamma synergistically stimulate MMP-1 expression in U937 macrophages by increasing transcription factor STAT1 activity. *Atherosclerosis* **202**, 363-371 (2009).

452. C. Silvestre-Roig *et al.*, Atherosclerotic plaque destabilization: mechanisms, models, and therapeutic strategies. *Circ Res* **114**, 214-226 (2014).

453. C. Mertoglu, M. Gunay, Neutrophil-Lymphocyte ratio and Platelet-Lymphocyte ratio as useful predictive markers of prediabetes and diabetes mellitus. *Diabetes Metab Syndr* **11 Suppl 1**, S127-S131 (2017).

454. M. Delamaire *et al.*, Impaired leucocyte functions in diabetic patients. *Diabet Med* **14**, 29-34 (1997).

455. N. Ozsoy, H. Bostanci, C. Ayvali, The investigation of the ultrastructural neutrophil changes in alloxan-induced diabetes in rats: response to a chemotactic challenge. *Cell Biochem Funct* **22**, 81-87 (2004).

456. J. M. Alexiewicz, D. Kumar, M. Smogorzewski, M. Klin, S. G. Massry, Polymorphonuclear leukocytes in non-insulin-dependent diabetes mellitus: abnormalities in metabolism and function. *Ann Intern Med* **123**, 919-924 (1995).

457. N. Ridzuan *et al.*, Preliminary study on overproduction of reactive oxygen species by neutrophils in diabetes mellitus. *World J Diabetes* **7**, 271-278 (2016).

458. E. A. Bostrom, A. Tarkowski, M. Bokarewa, Resistin is stored in neutrophil granules being released upon challenge with inflammatory stimuli. *Biochim Biophys Acta* **1793**, 1894-1900 (2009).

459. C. M. Steppan *et al.*, The hormone resistin links obesity to diabetes. *Nature* **409**, 307-312 (2001).

460. W. C. Chao *et al.*, Increased resistin may suppress reactive oxygen species production and inflammasome activation in type 2 diabetic patients with pulmonary tuberculosis infection. *Microbes Infect* **17**, 195-204 (2015).

461. S. R. Thom *et al.*, Neutrophil microparticle production and inflammasome activation by hyperglycemia due to cytoskeletal instability. *J Biol Chem* **292**, 18312-18324 (2017).

462. T. S. Cohen *et al.*, Staphylococcus aureus drives expansion of low-density neutrophils in diabetic mice. *J Clin Invest* **129**, 2133-2144 (2019).

463. Y. Kumagai *et al.*, Surgical Stress Increases Circulating Low-Density Neutrophils Which May Promote Tumor Recurrence. *J Surg Res* **246**, 52-61 (2020).

464. D. S. Schwarz, M. D. Blower, The endoplasmic reticulum: structure, function and response to cellular signaling. *Cell Mol Life Sci* **73**, 79-94 (2016).

465. D. L. Eizirik, A. K. Cardozo, M. Cnop, The role for endoplasmic reticulum stress in diabetes mellitus. *Endocr Rev* **29**, 42-61 (2008).

466. B. M. Brooks-Worrell, J. P. Palmer, Setting the Stage for Islet Autoimmunity in Type 2 Diabetes: Obesity-Associated Chronic Systemic Inflammation and Endoplasmic Reticulum (ER) Stress. *Diabetes Care* **42**, 2338-2346 (2019).

467. A. Goel, H. Chiu, J. Felton, J. P. Palmer, B. Brooks-Worrell, T-cell responses to islet antigens improves detection of autoimmune diabetes and identifies patients with more severe beta-cell lesions in phenotypic type 2 diabetes. *Diabetes* **56**, 2110-2115 (2007).

468. D. A. Dance, D. Limmathurotsakul, Global Burden and Challenges of Melioidosis. *Trop Med Infect Dis* **3**, (2018).

469. M. L. Meizlish *et al.*, A neutrophil activation signature predicts critical illness and mortality in COVID-19. *Blood Adv* **5**, 1164-1177 (2021).

470. P. E. Parsons, M. A. Matthay, L. B. Ware, M. D. Eisner, L. B. I. A. R. D. S. C. T. N. National Heart, Elevated plasma levels of soluble TNF receptors are associated with morbidity and mortality in patients with acute lung injury. *Am J Physiol Lung Cell Mol Physiol* **288**, L426-431 (2005).

471. J. R. Tisoncik *et al.*, Into the eye of the cytokine storm. *Microbiol Mol Biol Rev* **76**, 16-32 (2012).

472. I. J. Jensen, F. V. Sjaastad, T. S. Griffith, V. P. Badovinac, Sepsis-Induced T Cell Immunoparalysis: The Ins and Outs of Impaired T Cell Immunity. *J Immunol* **200**, 1543-1553 (2018).

473. K. P. Chung *et al.*, Severe lymphopenia is associated with elevated plasma interleukin-15 levels and increased mortality during severe sepsis. *Shock* **43**, 569-575 (2015).

474. R. S. Hotchkiss *et al.*, Prevention of lymphocyte cell death in sepsis improves survival in mice. *Proc Natl Acad Sci U S A* **96**, 14541-14546 (1999).

475. J. Unsinger *et al.*, The role of TCR engagement and activation-induced cell death in sepsis-induced T cell apoptosis. *J Immunol* **177**, 7968-7973 (2006).

476. Y. J. Choi *et al.*, Impaired polyfunctionality of CD8(+) T cells in severe sepsis patients with human cytomegalovirus reactivation. *Exp Mol Med* **49**, e382 (2017).

477. H. Turner, J. P. Kinet, Signalling through the high-affinity IgE receptor Fc epsilonRI. *Nature* **402**, B24-30 (1999).

478. K. Dong *et al.*, FCER1G positively relates to macrophage infiltration in clear cell renal cell carcinoma and contributes to unfavorable prognosis by regulating tumor immunity. *BMC Cancer* **22**, 140 (2022).

479. V. Duhan *et al.*, NK cell-intrinsic FcepsilonRIgamma limits CD8+ T-cell expansion and thereby turns an acute into a chronic viral infection. *PLoS Pathog* **15**, e1007797 (2019).

480. Y. X. Yang, L. Li, Identification of potential biomarkers of sepsis using bioinformatics analysis. *Exp Ther Med* **13**, 1689-1696 (2017).

481. F. Pinheiro da Silva *et al.*, CD16 promotes Escherichia coli sepsis through an FcR gamma inhibitory pathway that prevents phagocytosis and facilitates inflammation. *Nat Med* **13**, 1368-1374 (2007).

482. D. G. Mashek, L. O. Li, R. A. Coleman, Long-chain acyl-CoA synthetases and fatty acid channeling. *Future Lipidol* **2**, 465-476 (2007).

483. J. Roelands *et al.*, Long-Chain Acyl-CoA Synthetase 1 Role in Sepsis and Immunity: Perspectives From a Parallel Review of Public Transcriptome Datasets and of the Literature. *Front Immunol* **10**, 2410 (2019).

484. P. Khaenam *et al.*, A transcriptomic reporter assay employing neutrophils to measure immunogenic activity of septic patients' plasma. *J Transl Med* **12**, 65 (2014).

485. F. Al-Rashed *et al.*, TNF-alpha Induces a Pro-Inflammatory Phenotypic Shift in Monocytes through ACSL1: Relevance to Metabolic Inflammation. *Cell Physiol Biochem* **52**, 397-407 (2019).

486. M. J. Kim *et al.*, Caseation of human tuberculosis granulomas correlates with elevated host lipid metabolism. *EMBO Mol Med* **2**, 258-274 (2010).

487. K. B. Rubinow *et al.*, Acyl-CoA synthetase 1 is induced by Gram-negative bacteria and lipopolysaccharide and is required for phospholipid turnover in stimulated macrophages. *J Biol Chem* **288**, 9957-9970 (2013).

488. A. Tesse, P. Gena, M. Rutzler, G. Calamita, Ablation of Aquaporin-9 Ameliorates the Systemic Inflammatory Response of LPS-Induced Endotoxic Shock in Mouse. *Cells* **10**, (2021).

489. L. F. Mariajoseph-Antony *et al.*, Role of Aquaporins in Inflammation-a Scientific Curation. *Inflammation* **43**, 1599-1610 (2020).

490. S. De Santis *et al.*, Aquaporin 9 Contributes to the Maturation Process and Inflammatory Cytokine Secretion of Murine Dendritic Cells. *Front Immunol* **9**, 2355 (2018).

491. A. Matsushima, H. Ogura, T. Koh, T. Shimazu, H. Sugimoto, Enhanced expression of aquaporin 9 in activated polymorphonuclear leukocytes in patients with systemic inflammatory response syndrome. *Shock* **42**, 322-326 (2014).

492. S. I. Miller, R. K. Ernst, M. W. Bader, LPS, TLR4 and infectious disease diversity. *Nat Rev Microbiol* **3**, 36-46 (2005).

493. A. Savva, T. Roger, Targeting toll-like receptors: promising therapeutic strategies for the management of sepsis-associated pathology and infectious diseases. *Front Immunol* **4**, 387 (2013).

494. V. Kumar, Toll-like receptors in sepsis-associated cytokine storm and their endogenous negative regulators as future immunomodulatory targets. *Int Immunopharmacol* **89**, 107087 (2020).

495. S. W. Wright *et al.*, Lactoferrin is a dynamic protein in human melioidosis and is a TLR4-dependent driver of TNF-alpha release in Burkholderia thailandensis infection in vitro. *PLoS Negl Trop Dis* **14**, e0008495 (2020).

496. B. Verstak *et al.*, MyD88 adapter-like (Mal)/TIRAP interaction with TRAF6 is critical for TLR2- and TLR4-mediated NF-kappaB proinflammatory responses. *J Biol Chem* **284**, 24192-24203 (2009).

497. M. J. Delano *et al.*, MyD88-dependent expansion of an immature GR-1(+)CD11b(+) population induces T cell suppression and Th2 polarization in sepsis. *J Exp Med* **204**, 1463-1474 (2007).

498. L. Yang, C. M. Edwards, G. R. Mundy, Gr-1+CD11b+ myeloid-derived suppressor cells: formidable partners in tumor metastasis. *J Bone Miner Res* **25**, 1701-1706 (2010).

499. B. J. Currie *et al.*, The Darwin Prospective Melioidosis Study: a 30-year prospective, observational investigation. *Lancet Infect Dis* **21**, 1737-1746 (2021).

500. M. Sunpuwan, S. Punpuing, W. Jaruruengpaisan, J. Kinsman, H. Wertheim, What is in the drug packet?: access and use of non-prescribed poly-pharmaceutical packs (Yaa Chud) in the community in Thailand. *BMC Public Health* **19**, 971 (2019).

501. N. Klinsunthorn, A. Petsom, T. Nhujak, Determination of steroids adulterated in liquid herbal medicines using QuEChERS sample preparation and high-performance liquid chromatography. *J Pharm Biomed Anal* **55**, 1175-1178 (2011).

502. W. Chierakul *et al.*, Short report: disease severity and outcome of melioidosis in HIV coinfected individuals. *Am J Trop Med Hyg* **73**, 1165-1166 (2005).

503. S. H. E. Kaufmann, Protection against tuberculosis: cytokines, T cells, and macrophages. *Ann Rheum Dis* **61**, 54-58 (2002).

504. L. Heitmann *et al.*, The IL-13/IL-4Ralpha axis is involved in tuberculosis-associated pathology. *J Pathol* **234**, 338-350 (2014).

505. R. van Crevel, H. M. Dockrell, T. Consortium, TANDEM: understanding diabetes and tuberculosis. *Lancet Diabetes Endocrinol* **2**, 270-272 (2014).

506. C. Eckold *et al.*, Impact of Intermediate Hyperglycemia and Diabetes on Immune Dysfunction in Tuberculosis. *Clin Infect Dis* **72**, 69-78 (2021).

507. G. Roglic, World Health Organization, *Global report on diabetes*. (World Health Organization, Geneva, Switzerland, 2016), pp. 86 pages.

508. A. Javid *et al.*, Hyperglycemia Impairs Neutrophil-Mediated Bacterial Clearance in Mice Infected with the Lyme Disease Pathogen. *PLoS One* **11**, e0158019 (2016).

509. W. M. T. Kuwabara, C. N. F. Yokota, R. Curi, T. C. Alba-Loureiro, Obesity and Type 2 Diabetes mellitus induce lipopolysaccharide tolerance in rat neutrophils. *Sci Rep* **8**, 17534 (2018).

510. A. Lecube, G. Pachon, J. Petriz, C. Hernandez, R. Simo, Phagocytic activity is impaired in type 2 diabetes mellitus and increases after metabolic improvement. *PLoS One* **6**, e23366 (2011).

511. J. A. Beckman, M. A. Creager, P. Libby, Diabetes and atherosclerosis: epidemiology, pathophysiology, and management. *JAMA* **287**, 2570-2581 (2002).

512. W. M. Nauseef, N. Borregaard, Neutrophils at work. *Nat Immunol* **15**, 602-611 (2014).

513. P. Lacy, Mechanisms of degranulation in neutrophils. *Allergy Asthma Clin Immunol* **2**, 98-108 (2006).

514. P. Song *et al.*, Association of Plasma Myeloperoxidase Level with Risk of Coronary Artery Disease in Patients with Type 2 Diabetes. *Dis Markers* **2015**, 761939 (2015).

515. L. Peng *et al.*, Increased concentrations of myeloperoxidase in serum and serum extracellular vesicles are associated with type 2 diabetes mellitus. *Clin Chim Acta* **522**, 70-76 (2021).

516. J. J. Wiersma *et al.*, Diabetes mellitus type 2 is associated with higher levels of myeloperoxidase. *Med Sci Monit* **14**, CR406-410 (2008).

517. Y. Kataoka *et al.*, Myeloperoxidase levels predict accelerated progression of coronary atherosclerosis in diabetic patients: insights from intravascular ultrasound. *Atherosclerosis* **232**, 377-383 (2014).

518. U. Bank *et al.*, Selective proteolytic cleavage of IL-2 receptor and IL-6 receptor ligand binding chains by neutrophil-derived serine proteases at foci of inflammation. *J Interferon Cytokine Res* **19**, 1277-1287 (1999).

519. T. R. Sippel *et al.*, Arginase I release from activated neutrophils induces peripheral immunosuppression in a murine model of stroke. *J Cereb Blood Flow Metab* **35**, 1657-1663 (2015).

520. R. A. Ali, L. M. Wuescher, R. G. Worth, Platelets: essential components of the immune system. *Curr Trends Immunol* **16**, 65-78 (2015).

521. E. M. Golebiewska, A. W. Poole, Platelet secretion: From haemostasis to wound healing and beyond. *Blood Rev* **29**, 153-162 (2015).

522. A. Zarbock, R. K. Polanowska-Grabowska, K. Ley, Platelet-neutrophil-interactions: linking hemostasis and inflammation. *Blood Rev* **21**, 99-111 (2007).

523. C. A. Gleissner, P. von Hundelshausen, K. Ley, Platelet chemokines in vascular disease. *Arterioscler Thromb Vasc Biol* **28**, 1920-1927 (2008).

524. S. Fateh-Moghadam *et al.*, Platelet degranulation is associated with progression of intima-media thickness of the common carotid artery in patients with diabetes mellitus type 2. *Arterioscler Thromb Vasc Biol* **25**, 1299-1303 (2005).

525. N. Kakouros, J. J. Rade, A. Kourliouros, J. R. Resar, Platelet function in patients with diabetes mellitus: from a theoretical to a practical perspective. *Int J Endocrinol* **2011**, 742719 (2011).

526. M. J. Kraakman *et al.*, Neutrophil-derived S100 calcium-binding proteins A8/A9 promote reticulated thrombocytosis and atherogenesis in diabetes. *J Clin Invest* **127**, 2133-2147 (2017).

527. L. C. Burzynski *et al.*, The Coagulation and Immune Systems Are Directly Linked through the Activation of Interleukin-1alpha by Thrombin. *Immunity* **50**, 1033-1042 e1036 (2019).

528. Y. Chung *et al.*, Critical regulation of early Th17 cell differentiation by interleukin-1 signaling. *Immunity* **30**, 576-587 (2009).

529. Y. Zheng, M. Humphry, J. J. Maguire, M. R. Bennett, M. C. Clarke, Intracellular interleukin-1 receptor 2 binding prevents cleavage and activity of interleukin-1alpha, controlling necrosis-induced sterile inflammation. *Immunity* **38**, 285-295 (2013).

530. P. R. Nagareddy *et al.*, Hyperglycemia promotes myelopoiesis and impairs the resolution of atherosclerosis. *Cell Metab* **17**, 695-708 (2013).

531. M. C. Flynn *et al.*, Transient Intermittent Hyperglycemia Accelerates Atherosclerosis by Promoting Myelopoiesis. *Circ Res* **127**, 877-892 (2020).

532. G. A. Rook, Th2 cytokines in susceptibility to tuberculosis. *Curr Mol Med* **7**, 327-337 (2007).

533. S. Ashenafi *et al.*, Progression of clinical tuberculosis is associated with a Th2 immune response signature in combination with elevated levels of SOCS3. *Clin Immunol* **151**, 84-99 (2014).

534. J. L. Flynn *et al.*, An essential role for interferon gamma in resistance to Mycobacterium tuberculosis infection. *J Exp Med* **178**, 2249-2254 (1993).

535. A. M. Caruso *et al.*, Mice deficient in CD4 T cells have only transiently diminished levels of IFN-gamma, yet succumb to tuberculosis. *J Immunol* **162**, 5407-5416 (1999).

536. H. Lu *et al.*, High glucose induces upregulation of scavenger receptors and promotes maturation of dendritic cells. *Cardiovasc Diabetol* **12**, 80 (2013).

537. K. Fukuhara-Takaki, M. Sakai, Y. Sakamoto, M. Takeya, S. Horiuchi, Expression of class A scavenger receptor is enhanced by high glucose in vitro and under diabetic conditions in vivo: one mechanism for an increased rate of atherosclerosis in diabetes. *J Biol Chem* **280**, 3355-3364 (2005).

538. X. Huang, G. Liu, J. Guo, Z. Su, The PI3K/AKT pathway in obesity and type 2 diabetes. *Int J Biol Sci* **14**, 1483-1496 (2018).

539. M. Zheng, P. Wang, Role of insulin receptor substance-1 modulating PI3K/Akt insulin signaling pathway in Alzheimer's disease. *3 Biotech* **11**, 179 (2021).

540. J. Szendroedi *et al.*, Role of diacylglycerol activation of PKCtheta in lipid-induced muscle insulin resistance in humans. *Proc Natl Acad Sci U S A* **111**, 9597-9602 (2014).

541. P. Barma *et al.*, Lipid induced overexpression of NF-kappaB in skeletal muscle cells is linked to insulin resistance. *Biochim Biophys Acta* **1792**, 190-200 (2009).

542. S. Varma *et al.*, Hyperglycemia alters PI3k and Akt signaling and leads to endothelial cell proliferative dysfunction. *Am J Physiol Heart Circ Physiol* **289**, H1744-1751 (2005).

543. D. Hamamdzic *et al.*, Akt pathway is hypoactivated by synergistic actions of diabetes mellitus and hypercholesterolemia resulting in advanced coronary artery disease. *Am J Physiol Heart Circ Physiol* **299**, H699-706 (2010).

544. A. Opasawatchai *et al.*, Neutrophil Activation and Early Features of NET Formation Are Associated With Dengue Virus Infection in Human. *Front Immunol* **9**, 3007 (2018).

545. A. Therrien *et al.*, Recruitment of activated neutrophils correlates with disease severity in adult Crohn's disease. *Clin Exp Immunol* **195**, 251-264 (2019).

546. R. Sun *et al.*, Dysfunction of low-density neutrophils in peripheral circulation in patients with sepsis. *Sci Rep* **12**, 685 (2022).

547. A. J. van Oostrom, J. P. van Wijk, T. P. Sijmonsma, T. J. Rabelink, M. Castro Cabezas, Increased expression of activation markers on monocytes and neutrophils in type 2 diabetes. *Neth J Med* **62**, 320-325 (2004).

548. P. Horvath *et al.*, Fasting glucose level modulates cell surface expression of CD11b and CD66b in granulocytes and monocytes of patients with type 2 diabetes. *J Investig Med* **61**, 972-977 (2013).

549. P. Elsbach, J. Weiss, Role of the bactericidal/permeability-increasing protein in host defence. *Curr Opin Immunol* **10**, 45-49 (1998).

550. R. Savedra, Jr., R. L. Delude, R. R. Ingalls, M. J. Fenton, D. T. Golenbock, Mycobacterial lipoarabinomannan recognition requires a receptor that shares components of the endotoxin signaling system. *J Immunol* **157**, 2549-2554 (1996).

551. H. Nishimura *et al.*, Bactericidal/permeability-increasing protein promotes complement activation for neutrophil-mediated phagocytosis on bacterial surface. *Immunology* **103**, 519-525 (2001).

552. N. P. Juffermans *et al.*, Serum concentrations of lipopolysaccharide activity-modulating proteins during tuberculosis. *J Infect Dis* **178**, 1839-1842 (1998).

553. A. Balakrishnan, S. A. Marathe, M. Joglekar, D. Chakravortty, Bactericidal/permeability increasing protein: a multifaceted protein with functions beyond LPS neutralization. *Innate Immun* **19**, 339-347 (2013).

554. E. Esteve *et al.*, Circulating bactericidal/permeability-increasing protein (BPI) is associated with serum lipids and endothelial function. *Thromb Haemost* **103**, 780-787 (2010).

555. S. Yu *et al.*, Positive correlations between plasma BPI level and MPO-DNA and S100A8/A9 in myocardial infarction. *Platelets*, 1-9 (2021).

556. A. Navratilova *et al.*, S100A11 (calgizzarin) is released via NETosis in rheumatoid arthritis (RA) and stimulates IL-6 and TNF secretion by neutrophils. *Sci Rep* **11**, 6063 (2021).

557. L. Zhang, T. Zhu, H. Miao, B. Liang, The Calcium Binding Protein S100A11 and Its Roles in Diseases. *Front Cell Dev Biol* **9**, 693262 (2021).

558. D. L. Cecil, R. A. Terkeltaub, Arterial calcification is driven by RAGE in Enpp1-/- mice. *J Vasc Res* **48**, 227-235 (2011).

559. J. J. Kim, Z. Lipatova, N. Segev, TRAPP Complexes in Secretion and Autophagy. *Front Cell Dev Biol* **4**, 20 (2016).

560. J. Brown, M. A. Wallet, B. Krastins, D. Sarracino, M. M. Goodenow, Proteome bioprofiles distinguish between M1 priming and activation states in human macrophages. *J Leukoc Biol* **87**, 655-662 (2010).

561. A. V. Washington *et al.*, TREM-like transcript-1 protects against inflammation-associated hemorrhage by facilitating platelet aggregation in mice and humans. *J Clin Invest* **119**, 1489-1501 (2009).

562. M. Derive *et al.*, Soluble TREM-like transcript-1 regulates leukocyte activation and controls microbial sepsis. *J Immunol* **188**, 5585-5592 (2012).

563. C. W. Smith *et al.*, TREM-like transcript 1: a more sensitive marker of platelet activation than P-selectin in humans and mice. *Blood Adv* **2**, 2072-2078 (2018).

564. L. Shen *et al.*, P-selectin (CD62P) and soluble TREM-like transcript-1 (sTLT-1) are associated with coronary artery disease: a case control study. *BMC Cardiovasc Disord* **20**, 387 (2020).

565. M. V. Joglekar, J. Ware, J. Xu, M. E. Fitzgerald, T. K. Gartner, Platelets, glycoprotein Ib-IX, and von Willebrand factor are required for FeCl(3)-induced occlusive thrombus formation in the inferior vena cava of mice. *Platelets* **24**, 205-212 (2013).

566. N. Li, Platelet-lymphocyte cross-talk. *J Leukoc Biol* **83**, 1069-1078 (2008).

567. S. C. Starossom *et al.*, Platelets Play Differential Role During the Initiation and Progression of Autoimmune Neuroinflammation. *Circ Res* **117**, 779-792 (2015).

568. M. Kanoksil, A. Jatapai, S. J. Peacock, D. Limmathurotsakul, Epidemiology, microbiology and mortality associated with community-acquired bacteremia in northeast Thailand: a multicenter surveillance study. *PLoS One* **8**, e54714 (2013).

569. F. Venet, G. Monneret, Advances in the understanding and treatment of sepsis-induced immunosuppression. *Nat Rev Nephrol* **14**, 121-137 (2018).

570. M. J. Delano, P. A. Ward, The immune system's role in sepsis progression, resolution, and long-term outcome. *Immunol Rev* **274**, 330-353 (2016).

571. P. Chaichana *et al.*, Antibodies in Melioidosis: The Role of the Indirect Hemagglutination Assay in Evaluating Patients and Exposed Populations. *Am J Trop Med Hyg* **99**, 1378-1385 (2018).

572. V. Wuthiekanun *et al.*, Development of antibodies to Burkholderia pseudomallei during childhood in melioidosis-endemic northeast Thailand. *Am J Trop Med Hyg* **74**, 1074-1075 (2006).

573. T. E. West *et al.*, Impaired TLR5 functionality is associated with survival in melioidosis. *J. Immunol.* **190**, 3373-3379 (2013).

574. T. E. West *et al.*, NLRC4 and TLR5 each contribute to host defense in respiratory melioidosis. *PLoS Negl Trop Dis* **8**, e3178 (2014).

575. D. Braga *et al.*, A longitudinal study highlights shared aspects of the transcriptomic response to cardiogenic and septic shock. *Crit Care* **23**, 414 (2019).

576. R. P. Dellinger *et al.*, Surviving Sepsis Campaign: international guidelines for management of severe sepsis and septic shock, 2012. *Intensive Care Med* **39**, 165-228 (2013).

577. X. Liu *et al.*, Prognostic Significance of Neutrophil-to-Lymphocyte Ratio in Patients with Sepsis: A Prospective Observational Study. *Mediators Inflamm* **2016**, 8191254 (2016).

578. L. R. Ljungstrom, G. Jacobsson, R. Andersson, Neutrophil-lymphocyte count ratio as a biomarker of severe sepsis in Escherichia coli infections in adults. *Critical Care* **17**, P25 (2013).

579. M. Warny, J. Helby, B. G. Nordestgaard, H. Birgens, S. E. Bojesen, Lymphopenia and risk of infection and infection-related death in 98,344 individuals from a prospective Danish population-based study. *PLoS Med* **15**, e1002685 (2018).

580. S. K. Mittal, P. A. Roche, Suppression of antigen presentation by IL-10. *Curr Opin Immunol* **34**, 22-27 (2015).

581. K. R. Kasten, J. T. Muenzer, C. C. Caldwell, Neutrophils are significant producers of IL-10 during sepsis. *Biochem Biophys Res Commun* **393**, 28-31 (2010).

582. X. Li *et al.*, Interleukin-10/lymphocyte ratio predicts mortality in severe septic patients. *PLoS One* **12**, e0179050 (2017).

583. E. Tamayo *et al.*, Pro- and anti-inflammatory responses are regulated simultaneously from the first moments of septic shock. *Eur Cytokine Netw* **22**, 82-87 (2011).

584. M. E. Keir, M. J. Butte, G. J. Freeman, A. H. Sharpe, PD-1 and its ligands in tolerance and immunity. *Annu Rev Immunol* **26**, 677-704 (2008).

585. X. Huang *et al.*, PD-1 expression by macrophages plays a pathologic role in altering microbial clearance and the innate inflammatory response to sepsis. *Proc Natl Acad Sci U S A* **106**, 6303-6308 (2009).

586. I. Sabroe, E. C. Jones, L. R. Usher, M. K. Whyte, S. K. Dower, Toll-like receptor (TLR)2 and TLR4 in human peripheral blood granulocytes: a critical role for

monocytes in leukocyte lipopolysaccharide responses. *J Immunol* **168**, 4701-4710 (2002).

587. J. C. Alves-Filho *et al.*, Regulation of chemokine receptor by Toll-like receptor 2 is critical to neutrophil migration and resistance to polymicrobial sepsis. *Proc Natl Acad Sci U S A* **106**, 4018-4023 (2009).

588. J. C. Alves-Filho *et al.*, Interleukin-33 attenuates sepsis by enhancing neutrophil influx to the site of infection. *Nat Med* **16**, 708-712 (2010).

589. R. S. Hotchkiss *et al.*, Accelerated lymphocyte death in sepsis occurs by both the death receptor and mitochondrial pathways. *J Immunol* **174**, 5110-5118 (2005).

590. Y. Y. Luan, Y. M. Yao, X. Z. Xiao, Z. Y. Sheng, Insights into the apoptotic death of immune cells in sepsis. *J Interferon Cytokine Res* **35**, 17-22 (2015).

591. J. Zheng, Y. Liu, Y. L. Lau, W. Tu, gammadelta-T cells: an unpolished sword in human anti-infection immunity. *Cell Mol Immunol* **10**, 50-57 (2013).

592. J. M. Coquet *et al.*, Diverse cytokine production by NKT cell subsets and identification of an IL-17-producing CD4-NK1.1- NKT cell population. *Proc Natl Acad Sci U S A* **105**, 11287-11292 (2008).

593. B. Martin, K. Hirota, D. J. Cua, B. Stockinger, M. Veldhoen, Interleukin-17-producing gammadelta T cells selectively expand in response to pathogen products and environmental signals. *Immunity* **31**, 321-330 (2009).

594. C. L. Langrish *et al.*, IL-12 and IL-23: master regulators of innate and adaptive immunity. *Immunol Rev* **202**, 96-105 (2004).

595. X. Wang *et al.*, Characterization of human peripheral blood gammadelta T cells in patients with sepsis. *Exp Ther Med* **19**, 3698-3706 (2020).

596. P. H. Papotto, J. C. Ribot, B. Silva-Santos, IL-17(+) gammadelta T cells as kick-starters of inflammation. *Nat Immunol* **18**, 604-611 (2017).

597. A. Schmidt, N. Oberle, P. H. Krammer, Molecular mechanisms of treg-mediated T cell suppression. *Front Immunol* **3**, 51 (2012).

598. D. K. Sojka, Y. H. Huang, D. J. Fowell, Mechanisms of regulatory T-cell suppression - a diverse arsenal for a moving target. *Immunology* **124**, 13-22 (2008).

599. L. F. Huang *et al.*, Association between regulatory T cell activity and sepsis and outcome of severely burned patients: a prospective, observational study. *Crit Care* **14**, R3 (2010).

600. X. F. Shen, K. Cao, J. P. Jiang, W. X. Guan, J. F. Du, Neutrophil dysregulation during sepsis: an overview and update. *J Cell Mol Med* **21**, 1687-1697 (2017).

601. E. Herlaar, Z. Brown, p38 MAPK signalling cascades in inflammatory disease. *Mol Med Today* **5**, 439-447 (1999).

602. H. W. Murray, Interferon-gamma and host antimicrobial defense: current and future clinical applications. *Am J Med* **97**, 459-467 (1994).

603. P. Bhat, G. Leggatt, N. Waterhouse, I. H. Frazer, Interferon-gamma derived from cytotoxic lymphocytes directly enhances their motility and cytotoxicity. *Cell Death Dis* **8**, e2836 (2017).

604. T. M. Scharton, P. Scott, Natural killer cells are a source of interferon gamma that drives differentiation of CD4+ T cell subsets and induces early resistance to Leishmania major in mice. *J Exp Med* **178**, 567-577 (1993).

605. R. Sporri, N. Joller, U. Albers, H. Hilbi, A. Oxenius, MyD88-dependent IFN-gamma production by NK cells is key for control of Legionella pneumophila infection. *J Immunol* **176**, 6162-6171 (2006).

606. S. K. Gohil, M. Heo, E. E. Schoenbaum, D. Celentano, L. A. Pirofski, CD8+ T cells and risk for bacterial pneumonia and all-cause mortality among HIV-infected women. *J Acquir Immune Defic Syndr* **60**, 191-198 (2012).

607. F. Prall *et al.*, CD66a (BGP), an adhesion molecule of the carcinoembryonic antigen family, is expressed in epithelium, endothelium, and myeloid cells in a wide range of normal human tissues. *J Histochem Cytochem* **44**, 35-41 (1996).

608. R. Kammerer, S. Hahn, B. B. Singer, J. S. Luo, S. von Kleist, Biliary glycoprotein (CD66a), a cell adhesion molecule of the immunoglobulin superfamily, on human lymphocytes: structure, expression and involvement in T cell activation. *Eur J Immunol* **28**, 3664-3674 (1998).

609. H. G. Leusch, Z. Drzeniek, Z. Markos-Pusztai, C. Wagener, Binding of Escherichia coli and Salmonella strains to members of the carcinoembryonic antigen family: differential binding inhibition by aromatic alpha-glycosides of mannose. *Infect Immun* **59**, 2051-2057 (1991).

610. H. S. Lee, M. A. Ostrowski, S. D. Gray-Owen, CEACAM1 dynamics during neisseria gonorrhoeae suppression of CD4+ T lymphocyte activation. *J Immunol* **180**, 6827-6835 (2008).

611. T. Nagaishi, H. Iijima, A. Nakajima, D. Chen, R. S. Blumberg, Role of CEACAM1 as a regulator of T cells. *Ann N Y Acad Sci* **1072**, 155-175 (2006).

612. C. Benarafa, G. P. Priebe, E. Remold-O'Donnell, The neutrophil serine protease inhibitor serpinb1 preserves lung defense functions in Pseudomonas aeruginosa infection. *J Exp Med* **204**, 1901-1909 (2007).

613. K. Farley, J. M. Stolley, P. Zhao, J. Cooley, E. Remold-O'Donnell, A serpinB1 regulatory mechanism is essential for restricting neutrophil extracellular trap generation. *J Immunol* **189**, 4574-4581 (2012).

614. M. Baumann, C. T. Pham, C. Benarafa, SerpinB1 is critical for neutrophil survival through cell-autonomous inhibition of cathepsin G. *Blood* **121**, 3900-3907, S3901-3906 (2013).

615. S. Herda *et al.*, The sorting receptor Sortilin exhibits a dual function in exocytic trafficking of interferon-gamma and granzyme A in T cells. *Immunity* **37**, 854-866 (2012).

616. H. Talbot *et al.*, Regulatory Roles of Sortilin and SorLA in Immune-Related Processes. *Front Pharmacol* **9**, 1507 (2018).

617. M. B. Mortensen *et al.*, Targeting sortilin in immune cells reduces proinflammatory cytokines and atherosclerosis. *J Clin Invest* **124**, 5317-5322 (2014).

618. J. Ma *et al.*, Lysosome and Cytoskeleton Pathways Are Robustly Enriched in the Blood of Septic Patients: A Meta-Analysis of Transcriptomic Data. *Mediators Inflamm* **2015**, 984825 (2015).

619. S. D. Kobayashi *et al.*, Rapid neutrophil destruction following phagocytosis of Staphylococcus aureus. *J Innate Immun* **2**, 560-575 (2010).

620. Y. Tang *et al.*, Bioinformatic analysis identifies potential biomarkers and therapeutic targets of septic-shock-associated acute kidney injury. *Hereditas* **158**, 13 (2021).

621. B. J. Currie, Melioidosis: an important cause of pneumonia in residents of and travellers returned from endemic regions. *Eur Respir J* **22**, 542-550 (2003).

622. R. Lin *et al.*, 6-Phosphogluconate dehydrogenase links oxidative PPP, lipogenesis and tumour growth by inhibiting LKB1-AMPK signalling. *Nat Cell Biol* **17**, 1484-1496 (2015).

623. M. Nalos *et al.*, Transcriptional reprogramming of metabolic pathways in critically ill patients. *Intensive Care Med Exp* **4**, 21 (2016).

624. S. Daneshmandi *et al.*, Blockade of 6-phosphogluconate dehydrogenase generates CD8(+) effector T cells with enhanced anti-tumor function. *Cell Rep* **34**, 108831 (2021).

625. S. Daneshmandi, T. Cassel, R. M. Higashi, T. W. Fan, P. Seth, 6-Phosphogluconate dehydrogenase (6PGD), a key checkpoint in reprogramming of regulatory T cells metabolism and function. *Elife* **10**, (2021).

626. E. L. Pearce, E. J. Pearce, Metabolic pathways in immune cell activation and quiescence. *Immunity* **38**, 633-643 (2013).

627. M. M. Rahman, G. McFadden, Modulation of tumor necrosis factor by microbial pathogens. *PLoS Pathog* **2**, e4 (2006).

628. H. T. Idriss, J. H. Naismith, TNF alpha and the TNF receptor superfamily: structure-function relationship(s). *Microsc Res Tech* **50**, 184-195 (2000).

629. J. M. Debets, R. Kampmeijer, M. P. van der Linden, W. A. Buurman, C. J. van der Linden, Plasma tumor necrosis factor and mortality in critically ill septic patients. *Crit Care Med* **17**, 489-494 (1989).

630. P. Damas *et al.*, Tumor necrosis factor and interleukin-1 serum levels during severe sepsis in humans. *Crit Care Med* **17**, 975-978 (1989).

631. F. Offner *et al.*, Serum tumor necrosis factor levels in patients with infectious disease and septic shock. *J Lab Clin Med* **116**, 100-105 (1990).

632. E. Abraham *et al.*, Double-blind randomised controlled trial of monoclonal antibody to human tumour necrosis factor in treatment of septic shock. NORASEPT II Study Group. *Lancet* **351**, 929-933 (1998).

633. C. J. Fisher, Jr. *et al.*, Treatment of septic shock with the tumor necrosis factor receptor:Fc fusion protein. The Soluble TNF Receptor Sepsis Study Group. *N Engl J Med* **334**, 1697-1702 (1996).

634. L. Zheng *et al.*, Induction of apoptosis in mature T cells by tumour necrosis factor. *Nature* **377**, 348-351 (1995).

635. S. Gupta, Tumor necrosis factor-alpha-induced apoptosis in T cells from aged humans: a role of TNFR-I and downstream signaling molecules. *Exp Gerontol* **37**, 293-299 (2002).

636. T. Yoshimoto, The Hunt for the Source of Primary Interleukin-4: How We Discovered That Natural Killer T Cells and Basophils Determine T Helper Type 2 Cell Differentiation In Vivo. *Front Immunol* **9**, 716 (2018).

637. C. A. Lazarski, J. Ford, S. D. Katzman, A. F. Rosenberg, D. J. Fowell, IL-4 attenuates Th1-associated chemokine expression and Th1 trafficking to inflamed tissues and limits pathogen clearance. *PLoS One* **8**, e71949 (2013).

638. F. A. Bozza *et al.*, Cytokine profiles as markers of disease severity in sepsis: a multiplex analysis. *Crit Care* **11**, R49 (2007).

639. J. Woytschak *et al.*, Type 2 Interleukin-4 Receptor Signaling in Neutrophils Antagonizes Their Expansion and Migration during Infection and Inflammation. *Immunity* **45**, 172-184 (2016).

640. A. Grenier *et al.*, Oncostatin M production and regulation by human polymorphonuclear neutrophils. *Blood* **93**, 1413-1421 (1999).

641. H. M. Hermanns, Oncostatin M and interleukin-31: Cytokines, receptors, signal transduction and physiology. *Cytokine Growth Factor Rev* **26**, 545-558 (2015).

642. N. R. West *et al.*, Oncostatin M drives intestinal inflammation and predicts response to tumor necrosis factor-neutralizing therapy in patients with inflammatory bowel disease. *Nat Med* **23**, 579-589 (2017).

643. Y. Gong *et al.*, Oncostatin M Is a Prognostic Biomarker and Inflammatory Mediator for Sepsis. *J Infect Dis* **221**, 1989-1998 (2020).

644. S. Verstockt *et al.*, Oncostatin M Is a Biomarker of Diagnosis, Worse Disease Prognosis, and Therapeutic Nonresponse in Inflammatory Bowel Disease. *Inflamm Bowel Dis* **27**, 1564-1575 (2021).

645. Y. Cao *et al.*, Serum oncostatin M is a potential biomarker of disease activity and infliximab response in inflammatory bowel disease measured by chemiluminescence immunoassay. *Clin Biochem* **100**, 35-41 (2022).

646. J. Hoppstadter, A. J. Ammit, Role of Dual-Specificity Phosphatase 1 in Glucocorticoid-Driven Anti-inflammatory Responses. *Front Immunol* **10**, 1446 (2019).

647. M. Hammer *et al.*, Increased inflammation and lethality of Dusp1-/- mice in polymicrobial peritonitis models. *Immunology* **131**, 395-404 (2010).

648. W. J. Wiersinga, T. van der Poll, N. J. White, N. P. Day, S. J. Peacock, Melioidosis: insights into the pathogenicity of Burkholderia pseudomallei. *Nat. Rev. Microbiol.* **4**, 272-282 (2006).

649. S. H. Kaufmann, Protection against tuberculosis: cytokines, T cells, and macrophages. *Ann Rheum Dis* **61 Suppl 2**, ii54-58 (2002).

650. J. P. Ingram, I. E. Brodsky, S. Balachandran, Interferon-gamma in Salmonella pathogenesis: New tricks for an old dog. *Cytokine* **98**, 27-32 (2017).

651. T. Kaewarpai *et al.*, Longitudinal profiling of plasma cytokines in melioidosis and their association with mortality: a prospective cohort study. *Clin Microbiol Infect* **26**, 783 e781-783 e788 (2020).

652. E. J. Hillmer, H. Zhang, H. S. Li, S. S. Watowich, STAT3 signaling in immunity. *Cytokine Growth Factor Rev* **31**, 1-15 (2016).

653. R. Lu, Y. G. Zhang, J. Sun, STAT3 activation in infection and infection-associated cancer. *Mol Cell Endocrinol* **451**, 80-87 (2017).

654. J. J. Balic *et al.*, STAT3 serine phosphorylation is required for TLR4 metabolic reprogramming and IL-1beta expression. *Nat Commun* **11**, 3816 (2020).

655. S. Xu *et al.*, Phospho-Tyr705 of STAT3 is a therapeutic target for sepsis through regulating inflammation and coagulation. *Cell Commun Signal* **18**, 104 (2020).

656. X. O. Yang *et al.*, STAT3 regulates cytokine-mediated generation of inflammatory helper T cells. *J Biol Chem* **282**, 9358-9363 (2007).

657. S. Das, S. Khader, Yin and yang of interleukin-17 in host immunity to infection. *F1000Res* **6**, 741 (2017).

658. K. Yasuda, Y. Takeuchi, K. Hirota, The pathogenicity of Th17 cells in autoimmune diseases. *Semin Immunopathol* **41**, 283-297 (2019).

659. J. L. Wynn *et al.*, Targeting IL-17A attenuates neonatal sepsis mortality induced by IL-18. *Proc Natl Acad Sci U S A* **113**, E2627-2635 (2016).

660. R. Lv *et al.*, IL-33 Attenuates Sepsis by Inhibiting IL-17 Receptor Signaling through Upregulation of SOCS3. *Cell Physiol Biochem* **42**, 1961-1972 (2017).

661. M. Ahmed Ali *et al.*, Interleukin-17 as a predictor of sepsis in polytrauma patients: a prospective cohort study. *Eur J Trauma Emerg Surg* **44**, 621-626 (2018).

662. S. Rose-John, K. Winthrop, L. Calabrese, The role of IL-6 in host defence against infections: immunobiology and clinical implications. *Nat Rev Rheumatol* **13**, 399-409 (2017).

663. C. A. Hunter, S. A. Jones, IL-6 as a keystone cytokine in health and disease. *Nat Immunol* **16**, 448-457 (2015).

664. N. C. Riedemann *et al.*, Protective effects of IL-6 blockade in sepsis are linked to reduced C5a receptor expression. *J Immunol* **170**, 503-507 (2003).

665. P. R. Taylor *et al.*, Activation of neutrophils by autocrine IL-17A-IL-17RC interactions during fungal infection is regulated by IL-6, IL-23, RORgammat and dectin-2. *Nat Immunol* **15**, 143-151 (2014).

666. F. Eddahri *et al.*, Interleukin-6/STAT3 signaling regulates the ability of naive T cells to acquire B-cell help capacities. *Blood* **113**, 2426-2433 (2009).

667. C. E. Hack *et al.*, Increased plasma levels of interleukin-6 in sepsis. *Blood* **74**, 1704-1710 (1989).

668. D. G. Remick, G. Bolgos, S. Copeland, J. Siddiqui, Role of interleukin-6 in mortality from and physiologic response to sepsis. *Infect Immun* **73**, 2751-2757 (2005).

669. J. Song *et al.*, Diagnostic and prognostic value of interleukin-6, pentraxin 3, and procalcitonin levels among sepsis and septic shock patients: a prospective controlled study according to the Sepsis-3 definitions. *BMC Infect Dis* **19**, 968 (2019).

670. J. A. Kellum *et al.*, Understanding the inflammatory cytokine response in pneumonia and sepsis: results of the Genetic and Inflammatory Markers of Sepsis (GenIMS) Study. *Arch Intern Med* **167**, 1655-1663 (2007).

671. M. Veldhoen, Interleukin 17 is a chief orchestrator of immunity. *Nat Immunol* **18**, 612-621 (2017).

672. S. L. Gaffen, The role of interleukin-17 in the pathogenesis of rheumatoid arthritis. *Curr Rheumatol Rep* **11**, 365-370 (2009).

673. Y. Ge, M. Huang, Y. M. Yao, Biology of Interleukin-17 and Its Pathophysiological Significance in Sepsis. *Front Immunol* **11**, 1558 (2020).

674. M. A. Flierl *et al.*, Adverse functions of IL-17A in experimental sepsis. *FASEB J* **22**, 2198-2205 (2008).

675. C. J. Luo *et al.*, Knockout of interleukin-17A protects against sepsis-associated acute kidney injury. *Ann Intensive Care* **6**, 56 (2016).

676. P. E. S.W. Wright, S. Sengyee, B. Cai, R. Phunpang, T. Kollmann, N. Chantratita, T.E. West in *American Thoracic Society 2019 International Conference*. (The American Thoracic Society, Dallas, Texus, USA, 2019).

677. J. C. Andreu-Ballester *et al.*, Association of gammadelta T cells with disease severity and mortality in septic patients. *Clin Vaccine Immunol* **20**, 738-746 (2013).

678. X. L. Liao *et al.*, Phenotypic Changes and Impaired Function of Peripheral gammadelta T Cells in Patients With Sepsis. *Shock* **48**, 321-328 (2017).

679. R. S. Hotchkiss *et al.*, Sepsis-induced apoptosis causes progressive profound depletion of B and CD4+ T lymphocytes in humans. *J Immunol* **166**, 6952-6963 (2001).

680. D. B. Danahy, R. K. Strother, V. P. Badovinac, T. S. Griffith, Clinical and Experimental Sepsis Impairs CD8 T-Cell-Mediated Immunity. *Crit Rev Immunol* **36**, 57-74 (2016).

681. M. Xue *et al.*, Circulating Th1 and Th2 Subset Accumulation Kinetics in Septic Patients with Distinct Infection Sites: Pulmonary versus Nonpulmonary. *Mediators Inflamm* **2020**, 8032806 (2020).

682. M. Xue *et al.*, Early and dynamic alterations of Th2/Th1 in previously immunocompetent patients with community-acquired severe sepsis: a prospective observational study. *J Transl Med* **17**, 57 (2019).

683. H. Wang *et al.*, ZAP-70: an essential kinase in T-cell signaling. *Cold Spring Harb Perspect Biol* **2**, a002279 (2010).

684. M. L. Giardino Torchia *et al.*, Intensity and duration of TCR signaling is limited by p38 phosphorylation of ZAP-70(T293) and destabilization of the signalosome. *Proc Natl Acad Sci U S A* **115**, 2174-2179 (2018).

685. C. de Roquetaillade *et al.*, Intracellular calcium signaling and phospho-antigen measurements reveal functional proximal TCR activation in lymphocytes from septic shock patients. *Intensive Care Med Exp* **7**, 74 (2019).

686. R. S. Hotchkiss, G. Monneret, D. Payen, Immunosuppression in sepsis: a novel understanding of the disorder and a new therapeutic approach. *Lancet Infect Dis* **13**, 260-268 (2013).

687. R. M. Koch *et al.*, Patterns in Bacterial- and Viral-Induced Immunosuppression and Secondary Infections in the ICU. *Shock* **47**, 5-12 (2017).